BNL 52167
UC-400
(General Energy Research -
DOE/OSTI-4500-INTERIM 3)

BNL--52167

DE90 000001

National Synchrotron Light Source Annual Report 1988

(For the period of October 1, 1987 through September 30, 1988)

Editors:
S. Hulbert, N. Lazarz, and G. Williams

The National Synchrotron Light Source Department
is supported by the
Office of Basic Energy Sciences
United States Department of Energy
Washington, D.C.

Brookhaven National Laboratory
Associated Universities, Inc.
Upton, New York 11973
Under Contract No. DE-AC02-76CH00016 with the
United States Department of Energy

Printed in the United States of America
Available from
National Technical Information Service
U.S. Department of Commerce
5285 Port Royal Road
Springfield, VA 22161

NTIS price codes:
Printed Copy: A15; Microfiche Copy: A01

Contents

SECTION VI

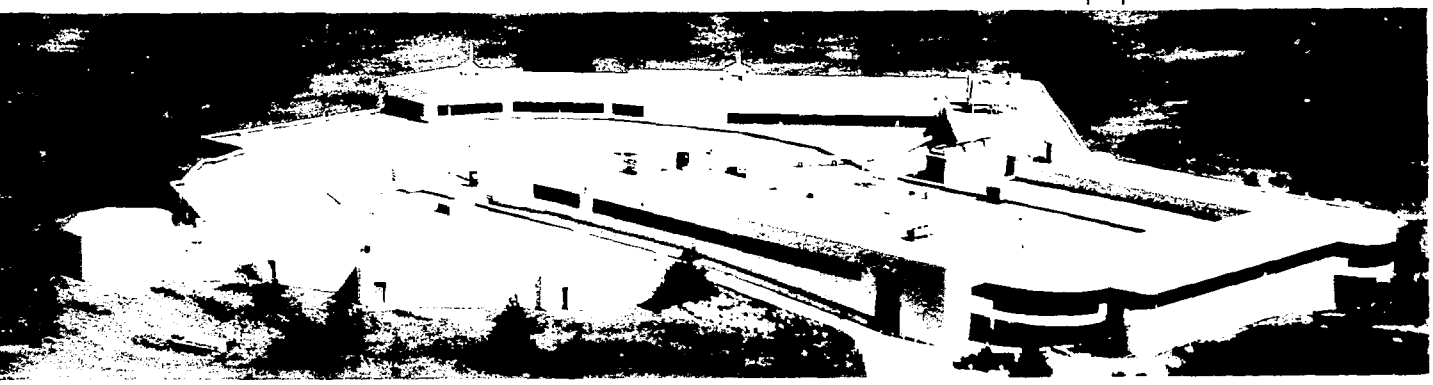

Section I

Introduction

Introduction

Michael Knotek
Chairman, NSLS

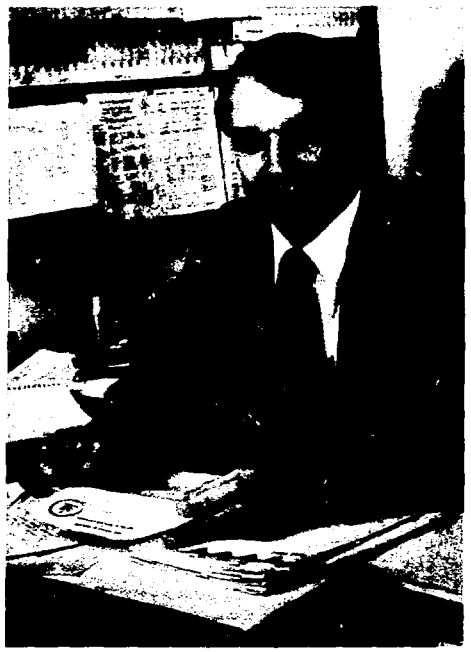

1988 was an especially important year for the NSLS and the User community. The VUV ring enjoyed a year of virtually uninterrupted running, and the X-ray ring came back into operation after a long and difficult shutdown for installation of insertion devices and hardware revamping. The Phase II program included the installation of 26 new beamlines on the two rings and by mid-1989 we will have twelve insertion device beamlines on seven insertion devices on the two rings. Sometime in 1989 we will have over 95 beamlines in operation on the two rings. A major effort throughout 1988 was the development of new orbit stability hardware and methodology. The replacement of virtually all electronics on both rings to remove any sources of noise is being followed by installation of dynamic feedback systems for both local and global control of the orbit on both rings. All of this activity is aimed at providing state-of-the-art, stable, reliable, and *continuous* operations for many years to come.

Management Activity

1988 was a busy year for the NSLS management and the User community. The Program Advisory Committee , which saw Paul Horn and Ken Kliewer rotate off and Hugh Huxley, a structural biologist, and Tom Baer, a chemist, become new members, gave final approval to the NSLS Policy and Procedures Document, and gave approval to several additional PRT's and Stewardship groups. The PAC is now beginning it's review of the PRT's after the completion of their first three years of activity at the NSLS. There are nearly 60 PRT's to be reviewed during 1989 and early 1990.

Throughout 1988, the Scientific Program Support Committee, which is comprised of NSLS Staff and Users, diligently examined all aspects of the User program at the NSLS and ways in which the NSLS can improve the lot of our User community. They produced numerous reports on staffing, safety and housekeeping, meetings, communications, support services, work environment, and looked into many more areas. They have noticeably improved communications, with a new experimenters handbook, an NSLS Community Directory, and greatly improved communications and procedures in the operations/user community interface. We are deeply indebted to Bill Thomlinson and Denis McWhan, the Co-Chairmen of the committee, and the committee members for their selfless commitment and hard work. The NSLS is firmly committed to carrying out the recommendations of the SPSC, and will continue work with the UEC to continue the SPSC as an ongoing way to keep up with the needs of NSLS staff and Users.

Science at the NSLS

The VUV ring Users had a very productive year. In X-ray lithography, IBM produced working 0.5 micron design rule chips during several wafer runs at U6 in which all exposure levels were done with X-rays. The effort is now expanding with a second "production" line at U2. The spin-resolved photoemission effort at U5 produced some beautiful results for adsorbates on magnetic surfaces. The EXXON people at U1 continued their high pressure surface work employing Fluorescence Yield Near Edge Spectroscopy (FYNES). At U4B the Bell Labs group achieved new levels of resolving

power (~ 10,000 at the nitrogen K edge) and are now opening new areas of study of excited state potentials of adsorbates. On U3 some interesting studies of X-ray induced bonding to teflon were performed by the Sandia group. The U41R beamline, installed as part of Phase II, came into full operation and is proving to be extremely useful. U7 has conducted numerous important investigations of low temperature oxidation and high T_c materials. Electron-electron measurements at U12 and U14 and electron-ion measurements at U15 have provided state specific electronic structure information and insight into bond dissociation mechanisms, respectively. At numerous beamlines around the VUV ring, extremely sophisticated studies of adsorption, and surface and interfacial reactions have taken place.

The X-ray ring came back on the air in March 1988 after a long shutdown. The Users were ready with numerous experiments and most groups had significantly improved their beamlines. The X1 undulator was in place and running early and the X25 wiggler line had taken light by the end of the year. All five insertion devices will be in place early in 1989.

Numerous efforts are now pushing magnetic scattering measurements into new areas. A collaboration of groups working at X14 has measured resonant magnetic scattering peaks in the antiferromagnet, UAs, which have 10% of the strength of charge scattering peaks. X16 was used for a number of studies of surface structures and roughening which set a new level of rigor in the field. X11 efforts included studies of high T_c materials, multilayers and zeolite materials. X12 carried out some important structural studies of the Rhinovirus. X3 has carried out anomalous contrast crystallography on high T_c materials and time dependent SAXS and WAXS studies of protein folding. X15B came online with a beautiful beamline for SEXAFS studies in the 1-4 keV region. X26 used X-rays for the production and trapping of multiply charged ions. The microtomography effort at X10 has pushed ahead with the EXXON group now targeting resolution far below 1 micron.

Finally, the excellence of the innovative instrumentation of our user community was recognized with two IR-100 awards by *Research and Development Magazine*. The Bell Labs group at U4B received one for the "Dragon" monochromator, and the BNL Department of Applied Sciences received one for the collimated X-ray microprobe at X26. Our congratulations to both groups.

Users Executive Committee

Dale Sayers
Chairman, UEC

The Users Executive Committee met on four occasions during the past year. Its main activities centered around establishing a more user friendly environment as the Light Source moved out of Phase II and into a fully operational mode. One of the main activities was participating in and working with the SPSC. Denis McWhan of the UEC served as vice-chairman of the committee and other members of the user community were active participants. The UEC met regularly with representatives of the SPSC and on a number of occasions provided constructive comments and input to their activities. We also worked on other environmental factors for Users such as space allocation, improved accounting procedures and communication, including both computer support and telephone service.

Other significant activity for this period included:

1. Interaction with the Cardillo Committee and the Richard's Committee of the AUI;

2. Continued discussion and development of procedures for General Users, including beamline utilization and training and review of the GUOC and PSP process;

3. Discussions with the NSLS on machine scheduling including attempts to develop a fixed long range scheduling process, a review of the shutdown plans on the VUV ring and the approval and submission of a report on X-ray scheduling;

4. Initiation of a community meeting prior to the UEC meetings to improve communication between the UEC and the General User community; and,

5. Revision of the UEC charter which will be submitted this spring to the general body for approval.

The following people are members of the NSLS Users Executive Committee:

Dale Sayers North Carolina State University	Chairman
Denis McWhan AT&T Bell Labs	Vice Chairman
Janos Kirz SUNY at Stony Brook	Past Chairman
Wolfgang Eberhardt EXXON Research and Engineering Company	Member
Richard Hewitt EXXON Research and Engineering Company	Member
Gene Ice Oak Ridge National Laboratory	Member
Peter Johnson Brookhaven National Laboratory	Member
Keith Jones Brookhaven National Laboratory	Member

UEC Subgroup Reports

Atomic and Molecular Science

David M. Hanson, Stony Brook, SUNY
Subgroup Representative

A wide variety of research that can be classified as atomic and molecular science is being conducted at NSLS. This overview highlights some of the work that does not overlap that of other subgroups. Readers are directed to the Abstracts (Section V), which are organized by beamline, for details.

Autoionization and Auger decay of core hole states in molecules (U1, U15).

Molecular fragmentation following core electron excitation (U1, U15).

VUV and soft X-ray photochemistry of polymers (U3C, U6).

Use of the high resolution Dragon monochromator to measure structure in the soft X-ray absorption spectra of transition metal compounds, CO, N_2, and benzene (U4B).

Fluorescence lifetimes of molecules following VUV excitation (U9A).

VUV photochemistry of excimer-forming mixtures of gases, state specificity of the reactions (U9A).

Circular dichroism of nucleic acids and membranes in the VUV (U9B).

Valence photoionization of small molecules and van der Waals complexes (U11).

Photoionization of atoms above the second ionization potential (U11).

Fluorescence of Auger decay products (U15).

Nucleic acid structures in solution by X-ray scattering (X3).

Small angle X-ray scattering of block co-polymers (X3).

Time resolved small angle X-ray scattering (SAXS) and wide angle X-ray scattering (WAXS) studies of the crystallization of polyethylene blends (X3).

Morphology of ionomers and polydiacetylene by X-ray scattering (X3).

X-ray diffraction of a single Kevlar fiber (X3).

Orientation of Langmuir-Blodgett films, liquid crystals, and monomolecular films on liquid substrates from near edge X-ray absorption fine structure (NEXAFS) and X-ray scattering (X3, X20, X23B, U14).

Studies with X-ray absorption near edge structure (XANES) of metallo-enzymes and valency in copper compounds (X9A, X18B).

Production and trapping of multiply charged atoms (X26C).

Energy Dispersive Diffraction

David Cox, BNL Physics Department
Contributor

Energy-dispersive diffraction at the NSLS is carried out mainly at white-light beamline X7A (formerly X13A). Unfortunately, the new beamline only achieved operational status in December 1988 because of front-end alignment problems, and there are no new experimental results to report. Most of the energy-dispersive program is directed towards diffraction in diamond-anvil cells at very high pressures (up to 2Mbar) involving, in particular, groups from the high pressure laboratories at Carnegie Institution, Naval Research Laboratory, Los Alamos National Laboratory and their collaborators. Several improvements have been made at the new beamline; among those especially useful for high-pressure studies are the installation of a tanzboden, which will allow precise control of the movement of the diffractometer in the horizontal scattering plane, and the new slit system for the incident beam which can be moved in steps as small as 0.2μm.

Extended X-Ray Absorption Fine Structure (EXAFS)

Pedro Montano, Brooklyn College, CUNY
Subgroup Representative

There has been considerable activity in the X-ray absorption beamlines during the past few months, after recommissioning of the X-ray ring. The experimental work was concentrated at beam lines X9, X11, X18B, and X29B. A brief summary of some of the important results obtained during this period is given in the following paragraphs.

The use of X-ray absorption techniques to characterize high T_c superconductors was emphasized: Polarized X-ray absorption studies were carried out at the Cu K-edge to study the effect of Sr doping in La_2CuO_4 and oxygen doping in $YBa_2Cu_3O_{6+x}$. The experimental results were explained using detailed embedded cluster calculations (E.E. Alp, S.M. Mini, M. Ramanathan, B.W. Veal, L. Soderholm, B. Dabrowski, G.K. Shenoy, J. Guo, D.E. Ellis, A. Bommannavar, and O.B. Hyun). Oriented high T_c superconductors were prepared by casting 400 mesh powders in epoxy in an 8T magnetic field. Four classes of superconductors were studied: $YBa_2Cu_3O_{6+x}$, $BiSr_{1.75}Ca_{1.25}Cu_2O_{8+x}$, $Tl_2Ba_2CaCu_2O_x$, $Tl_2Ba_2Ca_2Cu_3O_x$, and $La_{1.85}Sr_{0.15}Cu_2O_4$. Measurements were performed with the X-ray polarization vector, parallel and perpendicular to the c-axis of the samples. For the perpendicular case, all the edges were very similar since the X-rays probe the Cu-O planes which are common to all the materials. For the parallel case, the spectral features of the edges are different, but all edges show a weak 1s-4pπ shakedown peak (S.M. Heald, J.M. Tranquada, A.R. Moodenbaugh, Y. Xu, M.A. Suramenian, and A.W. Sleight). The chemical and structural modification of the 1-2-3 high T_c superconductor by water was examined by EXAFS. Examination of the Cu K-edge is consistent with a partial reduction of copper from 2+ to 1+ oxidation state (M.W. Ruckman, S.M. Heald, D. Di Marzio, and A.R. Moodenbaugh). Cu K-edge X-ray absorption measurements were also performed on thin films of superconducting $Tl_2CaBaCu_2O_x$ (T_c=105 K). The near edge and EXAFS spectra of the films exhibit diminished oscillations which are characteristic of reduced long range order (D. Di Marzio, D.H. Chen, S.M. Heald, R.L. Sabatini, and H. Wiesman). X-ray absorption measurements were also performed on Ba-K-Bi-O superconductors. The L_3, L_2, L_1 absorption edges of Bi were measured for different compounds in an effort to establish the difference between formally +3, +4, and +5 bismuth oxides. The series of $Ba_{1-x}K_xBiO_3$ compounds is superconducting at 30 K for $0.30< x <0.45$. Very little change in the Bi L_3 edge was observed for all the samples. This may support the view that the charge compensation for K doping may come predominantly from the oxygen atoms rather than from the Bi atoms directly (E.E. Alp, S.M. Mini, L. Soderholm, G.K. Shenoy, M. Pamanathan, B. Dabrowski, D.G. Hinks, and A.S. Bommannavar).

Reflection and glancing incidence EXAFS is finding wide application in the study of interfaces. Reflection mode EXAFS with fluorescence detection has been used to probe the Al/GaAs interface to determine directly the interdiffusion, compound formation, and phase segregation near the interface. Preliminary results of both the As and Ga K-edges show clear interdiffusion of the Al into the GaAs (P. Bandyo-padhyay and B.A. Bunker). The glancing angle EXAFS technique has been applied to investigate the structure of W/C multilayers and the effects of moderate annealing. It is found that after annealing to 350 C for several hours, drastic changes can occur in the environment of the W atoms, with minimal changes in the reflectivity of the layers. There is formation of W2C depending on the W thickness and the W/C ratio (G.M. Lamble, S.M. Heald, D.E. Sayers, E. Ziegler and P.J. Viccaro). Glancing angle EXAFS was also used to study the reactions at the interface in Al/Nb films. It was observed that ion beam irradiation tends to induce disordered or short-range-only ordered phases which depend strongly on the irradiation condition (Z. Tan, J.I. Budnick, Y. Bruynserade, W. Sevenhans, S.M. Heald, and J.M. Tranquada). Conversion electron X-ray absorption fine structure was successfully employed to determine the crystallographic structure of Co films deposited on GaAs. The crystallographic structure of the cobalt films was unambiguously determined as bcc, with an extracted lattice constant of 2.83 Å (Y.U. Idzerda, B.T. Jonker, W.T. Elam, and G.A. Prinz).

EXAFS was used to determine the structure of Cu/alumina sorbents used for the removal of SO_2 from flue gases. The measurements over a wide range of temperatures indicated that the copper is surrounded by an average of 2.4-2.7 oxygen atoms and that the CuO units are very small or amorphous. The low coordination number may be related to the fact that the material is a good sorbent for SO_2 (S.S. Pollack, W.P. Chisholm, R.T. Obermyer, S.W. Hedges, M. Ramanathan, and P.A. Montano).

There was great activity in the past year in the application of X-ray absorption techniques to the biological sciences. A diversity of experiments were performed at NSLS, only a couple of which are reported here. The active site of carboxilato-bridged diferrous proteins was studied to determine how changes in the iron environment of these proteins affect their catalytic function. EXAFS measurements were performed on deoxyhemarythrin and diferrous forms of methane moncoxygenase and ribonucleotide reductase. Further experiments were used to probe the structure of a model compound of bridged diferric proteins $Fe_2(HPTB)(Me)_2(NO_3)_5$, and to study the changes in the iron environment when hydrogen peroxide is complexed with this compound (L. Que and A. True). Experiments were performed using X-ray absorption techniques to study the effect of synchrotron radiation on cytochrome c oxidase. These experiments confirmed that cytochrome oxidase gets reduced at room temperature. In addition to the reduction of the heme, the activity was also found to be diminished by prolonged exposure (8 hours). These damages can be reduced by cystamine, which was found to be more effective than other radical scavengers (I. Ayene and B. Chance).

Microscopy and Lithography

Christopher Buckley, Stony Brook, SUNY
Subgroup Representative

In order to take advantage of imaging at high spatial resolution with soft X-rays, the imaging system must allow the scientist to roam the specimen and select areas for detailed study. In visible light microscopy and electron microscopy, the image time in the inspection mode is usually a few seconds, while the micrographs of the area of useful detail take less than a minute. In order to approach this kind of imaging rate using X-ray microscopy, a very bright source of soft X-rays is required. This source has been realized at the Soft X-Ray Undulator on beamline X-1 at the NSLS.

The undulator was installed in July 1988. The source has a peak brightness of 10^{17} photons/s/mm^2/mrad^2/0.1% bandpass. The stability of the source is maintained by a closed orbit feedback system. The imaging branch of the X1 beamline (X-1A) uses a spherical grating monochromator with two exit slits, so that two imaging experiments can operate at the same time. The imaging program includes scanning transmission X-ray microscopy, scanning photoemission microscopy, holography (Gabor and Fourier transform) and soft X-ray diffraction.

The construction of the beamline has taken place in three phases. The first was to establish a good electron beam orbit and implement the feedback system. This was successfully completed in September and the feedback system continues to be refined during study periods. The second phase involved the construction of the monochromator, which was characterized and used to investigate the output of the undulator. Both the monochromator and the undulator have performed well. This data was taken in September and October 1988 after which the exit arm of the monochromator was disassembled to allow for the final construction phase of the beamline. Two exit slits will be installed on the monochromator and two mirrors will be used to illuminate two experimental stations. The construction is almost complete and first experiments are expected to begin in early December, 1988.

In lithography, IBM have used synchrotron radiation in each of the several exposure stages required to fabricate a micro circuit. The work has resulted in the fabrication of working microchips. At U2, IBM have nearly completed a production beam line for lithography. Commissioning is expected to take place in January, 1989.

Activity in synchrotron X-ray microtomography by the Exxon PRT has concentrated on the design of the dedicated beamline X2. This line will be optimized for microtomography studies and will be coming on line in early 1989.

Photoemission and Surface Science Subgroup

Thor Rhodin, Cornell University
Subgroup Representative

This summarizes work accomplished primarily in photoemission spectroscopy and related areas which is one of the main research activities of 14 beamlines in the VUV ring. Of the remaining 5 beamlines, 4 are mainly devoted to microlithography and other non-photoemission purposes and one to infrared spectroscopy. Of the 120 submitted abstracts summarized for this subgroup, 70 relate more or less directly to photoemission and 50 refer to the closely related areas of photofragmentation, fluoresence yield near edge spectroscopy (FYNES), soft X-ray surface extended X-ray absorption fine structure (SEXAFS) and near-edge X-ray absorption fine structure (NEXAFS) spectroscopy, photoabsorption, soft X-ray fluoresence spectroscopy, photoionization studies, electron-ion and photon-electron coincidence studies, and soft X-ray reflectivity and microscopy.

Rather than summarize each study, reference will be confined here to either the largest efforts or the more innovative work. For details, see the individual abstracts in Section V.

Photoemission Work: Valence band photoemission has been used in a variety of ingenious ways to investigate the electronic structure, composition, orientation and atomic structure of clean metal and semiconductors surfaces and interfaces, epitaxial films, condensed and chemisorbed layers, thin films, and chemically reacted layers. A clever measurement of sigma-bond energy splitting for adsorbed oxygen was used to determine molecular bond length distortion for O_2 on Ag (110). In another study, high resolution photoemission of GaAs and Si semiconductor surfaces was used to determine changes in electron structure and chemical bonding upon thermal and chemical treatment.

Another highly refined application is band mapping and Fermi surface characterization of Mo(011) and W(011) surfaces using very high momentum resolution angle-resolved measurements. A related fruitful area for quantitative electronic and atomic structure studies concerns the early stages of metal-semiconductor and metal-metal interface formation using quantitative band mapping techniques. A significant investigation of a related property, that of surface electronic excitations, was successfully achieved using Auger photoelectron coincidence spectroscopy (APECS) of Ta(001) and Cu(001).

A significant new advance is the implementation of spin polarization instrumentation to study magnetic and other electron spin effects at surfaces. For example, the observation of exchange splitting in oxygen and sulfur adsorption on Fe(001) has been recently observed.

Another promising new development is the measurement of surface and interface electronic structure induced by the growth of ultrathin metal film overlayers on single crystal metal substrates using both VUV and soft X-ray photoelectron spectroscopy. The occurrence of pseudomorphic overlayers can have marked effects on surface crystallography, electronic properties, and chemical behavior. Extension of these studies to bimetallic alloys and intermetallic surfaces has also begun.

A new understanding of oxygen interactions with metals, semiconductors and inorganic compound surfaces has been another fruitful area for photoemission studies. Interesting applications have been made to the oxidation of various metal overlayer systems, oxygen interactions with cerium and cesium, properties of metals deposited on solid oxygen, formation of metal-oxygen species at low temperatures, and the surface electronic structure and chemistry of high T_c superconductors ($YBa_2Cu_3O_7$). Important valence band electronic structure and core level shift measurements of single and polycrystalline metal oxide surfaces critical to catalyst support and superconductor studies have also been performed.

Photoemission-Related Work: Significant work has also been achieved involving concepts and techniques similar to that of photoemission and producing closely related new information on surfaces, films and overlayers.

The decay mechanisms of 5-membered ring cyclic compounds as well as CS_2 have been measured via the dependence of core photofragmentation processes on the site of core excitation. Another new technique, that of fluoresence yield near edge spectroscopy (FYNES) has also been effectively applied to dispersed-catalyst characterization. High resolution NEXAFS exploiting fluoresence detection has also been developed for probing the nature of chemical bonding in condensed and adsorbed layers. Two similar techniques which are proving very useful involve the use of ultra-soft X-ray fluorescence EXAFS and total electron yield EXAFS, depending on the relative cross-sections and backgrounds for photons and electrons.

In another approach, crystal field splittings in ionic crystals have been measured using high resolution photoabsorption. This technique has also been used to probe molecular potentials in the presence of core holes as well as for the exact determination of intrinsic line shapes for C_{1s} and N_{1s} excitations.

Fluorescence measurements have also been applied to a variety of photon-excited phenomena including rare-gas matrix isolated small hydrocarbons, lifetime excited states of chlorine, excited cyclohexane in an argon matrix and VUV light-induced reactions of halogenated gases. The technique of soft X-ray fluorescence spectroscopy has also been used to explore the electronic density of states of carbon-silicon interfaces, a very important aspect of VLSI device development.

NEXAFS spectroscopy for the measurement of structure and bonding is being continuously extended to new practical coating applications involving, for example, ordering in polypyrrole and polythiophene Langmuir-Blodgett films, orientational behavior of poly(3-methylthiophene), and hexadecyl-pyrrole films on platinum as well as thickness and annealing effects of polyacrylonitrile films on nickel.

Soft X-ray reflectivity studies have been applied to the characterization of InGaAs/InP and of InGaAs/GaAs for determining electron density profiles vs. depth in layered or stratified materials. Total electron yield (TEY) from soft X-ray excitation of AlAs/GaAs and Ga/AlAs heterjunctions has also proved to be very useful for the same purpose. The availability of a very bright soft X-ray source is critical to the use of soft X-ray microscopy as a general tool for examining such buried interfaces. Another somewhat related measurement which is in a preliminary stage of development is the use of reflection-EXAFS to investigate the structural influence of alloy additions to surfaces of metal films.

(Editorial Note: The above is limited to abstracts of photoemission and related work received at this time for the following beamlines: U1, U3, U4B, U5, U6, U7A, U7B, U8, U10, U11, U12, U14, U15 and U16B. The microlithography, TOK and infrared work is not included).

X-Ray Crystallography

Hubert King, Exxon Research and Engineering
Subgroup Representative

The crystallographic activities reported here are those pertaining to experiments on single-crystal samples. Other crystallographic studies, for example those on polycrystalline powder samples, are reported elsewhere (see Abstracts, Section V).

The single most important activity to report in this period is the reappearance of user beam at NSLS. This comes after an extended, 16 month, shutdown. The Phase II shutdown began in March 1987 and ended with usable beam becoming available again in mid July 1988, but the first scheduled user beam was not until October. Although such a long shutdown disrupted many research efforts, it will ultimately bring benefits. Among the important work accomplished was the installation of several insertion devices. Crystallographic uses for two of the wiggler beamlines are already planned. A 6-circle diffractometer is being installed on X17 and Laue diffraction measurements are

planned for X25. In addition, several beamlines were moved during this shutdown and new crystallography beamlines continue to be constructed. The first light in beamline X10B was obtained just before the shutdown, and X4 is now under construction. In anticipation of greater User need for darkrooms, two are now available and new procedures for their use have been established. Details can be obtained from the darkrooms czars, R. Sweet (X12C) and A. Kvick (X7B). There has also been progress on setting up a sample alignment facility. An X-ray generator has been donated by the Brookhaven Chemistry Department and a room to house it is under construction. Still needed are a radiation enclosure and various types of cameras.

The severely restricted beamtime for this period has obviously significantly reduced the experimental activity reported in this year's annual report.

Among the small-molecule crystallographic experiments are those on the 2-2-1-2 bismuth-copper-oxide superconductor performed by workers on beamline X3. Intensities for several Bragg reflections were measured from a small single crystal for two incident-radiation energies, above and below the bismuth K adsorption edge (≈13 KeV). A differential analysis technique, relying on the change in bismuth's anomalous scattering was then used to pinpoint the bismuth atom locations. Especially important was the determination of the bismuth atom concentration on mixed-atom structural sites which also contain strontium and calcium atoms. Localization of the bismuth atoms within particular layers in the structure is thought to be influential in the superconducting behavior.

Work on macromolecular crystals has also continued through use of the facilities of beamline X12C. A group from UCLA and UCSD refined the structure of the photosynthetic reaction center from *rhodobactor sphaeroides* to an improved resolution over that of previous refinements through use of data taken at NSLS. The structure of Asp-43 mutant staphylococcal nuclease was determined and refined to a resolution of 1.65Å by a group from John Hopkins Medical School. An extensive study to characterize crystallographically the effect of a series of antiviral agents on human rhinovirus 14 was carried out by a large group from Purdue, Sterling-Winthrop Research Institute and the Institute for Molecular Virology. Also, workers from Fox Chase Cancer Center and Albert Einstein College of Medicine began solving the structure for crystalline AMP nucleosidases from *escherichia coli* and *azotobacter vinelandii* by determining the subunit symmetries and orientations in their unit cells.

X-ray Fluorescence Subgroup

Mark L. Rivers, University of Chicago
Subgroup Representative

General Progress

The X-ray fluorescence (XRF) work at the NSLS is principally performed on beamline X26. Prior to the X-ray ring shutdown, fluorescence microprobe studies were done on X26C, using mainly unfocussed filtered white radiation. X26C was shared by the XRF microprobe and atomic physics experiments. Work on X26 during the X-ray ring shutdown concentrated on hardware and software upgrades and construction of beam line X26A.

The X26C beam line is now equipped with a cylindrical mirror designed for 1:1 focussing of white light. The mirror performance seems to be excellent. While this beam line will mainly now be used for atomic physics experiments, it will also be very useful for XRF microprobe studies when a pinhole is used in the focussed beam.

The X26A beam line is advantageous for XRF microprobe studies for two reasons: 1) the hutch is half the distance to the X-ray source so the flux is 4 times greater and 2) an 8:1 focussing mirror will be installed. The focussing mirror is currently being coated and is expected to be installed over the Christmas 1988 shutdown. The increased flux from the mirror will allow the effective use of a wavelength dispersive spectrometer (WDS) detection system, and a Cameca crystal spectrometer is currently in hand for this purpose. WDS is desirable for improved signal-to-background and for elimination of diffraction interference, but simultaneous analysis of many elements is compromised.

In principle, the flux should be increased by a factor of 1,000 using the mirror but the raw spot size produced will be about 100 microns. Laser-drilled holes in Au and Pt will be mounted a few mm upstream of the sample to produce a 10 micron spot. An x-z-θ-ϕ stage will be used to accurately align the large aspect ratio (about 20) pinhole. The grazing incidence mirror has a high energy cutoff of about 17 keV.

The increased flux provided by the mirror will also permit the use of a monochromator when desirable to allow the incident energy to be tuned for selective elemental excitation and thereby improve signal-to-background even further. However, the monochromator will reduce the flux by a factor of 1000 nearly cancelling the flux gain of the mirror and ruling out the use of a WDS detector in this configuration.

The combination of these upgrades is expected to lead to improvements in elemental sensitivity of about one order of magnitude, i.e., near the 100 ppb level for 10 micron spots and 10 minute acquisitions.

The light optics have been upgraded to a Nikon Optiphot petrographic microscope equipped with reflected and transmitted light illuminators and a TV camera. An image processing system consisting of a frame grabber board for the MicroVAX, Sony RGB color monitor, and AUTOCAM image recorder with 35 mm and Polaroid camera backs has been added. The image processing capability has two main uses: 1) real time contrast enhancement of specimen images for accurate identification of analyzed regions and 2) computer enhancement, false coloring, and hardcopy production of elemental maps resulting from 2-D XRF elemental scans.

The data analysis procedures have been significantly improved. A program called SPCALC has been written to perform background removal and peak fitting. It can be used either in interactive or "batch" modes for critical or routine analyses. The net peak areas can then be read into the 20 20 spreadsheet on the MicroVAX, where corrections for standards, beam current, theoretical sensitivities, etc. are made. These improvements should increase the speed and remove much of the drudgery which has been required to analyze the synchrotron XRF data in the past. We expect that most users will now have final results in ppm before they leave the NSLS.

X-ray Microprobe Receives R&D 100 Award

The collimated X-ray microprobe has been nationally recognized by *Research and Development Magazine* as one of the top 100 inventions in 1988. Keith Jones attended the gala ceremony in Chicago.

CHESS Run (May, 1988)

Mark Rivers, Steve Sutton, and Barry Gordon were privileged to perform some XRF measurements using the Advanced Photon Source (APS) prototype undulator (3.3 cm period, 61 periods) during its testing on the CESR storage ring at Cornell (5.5 GeV, 100 mA). The undulator was operated with the gap either fully closed (first harmonic at 4.4 keV) or open (first harmonic at 7.1 keV). Ring currents below 5 mA were necessary to avoid high radiation levels outside the hutch and saturation of the Si(Li) fluorescent X-ray detector. The microprobe beam was defined with two pairs of 6 mm thick tungsten slits which were rotated to vary the apparent hole diameter down to below 10 microns. Fluorescence spectra were collected from a number of standards and unknowns. Several one-dimensional multi-elemental scans and two dimensional images were made with 10 micron resolution and 30 ppm minimum detectable limit (MDL). These results demonstrated that the APS, with lower emittance, higher energy, and higher currents than CESR, will be a suitable source for a submicron XRF microprobe.

X-ray Scattering

Gerald Liedl, Purdue University
Subgroup Representative

Throughout this past year the members of this group have redirected their activities while the X-ray ring has been down. For many, this time was fruitful for making changes in beamlines to improve performance while for others it has been time needed for the construction of new beamlines. There are now, in operation or under construction, twenty-seven beamlines which have as their primary focus the use of X-ray scattering in the research being conducted. The large addition to the scattering beamlines comes from the completion and opening of the ports on the first segment of the X-ray ring, i.e., X1 to X9. Also, the shutdown was used to construct the front-end and beamline for the X17 superconducting wiggler. Many of the beamlines made use of the down-time to improve beamline optics and solve those problems that became apparent during initial stages of operations; for example, the MATRIX beamline (X18A) replaced the entire optical system, with an emphasis on simplicity and stability of operations coupled with ease of monitoring the beam at critical locations.

During the summer and early fall, while the NSLS was reestablishing the operation of the X-ray ring, most of the operational beamlines were using the available beam to get their beamlines functional again and to conduct some experiments. As one might expect, there was some action regarding the ever popular area of high T_c superconductors with work being done on X3, X7A, and X22C. One can expect more work in this area in the coming year as all the beamlines become fully functional. Both the resolution capabilities and the anomalous contrast capabilities are being exploited.

Surface scattering studies, which were a major area of work before the shutdown, are expanding in scope. New instrumentation such as the one reported for X22C will provide expanded capabilities compared to those of the earlier systems. Expanded types of information are now being reported, such as the ordering work of the MIT group on X20 and the roughening transition work of the AT&T Bell Labs group on X16A.

Two techniques which are just becoming major ones at the NSLS are small angle X-ray scattering (SAXS) and powder diffraction. The high resolution powder diffraction pattern taken with a linear position-sensitive detector was shown by D.E. Cox, et. al. on X7A to yield comparable data to a conventional scan. These results are just beginning to show the potential for powder diffraction studies. The SAXS experiments of the SUNY Stony Brook group on X3 were used to provide some interesting insight into morphology and crystallization kinetics of polymers.

Finally, some novel new approaches have been made in the realm of microdiffraction. G.E. Ice on X14 has shown that submicron regions can be studied and has shown applications to strain fields around a particle. A novel extension by the NRL group on X23 has shown how one can get orientation data from the individual spots of the Debye-Scherrer ring.

These results are just the tip of the iceberg as we approach full operations of the ring this year. The research, rather than the instrumentation, is becoming the dominant factor, a sign of coming-of-age of the X-ray scattering area at the NSLS.

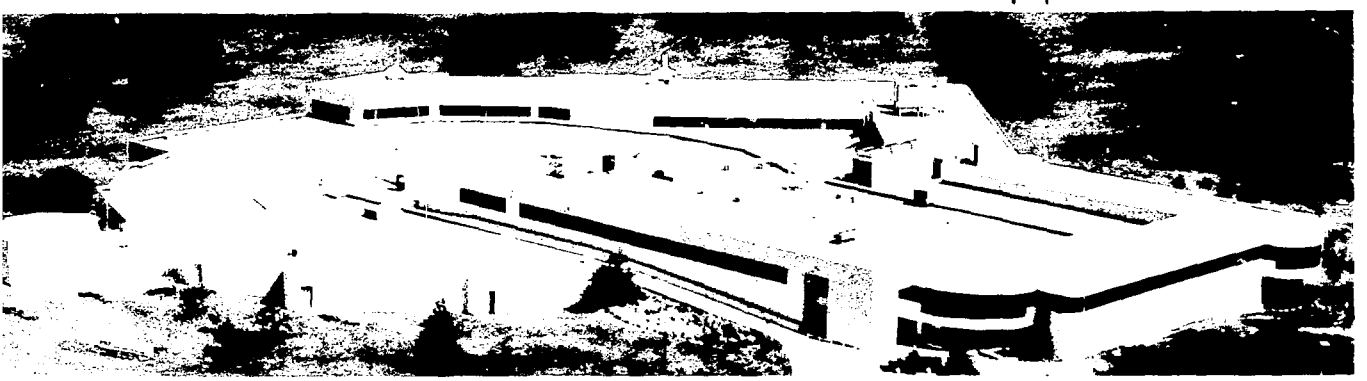

Section II

Operations Summary

15/16

VUV Machine Operations

Anne Marie Fauchet
NSLS VUV Ring Manager

VUV Ring Performances and Studies

Average performances of the VUV ring for fiscal year 1988 are given below:

Average Filling Current	730 mA
Average Charge Rate	33 mA/minute
Average 200 mA Lifetime	209 minutes
Total Amp Hours	1977 AH

A peak current of 1.3 A in multibunch mode was reached in February following improvements to the radio-frequency source for the main 53 MHz cavity.

Testing of the 211 MHz RF cavity is continuing. The goal of this R&D program is to lengthen the electron bunch, and thus improve the lifetime by running the VUV ring with two RF cavities, the main cavity and a fourth harmonic cavity appropriately tuned and phased. Bunch lengthening by more than 60% with 700 mA in 5 bunches has been achieved with beam-induced voltage in the harmonic cavity. The theoretical trapezoidal shape of the bunch has been observed under the same conditions. A 211 MHz, RF power driven transmitter slaved to the main cavity is under development to provide bunch lengthening in a more controlled manner.

Bunch length measurements have been performed under normal operating conditions and at several values of the electron energy and momentum compaction. The graph below gives the measured bunch length versus average current per bunch under conditions close to the present operating conditions.

RF receivers for a fast orbit measurement system have been extensively tested; the global harmonic feedback has reduced vertical orbit motion by a factor of 5 or better during studies. The final system, including 8 RF receivers, will be operational by mid 1989.

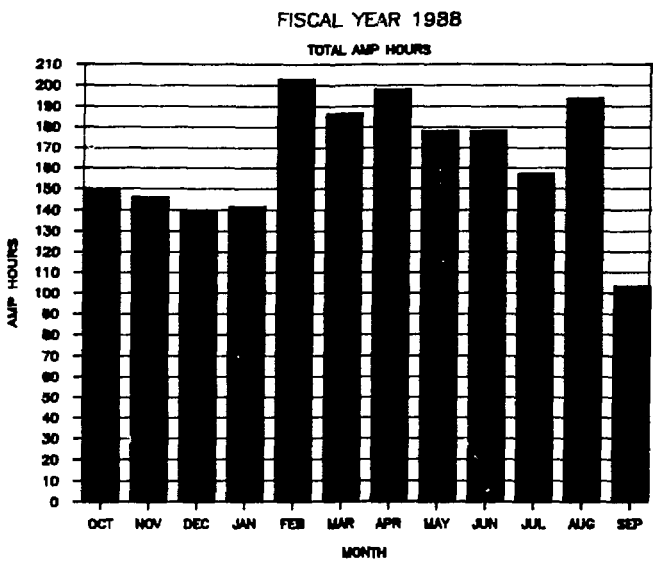

FIGURE 1: Total Monthly Amp Hours NSLS VUV Ring During FY 1988

RF receivers for a fast orbit measurement system have been extensively tested; the global harmonic feedback has reduced vertical orbit motion by a factor of 5 or better during studies. The final system, including 8 RF receivers, will be operational by mid 1989.

In the TOK experiment, gain was measured at the argon laser wavelength using either the first or the third harmonic of the wiggler. Interaction between the pulsed, high power Nd:YAG laser and the electron beam was first observed in February as evidenced by an increase in electron beam energy spread synchronous with the laser firing.

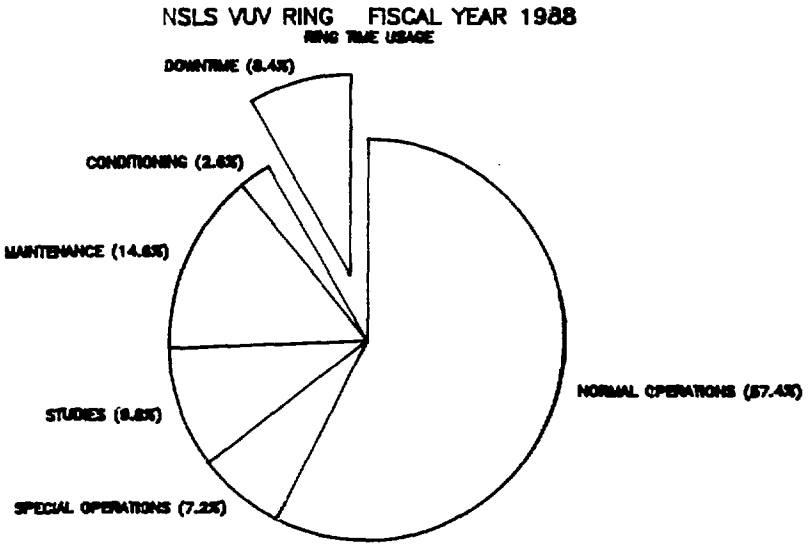

FIGURE 2: Utilization of the VUV Ring for FY 1988 Percentage in Time

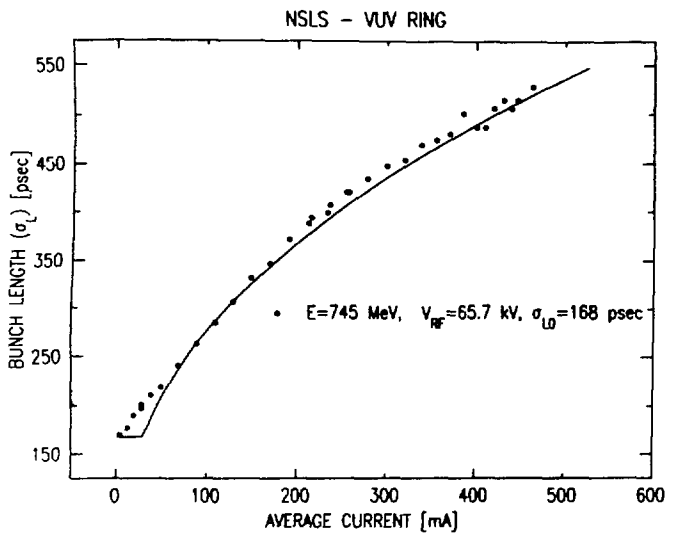

FIGURE 3: Bunch Length versus Average Current per Bunch RF Cavity Power was 2.2 kW. Data taken 10/87. Full width at half - maximum is 2.35σ

VUV Beamline Operations

Richard Garrett
NSLS VUV Ring Operations Manager

Machine Operations

The VUV community enjoyed very reliable machine operations in 1988, only interrupted by a month long shutdown in September to replace a damaged ceramic section of the ring and to install a fast valve at U3. Routine operations beam has consisted of fills to 750 mA, with a lifetime of 3 hours at 250 mA, and fill durations of 5 hours. Several events during the past year have produced, or will produce, significant improvements in the operations of the VUV ring:

- The fast valve system was implemented on all beamlines, and has already played its part in preventing a vacuum accident.
- The ion pump power supply modules were upgraded and the resulting increased pumping efficiency has produced a 10% increase in the beam lifetime.
- The closed orbit feedback system was successfully tested by the Diagnostics and Controls Group and achieved more than a three fold reduction in the vertical beam motion, including motions induced by the booster. It is planned to implement global orbit feedback as part of routine operations in 1989, after the new trim magnet power supplies are installed.

Beamline Operations

1989 saw continued activity in planning, construction and commissioning of new beamlines. The experimental programs on the established beamlines were extremely productive, as evinced by the abstracts published herein, and summarized in the various subgroup reports. The highlights of new beamline construction were:

- IBM was assigned the U2A beam port and has begun construction of a new submicron lithography beamline. It is expected to be in operation in mid-1989.
- The "Dragon" SGM at U4B is fully operational, and resolving powers in excess of 3000 have been measured using gas phase targets.
- The spin-polarized detection system at U5U has achieved reliable operations and is being used in studies of adsorbate effects on magnetic surfaces.
- The U7A TGM is operational and has entertained its first general users, and the U7B PGM has been upgraded with the addition of a refocusing system, which allows better vacuum isolation of the end station from the monochromator.
- The U12A TGM has been completed and commissioning is underway.
- A spectroscopy branch line, designated U13, for the TOK wiggler is in the final stages of component fabrication, and construction of the beamline will commence in 1989.
- The U16 ERG and TGM beamlines have been completed and are in the alignment/commissioning phase.

General

The high level of activity of the PRTs in 1988 was matched by an expansion of the General User Program to the point where some of our VUV resources have become oversubscribed. This is especially true of the high energy/high resolution beamlines. It therefore became necessary to institute a "Proposal Study Panel" to rate General User proposals to aid in distributing the limited beamtime resources.

Several efforts have been made, mostly through the Scientific Program Support Committee, to improve the working conditions on the VUV floor. We have seen the appearance of vending machines and a coffee service, but more importantly, efforts have begun to reduce the noise levels on the experimental floor.

VUV Storage Ring Parameters as of December 1988	
Parameters	**VUV Storage Ring**
Normal Operating Energy	0.750 GeV
Maximum Operating Current (multibunch operation)	1.0 amp (1.1×10^{12} e^-)
Circumference	51.0 meters
Number of Beam Ports on Dipoles	17
Number of Insertion Devices	2
Maximum Length of Insertion Devices	~2.5 meters
$\lambda_c(E_c)$	25.3 A (486 eV)
$B(\rho)$	1.28 Tesla (1.91 meters)
Electron Orbital Period	170.2 nanoseconds
Damping Times	$\tau_x \cong \tau_y \cong 17$ msec; $\tau_\varepsilon \cong 9$ msec
Touschek lifetime dependent on current/bunch and vertical emittance	200 min @ 200 mA (6 bunches, present operating conditions)
Lattice Structure (Chasman-Green)	Separated Function, Quad, Doublets
Number of Superperiods	4
Magnet Complement	8 Bending (1.5 meters each) 24 Quadrupole (0.3 meters each) 12 Sextupole (0.2 meters each)
Nominal Tunes ν_x, ν_y	3.14, 1.20
Momentum Compaction	0.023
R.F. Frequency	52.887 MHz
Radiated Power	14.7 kW/amp of Beam
R.F. Peak Voltage (typical)	100 kV
Design R.F. Power	50 kW
ν_s (Synchrotron Tune)	0.002
Natural Energy Spread $(\sigma_\varepsilon/E)^*$	4.5×10^{-4} (I < 20 mA)
Natural Bunch Length $(2\sigma)^*$	7.6 cm (I < 20 mA)
Number of RF Buckets	9
Horizontal Damped Emittance (ε_x)	1.5×10^{-7} meter-radian
Vertical Damped Emittance (ε_y)	$\geq 2.8 \times 10^{-10}$ meter-radian (adjust.)
Power per Horizontal milliradian, 1A	2.3 Watts
Source Size: σ_h, σ_v	0.5 mm, > 0.06 mm

*current and RF voltage dependent

Source of Data: NSLS Parameters, January 1983, compiled by A. van Steenbergen; updated values provided by Gaetano Vignola and Anne-Marie Fauchet (NSLS).

X-Ray Machine Operations

Sam Krinsky
Deputy Chairman, NSLS

X-Ray Storage Ring

The Phase II shutdown of the X-ray ring ended April 10, 1988. Recommissioning of the storage ring and the alignment of the X-ray beamlines was accomplished by the end of July. Since August, the experimental program has been in full swing. Storage ring performance has been good, and at the present time operations are taking place at 150 mA, with a beam lifetime of 20 hours.

The soft X-ray undulator for X1 is in operation. Radiation from the hybrid wiggler at X25 has been observed at low current (<5 mA) during machine studies periods. High current operation must await the commissioning of an active interlock system to protect the vacuum chamber from high power radiation in the event of an orbit deviation in the insertion device. The hybrid wiggler for X21 and the superconducting wiggler for X17 will be installed during a two-week shutdown in February 1989. The X5 LEGS Compton backscattering experiment is in an advanced stage of commissioning.

Installation of new power supplies for the quadrupole, sextupole and orbit correction dipole magnets has resulted in an improvement of orbit stability. Work aimed at further improvement of orbit stability is being given the highest priority. In particular, R&D for a global orbit feedback system based on an harmonic analysis of orbit fluctuations is underway on the VUV ring. Promising results have been obtained, and it is hoped that this work will lead to the implementation of operational global orbit feedback systems on both storage rings.

X-Ray Beamline Operations

Roger Klaffky
NSLS X-Ray Ring Operations Manager

Machine Operations

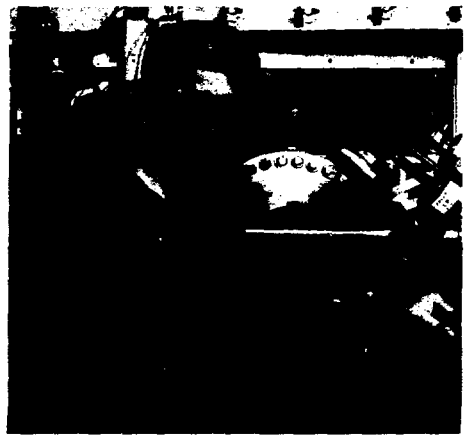

During the 1988 fiscal year, there were only three months of X-ray operations because of the Phase II shutdown work and the subsequent months of recommissioning. During these three months there were steady improvements in the integrated beam current as displayed in Figure 1 (which shows the total amp hours and the high energy amp hours). The breakdown of the fiscal year into percentages of operations, studies, downtime (which includes injection/ramping time), maintenance and conditioning is shown in Figure 2. The large percentage of time devoted to maintenance reflects six months of Phase II shutdown work.

Beam Line Upgrades/Operations

The Phase II shutdown continued during the first six months of FY 1988. A number of new beam lines are under construction by PRTs and the NSLS during this period, including: X1A, X2B, X3A1, X3A2, X3B1, X3B2, X4A, X4C, X5A, X5B, X6B, X7A, X7B, X8A, X8C, X13, X17B1, X17B2, X17C, X27A, X27B, X27C, X28A, X28C, and X30B. Each of these new lines required the installation of a new front end and a Phase II interlock system.

A prototype for the upgraded Phase II interlock system was successfully tested on X7 in early FY 1988. This system differs from the Phase I system in that it utilizes a modular design to permit disconnection from the main ring interlock system for testing during normal ring operation.

During the shutdown, there were also a number of new beamlines added to the Phase I front ends (X9B, X10C, X20B, X32A2 and X26A), and there were extensive modifications at beamline components on other beamlines.

The Phase II shutdown ended at the beginning of April 1988. First light was observed on X14A on April 19, 1988, at which time there were 20 minute lifetimes and 15 mA of stored 2.5 GeV beam. For the next month, as beam lifetimes and currents steadily improved, beamline radiation surveys were conducted while the electron beam was swept vertically. At the end of May, a series of grid searches began in which the strengths at two vertical trim magnets (X2V5 and X3V5) were varied to change the vertical position and angle of the electron orbit in each dipole. On the basis of the grid searches, an optimal orbit was chosen [orbit (5.5)] which gave good illumination to most of the 15 X-ray ports whose beamlines participated in the study. On ports where there was not full illumination and where there were not limiting beamline apertures that could be moved, local orbit bumps were implemented (X3, X12, X16) or the storage ring dipole chambers were surveyed in closer to their theoretical positions (X7/X8; X19/X20). In the middle of June, an initial operational mode began after a preliminary vertical orbit was established. The X1 undulator was installed July 1 with first light being observed on July 10th. By the end of September 1988, there were twenty-five beamlines in regular operation and a large number of lines close to resuming operations or to accepting X-rays for the first time. By the end of FY 1989, the number of operating lines will have doubled.

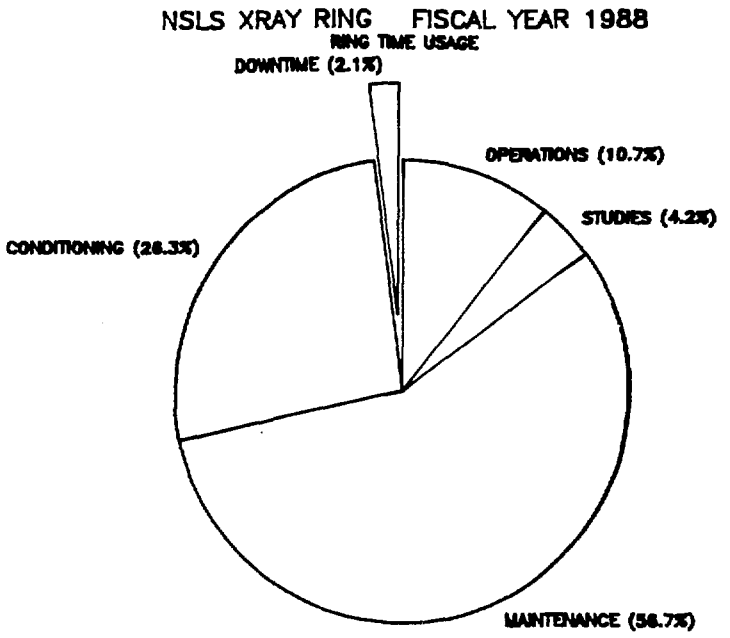

FIGURE 1: Utilization of the X-Ray Ring for FY 1988

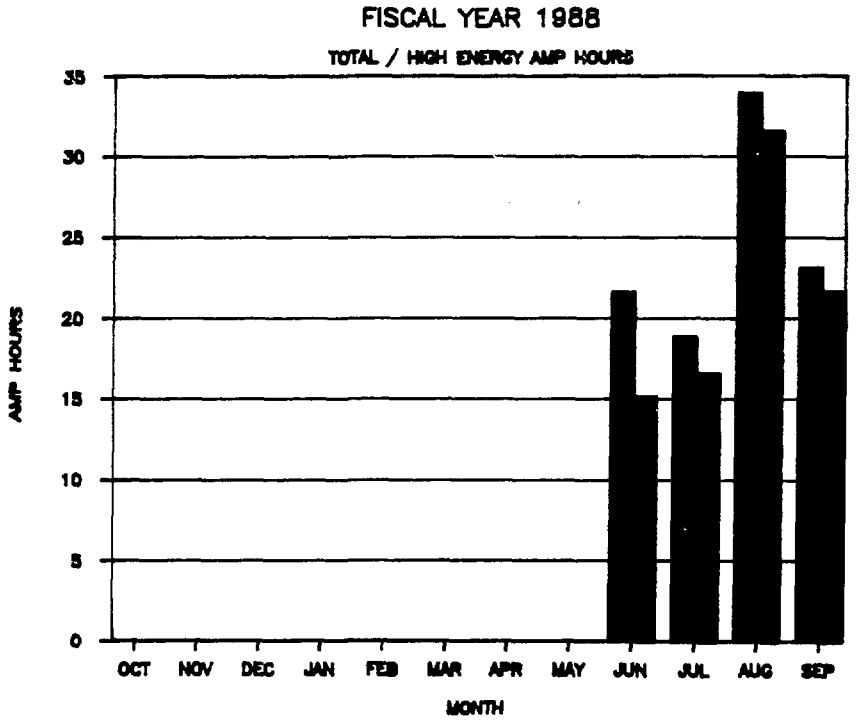

FIGURE 2: Total Monthly Amp Hours NSLS X-Ray Ring During FY 1988

X-Ray Storage Ring Parameters as of December 1988	
Parameters	**X-Ray Storage Ring**
Normal Operating Energy	0.75 - 2.5 GeV
Maximum Operating Current	0.25 amp (10^{12} e^-)
Lifetime	> 10 hours
Circumference	170.1 meters
Number of Beam Ports of Dipoles	30
Number of Insertion Devices	5
Maximum Length of Insertion Devices	< 4.50 meters
$\lambda_c(E_c)$ at 1.22 T (B)	2.48 A (5 keV)
λ_c (E_c) at 5.0 T (W)	0.60 A (20.8 keV)
$B(\rho)$	1.22 Tesla (6.875 meters)
Electron Orbital Period	567.7 nanoseconds
Damping Times (2.5 GeV)	$\tau_x = \tau_y = 6$ msec; $t_\varepsilon = 3$ msec
Touschek (2.5 GeV, 0.25A)	$\geq$ 16 hrs (v_{RF} = 700 kV)
Lattice Structure (Chasman-Green)	Separated Function, Quad Triplets
Number of Superperiods	8
Magnet Complement	16 Bending (2.7 meters each) 40 Quadrupole (0.45 meters each) 16 Quadrupole (0.80 meters each) 32 Sextupole (0.20 meters each)
Nominal Tunes v_x, v_y	9.15, 6.20
Momentum Compaction	0.0065
R.F. Frequency	52.88 MHz
Radiated Power for Bending Magnets	126 kW/0.25 amp of Beam
R.F. Peak Voltage	700 kV
Design R.F. Power	300 kW
v_s (Synchrotron tune)	0.002
Natural Energy Spread (σ_ε/E)	8.2×10^{-4}
Natural Bunch Length (2σ)	10.5 cm
Number of RF Buckets	30
Horizontal Damped Emittance (ε_x)	10^{-7} meter-radian
Vertical Damped Emittance (ε_y)	10^{-9} meter-radian
Power per Horizontal milliradian, 0.25A	20 watts
Typical Arc Source Size: σ_h, σ_v	~ 0.35 mm, ~ 0.15 mm

Source of Data: NSLS Parameters, January 1983, compiled by A. van Steenbergen; updated values provided by Sam Krinsky and John Keane (NSLS).

NSLS Phase II Insertion Devices: A Pictorial

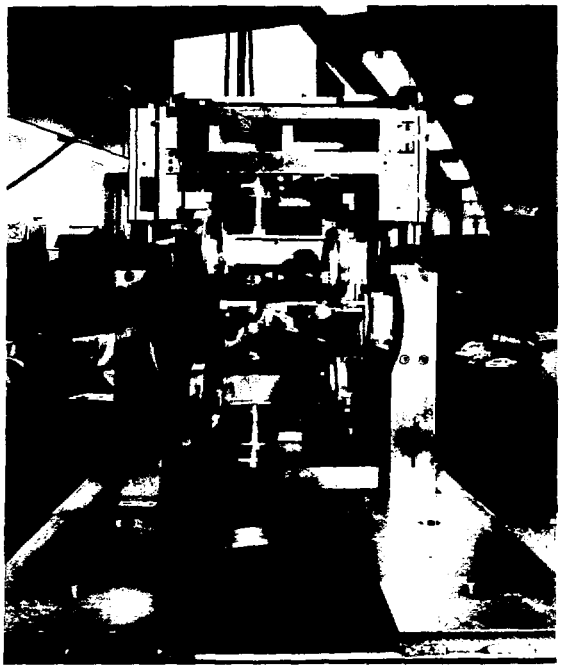

The X17 High Field Superconducting Wiggler front end aperture and splitter assembly. The copper "bow-tie" elements are the vertical apertures where the wiggler beam enters. The small (6°) angle that the water cooled copper elements make to the incident beam lowers the power density on these elements to acceptable levels. Downstream of the vertical apertures are two splitters which break the 13 mrad horizontal beam into the A, B, and C beams. Further downstream are the pneumatic photon shutters which are used to mask the photon power in each beam prior to the bremsstrahlung shutters.

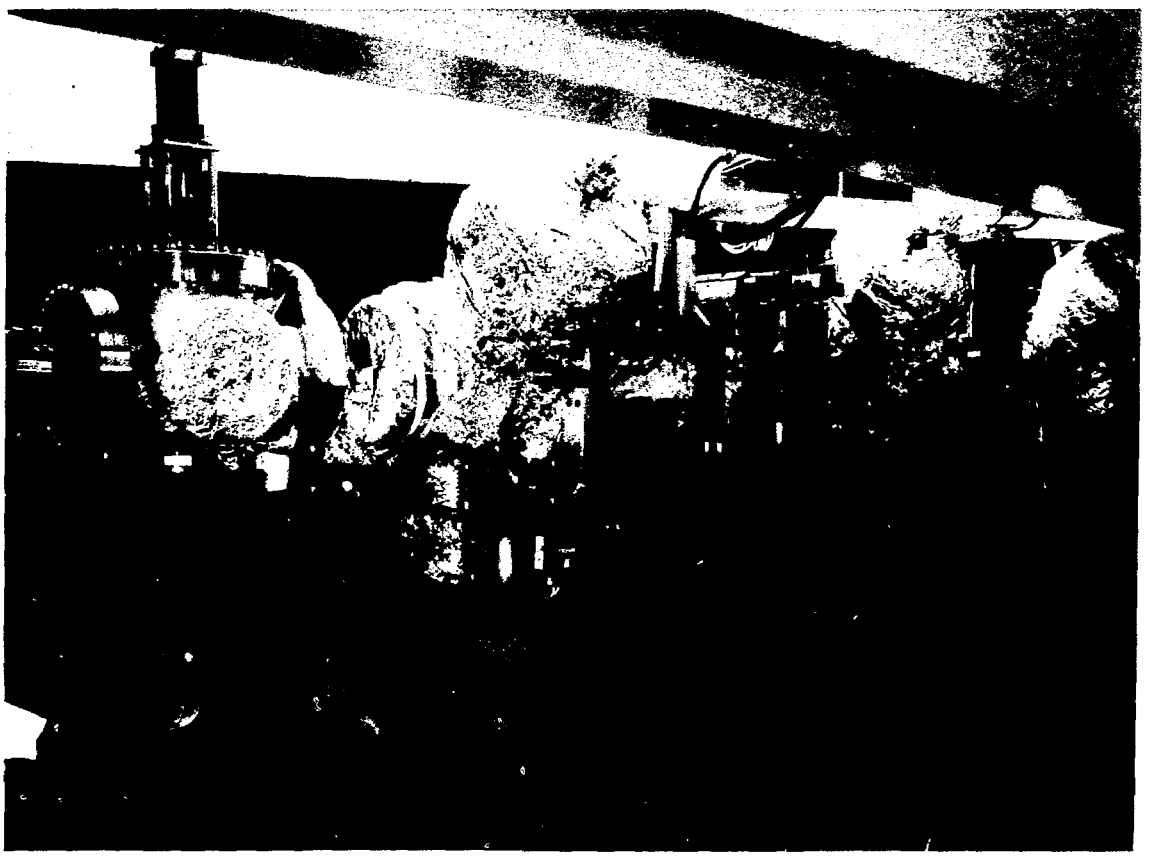

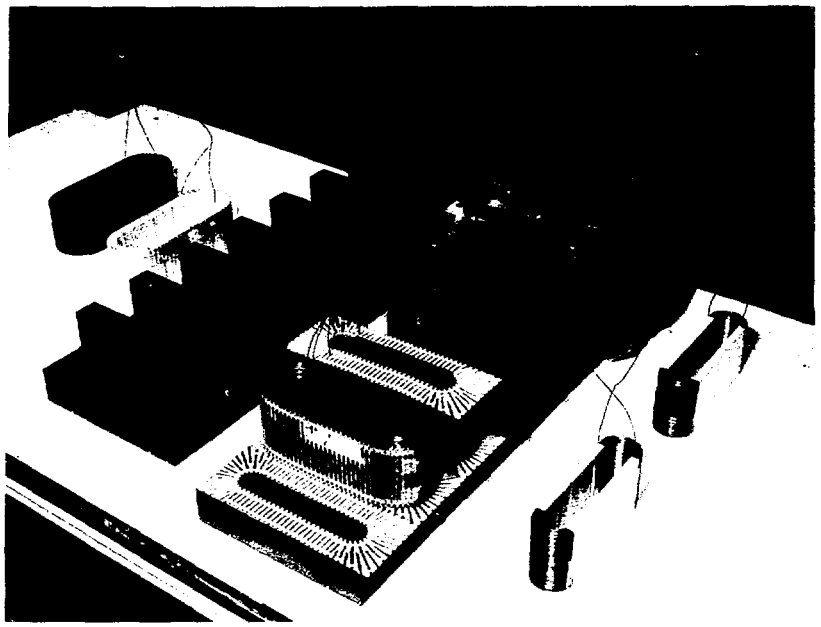

The NbTi coil windings and pole assembly from the superconducting wiggler during fabrication. The electron beam tube is installed in the oval opening between the poles. The entire assembly, when placed in the cryostat, is immersed in liquid helium. The device has seven poles (five at full field and two end poles at half field) with a maximum field during operations of 5.22 Tesla. Total power from this device at its maximum operational field and a ring current of 250 mA is expected to be 13.2 kWatts.

The X-25 wiggler magnet shown installed in an X-Ray ring straight section. Visible are the C-frame support structure and the upper and lower magnet jaws. The magnet uses rare earth-cobalt permanent magnet material to generate a peak field of 1.1 Tesla at a 24 mm gap, resulting in photons with critical energy E_c=4.7 KeV using 2.5 GeV electrons.

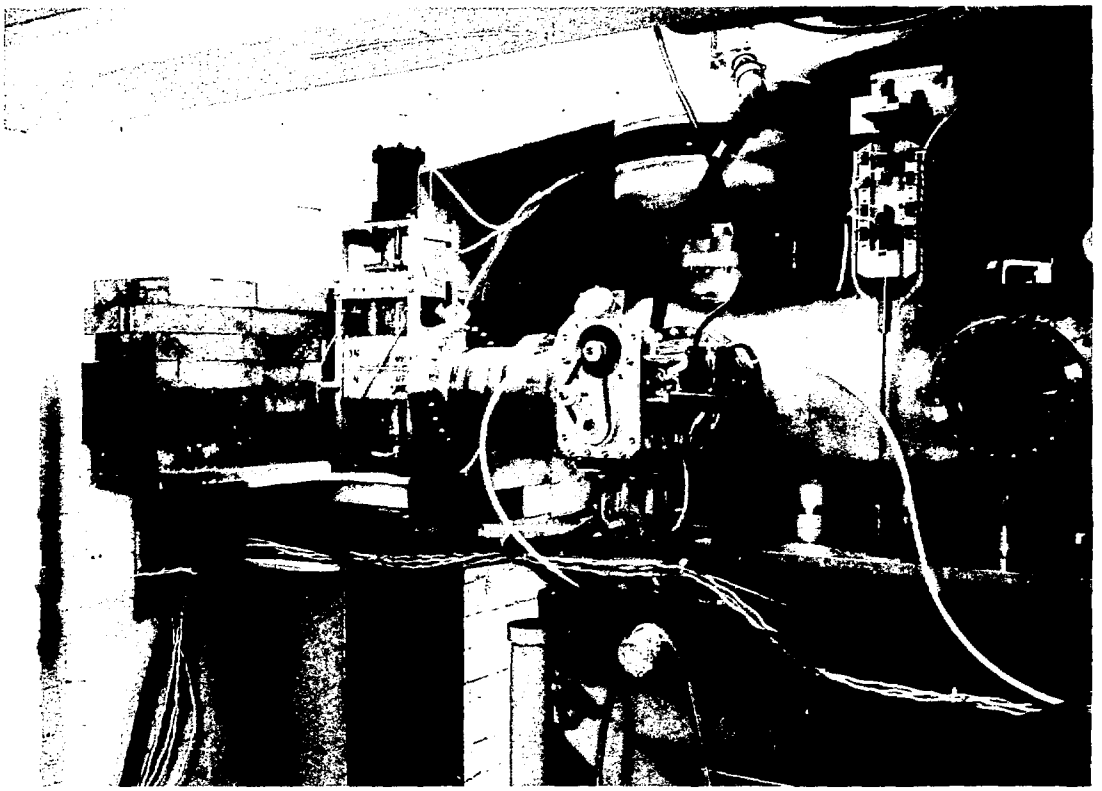

Front end of beamline X-1, which is illuminated by the Soft X-Ray Undulator. The large tank at the right holds the Beam Defining Apertures, which have been designed to take the high power of the Phase II insertion devices.

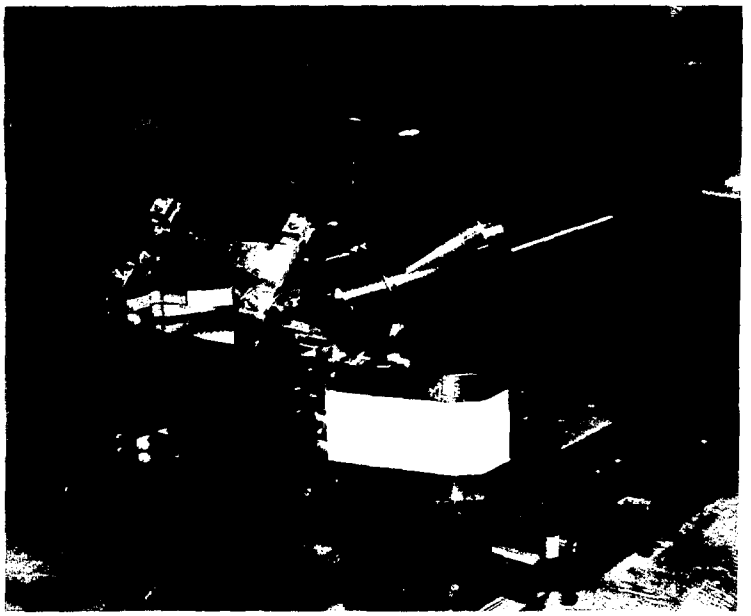

First mirror of the X-1A beamline. This flat mirror has been designed to take the high power density of the Soft X-Ray Undulator without significant distortion. The mirror has water cooling channels within a few millimeters of the surface. The surface coatings of the mirror are beryllium (along the center of the mirror) and gold, either of which can be put in the beam to vary the cutoff energy. A protective bumper (to the right in the photograph) is plasma sprayed with ruby to take high temperatures and fluoresce red in the undulator beam. This mirror was designed and fabricated at LBL as part of their contribution to the X1-A IDT.

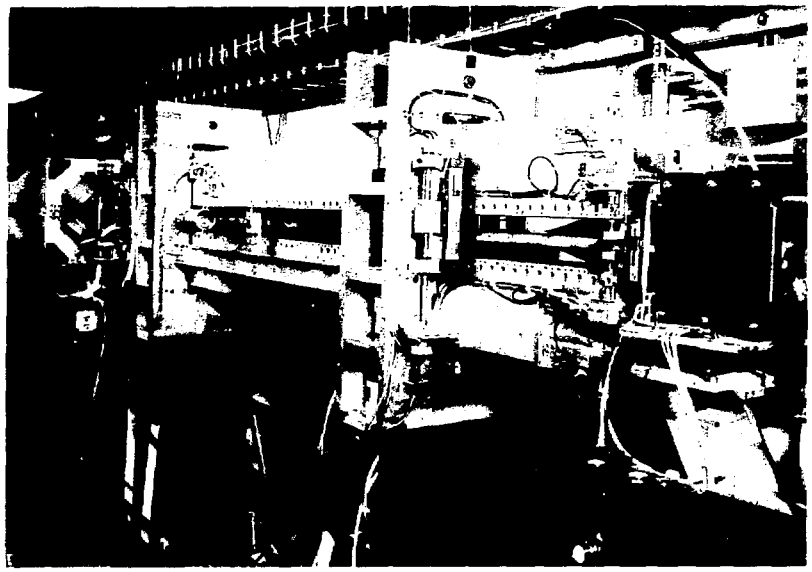

The Soft X-Ray Undulator, the first Phase II device to be installed in the X-Ray ring. The 3 cm high storage ring vacuum chamber sits inside the two movable beams, each bearing 70 poles of samarium cobalt permanent magnets. The device is about 3 meters long.

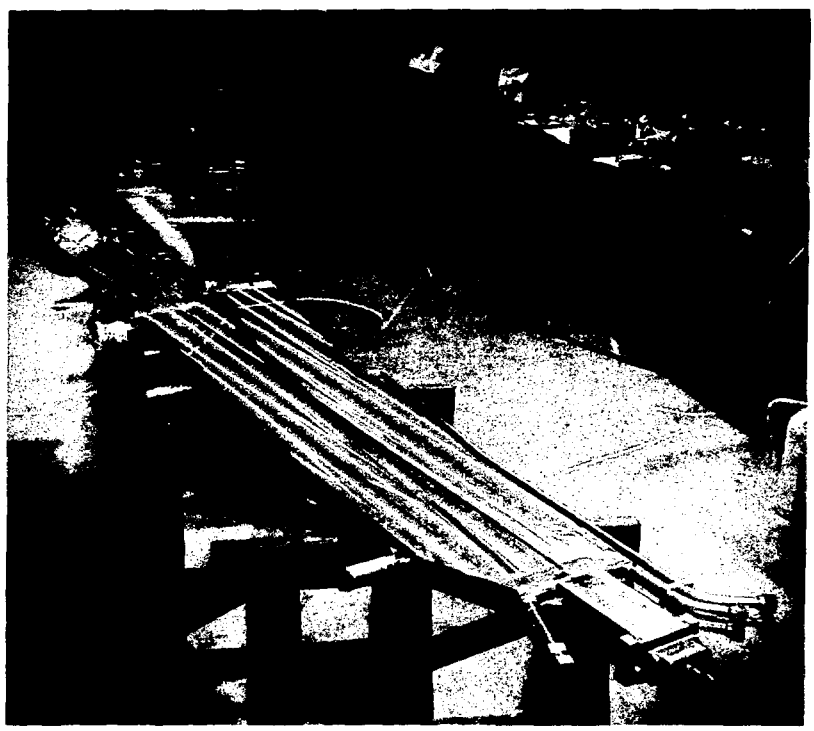

Aluminum Vacuum Chamber for use downstream of NSLS Insertion Devices. Note that the entire top and bottom of the arc section is completely machined from flat plate to ensure critical cooling and dimensional stability.

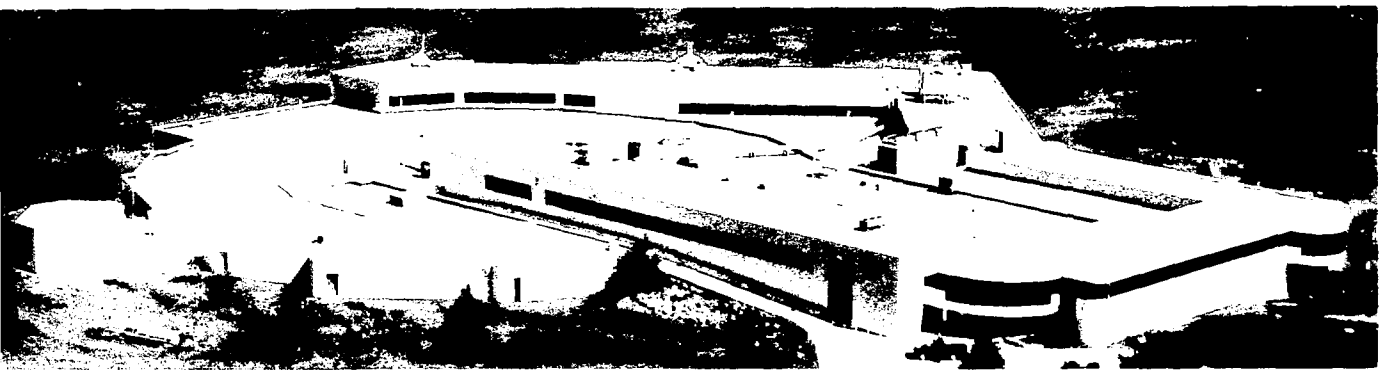

Section III

Symposia, Workshops, and Projects

31/32

The NSLS Superconducting X-Ray Lithography Source (SXLS) Project

Richard Heese
SXLS Project Head, NSLS

Introduction

The Superconducting X-Ray Lithography Source (SXLS) Project at Brookhaven National Laboratory is funded by the United States Department of Defense in the context of an ongoing national effort aimed to strengthen a declining leadership of the U.S. semiconductor industry on the world market.

The two main objectives of this project are:

- To build a compact electron storage ring optimized for X-ray lithography.
- To establish domestic vendors of such accelerators by transferring to industry the capability of designing, building, commissioning and operating compact synchrotron X-ray sources.

X-ray lithography is at the present time emerging as the technology that will replace optical lithography and is the most viable candidate for the industrial production of integrated circuits with component sizes in the submicron range.

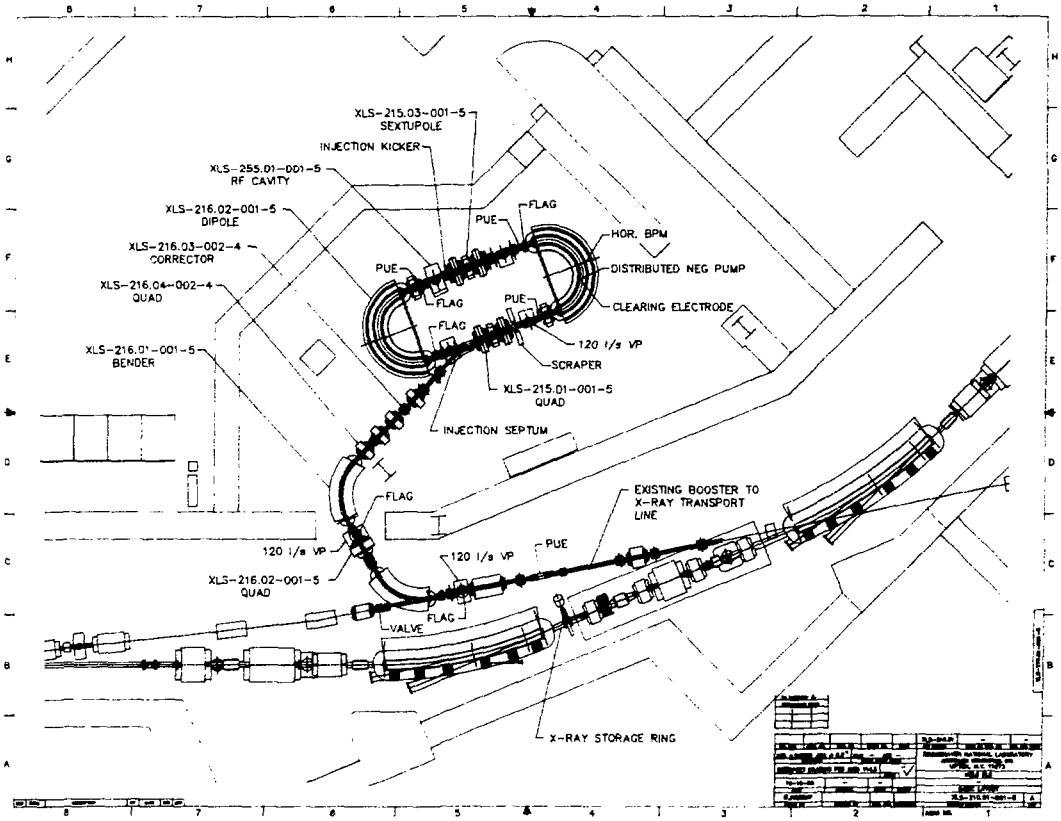

Figure 1.

The major credit for the development of synchrotron based X-ray lithography must be given to the IBM Corporation, who started to pursue this technology in the early 1970's and has been carrying out proof-of-principle experimentation at several radiation facilities since then. In the early 1980's, IBM established an X-ray lithography beamline on the NSLS VUV storage ring. In 1988, IBM announced the successful fabrication of the first fully scaled 0.5 micron metal-oxide semiconductor (MOS) circuit by synchrotron radiation X-ray lithography.

X-ray lithography is a broad technology with many challenging engineering and materials problems still open, in spite of these successes. Key pieces of technology include masks, resists, aligner-stepper systems, processing, metrology, chip design and X-ray sources.

A viable X-ray source is one of several major technologies which must be brought to the manufacturing level. It is also the area in which the NSLS at BNL has the unique combination of an experienced staff and an infrastructure of high technology support. Due to the IBM effort at NSLS and other synchrotron facilities, BNL is aware of early successful experiments in the field and of the rapid push to move from research to development.

BNL held several workshops in the past to define the parameters of a dedicated X-ray lithography source, to present strawman designs to the semiconductor industry and to detail a 0.25 micron X-ray lithography facility. These workshops resulted in the DOD funding a conceptual design study for a complete prototype semiconductor production facility, followed by their funding of a five year $21 million project for the development of a superconducting ring, the SXLS.

We are addressing the problem of building the supercompact ring in two phases, corresponding to the main difficulties associated with these machines. Phase I consists of the construction of a room temperature mock-up of a superconducting magnet ring. Phase II will develop the superconducting magnet and the final ring.

To keep costs and schedule to an absolute minimum, we intend to install the Phase I ring in an alcove in the NSLS building adjacent to the X-ray tunnel, as seen in Figure 1. This will permit us to extract an electron beam from the existing injection line of the X-ray storage ring, thus saving for the present time, the cost of a new injector and building. To save additional cost and time, we intend to borrow existing 200 MHz RF components which would be suitable for the first phase storage ring. All other systems, such as the vacuum chambers, multipole magnets and their power supplies, and diagnostics will be similar to those for the second step storage ring. As part of Phase I, initial design of the cryogenic magnet will begin.

The performance of a very small circumference ring is related to the maximum current obtainable at injection energy. The current at injection is limited by coherent instabilities, by disruption of the electron optics due to ion trapping and by beam losses due to the long radiation damping time of the injected electrons. These phenomena are properties of the low field characteristics of the magnets and the exact injection process selected, quite apart from the high field requirements of superconducting magnet design. The purpose of building a warm analog ring and carrying out a program of injection studies, is to select the optimum injection process, to confirm the design of the lattice and beam chamber, and to study the effects of extended fringe fields which are a property of the superconducting dipole. Diagnostics and a control system suitable for an industrial environment will be defined. In parallel with this work, initial design of the superconducting dipoles will begin and different design approaches will be explored. A successful conclusion of Phase I will provide us with the critical empirical knowledge needed to proceed with Phase II, a working cryogenic magnet synchrotron.

Phase II is the more difficult part of developing, building, measuring and commissioning the superconducting magnet, an essential prerequisite of the final ring. Phase I will have yielded a flexible lattice, information on gradients and higher harmonic content in the dipoles, effect of fringing fields, and how the lattice must be modified to adapt to the final magnet as measured. The measurement of the magnet is one of the crucial technical challenges of this program. The magnet must be designed such that the measurement of the dipole can be performed in the circular geometry of the magnet and with the accuracy required by accelerator physics consideration, in spite of the fact that the measurement probe may be in a cryogenic environment.

Phase I will also have defined the vacuum system (whether pumping in the magnet is required and the aspect of clearing electrodes) and an injection scheme (and energy). It is planned for the Phase II machine to have its own injector, probably a small linac. Linacs produce approximately ten times the average current than any other injector and the gradients for short pulse operation are getting high enough so that a 100 MeV linac will fit into the same space as a 100 MeV microtron.

To house the Phase II machine, a building must be erected, or an existing building modified, since the cryogenics, the injector and the control system will not have space in the existing area. Figure 2 shows the synchrotron radiation spectrum generated by both storage rings.

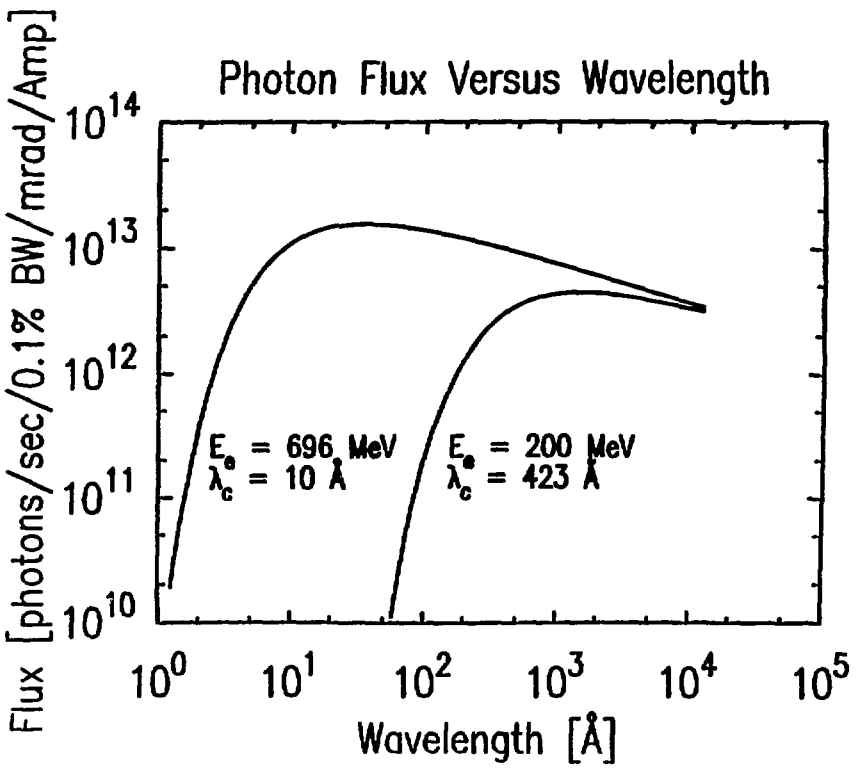

Figure 2.

Present Status of the SXLS

The lattice parameters of the Phase I and Phase II storage rings are shown in Table I. The Phase I ring is under construction, and commissioning will commence in December 1989. The superconducting dipole is moving into the engineering design phase with the help of our industrial partner, Grumman Aerospace Corporation and their subcontractor, General Dynamics.

Machine Phase	Phase I	Phase II*
Energy, E [MeV]	200	696
Dipole Magnet Type	EM	SC
Dipole Field, B_0 [T]	1.1	3.85
Bending Radius, ρ [m]	.6037	
Field Index, n	.1759	
Lattice Structure	FODO-like	
Superperiods, N_s	2	
Circumference, C [m]	8.503	
Critical Wavelength, λ_c [A]	423	10
Number of Superperiods	2	
Horizontal Betatron Tune, ν_x	1.415	
Vertical Betatron Tune, ν_y	.415	
Energy Loss Per Turn, U_0 [KeV]	.234	34.4
Natural Energy Spread, $\sigma_{\varepsilon 0}$	2.0×10^{-4}	6.9×10^{-4}
Damping Partition Numbers, J_x, J_y, J_ε	.53,1.,2.47	
Damping Times, τ_x, τ_y, τ_ε [ms]	91,48,20	2.16,1.15,.46
Uncorrected Chromaticity, ξ_x,ξ_y	-.49, -1.32	
Momentum Compaction, α	.32	
Natural Emittance, ε [m-rad]	5.92×10^{-8}	7.17×10^{-7}

* unfilled boxes same as Phase I

Table I. Storage Ring Parameters

The project is proceeding well and will result in a superconducting dipole synchrotron suitable for X-ray lithography and the technology will have been transferred to a U.S. industrial firm, so that prospective customers can turn to a domestic supplier of these devices.

Acknowledgements

Most of this report was culled from the SXLS Design Handbook assembled by J. Murphy of the SXLS staff.

Photoemission Microscopy Workshop

August 15-16, 1988

B.P. Tonner,
University of Wisconsin-Milwaukee
Workshop Organizer

Speakers:

B.P. Tonner, G.R. Harp, Univ. of Wisconsin-Milwaukee

Janos Kirz, Harald Ade, SUNY-Stonybrook

E. Johnson, S. Hulbert, NSLS

Topics:

- Fundamental and practical issues in spatial and spectral resolution
- Worldwide efforts in soft X-ray microscopy
- Scanning photoemission microscopy
- Paraxial-ray imaging photoemission microscopy
- Undulator light sources at NSLS for microscopy

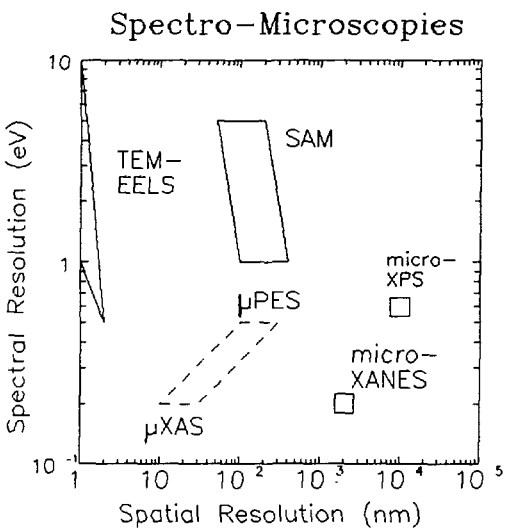

Figure 1: Impact on Undulator Photoemission Microscopies

The new spatially-resolved surface spectroscopies which are being developed on beamlines at NSLS will fill a void as shown in the illustration above. The two techniques discussed in the workshop were micro-Photoemission Spectroscopy (μPES) and micro-X-ray Absorption Spectroscopy (μXAS). The range of spatial and spectral resolution spanned by these techniques is shown as the dashed area in the graph. The undulator microscopies have significant advantages when compared with common electron-probe techniques. Energy loss spectroscopy in the electron microscope (TEM-EELS) has high spatial resolution but poorer spectral resolution, and furthermore does not have intrinsic surface sensitivity. Scanning Auger Microscopy (SAM) has intrinsic surface sensitivity, but significantly poorer energy resolution. In addition, the photon probes enjoy a two order of magnitude advantage in sensitivity for a given level of sample damage, as compared to SAM.

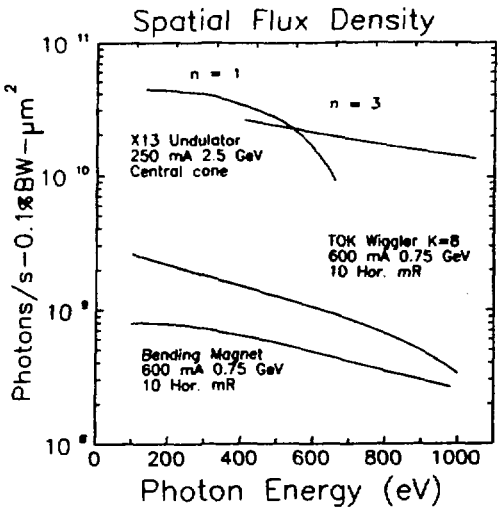

Figure 2: Importance of Insertion Device Synchrotron Radiation Sources to Photoemission Microscopy

One of the practical limitations to spatially-resolved spectroscopy is the spatial photon flux density which ultimately arrives at the sample. This figure shows the photon flux per unit area for several soft X-ray sources at NSLS, under practical operating conditions. The curves for the X13 undulator are taken from measurements made by Rarback, Jacobsen, Kirz and McNulty. The increase in flux density of the undulator translates directly into a smaller analysis *area* in spatially-resolved spectroscopy. The recently commissioned X1 undulator should have ≈4 times the flux-density of X13.

Comparison
of synchrotron
Spectro–Microscopies

TECHNIQUE	Detected Particle	Lateral Resolution	Depth Resolution	Spectral Resolution
μXAS	Secondary electron	10 nm	λ_{Auger}	0.1 eV
μPES	Primary photo–electron	100 nm	λ_{PES}	0.5 eV
μPSD	Secondary ion	1 μm	1 ML	1.0 eV

Figure 3: Comparison of Synchrotron Spectro-Microscopies

One of the attractive features of the photoemission microscopes is that they encompass a variety of analytical techniques with overlapping capabilities. Three techniques which are under development are micro-photoemission spectroscopy, micro-X-ray absorption spectroscopy, and micro-photon stimulated ion-desorption spectroscopy. These techniques cover a wide range of sampling depths and intrinsic spectral resolution, as shown in the figure. These techniques are easily combined in a single instrument, so that multiple microprobes can be applied to the same sample.

Synchrotron Radiation in Structural Biology

May 22-25, 1988
Robert M. Sweet, BNL Biology Department
Conference Chairman

Synchrotron Radiation in Structural Biology. From left to right: Robert Sweet, Malcolm Capel, Benno Schoenborn, Steven White (session chairman, Biology, BNL); Elizabeth Theil (session chairman, Biochemistry, N. Carolina State University); Hugh Huxley (Rosentiel Institute, Brandeis University); Richard Setlow (Associate Director for Life Sciences, BNL).

A symposium was held at Brookhaven National Laboratory during May 22-25, 1988 to discuss applications of synchrotron radiation to structural biology. The program included descriptions of the facilities available for biological studies at seven synchrotron radiation sources around the world. There are a dozen beamlines effectively dedicated to this sort of research.

There were four invited lectures for each of several topics: X-Ray Crystallography, Small-Angle X-Ray Scattering, VUV Spectroscopy and Photobiology, Extended X-Ray Absorption Fire Structure Spectroscopy, Advances in Instrumentation, and New Techniques. In the Symposium Lecture, Hugh Huxley, Brandeis Univ., reviewed the history of the development of X-ray instrumentation for biological structure research. A symposium volume will be available from Plenum Press in a few months.

Several highlights of the symposium demonstrate the scope and power of synchrotron studies, as follows. J. Bordas of SRS Daresbury, UK, displayed diffraction from muscle fibers that reveals a 25,000A lowest-order maximum. This extends use of the technique to the scale accessible by light microscopes. P. Bjorkman of Stanford and Harvard described her successful solution of the structure of human leukocyte antigen using crystals only 50 microns thick. J. Johnson of Purdue described how his group solved the structure of Bean-Pod Mottle Virus in only ten months and showed in this structure the first example of ordered RNA in a viral genome. W. Hendrickson of Columbia

showed how he and coworkers had solved the structure of the streptavidin/seleno-biotin complex, using for phasing only the anomalous scattering from the selenium atom on biotin measured at several different wavelengths. Finally, J. Hajdu of Oxford revealed some of the structural changes that accompany Ca-dependent swelling of tomato bushy stunt virus. These results come from a single Laue ("white" X-ray) photograph, exposed for only 24 seconds.

A particular theme, related to these sorts of research, arose and was repeated during the meeting. This was that there are two sorts of advance that can be made in experimentation: advances in equipment and advances in methods. The very existence of synchrotron radiation sources represents a triumph in equipment development, the full impact of which can only be imagined. The development of X-ray storage phosphors by the Fuji and Eastman Kodak companies will provide a new generation of precise X-ray detectors for diffraction science. On the other hand, development of clever methods can amplify the use of equipment many-fold. One such method is that of quick freezing of protein crystals, making them almost completely resistant to radiation damage. Another is the use of Laue photography for diffraction intensity measurement, developed by K. Moffat of Cornell, and J. Helliwell and D. Cruickshank in England. This method requires no new apparatus, but demands a precise analysis of the physics of diffraction and careful experimentation. Finally, the solving of a protein crystal structure by multi-wavelength anomalous diffraction represents the culmination of years of effort by many workers, finally brought to fruition by Hendrickson and by Phizackerly of Stanford. Again in this case, the apparatus wasn't particularly unusual; the use made of it was.

A final message from the symposium is that new advances in instrumentation are absolutely required. The most glaring need is for X-ray detectors. Existing synchrotron sources produce sufficient X-rays that complete data sets could be measured from most protein crystals in a fraction of an hour if X-ray area detectors coupled to sufficient computing power existed to the job. The film methods that are in use must be supplanted by true electronic detectors. Only then will we be able to realize the full potential of synchrotron radiation for the study of biological structures.

Vacuum Design of Advanced and Compact Synchrotron Light Sources

May 16-18, 1988

Henry Halama, Joe Schuchman and Peter Stefan, NSLS
Conference Organizers

Invited speakers. Left to right, rear row: H. Heidmann (S.R.C.), R. Suchet (LURE), M. Kobayashi (KEK), N.B. Mistry (Cornell University). Left to right, front row: K. Kennedy (C.B.C.), R. Wehril (ANL), H.F. Dyle (PPL), C.H. Pruett (University of Wisconsin), E. Hoyer (LBC), E.M. Rowe (University of Wisconsin), D.M. Poncet (CERN), A. Mathewson (CERN).

The first conference on vacuum design of advanced and compact synchrotron light sources, sponsored by the American Vacuum Society (AVS) and Brookhaven National Laboratory (BNL), was held at Brookhaven on May 16-18, 1988. The meeting was truly international in scope with speakers and attendees from major light source facilities in the US, Europe and the Far East. There were 125 people registered for the conference.

The purpose of this meeting was to bring together accelerator designers and builders from around the world to exchange ideas and promote discussion on existing and new vacuum system designs. In addition to general machine design, specific sessions were devoted to problems unique to synchrotron radiation sources. For example, gas desportion and surface cleaning, ion trapping and lifetime, impedance and instabilities, wigglers and undulators, and chamber cooling.

An entire evening session was devoted to compact light sources for X-ray lithography, with both research laboratories and industrial participation. Three designs incorporating superconducting magnets were presented, two having cold bore (LHe) vacuum chambers and the third a room temperature beam envelope. Of equal interest was the fact that the three designs are from German, Japanese and English firms. The session concluded with an open discussion moderated by R. Heese (BNL). The injection energy seemed to be the fundamental question affecting all aspects of these small machines.

N. Misty (Cornell University) and H. Wiedemann (SSRL) opened the conference with invited papers on vacuum systems for synchrotron radiation sources, and vacuum considerations of impedances and higher mode losses in electron storage rings, respectively. Since these two topics affect all phases of light source vacuum system design, the stage was set for the papers that followed. First were presentations and discussions on vacuum system designs for new machines, namely LEP Injector (CERN-Switzerland), Super ACO (LURE-France), HBL (Daresbury-England), ALS (Berkeley-USA), 7 GeV APS (Argonne-USA), 6 GeV SRS (RIKEN-Japan), 1.3 GeV SRS (SSRC-Taiwan), and the ESRF (Grenoble-France).

Although all these machines are different in design and purpose, they are all faced with the same question: choice of material, aluminum or stainless steel, antechamber or not, choice of pumps, choice of radiation absorber, etc. The non-evaporable getter pump (NEG) has come into its own as a viable means of pumping in storage rings, and many machines rely heavily on its use for both the ring and undulator chambers. Kobari and Matsumoto (Hitachi) reported on their experimental work on indirectly and directly irradiating the NEG pump strip (St-122). Their results, on small samples, show that there is no undue gas desorption from the NEG strip when irradiated with synchrotron radiation.

E. Rowe (University of Wisconsin) reported on trapped ions and their elimination. To some extent, trapped ions affect the performance of all electron storage rings, especially those operating at low energies, and the vacuum design must take into account this very important current-limiting phenomena.

On Wednesday morning, the thermal problems associated with wigglers and undulators were discussed. Current insertion devices produce intense photon beams (1.5 to 2 Kw/mrad^2) which are capable to melting vacuum chamber components if they are mis-directed.

E. Hoyer (LBL) gave an overview of the problem in designing vacuum chambers for the insertion devices themselves and listed existing designs and current thoughts in this area. Continuing with the thermal problem theme, papers were presented on the design of vacuum chambers downstream of insertion devices, crotches and absorbers, beamline designs and, finally, the thermal problems of the first beryllium window. Overall, these papers provide a definitive source of reference to the designer of vacuum components for high power beamlines.

X-Ray Microscopy II

August 31 - September 4, 1987

Harvey Rarback, NSLS
Workshop Co-Organizer

(adapted from David Sayre's Synchrotron Radiation News report)

An International Symposium on X-ray Microscopy was held at Brookhaven in September, 1987. Approximately 100 participants from eight countries spent a week learning what has happened in the field since the first Symposium was held at Gottingen in 1983. Synchrotron radiation played an important part in many of the recent advances.

The best reported resolution, for techniques other than contact microscopy, remains at the 1983 value of 500 Angstroms. However, progress in Fresnel zone plate fabrication at several laboratories promises 200 Angstrom resolution in the next several years. Even the 500-1000 Angstrom resolution currently attainable is quite interesting and should allow intact biological cells and organelles to be examined at higher resolution than is possible with the optical microscope and with less damage than with the electron microscope.

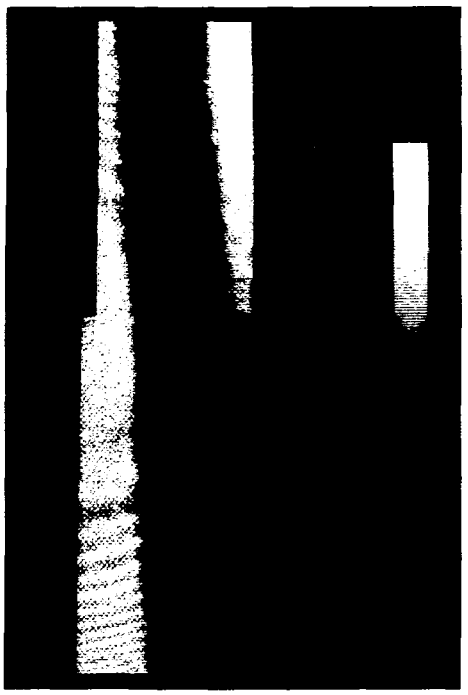

Figure 1: Scanning transmission X-ray micrograph of the demyelinated axon of the shrimp nerve taken with the NSLS/Stony Brook microscope. The wavelength used was 32 Angstroms. Clusters of microtubules run down the axon, which is about four microns wide. (Specimen courtesy of S. Fan).

Scanning microscopes with Fresnel zone plate optics are now operating at the NSLS, Daresbury, and BESSY with several more planned worldwide. They have all achieved resolutions near 750 Angstroms. In another development, phase contrast imaging microscopy has been demonstrated by the Gottingen group.

Source development has been very rapid in the past three years. Undulators with a very high coherent power in soft X-rays are now operating at the NSLS, Photon Factory, and Daresbury. The ten period mini-undulator at the NSLS has demonstrated the world's highest intensity of any continuous source of soft X-rays. Groups at Lawrence Livermore and Princeton have built soft X-ray lasers showing gain near 100 Angstrom wavelength and the promise to cross the carbon K-edge before the next symposium to be held in London in 1990.

These bright sources permit improved performance in scanning systems and make diffracted-photon imaging using soft X-rays feasable. Holograms and diffraction patterns of single biological cells have been obtained, and sub-1000 Angstrom computer reconstructions made by a group from Lawrence Berkeley Lab using the NSLS mini-undulator.

Progress in components was extensively reported, including: high counting rate detectors (Gottingen); high spatial resolution detectors (EXXON); high efficiency phase zone plates (Gottingen); linear zone plates for 8 keV X-rays (Livermore); beam splitters, transmission guides, and high dispersion multilayers (Livermore).

Two imaging techniques using harder radiation have come close to reaching maturity: fluorescence imaging with elemental sensitivity better than 1 ppm and three dimensional tomographic imaging with spatial resolution of a few microns. Both these techniques have been demonstrated at the NSLS.

More than twenty papers reported on applications of X-ray microscopy to biological and materials science. Contact microscopy continues as the most frequently used technique, but applications of almost all the imaging techniques were presented.

The Symposium was sponsored by the NSF, the Center for X-ray Optics at LBL, the Department of Physics at the State University of New York at Stony Brook, and by the NSLS. The Proceedings are available as Volume 56 in the *Springer Series in Optical Sciences.*

New Opportunities in Chemistry: An International Symposium of the Uses Of Synchrotron Radiation in Chemistry

November 4-6, 1987

Jack M. Preses, BNL Chemistry Department
Conference Chairman

The first decade of widespread use of synchrotron radiation was dominated by applications in physics and materials science. Chemists have only recently begun to apply synchrotron radiation to a wide range of chemical problems, so that is seemed an appropriate time to provide a forum for chemists to communicate the very broad range of problems being studied and to focus on their unique approaches to the examination of molecular and atomic systems of interest to them and to scientists in other disciplines.

The meeting was held November 4-6, 1987 at Brookhaven National Laboratory. Speakers discussed the chemical problems being studied and the new X-ray and VUV techniques brought to bear on those problems.

The high intensity, collimation, and tunability of synchrotron radiation have permitted X-ray diffraction studies of complex crystal structures and of molecules which form only microscopic crystals. Studies which were inaccessible before the use of synchrotron radiation, such as ultrahigh pressure experiments, determinations of the structure of amorphous materials, and time resolved diffraction were discussed. The tunability of synchrotron radiation permits multiwavelength anomalous scattering determinations of the structure of complex proteins. The high flux of synchrotron radiation allows the use of small angle scattering techniques to study morphological changes during chemical reactions or phase changes in polymers. Similarly, X-ray microprobe methods have been applied to a wide range of problems in biochemistry and geochemistry.

Extended X-ray Absorption Fine Structure (EXAFS) and Near Edge X-ray Absorption Fine Structure (NEXAFS) are being utilized in a number of novel chemical applications. Surface EXAFS and X-ray standing wave techniques have been used to elucidate the structure and mechanisms of electrochemical interfaces. NEXAFS can provide details about the structure of molecules chemisorbed on surfaces. New detection methods for simultaneous acquisition of entire X-ray absorption spectra will open areas of kinetics measurements, such as oxidation and reduction of porphyrins and ferretin, electrochemistry, interfacial reaction rates, high pressure phase transitions, and high temperature superconductors. Polarization dependent EXAFS and XANES are being used to characterize sulfur adlayers on Ni and Fe single crystals. High resolution Auger spectroscopy may be able to extend the measurement of electronic state lifetimes down to .01 picoseconds. Fluorescence Yield Near Edge Spectroscopy (FYNES) can be used to probe surface reactions and species both in UHV and at high pressure. Ultraviolet photoemission spectra of high temperature superconductors have already revealed detailed information about the electronic structure of such materials.

Gas phase chemistry was well represented at the meeting. Single photon photoionization of van de Waals and hydrogen bonded species can be used to determine thermodynamic quantities of these evanescent species. The structure and thermochemistry of cluser molecules has also been examined by this method. Simultaneous measurements of angular resolved photoelectrons from small gas-phase molecules such as carbon disulfide, carbonyl sulfide, silicon tetrafluoride, and chloromethanes have elucidated the roles of separate valence shell photoelectron spectra and Auger spectra during the decay of electrons to virtual, but bound states in these molecules. The use of synchrotron radiation has permitted high resolution studies of unimolecular dissociation of molecular ions, and studies of photoionization dynamics of small gas phase molecules. The next generation of synchrotrons will open the possibility of studying relativistic effects in atomic and molecular systems.

The symposium was sponsored by the Division of Chemical Sciences and the Division of Materials Sciences, U.S. Department of Energy.

DOE High School Honors Research Program

Dean Chapman, NSLS
NSLS Program Coordinator

Brookhaven National Laboratory hosted 56 high school students for two weeks (July 27 - August 9) as part of the DOE High School Honors Research Program. This program, now in its third year at BNL, is designed to allow these students access to some of the premier facilities available at the DOE sponsored national laboratories. The program at BNL is centered around experiments performed on beamlines at the NSLS. One outstanding student was chosen from each state plus the District of Columbia and Puerto Rico. In addition, students were present from Canada, Italy, Japan, and Mexico.

The first full three days of the program were devoted to lectures on the nature of synchrotron radiation and its scientific applications, machine physics, operations and procedures at the NSLS, and on the experiments which the students would be conducting. The weekend was devoted to calculations which would allow the students to estimate the photon flux from the VUV ring, as well as a not-so-scientific tour of New York City.

The second week was devoted primarily to the experiments, analysis of experimental results, and the writing of a report on those results. The experiments involved were: 1) optical diffraction and computer control, which demonstrated optical X-ray diffraction and the uses of a computer controlled data acquisition system, 2) an experiment on beamline IR4 which demonstrated the use of Fourier transform spectroscopy to obtain infared transmission spectra, 3) an experiment on the undulator beamline U5U which involved a measurement demonstrating the quasi-monochromatic nature of undulator radiation and its dependence on opening angle, 4) an experiment on the EXXON beamline U1 based on understanding gas phase spectroscopy and using the technique to identify an unknown gas molecule, and 5) an experiment on the BNL biology beamline U9B in which circular dichroism was used to study and identify various DNA-RNA molecules.

Other activities included tours of other departments at BNL (Physics, Biology, Chemistry, Applied Science, HFBR, Medical, Fire Island).

Information regarding the program and copies of the student reports can be obtained by contacting Karl Swyler or Donald Metz in the Office of Educational Programs.

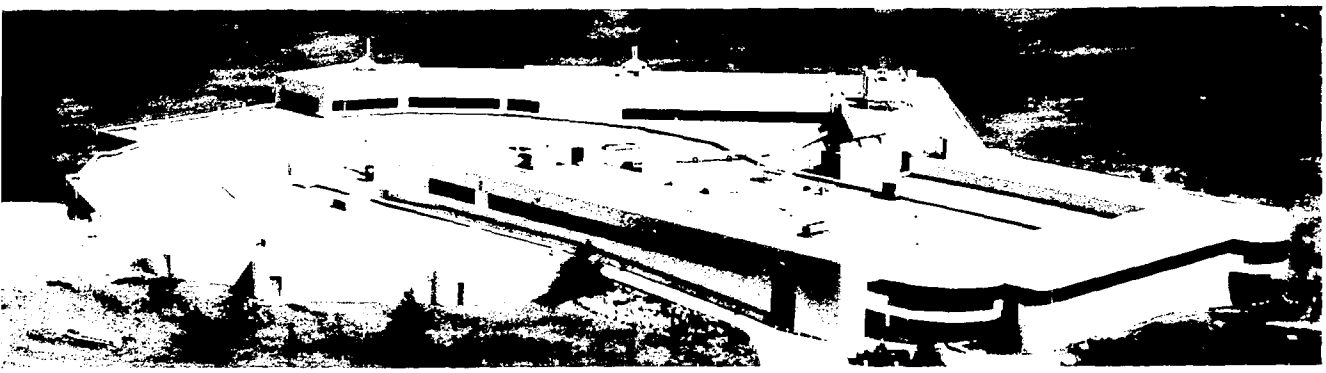

Section IV

NSLS Committees and Administration

Scientific Program Support Committee (SPSC)

William Thomlinson, NSLS
Committee Chairman

The Scientific Program Support Committee was formed in October 1987 by the NSLS Chairman. Its charge, as stated in the original memo, was to ". . . study every possible area of NSLS operation which directly or indirectly involves the NSLS scientific community. The charge of the committee is to define ways in which use of the facility can be optimized and to identify any existing problems and weaknesses. The committee should solve as many problems as possible with the existing resources of the NSLS and the scientific community, and make explicit recommendations for longer range solutions." The SPSC, under the Chairmanship of Dr. William Thomlinson, agreed to function for a one year period. The membership consisted of seven members of the NSLS Staff and six members of the scientific community, with Dr. Denis McWhan of AT&T acting as Vice-Chairman.

The Committee met bi-weekly for one year, with subcommittees dealing with issues related to Communications, User Meetings, Safety and Houskeeping, Staffing, the Experimenter's Handbook, Work Environment, NSLS Community Directory, and Support Services. The details of the recommendations and decisions are contained in a series of four reports made quarterly to the NSLS Chairman. The Final Report was released on October 7, 1988, the anniversary date of the Committee. These reports are available upon request.

The Scientific Program Support Committee has been highly successful in bringing about changes at the NSLS in the area of facility/experimenter interaction. Although many of the items which have been dealt with are in themselves small, they add up to a noticeably friendlier, more efficient environment in which to work. The most obvious output of the SPSC is the extensive list of publications and reports designed to facilitate utilization of the NSLS for general users, staff, and resident experimentalists. Among these items are the *NSLS Committee Directory*, the *NSLS Experimenter's Handbook*, the *NSLS Operations Directory*, and the *NSLS Community Directory*. In addition, the Committee contributed significantly to the upgrading of communications, the changes in the General User Information and Proposal Paths handled by the User Administration, and the clarification of policies which affect the users. Major recommendations have been made to the NSLS in areas of operations support staff upgrades, increased User Administration support, NSLS organizational changes to reflect the needs of the experimental community, and expanded support services and shops available to the experimenters.

The SPSC was very pleased with the cooperation of the entire community during the year. Many sensitive areas were discussed openly in an atmosphere of cooperation and unified purpose. The Committee feels that it has created a new, important type of interactive mode which must be continued at the NSLS and which hopefully other large facilities can emulate to their benefit. In its final act, the SPSC has recommended to the NSLS and the Users Executive Committee that the SPSC be reestablished each year to carry on its activities.

Membership

NSLS	Community
William Thomlinson (Chairman)	Denis McWhan, AT&T (Vice Chairman)
Richard Garrett	Marten denBoer, Hunter College
Nicholas Gmur (Secretary)	Jean Jordan-Sweet, IBM
Roger Klaffky	James Phillips, SUNY Stony Brook
Michael Knotek	Jack Preses, BNL Chemistry Dept.
Vincent Racaniello	Dale Sayers, North Carolina
Susan White-DePace	

PRT/IDT Council

Kent Blasie, University of Pennsylvania
Chairman, PRT/IDT Steering Committee

Over approximately the past year, the Council of PRT IDT Directors has concerned itself primarily with the matter of self-organization. The Council selected a Steering Committee composed of Richard Deslattes (NBS), Jerry Hastings (BNL-NSLS), Richard Hewitt (EXXON), Denis McWhan (AT&T), Dale Sayers (North Carolina State Univ.) and Chaired by Kent Blasie (Univ. of Penn.). The Steering Committee drafted a Charter for the Council which has been circulated to the PRT/IDT Directors for their approval. In addition, a "white paper" stating the significance and purpose of the Council has been drafted and is currently under consideration by the Steering Committee. These two documents are necessary to fully establish the "legitimacy" of the PRT/IDT Council to the NSLS, BNL, DOE and the sponsoring institutions funding agencies of the PRT IDTs. As a result, the consensus opinions generated by the Council should then carry substantial weight in DOE BNL NSLS decisions on important matters affecting the PRT IDTs abilities to carry out their respective scientific technological missions. Over the next year, the Council should therefore be concerned primarily with establishing consensus opinions on a number of such matters currently on the Council's agenda.

General User Oversight Committee (GUOC)

Erik Johnson, NSLS
Committee Member

In years past general users were usually handled on a first come first served basis. However, as the facility has matured the requests for beam time have begun to exceed the available resources. The General User Oversight Committee (GUOC) was established a few years ago in anticipation of this problem. Its major function is to distribute the available beam time on as equitable a basis as possible, and to voice the concerns of the general user community to the NSLS management. At present it is composed of eight members who serve on a rotating basis. Representatives are roughly divided between the two rings, with replacement members nominated by the committee.

During fiscal 1988 the X-ray ring was in the Phase II shutdown, so most of the activity was related to the VUV ring. Sixty-one VUV general user proposals were active during this period with 47 requesting beam time, over 90% of which were actually scheduled. More than 540 days were allocated with the average proposal receiving about 13 days of beam time.

To deal with the increased demand for the resource anticipated for fiscal 1989, Proposal Study Panels (PSP) for both the X-ray and VUV have been established to rate the general user proposals for scientific merit. This information will be used to determine priorities in areas where demand is the greatest, such as EXAFS or photoemission.

User's Space Committee

Richard Hewitt, EXXON
Committee Chairman

Over the past year the User's Space Committee has served to allocate most of the office, laboratory, and NSLS experimental floor space made available to it by BNL and the NSLS. The amount of available space remaining in the above areas is either none or very little. With both rings at the

NSLS in full operational mode, we see a potential demand for increased laboratory and office space in 1989. To date, very few of those requests have been forwarded to the User's Space Committee. It is important for the user community to evaluate their needs concerning space utilization for 1989 and beyond. These evaluations should be forwarded to the User's Space Committee to help document the expansion of the user community.

NSLS/HFBR Faculty Student Support Program

Susan White-DePace, NSLS
User Administrator

This program, funded by the Department of Energy, provides support for faculty/student research groups performing experiments at the NSLS as General Users, or neutron experiments at the BNL High Flux Beam Reactor (HFBR). The program is designed to encourage new users to use these facilities and to defray expenses incurred during exploratory visits to BNL and during initial experiments at the NSLS and HFBR. It is aimed at university users who have only limited grant support.

A three member committee, consisting of representatives from the NSLS staff, one from the HFBR staff, and one designee of the NSLS User's Executive Committee, reviews applications and selects participants for the program.

Fifty faculty members and students participated in research on the X-ray and VUV rings at the NSLS and at the HFBR during FY 1988 with the help of this funding. Application forms or further information can be obtained from Susan White-DePace, NSLS User Administrator.

Housekeeping Committee

Don Cassidy, Sachs/Freeman Associates, Inc.
Committee Chairman

The purpose of the Housekeeping Committee is to perform periodic inspections of the X-ray and VUV work and setup areas in building 725, so as to limit the clutter and unsafe conditions which inevitably occur when large groups of workers perform day-to-day tasks unchecked.

Early in 1988, the X-ray ring was recovering from a one year shutdown and many beamlines were under construction and/or renovation. Considering these facts, the Housekeeping Committee feels that the general condition of the X-ray area is good but there is room for improvement. The VUV area, being older and more established, is in better overall condition from a housekeeping standpoint and always has fewer violations then does the X-ray area.

Housekeeping inspections are performed every 4 to 6 weeks and there are an average of 45 to 50 violations of housekeeping rules per inspection. The fact that the number of violations has remained constant as the number of NSLS staff and experimenters has steadily increased indicates a general improvement in the attitude and performance of all personnel at the NSLS with regard to housekeeping.

The committee will continue to inspect NSLS during the upcoming year with an emphasis on further improvement of the safety and housekeeping conditions which are important to insure a safe and orderly working environment.

Safety Committee

Ken Batchelor, NSLS
Committee Chairman

The Safety Committee, along with the Beam Line Review Committee, has continued to review new experimental beamlines prior to their operation with synchrotron radiation. In addition, the committee has reviewed NSLS procedures for the handling and disposal of chemicals and hazardous wastes. Recommendations for improvement in the emergency lighting and building drainage systems have been made. A radiation monitoring system utilizing thermo-luminescent dosimeters (TLDs) located around the VUV experimental floor and office areas has been extended to the X-ray experimental floor; recommendations for improved support stands for lead shielding around the Booster and VUV rings have been made. The committee has overseen the writing of the Phase II Safety Analysis Report, which is nearing completion. The committee carried out an extensive review of the X5 Laser Electron Gamma Source (LEGS) hydrogen target and has submitted a proposal for staffing and training needs to the NSLS management.

Facilities Planning Committee

William Foyt, NSLS
Committee Chairman

The Facilities Planning Committee was formed in March 1988 in order that all requests for modifications and/or additions to the NSLS facilities could be evaluated properly. In April 1988 the committee met to discuss the request for an appendage to the X5 LEGS building in order to create floor space for Argonne National Laboratory (ANL) beamline X6A. A number of schemes were reviewed, with final approval given to one scheme in May 1988. Subsequently, ANL found the estimated cost of this addition ($150K) to be prohibitive and the job is on hold. The Light Source has recommended sharing with ANL a proposed building addition to be funded with BNL General Plant Projects (GPP) funds if ANL were willing to contribute approximately 15% of the $450K price tag of this project. ANL is prepared to contribute approximately 4%; negotiations with the chairman's office are on-going.

In August, the committee met to review the proposed construction of a walkway to connect the two furthest wings of the Light Source's second floor. This project has been approved and should be completed by June 1989. In addition, at this same meeting the committee reviewed and approved the list of GPP requests for FY 1989 - FY 1991.

Library Committee

William Foyt, NSLS
Committee Chairman

With the completion of the convential construction portion of Phase II, the library ceased to be a conference room and became a full fledged library. Most of the effort spent since then has been in arranging furniture, reorganizing shelves, and insuring that all NSLS publications (the original and six copies) reside in the library.

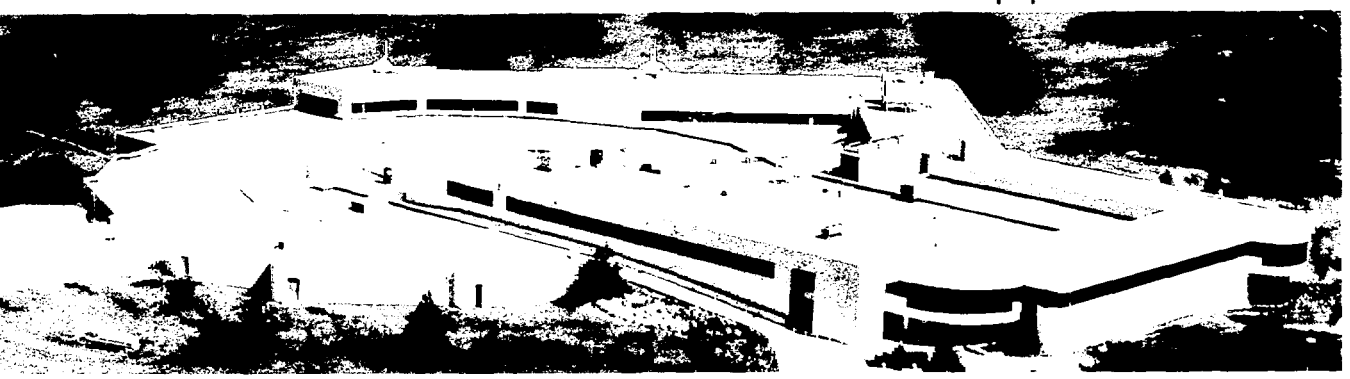

Section V

Abstracts: Science at the NSLS

Research Reports For The VUV Beamlines

Beamline U1

Beamline U3C

Beamline U4A

Beamline U4B

Beamline U4IR

Beamline U5

Beamline U6

Beamline U7B

Beamline U8

Beamline U8B

Beamline U8C/D

Beamline U9A

Beamline U9B

Beamline U10A

Beamline U10B

Beamline U11

Beamline U12

Beamline U14

Beamline U14B

Beamline U15

Beamline U16A

LARGE ANGLE SCATTERING OF SOFT X-RAYS FROM CHARACTERIZED SURFACES

Jeffrey Colbert (Instrumentation Division), Daniel A. Fischer (NSLS/Exxon PRT)

In soft x-ray fluorescence yield near edge spectroscopy (FYNES) experiments it is desirable to reduce the ratio of scattered relative to fluorescent radiation emerging from the sample. It is the purpose of this study to optimize the sample and detector geometry in order to minimize the scattered light contribution.

We have quantified specular and low level off specular scattering of soft x-rays incident on a polished Pt(111) single crystal, Pt coated float glass, graphite, pure alumina, and zeolite catalysts, both coked and uncoked. The scattering measurements were performed for both S and P polarizationwith the detector in and out of the plane of incidence, a total of four scattering geometries for each sample. These measurements were all made at an energy of 275 eV (9 eV below the carbon K edge).

A sampling of our results for a Pt(111) single crystal and a coked zeolite powder catalyst is shown in the figures. For the single crystal sample we clearly wish to avoid geometries where the detector is in the plane of incidence to eliminate the specular peak or its wings. P polarization with out of the incidence plane geometry seems a favorable geometry that has already been used with success. For the coked zeolite the specular peak is much broader, less intense and there is an S polarization enhancement for the zeolite versus a P enhancement for the single crystal. A P polarization out of the incidence plane geometry is preferred for the zeolite although the scattered light level is about five times worse than for the single crystal. There was little difference in the scattered light response for pure alumina, coked or uncoked zeolite catalysts. This study has shown that through the use of appropriate detector and sample geometry sufficient signal to noise is available to utilize the FYNES technique for powdered catalyst samples.

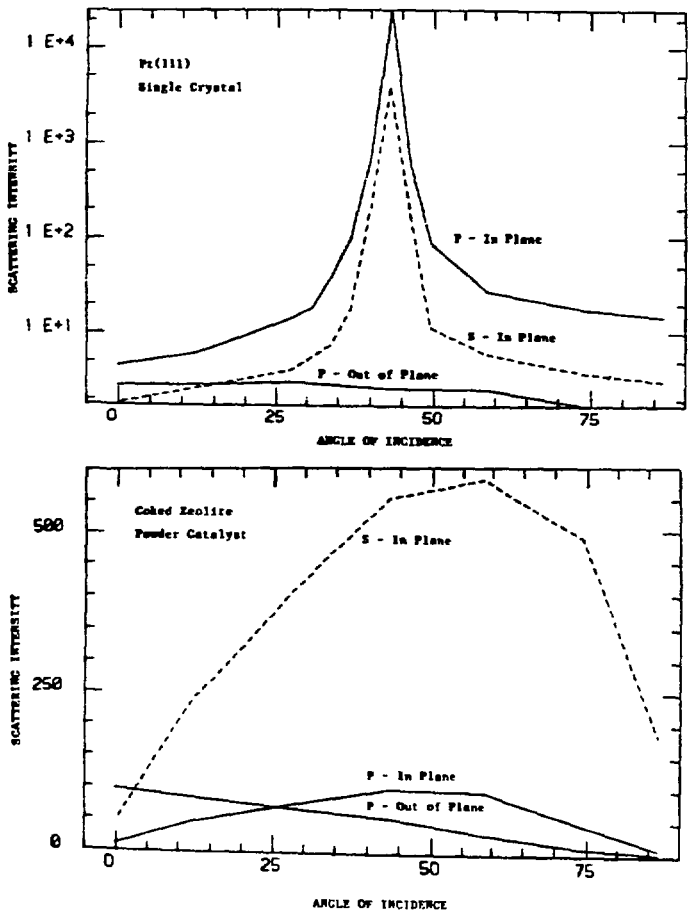

*This research was supported by the U. S. Department of Energy: Contract No. DE-AC02-76CH00016.

SOFT X-RAY EVALUATION OF MULTILAYER MIRRORS*

Jeffrey Colbert (Instrumentation Division), Daniel A. Fischer (NSLS/Exxon PRT)

In soft x-ray fluorescence yield near edge spectroscopy (FYNES) experiments it is desirable to reduce the ratio of scattered relative to fluorescent radiation emerging from the sample. Just above an absorption edge the fluorescent and elastically scattered photons have similar energies and cannot be electronically discriminated in our proportional counter detector. For low concentration (10 ppm) samples a large detector area maximizes collected light but allows scattered radiation over a large solid angle to contribute.

One approach to improve photon collection in FYNES employs a focusing multilayer mirror analyzer. This device would intercept a significant fraction of solid angle around the sampling point. Photons would arrive at near-normal incidence, be energy analyzed, reflected, and focused onto the detector element. The problem of a multilayer's low reflectivity may be counterbalanced by its large area, ability to concentrate flux and, particularly, its ability to discriminate between fluorescent and scattered light.

Model multilayer mirror devices have been obtained and we have undertaken an examination of their soft x-ray performance. The mirrors were energy calibrated and found to possess unwanted azimuthal grading of 2d spacing, but signal-to-background enhancement greater than fifteen. In fluorescence yield tests a multilayer mirror used as an analyzer exhibited filtering behavior at special angles which utilized only small regions of the mirror surface. It is expected that improvements in mirror fabrication or reevaluation of experimental geometry will make multilayer mirror analysis the procedure of choice for low background, low concentration FYNES studies.

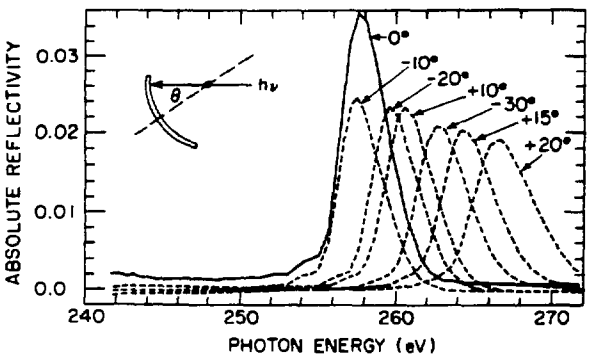

Measured reflectivity versus photon energy for the nominal 48.4 angstrom multilayer mirror at 2 degrees angle of incidence. Mirror was rotated away from nominal zero degrees (starting position) to sample different points on the surface.

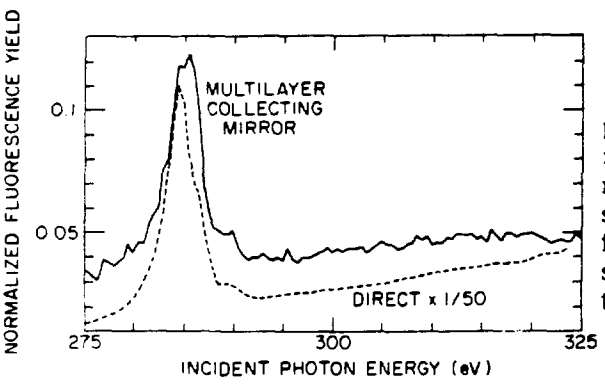

Fluorescence yield spectrum of graphite analyzed by nominal 48.4 angstrom multilayer mirror. Prominent π^* resonance rises above background. For comparison, same spectrum taken with direct capture of fluorescent photons by proportional counter, scaled by 1/50th. Incident beam monochromatized by ERG grating G3.

*This research was supported by the U. S. Department of Energy: Contract No. DE-AC02-76CH00016.

Fluorescence Yield Near Edge Spectroscopy of π-Bonded CO on Fe(100)

D.J. Dwyer and B. Rausenberger (U of Maine), J.P. Lu (Princeton), D. Fischer (NSLS), D. Parker (U. of Colorado), S. Cameron and J. Gland (Exxon).

Near edge X-ray absorption fine structure (NEXAFS) has become an important tool in determining molecular orientation of adsorbed molecules. The extension of this UHV technique to in-situ measurements via fluorescence yield detection (FYNES) has already been demonstrated.[1] In this work we use the FYNES technique to characterize the various adsorption states of CO on Fe(100). This data was obtained in vacuo and was seen as a preliminary to future in-situ reactivity measurements. There are three molecular adsorption states of CO on Fe(100) labeled α-1 through α-3 and a dissociated beta state[2]. The α-3 state is of particular interest since it is the precursor to dissociation and exhibits an extremely low stretching frequency of 1200 cm^{-1}. Earlier NEXAFS studies have been interpreted to indicate that the CO bond axis is tilted with respect to the surface normal[3]. However, these earlier data were limited to the CO saturated surfaces (mixed α states) and the α-3 state. In the present study we have obtained high quality carbon edge FYNES data for the CO/Fe(100) system after various thermal treatments. These thermal treatments allowed us to extract the near edge spectra of the individual adsorption states via difference spectra. Fig. 1 contains the difference spectra obtained for each of the four adsorption states of CO on the Fe(100) with the E vector of the radiation 90° from the surface normal. Fig 2. contains the same data obtained with the E vector 30° from the surface normal.

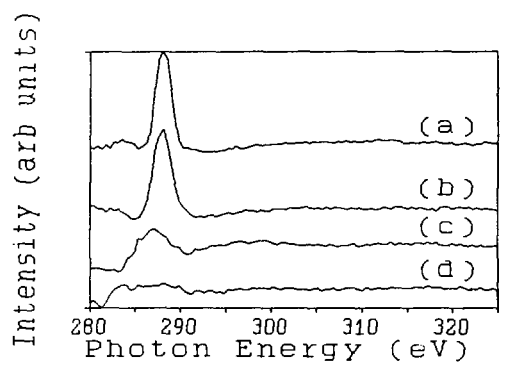

Figure 1: FYNES difference spectra taken with the E vector in the surface plane for the various adsorption states of CO on Fe(100): (a) α-1 CO, (b) α-2 CO, (c) α-3 CO, (d) β CO.

The polarization dependence of the FYNES data for the α-1 and α-2 CO states displays the characteristic response of CO adsorbed with it's molecular axis perpendicular to the metal surface, i.e. an intense carbon 1s to $2\pi^*$ transition (288 eV) with the E vector in the surface plane with an intensification of 1s to $6\sigma^*$ as the E approaches the surface normal. These results are fully consistent with other spectroscopic data which demonstrate that CO bound in these states is typical of CO adsorbed on transition metal surfaces [2]. The FYNES spectra labeled (c) in both Fig. 1 and Fig. 2 are those obtained for the π-bonded CO state (α-3 CO). Note that the characteristic near edge 1s→$2\pi^*$ transition of molecular CO is extremely weak in both polarizations even though the surface coverage of α-3 CO is greater than the α-1 and α-2 states ($6x10^{14}$ cm^{-2}). These results imply that the carbon oxygen bond in the CO α-3 state is rehybridized with respect to "normal" chemisorbed CO. The rehybridization may be viewed as either extensive occupation of the $2\pi^*$ antibonding orbital or a lowering of the carbon-oxygen bond order due to the direct coordination of the oxygen and carbon end of the molecule to the surface. The spectra obtained for α-3 CO (π-bonded CO) are reminiscent of those observed for surface methoxide (carbon-oxygen single bond). A carbon-oxygen single bond is consistent with the low CO stretching frequency of this adsorption state. The lack of a strong polarization dependence for the α-3 CO as seen in the earlier study indicates that the carbon oxygen bond is tilted with respect to the surface normal. A more detailed analysis of the data presented here as well as that obtained at other polarizations is in progress. One additional noteworthy observation was the strong polarization dependence of the dissociated β CO (atomic carbon). The origin of this effect is being explored.

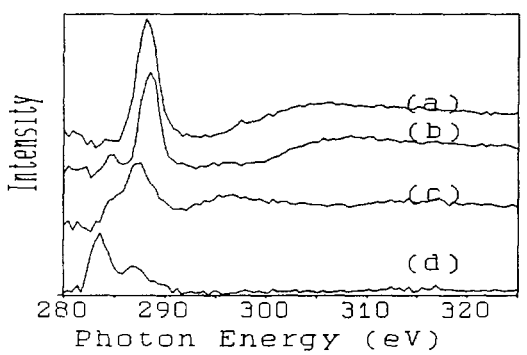

Figure 2 Spectra obtained with the E vector 30° from the surface normal. Trace (a) is that of α-1 CO, (b) α-2 CO, (c) α-3 CO and (d) is β CO.

[1]. F. Zaera, D. Fischer, S. Shen, J. L. Gland, Surface Science, **194**, 205 (1988).
[2]. D. W. Moon, S. L. Bernasek, D. J. Dwyer, J. L. Gland, Surface Science, **165**, 215 (1985). S. D. Cameron, D. J. Dwyer, Langmuir, **4**, 282 (1988).
[3]. D. W. Moon, S. Bernasek, S. D. Cameron, W. Eberhardt, D. J. Dwyer, J. L. Gland, Surface Science, **180**, L123 (1986).

FLUORESCENCE YIELD NEAR EDGE SPECTROSCOPY (FYNES): A Study of Sample and Detector Geometry to Minimize Scattered Light Background

Daniel A. Fischer,* National Synchrotron Light Source and Jeffrey Colbert,† Instrumentation Department, Brookhaven National Laboratory, Upton, NY 11973
John Gland, Exxon Research and Engineering Co., Annandale, NJ 08801

In Soft X-ray Fluorescence Yield Spectroscopy (FYNES) experiments it is desirable to reduce the amount of scattered relative to fluorescent radiation from the sample. In the case of low concentration (10 ppm) bulk or submonolayer surface coverage samples, a large area detector maximizes the collected light but allows scattered radiation over a wide angular range to be counted as well. Just above an absorption edge the fluorescent and scattered incident photons have similar energies (within 7 eV for C K_α) and therefore cannot be pulse height discriminated by our proportional counter detector. It is the purpose of this study to optimize the sample and detector geometry in order to minimize the scattered light contribution.

We have quantified specular and low level off specular scattering of soft X-rays incident on a Pt(111) single crystal, Pt coated float glass, graphite, pure alumina, and zeolite catalysts (coked and uncoked). The scattering measurements were performed for S and P polarization with the detector in and out of the plane of incidence, thus four scattering geometries were used for each sample. The scattering measurements were all made at an energy of 275 eV (9 eV below the C K edge). An additional set of data was collected for graphite at 300 eV (16 eV above the C K edge) where the measured radiation from the sample was predominantly due to carbon fluorescence allowing us to quantitatively compare the four scattering geometries.

A sampling of our results is described for a Pt(111) single crystal and a Coked Zeolite Powder catalyst. For the Pt(111) single crystal we clearly wish to avoid in the plane of incidence geometries in order to eliminate the specular peak and its wings. In fact for P polarization with out of the plane of incidence detection seems to be a good geometry and one that we have used with success already. For the coked zeolite case we see a much broader, less intense, specular peak and reverse polarization enhancement S to P as compared with the single crystal Pt(111). Once again a P polarization out of plane geometry is favored, however the scattered light for this geometry is still about five times worse for the zeolite powder versus the smooth Pt(111) single crystal. We also saw very little difference in the amount of scattered light for pure alumina, the coked and uncoked zeolites catalysts. Finally this study has shown that through the use of appropriate detector and sample geometry sufficient signal to noise is available to utilize the FYNES technique for powdered catalyst samples.

*Work supported by Exxon Research and Engineering Co.
†Research supported by U.S. DOE under contract #DE-AC02-76CH00016.

HYDROGEN INDUCED DISPLACEMENT OF CO ON Pt(111) IN SITU OBSERVATIONS USING FYNES

D. Fischer (NSLS), J. Colbert (Instrumentation), D. Parker (U. of CO) and J. Gland (Exxon)

We report the first in situ observation of hydrogen induced displacement of CO on a platinum surface. Data was collected for range of sample temperatures and hydrogen pressures. Preliminary analysis indicates that the displacement is temperature activated with rapid displacement occurring above 55°C. Shown below is a figure representative of the displacement data we obtained.

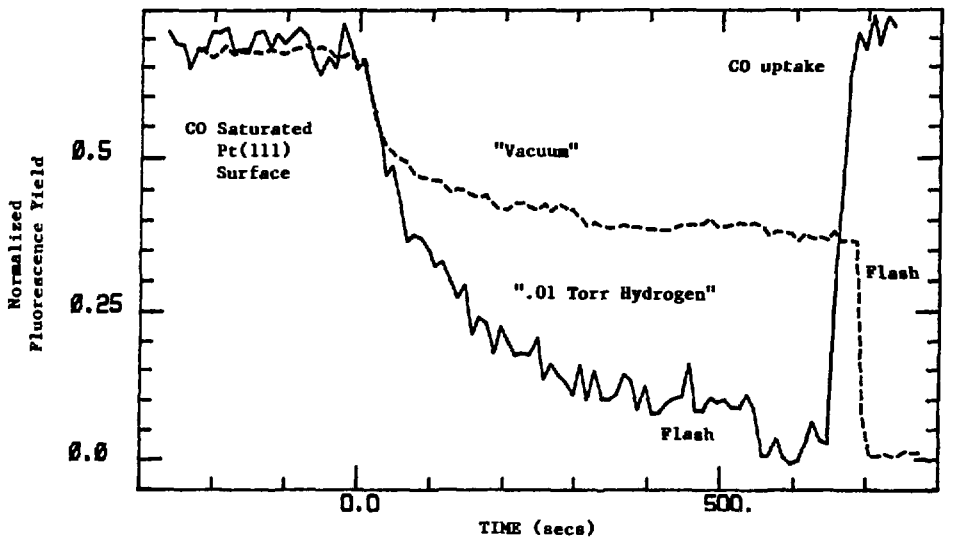

ULTRA SOFT X-RAY FLUORESCENCE EXAFS

D. Fischer (NSLS), M. Davis (Exxon), G. Meitzner (Exxon), and J. Gland (Exxon)

We have used soft X-ray fluorescence EXAFS for the first time to characterize the structure of fluorine in a series of solids. These pioneering experiments were performed using new instrumentation and a unique approach developed over the past several years.* In part these studies were performed on proprietary beamtime on the Exxon VUV facility at the NSLS at Brookhaven National Laboratory. EXAFS in the soft x-ray region gives researchers the ability to characterize the local environment around C, N, O, and F even for disordered materials. In favorable situations both the bonding distances and number of neighbors can be determined. Moreover, fluorescence yield detection precludes difficulties associated with sample charging rendering this technique especially suitable for studies of high area practical catalysts.

Fluorine EXAFS results were obtained for a series of hydroisomerization catalysts containing 0.9-7.0 wt% fluorine dispersed on high area γ-Al_2O_3. Teflon and aluminum trifluoride were also investigated as reference standards. Satisfactory x-ray absorption fine structure was resolved even at the 1% loading level. Discrimination of the fluorine EXAFS lineshape from nearly overlapping oxygen EXAFS oscillations was facilitated by using an energy dispersive detector along with pulse height discrimination to selectively filter the oxygen fluorescence. Further development of this discrimination technique should permit structural characterization of dispersed phase species at even lower loading levels well below 1 wt%. As such we believe that the development and application of soft x-ray fluorescence-yield EXAFS represents a significant technical achievement in catalysis science.

Preliminary Fourier analysis indicates that the local fluorine atomic structure in fluorided alumina is characterized by an unusually long Al-F bond length and that the number of aluminum nearest neighbors is lowered as compared to AlF_3. These results complement earlier ion scattering and photoemission results which demonstrated that fluorine substitutes for oxide anions and hydroxyl groups at the surface of γ-Al_2O_3. A more detailed account of this research will be reported in the near future.

*Ultra Soft X-Ray Fluorescence Detection: Proportional Counters, Focusing Multilayer Mirrors, and Scattered Light Systematics, in press, Rev. Sci. Inst. (April/May 1989).

TITLE OF EXPERIMENT: Dependence of core photofragmentation processes on the site of core excitation

BEAM LINE: U1 DATE OF EXPERIMENT: from: 1/21/88 to: 2/3/88

EXPERIMENTER(S): AFFILIATION:

Robert G. Hayes Dept. of Chemistry and Radiation Laboratory, U. Notre Dame

WORK SPONSORED BY: DOE

We used not only beam line U1, but also a chamber which belongs to that beam line, and which is designed for electron-ion coincidence studies of gaseous molecules, in this experimental run. We took considerable data on CS_2, which included photoabsorption data around the C 1s and the S 2p thresholds, the S 2p and C 1s Auger spectra, autoionization electron spectra which arise from exciting resonances out of the C 1s and S 2p excitations, and various electron-ion and ion-ion coincidence data associated with the various electron spectra. The most extensive set of coincidence data is a set of electron-ion coincidence spectra which correlate ion production with electrons from various points in the S 2p Auger spectrum. They show a change in ion yields as the point in the Auger spectrum is varied from the Auger feature which has highest kinetic energy (and thus corresponds to production of the ground state of CS_2^{++}) to a feature which corresponds to production of CS_2^{++} with 12 eV of excitation, which is the last well resolved feature in the Auger spectrum. The ground state of the ion yields CS_2^{++} exclusively. Higher ionic states yield increasing amounts of $CS^+ + S^+$. At the highest ionic states C^+, from the fragmentation $C^+ + S^+ + S$, begins to appear. The kinetic energies of the fragmentation products, CS^+ and S^+, are almost independent of the energy of the state from which they have arisen and only the amount of fragmentation changes. This behavior is somewhat unexpected, although Eberhardt observed similar behavior in CO_2(1). On the other hand, in SO_2 Dujardin and coworkers observed that the energies of the ions in the $SO^+ + O^+$ channel depended strongly on the state of the molecular ion.

We also measured coincidence spectra from acetonitrile, using electrons which are produced by collapse of the π^* resonance, which is a prominent feature in the absorption spectrum of this molecule in the neighborhood of both the C 1s and the N 1s edges.

(1) W. Eberhardt, private communication
(2) G. Dujardin, S. Leach, O. Dutuit, P.-M. Guyon, M. Richard-Viard, Chem. Phys. 88, 339 (1984)

DEPENDENCE OF CORE PHOTOFRAGMENTATION PROCESSES ON THE SITE OF CORE EXCITATION

R. G. Hayes (Notre Dame), W. Eberhardt (Exxon), and J. Bellina (St. Mary's College)

We have studied the ionic products of the excitation of thiophene, C_4H_4S, and of tetrahydrothiophene, C_4H_8S, both five-membered ring cyclic compounds, upon excitation of the S 2p and of the C 1s electrons. We have also measured the ion yield spectra and Auger spectra of the compounds, and the spectra of electrons from excitation of core-valence resonances. Ion products were detected in coincidence with Auger electrons from decay of the core excitations. Figure 1 shows the mass spectrum of thiophene, on a mass scale, in coincidence with Auger electrons with kinetic energy of 138. eV from ionization of the s 2p level. This energy corresponds to an internal energy of the dipositive molecular ion from Auger decay of 7. eV. All the observed products appear in Figure 1 except H^+, which is produced in small quantity. Some dipositive molecular ion is produced, which is obscured in the spectrum by $C_3H_3^+$ at m/e=39. The peaks show clearly the presence of kinetic energy in the products. The sum of the kinetic energies of the most abundant ion pair, $C_3H_3^+/HCS^+$, is 2.7 eV. Figure 2 shows the branching ratios of the observed ionic products at various internal energies. The branching ratios to the most abundant ion pairs, $C_3C_3^+/HCS^+$ and $C_2H_2^+/C_2H_2S^+$, are in the order of the energy releases of the two processes. The energy dependence of the ratios between 7. eV and 20. eV is consistent with a statistical decay mechanism with activation energies of 1.9 eV and 2.4 eV respectively.

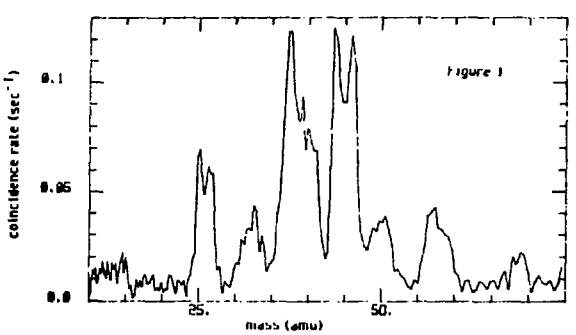

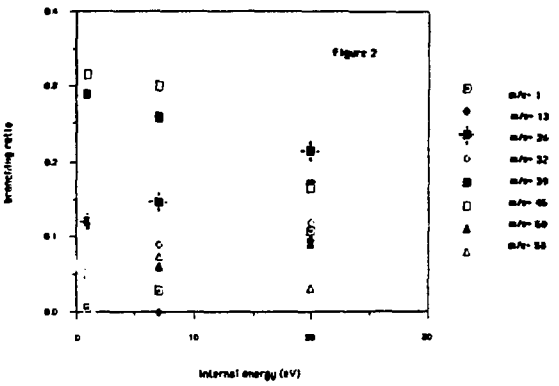

This work was sponsored in part by DOE through the Notre Dame Radiation Laboratory.

HIGH RESOLUTION NEXAFS SPECTRA OF CONDENSED $Ru_3(CO)_{12}$

D. Sondericker, Z. Fu, J. Bradley, W. Eberhardt (Exxon R&E Co.)

We have measured high resolution C and O NEXAFS spectra of $Ru_3(CO)_{12}$. The carbonyl was condensed onto a stainless steel substrate and transferred under UHV into the measurement chamber at U1. The experiments were carried out using the ERG monochromator at U1 and a partial yield electron detector.

Fig. 1 shows a high resolution scan of the C 1s → π^* transitions in $Ru_3(CO)_{12}$. Compared to isolated CO molecules this peak exhibits a pronounced shoulder at the high energy side. We attribute this shoulder to transitions into higher energy parts of the manifold of the unoccupied π orbitals in this molecule. The energy difference (0.4 eV) and intensity make it unlikely that this shoulder is due to vibrational substructure.

Fig. 2 shows the O absorption edge in $Ru_3(CO)_{12}$. Again the spectrum is dominated by the strong O 1s → π^* transition. Above the continuum onset at 538 eV we see the σ shape resonance located at 549 eV. This value is about 2 eV lower than for gas phase CO.

The basic trend observed here is that the C π^* resonance shifts to larger energy, whereas the energy of the O-π^* resonance is lower than in gas phase CO. This observation also holds for CO adsorbed on metal surfaces. However it is for the first time that a clear splitting of the π^* resonance has been observed. This splitting is due to the discrete number of CO molecules in the $Ru_3(CO)_{12}$ carbonyl. The empty π bands split due to various linear combinations of the atomic orbitals, which constitute a whole manifold of empty π states in the molecule. The analogue to that is the formation of a CO 2σ "band" in an adsorbed monolayer of CO molecules on the surface.

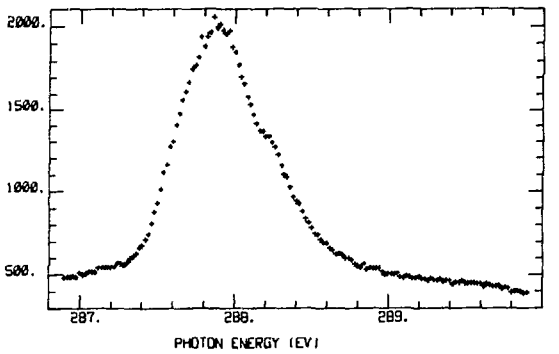

Fig. 1 High resolution scan of the C 1s → π^* transitions in $Ru_3(CO)_{12}$.

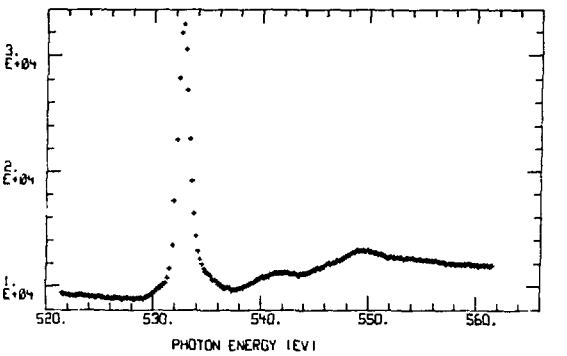

Fig. 2 Electron yield NEXAFS curve of $Ru_3(CO)_{12}$ near the onset of the O 1s excitations.

THE ELECTRONIC STRUCTURE OF MOLECULAR O_2 on Ag(110)

D. Sondericker (NSLS); Z. Fu (PRC); T. Upton and W. Eberhardt (Exxon)

We have studied valence band photoemission of O_2 on Ag(110) in order to determine the bond length of the adsorbed O_2 molecule. At 190°K O_2 chemisorbes on Ag in a molecular form. It is lying down parallel to the surface in the [110] direction and is in a π-bonded configuration.[1,2] From the very low vibrational frequency, we know that the O-O bond is severely stretched. Because the inner σ orbitals are not directly involved in the bonding to the surface, their energy splitting contains information about the O_2 molecular bond length.

The sample was cleaned by Ar ion sputtering and annealed at ~400°C. Carbon contamination was checked by C 1s photoemission. The sample were cooled to 170°K and valence band spectra from the clean surface was collected for various incident photon energies between 30 eV and 150 eV. The sample was exposed to 2000 L O_2 and photoemission spectra from the O_2 covered surface collected and compared to the clean spectra.

The figure shows spectra for the clean surface, the O_2 covered surface and their difference for incident photon energy of $h\nu$=120 eV. The large peak centered at 5 eV below the Fermi edge is a mixing of the Ag-4d bands and the oxygen π orbitals. The peaks at 10.5 eV, 22 eV, and 27 eV are the oxygen $3\sigma_g$, $2\sigma_u$ and $2\sigma_g$ respectively.

Calculations have been made for the O_2 neutral gas molecule and the O_2^{--} dianion which show that the splitting of the σ levels ($2\sigma_u$-$2\sigma_g$) and ($3\sigma_g$-$2\sigma_u$), is relatively independent of the charge of the molecule but is a function of the O_2 molecular bond length. These calculations have been used successfully in determining the bond length of molecular O_2 on Pt(111). We have compared the energy splitting of the σ orbitals in O_2 on Ag(110) to the gas phase calculations and have deduced a bond length of 1.55Å. As expected, this is substantially larger than the 1.21Å bond length of the free molecule and also larger than the 1.40Å of O_2 on Pt(111).

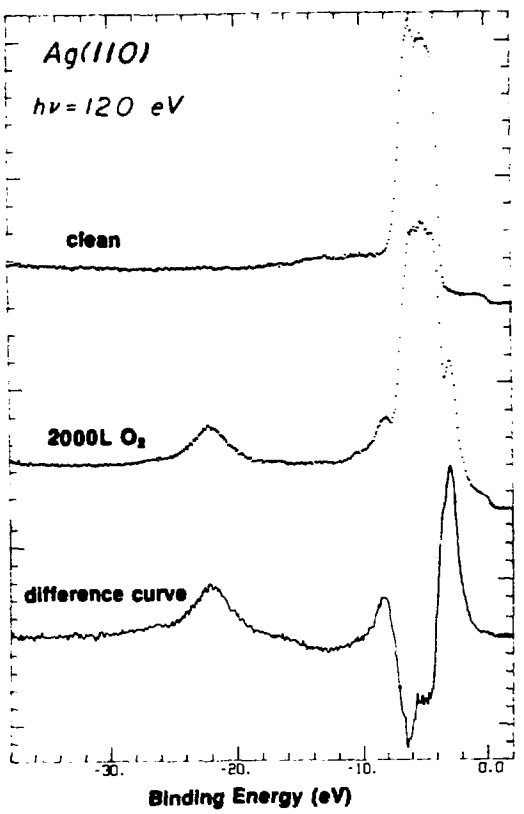

1. D.A. Outka, J. Stohr, W. Jark, P. Stevens, J. Soloman, and R.J. Madix, Phys. Rev. B 35, 4119 (1987).
2. K.C. Prince, G. Paolucci, A.M. Bradshaw, Surf. Sci. 175, 101 (1986).
3. W. Eberhardt, T. Upton, S. Cram, L. Incoccia, Chem. Phys. Letts. (in press).

UV PHOTOEMISSION STUDY OF SULFUR PASSIVATED GaAs SURFACES

T. Tiedje,[1] W. Eberhardt,[3] P. Wong,[2] Zugen Fu,[3] K.A.R. Mitchell,[2] and D. Sondericker[3]
[1]Phys. Dept., U. of British Columbia; [2]Chem. Dept., U. of British Columbia; [3]Exxon Research & Engineering Co.

The surface of GaAs can be passivated by an aqueous Na_2S treatment in which the metastable passivation effect shows up as a decrease in the surface recombination velocity and increase in the photoluminescence efficiency.[1] In order to understand in microscopic detail the atomic and electronic structure of these passivated surfaces, we have carried out a high resolution VUV photoemission study of as-treated GaAs (100) surfaces, using synchrotron radiation at the NSLS, Brookhaven. The synchrotron radiation source has enabled us to resolve relatively small chemical shifts in the core level photoemission and also to select the excitation energy for maximum surface sensitivity. From a study of the chemical shifts of the Ga 3d and As 3d core levels we find that the Na_2S treatment produces primarily a surface oxide 2-3Å thick, containing relatively small amounts of sulfur and carbon. About 1/3 of a monolayer of sulfur is present in the form of GaS_x and AsS_x species, with no indication of sulfur-oxygen bonds, or a physisorbed sulfur species. The surface Fermi level shifts by 0.3 eV toward the valence band after the treatment. This observation shows that the Na_2S treatment modifies the surface state density, as expected, which also can be seen directly in the valence band photoemission spectrum.

[1]C.J. Sandroff, et al., Appl. Phys. Lett. 51, 33 (1987), E. Yablonovitch et al., Appl. Phys. Lett. 51, 441 (1987).

NEXAFS Study of 3-hexadecyl-pyrrole/ferrocene-pyrrole Langmuir-Blodgett Films

J. M. Chen, X. Q. Yang, T. Inagaki, T. A. Skotheim (BNL), M. L. denBoer (CUNY), Y. Okamoto (Polytech. U), L. Samuelson, S. Tripathy (U Lowell).

The orientational behavior of Langmuir-Blodgett(LB) films consisting of mixtures of 3-hexadecyl-pyrrole(3HDP) and ferrocene-pyrrole(FcP) have been studied at beam line U3 by near edge X-ray absorption fine structure (NEXAFS) spectroscopy above the carbon *K*-edge. The spectra were obtained by measuring the total electron yield of the sample and normalized to the photo-yield of a gold grid placed in the incident beam.

The dipole transition rule implies that the probability of photoexcited transitions from the C 1*s* state to unoccupied molecular states such as the σ^* C-C bond, the σ^* or π^* C=C bond, or the C-H bond depends on the orientation of the electric field E of the photon with respect to the molecular axis[1]. This phenomenon has been widely used to study the orientational behavior of low-Z organic compounds.

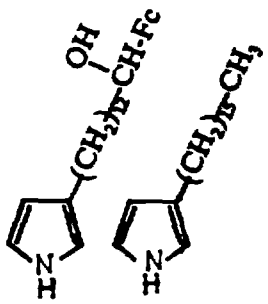

Fig. 1 The molecular structure of 3HDP/FcP. Fc is ferrocene.

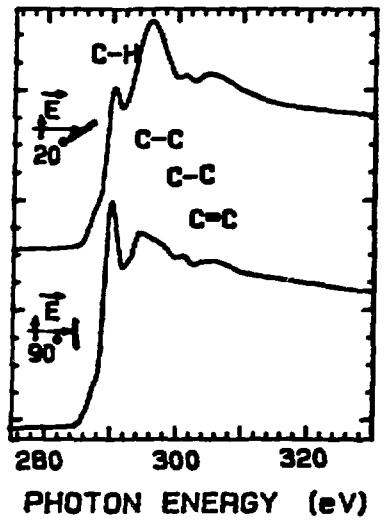

Fig. 2 NEXAFS of 3HDP/FcP Langmuir-Blodgett films above the C *K*-edge.

The structures of the 3HDP and FcP monomers of the mixed LB film are shown in fig. 1. One chain terminates in a hydroxide-ferrocene unit. NEXAFS measurements as a function of orientation (Fig. 2) show that the 290 eV peak, involving transitions to C-H states, which are perpendicular to the hydrocarbon chains, is higher at normal incidence when the E field is parallel to the substrate, while the 295.6 eV peak, involving C-C states, which are oriented along the hydrocarbon chains, is higher at grazing incidence, when the E field is nearly normal to the substrate. This indicates a high degree of orientation of the hydrocarbon chains: i.e. they are oriented nearly normal to the substrate.

References

1. J. Stöhr and R. Jaeger, Phys. Rev. B. 26, 4111 (1988).

Acknowledgement: This work was supported by the Division of Materials Science, U. S. Dept. of Energy under contract No. DE-AC02-76CH00016.

LEX Detector Calibrations and a U3C Beam Line Flux Characterization*

R. Hockaday (LANL), R. Blake (LANL), G. Stradling (LANL), G. Idzorek (LANL), L. Sigman (EG&G), J. Studabaker (LANL), J. Vaninetti (LANL)

The purpose of this experiment was to characterize the UC3 beam line for it's absolute flux output and to obtain a LEX detector system calibration.

LEX (Low Energy X-ray) detectors are designed to measure absolute x-ray fluxes from high temperature plasmas. Combinations of filters, fluorescers, and x-ray diodes or photodiodes are used to define notch spectral responses. The calibrations in the past have depended on film thickness measurements, the diode calibrations, published fluorescence efficiencies, and published scattering and absorption coefficents to calculate a system response. These calibrations could lead to uncertainties of order 2 to 3 for the low atomic weight fluorescers such as C_k from polypropylene and F_k from teflon. This variation reflects the different fluorescence yield values that have been reported in the literature and the accumulated uncertainties from each component measurement. Thus, a system calibration can dramatically reduce the LEX system response uncertainties. Up until this experiment LEX detectors had never been system calibrated due to their low sensitivity and the insufficient flux outputs of conventional x-ray tube sources. With the development of monochromated synchrotron light sources LEX system calibrations are now possible.

This experiment consisted of two steps. The first was to characterize the output of the UC3 monochrometer with an array of different detectors. These detectors were a X-Y positioned apertured x-ray diode, a large windowed ion chamber, a X-Y positioned pinhole windowed gas proportional counter, a large aperture filtered x-ray diode and a transmission grating coupled to a x-ray streak camera used in DC mode. With these detectors the 1st, 2nd, and 3rd spectral orders of the monochrometer output and a 40ev background were measured. After the source was characterized the second step was to calibrate a polypropylene-teflon-aluminum fluorescer LEX detector system. From this experiment the uncertainties of this LEX system has been reduced to the ±20% to ±30% level. Further calibrations and more refined measurements of LEX detectors and the beam line output are planned for the UC3 beamline.

*Work performed under the auspices of US DOE.

SYNCHROTRON RADIATION STUDIES OF TEFLON PHOTOCHEMISTRY*

R. R. Rye and N. D. Shinn,
Sandia National Laboratories, Division 1134, Albuquerque, NM 87185

Mechanistic and kinetic aspects of the radiation-induced cross-linking in poly(tetrafluoroethylene) (Teflon) have been studied using photon stimulated desorption and photochemical methods. This cross-linking protects the Teflon surface against chemical etching and is the basis of a photolithographic process which allows control of both the spatial extent of adhesion and the adhesion strength. Pre-irradiated regions of the surface have, after chemical etching, the normal white appearance of Teflon with poor adhesion characteristics, while non-irradiated areas are dark and discolored with good adhesion characteristics.

Teflon samples were exposed to constant doses of soft X-rays over the energy range 25 eV < $h\nu$ < 1000 eV. Photon induced cross-linking was observed for all photon energies, indicating that the mechanism for this process does not require creation of a core hole, but probably results from secondary electron induced valence excitations. However, the efficiency of the process, as reflected in the etching behavior, is energy dependent through an energy dependence of the adsorption cross section. In crossing the F(1s) level there is a factor of five increase in the cross-section and photon energies just above the F(1s) level are five times more effective at producing an equivalent degree of protection against etching than those just below the F(1s) level. The observed energy dependence follows the calculated energy deposition profile; increased cross-sections lead to increased energy deposition in the near surface region consistent with a mechanism involving low energy secondary electrons within the near-surface region.

Photon stimulated desorption studies monitored the desorption of neutral fluorocarbon species produced as a byproduct of cross-linking during irradiation. A sharp increase in the rate of fluorocarbon desorption is observed as the energy advances through the F(1s) threshold, reflecting the previous observation that above the threshold the energy is deposited closer to the surface. Similar behavior in photo-fragment desorption and chemical etching behavior as the photon energy is swept through the F(1s) threshold is direct evidence that cross linking is the important step in photolithographic adhesion. Thus, information about the cross linking kinetics may be extracted from the photo-fragment desorption profiles. Modeling of the desorption profiles will also examine the role, if any, of photo-fragment diffusion through the near surface region.

* Work supported by the United States Department of Energy under contract DE-AC04-76DP00789 with Sandia National Laboratories.

PHOTOEMISSION OF Cr EPITAXY ON W(110)*

N. D. Shinn
Sandia National Laboratories, Division 1134, Albuquerque, NM 87185

Surface and interface electronic structure changes induced by the growth of ultra-thin chromium overlayers on the W(110) substrate have been measured by VUV and soft X-ray photoelectron spectrocopy. Both angle-integrated valence band and interface sensitive core-level photoelectron spectroscopies were used to measure Cr-induced electronic structure changes and to correlate these observations with the growth of epitaxial and/or other ordered overlayers. Previous studies [1] using Auger electron spectroscopy, low energy electron diffraction, temperature programmed desorption, work function measurements and field electron emission microscopy have shown that two-dimensional, layer-by-layer Cr adlayer growth occurs on the W(110) plane at low temperatures ($100K < T < 500K$) whereas 3-dimensional Cr microcrystallites nucleate on top of a Cr monolayer and grow epitaxially above 500K. The growth of the pseudomorphic monolayer results in the addition of new states near the Fermi level (Cr 3d and 4s derived) and more subtle changes deeper in the valence bands. Above one monolayer coverage, the valence band spectrum resembles a superposition of attenuated W(110) structure and bulk-like Cr structure. In particular, the metastable (2x2) Cr bi-layer, which is stable in the temperature range $500K < T < 800K$, does not exhibit a characteristically different valence band structure. This is consistent with the proposed model for this ordered overlayer which involves only minor translations of the second adlayer of Cr atoms to achieve (2x2) periodicity.

The stability of the pseudomorphic Cr monolayer up to 1150K is further demonstrated by no observable spectroscopic change after annealing. Thicker layers form three-dimensional nuclei upon annealing, resulting in a superposition of the monolayer Cr/W(110) and bulk-like Cr(110) valence bands. These structural transformations are further exhibited in interface-sensitive W(4f) core-level and Cr(3p) spectra. Growth of the pseudomorphic Cr monolayer results in a smooth attenuation of the surface-shifted W(4f) level and the growth of a new W(4f) component at a binding energy close to that for tungsten atoms in the bulk. The clustering of Cr multilayers with annealing is quite apparent in the relative increase in the W(4f) transition intensity with temperature, as expected from photoelectron mean free path considerations.

1. N. D. Shinn and P. J. Berlowitz, J. Vac. Sci. Technol A (in press);
A. J. Melmed and N. D. Shinn, Surf. Sci. 193, 475 (1988);
P. J. Berlowitz and N. D. Shinn, Surf. Sci. (submitted).

* Work supported by the United States Department of Energy under contract DE-AC04-76DP00789 with Sandia National Laboratories.

OXIDATION AT THE Fe/W(110) INTERFACE*

N. D. Shinn, C. H. F. Peden and P. J. Berlowitz[1]
Sandia National Laboratories, Albuquerque, NM 87185

Valence-band and near-surface sensitive core-level photoelectron spectroscopic studies of Fe/W(110) and Fe/WO_x/W(110) interfacial bonding are reported. These experiments are part of our systematic study of the metallization of model oxide surfaces and the reactivity of buried metal:metal interfaces. A monolayer (ML) of iron epitaxed in a pseudomorphic (1x1) overlayer on W(110) lowers the binding energy of the surface W($4f_{5/2}$) and W($4f_{3/2}$) peaks to the bulk-like tungsten value (ΔE_B < 100 meV). Surface tungsten atoms at a vacuum interface are slightly electronegative with respect to bulk tungsten atoms. The coverage dependence of the W(4f) chemical shifts during Fe/W interface growth indicates that the adlayer grows in two-dimensional islands and no alloying occurs. Valence band spectra show the expected superposition of the Fe 3d features upon the attenuated W(110) substrate features.

Further studies focused upon the oxidation of 1 ML, 2 ML and thick film Fe/W(110) interfaces. Because the pseudomorphic (1x1) Fe/W(110) surface has both Fe and W atoms exposed, oxygen chemisorption results in charge transfer from both metals. An electronic effect in the underlying tungsten is still observed for bilayer and thicker films where direct O-W bonding is prevented. Annealing of oxygen dosed overlayers results in increased oxidation of the tungsten, suggestive of oxygen diffusion to the Fe/W interface. Quantitative analyses of these data will yield a layer-by-layer compositional analysis of the interface.

Finally, photoemission of iron deposited on a partially-oxidized W(110) surface confirms that Fe does wet the WO_x surfaces (where 1 < x < 3) as suggested by previous Auger electron spectroscopic and temperature programmed desorption data [2]. Complex chemical interactions between the Fe and WO_x surfaces were found which were dependent upon the initial distribution of tungsten oxides. In general, the adsorption of iron affects the intermediate oxides; the Fe/WO_x interface appears to have only metallic and highly oxidized W atoms. In effect, the bonding of the iron atoms donates charge to those tungsten atoms that were initially in intermediate oxidation states. These electronic effects are found to be completely reversible. Thermal desorption of the iron (1400K) regenerates the original distribution of WO_x states, demonstrating that compositional changes or interdiffusion of the Fe into the substrate is not occurring.

1. Present address: EXXON Research and Engineering Co., Linden, NJ.
2. P. J. Berlowitz, C. H. F. Peden and D. W. Goodman, to be published.

* Work supported by the United States Department of Energy under contract DE-AC04-76DP00789 with Sandia National Laboratories.

STRUCTURE AND REACTIVITY OF STRAINED METAL OVERLAYERS ON W(110)*

N. D. Shinn, C. H. F. Peden, K. L. Tsang[1] and P. J. Berlowitz[2]
Sandia National Laboratories, Albuquerque, NM 87185

The epitaxy of transition metal surfaces on single crystal substrates is a novel method of preparing stable, well-characterized surfaces with chemical properties unlike those of either constituent alone. These hybrid surfaces and intermetallic interfaces can be tailored for specific materials and chemical applications including passivation, coatings and catalysis. Previous work at Sandia on iron and chromium epitaxy on W(110) using Auger electron spectroscopy (AES), low energy electron diffraction (LEED), temperature programmed desorption (TPD) and work function measurements has shown that a (1x1) pseudomorphic monolayer (1 ML) is stable at temperatures up to desorption at temperatures exceeding the bulk sublimation temperatures of the respective overlayer metals. In addition, for chromium a metastable bilayer of (2x2) symmetry is stable in the range $500K < T < 800K$. High resolution core-level photoemission has been used to measure the chemical shifts during the evolution of these well characterized metal:metal interfaces during the layer-by-layer growth. This information will be compared to theoretical calculations of the electronic structure and charge transfer involved in bonding for these overlayer systems.

In addition, the novel reactivity of these extremely stable hybrid (1x1) surfaces is being explored in detail. Chemisorption of simple molecules such as CO, O_2, and N_2 demonstrates that while the pseudomorphic overlayers have essentially the same morphology as the respective Fe(110) and Cr(110) surfaces, the hybrid surface electronic structure is manifested in markedly different adsorption states and dissociation energetics. Oxidation and nitridation studies of the pseudomorphic monolayers show enhanced reactivity as compared to the single crystal Fe(110) and Cr(110) surfaces. Because the pseudomorphic (1x1) Fe/W(110) and Cr/W(110) surfaces have both overlayer and tungsten atoms exposed, oxygen chemisorption results in charge transfer from both metals. An electronic effect in the underlying tungsten is still observed for bilayer and thicker films where direct oxygen-tungsten bonding is prevented. Annealing of oxygen dosed overlayers results in increased oxidation of the tungsten, suggestive of oxygen diffusion to the buried metal interface. Quantitative analyses of these data will yield a layer-by-layer compositional analysis of the interface.

1. Joint Cornell/Sandia Senior Research Associate.
2. Present address: EXXON Research and Engineering Co., Linden, NJ.

* Work supported by the United States Department of Energy under contract DE-AC04-76DP00789 with Sandia National Laboratories.

ELECTRONIC EFFECTS OF ALKALI ADSORPTION ON Cu(311)*

N. D. Shinn, Sandia National Lab., Division 1134, Albuquerque, NM 87185

and

S. H. Southworth[1], Los Alamos National Lab., Los Alamos, NM 87545

Both experimental and theoretical work have shown that the adsorption of alkali metals onto transition metal single crystal surfaces can alter both the morphology and chemical reactivity of the surface. Examples include long range reconstructions of the atomically-corrugated fcc(110) planes and the stabilization of reaction intermediates by coordination with nearby alkali adatoms. The present valence band photoemission measurements complement previous low energy electron diffraction (LEED), temperature-programmed desorption (TPD) and Auger electron spectroscopic (AES) studies [2] examining (1) the alkali-induced reconstructions of Cu(311) and the (2) structure of small molecules co-adsorbed with sodium and potassium on Cu(311).

Like the fcc(110) planes, the Cu(311) surface is atomically corrugated with alternating rows of raised and lowered atoms. It differs from the fcc(110) morphology in that microfacets of both (111) and (100) orientation are exposed. At very low coverages of potassium, sodium, or mixed alkalis, a reversible, coverage-dependent sequence of (1x1) → (1x3) → (1x2) → (1x1) diffraction patterns is observed [2], where the increased surface unit cell dimension is perpendicular to the row direction. Photoelectron spectra of the Cu(311) valence bands, K(3p) and Cu(3p) core-levels exhibited only subtle changes in the surface electronic structure for the low alkali coverages corresponding to the surface reconstructions. Potassium multilayers were easily distinguished by chemical shifts in the K(3p) binding energy. Co-adsorption of oxygen and carbon monoxide with sub-monolayer potassium coverages gives rise to new adsorption states characterized by simultaneous desorption in TPD experiments. This behavior is suggestive of the formation of surface complexes which are stabilized on the Cu(311) surface. Corroborating evidence is found from both K/O_2 and K/CO coverage and annealing photoemission studies. Subsequent experiments will address the local bonding geometries and electronic structure of these surface complexes in detail.

1. Present address: National Bureau of Standards, Room 221/A221, Gaithersburg, MD 20899
2. N. D. Shinn and P. D. Szuromi, J. Vac. Sci. Technol. A5, 796 (1987).
3. N. D. Shinn, P. D. Szuromi and S. H. Southworth, to be published.

* Work supported by the United States Department of Energy under contract DE-AC04-76DP00789 with Sandia National Laboratories.

SYNCHROTRON RADIATION STUDIES OF TEFLON PHOTOLITHOGRAPHY*

N. D. Shinn and R. R. Rye,
Sandia National Laboratories, Division 1134, Albuquerque, NM 87185

Preliminary experiments investigating the photon energy dependence of radiation-induced cross-linking in poly(tetrafluoroethylene) (Teflon) have been performed using the U-3 LANL/SNLA ERG beamline. These measurements investigated the initial electronic excitation that leads to cross-linking by incident energetic radiation. Polished Teflon samples, mounted in an ultra-high vacuum chamber, were exposed to constant doses of soft X-ray radiation over the energy range 25 eV < $h\nu$ < 1000 eV. Based upon prior laboratory experiments [1] utilizing a Mg($K\alpha$) X-ray source, this dose was determined to be approximately 4800 Mrads, corresponding to exposure times of 300 sec (at 1000 eV) to 10 sec (at 25 eV). The standard dose selected was just above the threshold necessary to obtain a visual photolithographic effect in chemical etching. Exposed regions of the Teflon sample remained white after chemical etching whereas unexposed regions were discolored indicating severe chemical and physical modification of the polymer surface. If the mechanism for cross-linking involves an initial core-hole excitation in either carbon or fluorine, strong threshold effects should be visible as the photon energy is reduced below the corresponding ionization potentials [e.g., C(1s) = 284 eV, F(1s) = 697 eV]. No such threshold behavior was observed, indicating that the predomiant mechanism operative in this photolithographic effect involves low-energy valence exciations via secondary electrons. This result implies that the energy of the incident radiation serves only to determine the energy deposition depth. Thus the depth of cross-linking (and subsequent adhesion resistence) could be controlled without fundamentally altering the cross-linking process.

In addition, these studies have demonstrated that Teflon photolithography can be used as a useful soft X-ray beamline diagnostic tool. Since the apparent etching resistence is independent of photon energy and roughly proportional to total incident dose, the cross-linked region serves as a two-dimensional intensity map of the photon beam profile. Such quantitative information is important for improving the focussing characteristics of the beamline optics.

1. R. R. Rye and R. J. Martinez, J. Appl. Polymer Sci. (submitted).

---

* Work supported by the United States Department of Energy under contract DE-AC04-76DP00789 with Sandia National Laboratories.

OXIDATION OF Cr OVERLAYERS ON W(110)*

N. D. Shinn and K. L. Tsang[1]
Sandia National Laboratories, Division 1134, Albuquerque, NM 87185

The epitaxy of transition metal surfaces on single crystal substrates is a novel method of preparing stable, well-characterized surfaces with chemical properties unlike those of either constituent alone. These hybrid surfaces and intermetallic interfaces can be tailored for specific materials applications including passivation and coatings. Previous work [2] on Cr/W(110) epitaxy using Auger electron spectroscopy (AES), low energy electron diffraction (LEED), temperature programmed desorption (TPD) and work function measurements has shown that a (1x1) pseudomorphic Cr monolayer (1 ML) is stable at temperatures up to desorption at 1300K, and a metastable bilayer of (2x2) symmetry is stable in the range 500K < T < 800K. Oxidation of the Cr overlayers has been studied using TPD [3] by monitoring Cr(g) desorption during the decomposition of surface and interface oxides of chromium; the oxygen remains on the W(110) substrate after all Cr has desorbed (T > 1600K), as expected from thermodynamic considerations. Two high temperature Cr desorption states for monolayer oxidation were identified as representative of an "interfacial" oxide (T ≈ 1370K) and bulk Cr_2O_3-like oxide (T > 1450K). Oxidation of the bilayer introduces lower temperature Cr desorption states that are believed to be due to surface disproportionation reactions. During the TPD experiment, the non-stoichiometric surface region forms stable oxides as the temperature increases. Excess Cr then desorbs at characteristic temperatures (1100K < T < 1259K) well below those for interfacial-oxide and Cr_2O_3 decomposition.

We have investigated these reactions using interface-sensitive photoemission to monitor the W(4f) and Cr(3p) chemical shifts of the interface tungsten atoms and Cr overlayer, respectively, following oxidation and subsequent annealing. Substantial charge transfer from both the Cr and the upper layers of tungsten is observed upon oxygen adsorption on 1 ML Cr; note that the pseudomorphic Cr ML does not "cover" the W(110) surface atoms whereas the bilayer does prevent direct oxygen-tungsten coordination. This result supports the identification of an "interface" oxide phase involving Cr:O:W bonding. Annealing studies provide evidence for clustering of excess Cr atoms on the oxidized 1 ML Cr and diffusion of oxygen through thick Cr overlayers to the Cr:W interface. Future work will examine these solid-state interfacial reactions in detail.

1. Joint Cornell/Sandia Senior Research Associate.
2. N. D. Shinn and P. J. Berlowitz, J. Vac. Sci. Technol., in press; P. J. Berlowitz and N. D. Shinn, Surf. Sci. (submitted).
3. N. D. Shinn and P. J. Berlowitz, (to be published).

* Work supported by the United States Department of Energy under contract DE-AC04-76DP00789 with Sandia National Laboratories.

INTERFACE FORMATION ON CO/SI (111) USING ANGLE RESOLVED PHOTOEMISSION FOR BAND MAPPING

D. Chambliss and T. Rhodin, School of Applied Physics, Cornell University, Ithaca, NY 14847 and
J. Rowe, AT&T Bell Laboratories, Murray Hill, NJ 07974 and
H. Schigekawa, Physics Dept., University of Florida, Gainsville, FL 32611.

The electronic and atomic structure of epitaxial layers of $CoSi_2$ on Si(111) substrates is of intense scientific and technical importance. Initiatcn of the optimized interface has been studied by doing precise band mapping of the surface layers formed by deposition and annealing of ultrathin deposits of cobalt on carefully prepared and characterized Si(111) substrates.[1]

Precise angle resolved photoemission measurements were systematically made on carefully monitored submonolayer deposits of cobalt produced and characterized in situ in order to achieve precise control of the surface structure. The objective being to model the atomic structure of the interface characteristic of that with the optimized electron properties.

The $CoSi_2$-Si sample showed electronic states in close agreement with the energy bands for bulk CoSi computed by Mattheiss and Hamann[2]. The $CoSi_2$-Co samples have similar bulk states, but their outermost layers showed a shift by about 0.5 eV toward that of the Co(3rd) states, which is taken to indicate that the outermost Co-atoms are less strongly bonded to the underlying silicon. Finally, a state at -3.0 eV was identified and attributed tentatively to an interface state of the Si(111)/$CoSi_2$ interface formed by annealing at 450 C.

These studies are continuing in order to more precisely determine the electronic character of the interface and the conditions for its preparation.

This work is supported by both the AT&T Bell Laboratories and the Materials Science Center at Cornell University.

References

1. D. Chambliss, T. Rhodin, J. Rowe and H. Shigewawa, J. Vac. Soc & Tech., Proc. 34th Annual Conference, Atlanta, GA (1988).
2. L. F. Mattheiss and D. R. Hamann, Phys. Rev. B37 (1988) 1623.

FERMI SURFACE AND RECONSTRUCTION OF W(011)

R.H. Gaylord, K. Jeong, and S.D. Kevan, University of Oregon

Using high resolution angle-resolved photoemission, we have investigated the interplay between the Fermi surfaces for surface-localized electronic levels on W(011) and the observed hydrogen-induced reconstruction of the surface. Our results for the clean and hydrogen-covered surfaces are presented in Fig. 1.

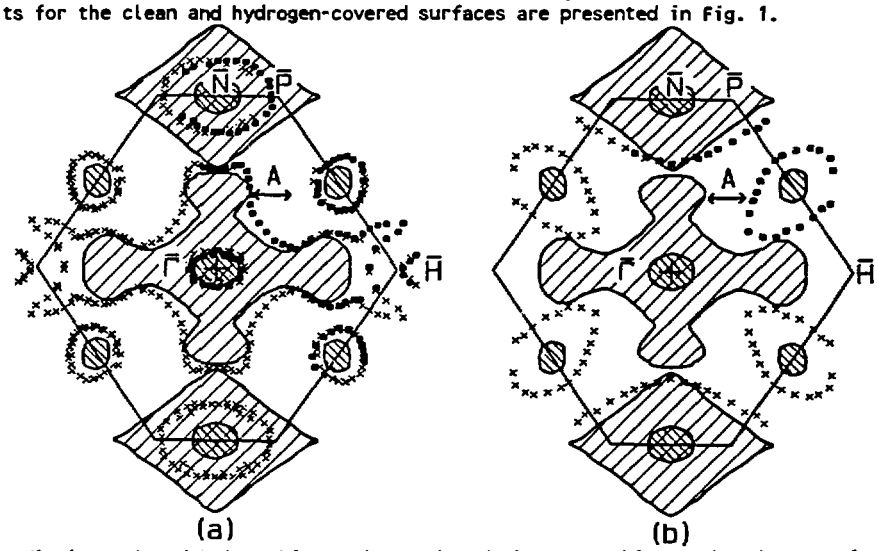

Fig. 1: Fermi surface orbits for clean (a) and hydrogen-covered W(011). The solid dots are real data while the crosses have been produced by mirror plane symmetry. The shaded regions are the projected bulk Fermi surface.

We observe a total of three distinct closed hole orbits and one closed electron orbit on the clean surface (Fig. 1a). The hole orbits are elliptical and are centered on different projections of the same bulk Fermi surface ellipsoid. They are located at the center and along each of the edges of the surface Brillouin zone. The surface electron pocket is closed but has a very complex shape. It orbits the projection of the bulk electron jack, and is centered in the surface Brillouin zone. These orbits are affected to different extents by hydrogen adsorption. The hole pockets are rapidly quenched by hydrogen, while the electron pocket grows in area until it merges with its image in the second Brillouin zone. At saturation (Fig. 1b), there exist two hole pockets which are the remnants of the clean-surface electron pocket. The change of the Fermi wavevector at arbitrary point in the zone is observed to be monotonically related to work function change and to coverage. The coverage dependence is shown in Fig. 2.

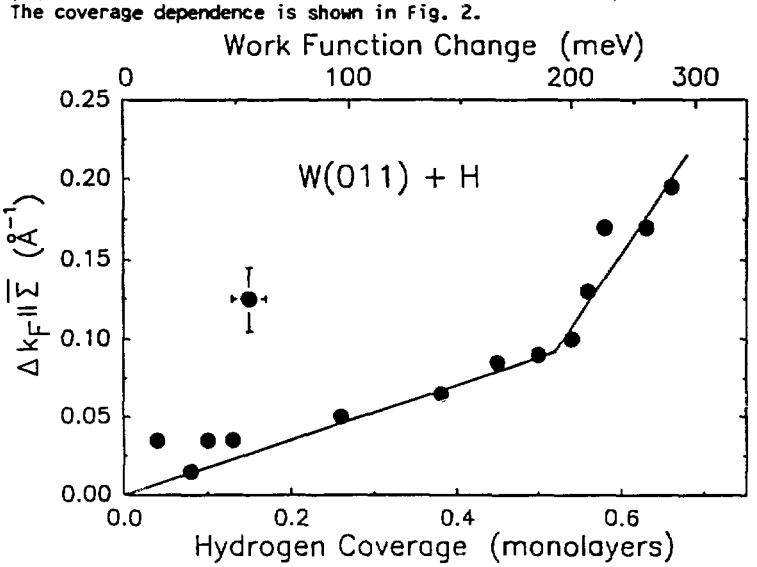

Fig. 2: Fractional change in the Fermi wave vector and the work function as a function of hydrogen dose.

The abrupt change in slope observed in Fig. 2 occurs very close to where the surface is observed to undergo a (1x1) reconstruction. The Fermi surface electrons are clearly responding to the change in lattice structure; whether or not they contribute to driving the reconstruction will need to await further theoretical work.

FERMI SURFACE AND ELEMENTARY EXCITATIONS OF Mo(011) U4A

K. Jeong, R.H. Gaylord, and S.D. Kevan, University of Oregon

The Fermi surface in metallic, crystalline systems is of fundamental importance since it determines many macroscopic and microscopic properties. Starting from Fermi surface contours, observables such as heat capacities, transport behavior, and intraband optical properties can be predicted. In addition, issues relating to phase stability and phonon behavior can be partially understood. Rarely have such correspondences been derived for surfaces, in part due to a lack of experimental Fermi surface contours.

We have used high resolution angle-resolved photoemission (ARP) to determine the complete Fermi surfaces for the surface-localized electronic levels on the clean and hydrogen-covered Mo(011) surface (Fig. 1).

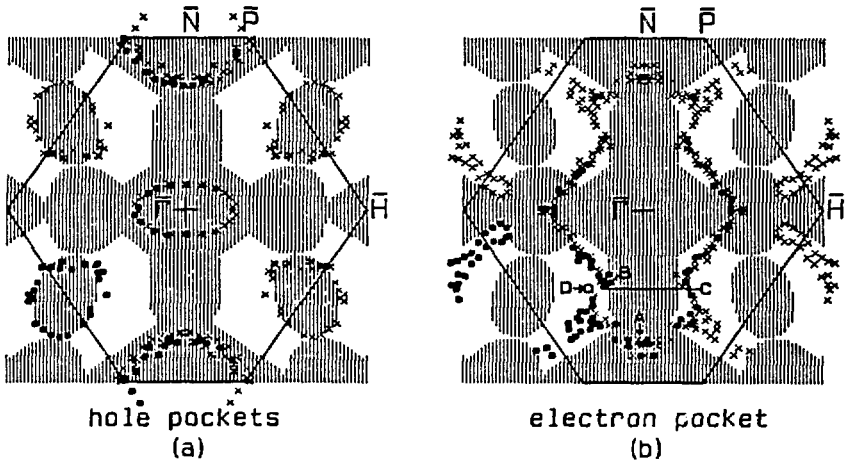

Fig. 1: Fermi surface orbits on the clean Mo(011) surface. Shaded regions the prejection of the bulk Fermi surface onto the surface plane.

We observe a total of three distinct closed hole orbits and one closed electron orbit. The hole orbits are elliptical and are centered on different projections of the same bulk Fermi surface ellipsoid. They are located at the center and along each of the edges of the surface Brillouin zone, and are rapidly quenched by hydrogen adsorption. The surface electron pocket is closed but has a very complex shape which is somewhat different than was observed on W(011).[1] It orbits the projection of the bulk electron jack, and is centered in the surface Brillouin zone. As was observed on W(011), the size and shape of the electron pocket is a sensitive function of hydrogen coverage. At saturation, there exist two hole pockets which are the remnants of the clean-surface electron pocket.

Hydrogen adsorption on the bcc (011) surfaces poses several interesting static and dynamical problems. When coupled to computations, our measurements would probably yield the static hydrogen adsorption site, commonly accepted to be at or near the long bridge site. The observed changes in Fermi surface require large changes in occupation of certain surface bands and thus suggest changes in the surface dipole layer. We observe that the Fermi wave vector varies approximately linearly with the change in work function. A twofold-symmetric or mirror-symmetric adsorption site implies different restoring forces for hydrogen motion in the two orthogonal symmetry azimuths. In this case, the adsorption well is presumed to be very flat along the [011] azimuthal direction so that large-amplitude motion along this direction would be expected. Non-adiabatic coupling of the electron-hole pair continuum to such phenomena as diffusion and surface vibrations might therefore be particularly interesting. A prediction concerning coupling at zero momentum, i.e., for a uniform displacement of the hydrogen layer normal to the surface, arises naturally from our observation relating the work function change to the size of the electron orbit. Our data can be analyzed to predict non-zero momenta where electronic coupling to elementary excitations (Kohn anomalies) might be particularly strong. This should motivate high resolution studies of surface phonons to search for anomalies in surface phonon dispersion relations.

1. R.H. Gaylord, K. Jeong, and S.D. Kevan, submitted to Phys. Rev. Lett.

RELATIVISTIC EFFECTS ON THE SURFACE ELECTRONIC STRUCTURE OF Mo(011) U4A

K. Jeong, R.H. Gaylord, and S.D. Kevan, Univ. of Oregon

High resolution angle-resolved photoemission (ARP) studies of the Mo(011) surface have allowed us to isolate and to study the effects of the spin-orbit interaction on the surface electronic structure of Mo(011). A summary of our experimental surface band dispersion relations in the mirror symmetry planes is shown in Fig. 1.

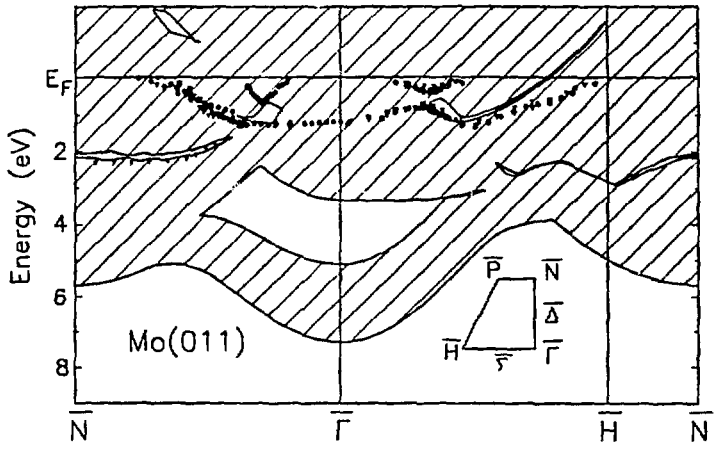

Fig. 1: Experimental surface bands for Mo(011) plotted on the projected bulk molybdenum band structure. Photon energies: ●, $h\nu$ = 24 eV; △, $h\nu$ = 40eV; ▽, $h\nu$ = 50 eV; □, $h\nu$= 60 eV.

Fig. 1 exhibits three distinct phenomena related to the breaking of symmetry by the spin-orbit interaction. The first is a zone-center surface resonance which exists in a pseudogap between the bulk Γ_{8+} and the Γ_{7+} points, and is similar to one observed previously on W(011).[1] We also observe a surface state in a projected band gap opened by spin-orbit induced hybridization between nominally odd and even bulk bands at N. Finally, we have observed avoided crossings of surface bands along both symmetry azimuths. The two observed bands along $\bar{\Delta}$ and $\bar{\Sigma}$ bands would be of opposite mirror plane symmetry in the absence of the spin-orbit interaction, but hybridize under its influence. The result is the opening of a gap in both case of magniduge 0.3-0.4 eV. Spectra taken in the vicinity of these gaps are among the most spectacular observed in ARP due to their extreme sensitivity to initial momentum, as shown in Fig. 2. We have observed and characterized the transfer of both the polarization behavior and contamination sensitivity from one band to another in these regions. We speculate upon the relevance of these results to other surface properties including reconstruction and work function change.

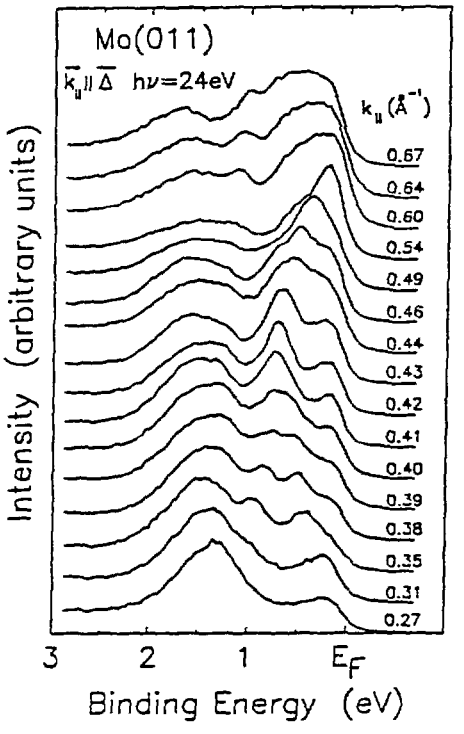

Fig. 2: ARP spectra of Mo(011) collected along △ near the avoided crossing.

1. R.H. Gaylord and S.D. Kevan, Phys. Rev. B36, 9337 (1987).

PHOTOEMISSION STUDY OF THE $CoSi_2$(111)-Si SURFACE

J. E. Rowe, G.K. Wertheim, R. T. Tung, and D. N. E. Buchanan *(AT&T Bell Laboratories)*

Epitaxial $CoSi_2$ terminated with a thin Si bilayer [1,2] has been studied by synchrotron radiation photoemission. This well-defined surface phase of $CoSi_2$ is obtained by high temperature annealing in the range 450-650°C. The samples used were prepared by MBE techniques with a film thickness of ~800Å on Si(111) substrates and capped with a ~100Å film of a-Si to act as an oxide barrier while samples were transferred to the photoemission chamber. The surfaces studied by photoemission were prepared by careful sputtering to remove the oxide and a-Si layer and then anealed to ~450–650°C for one minute. Photoemission spectra were taken with total resolution in the range 200-237 meV and show evidence for four spin-orbit doublets. Our samples and results are somewhat different from those of previous studies [3-5] of thin $CoSi_2$ films or studies of bulk $CoSi_2$ samples. We find three surface Si(2p) components: one shifted to higher binding energy and two shifted below the main Si(2p) spin-orbit doublet in $CoSi_2$. We find the $Si(2p_{3/2})$ energy in $CoSi_2$ is 99.40 eV measured with respect to the Fermi level; the three surface-shifted Si components are at -0.75, 0.17 and -0.18 eV relative to the main component in order of decreasing intensity and thus layer distance from the surface. A structural model [1,2] previously proposed for thin $CoSi_2$ layers is shown to be qualitatively consistent with these results.

[1] S. A. Chambers, S. B. Anderson, H. W. Chen and J. H. Weaver, Phys. Rev. B **34**, 913 (1986).

[2] F. Hellman and R. T. Tung, Phys. Rev. B **37**, 10786 (1988); R. T. Tung and J. L. Batstone, Appl. Phys. Lett. **52**, 648 (1988).

[3] C. Pirri, G. Gewinner, J. C. Peruchetti, D. Bolmont and J. Derrien, Phys. Rev. B **38**, 1512 (1988).

[4] G. Gewinner, C. Pirri, J. C. Peruchetti, D. Bolmont, J. Derrien and P. Thiry, Phys. Rev. B **38**, 1879 (1988).

[5] R. Leckey, J. D. Riley, R. L. Johnson, L. Ley and B. Ditchek, J. Vac. Sci. Technol. A **6**, 63 (1988).

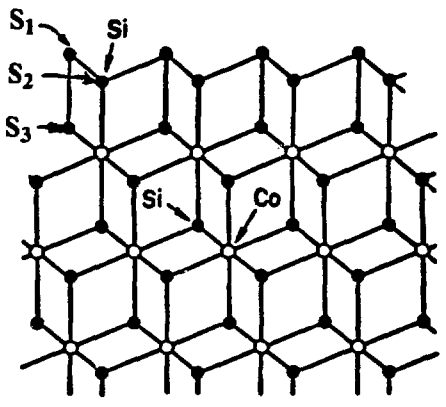

$CoSi_2$(111)-Si Surface

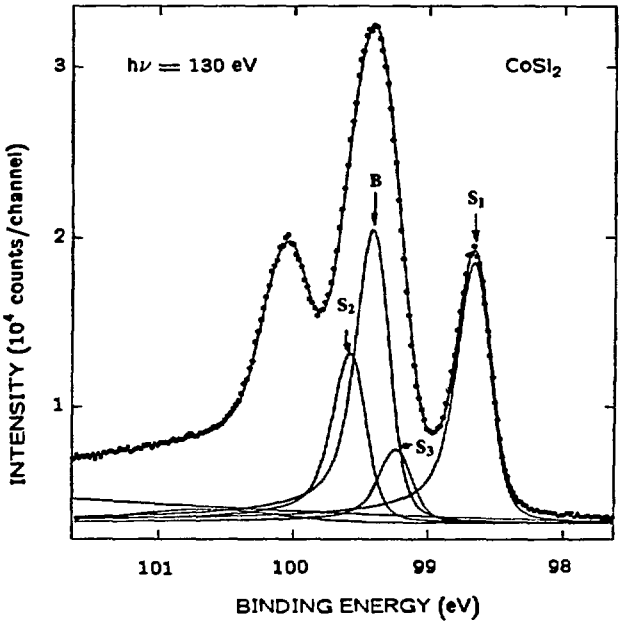

CHARGE TRANSFER IN $HfPt_3$

U4A

G.K. Wertheim and D. N. E. Buchanan *(AT&T Bell Laboratories)*
J. H. Wernick *(Bell Communications Research)*

For intermetallic compounds there are conflicting theoretical points of view regarding the cohesive interaction. In the semi-empirical scheme of Miedema and coworkers [1] the enthalpy of formation arises in part from the flow of charge due to the difference in work function, and in part from the need to equalize the charge density at the surface of the Wigner-Seitz cell. In the Engel-Brewer [2] approach charge flows to maximize the occupancy of bonding orbitals. Both have been successful in predicting heats of formation, even in cases where the sign of the charge transfer turns out to be in opposite directions for the same material [3,4]. A typical example is the compound $HfPt_3$ in which the Miedema scheme results in a charge transfer from Hf to Pt, while the Engle-Brewer correlation requires transfer in the opposite direction.

The compound $HfPt_3$ was prepared by arc melting, and annealed for several days in an evacuated quartz capsule. The structure was verified by powder x-ray diffraction. The compound has the $TiNi_3$ ($P6_3/mmc$) structure, with lattice constants a = 5.636 Å and c = 9.208 Å. The c/a ratio is 1.634, i.e., very close to the value of 1.633 obtained with atoms of equal size, even though the Goldschmitt radius of the Hf is significantly larger than that of Pt. This may be taken as a preliminary indication of charge transfer from Hf to Pt, i.e., in the direction to equalize the atomic radii. In this close-packed hexagonal structure with ABAC stacking sequence the Hf atoms have 12 Pt neighbors, and the Pt atoms have 4 Hf and 8 Pt neighbors. Photoemission spectra were obtained from sputtered and annealed polycrystalline surfaces. Typical Hf 4f spectra are shown below.

One of the salient observations is that the density of states at E_F is very much smaller than that of fcc Pt. This accounts for the reduced asymmetry of the Pt 4f photoemission lines in the compound. The core-electron binding-energy shifts are positive for both constituents, 0.88 eV for Hf and 0.54 eV for Pt. The Born-Haber cycle formalism is used to relate these shifts to the enthalpy of formation and to other thermodynamic quantities. The Hf 4f spectrum exhibits a strong, well-resolved surface-atom signal with a shift of 0.79 eV. In contrast, the intensity of the Pt 4f surface signal is relatively weak, indicating that the surface contains mainly Hf atoms. This is in accord with the surface free energies.

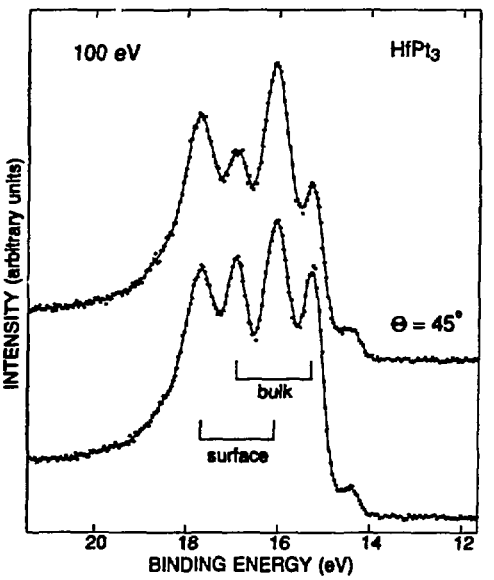

When corrected by the contact potentials between the elements and the compound the sign of the shifts indicates that electronic charge flows from Hf to Pt when the $HfPt_3$ is formed. This is in accord with the c/a ratio, with the electronegativity difference between the two elements, as well as with the results of Miedema's semiempirical description of bonding. It cannot be reconciled with the Engel-Brewer correlation.

[1] A. R. Miedema, P. F. de Chatel, and F. R. de Boer, Physica **100B**, 1 (1980).

[2] L. Brewer in *Electronic Structure and Alloy Chemistry of the Transition Elements*, P. A. Beck Ed., p. 221, Interscience, New York, 1963; and Acta Met. **15**, 553 (1967).

[3] Miedema, R. Boom, and F. R. de Boer, J. Less-Common Metals **41**, 283 (1975).

[4] V. Srikrishnan and P. J. Ficalora, Met. Trans. **5**, 1471 (1974).

CRYSTAL-FIELD SPLITTING OF CORE-ELECTRON SPECTRA: Sn 4d

G.K. Wertheim and D. N. E. Buchanan *(AT&T Bell Laboratories)*

We have studied the 4d core electron spectra of elemental Sn in order to assess the magnitudes of the surface-atom core-level shift, the phonon broadening and the crystal field splitting. Crystal-field effects have been previously studied in *compounds* of a number of metals [1], but the smaller splitting in *metals* has not been reported. Data were taken on U4A with a bulk, polycrystalline slab cleaned by argon ion sputtering. A least-squares fit with Doniach-Šunjic´ lines to data taken with 55 eV photons is superficially satisfactory, see the figure on the left. However, the residuals of this fit exhibit pronounced structure in the region of the j=5/2 line, which points to an inadequacy of the model function. The lifetime width of the j=3/2 line is 3 percent *smaller* that that of the 5/2 line. This is unphysical, since the 3/2 line has an additional Coster-Kronig decay channel, and should, if anything, be broader. The gaussian line width is well in excess of the combined effects of the instrumental resolution and theoretical phonon width. Measurements over a range of temperature established that the broadening is *not* due to phonons. Measurements at photon energies near threshold (and at various take-off angles) proved that it is *not* due to an unresolved surface-atom core-level shift.

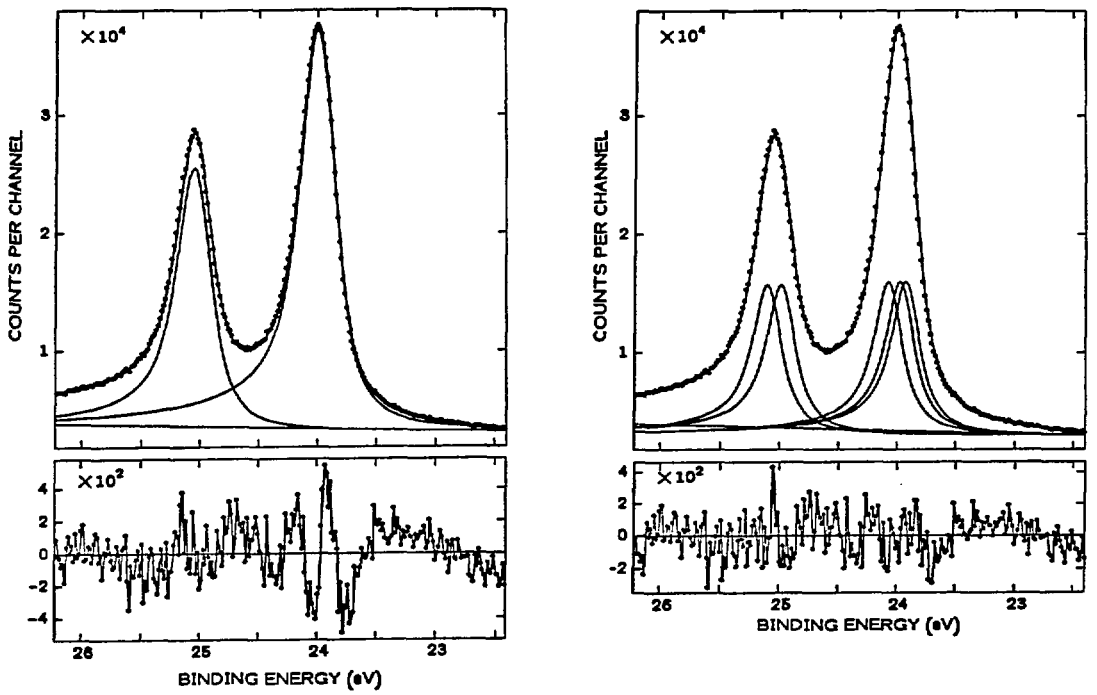

Since the atoms in β-tin are in equivalent sites with four-fold inversion symmetry, one must consider the effect of the crystal field. An axial crystal field splits the spectrum into five components, but adds only one parameter to the model function. Since the crystal-field splitting is small compared to the spin-orbit interaction, we assign equal weights to the components of the each line, and use the eigenvalues from Ref. 1 to fit our data. The improvement in the fit is seen most clearly in the residuals of the figure on the right. The crystal field splitting is very much smaller than in chemical compounds [1]. The phonon width now is very close to the theoretical value.

We have shown that the crystal field splitting must be considered in core-electron spectroscopy which make full use of the instrumental resolution now available. This is particularly relevant to the interpretation of spectra of surface atoms, which are in a site of lower symmetry.

[1] G. M. Bancroft, T. K. Sham, D. E. Eastman, and W. Gudat, J. Am. Chem. Soc. **99**, 1752 (1977).

ADSORPTION OF ANTIMONY ON Au(001)

G.K. Wertheim, J. E. Rowe, D. N. E. Buchanan, and H. L. Polite *(AT&T Bell Laboratories)*
H. Shigekawa[a] *(University of Florida)*

Antimony overlayers on a clean Au(001) surface were prepared by surface segregation on a sputtered and annealed, Sb-doped gold single crystal. This treatment results in a reproducible coverage near 1/3 ML, and a well defined LEED pattern. Comparison of valence band photoemission data from clean and Sb-covered surfaces, taken with photon energies between 35 and 150 eV, exhibit an Sb 5p contribution at the Fermi energy at the higher photon energies. [1] Sb 4d core level spectra have the asymmetric line shape associated with metallic screening with a many-body singularity index of 0.08. This value is significantly larger than that of bulk gold, and suggests screening by electrons in Sb-derived states at the Fermi level. Au 4f core-level photoemission data yield a major surface-atom component with a shift of +0.44 eV and a weaker one at +0.90 eV. The sign of these shifts is opposite to that of the clean Au surface, [2] and is suggestive of loss of charge from the Au surface layer. All aspects of these measurements indicate that the Sb is strongly chemisorbed and probably forms an ordered surface alloy. The reconstruction of the Sb-covered surface was investigated by LEED, and showed a compressed hexagonal layer [3] with 4×22 periodicity, which fits a modified (111) double layer of $AuSb_2$ with a small number of additional reconstructed Au atoms.

(a) On leave from Department of Applied Physics, University of Tokyo.

[1] G.K. Wertheim, J. E. Rowe, D. N. E. Buchanan, and H. L. Polite, Phys. Rev. B **38**, 9606 (1988).

[2] P. Heimann, J. F. van der Veen, and D. E. Eastman, Solid State Commun. **38**, 595 (1981).

[3] P. W. Palmberg and T. N. Rhodin, J. Chem. Phys. **9**, 147 (1968).

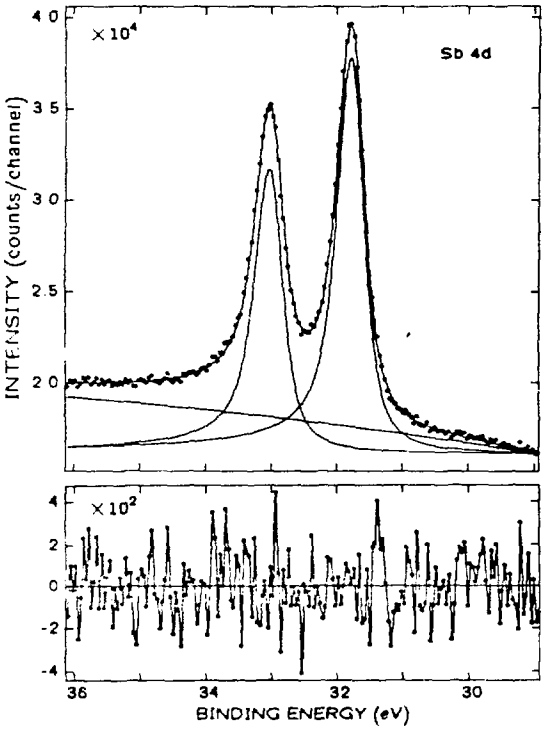

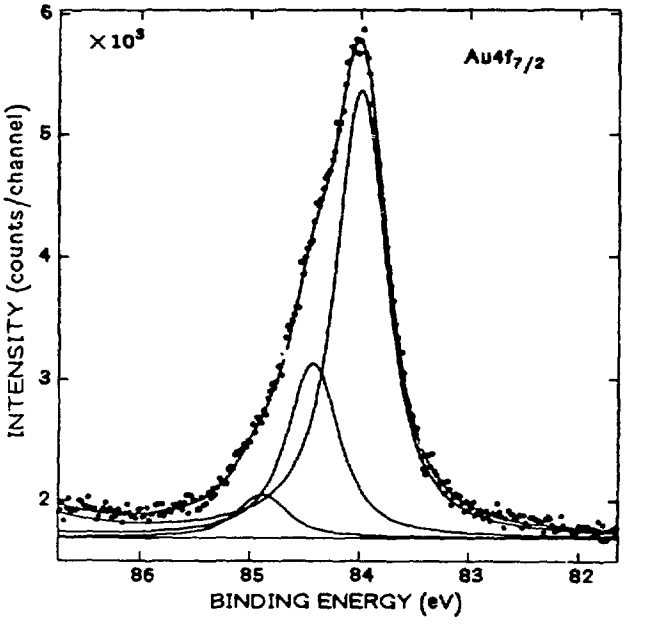

RESOLUTION OF THE 6 m TORIODAL GRATING MONOCHROMATOR ON U4A U4A

G.K. Wertheim, J. E. Rowe, and D. N. E. Buchanan *(AT&T Bell Laboratories)*

Although the U4A 6 m TGM [1] has been operational since 1983, only modest efforts have been made to determine the inherent resolution of the three gratings, G1, G2, and G3, that are installed. In an earlier study [1] the total widths of the Fermi cut-off in the conduction band of Cu(001) were reported to be 230, 140, and 90 meV, for G1, G2, and G3 respectively, but no attempt was made to separate the contributions of the TGM itself. Recent studies of the reconstruction of Si surfaces has resulted in partially resolved surface-atom core-electron binding-energy shifts that are not completely determined without reliable information about the instrumental width. Accurately known core-level line shapes are also required to estimate the disorder broadening associated with various adsorbate-covered surfaces. The resolution was determined from the photoemission response at the Fermi cut-off in the conduction band of various clean metals: Cu(100), Au(100), $Cu_3Au(100)$ and polycrystalline Sn using a VSW 100 mm electron spectrometer which had been previously calibrated. Since the thermal full-width at half maximum (FWHM) of the Fermi function at 300°K is 88 meV, instrumental widths that are significantly smaller cannot be accurately determined from room temperature data with normal statistical significance. By cooling the sample to the vicinity of liquid nitrogen temperature, T≈78°K, the thermal width is readily made small compared to other contributions.

For G1 the measured resolution generally follows the shape of the theoretical curve, but lies above it by a factor of about 1.7. The best resolution is obtained near 72 eV, where the theoretical curve has its minimum. At this photon energy the image of the entrance slit is in best focus on the exit slit. The entrance slit was here, of necessity, set to a value smaller than the 1.75 mm required for a resolution of 100 meV. The other minimum in the theoretical curve, at 170 eV, is not realized in the experiment, in part, because the requisite small slit opening could not be used. This may also, in part, be due to the combined defocus errors in the coupled optical pair: grating and ellipsoidal input mirror. [2] The practical resolution for G1 is estimated to be 80 meV near 75 eV, 200 meV in the vicinity of 120 eV, and significantly worse above 150 eV where slit widths less than 0.25 mm are required even for a theoretical resolution of 100 meV.

The data for G2 follow the shape of the theoretical curve more closely, giving a weak indication of improved resolution at photon energies approaching those where the focal condition is satisfied. The measured values range from 1.5 to 2.0 times greater that the theoretical values. Attempts to measure the Fermi-cut-off with photon energies below 30 eV or above 60 eV did not yield satisfactory data. The practical resolution lies between 70 and 90 meV for photon energies between 30 and 60 eV.

[1] P. Thiry, P. A. Bennett, S. D. Kevan, W. A. Royer, E. E. Chaban, J. E. Rowe, and N. V. Smith, Nucl. Instr. and Meth. 222, 85 (1984).

[2] D. E. Aspnes, Applied Optics, 71, 2642 (1982).

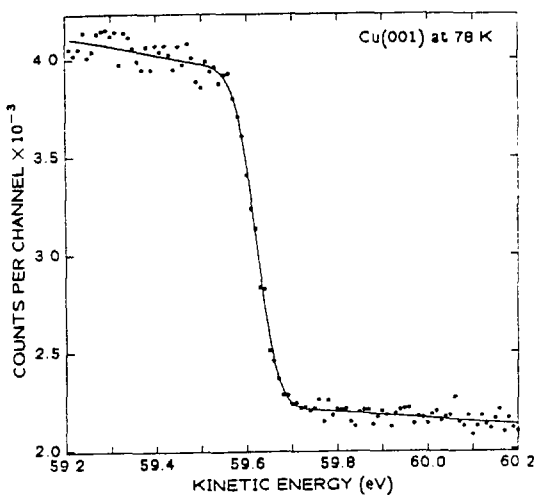

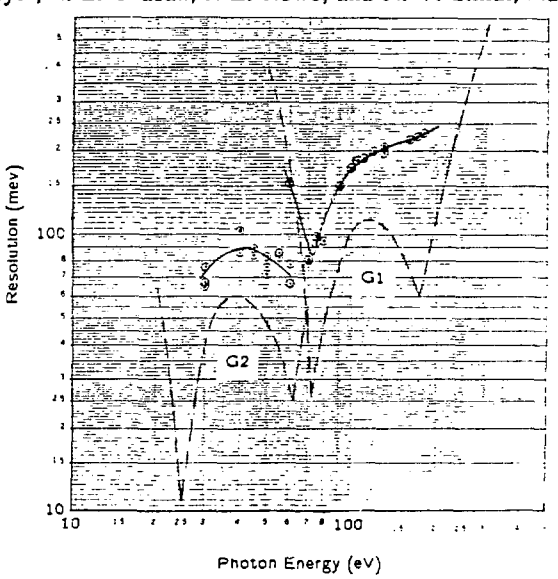

Multiplet Structure in the L-edges of 3d Metal Compounds

C. T. Chen, F. Sette and B. Sinkovic

AT&T Bell Laboratories
Murray Hill, New Jersey 07974

Studies on the $L_{2,3}$ white lines of $3d$ transition-metal compounds have been limited in the past by the poor spectral resolution of soft x-ray monochromators. Recently, utilizing the Dragon soft x-ray beamline, we measured the detailed structure and lineshape of these white lines. Representative $L_{2,3}$ edge photoabsorption spectra of $3d$ metal compounds are shown in the figure below. The structure observed in these spectra can be divided into two major groups. The peaks with lower excitation energies are due to transitions from the $2p_{3/2}$ core level to the unoccupied $3d$ levels (L_3 line), while those with higher excitation energies are from the $2p_{1/2}$ level (L_2 line). The energy seperation between these two groups, determined by the spin-orbit coupling of the $2p$ levels, is in the range of 5 to 20eV going from Sc to Cu. The complex structure observed in these spectra is caused by the interplay between the crystal field potential and the different spin-spin and spin-orbit couplings mechanisms of the $3d$ electrons in the final state. As an example, the doublet observed in the ScF_3 spectrum is due to the crystal field splitting of the Sc $3d$ orbitals, similarly to what was observed in the potassium $L_{2,3}$ spectrum of KCl. By increasing the number of $3d$ electrons in the final state from 1 to 10, i.e. going from ScF_3 to CuO, the multiplet structure gets first more complicated, reaching its climax near CrF_2, and then turns around being again very simple in CuO. A recent calculation done by the Prof. Sawatzky's group has successfully reproduced our MnF_2 data. In this work, it was demonstrated that the sensitive dependence of the calculated spectra on the Coulomb and exchange parameters and on the crystal field strength, can be used to determine the relative importance of the various coupling schemes from the direct comparison between theory and experimental results.

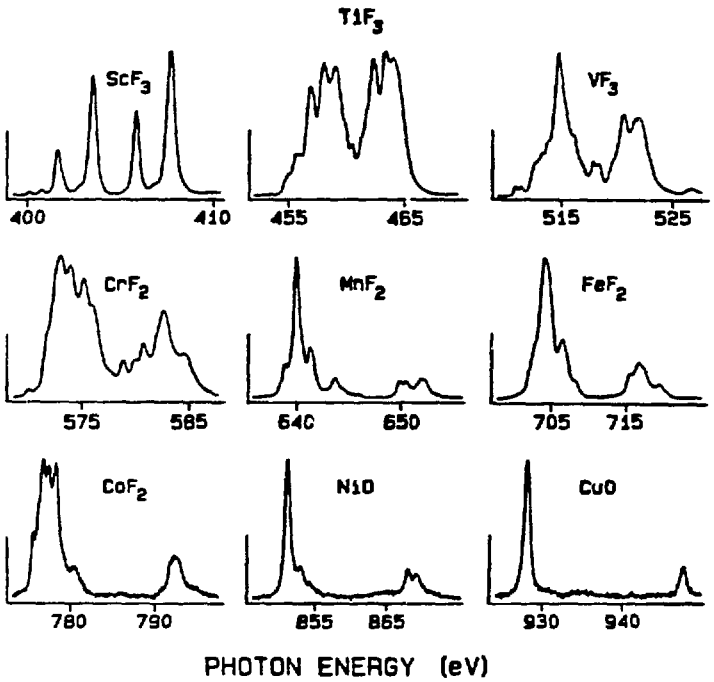

High Resolution Measurements of the C1s and N1s Photoabsorption in Condensed CO and N_2

C. T. Chen, B. Sinkovic and F. Sette

AT&T Bell Laboratories
Murray Hill, New Jersey 07974

We measured the $1s \rightarrow 2\pi^*$ absorption spectrum of condensed CO and N_2 molecules, using total electron yield detection. The spectra, shown in Fig. 1a,b, for carbon in CO and nitrogen in N_2, were taken utilizing the full 15 mR horizontal acceptance of our monochromator, and 0.5 mR in the vertical direction. Comparison of our data with previously measured electron-impact data, establishes that the Dragon monochromator can routinely operate with resolving power above 10^4 in the 250–700 eV photon energy region.

The data of Fig. 1 allow for the exact determination of the intrinsic lineshape of the $1s \rightarrow 2\pi^*$ excitation. The measured linewidths are 159 meV in N_2 and 144 meV for C 1s in CO. The intrinsic widths, obtained by removing the instrumental resolution, appear to be 10~20 meV larger than those for the isolated molecules. This indicates a final state broadening in the condensed phase, probably due to inter-molecular interactions.

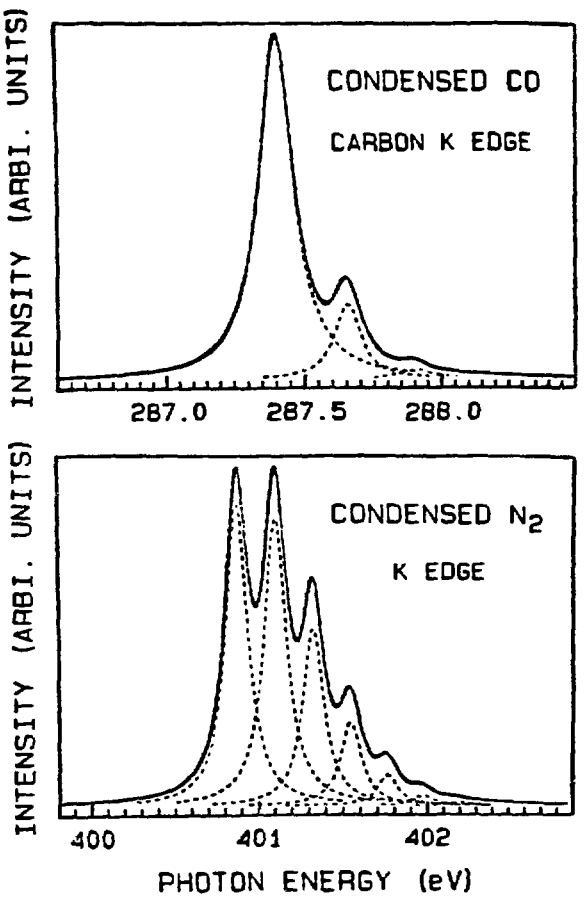

Fig. 1 Carbon K-edge photoabsorption spectrum of condensed CO. The data points are indistinguishable from the solid-line, representing a fit with three lorentzian linashapes having same width (dashed-lines).

Fig. 1b Nitrogen k-edge photoabsorption spectrum of condensed N_2. The data points, in this case, were fitted using seven lorentzian lineshapes.

Observation of Anisotropic Modification of the Excited state Potential in Benzene

Y. J. Ma, C. T. Chen, G. Meigs, S. Modesti[*], *and F. Sette*

AT&T Bell Laboratories
Murray Hill, New Jersey 07974

We measured the C $1s \rightarrow 2\pi^*$ photoabsorption spectrum of C_6H_6 and of C_6D_6 by total electron yield detection. Spectra are shown in Fig. 1. We observe a complex vibrational structure characterized by four most distinct features labelled A, B, C and D in Fig. 1. In C_6H_6, the energy positions relative to peak A for peaks B, C and D are 110 ± 10 meV, 181 ± 5 meV, 415 ± 10 meV respectively. The same excitations are observed in C_6D_6 at 70 ± 10 meV, 176 ± 5 meV and 298 ± 5 meV. Comparison with infrared data allows us to assign peak B to the C-H (C-D) out-of-plane bending, peak C to the C-C stretching and peak D to the C-H (C-D) stretching. This assignment is in agreement with the differences between the spectra of C_6H_6 and C_6D_6, where only the frequencies of the C-H and C-D modes are expected to change in the two molecules. While the energies of peaks B and C are almost identical to the correspondent infrared measurements, peak D has a significantly higher value. This observation indicates an anisotropic modification of the potential in the excited state, where the C-H bond strength is modified but that of the C-C is not. Our results show the unique opportunity one has with high-resolution to directly probe the molecular potential in presence of the core-hole.

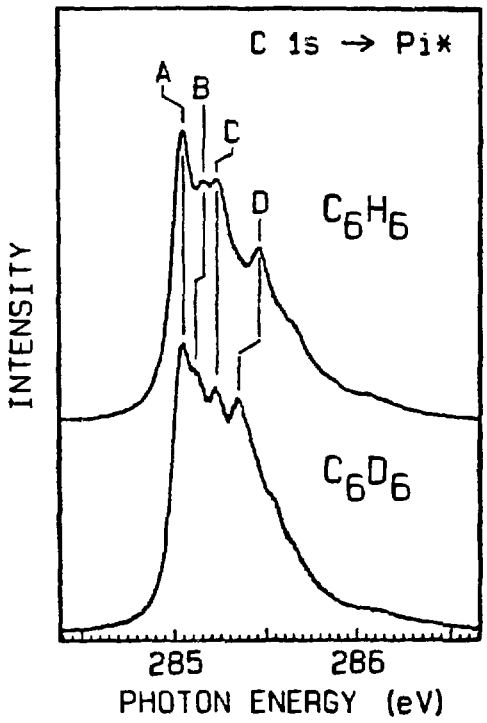

Fig. 1 Carbon K-edge photoabsorption spectra of C_6H_6 and of C_6D_6. Observe the shift of peaks B and D, while peaks A and C are the same for the hydrogenated and deuterated molecules.

[*] Visiting from the University of Trieste, Italy.

Measurement of the C 1s Photoemission Spectrum in Graphite

G. Meigs, Y. J. Ma, C. T. Chen, S. Modesti and F. Sette*

AT&T Bell Laboratories
Murray Hill, New Jersey 07974

We measured the C 1*s* XPS spectrum in graphite using an electron-kinetic-energy spherical-analyzer with multi-channel detection. The combined photon-beam and electron-analyzer resolution was better than 120 meV. The spectrum is shown in Fig. 1. This spectrum, at least three times narrower than any other C 1*s* XPS measurement in graphite, has a measured full-width-half-maximum of 284 meV. This lineshape is being analyzed in collaboration with G. K. Wertheim to assess the relevance of valence excitons associated with the screening of the photoexcited core-hole.

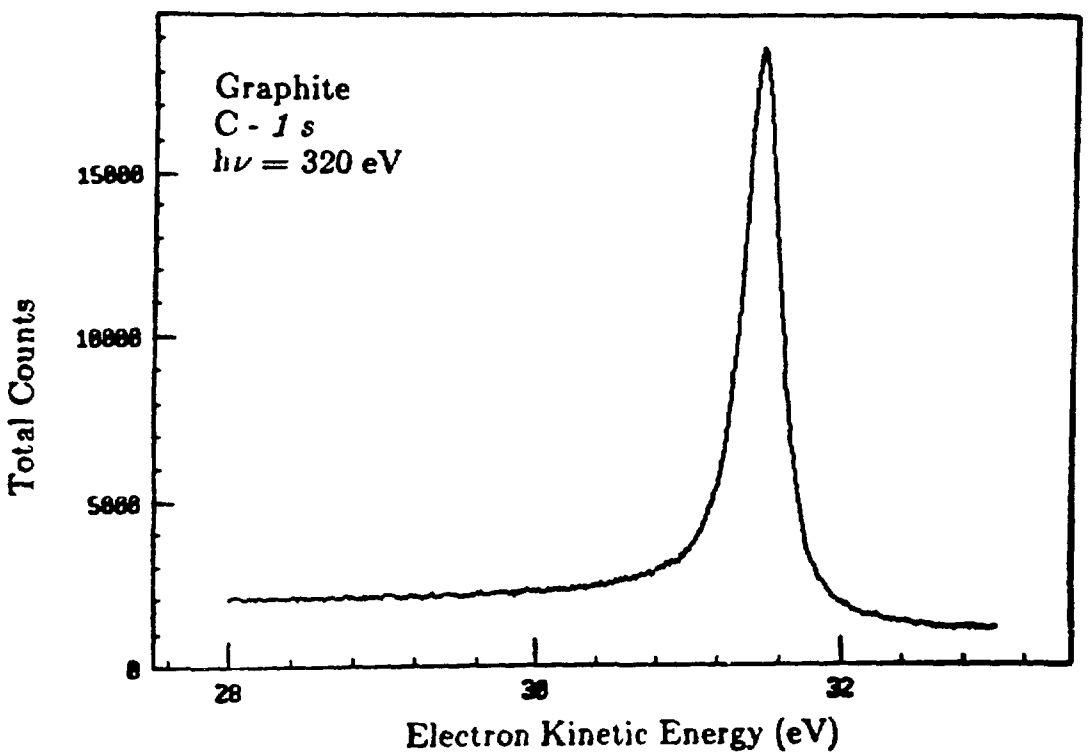

Fig. 1 Carbon 1s photoemission peak taken at 320 eV photon energy on UHV cleaved graphite.

* Visiting from the University of Trieste, Italy.

Crystal Field in Ionic Crystals Studied by High-Resolution Soft-X-Ray Spectroscopy

F. Sette, B. Sinkovic and C. T. Chen

AT&T Bell Laboratories
Murray Hill, New Jersey 07974

High resolution photo-absorption measurements at the potassium $L_{2,3}$ edges in KF, KCl, KBr, KI and $KMnF_3$ are used to study and identify crystal field splittings of empty potassium $3d$-orbitals. The data, collected by total electron yield detection are shown in Fig. 1. The direct observation of these d-split states, peaks A and B (A' and B'), and the variation with temperature of their energy position and lineshape are used to investigate the dependence of the crystal field potential and of the $3d$-orbitals spatial distribution on crystal symmetry, thermal expansion, atomic vibrational amplitudes and halide atom. The measured relations between crystal field splittings, lattice size, crystal structure and potassium-halide atom pair are accounted for by the simple $10Dq$ theoretical model. We also find that the spatial extent of the $3d$ orbitals is affected by *both* lattice-size and halide-atom. The observed trends are explained by changes in the dynamical screening of the potassium $2p$-core-hole in the different environments.

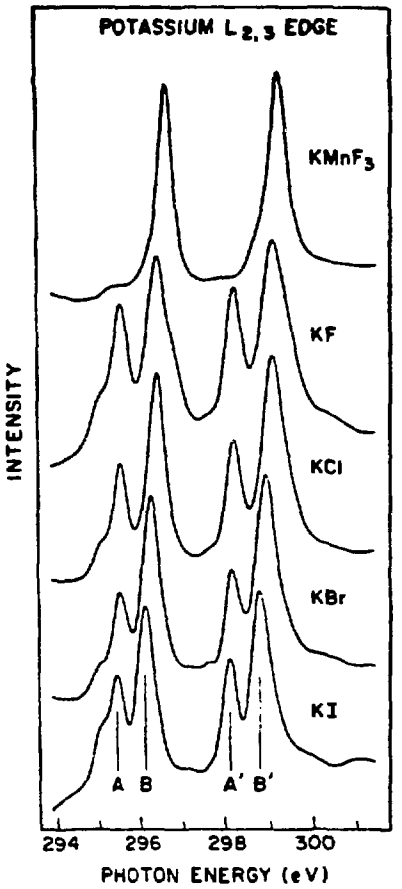

Fig.1 Potassium $L_{2,3}$ edges photoabsorption spectra of $KMnF_3$, KF, KCl, KBr and KI. Peaks A and B (A' and B') are the two crystal field split components of the $2p\,\bar{3}/\bar{2}3d$ ($2p\,\bar{1}/\bar{2}3d$) core exciton. The monochromator resolution was 30 meV.

Infrared Synchrotron Radiation Transmission Studies of High Tc Superconductors†

G. L. Carr*, R. Budhani, G. P. Williams, C.J. Hirschmugl, T. Yang‡, B. Lou‡ & S. Perkowitz‡, Brookhaven National Laboratory, Upton, New York 11973. * Physics Department, University of Florida, Gainesville, FL 32611, ‡ Department of Physics, Emory University, Atlanta, GA 30322,

We have recorded transmission spectra in the spectral region of the gap (from 20-300 cm^{-1}) for a series of thin films of 1-2-3 High Tc materials based on Dy and Y. The films were prepared by evaporation onto MgO substrates. The data clearly show the onset of superconducting behavior, evidence of a gap being the deviation from unity of the ratio Ts/Tn shown in Fig.1 - tending to zero at zero frequency and tending above unity toward higher frequencies. For comparison in Fig.2, we show similar spectra taken on a thin film of the conventional superconductor Nb_3Ge, which has a gap at 56 cm^{-1}. Analysis of the data, and in particular fitting to the spectra, should reveal the gap energy.

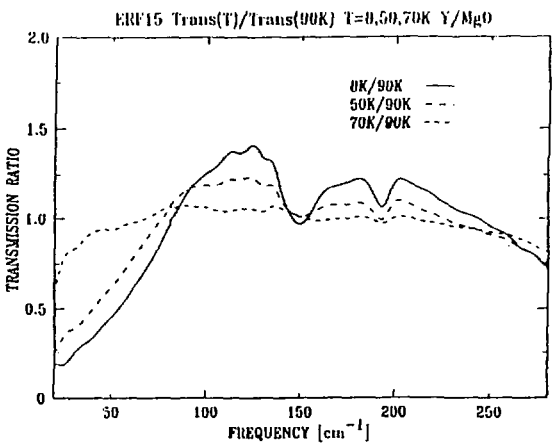

Fig. 1

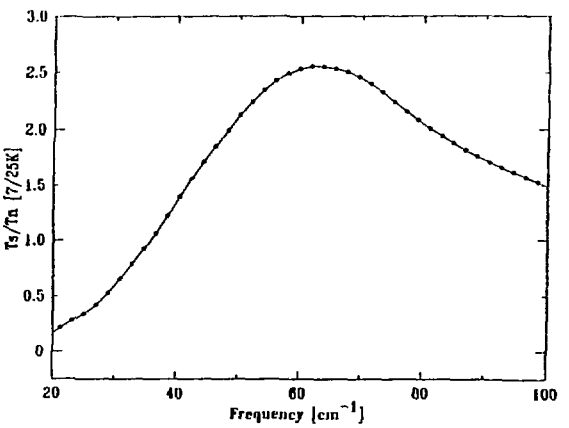

Fig. 2

† Research supported by the US DoE under contract number DE-AC02-76CH00016 including the NSLS/HFBR Faculty Support Program, by DARPA contract #MDA972-88-0-1006, and by NSF grant ECS-872008.

Search for Fractional-Charge Impurities in Silicon Using Infrared Photoionization and Field Ionization

D. D. Coon, Byungsung O and A. G. U. Perera, Department of Physics, University of Pittsburgh, Pittsburgh, PA 15260.
G. P. Williams and C. J. Hirschmugl, National Synchrotron Light Source, Brookhaven National Laboratory, Upton, NY 11973.

A search for unconfined fractional charges in silicon has been carried out at the IR4 beam line of the National Synchrotron Light Source. The search is based on fractional charge impurity energy level predictions of Chaudhuri, Coon and Derkits.[1] The experimental technique involves a combination of infrared photoionization and field ionization at 2.3K.

For a u-quark (charge 2/3) attached to a silicon nucleus, the binding energy of the outermost electron is 17 meV. The 1s to $2p^{\pm}$ transition energy corresponds to a wavelength of 78 μm in the infrared. The ground state field ionization signal is expected[1] at about 2500 V/cm. An example of experimental data for a scan of electric field showing no fractional charge signal near 2500 V/cm is given below.

Our experiment utilizes a silicon p-i-n diode with the i-region representing the sample. Charge is initially injected into the device by a fast forward biased pulse which neutralizes the ionized impurity sites in the i-region. Next the diode is reverse biased to establish the appropriate field to lower the Coulomb potential barrier and to sweep photoexcited carriers out of the i-region. This reverse bias voltage is maintained throughout the IR exposure. Field ionization and readout are accomplished by a large negative ramp or pulse. A second silicon p-i-n diode provides a reference signal for differential amplification. The differential output signal is digitized at 6144 points with a sampling frequency of 32 MHz. The NSLS IR4 beam line[2] is used as the infrared source. A liquid He cooled, low IR background monochromator is used in the experiment. For each wavelength, large numbers of data sets can be taken with and without infrared exposure. Shorter wavelengths are blocked by three sets of filters. The search involves extensive data collection, IR-on and IR-off comparisons, digital filtering and signal averaging.

Acknowledgement: This work was supported in part by the U.S. Department of Energy under contract number DE-ACO2-80ER10667.

1. S. Chaudhuri, D. D. Coon and G. E. Derkits, Phys. Rev. Let. **45**, 1374 (1980).
2. Gwyn P. Williams, Int. J. Infrared and Millimeter Waves **5**, 829 (1984).

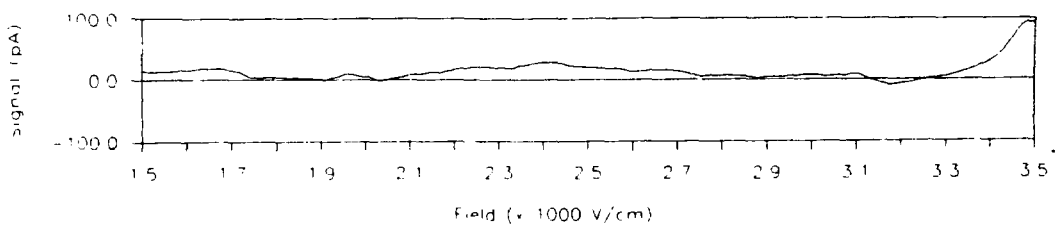

Far Infrared Submillimeter Spectrum of Water Vapor Absorption† U4-IR

K.D. Moller*, D.P. Siddons, C.J. Hirschmugl, P.Petrone*, G.P. Williams, NSLS, Brookhaven National Laboratory, Upton, New York 11973. * Physics Department, Fairleigh Dickinson University, Teaneck New Jersey 07666. † Research supported by the US DoE under contract number DE-AC02-76CH00016

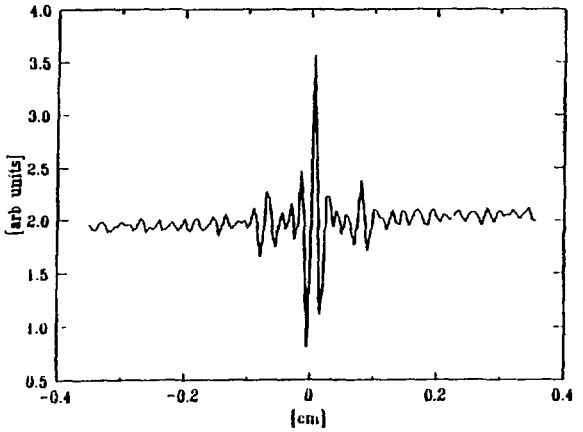

Figure 1. Interferogram taken using a wavefront dividing interferometer comprising two plates, one fixed and one scanning. The instrument uses gold-coated off-axis parabolic mirrors to collimate and focus the beam, and operates in air, the path length being two meters. The total distance travelled by the scanning plate was 2cm. The instrument uses *f* 10 optics and a liquid helium cooled bolometer operated at 1.8K as a detector.

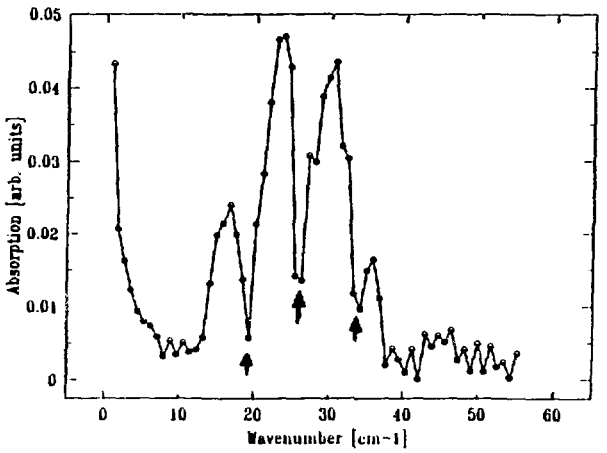

Figure 2. Spectrum resulting from the Fourier Transform of the interferogram of Fig. 1, and showing the characteristic rotational absorption bands of water vapor at frequencies of 18.6, 25.1 and 37.0 cm^{-1} corresponding to wavelengths of .538, .398 and .27mm. The signal to noise of this spectrum was two to three orders of magnitude better than that obtained with a mercury lamp using similar conditions.

Spatial Coherence in the Very Far Infrared (1-2mm) Spectral Region† U4-IR

K.D. Moller*, D.P. Siddons, C.J. Hirschmugl, P.Petrone*, G.P. Williams, NSLS, Brookhaven National Laboratory, Upton, New York 11973. * Physics Department, Fairleigh Dickinson University, Teaneck New Jersey 07666.

† Supported by the US DoE under contract number DE-AC02-76CH00016

Since the vertical height of the source at the NSLS VUV ring is ~ 0.3mm, one would expect the long wavelength emission to be highly spatially coherent. The condition for there to be less than a wavelength of wavefront error is $s\alpha<\lambda$ where α is the opening angle (100 mradians in this case), s the source size and λ the wavelength.

We have tested this in a series of experiments in the millimeter-wave spectral region. A scanning lamellar grating (f 10) interferometer was built using gold plated off-axis parabolic mirrors to collimate the beam on to the grating and to focus the beam onto the sample. The instrument was operated in air and was used in conjunction with a liquid helium cooled bolometer operated at 1.8K. The lamellar grating had a reflecting area of ~ $22\times22cm^2$, and comprised 24 plates each of thickness ~ 0.9cm which could be rearranged to give grating constants of 1.8cm, 5.4cm and 10.8cm. The data for all

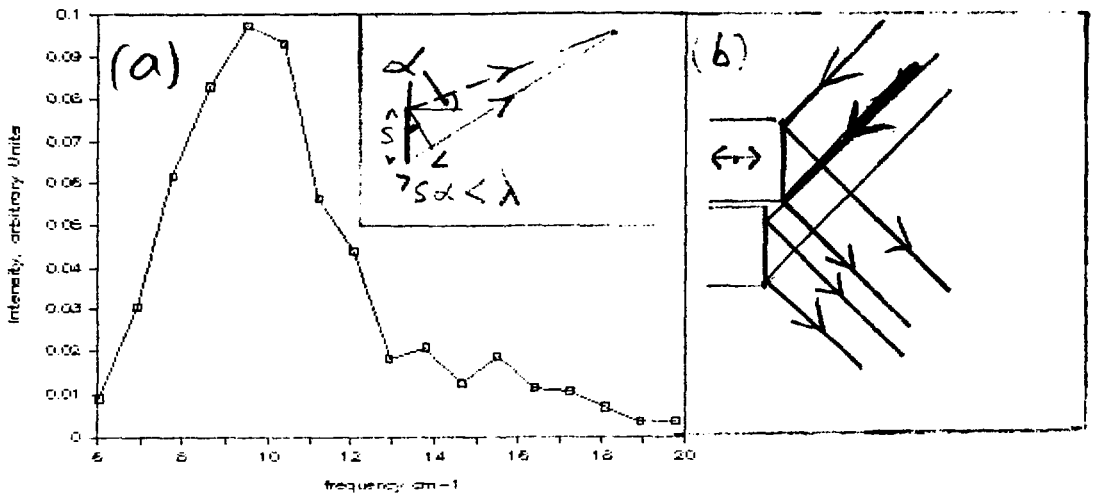

three grating constants were identical. Figure 1(a). Millimeter region spectrum taken using the two-beam interferometer shown in (b) and confirming spatial coherence, the condition for which is also indicated in the inset. The spectrum is cut off at short wavelengths by a microscope slide filter and at long wavelengths by the concentration optics of the bolometer.

Spatial coherence has important applications in the design of a completely new class of instrument, namely wavefront dividing intefrerometers. Such instruments have larger through put than either amplitude dividing or polarizing interferometers, and cover a large range. We have recently designed a long path folded beam, double reflection interferometer for high resolution spectroscopy. The goal is to obtain a resolution of 10^5 to 10^6 at a wavelength of 100 microns.

FIRST MEASUREMENTS OF POWER OUTPUT OF THE NSLS IN THE INFRA-RED SPECTRAL REGION FROM 10-200μm WAVELENGTH.

G.P. Williams, C.J. Hirschmugl, E.M. Kneedler (NSLS), Y. Chabal (AT&T), F.M. Hoffman (Exxon)

We report the first diffraction-free measurements of synchrotron radiation emission in the wavelength region from 20μm to 200μm wavelength where coherent enhancement was predicted. Power and brightness ratios were calculated and measured relative to a globar (black-body) source. The data confirm the predictions of synchrotron radiation emission theory in the long wavelength limit assuming no coherence. The data are shown, however, to be consistent with new calculations of coherent emission in which account is taken of the relative phases of all the emitting particles.

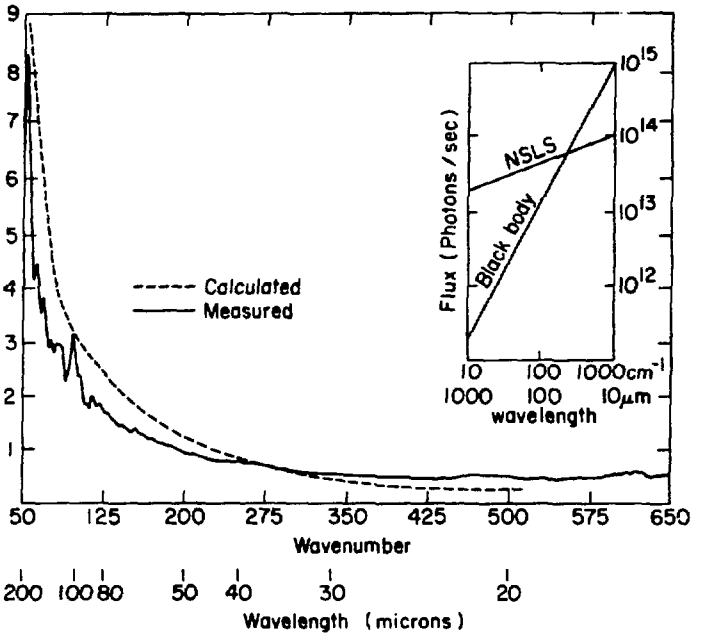

The figure shows the measured (solid line) and calculated (dashed line) ratios between the NSLS output at 330mA and a globar source. The calculated ratios are based on the flux calculations shown in the inset. The data were taken using a Nicolet 20F vacuum Michelson interferometer (rapid scan) using a triglycine sulphate detector with a polythene window.

Research sponsored by the United States Department of Energy under contract #DE-AC02-76CH00016.

Spin Polarized Photoemission Study of Oxygen and Sulfur on Fe(001)

P. D. Johnson, A. Clarke, N. B. Brookes, S. L. Hulbert (BNL)
B. Sinkovic and N. V. Smith (AT&T)

Using spin-polarized angle-resolved photoemission, we have observed spin-split adsorbate induced bands for p(1 x 1) oxygen and c(2 x 2) sulfur on Fe(001). Fig. 1 shows the exchange split bands measured at (a) the center and (b) the edge of the Brillouin Zone. By altering the incident light polarization, we are clearly able to identify the different symmetries of the adsorbate features. The exchange splitting of the Pz orbitals shows a considerable variation across the zone. We highlight this in fig. 2 where we show in (a) the experimentally determined adsorbate induced band structure and (b) a comparison of the measured exchange splitting with different theoretical predictions (dashed lines). We believe the observed Pz exchange splittings are a measure of the level of hybridization with the substrate dz^2 orbitals. The observation of exchange splitting is evidence of a magnetic moment on the adsorbate atom.

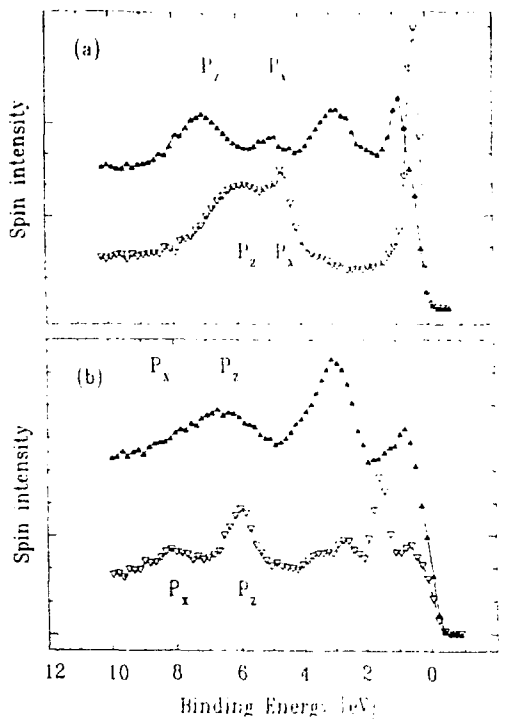

Figure 1

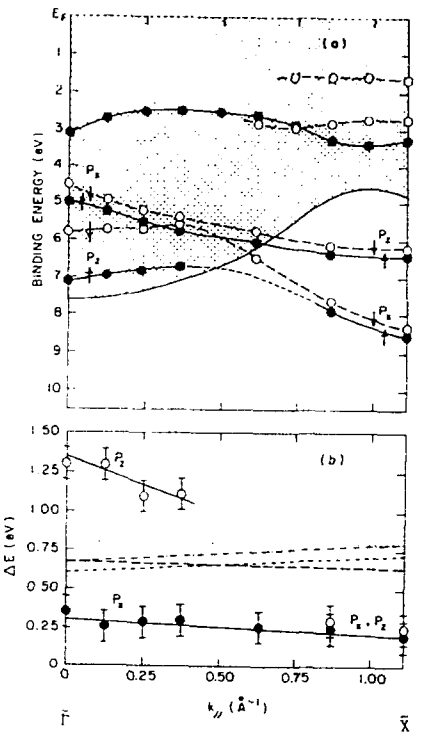

Figure 2

This work is sponsored by the Division of Materials Sciences, U.S. Dept. of Energy under contract DE-AC02-76CH00016.

FULLY SCALED 0.5 μm MOS CIRCUITS BY SYNCHROTRON RADIATION X-RAY LITHOGRAPHY

R. Acosta, I. Babich, V. DiMilia, F. Hohn, D. Katcoff, K. Kwietniak, J. Maldonado, D. Seeger, J. P. Silverman, R. Viswanathan, O. Vladimirsky, H. Voelker, L. K. Wang, J. M. Warlaumont, and A. D. Wilson (IBM Research Division) and D. Crockatt, R. Devenuto, R. Fair, B. Hill, L. C. Hsia, and R. Rippstein (IBM General Technology Division)

Functional NMOS and CMOS circuits with fully-scaled 0.5 μm ground rules have been fabricated using synchrotron radiation X-ray lithography for all device levels. The exposures were done at port U6 using a mask/wafer aligner developed at IBM Research. The system is capable of step-and-repeat exposures covering 125 mm wafers. The mask and wafer are held in a near-vertical plane and a scanning dark-field alignment technique is used to register mask to wafer with a proximity gap of 40 μm. A scanning mirror in the beamline sweeps the X-ray beam up and down over the exposure area to achieve uniform illumination over the 25 × 25 mm^2 area used for this experiment. Exposures are done in 20 Torr of helium to provide cooling for the mask. The overlay capability of the aligner was measured on test wafers and found to be ~ 0.05 μm (1σ). On device wafers, the alignment error was dominated by distortion caused by mask fixturing and by some systematic errors, with a total error of ~ 0.12 μm (1σ).

The CMOS mask set consists of eight light-field masks patterned on silicon substrates with electroplated gold absorbers. A four-mask subset was used for the NMOS devices. The patterns were written by a vector scan electron-beam lithography system. The precision of the mask set has been characterized by measuring more than 600 fiducials on each mask. Analysis of this data shows the level-to-level overlay error is less than 0.12 μm (3σ) including measurement error. SEM measurements show the linewidth on the masks to be controlled to within 250 Å (1σ).

Both positive and negative tone single-layer resists were used in thicknesses of 1 to 3 μm. The linewidth control on the wafer for the positive IBM novolak resist was measured both across a given wafer and from wafer to wafer and was found to be ~ 100 Å (1σ) for a 1 μm thickness. The resist also displayed extremely large process latitude, with linewidth changes of less than 200 Å caused by doubling the development time and changes less than 1000 Å caused by doubling the exposure dose. Linewidth control over topography was also excellent.

An example of a finished circuit is shown in Fig. 1. Both NMOS and CMOS devices worked as expected, with effects due to radiation eliminated by the standard annealing process. Transistor characteristics were normal, and the stage delay times for 61-stage ring oscillators (Fig. 2) were under 100 ps.

Fig. 1. Finished 0.5 μm CMOS circuit.

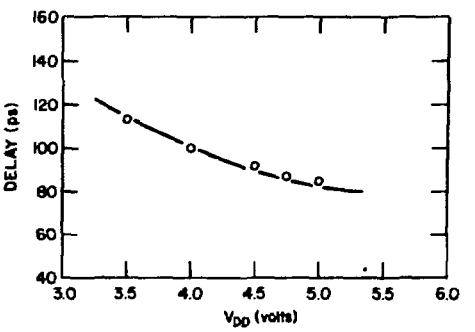

Fig. 2. Stage delay as function of power supply voltage for NMOS ring oscillators with channel length 0.7 μm.

DEGRADATION OF POLY(METHYL METHACRYLATE) BY DEEP UV, X-RAY, E-BEAM AND PROTON BEAM IRRADIATIONS.

J.O. Choi, J.A. Moore and J.C. Corelli (RPI), J. Silverman (IBM), and H. Bakhru, SUNY-Albany.

Many papers and review articles have been published on the mechanism of degradation of poly(methyl methacrylate) PMMA by UV and gamma irradiation. The purpose of this effort was to study the degradation mechanism of PMMA caused by synchrotron X-rays and to compare the results with UV, e-beam and ion beam irradiations using gel permeation chromatography, infrared and ultraviolet spectroscopy to measure directly the changes in PMMA films upon irradiation. The observed changes are related to the decrease of specific functional groups and to the generation of new functional groups. PMMA undergoes loss of ester side groups and scission of the main chain as a result of irradiation. Evidence for these processes includes reduced molecular weight, evolution of gaseous byproducts and the electron spin resonance spectroscopy. The decrease of the carbonyl (C=O) stretching band at 1730 cm^{-1} was found to be proportional to the incident dose. The increase of the 195 nm absorption in the UV spectrum was also proportional to the incident dose. The number of main chain scissions of PMMA was similarly proportional to the incident dose. The ratio of main chain scission to the change in the number of specific functional groups was compared for different types of radiation (Table 1). Main chain scission of PMMA produced by ultraviolet radiation was far less effective compared with the high energy radiations. X-rays were the most efficient at causing main chain scission accompanied by less removal of ester groups.

Table 1: Degradation of PMMA by UV, E-beam, X-ray and Proton beam (main chain scission, ester group removal and carbon carbon double bond generation per 100 monomer units in PMMA)

	DUV 4 ∿6 eV 0.6 J/cm²	E-Beam 25 KeV 20μC/cm² (0.5 J/cm²)	X-Ray 0.8 ∿ 1.8 KeV 1 J/cm²	Proton-Beam 300 KeV 1x10¹³H/cm² (0.48 J/cm²)
Main Chain Scission (MCS)	0.22	0.46	1.08	0.75
Ester Removal (C=O)	8.53	2.59	3.68	3.22
Ratio ($\frac{MCS}{C=O}$)	0.026	0.178	0.293	0.233
C=C generation (C=C)	7.06	2.24	3.72	2.83
Ratio ($\frac{MCS}{C=C}$)	0.031	0.205	0.290	0.265

Supported in part by Semiconductor Research Corporation

X-RAY TRANSMISSION THROUGH LOW Z PARTICLES DURING X-RAY LITHOGRAPHY

R.A. DellaGuardia, D.E. Seeger, J.L. Mauer, IV, J.P. Silverman and B. Hill

IBM Research and General Technology Divisions

The extent of the insensitivity of x-ray lithography to particulate contamination has been speculated upon by proponents of this technology for some time. The ability of x-rays to penetrate low atomic number and low density matter provides an advantage to x-ray lithography that is not shared by optical, ion beam or low voltage electron beam lithography. Results from a systematic study relating particle size, density and composition to the size of the particle-induced resist image (" defect ") have been combined with actual linewidth control data obtained from the fabrication of 0.5 μm MOS devices. The data show that image size tolerance of device geometries can be maintained while processing a wafer in a way that removes a significant number of the defect images.

Exposure of the resist coated wafers was performed at beamline U6 using a mask/wafer holder which maintained a 40 μm gap between the two. Particulate contamination was simulated with either polystyrene spheres, silicon dioxide spheres or aluminum oxide particles. Specific particles were identified on an x-ray mask and the size of the printed images on the wafer which resulted from the particles were monitored using a high resolution SEM.

The resist used was an IBM novolak positive resist. The wafers were processed with the same manufacturing process used to fabricate functional devices. The nominal process endpoint was determined by optical inspection of a test wafer and the amount of over development was calculated from this time. To determine the effect of over development of the resist on the size of the defect image and the linewidth uniformity of the device pattern, numerous measurements were made of the defect images and pattern geometries.

Figure 1 shows the maintenance of good linewidth control when processing a typical wafer to 50 % past nominal endpoint. Figure 2 shows the "disappearance" of a defect image in resist by over developing a wafer. The results of this work have demonstrated the potential yield leverage that x-ray lithography offers by reducing particulate-induced defects.

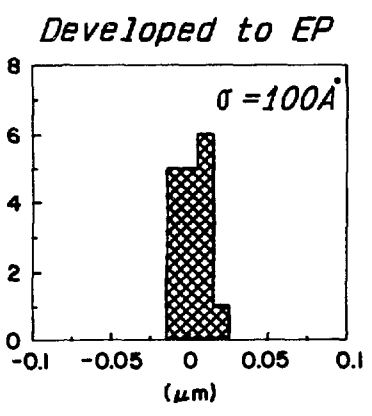

Fig. 1. Linewidth control with over development

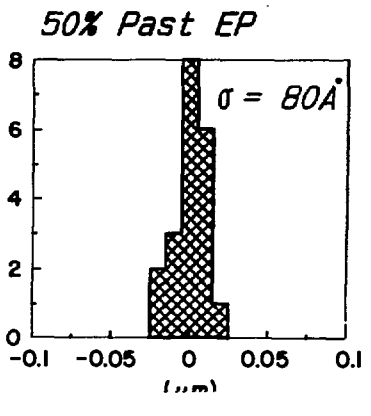

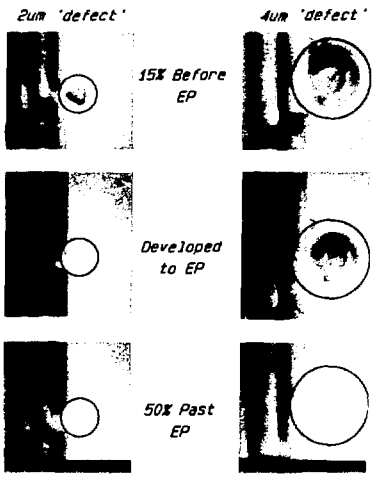

Fig. 2. Disappearance of resist defect images with over development.

Effect of Oxygen on the Cs 4d Photoemission process

Arun S. Bommannavar (Brooklyn College CUNY) and Erik D. Johnson (NSLS)

The data we present here show the results of oxygen exposure on Cesium 4d photoemission. The samples were prepared at the U7B PGM beamline by evaporating Cs on to a liquid nitrogen cooled Tantalum foil until the Ta 4f lines can no longer be observed. The films are then dosed with oxygen at 10-8 Torr to obtain exposures of 0, 0.6, 1.2, and 3.6 Langmuirs. Individual EDCs were recorded with an HA 100 hemispherical analyzer for photon energies ranging from 100 to 140 eV. These spectra were used to obtain the cross sections rather than a CIS scan since the background varies substantially with oxygen exposure and the Cs NVV auger line sweeps through this window. The first figure shows and example of these spectra with the background subtracted, and the auger peak removed. The solid curve is the Auger line, shown for reference. As the second figure shows, we find that the 4d 5/2 cross section increases by over a factor of 30 when oxidized. In addition the photon energy for maximum cross section shifts from 125 eV for the clean metal to 135 eV for the oxidized film. The implication is that the 4d wavefunction has become more compact as a result of the charge transfer from the cesium to the oxidation. In addition we also observe a minimum in the Auger cross section when the NVV energy roughly matches that of the 4d photoelectron (photon energy 125 eV). This may be the result of an interference effect between the Auger and photoelectron. An Auger Photoelectron Coincidence (APECS) experiment would be required to understand this aspect of the system more fully.

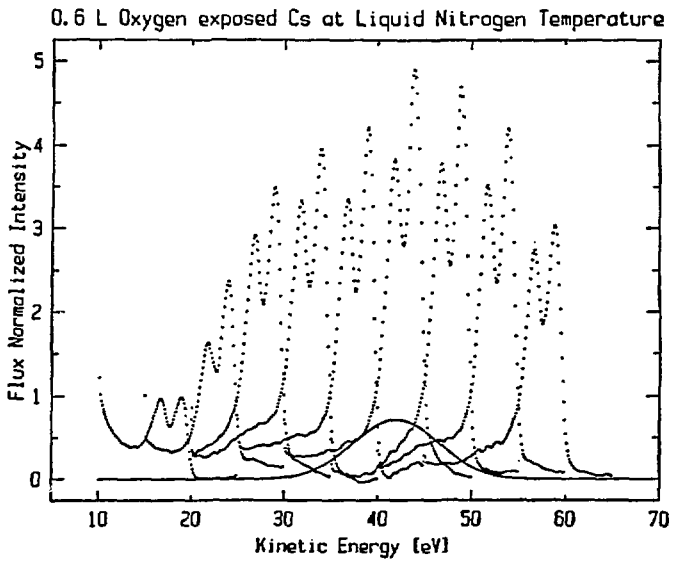

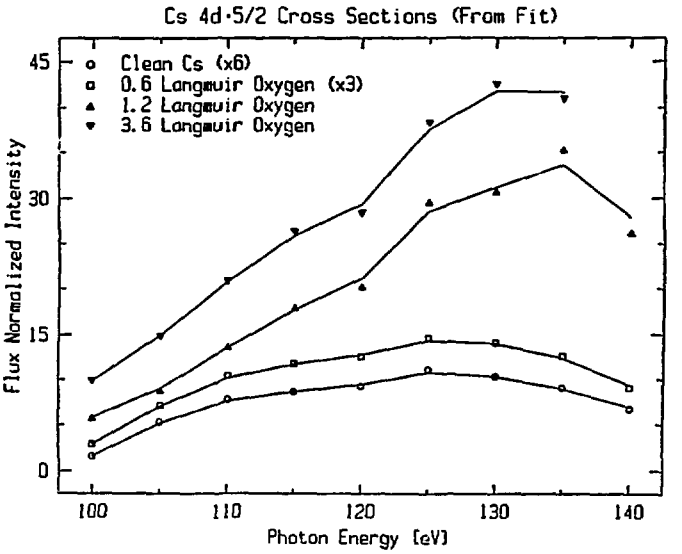

This work supported by the US Dept. of Energy under contract #DE-AC02-76CH00016.

OXIDATION OF THE Ce/Ta SYSTEM.

N.A. Braaten, S. Raaen, J.K. Grepstad (U. of Trondheim, Norway),
and S.L. Qiu (BNL)

Recent results on the oxidation of the Ce/Nb system (1) show that the rare earth overlayer has a dramatic effect on the oxidation of the substrate. We have studied the Ce/Ta system, and have found a similar behavior, which is not unexpected, considering the similarities between Ta and Nb. Both are refractory metals with the same crystal structure, and they form similar oxides. The catalytic oxidation mechanism on Nb and Ta may be different from the one on Al, where the absence of a tetravalent Ce oxide emission is noted. The proposed model for the catalytic oxidation of Nb (1) is based on a conversion from tetravalent to trivalent Ce oxides, thereby providing oxygen ions that can in turn oxidize the substrate. The oxide growth curve is logarithmic for the Ce/Ta system, as it is for pure Ta. The Ce layer stays on top of the substrate and does not form an interface alloy or compound as in the case of Al; as evidenced by the absence of a shift in the Ta core levels upon evaporation of Ce.

1. E.-E. Latta and Maria Ronay, Phys.Rev.Lett. 53, 948 (1984)

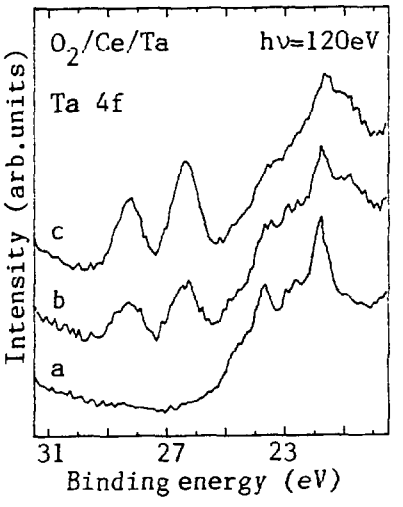

Fig.1 Spectra showing the Ta 4f oxide emission for an oxygen exposure of a) 2L, b) 5L, and c) 25 L.

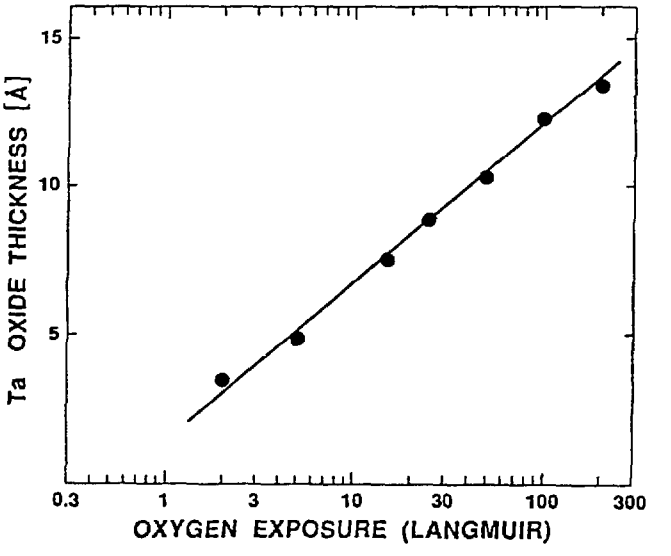

Fig.2 Growth curve showing a logarithmic relation between thickness and oxygen exposure.

This work was supported by the Norwegian Research Council (NAVF)

PHOTOEMISSION STUDIES OF METALLIC OXIDES

M. Croft, F. Lu, Y. Jeon (Rutgers U.), D. Di Marzio, M. W. Ruckman, (BNL-DAS), and M. S. Hegde (Bellcore)

Photoemission was conducted on lead oxide samples with Ba additions in an effort to understand electronic structure modifications in these materials which may be connected with the appearance of superconductivity in $Ba(Bi_{0.25}Pb_{0.75})O_3$. For PbO_2 (Fig. 1), photoemission shows a low density of states at E_f but a discernible Fermi level. Sharp Pb 5d core levels are seen at -17 and -23 eV and the Pb 6s6p-O 2p bands are centered at -3.8 eV. With Ba addition (Fig. 2), sharp Ba core levels (5s, 5p) are seen along with a feature at -9.5 eV which may be due to contamination. The Ba features are enhanced by the Ba 4d giant Fano resonance near 105 eV. The valance band centroid (Fig. 3) shifts about 1 eV to higher binding energy. From the data, we propose that addition of cations like Ba increases correlation effects in the Pb 6s6p-O 2p bands.

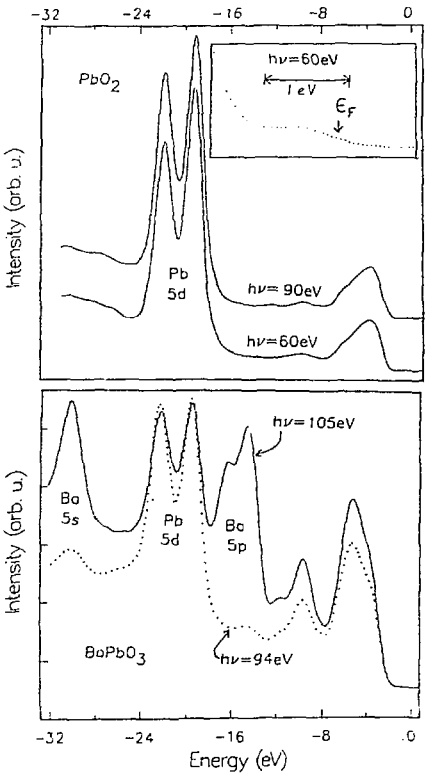

Fig. 1. PbO_2

Fig. 2. $BaPbO_3$

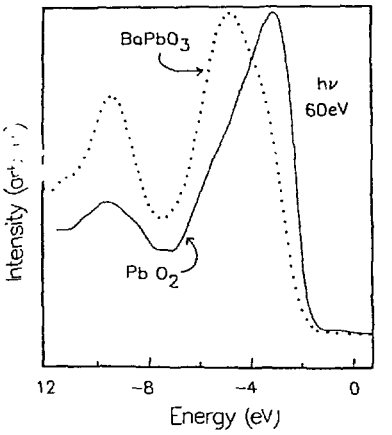

Fig. 3. PbO_2 and $BaPbO_3$.

This work was supported by the National Science Foundation under Grant No. MSM-87-16317 1/1.

CONVERSION FROM TRIVALENT TO TETRAVALENT Ce-OXIDE ON Cu.

J.K. Grepstad, N.A. Braaten, S. Raaen (U. of Trondheim, Norway),
and S.L. Qiu (BNL)

Oxidation of the Ce/Cu system has been studied by photoelectron spectroscopy. Ce may interact with Cu to form an interface compound or alloy upon evaporation at room temperature. This is indicated by the amount of evaporated Ce it takes to completely cover the Cu 3d emission. The Cu 3d emission (MFP about 3 Å) is clearly visible after the Cu 2p core levels (MFP about 12 Å) have been attenuated by a factor of 5. The interface may extend over several monolayers. No chemical shift is observed in the 2p core levels upon oxidation. The formation of CuO can be ruled out. However, the presence of Cu_2O is not easily verified by core level photoemission due to the minute size of the chemical shift. The Ce ions start out being trivalent, but change slowly into the tetravalent species during the course of the oxidation. No indication that Ce has an effect on the oxidation of the Cu substrate has been seen, and the tendency of formation of the oxygen rich tetravalent Ce oxide, may be an indication that the substrate is not oxidizing appreciably.

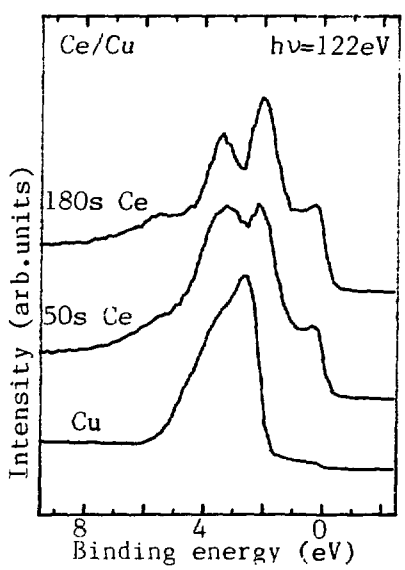

Fig.1 Photoemission spectra of the valence band region for Cu and two Ce depositions. The two peaks near 0 and 2 eV correspond to 4f-emission.

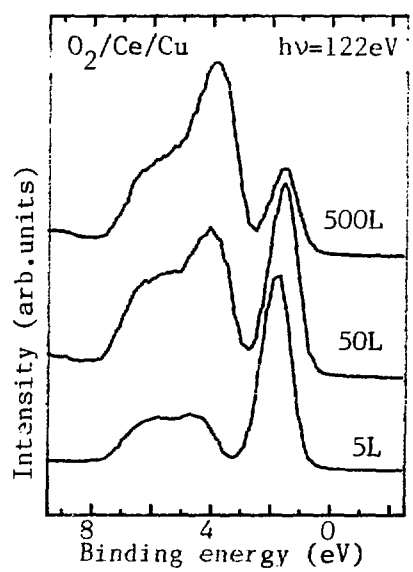

Fig.2 Spectra showing the change in 4f occupation with oxygen exposure. The 4f emission is near 2 eV.

This work was supported by the Norwegian Research Council (NAVF)

PHOTOEMISSION STUDY OF Cu/Al INTERFACES

S. M. Heald, M. W. Ruckman, D. Di Marzio, and H. Chen (BNL-DAS)

Photoemission spectroscopy is used to study the effects of oxygen exposure on the formation of Al/Cu and Cu/Al thin films and their interface. For Al/Cu, the initial valence band spectrum typical of copper (Fig. 1) changes with increasing Al coverage and a new state at higher binding energy attributable to a $CuAl_2$-like phase is observed. Examination of the Al 2p core levels also shows that bulk Al is not seen during initial stages of Al/Cu interface formation. In absence of oxygen contamination, photoemission shows that significant mixing occurs at Al/Cu and Cu/Al interface at room temperature. Oxidation of the Cu substrate does not stop the interfacial reaction between Al and Cu because a Cu-Al phase similar to that found for Al/Cu is seen (Fig. 2). Oxidation of the Al substrate weakens the interfacial reaction between Cu and Al and an abrupt Cu/Al interface forms.

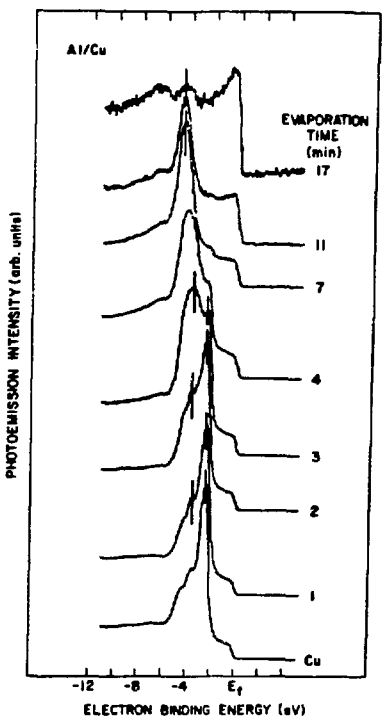

Fig. 1.

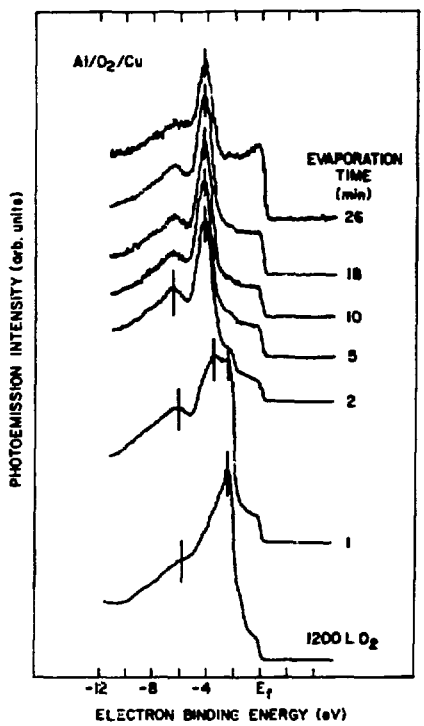

Fig. 2.

This work was supported by the U.S. Department of Energy under Contract No. DE-AC02-76CH00016.

Dependence of Sm Valence on Cu Subtrate Morphology

S. Horn,[1] L. Tao,[1] and M. L. denBoer[2]

1. Department of Physics, New York University, 4 Washington Place, New York NY 10003
2. Department of Physics, Hunter College of CUNY, 695 Park Ave., New York NY 10021

The objective of our measurements is to investigate the electronic state of rare earth atom overlayers on transition metal (TM) surfaces as a function of coverage and transition metal substrate. At the same time possible changes of the surface electronic structure of the transition metal substrates are examined. Although ultimately TM single crystalline surfaces will be used as substrates, initially we used polycrystalline TM substrates as simpler models in order to find systems providing interesting physical effects which later can be studied in greater detail using single crystal TM substrates for ordered RE overlayers. In this report we describe briefly the results of measurements on a Cu-Sm substrate-overlayer systems.

Earlier XPS measurements[1] on Sm on Cu showed the Sm to be in an intermediate valent state between Sm^{2+} and Sm^{3+} with the trivalent component increasing with increasing Sm coverage. This systematic variation of the valence of the RE component with coverage makes this system well suited to examine the interplay between RE valence and surface electronic structure of the substrate. As substrate we used a recrystallized Cu sheet displaying large single crystalline grains. The surface was cleaned by argon ion sputtering, but no attempt was made to repair the surface damage by annealing. We investigated the valence band region of the system using incident energies between 40 eV and 140 eV. To emphasize the Sm- component of the system we took spectra at the Sm resonance energy of hw = 137 eV. Surprisingly only trivalent Sm was observed at low and intermediate coverages. This result was confirmed by measuring the energy dependence of the cross section, which is characteristically different for Sm^{2+} and Sm^{3+}, in the region of the valence band where a Sm^{2+} component is expected. Oxidation studies showed that the absence of divalent Sm in the low coverage spectra was not due to the presence of oxygen on the surface. A divalent Sm component was only observed at high coverages, and we interprete this divalent contribution as due to the presence of multilayers of Sm. In this construction, the surface layer consists of Sm^{2+} ions as is the case for the surface of bulk Sm samples. The fact that no divalent Sm is observed for low and intermediate coverage indicates that the first Sm layer on the Cu substrate is trivalent. This apparent contradiction to reference 1 might be due to the fact that in our measurement the Sm was evaporated on a rough Cu surface, implying a marked sensitivitiy of the Sm-Cu interaction to the morphology of the surface. This important result should clearly be tested using well-defined single crystal substrates of different orientations and controlled roughness.

1. A. Fäldt and H. P. Myers, Phys. Rev. Lett. 52, 1315 (1984).

Electronic State of Sm on Tantalum

S. Horn,[1] L. Tao,[1] and M.L. denBoer[2]
1. Department of Physics, New York University, 4 Washington Place, New York, N.Y. 10003
2. Department of Physics, Hunter College of CUNY, 695 Park Ave, New York, N.Y. 10021

The objective of our measurements is to investigate the electronic state of rare earth atom overlayers on transition metal (TM) surfaces as a function of coverage and transition metal substrate. At the same time possible changes of the surface electronic structure of the transition metal substrates are examined. Although ultimately TM single crystalline surfaces will be used as substrates, it appeared practical to study RE atoms on polycrystalline TM substrates in the beginning to find systems providing interesting physical effects which later can be studied in greater detail using TM single crystals as substrate for ordered RE overlayers. In this report we describe briefly the results of measurements on a Ta-Sm substrate-overlayer system.

Ta foil was used as a substrate. A clean Ta surface was obtained by repeatedly heating the foil close to the melting point. After many cleaning cycles no traces of oxygen were found, and from oxidation studies we estimate the residual oxygen coverage was less than 1/1000 of a monolayer. On this clean substrate, Sm overlayers at a range of coverages from as low as 1% of a monolayer to several monolayers of Sm were measured. It was found that at the lowest coverage both a Sm^{2+} and a Sm^{3+} component is present. When the coverage is increased, the 3+ component initially increases with increasing Sm coverage with respect to the 2+ component. However, at high coverage the 3+ component decreases again, probably when the coverage exceeds one monolayer, and a divalent surface layer is formed. The figure shows spectra taken at the resonace energy of Sm^{3+} for four different coverages, with *a* the lowest coverage and *d* the highest, highlighting the increase in the trivalent Sm contribution with increasing coverage.

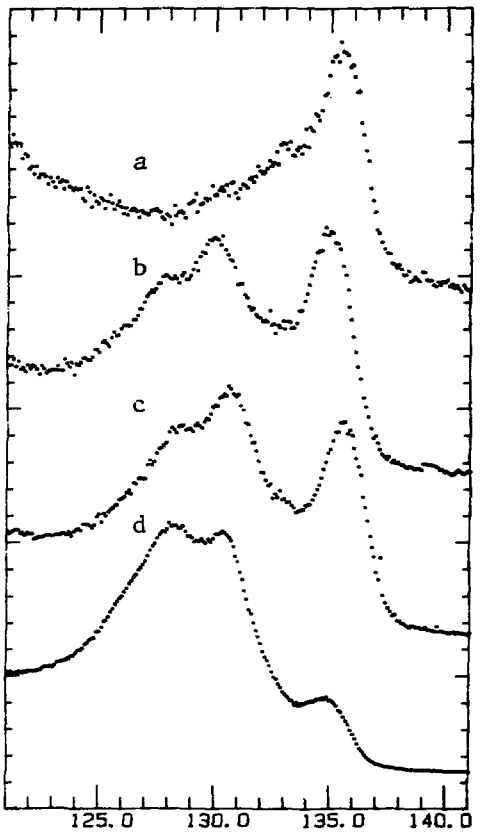

The clean Ta sample showed three distinct valence band contributions, which have been interpreted earlier as surface states. We investigated the energy dependent cross section of these three contributions and found significant differences. Surprisingly for surface states, none of the contributions was very sensitive to oxidation. The effect of the Sm deposition on the surface states has not yet been investigated.

INTRINSIC FEATURES OF THE O 1S CORE LEVEL AND THE O 2p HOLE STATES IN Y-Ba-Cu-O COMPOUNDS

C.L. Lin, S.L. Qiu, M.W. Ruckman, J. Chen, D.H. Chen, Youwen Xu, A.R. Moodenbaugh, and Myron Strongin (BNL), D. Nichols and J.E. Crow (Temple Univ.)

There have been reports[1] and much controversy, concerning features in the the O 1s spectra near 532 eV, and also at 533 eV at low temperatures[2] in the 1-2-3 compounds. With adequate scraping we find no evidence for intrinsic features at these energies, except for a possible weak shoulder at 531 eV as shown in Fig. 1. In view of this, we argue that the previous reports of features near 531 to 533 eV are due to impurities. In addition, upon scraping, the O K-edge feature at 529 eV, of the superconducting 1-2-3 material shown in Fig. 2, increases in intensity. It has been claimed by Sarma et al.[3] that the scraping process removes the stoichiometric species of O on the surface and thereby explains the lack of change with temperature. The data in Fig. 2 argues against this conclusion since removing oxygen would be expected to reduce the 1s-2p near-edge feature and make the spectrum look like the $O_{6.25}$ sample, shown in Fig. 2, which does not show this feature. The growth of the 1s-2p peak as the O_7 sample is scraped, in fact, indicates that the surface band structure originally has less oxygen 2p holes, and scraping produces a more stoichiometric O surface where there are more oxygen holes. We conclude that the O 1s peak at 529 eV is the only intrinsic O 1s feature directly attributable to the 1-2-3 phase and the oxygen 2p hole states are just at and above the Fermi level for the superconducting 1-2-3 material.

1. Y. Dai et al., Phys. Rev. B 38, 5091, 1988.
2. D. D. Sarma et al., Phys. Rev. B 36, 2371, 1987.
3. D. D. Sarma et al., Solid State Commun. 67, 263, 1988.

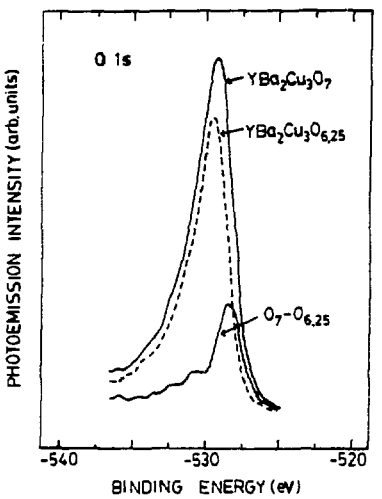

Figure 1

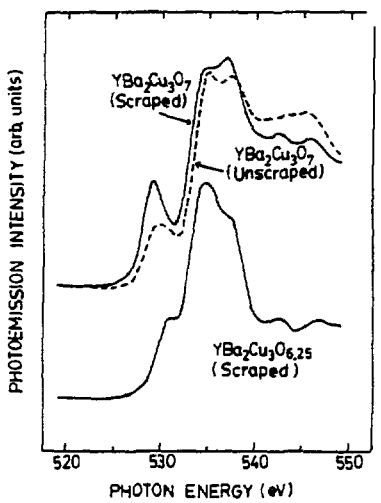

Figure 2

This work was supported by the Department of Materials Sciences, U. S. Dept. of Energy under Contract No. DE-AC002-76CH00016.

$4p-4d$ RESONANCE IN RHODIUM

V. Murgai (Boston U.), Young-Sea Huang (Boston U.), and M.W. Ruckman* (BNL)

Photoemission measurements of Rh films in the photon energy range 40 to 120 eV were made on the U7B beamline with an angle resolving 50 mm 150° sector analyzer operated at a pass energy of 20 eV. The figure below shows valence band EDCs in the vicinity of the Rh 4p core levels. Examination of the valence band photoemission in the vicinity of the $4p$ core levels ($4p_{3/2}$ at 47.0 eV $4p_{1/2}$ at 50.2 eV) shows that a $4p-4d$ intershell interaction takes place: the cross-section for the density of states at the fermi level decreases monotonically below the $4p_{3/2}$ threshold, starts increasing above 47 eV and then decreases at the $4p_{1/2}$ threshold before going through another local maximum around 60 eV. Basically we see a Fano-like resonance analogous to that seen in the $3p-3d$ resonances in the $3d$ transition metals.[1] We also observe an Auger feature of kinetic energy 40 eV appear for the first time at the $4p_{3/2}$ threshold of 47 eV. As the photon energy is increased further, the cross-section for the $4d$ states near the Fermi level decreases again as the Cooper minimum is approached. By contrast the $4d$ density of states seen at approximately 4 eV binding energy do not undergo a Fano like resonance. The apparent resonance is simply the Auger feature at 40 eV kinetic energy moving through.

[1] for a review article see L.C. Davis, J. Applied Physics **59**, R25 (1986).

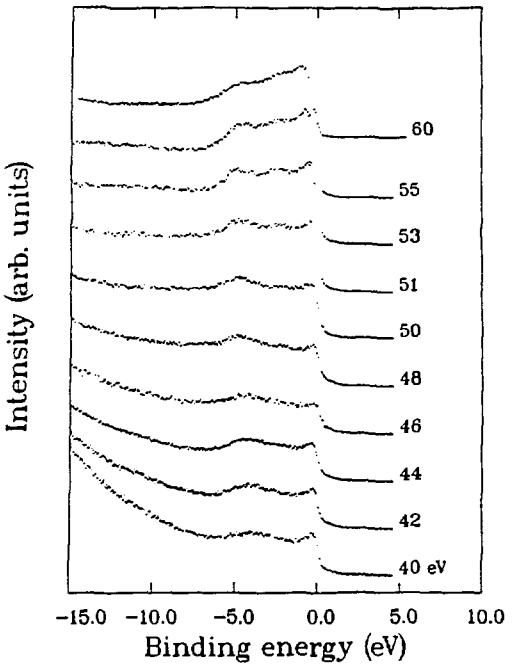

*Supported by the Division of Materials Sciences U.S. Department of Energy under Contract No. DE–AC02–76CH00016.

EFFECT OF IMPURITIES ON THE ELECTRONIC STRUCTURE OF $YBa_2Cu_3O_7$

S.L. Qiu, C.L. Chin, M.W. Ruckman, J. Chen, D.H. Chen, Youwen Xu, A.R. Moodenbaugh and Myron Strongin (BNL), D. Nichols and J.E. Crow (Temple Univ.)

Photoemission from high Tc superconductors crucially depends on surface stoichiometry as well as the interaction of impurities with the reactive surface. Figs. 1 and 2 show the effect of selected impurities on the O 1s core level and the valence band spectra of $YBa_2Cu_3O_7$. The 532 eV O 1s component (Fig. 1 (5)) and the 9.5 eV feature in Fig. 2 (5) along with a huge carbon 1s peak (data are not shown) can be significantly reduced by scraping as shown in spectrum (1) in both figures. The interaction of water, CO and CO_2 with the 1-2-3 compound at room temperature produces species with binding energies from 531 to 533 eV as shown in Fig. 1 and a feature at 9.5 eV as shown in Fig. 2. These results indicate that the higher binding energy O 1s features and the 9.5 eV feature in the valence bank spectrum taken at 105 eV photon energy are extrinsic.

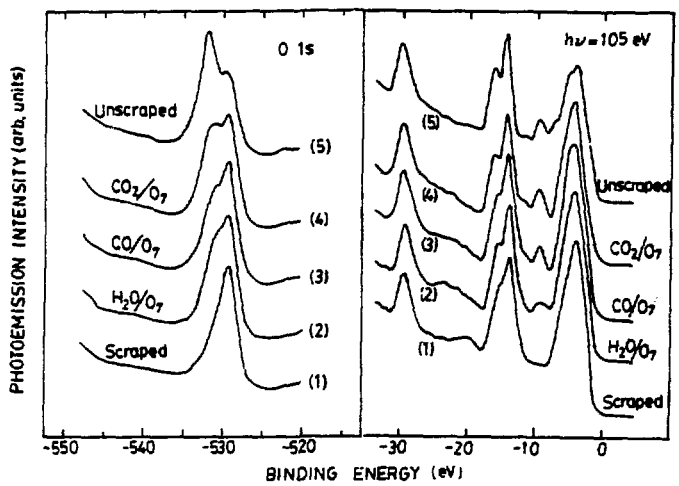

Figure 1

Figure 2

This work is sponsored by the Division of Materials Sciences, U. S. Dept. of Energy under contract DE-AC02-76CH00016.

Oxidation of Bi at 35K: Comparison to Ba-Bi-Pb-O

S. L. Qiu, C. L. Lin, J. Chen, and Myron Strongin

The oxidation of Bi is of current interest because of the superconducting properties of some Bi oxides and the suggestion that Bi can have a fluctuating valence state in these compounds. We have formed Bi oxides by exposing Bi layers to oxygen at 35K. At this temperature the vapor pressure of solid molecular oxygen is high enough so that only a monolayer of molecular oxygen condenses on the surface. The O $1s_2$ core level spectra shows only a weak peak at 530 eV characteristic of O^{2-} in an oxide, and a weak peak between 535 eV and 540 eV due to molecular oxygen. There is no evidence of the peroxide and superoxide features which are seen in the oxidation of the alkali metals. Figure 1 shows the valence band spectrum as molecular oxygen at 35K is condensed on the Bi surface. There is some evidence that the weak oxidation seen in the core level spectra, appears here as a shoulder at 5 eV. The additional features can be identified as molecular oxygen features. In Figure 2 the Bi 5d spectra are shown and it can be seen that the oxide features A and B coincide with the Bi 5d features of the superconducting compound Ba $Bi_{.25}Pb_{.75}O_3$.

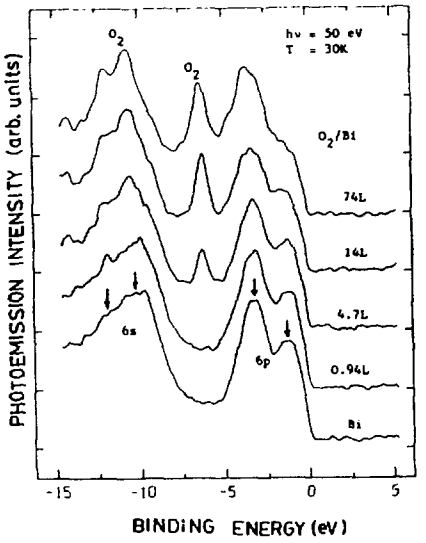

Figure 1

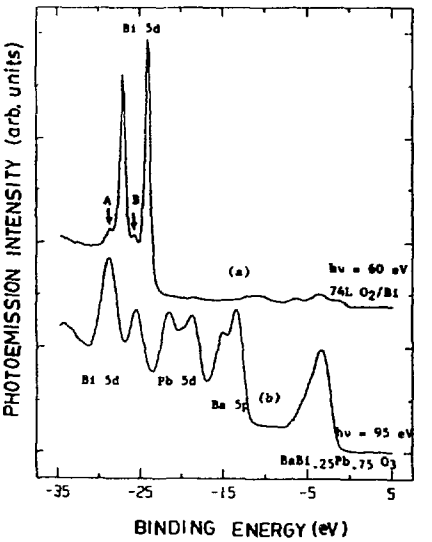

Figure 2

This work is sponsored by the Division of Materials Sciences, U.S. Dept. of Energy under contract DE-AC02-76CH00016.

THE FORMATION OF ALKALI METAL -- OXYGEN SPECIES AT LOW TEMPERATURES

S. L. Qiu, C. L. Lin, J. Chen and M. Strongin

The interaction of solid molecular oxygen with Li, Na, K and Cs near 30K has been studied using photoemission. Three different alkali metal - oxygen species were observed in O 1s core level spectra when alkali metals are deposited in solid oxygen. A feature at about 534.5 eV was identified with one electron donated to an oxygen molecule, i.e. the superoxide which as far as we know has not been previously reported for Li. The feature at about 531.5 to 532.5 eV was identified as peroxide where two electrons were donated to an oxygen molecule. Another feature at about 528 eV for Cs, Na and K, at 530 eV for Li, was identified as the oxide where the molecular oxygen was dissociated into atomic oxygen with formal valence of -2. We argue that the difference in binding energy of 528 eV and 530 eV when oxygen is reacted with these alkali layers is due to the oxygen being incorporated under the surface for Cs,[1] Na and K, whereas the oxide forms on the surface for Li. It is plausible that an O^{2-} species under the surface is screened more effectively and has a smaller binding energy. Oxygen incorporated under the surface shows a valence bond feature near 3 eV; the regular oxide is near 6 eV. For Li only a feature at 5.5 eV is observed. As an example, the valence band and O 1s core level spectra due to the interaction of Cs with solid oxygen at 30K are shown in Fig. 1 and 2.

[1] See for example G. Woratschek, W. Sesselmann, J. Keeppers, G. Ertl and H. Haberland, J. Chem. Phys. 86, 2411, 1987.

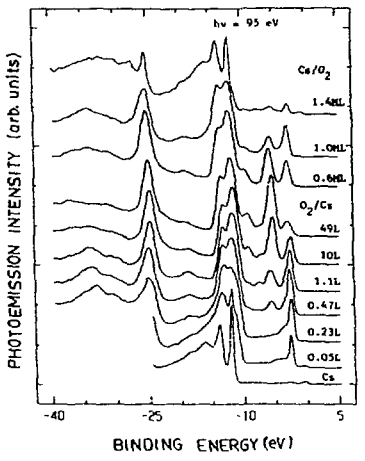

Figure 1

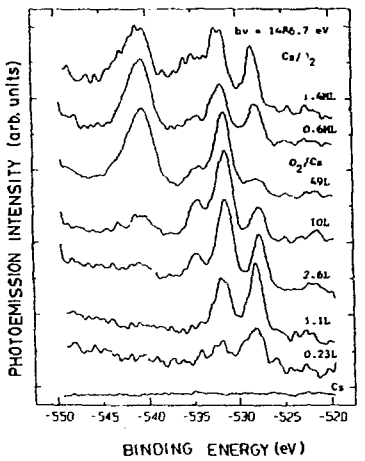

Figure 2

This work is sponsored by the Division of Materials Sciences, U.S. Dept. of Energy under contract DE-AC02-76CH00016.

STUDIES OF Cu ON SOLID OXYGEN

S. L. Qiu (BNL), C. L. Lin (BNL), and M. Strongin (BNL)

Various explanations of superconductivity in the new ceramic high temperature superconductors involve the properties of the "CuO_2" layers. The present series of experiments is an attempt to study the properties of isolated Cu-oxide by depositing Cu on Solid O_2 layers. In Fig. 1 the valence band spectra is shown for molecular oxygen and the appearence of Cu d-states is shown as successive amounts of Cu are deposited. The valence band for a thick Cu layer is seen at the coverage of 24 ML. From the point of view of the layers the single most important measurement are the features of the Cu 2p core levels. The appearence of the satellite feature in Fig. 2 is characteristic of Cu^{II}. The observation of Cu^{II} implies the existence of the four fold planar coordinated dsp^2 bonding. Although the Cu remains as Cu^{II} in the regime up to several monolayers, it is interesting that the oxygen 1s level shifts from 531.7 to 529.7 eV. This is thought to be the change from an initial peroxide level where a Cu atom donates its two electrons to the oxygen molecules, to a CuO state which occurs as more copper is deposited and the oxygen molecules start to dissociate. Since a planar four fold mesh of CuO_2 probably be unstable, it is expected that the layer made here must be a disordered array of CuO complexes or tenorite, the bulk CuO structure. It is possible that alkali metal doping can lead to a neutral layer with a fourfold planar CuO_2 structure and experiments to try this are underway. Finally, we mention the absence of evidence for Cu^{III}, and argue that this is a relatively unstable configuration. Cu^{I} was formed at 25K when O_2 was deposited on Cu, i.e., Cu_2O formed.

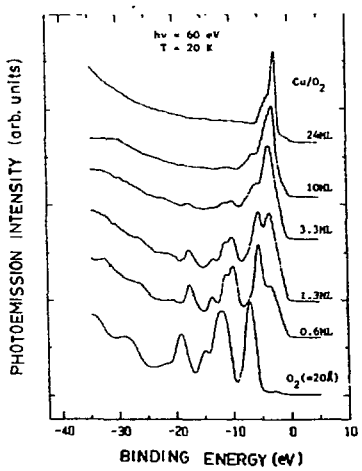

Figure 1

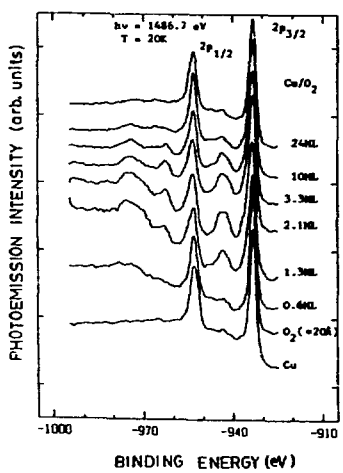

Figure 2

This work is sponsored by the Division of Materials Sciences, U.S. Dept. of Energy under contract DE-AC02-76CH00016.

INTERACTION OF CO, H_2O AND CO_2 WITH Ba

S.L. Qiu, C.L. Lin, M.W. Ruckman, J. Chen, D.H. Chen, Youwen Xu, A.R. Moodenbaugh and Myron Strongin (BNL), D. Nichols and J.E. Crow (Temple Univ.)

To better understand how the photoemission spectra of the 1-2-3 compounds are affected during the interaction with various gases, we studied the O 1s core level, the valence band, and the Ba 3d and 4d spectra for O_2, CO, and H_2O on Ba films. The dominant peak at about 532.5 eV in the O 1s spectrum shown in Fig. 1 (3) is accompanied by a huge carbon 1s feature (data are not shown) which resembles the case of the dirty $YBa_2Cu_3O_7$ sample. This makes plausible the conjecture that the carbon related contamination on the surface of the 1-2-3 compounds is a Ba carbonate (possibly $BaCO_3$). The spectra in Fig. 2 show the dramatic affects of impurities on the Ba valence band. Only the peak at 9.5 eV in spectrum (4), denoted by an arrow, is accompanied by a huge carbon 1s peak and therefore, it can be assigned to a feature of Ba carbonate. After the interaction of CO with Ba metal, a shift of 0.8 eV between peak A and C in Fig. 3 is observed. Both Figs. 2 and 3 show that there is a positive Ba core electron chemical shift due to Ba carbonate which makes the Ba core level spectra asymmetric. This would explain the asymmetry in the Ba 3d and 4d spectra of the dirty 1-2-3 compounds.

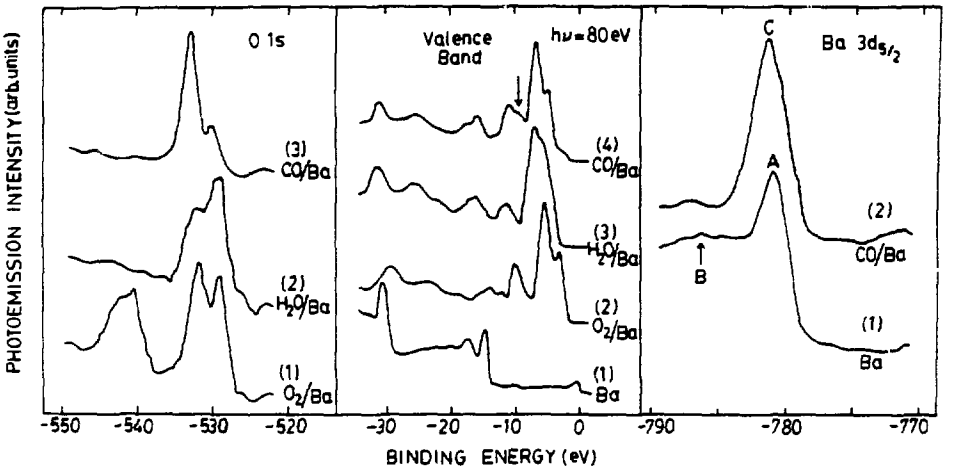

Figure 1 Figure 2 Figure 3

This work is sponsored by the Division of Materials Sciences, U.S. Dept. of Energy under contract DE-AC02-76CH00016.

INTERACTION OF H_2O WITH A HIGH TEMPERATURE SUPERCONDUCTOR

S.L. Qiu (BNL), M.W. Ruckman (BNL), N. Brookes (BNL), P.D. Johnson (BNL), J. Chen (BNL), C.L. Lin (BNL), M . Strongin (BNL), B. Sinkovic (AT&T), J.E. Crow (Temple U.), and Cham-Soo Jee (Temple U.)

The effect of water on the high temperature superconductor YBa_2CuO_7 has been studied. Valence band photoemission spectra between 50 and 150 eV are shown for clean $YBa_2Cu_3O_7$ at 20 K (Fig. 1) and for the same surface following the adsorption and desorption of water (Fig. 2). This study provides evidence that $YBa_2Cu_3O_7$ can be modified by water at cryogenic temperatures and suggests that a OH^- species most probably reacts with the oxygen vacancies and modifies both the Ba and Cu electronic environments. We find that most of the water desorbs between 160 and 210 K but a small amount may also preferentially desorb near 240 K. This work illustrates the problems that unintentional water incorporation may pose for devices employing interfaces between $YBa_2Cu_3O_7$ and dissimilar material, or the builk material prepared by ceramic techniques. Reports of dimerization and other reported changes with temperature must be reexamined in view of the effect of water on the surface.

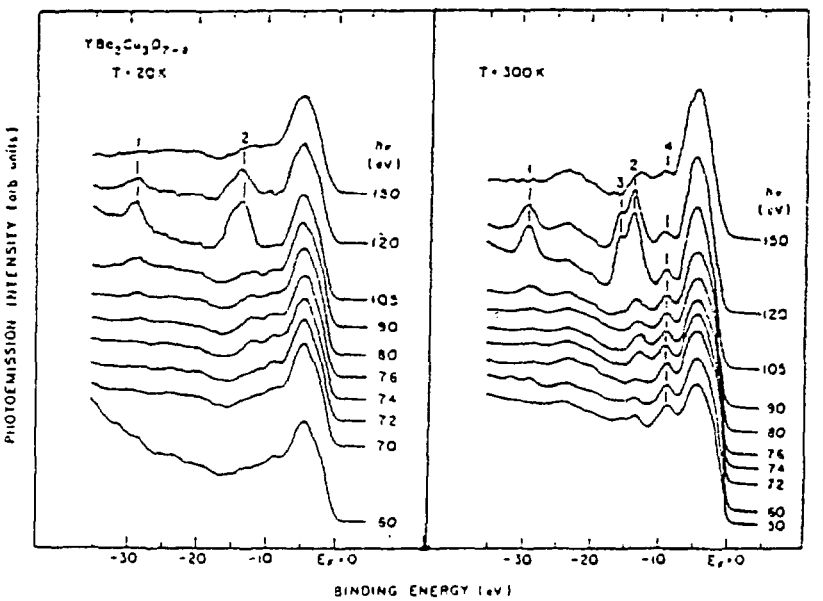

Figure 1

Figure 2

This work is sponsored by the Division of Materials Sciences, U.S. Dept. of Energy under contract DE-AC02-76CH00016.

ELECTRONIC STRUCTURE OF $YBA_2CU_3O_6$ U7B

S. L. Qiu (BNL), M. W. Ruckman (BNL), P. D. Johnson (BNL), N. Brookes (BNL), J. Chen (BNL), C. L. Lin (BNL), M. Strongin (BNL), B. Sinkovic (AT&T), J. E. Crow (Temple U.) and Cham-Soo Jee (Temple U.)

The electronic stucture of $YBa_2Cu_3O_6$ has been studied using synchrotron radiation and x-ray photoemission. There are significant differences in the electronic structure between $YBa_2Cu_3O_6$ and $YBa_2Cu_3O_7$ which are mainly due to the removal of oxygen from the lattice. Fig. 1 shows the spectra obtained from both $YBa_2Cu_3O_6$ (curve B) and $YBa_2Cu_3O_7$ (curve A) at (a) 76 eV and (b) 105 eV. The absence of the Cu 3d satellite in curve B (Fig. 1(a)) implies that the average charge state of Cu in $YBa_2Cu_3O_6$ is less than 2+. This is confirmed by the absence of the satellite of Cu 2p core level. The line width of all Ba peaks in curve B (Fig. 1 (b)) is narrower than that in curve A, and the intensities of Ba $5p_{3/2,1/2}$ and Ba 5s of $YBa_2Cu_3O_6$ are much stronger than that of $YBa_2Cu_3O_7$. This indicates that the Ba environment is quite different in $YBa_2Cu_3O_6$ and $YBa_2Cu_3O_7$. Fig. 2 shows that when the oxygen atoms are removed from $YBa_2Cu_3O_7$ The O 1s core level shifts from 529 eV to 531.4 eV and this can be partially reversed by oxygen adsorption.

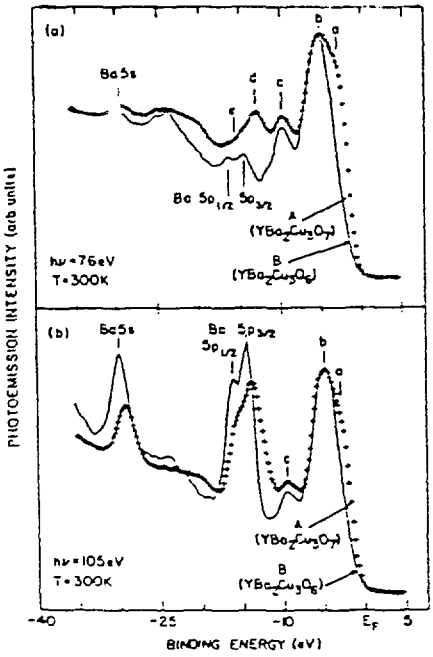

Figure 1

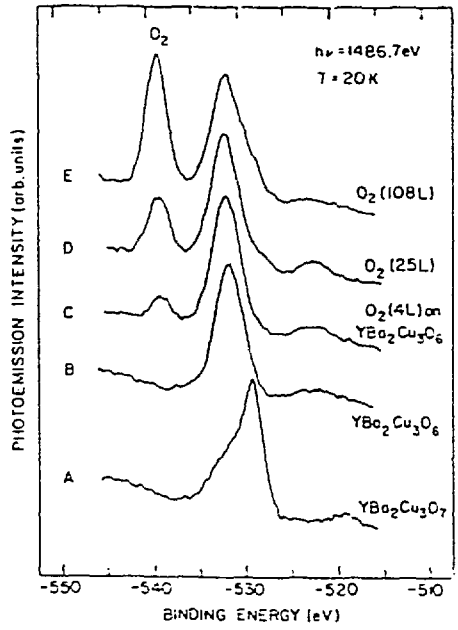

Figure 2

This work is sponsored by the Division of Materials Science, U.S. Dept. of Energy.

CATALYTIC OXIDATION OF ALUMINUM.

S. Raaen, N.A. Braaten, J.K. Grepstad (U. of Trondheim, Norway),
and S.L. Qiu (BNL)

Oxidation studies of polycrystalline Al-films covered by thin overlayers of Ce (10 Å) have been performed by photoelectron spectroscopy. Our findings are that the rare earth overlayer has a dramatic catalytic effect on the rate of oxidation of the substrate at room temperature. First, a mixed Ce/Al-oxide seems to form at the interface, and subsequently, the Al substrate oxidizes. The crossover between these two regions is characterized by a kink in the growth curve. The growth law is logarithmic on both sides of the kink, and is consistent with an electric field assisted mechanism of the Cabrera-Mott type. The Ce overlayer also has an enhancement effect on the initial oxidation at liquid nitrogen temperatures, however, in this case the growth does not persist beyond one to two monolayers. The enhancement in the oxidation rate is caused by an increase in the oxygen uptake rate induced by the cerium overlayer. Our findings may provide a means of performing detailed oxidation studies of Al under well controlled vacuum environments, and may be of importance to applications where a controlled thickness of Al-oxide is needed.

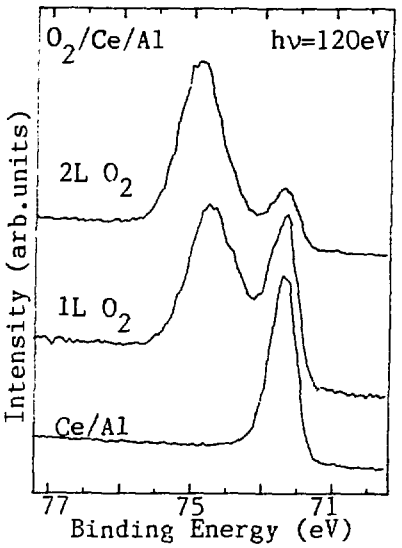

Fig.1 Al 2p emission showing the rapid evolution of the oxide peak.

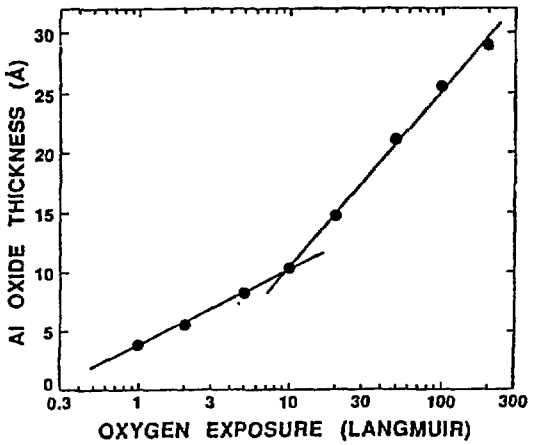

Fig.2 Growth curve showing the two logarithmic regions. The branch below 10L correspond to a mixed Ce-Al oxide.

This work was supported by the Norwegian Research Council (NAVF)

OXIDATION OF Ce/METAL OVERLAYER SYSTEMS.

S. Raaen, N.A. Braaten, and J.K. Grepstad (U. of Trondheim, Norway), and S.L. Qiu (BNL)

Recent results on the oxidation of the Ce/Nb system (1) show that the rare earth overlayer has a dramatic catalytic effect on the oxidation of the substrate. The present experiment concerns the Ce/Cu, Ce/Ta and Ce/Al systems. No enhancement was observed on the oxidation of Cu; however, both Ta and Al oxidation were increased markedly in the presence of the Ce overlayer. Nb and Ta are similar in many respects; e.g. they form oxides of the same structure, and the oxide growth is by anion migration. They may thus be expected to behave in similar ways. Al forms a different oxide which grows by another mechanism. The catalytic process may be of a different type in this latter case. The conversion from tetravalent to trivalent Ce-oxide does not seem to take place for Al, as evidenced by the absence of a tetravalent signal in the photoemission. A possible surface alloy formation between Ce and Al may be important for the catalytic oxidation of aluminium.

1. E.-E. Latta and Maria Ronay, Phys.Rev.Lett. 53, 948 (1984)

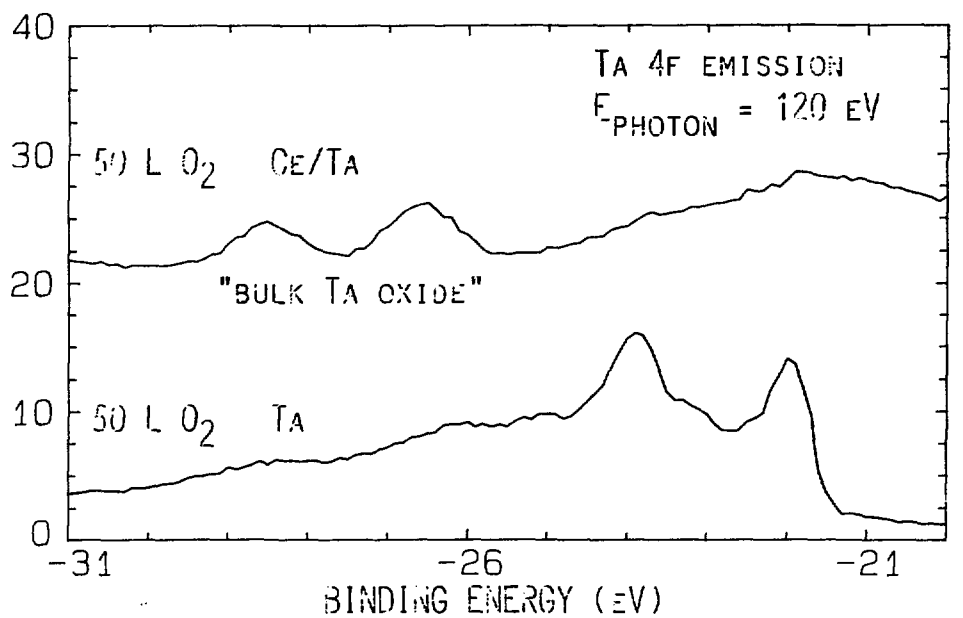

Fig. Photoemission spectra in the region of the Ta 4f levels, showing the effect of a thin Ce overlayer on the oxidation of the Ta substrate.

This work was supported by the Norwegian Research Council (NAVF).

EXPERIMENTAL DETERMINATION OF THE BAND STRUCTURE OF THE ALLOY Cu_3Au

Z.Q. Wang, S.C. Wu, J. Quinn, C.K.C. Lok, Y.S. Li, F. Jona SUNY, Stony Brook, and J. Davenport (BNL)

We have done angle-resolved photoemission experiments on clean $Cu_3Au(001)$ with synchrotron light in the range 12.5 to 46 eV at normal emission. The data were evaluated to produce the band structure along Γ-X. The initial band positions were calculated with the assumption of free-electron-like final states. The resulting experimental band structure was compared with that calculated by Davenport, Watson and Weinert.[1] There is general agreement insofar as both experiment and theory show that the energy bands fall into two groups -- bands that lie below -5 eV and bands that lie above -3.5 eV. The calculation indicates that the deeper bands are predominantly of gold character and the more shallow bands are predominantly copper, although there is hybridization between the two groups and there is some gold character at all energies. But it is not possible to make a detailed comparison between calculated and experimental band structure because the former shows many more bands than the latter. There are two possible explanations for this fact: (i) insufficient experimental resolution and (ii) effect of band folding, which makes the folded-back bands very weak. The most glaring discrepancy between theory and experiments, the peak with binding energy of about -0.5 eV, is very probably due to failure of the free-electron approximation, as this state is only observed with small photon energies. Overall, the experimental results are consistent with first-principles electronic-structure calculations, but it is clear that studies of the electronic structure of metallic compounds with many atoms per unit cell require very high resolution to allow the kind of band-mapping which has become standard for elemental metals.

[1] J.W. Davenport, R.E. Watson and M. Weinert, Phys. Rev. B37, 9985 (1988).

This work was supported by the U.S. Department of Energy under Contract No. DE-AC002-76CH00016.

OBSERVATION OF A SURFACE STATE IN OVERLAYERS OF Au ON Pt(001)

S.C. Wu, C.K.C. Lok, S.H. Lu, J. Quinn, D. Tian, Y.S. Li and F. Jona (SUNY, Stony Brook)

Angle-resolved photoemission experiments on ordered Au overlayers deposited in vacuo on a Pt(001) substrate show a peak located 7.1 eV below the Fermi level which has many of the properties of a surface state. The peak has no energy dispersion in the photon-energy range from 40 to 110 eV; its intensity, relative to neighboring peaks, is a function of the thickness of the Au overlayers and decreases when the coverage exceeds 1 monolayer. The relative intensity is also a function of the photon energy and reaches a maximum at 84 eV, which corresponds to a final-state momentum predicted by the theory of Louie et al.[1] for surface-state oscillations (Fig. 1). Finally, energy position and dispersion agree well with calculations of Wang et al.[2] for Au-covered Pt(001) surfaces. We suggest that this peak is produced by a surface state below the d-band at the $\bar{\Gamma}$-point of the Au overlayers. We also suggest that this state exists on (001) and (111) surfaces of bulk Au, and that the surface states observed around 5 eV on (001) and (111) surfaces of Cu have the same origin.

[1] S.G. Louie, P. Thiry, R. Pinchaux, Y. Petroff, D. Chandesris and J. Lecante, Phys. Rev. Lett. 44, 549 (1980).
[2] D.S. Wang, A.J. Freeman and H. Krakauer, Phys. Rev. B29, 1665 (1984).

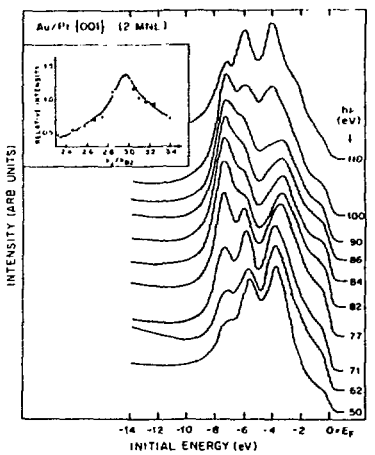

Fig. 1. Normal-emission electron distribution curves from a 2-MNL Au-1x1 overlayer on Pt(001) for different photon energies hν. The insert shows the ratio of the 7.1-eV to the 5.7-eV peak intensity versus the perpendicular momentum relative to the Γ-X distance in the bulk Brillouin zone.

This work was supported by the U.S. Department of Energy under Contract No. DE-AC02-76CH00016.

OBSERVATION OF RESONANCE PHOTOEMISSION FROM Pd(001)

S.C. Wu, C.K.C. Lok, J. Quinn, Y.S. Li, D. Tian and F. Jona SUNY, Stony Brook

In photoemission experiments on Pd(001) we have observed a satellite peak about 8.5 eV below the Fermi level which exhibits resonance when the photon energy is varied around the binding energy of the 4p level (about 53 eV). The enhancement of the satellite peak is approximately a factor of 5. Analogous behavior was observed by Chandesris et al.[1] on Pd(111), and ascribed by these authors to the resonance photoemission effect originally observed on Ni by Guillot et al.[2], who suggested that the phenomenon could be understood in terms of normal interband excitations from the top region of the lower Δ_1 band. If this argument were correct we would not observe the satellite peak on Pd(001) with pure s-polarized light. Our experiments show that we do, either in the angle-resolved or in the angle-integrated mode. No change is observed when the polarization of the light is changed from pure s to 40%p, a fact consistent with the fact that the 3p-3d excitation and the atomic-like Auger decay $3p^5\,3d^{10}\,4s \rightarrow 3p^6\,3d^8\,4sel$ do not depend much on selection rules or the position in the Brillouin zone.

[1] D. Chandesris, G. Krill, C. Maire, J. Lecante and Y. Petroff, Solid State Commun. 35, 397 (1980).
[2] C. Guillot, Y. Bella, J. Paigne, J. Lecante, K.P. Jain, P. Thiry, R. Pinchaux and Y. Petroff, Phys. Rev. Lett. 39, 1632 (1977).
[3] J. Kanski, P.O. Nilsson and C.G. Larsson, Solid State Commun. 35, 397 (1980).

This work was supported by the U.S. Department of Energy under Contract No. DE-AC002-76CH00016.

OBSERVATION OF A SURFACE STATE AND A SURFACE RESONANCE AT THE CENTER OF THE SURFACE BRILLOUIN ZONE ON Cu(001)

S.C. Wu, C.K.C. Lok, J. Sokolov, J. Quinn, Y.S. Li, D. Tian and F. Jona
(SUNY, Stony Brook)

Angle-resolved photoemission experiments from Cu(001) show two peaks s_1 and s_2 located 5.0 eV and 2.2 eV below the Fermi level, which are a surface state and a surface resonance at the center of the Brillouin zone $\bar{\Gamma}$, respectively. Neither peak exhibits energy dispersion with momentum perpendicular to the surface, but otherwise the energy positions and the dispersions are in good agreement with the calculations of Gay et al.[1] The intensities of both peaks relative to the intensity of the adjacent bulk peak are functions of the photon energy and exhibit maxima for a value of the final-state momentum predicted by the theory of Louie et al.[2] Both peaks are sensitive to the presence of impurities on the surface. Angle-resolved normal-emission EDC's were measured with 30%-p-polarized and pure s-polarized light from a clean Cu(001) surface and one covered with oxygen. The changes caused by the different polarization indicate that the s_1 state is Δ_1-like and the s_2 state is Δ_5-like. Reference to the electronic band structure calculated by Janak et al.[3] suggests that these states originate from the s-d hybridized Δ_1 band at the bottom of the valence band and from the Δ_5 band, respectively. The existence of these states is consistent with the surface-core-level-shift theory of Citrin and Wertheim[4] for noble metals.

[1] J.G. Gay, J.R. Smith and F.J. Arlinghaus, Phys. Rev. Lett. 42, 332 (1979).
[2] S.G. Louie, P. Thiry, R. Pinchaux, Y. Petroff, D. Chandesris and J. Lecante, Phys. Rev. Lett. 44, 549 (1980).
[3] J.F. Janak, A.R. Williams and V.L. Moruzzi, Phys. Rev. B11, 1522 (1975).
[4] P.H. Citrin and G.K. Wertheim, Phys. Rev. B27, 3176 (1983).

This work was supported by the Department of Materials Sciences, U.S. Department of Energy under Contract No. DE-AC02-76CH00016.

EVIDENCE FOR RELATIVISTIC EFFECTS IN THE ELECTRONIC STRUCTURE OF Cu(001)

S.C. Wu, C.K.C. Lok, J. Sokolov, J. Quinn, Y.S. Li, D. Tian and F. Jona
(SUNY, Stony Brook)

Measurements on clean Cu(001) with pure s-polarized light in the range from 13 to 40 eV show evidence for direct transitions from the Δ_2 band, which are forbidden by the dipole selection rules. If the spin-orbit interaction could be neglected, only states which are even (Δ_1 symmetry) or odd (Δ_5 symmetry) under the vertical mirror planes could be observed in normal emission. With the z axis perpendicular to the surface the orbitals that belong to Δ_1, are s, p_z and d_{z^2} and the orbitals that belong to Δ_5 are p_x, p_y, d_{xz} and d_{yz}. The Δ_1 states would be observed when the electric field of the incident light is normal to the surface (p polarization), and the Δ_5 states would be observed when the electric field lies in the plane of the surface (s polarization). The other orbitals (Δ_2 and Δ_2 ,) would not contribute to the normal emission. However, addition of the spin-orbit interaction mixes the Δ_2 and the Δ_2 , into the Δ_5 states, and the resulting symmetry label is conventionally written Δ_7, while the Δ_1 states are labelled Δ_6. The relativistic selection rules allow transitions from initial Δ_7-symmetry states to final Δ_6-symmetry states for pure s-polarized radiation. Our data show clear evidence for these transitions. We measured energy values for special points at the center of the Brillouin zone and find them in good agreement with the relativistic calculations of Eckardt et al.[1] (see Table).

Symmetry label	This work	Eckardt et al.[1]
Γ_{8+}	-2.85± 0.10 eV	-2.86 eV
Γ_{7+}	-3.40± 0.10 eV	-3.45 eV
Γ_{8+}	-3.70± 0.10 eV	-3.65 eV

[1] H. Eckardt, L. Fritsche and J. Noffke, J. Phys. F 14, 97 (1984).

This work was supported by the U.S. Department of Energy under Contract No. DE-AC002-76CH00016.

SOFT X-RAY ABSORPTION OF THIN POLYMER FILMS

Jeffrey Colbert (Instrumentation Division), Daniel A. Fischer (NSLS/Exxon PRT)

In the development of gaseous detectors of soft x-rays for absorption spectroscopy, it is important to use correct window materials for the photon energy region of interest. We have begun to study a selection of candidate materials. The proposed windows must be strong enough to withstand the pressure differentials of use, be free of defects or pinholes which would leak counter gas and be thin enough to pass detected radiation with minimal loss. For fluorescence yield near-edge spectroscopy (FYNES) of ultra-soft x-rays, a window should preferably have maximal transmission to the fluorescence radiation of carbon, nitrogen and oxygen. High contrast at an absorption edge is beneficial, since unwanted scattered radiation above the edge, unrelated to the sample absorption, can be suppressed by the detector window.

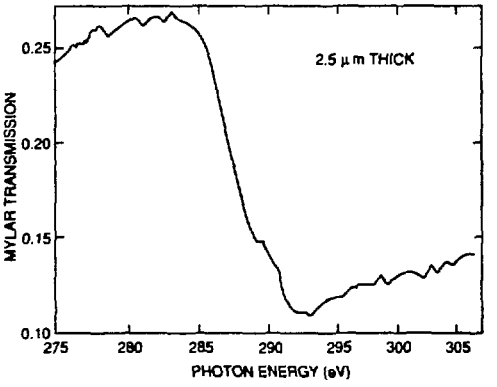

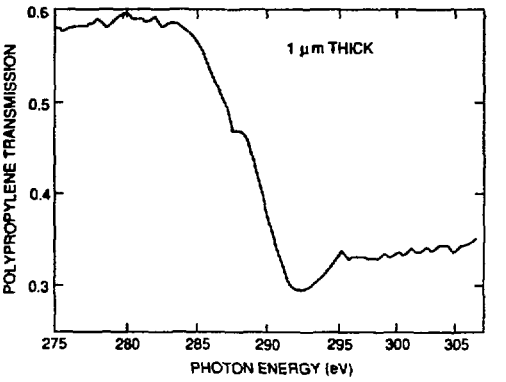

These figures show the absolute transmission measured for samples of 1 μm thickness polypropylene and 2.5 μm mylar around the absorption edge of carbon using the zone plate monochromator. For fluorescence rays just below the edge, the polypropylene transmission is clearly superior. Contrast at the edge is unexpectedly somewhat low, perhaps due to higher order contamination in the incident beam.

*This research was supported by the U. S. Department of Energy: Contract No. DE-AC02-76CH00016.

MICROSCOPIC STRUCTURE OF THE SiO_2/Si INTERFACE

F. J. Himpsel, F. R. McFeely, A. Taleb-Ibrahimi, J. A. Yarmoff, IBM Research Division, T. J. Watson Research Center, Yorktown Heights, NY 10598, G. Hollinger, Laboratoire d'Electronique Automatique, Ecole Centrale de Lyon, F 69131 Ecully Cedex, France

The structure of the SiO_2/Si interface has been elusive despite many efforts to come up with models. Several structural models have been proposed for the SiO_2/Si(100) interface. Most of them assume an atomically abrupt interface. We have studied the distribution of intermediate oxidation states (Si^{1+}, Si^{2+}, Si^{3+}) at the interface using core level spectroscopy. From our data, we can exclude abrupt interface models, since they cannot explain the large portion of Si^{3+} observed at the interface. For a truncated bulk structure, for example, one would obtain only Si^{2+}, since there are two broken bonds per surface atom. Recent calculations by Ohdomari, et al. have arrived at an extended interface model for SiO_2/Si (100) by minimizing the strain energy. This model is found to be in good agreement with our data. It is not unique, though. A new model is proposed for SiO_2/Si(100) based on the observed distribution and intensity of intermediate oxidation states. Both models are characterized by an extended interface, with protrusions of Si^{3+} reaching about 3Å into the SiO_2 overlayer. These protrusions may be viewed as the cores of misfit dislocations, which take up the large mismatch in the Si atom density (a factor of 2 between Si and and SiO_2).

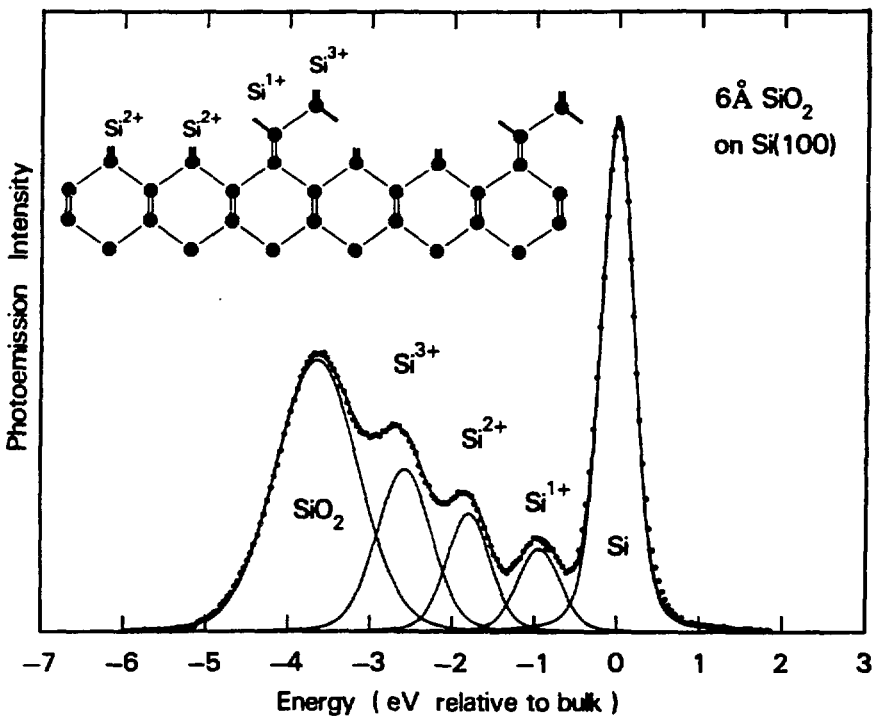

Silicon $2p_{3/2}$ core level spectrum and structural model of the SiO_2/Si(100) interface. The amorphous SiO_2 lattice is omitted.

INTERFACE CHEMISTRY OF MBE-GROWN POLYMER FILMS ON METALS

Jean L. Jordan-Sweet and Steven P. Kowalczyk

IBM Research Division, T.J. Watson Research Center
Yorktown Heights, NY 10598

The interface chemistry of electropositive metals and polyimide (poly(pyromellitimido oxydianiline)) is of great interest to the microelectronics industry because of the potential applications for metal-insulator multilayer structures. There are two inequivalent processes involved in the formation of multilayers: the deposition of a metal onto a cured polyimide surface, and the deposition and subsequent curing of polyamic acid on a metal surface. The former process has been studied quite extensively in the past several years, using techniques such as XPS, UPS, EELS, FTIR, NEXAFS and solution model studies. Very recently a method has been developed for co-depositing the monomers of polyamic acid (pyromellitic dianhydride and oxydianiline) ***in vacuo*** onto substrate surfaces. We report results of a synchrotron photoemission and NEXAFS study of MBE-grown polyamic acid on copper and chromium surfaces. Data were taken at Beamline U8 of the National Synchrotron Light Source*.

Results for the case of polyamic acid on copper show that there is no severe alteration of the polymer's structural integrity due to interaction with the metal. The C 1s and O 1s spectra show less intensity than expected, which indicates that the carbonyl groups are affected by the copper surface. Upon annealing, these peaks remain depleted and a relatively electron-rich peak appears in the N 1s spectrum which may be attributed to isoimide formation.

When a small amount (approximately a monolayer) of polyamic acid is deposited on chromium, both XPS and NEXAFS spectra show a severe depletion of carbonyl groups and appearance of oxide. After annealing, the spectra change drastically due to the formation of carbide, oxide and nitride species. As thicker layers of polyamic acid are deposited, this reacted interface becomes buried and the XPS and NEXAFS spectra resemble those of bulk polyamic acid and, when annealed, polyimide. The spectra for the chromium case are strikingly similar to those for chromium deposited on spun polyimide films.

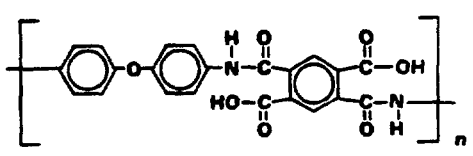

POLYAMIC ACID

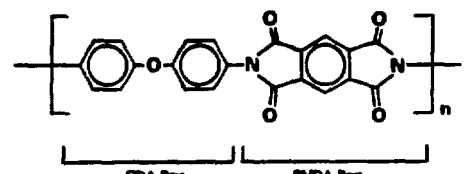

POLYIMIDE

PHOTOEMISSION SPECTROSCOPY OF THE SiO2/Si INTERFACE - CROSS SECTION MODULATIONS I

F. R. McFeely, B. Robinson, IBM T. J. Watson Research Center, Yorktown Heights, NY 10598, J. A. Yarmoff and S. Joyce National Bureau of Standards, Gaithersburg Md.

The structure of SiO2/Si interfaces continues to be a subject of active research interest. Photoemission spectroscopy is a valuable method for the investigation of this interface, owing to its ability to determine the oxidation state distribution in the interface region. This provides a stringent test for structural models of the interface. However, in order to correctly interpret the photoemission data it is necessary to understand both the depth-dependent attenuation of the photoemission intensity and the inherent photoelectric cross section variations among the interface oxides. In this experiment we measured the photoelectron escape depth through SiO2 by meauring the ratios of bulk Si to SiO2 Si 2p photoemission intensity for two different thicknesses of oxide. This method is independent of the relative photoelectric cross sections of the two materials, which are, in fact, quite variable.

The figure below shows the the escape depths determined by this analysis. The curve bears little resemblence to the "universal curve" of escape depths. Short escape depths occur both at around 35 eV, due to plasmon losses, and at low energy, where the excitation of LO phonons is the dominant loss mechanism.

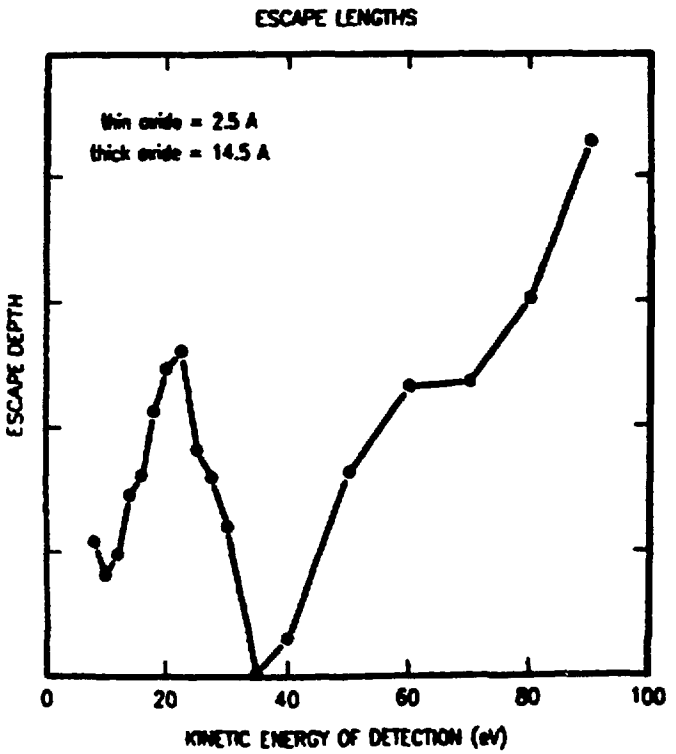

PHOTOEMISSION SPECTROSCOPY OF THE SiO2/Si INTERFACE - CROSS SECTION MODULATIONS II

F. R. McFeely, B. Robinson, IBM T. J. Watson Research Center, Yorktown Heights, NY 10598, J. A. Yarmoff and S. Joyce National Bureau of Standards, Gaithersburg Md.

The structure of SiO2/Si interfaces continues to be a subject of active research interest. Photoemission spectroscopy is a valuable method for the investigation of this interface, owing to its ability to determine the oxidation state distribution in the interface region. This provides a stringent test for structural models of the interface. However, in order to correctly interpret the photoemission data it is necessary to understand both the depth-dependent attenuation of the photoemission intensity and the inherent photoelectric cross section variationsamong the interface oxides. Only with this knowledge can the relative concentrations of the interface oxide species be inferred from the photoemission peak intensities. In this experiment we measured the relative intensities for the inermediate oxide species as a function of kinetic energy of detection from 6-80 eV. A CFS technique was employed to insure that there were no escape-depth effects within a given spectrum. The results, plotted below, indicate that there are substantial variations in the photoelectic cross section among the three species, and that analyses of the interface strcture which fail to take this into account are incorrect.

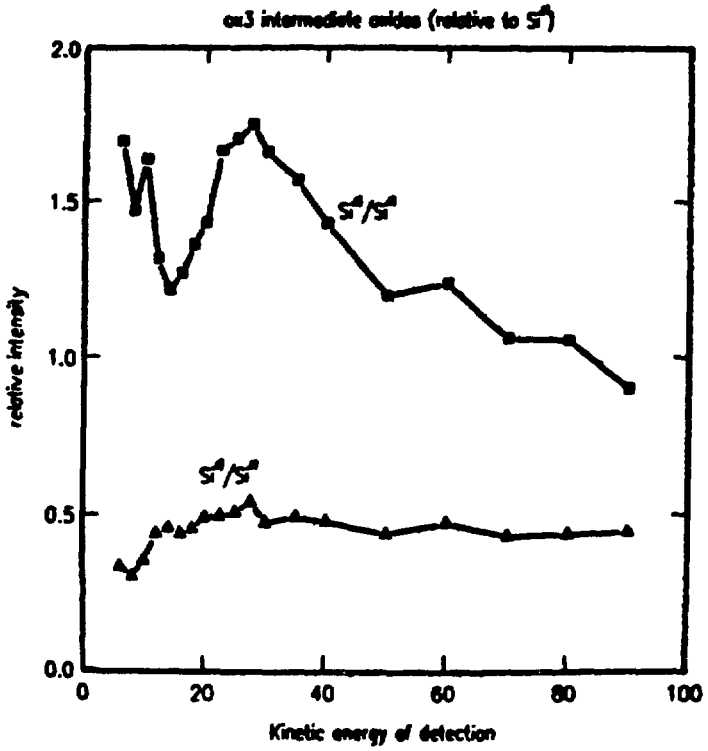

PHOTOELECTRON SPECTROSCOPIC STUDY OF THE Mn/MoS_2(0001) INTERFACE* U8B

J.R. Lince, T.B. Stewart, M.H. Hills, P.D. Fleischauer (Aerospace**),
J.A. Yarmoff (NIST), and A. Taleb-Ibrahimi (IBM)

Metal/semiconductor interfaces formed by the deposition of thin metal films on MoS_2(0001) surfaces exhibit interesting chemical and electronic properties that result from the anisotropic, layered structure of MoS_2.[1,2] We have conducted a study of a particularly reactive metal, Mn, on MoS_2(0001), using high-resolution core level and valence band photoelectron spectroscopies (CLPS and VBPS, respectively) at beamline U8-B.

All Mn depositions were done on MoS_2(0001) surfaces that exhibited good quality 1X1 LEED patterns, and no carbon, oxygen, or other contamination as seen by CLPS. Spectra for the Mo-3d and S-2p core levels were taken with a photon energy of 300 and 230 eV, respectively, resulting in a photoelectron kinetic energy of ~70 eV for both Mo and S photoelectrons.

In general, the Mo-3d, S-2p (see Fig. 1) and Mn-4p core level (not shown) results are consistent with Mn interacting with MoS_2(0001) via the following reaction:

$$Mn + \frac{1}{2}MoS_2 \rightarrow MnS + \frac{1}{2}Mo$$

The persistence of the substrate components of the Mo-3d and S-2p spectra (see Fig. 1 spectra c and g) for thicknesses >35 Å are consistent with the Volmer-Weber growth mode, i.e. three-dimensional island growth. Valence band spectra were similar to that for Mn metal[3] (see Fig. 2d) indicating that the reaction was incomplete at room temperature. The partially reacted layer (i.e. Mn+MnS+Mo) formed an abrupt interface with the remaining unreacted substrate (see Fig. 2b).

The reaction was driven by annealing ~50-~58 Å Mn films on MoS_2(0001) to temperatures in the range 770 K- 1040 K. Analysis of the core levels after annealing to 770 K (not shown) indicated that the MoS_2 substrate surface is sulfur-deficient,[3] while valence band spectra (see Fig. 2e) showed that some unreacted Mn exists in an overlayer consisting mostly of MnS. The reaction was driven to completion by annealing to temperatures ≥850 K (see Fig 2, spectra *f-i*). Annealing to temperatures ≥1130 K resulted in the formation of a MoS_2(0001)-2x2 LEED pattern. This LEED pattern, along with the CLPS data, indicates the presence of a sulfur-vacancy-defect surface structure, rather than a Mn-Mo-S compound.

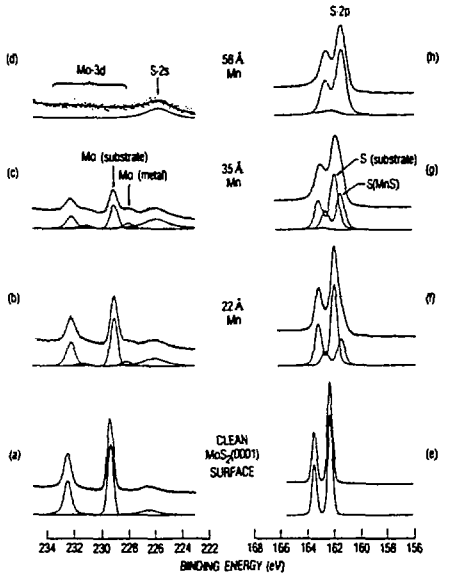

Figure 1. Mo-3d and S-2p core level spectra during various stages of Mn deposition on the MoS_2(0001) surface.

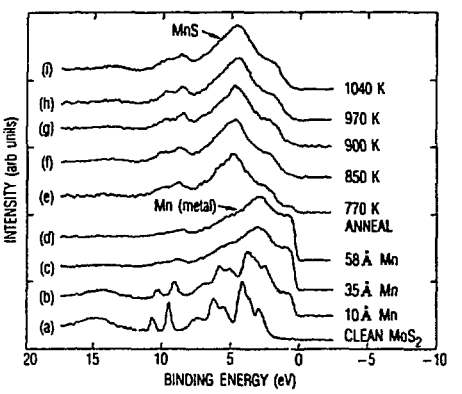

Figure 2: Valence band spectra ($h\nu$ = 152 eV) during deposition of Mn on the MoS_2(0001) surface and annealing of a 58 ÅMn film. The two peaks visible at ~9-11 eV result from the S-2p core level doublet produced by second-order light from the monochromator.

*Supported by the Air Force Space Division under contract number F04701-85-C-0086-P00016 and by DOE- Dept. of Materials Science.
**Aerospace Corp., P.O. Box 92957, Los Angeles, Calif., 90009
[1] J.R. Lince, D.J. Carré, and P.D. Fleischauer, Phys. Rev. B 36 (1987) 1647.
[2] I.T. McGovern, E. Dietz, H.H. Rotermund, A.M. Bradshaw, W. Braun, W. Radlik, and J. F. McGilp, Surf. Sci. 152/153(1985) 1203.
[3] H. F. Franzen, and C. Sterner, J. Solid State Chem. 25 (1978) 227.

DELOCALIZATION AND SCREENING EFFECTS AT METAL-SEMICONDUCTOR INTERFACES

R. Ludeke, A. Taleb-Ibrahimi and G. Jezequel (IBM)

The role of metallic screening on metallic behavior was investigated by initially " pinning " GaAs surfaces with transition metal atoms and then monitoring further changes in Fermi energy as Ag is deposited. Downward motion of the Fermi level is correlated with the onset of metallic behavior of the Ag for both n and p-type GaAs. Similar dependencies during Schottky barrier formation have previously been observed, but lacked a satisfactory explanation. We now attribute these effects to delocalization of the "pinning" interface states as these overlap the metallic states upon formation of the metallic state. We describe this situation in terms of a broadening of the defect level. If this level is charged a lowering of its energy due to screening effects may accompany the broadening. We performed a calculation based on a modified Newns-Anderson formalism and estimated a shift in Fermi level comparable to 130 meV observed experimentally. Most of this shift is due broadening, the screening contributions being almost negligeable because of the low average charge density per defect site.

2p-3d INTERSHELL INTERACTIONS IN THE 3d TRANSITION METALS U8B

DATE OF EXPERIMENT: from: Feb 1 to: Feb 9,88

EXPERIMENTER(S):	AFFILIATION:
V. Murgai	Boston University
Young-Sea Huang	Boston University
M.L. denBoer	Hunter College

WORK SPONSORED BY:

We have performed XAS measurements at the $L_{III,II}$ edges of evaporated polycrystalline samples of the middle 3*d* transition metals: V, Cr, Mn, and Fe. (See Fig. 1. The first maximum in intensity of the L edges have been aligned). Sample cleanliness was monitored by doing CFS scans over a wide energy range ($h\nu$ = 260 to 860 eV). No traces of carbon or oxygen were found except possibly some oxygen on the V. As expected and in agreement with EELS results[1], we find that the expected statistical intensity ratio of 2:1 for the $2p_{3/2}$:$2p_{1/2}$ peaks is not reached before Fe. There are some qualitative differences with respect to the EELS measurements particularly in V where EELS results have an extra low energy shoulder. For V we also meausred valence band EDCs in the vicinity of the 2*p* edges and find that the 3*d* cross-section undergoes a Fano like resonance.

1. J. Fink, Th. Müller-Heinzerling, B. Scheerer, W. Speier, F.U. Hillebrecht, J.C. Fuggle, J. Zaanen, and G.A. Sawatzky, Phys. Rev. B **32**, 4899 (1985).

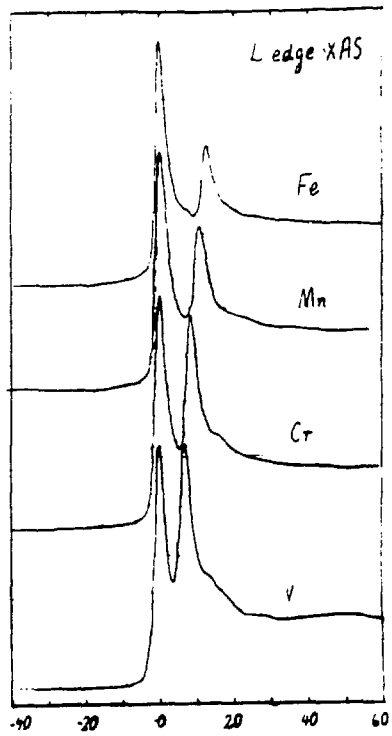

THE ANNEALED Sb/GaAs(110) INTERFACE

A. Taleb-Ibrahimi, R. Ludeke and G. Jezequel (IBM)

High resolution photoelectron spectroscopy has been used to study the influence of thermal annealing of the Sb/GaAs interface. Detailed spectral analysis of core level and valence band emission of both adsorbate and substrate show drastic changes of the interface morphology and the related electronic structure after annealing. In contrast to prevailing assumptions, room temperature (RT) does not lead to perfectly ordered growth of the first monolayer (ML). Annealing at 300 °C results in a highly ordered growth overlayer that is desorption limited to 1ML. This high degree of epitaxial perfection is characterized by the presence of occupied Sb derived states that reduce the Fermi level (E_f) pinning position for p-type GaAs to a value of ≅280 meV above the valence band maximum as compared to .6 eV at RT. On n-type GaAs the barrier height is slightly increased from .58 eV below the conduction band minimum at RT to .7 eV after annealing. This observation suggests the presence of an emty band of states in the gap in agreement with recent inverse photoemission results of Drube and Himpsel.

ROLE OF Ga IN THE FORMATION OF REACTIVE INTERFACES

A. Taleb-Ibrahimi, G. Jezequel, and R. Ludeke (IBM)

Ga is essentially the only reaction product observed during the metallization of GaAs with reactive metals. Since Ga has been reported to form a Schottky barrier, the role of the two metals in the barrier formation process cannot be separated a priori. To understand the role of elemental Ga, we have reexamined the Ga/GaAs(110) interface. The observed constancy of the Fermi level position over a broad range of Ga coverage suggests that a unique donor level at 250 meV above the valence band maximum is formed for submonolayer coverages. In contrast, reactive metals generate donor levels on p-type GaAs which lie substantially higher in the gap than the Ga donor level. From this observation we conclude that the Ga does not play a major role in the formation in the Schottky barrier formation process of reactive metals on GaAs. Furthermore, its low miscibility with many metals at RT suggests that the exchanged Ga is swept away from the interface as the thickness of the overlayer increases. The notion of such a "snowplow" effect is supported experimentally as well.

Refractive Index Measurements of Amorphous Carbon Near its K Edge

Eberhard Spiller

IBM T. J. Watson Research Center Yorktown Heights, NY 10598, USA

A zone plate monochromator with free-standing zone plates does not suffer from the contamination problem of mirror optics and can therefore be used at the carbon edge. The position of the reflectivity maximum of a multilayer mirror is slightly shifted from the position defined by the Bragg condition due to refraction and this shift can be used to determine the effective index of the materials within a multilayer mirror. Last summer we obtained the refractive index of carbon in the $\lambda = 42 - 50$Å range by analyzing the reflectivity curve of a 140-layer Co-C multilayer mirror with a period of 32.1 Å. We have now fabricated coarser coatings which show a larger shift in the position of the reflectivity maxima (50 layer Co-C, period 72.2 Å, thickness ratio C/Co 2:1) and measured the reflectivity versus angle of incidence curves for wavelengths in the 43-58 Å range. The refractive indices obtained are given in Fig. 1 and are in excellent agreement with the data of Henke et al.[1]. We used an adjustment in the zero of the angle-scale to produce agreement between our measurments and Henke's data for $\lambda = 58$Å. Corrections due to absorption and due to the roughness of the boundaries are included in the analysis of the data.

1. B.L. Henke, P. Lee, T. J. Tanaka, R. L. Shimabukuro and B. K. Fujikawa, AIP Proc. 75, 340, (1981), Atomic Data and Nucl. Tables 27,1,(1982).

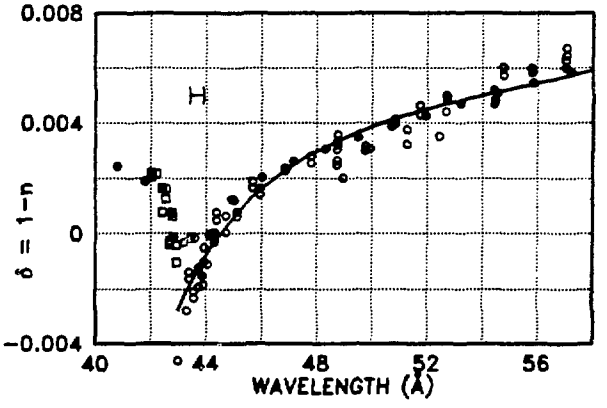

Fig.1. Refractive index of amorphous carbon near the carbon edge. Open circles represent data obtained from the mirror with 72.2 Å period, open squares are obtained from the mirror with 32.1 Å period, and the full circles are obtained from the absorption values using Kramers Kronig analysis and given in Ref. 1

Resolution Test of the Zoneplate Monochromator with "High Brightness" beam

Eberhard Spiller

IBM T. J. Watson Research Center Yorktown Heights, NY 10598, USA

The zone plate monochromator was tested with "High Brightness" beam in March 1988. It was hoped that with a source size of 0.1mm we could approach the theoretical resolution of $E/\Delta E > 1000$. However, very little improvement in the resolution was observed and the same spectra were obtained with normal beam on the day between the two "high brightness" nights. The resolution corresponds to a source size of 0.5mm. The beam monitor at U5 showed a reduction in the source size from 0.5 to 0.3mm during the night and this reduction should have resulted in a corresponding improvement in resolution. The reason for the failure could be either in the quality of the zone plates or in the beam size at U8. We will have to use an independent beam size monitor at U8 in order to decide between these possibilties.

Fluorescence Measurements in Rare-Gas Matrix Isolated Smaller Hydrocarbons

R. A. Holroyd and J. M. Preses

Chemistry Department, Brookhaven National Laboratory, Upton, NY 11973

The unique features of synchrotron radiation make it very suitable for studies of weakly fluorescing species with short lifetimes. Previous experiments in this program have revealed detailed information about gas, liquid, solid, and matrix isolated hydrocarbons such as cyclohexane and tetramethylethylene. Hydrocarbons with fewer than 4-5 carbon atoms have been observed to fluoresce only weakly, if at all, near room temperature. Since low temperature enhances the fluorescence quantum yield in such molecules, rare gas matrix studies of smaller hydrocarbons may produce the greater experimental sensitivity required to examine the details of electronic relaxation in these molecules. The behavior of smaller hydrocarbons is of interest because of the greater tractability of their spectra, and the better ability to describe the observations theoretically.

A series of experiments has been performed, studying the lifetimes, excitation spectra, and fluorescence spectra of argon isolated n-pentane and n-butane, and neat pentane, as functions of temperature in the range 20 - 100 K. Strong fluorescence signals have been obtained, including the first direct measurement of the fluorescence lifetime of butane. Shifts in the excitation spectra and the appearance of new features have been observed as functions of temperature. Observed lifetimes also change with temperature. The effects may be due to reversible or irreversible formation of aggregates or conversion of conformers. Fig. 1 is a plot of a typical butane lifetime in Ar. Fig. 2 is a fluorescence spectrum of butane in Ar.

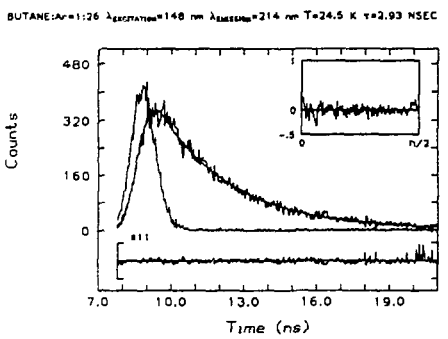

Figure 1

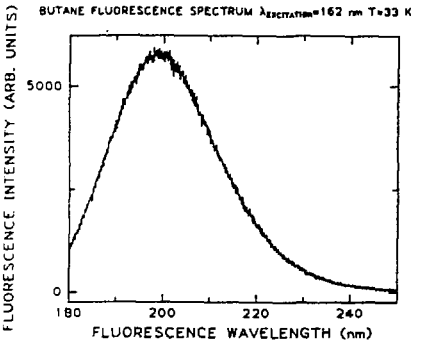

Figure 2

Acknowledgement: This research was carried out at Brookhaven National Laboratory under Contract No. DE-AC02-76CH00016 with the U. S. Department of Energy and supported by its Division of Chemical Sciences, Office of Basic Energy Research.

Fluorescence Lifetime of the 1 $^2\Sigma_u^+$ and 2 $^2\Sigma_u^+$ excited states of Cl_2

J.B. Nee[1], J.M. Preses[2], and R.E. Weston, Jr.[3]

1. Department of Physics, National Central University, Chung-Li, Taiwan 32054
2. Department of Chemistry, Brookhaven National Laboratory, Upton, NY 11973

Recently the strong fluorescence from the high lying ion-pair excited states of chlorine molecule have been investigated extensively. By using techniques of synchrotron radiation spectroscopy, Moeller et al.[1] and Wormer et al.[2] studied the 1 $^2\Sigma_u^+$ and 1 $^2\Sigma_u^+$ excited states by measuring the photoabsorption and fluorescence spectrum. Strong interaction of valence and Rydberg excited states have been observed.

In this experiment, we used the apparatus at the beamline U9A to measure the radiative lifetime of the 1 and 2 excited states. This is interesting since with a tunable source we may be able to excite the Cl_2 at various wavelengths and observe the variation of radiative decay rate.

Chlorine molecule with pressure 7-200 mTorr was introduced into a static cell with LiF entrance window. Fluorescence following the excitation in the wavelength range 124-127 and 134-149 nm was observed with a fast photomultiplier tube combined with an interference filter centered at 206 nm. Signals were processed with the technique of single photon counting time correlation spectroscopy, which has been previously published in detail[3].

Fluorescence lifetime obtained at various pressure ranges and resolutions at several wavelengths within the photoabsorption of the 1 and 2 excited states are shown in Table 1. What we have observed is an average lifetime of 2.11nS for the $1^2\Sigma_u^+$ excited state at wavelengths 133-149 nm, and an average lifetime of 2.78nS for the 2 excited state at 124-127 nm region. The radiative lifetime does not vary with excitation wavelength.

It is known from previous studies that the fluorescence spectra for the 1 and 2 excited states are similar. This is because a rapid internal conversion of the 2 excited state to 1 excited state resulted following the photoexcitation of the 2 state. The fluorescence in the 206 nm region corresponds to the bound-to-free emission from the 1 excited state to the outer dissociative region of ground electronic state. The difference in fluorescence lifetime obtained here should therefore be related to the time difference in populating the 1 excited state.

Acknowledgement

This experiment was conducted at the National Synchrotron Light Source which is supported by the US Department of Energy under contract number DE-AC02-76CH00016 from Division of Chemical Science and the Office of Basic Energy.

Reference

1. T. Moeller, B. Jordan, P. Gurtler, G. Zimmerrer, D. Haaks, J. LeCalve, and M.C. Castex, Chem. Phys. 76, 295, 1983.
2. J. Wormer, T. Moeller, J. Stapefeldt, G. Zimmerrer, D. Haaks, S. Kampf, J. LeCalve, and M.C. Castex, Z. Phys. D-Atoms, Molecules and Clusters 7, 383, 1988.
3. M.A. Wickramaaratchi, J.M. Preses, R.A. Holroyd, and R.E. Weston, Jr, J. Chem. Phys. 82, 4745, 1985.

Table 1. Radiative lifetime studied at various wavelengths, pressure ranges, and monochromator resolutions.

Wavelength nm	Pressure m/Torr	Resolution nm	Lifetime nS
124	57	1.3	3.03
125	45-55	1.3	2.71
126	38-60	1.3	2.63
133	38	1.3	2.18
134	36	0.85	2.28
136	7-92	0.85/1.3	2.07
138	33	1.3	2.11
141	38-65	1.3	1.97
149.3	200	1.3	2.24

THE FLUORESCENCE LIFETIME OF EXCITED CYCLOHEXANE IN AN ARGON MATRIX AND IN SOLID STATE CYCLOHEXANE AT LOW TEMPERATURE

Jack M. Preses, Chemistry Department, Brookhaven National Laboratory, Upton, NY 11973

Previous work in this program[1-3] has elucidated mechanisms for electronic energy relaxation in gas, liquid, and solid hydrocarbons using single-photon time correlation fluorescence spectroscopy to determine lifetimes of electronically excited states as functions of pressure, excitation wavelength, and quencher gas pressures. One common feature of these experiments has been the observation that fluorescence quantum yields increase toward lower temperatures. Measurements at cryogenic temperatures should, therefore, be subject to increased experimental sensitivity due to higher fluorescence intensity. However, saturated and unsaturated hydrocarbons condense close to room temperature, so that low temperature experiments cannot be performed using neat liquid or solid hydrocarbons without encountering the difficulties engendered by high molecular concentrations, such as strong intermolecular interactions and very high extinction coefficients. These disadvantages can be overcome by forming a cryogenic matrix consisting of a low concentration of hydrocarbon trapped in a solid rare gas.

The fluorescence lifetime of a few molecular percent of cyclohexane trapped in argon was studied as a function of temperature, cyclohexane concentration, and excitation wavelength. The behavior of the lifetime compares with that observed from gas phase cyclohexane rather than liquid phase cyclohexane. This result supports the idea of such a matrix approximating the relative weakly interacting environment of the gas phase rather than the strongly interacting environment of the liquid phase.

Experiments were also carried out to measure the fluorescence lifetime of neat cyclohexane at low temperature, in order to extend the range of the determination of the "activated" and "nonactivated" components of the cyclohexane relaxation. Lifetime measurements at 67 K added to the previous ones made near room temperature yield an expression of the form:

$$\frac{1}{\tau} = k_o + Ae^{-E_a/RT}$$

for the temperature dependence of the rate constant for the decay of cyclohexane fluorescence, where $k_o = 4.1 \times 10^8\ s^{-1}$, $A = 8.8 \times 10^{11}\ s^{-1}$, and $E_a = 4.1$ kcal mol^{-1}.

Further experiments are planned which exploit the greater sensitivity of the matrix method in order to explore the behavior of the fluorescence lifetimes of smaller saturated and unsaturated hydrocarbons, some of which have not been previously observed to fluoresce.

1. M. A. Wickramaaratchi, J. M. Preses, R. A. Holroyd, and R. E. Weston, Jr., J. Chem. Phys. 82 (1985) 4745

2. M. A. Wickramaaratchi, J. M. Preses, and R. E. Weston, Jr., J. Chem. Phys. 85 (1986) 2445

3. J. M. Preses, J. Chem. Phys. 89 (1988) 1251

Acknowledgement

This Research was carried out at Brookhaven National Laboratory under Contract No. DE-AC02-76CH00016 with the U.S. Department of Energy and supported by its Division of Chemical Sciences, Office of Basic Energy Sciences.

TIME-RESOLVED FLUORESCENCE STUDY OF VUV LIGHT INDUCED REACTIONS U9A

J. J. Tiee (LANL), C. R. Quick (LANL), D. Hof (LANL), and J. M. Preses (BNL)

Interest in high power excimer lasers in recent years has prompted several studies of light induced reactions between rare gas atoms and halogen containing molecules.[1] Much of this work was aimed at understanding the kinetic processes that are relevant to excimer laser systems, namely, reactive mixtures of Cl_2 and HCl with Ar, Kr, and Xe.[2] In an effort to better understand gas-phase excited state dynamics, we have initiated a set of experiments to investigate the vuv photochemistry of several polyatomic species. The main thrust of the current experiment was to examine the reaction dynamics of vuv light induced reactions. The specific systems of interest are the excited excimer forming reactive mixtures of Xe or Kr with Cl_2, HCl, CCl_4, $COCl_2$, COFCl, CF_3X (X = Cl, Br, I), and C_2N_2. The particular emphasis was directed at elucidating the importance of state-specificity in the electronic excitation of the reactive processes concerning critical elements such as internal energy contents, branching ratios, and quantum efficiency. We have determined that the quantum efficiency and branching ratios in forming excited products were directly related to the lifetimes of the excited states of the reactants and the energetics of the resultant products. In some cases, it appeared that some enhancement in excited excimer formation could occur due to either (1) longer-lived intermediates or (2) particular character of electronic states involved. In addition, it was demonstrated that the vuv excitation technique could be used as a selective means for producing novel excimers, allowing their characterization and identification. An example of this was the observation of an excited (Xe-C_2N_2) complex. In our preliminary study, an emission band near 376 nm was produced when a mixture of Xe and C_2N_2 was photolyzed at 147 nm.
Preliminary experiments were carried out to extend the gas-phase work to condensed media, specifically, in rare-gas solid matrices. This allows us to better characterize the charge transfer reaction dynamics of halogenated compounds in a more isolated enviornment and provides useful information concerning condensed phase photochemistry of novel molecular complex formed in low temperature matrices due to many-body interaction[3]. We were beginning to examine the formation of van der Waals complexes that occurred in both Ar and Xe host matrices.
One other experimental study was also conducted to determine the feasibility of implementing a technique of using a high power laser as the excitation source and probing the end product with the synchrotron light radiation. A quadrupled Nd:YAG laser at 266 nm (0.5 mJ/pulse at 10 Hz) or a KrF excimer laser (20 mJ/pulse at 50 Hz) was used to dissociate CF_3I to produce CF_3 radicals and the synchrotron light in the region of 140-160 nm was used to probe the CF_3 radicals. The high scattered laser light background obscured CF_3 emission near 230 nm. A modified optical arrangement which minimizes the scattered light problem will be tested in a future experimental run.

[1] J. K. Ku and D. W. Setser, Appl. Phys. Lett. 48, 689 (1986)
[2] V. S. Zuev, A. V. Kanaev, and L. D. Mikheev, Sov. JQE 14, 242 (1984)
[3] M. E. Fajardo and V. A. Apkarian, J. Chem. Phys. 85, 5660 (1986)
NOTE: This work is sponsored by the Los Alamos National Laboratory

TITLE OF EXPERIMENT: VUV Photofragmentation and Light Induced Reaction

BEAM LINE: U9A DATE OF EXPERIMENT: from: 12/11/87 to: 12/19/87

EXPERIMENTER(S):	AFFILIATION:
J. J. Tiee, C. R. Quick, and D. E. Hof	Los Alamos National Laboratory
J. Preses and R. Weston	Brookhaven National Laboratory

WORK SPONSORED BY: Los Alamos National Laboratory

In an effort to better understand gas-phase excited state dynamics, we have initiated a set of experiments to investigate the vuv photochemistry of several polyatomic species. The main thrust of the current experiment was to examine the reaction dynamics of vuv light induced reactions. The specific systems of interest are the excited excimer forming reactive mixtures of Xe or Kr with Cl_2, HCl, CCl_4, $COCl_2$, COFCl, CF_3X (X = Cl, Br, I), and C_2N_2. The particular emphasis was directed at elucidating the importance of state-specificity in the electronic excitation of the reactive processes concerning critical elements such as internal energy contents, branching ratios, and quantum efficiency. It was determined that the quantum efficiency and branching ratios in forming excited products were directly related to the lifetimes of the excited states of the reactants and the energetics of the resultant products. In some cases, it appeared that some enhancement in excited excimer formation could occur due to either (1) longer-lived intermediates or (2) particular character of electronic states involved. The high sensitivity detection of some atomic and molecular species was also achieved by monitoring the fluorescence from vuv light induced reactions. In addition, it was demonstrated that the vuv excitation technique could be used as a selective means for producing novel excimers, allowing their characterization and identification. An example of this was the observation of an excited (Xe-C_2N_2) complex. In our preliminary study, an emission band near 376 nm was produced when a mixture of Xe and C_2N_2 was photolyzed at 147 nm. This is shown in contrast to the CN (B-X) emission when the mixture was excited at 128 nm (see Figure).

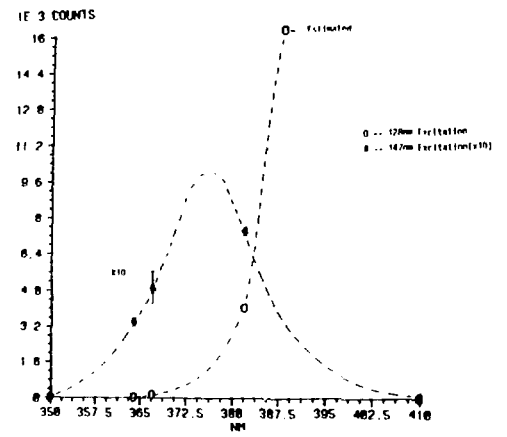

One other experimental study was also conducted to determine the feasibility of applying an excitation and probe technique with a high power laser. A quadrupled Nd:YAG laser at 266 nm (0.5 mJ) was used to dissociate CF_3I to produce CF_3 radicals and the synchrotron light in the region of 140-160 nm was used to probe the CF_3 radicals. The high scattered laser light background obscured CF_3 emission near 230 nm. A modified optical arrangement which minimizes the scattered light problem will be tested in a future experimental run.

The Vacuum Ultraviolet Circular Dichroism Spectra of Poly (dC)[1]

M.C. Armijo, J. Trunk, and J.C. Sutherland,
Brookhaven National Laboratory

The secondary structure of a synthetic double stranded DNA, polydeoxycytidylic acid [Poly (dC)] was studied as a function of pH by circular dichroism (CD) spectroscopy in the 180 - 330 nm wavelength region (figure 1). Conformational changes associated with differing degrees of hydrogen-bonding in the DNA at pH = 6.5 and 8.5 were reflected in the CD spectra. These are the first CD spectra of Poly (dC) obtained below the limits of commercial instrumentation and the structural changes are particularly noticeable in the previously unstudied 190 - 210 nm region.

The sample solution consisted of Poly (dC) (obtained from Sigma Chemical Co.) dissolved in a phosphate buffer which was composed of a mixture of potassium mono- and potassium di-hydrogen phosphate. Because Poly (dC) would not dissolve under acidic conditions but readily did so in basic solutions, the pH = 6.5 sample was prepared by adding HCl to a pH = 8.5 solution of already dissolved Poly (dC). All spectra were recorded in a 0.1 mm path length quartz sample cell.

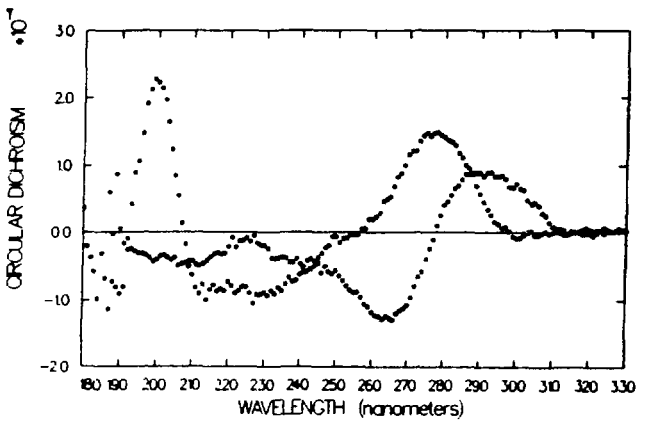

Figure 1. The circular dichroism spectra of Poly (dC) at pH = 8.5 (solid circles) and pH = 6.5 (open circles).

---

[1]Research supported by the Office of Health and Environmental Research, United States Department of Energy and a grant from National Institutes of Health (GM35662).

CIRCULAR DICHROISM (CD) STUDIES OF TFIIIA AND ITS NUCLEIC ACIDS INTERACTIONS

W.-J. Huang (SUNY,Stony Brook), Z. Shang (SUNY, Stony Brook), C.-W. Wu(SUNY, Stony Brook), F.Y.-H. Wu (SUNY, Stony Brook)

Transcription factor IIIA (TFIIIA of Xenopus oocytes is the first purified protein factor (38-Kd) which is necessary for the accurate transcription of a purified eukaryotic gene, the 5S RNA gene. The transcriptional regulation of the 5S RNA gene involves the specific binding of TFIIIA to the intragenic control region (ICR), and along with other factors, directs RNA polymerase III to initiate the 5S RNA synthesis upstream from the ICR. TFIIIA binds the gene product, 5S RNA, to form a 7S particle. We have previously shown that TFIIIA is a Zn-metalloenzyme, i.e. a DNA-activated ATPase, containing 2 Zn ions/mol protein. Based on amino acid sequence analysis, TFIIIA has been suggested to be composed of 9 repeated, linked, loop-like domains, each enclosing a Zn atom at its base for conformational stabilization, and these "Zn fingers" may be involved in DNA binding. The Zn-fingers structure and their relation to the binding of TFIIIA to 5S DNA (or RNA) has attracted great attention. We have used CD studies to gain insight into the structures of TFIIIA, apo-TFIIIA, and their interactions with the nucleic acids. By monitoring the CD spectra of TFIIIA (5 μM) under different conditions, we found that TFIIIA is quite stable at R.T. for several hours. The CD spectra show that TFIIIA and apo-TFIIIA have typical α-helical structures. The spectral similarity between these two proteins seems to indicate that Zn ions may not be involved in the conformational stabilization of protein. The intensity of 260-nm bands for 7S particle is much less (< 50%) than that of 5S RNA suggests substantial conformational changes of 5S RNA upon binding to TFIIIA. The interactions of TFIIIA and 5S DNA are being studied.

N.I.H. grant GM28057

CIRCULAR DICHROISM OF SYNTHETIC RNAs IN THE VACUUM ULTRAVIOLET

K.H. Johnson (UT-Dallas), D.M. Gray (UT-Dallas), P. Morris (NSLS), and J.C. Sutherland (NSLS)

Double-stranded DNAs in the A conformation generally have large positive circular dichroism (CD) bands at or about 185nm, the magnitudes of which increase with G·C content. We were interested in (a) whether large VUV CD spectral bands also generally appear upon base pairing of double-stranded RNAs and (b), if so, whether these bands depend simply on base composition or also depend on the sequence. Therefore, we measured the VUV CD of double- and single-stranded synthetic RNAs containing different nearest neighbors. The CD spectra of two additional single strands were estimated, using the nearest-neighbor approximation, from the measured spectra of oligomers. The RNAs measured were: poly[r(A-U)·r(A-U)], heat-denatured poly[r(A-U)], poly[r(A)·r(U)], poly[r(A)], poly[r(U)], poly[r(G)·r(C)], poly[r(C)], GpG, GpC, and CpG. The spectra of poly[r(G-C)·r(G-C)], CMP, and GMP were generously communicated by J. Riazance and W.C. Johnson, Jr. (OR State U.).

The VUV CD spectra of the double-stranded RNAs did have large positive bands. The main positive VUV band was centered at 185nm for (G·C)-containing RNAs and at 177nm for (A·U)-containing RNAs. Difference spectra obtained by subtracting spectra of the component single strands from the spectra of the double strands showed the CD changes induced by base pairing. For both the (G·C)-containing and (A·U)-containing polymers, the main positive VUV CD bands were present in the difference spectra and thus were due to base pairing. The similarities in the 174-220nm region between the difference spectra of the two (A·U)-containing polymers, and the similarities between the difference spectra of the two (G·C)-containing polymers, indicated that nearest neighbors had little effect on the VUV bands induced by base pairing. Since A·U and G·C base pairs each make distinct contributions to the CD in the 174-220nm region, it may be possible to use this region of the spectrum to estimate the amount of A·U and G·C base pairs in a natural RNA.

This work was supported by NIH Research Grant GM 19060, by Grant AT-503 from the Robert A. Welch Foundation, and by the NSLS Faculty-Student Support Program.

ULTRAVIOLET CIRCULAR DICHROISM IN THYLAKOID MEMBRANES

J. Kieleczawa, G. Garab, J. C. Sutherland and G. Hind
Biology Department, Brookhaven National Laboratory, Upton, NY

Our previous work on the circular dichroism (CD) spectrum of thylakoids within the visible wavelengths gave evidence of long-range structural ellipticity in the light-harvesting chlorophyll-protein complex of photosystem II (LHC-II). Ultraviolet CD, by contrast, can supply information on local domains of ellipticity, predominantly in the form of α-helices within the secondary structure of protein complexes. In order to deconvolute the spectral envelope of the ultraviolet-CD absorption signal it is necessary to monitor wavelengths below 200 nm. The unique dichrometer at the NSLS U9-B station offers this capability.

Ultraviolet-CD spectra from normal barley thylakoids were compared with spectra from: (i) a mutant (chlorina) lacking LHC-II and defective in membrane stacking; (ii) normal thylakoids treated with trypsin (which removes an amino-terminal, surface-exposed fragment responsible for Mg^{2+}-induced stacking of membranes). In normal thylakoids, Mg ion (> 1 mM) promoted membrane stacking, a decrease in ellipticity above 205 nm, and a complex change below 200 nm. Trypsin-treated and mutant membranes were indifferent to the presence of Mg ion, with respect both to stacking and the CD spectrum; thus, the ellipticity changes are assignable to LHC-II itself or to a change induced by LHC-dependent stacking.

We conclude from the ellipticity spectra that an intrinsic change in secondary structure occurs when membrane-bound LHC-II interacts with Mg ion. This change is complex, but probably includes modified β-sheet and random coil content in the polypeptide chains.

Work supported by the Division of Biological Energy Research, and the Office of Health and Environmental Research of the U.S. D.O.E. and by a grant to G. H. from the Competitive Research Grants Office of the U.S.D.A.

EXCITED STATES OF NUCLEIC ACID BASES IN LOW TEMPERATURE MATRIXES*

K. Polewski(BNL and Agricultural U.,Poznan, Poland), D.Zinger,
J. Trunk and J. C. Sutherland (Biology Department, BNL)

The absorption, fluorescence, phosphorescence and excitation spectra of the nucleic acid bases in the range from 160 nm to 500 nm have been measured.
The bases were deposited on the quartz window on the sample holder at 15K using Matrix Isolation Technique.
The excitation spectra were corrected for the excitation profile of the excitation source and optics. As a standard sodium salicylate was used, which fluorescence quantum yield is independent on the excitation wavelength.
An example of the excitation spectrum is shown on fig. 1. In the case of guanine one can find 5 good resolved peaks at wavelengths: 309nm, 278 nm, 236 nm, 207 nm and 186 nm. Fig. 2 displays flurescence spectra for diffrent excitation wavelenths, listed in the upper right corner. Relativly low, but highest among nucleic acid bases, flurescence quantum yield of guanine and well structured excitation spectrum sugests presence of very efficient non-radiative processes. From fig. 2 is easy to detect that emission spectrum of guanine is independent of the excitation wavelength, what means, only the lovest excited state is involved in the fluorescent properties of guanine.

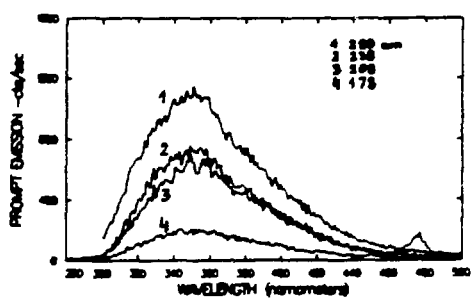

Fig.1. Excitation spectrum of guanine in nitrogen matrix, 15K.

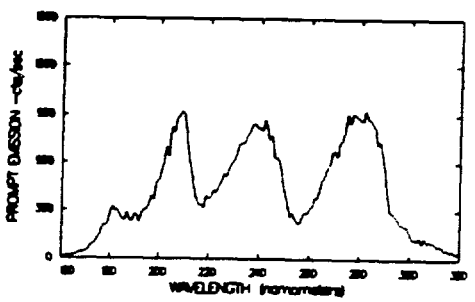

Fig.2. Emission spectra of guanine in nitrogen matrix,15K,at diffrent wavelengths.

---

* This work was supported by the O.H.E.R. of the U.S. Department of Energy and by grant from N.I.H.(GM 35662)

TITLE OF EXPERIMENT: Fluorescence decay times of nucleic acid bases in an argon matrix.

BEAM LINE: U9B DATE OF EXPERIMENT: from: Aug/87 to: 1/88

EXPERIMENTER(S):	AFFILIATION:
Krzysztof Polewski	BNL/Biology
David Zinger	BNL/Biology
John Trunk	BNL/Biology
John Sutherland	BNL/Biology

WORK SPONSORED BY: DOE and NIH

The matrix isolation technique has been used to obtain low temperature, 12K-5K, absorption, emission, and excitation spectra. Lifetime decay profiles of the nucleic acid bases in argon and nitrogen matrices.

For the measurements the vacuum spectroscopic setup at port U9B of the NSLS was employed.

The emission spectra, generally, come from single electronic state. Existence of the vibronic features vary for each case. Excitation and absorption spectra has been taken up to 160nm.

The results of the free nucleic bases luminescence and calculated spectroscopic parameters will be used in possible explanation of the absorption and energy transfer in DNA.

An example of the emission spectrum of guanine in an argon matrix is shown below.

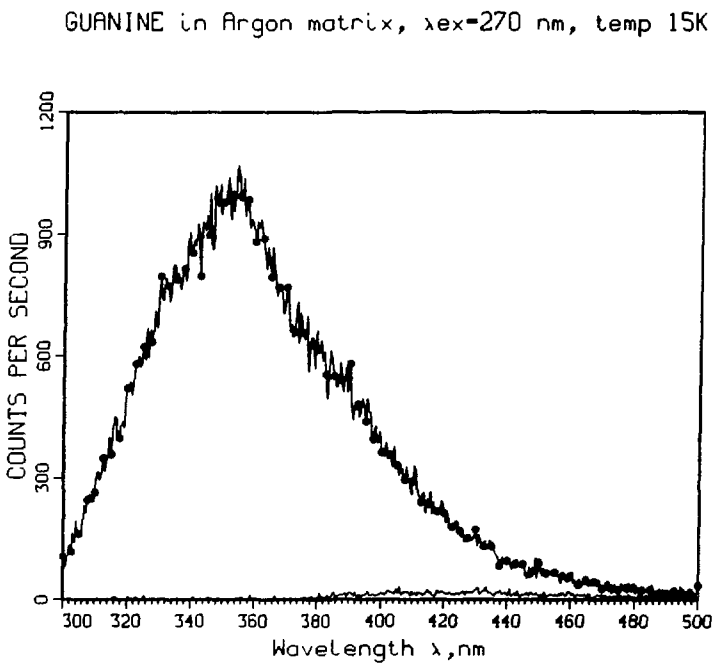

U9B

POLARIZED EXCITATION SPECTRA OF GUANINE IN LOW TEMPERATURE NITROGEN MATRIX*

K. Polevski(BNL and Agricultural U.,Poznan, Poland), D.Zinger,
J. Trunk and J. C. Sutherland (Biology Department, BNL)

Matrix Isolation Technique to deposit guanine in nitrogen matrix at 15K has been employeed. The polarized excitation spectra of guanine, 7-MeGuanine and hypoxanthine in the region from 170 nm to 350 nm has been measured.
The anisotropy is defined as $r = (I_{\parallel} - I_{\perp})/(I_{\parallel} + 2*I_{\perp})$, where $I_{\parallel}$and $I_{\perp}$ fluorescence intensity taken with polarizer parallel or perpendicular to the polarization of the exciting beam.
The strong absorption band about 260 nm in purines is suggested to be composed of two superimposed $\pi - \pi^*$transitions and that their transition moments are mutualy perpendicular(1).
The absorption spectrum and anisotropy values for guanine are shown on fig. 1.
Note that anisotropy decreases over the whole spectrum starting from value 0.4 at 270 nm and ending with value -0.15 at 200 nm. This shows us that we detected at least 3 transitions, where 2 of them are mutually perpendicular, at 270 nm and 200 nm, because of theory limited values. The region between 250 nm and 230 nm exhibits mixed behavior what can strongly support and be taken as a evidence for strong vibronic mixing for this transiton.

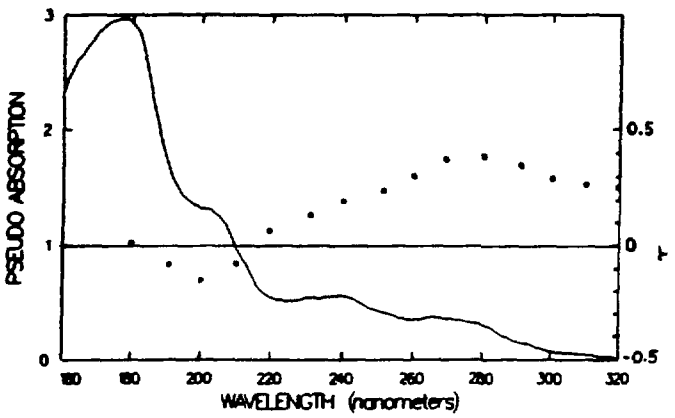

Fig. 1. Absorption spectrum (solid line) and anisotropy(dotted line) of guanine in nitrogen matrix, 15K.

---

1. Clark L.B. and Tinoco I.,J. Am. Chem. Soc., 87 (1965) 11

*This work was supported by the O.H.E.R. of the U.S. Department of Energy and by grant from N.I.H.(GM 35662)

VACUUM UV CIRCULAR DICHROISM AND ABSORPTION OF MELANINS

Tadeusz Sarna (Med. Coll. of WI & Jagiellonian U, Krakow, Poland), Krzysztof Polewski (BNL, Biol. & Agricultural U, Poznan, Poland) and Tom Schultz (Clairol Research Labs., Stamford, CN, USA)

Melanins are photoprotective pigments present in the skin, hair and eye of most animals. It has been shown that susceptibility of experimental animals to UV-induced skin cancer correlates inversely with the degree of their pigmentation. In humans, the skin sensitivity to solar radiation depends on the amount and type of melanin pigments. It is generally accepted that individuals with "reddish" pigmentation of the skin, containing pheomelanins are significantly more sensitive to solar radiation than those individuals containing brown pigment - eumelanins.

In model studies it has recently been shown that melanins are efficient quenchers of excited triplet states of certain photosensitizers and can interact rapidly with oxygen active species such as superoxide anion, hydroxyl radical and singlet molecular oxygen. However, under some experimental conditions melanin is also capable of generating these potentially cytotoxic radicals and in addition, H_2O_2.

Therefore, it is justified to expect melanins to play various roles in photobiological phenomena in pigmented cells. Melanins are considered amorphous substances; they are irregular polymers with a variety of monomers bound by different bonds. Little is known about the molecular structure of these important biological pigments.

Although the optical properties of melanins are important in view of their biological role in photoprotection the reported data on melanin absorbance are rather fragmentary. In this study we measured the absorption spectra of different synthetic polymers - models of eumelanin and pheomelanin - in the vis - vacuum UV region in an attempt to define any absorption maxima of this material. Two groups of melanin samples were used: films deposited on quartz surfaces and aqueous solution/suspensions of the polymers.

With the films, we were able to measure the absorption of melanin down to 160 nm while measurements of melanin in H_2O were made down to 170 nm. At 200 nm all melanin samples exhibit either a shoulder or local maximum with the intensity depending on the type of melanin polymer being used. We were also able to detect, for the first time, a weak but distinctive CD signal with the negative maximum around 190-200 nm.

The data should be useful in characterizing melanins of different origin. We will try to correlate the CD signals of melanins with such signals of polymeric precursors and monomeric subunits of these pigments.

VACUUM UV CIRCULAR DICHROISM OF TELOMERIC DNA OLIGONUCLEOTIDES*

John C. Sutherland and Ann M. Bergman, Brookhaven National Laboratory
and Robert Ratliff, Los Alamos National Laboratory

Telomeres are the structures at the ends of eukaryotic chromosomes. They are responsible for priming replication at the extreme ends of chromosomal DNA molecules and for stabilizing the chromosome ends by suppressing the recombinogenic properties of unmodified, free duplex DNA ends (Blackburn and Szostak, 1984).

Two single-stranded synthetic oligonucleotides corresonding to telomeric sequences from Tetrahymena thermophila were studied using the circular dichroism set up at the U9B beam line of the NSLS.

The two oligonucleotides, 5'(TAACCC)3' and 5'(GGGTTA)3' are thought to form not only a duplex with each other but also independently, G-G base pairing has already been observed by Henderson et al, 1987 and is thought to occur because of the formation of a unique structure stabilized by hydrogen bonds and containing G-residues in the syn conformation.

Figures 1 and 2 illustrate the circular dichroism spectra of the two oligonucleotides separately at 23 C in 10 mM PO4 buffer pH 7. It is believed that the 5'(GGGTTA)3' strand is a duplex under these conditions due to the absence of the 280 nm peak. However, the 5' (TAACCC)3' strand is single stranded as observed in the figure by the peak at 280 nm.

Future studies will show the circular dichroism of the two strands annealed to form a duplex.

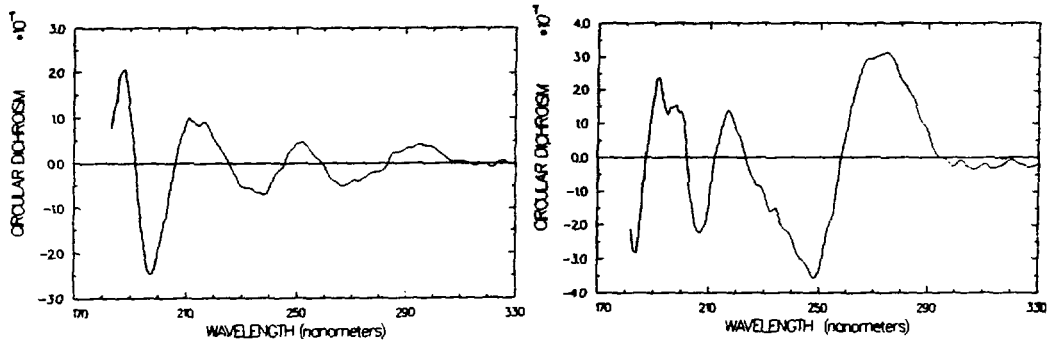

Figure 1 & 2. Circular dichroism spectra of 5'(GGGTTA)3' and 5'(TAACCC)3'.

Blackburn,E.H. and Szostak,J.W. (1984). Annu. Rev. Biochem. 53, 163-194.
Henderson,E., Hardin,C., Walk, S., Tinoco,I., Blackburn,E. (1987). Cell 51, 899-908.

*Research supported by the Office of Health and Environmental Research, United States Department of Energy and a grant from the National Institutes of Health (GM34662).

ACTION SPECTRUM FOR THE FORMATION OF PYRIMIDINE DIMERS IN T7 DNA IN BUFFERED AQUEOUS SOLUTION IN THE WAVELENGTH RANGE FROM 180 TO 360nm

John C. Sutherland, Ann M. Bergman and John G. Trunk, BNL.

The absorption of DNA has been measured by Inagaki et al (1974) in the spectral range of 620-15nm and by Sontag and Weibezahn (1975). Both studies demonstrated the existence of a stronger absorption band around 190nm than the well-known peak at 260nm. Below 180nm a steep increase has commonly been observed.

Using synchrotron radiation from the U9B beamline at the NSLS as a light source, we have induced strand breaks in T7 DNA (from E. coli) in the wavelength range of 180 to 360nm at 10nm intervals. By using synchrotron radiation we could select any wavelength, not only the discrete spectral lines usually available with conventional light sources.

An action spectrum is a plot of the reciprocal of the number of incident photons required to produce a given effect vs. wavelength. Peaks in the action spectrum represent the most efficient wavelengths, which require the fewest incident photons to produce the effect. The action spectrum for an effect usually resembles the absorption spectrum of the molecule that absorbs the radiation responsible for the effect. The figures below show that the absorption spectrum of DNA (Fig. 1) corresponds to the action spectrum data (Fig. 2) as would be expected.

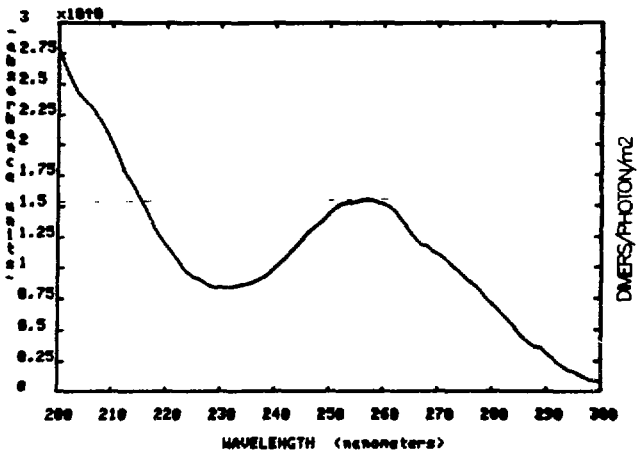

Fig. 1 The absorption spectrum of T7 DNA.

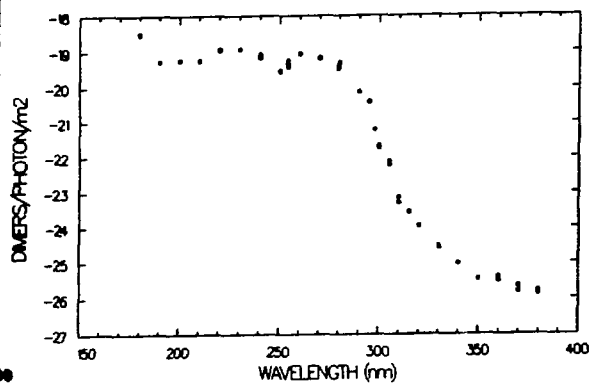

Fig. 2 The action spectrum for for pyrimidine dimer formation in T7 DNA.

Inagaki, T., Hamm, R.N., Arakawa, E.T. (1974). J. Chem. Phys. 61, 4246-4250.
Sontag, W. and Weibezahn, K.F. (1975). Rad. Environ. Biophys. 12, 169-174.

*Research supported by the Office of Health and Environmental Research, United Stated Department of Energy and a grant from the National Institutes of Health (GM35662).

TITLE OF EXPERIMENT: Fluorescence Decay Times of AAF-Nucleic Acid Covalent Adducts

BEAM LINE: U9B DATE OF EXPERIMENT: from:11/30/87 to:12/14/87

EXPERIMENTER(S):	AFFILIATION:
Leo Van Houte	Free University of Amsterdam
S. K. Kim	New York University
Nicholas Geacintov	New York University
David Zinger	BNL/Bio

WORK SPONSORED BY: National Cancer Institute, NIH CA20851,DOE
DOE #DE-AC02-78EV04959
DOE #DE-AC02-76V02386

Studies were conducted of Fluorescence lifetime of the exciplex of N-(deoxyguanosine-8-yl)-2 aminofluorene (d Guo-C8AF) which results from the covalent attachment of a chemical carcinogen to the DNA base guanosine. These studies, in combination with studies of steady polarization will be used to deduce possible three dimensional structures for the DNA-AF adduct.

Fig 7.

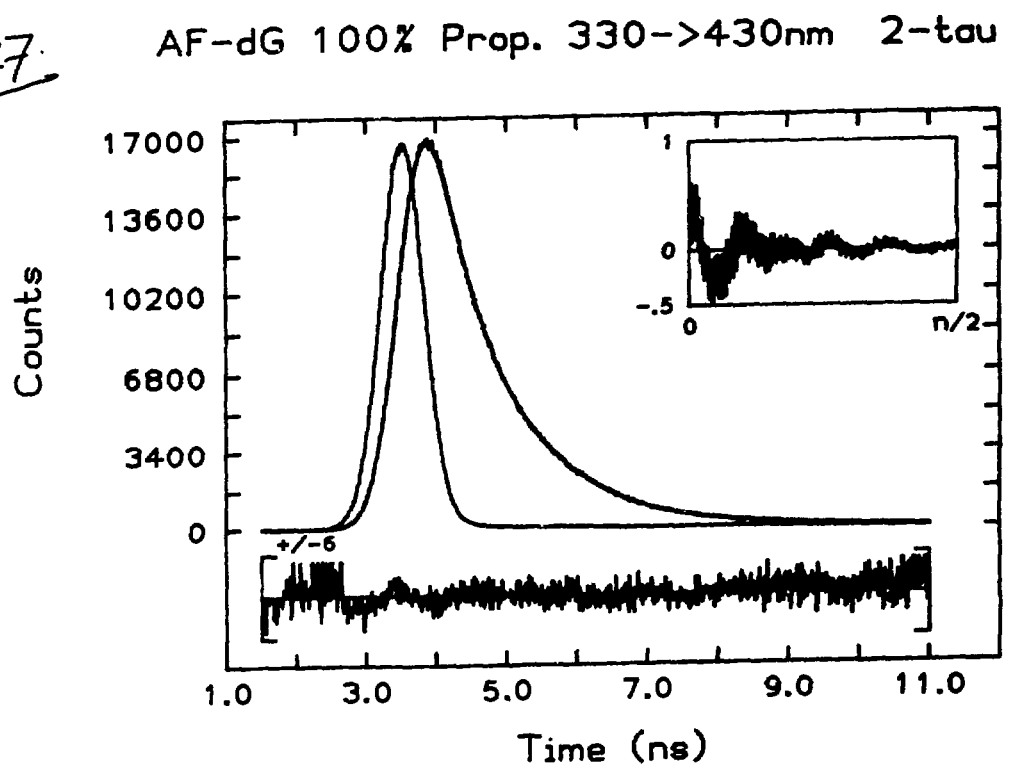

A TRANSMISSION GRATING SOFT X-RAY BEAMLINE MONOCHROMATOR

T.A. Callcott, K.-L. Tsang, C.H. Zhang (U. Tennessee), D.L. Ederer (NBS), and E.T. Arakawa (ORNL)

We have designed, built, and installed on beamline U-10 at NSLS a relatively simple monochromator with moderate resolution, which uses a single bent mirror toroid as a focusing element and a normal incidence transmission grating.

The monochromator is derived from a previously described VUV spectrometer design in which a transmission grating is inserted in the converging rays from a grazing incidence focusing mirror. [1] The monochromator is illustrated schematically in Fig. 1. The e-beam from the SLS is the input slit (IS-SLS), which is focused by a 1:1 bent mirror toroid (FM) onto an output slit (OS) located a few centimeters in front of the sample (S). A transmission grating (G) placed downstream from the focusing mirror disperses the spectrum. The spectrum is scanned by the linear motion of a plane mirror (SM) placed halfway between the grating and the input slit. A second plane mirror (OM) is used to maintain a fixed output axis for the light. A light trap (O-LT) blocks the zero order and monitors the beam position. Provisions are also made to insert thin film absorption filters (AF) and reflection filters to aid in order sorting and to reduce the heat load on the transmission grating. The reflection filter consists of two parallel mirrors with incidence angles adjustable between 5 and 15 degrees which replace the output mirror (OM).

The monochromator has been placed into operation using a single 1000 line/mm grating. A second 5000 line/mm grating has will be installed in June, 1988, and a third grating of intermediate line spacing will be acquired in the near future. Table 1 shows the nominal resolution of the monochromator for these gratings and a 0.5 mm output slit width.

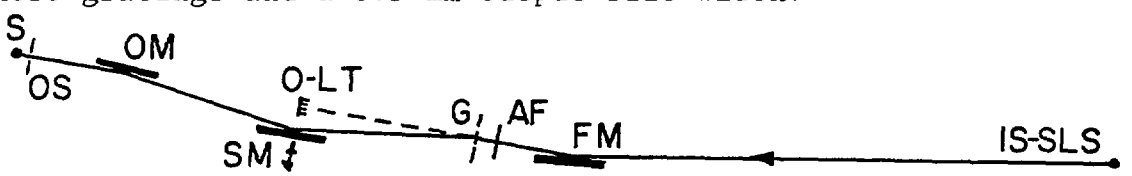

Fig. 1. Schematic diagram of transmission grating monochromator. Labeled elements are identified in text.

Table 1. Resolution with .5 mm slit.

Grating (1/mm)	Range (A)	Resolution (A)
1000	50-500	2.0
2400	21-210	0.83
5000	10-100	0.40

1. P.J. Caldwell et al., Appl. Opt. 20, 3047 (1981).

Research supported by NSF, USDOE, NBS and the State of Tennessee.

The Electronic Density of States of Si and C for the Interfacial Regions of Si-C Layers

R.C.C. Perera, P. Plag (LBL), C.H. Zhang, T.A. Callcott, K.-L. Tsang, (U. Tennessee), and D.L. Ederer (NBS),

The technique of soft x-ray fluorescence spectroscopy has been used to make preliminary studies of the electronic structure of C-Si at an interface. It is difficult to study the electronic structure of the interface between different materials, because it is buried under a layer of material. Surface sensitive probes like photoelectron spectroscopy can not be effective. X-ray fluorescence spectroscopy is not surface sensitive, but is inefficient. This drawback was overcome by making a multilayer consisting of 50 layers of carbon films interdigitated with silicon films. In one group of samples the thickness of the silicon film was varied from 3Å to 30Å, with the carbon film thickness fixed at 30Å . In another group of samples the silicon film thickness was fixed and the thickness of the carbon was varied. By this sample preparation technique it was possible to enhance the signal to noise ratio by a factor of 50 over a single C-Si interface The fluorescence was excited by near threshold soft x-rays from the National Synchrotron Light Source at Brookhaven National Laboratory, and detected by an ultra high sensitivity spectrometer. The interface signal was separated from the signal generated in the bulk. The silicon $L_{2,3}$ emission band from the layers 9Å silicon alternating with 30Å of carbon (Fig 1a) resembles that of SiC (Fig. 1b).

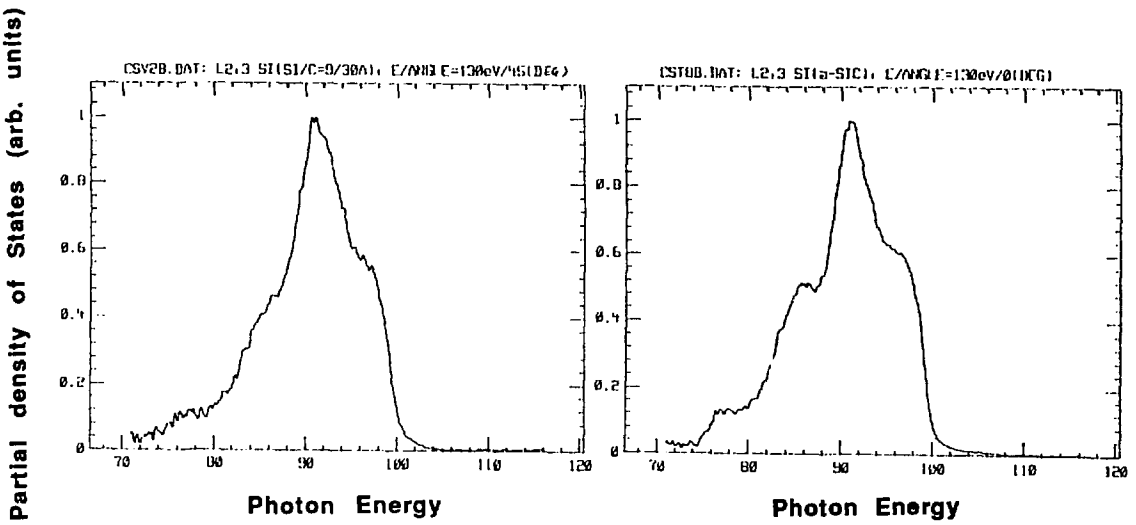

Fig. 1a) $L_{2,3}$ emission spectrum of silicon from 50 layers a 9Å silicon film alternating with a 30Å carbon film.

Fig 1b) $L_{2,3}$ emission spectrum of silicon from amorphous SiC.

Research supported by NSF, USDOE, NBS and the State of Tennessee.

The Partial Density of States of Si and C for Oxygen in the $YBa_2Cu_3O_x$ for $6<x<7$

C.H. Zhang, T.A. Callcott, K.-L. Tsang, (U. Tennessee), D.L. Ederer, J.E. Blendell (NBS), and T. Scimica (U. Hawaii)

We have measured the O K emission spectrum from a series of $YBa_2Cu_3O_x$, $6<x<7$ compounds. Dipole selection rules require that only p-type valence electrons can make transitions to s core states as in the K emission spectra of O. Thus the K spectrum of O is proportional to the p-type PDOS at the oxygen sites. These spectra have been adjusted to account for background emission and for energy dependence of the emission rate, to give the p-type PDOS depicted in Fig. 1, where the solid, dotted, and dashed curves were obtained for samples with values of x equal to 7, 6.5 and 6 respectively.

The spectra were obtained using a 2 kV electron beam to excite the O K emission spectrum. The emission intensity at photon energies greater than 530 eV are due primarily to shake up states produced by the excess energy of the excitation beam. As the excess excitation is decreased the intensity of the shake-up states grows smaller.

We note that, as x decreases from 7 to 6.5, the PDOS near E_F decreases. This suggests that as T_C for the material decreases, the density of states near E_F decreases. As x decreases from 6.5 to 6 the maximum in the density of states decreases. This suggests that the PDOS suppressing the antiferromagnetic behavior of the material lies deeper in the band.

The overall shape of the O K spectrum is in good agreement to O K emission that was modeled from band structure calculations obtained from a density functional approach[1]. In these calculation in coordination position 2 and 4 have a binding energy about 1 eV less than those in position 1 and 3. Our results suggest that the electrons associated with coordination position 2 and/or 4 are involved with the transition to superconductivity.

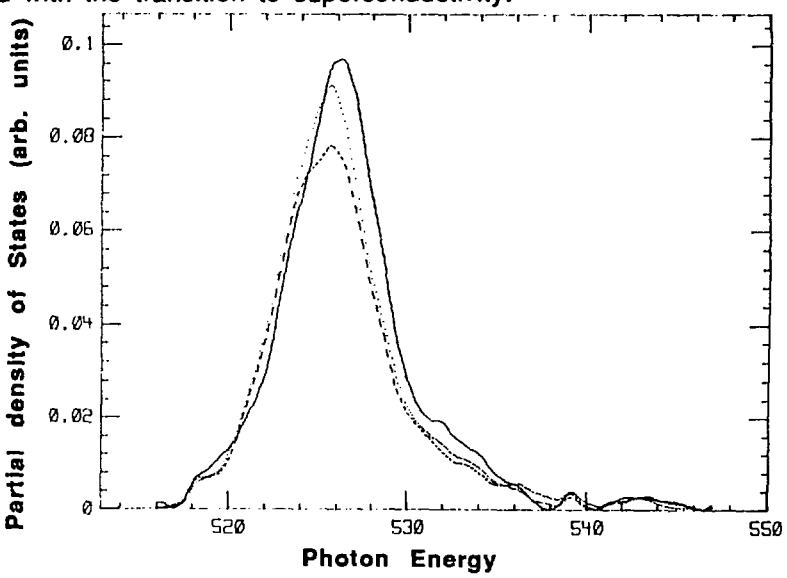

Fig.1) O K emission for x=7, solid line, x= 6.5, dotted line and x=6, dashed line. The spectra were normalized to the number of electrons.

1) J. Redinger, A. J. Freeman, J. Yu, and S. Massida, Phys. Lett A **124** , 469 (1987).

Research supported by NSF, USDOE, AFOSR, NBS and the State of Tennessee.

WORK CONDUCTED ON BEAM LINE: BEAM LINE U10B

MEASUREMENTS OF A PROTOTYPE PUMPED SYNCHROTRON RADIATION ABSORBER*

C.L. Foerster, T.S. Chou, H. Halama, and C. Lanni (NSLS)

In the existing synchrotron light sources, the conventional concept of removing the gas load caused by photon stimulated desorption (PSD) has several shortcomings. Large pressure rise inside the dipole vacuum chamber is responsible for short beam lifetime, ion trapping, and lengthy conditioning of the storage rings. A new concept proposed for future machines utilizes discrete photon absorbers[1] that intercept synchrotron radiation outside the beam chamber where more space for pumping is available. Large pumping speed using inexpensive titanium sublimation below the absorber can be provided to prevent desorbed molecules from diffusing into the beam chamber to interact with circulating electrons. The beam lifetime is extended, trapped ions are reduced, and conditioning time is decreased.

A model of this "photon absorber-pump combination" has been constructed and thoroughly tested in the U10B beam line. In future machines, this device can be installed into the front ends to define synchrotron radiation exit ports for respective beam lines.

As in previous experiments[2], the main gas species desorbed was H_2, CO, CO_2, and CH_4, and they were studied as a function of the beam dose. The synchrotron light was collimated to 10 mrad horiztonally and 3.3 mrad vertically. White light struck 65 cm^2 of the absorber face at angles of 5° and 45°. The 5° incident surface intercepted the light contained within a 0.8 mrad vertical angle.

The absorber model was first run with the TSP inactive to determine the desorption yield for the copper used. After restoring the absorber to its starting condition, the run was repeated with the TSP active and shielded to keep the titanium within the walls of the pump. The absorber was again restored to its starting condition and the run with the TSP unshielded to allow the titanium to coat the absorber and the walls of the test chamber.

The desorption yields for copper (runs 1 and 7) were within the same range that others[2-3] report for aluminum. Our clean up rate for all cases was less for all major gases desorbed. As for the unshielded run, the yields for H_2, CO, and CO_2 were initially significantly lower but they did not change a great deal during the run. When the absorber was biased negatively or positively to serveral kilovolts the desorption increased. Runs using Ti sublimation yielded inital total pressure improvement factors of 28 for shielded to 500 for unshielded. Initial partial pressure improvement factors for CO and CO_2 were 46 and 420 repsectively for shielded Ti. Without the Ti shield inital factors were ~450 and ~9000 respectively.

1. Light Source Report, Lawrence Berkeley Laboratory, Vol. 1, No. 1 (1986).
2. O. Grobner, et. al., Vacuum 33, 397 (1983).
3. T. Kobari and H. Halama, J. Vac. Sci. Technol. A5(4), 2355 (1987).

*Work performed under the auspices of U.S. Department of Energy.

RESOLUTION OF PHOTOIONIZATION SPECTRA OF MIXED VAN DER WAALS COMPLEXES: APPLICATION TO BUTADIENE-SULFUR DIOXIDE

J. R. Grover* and E. A. Walters**, *Chemistry Department, Brookhaven National Laboratory, Upton, NY 11973, **Chemistry Department, University of New Mexico, Albuquerque, NM 87131

When van der Waals complexes are synthesized in free jet expansions they are always present as mixtures in the resulting molecular beams. We have developed photoionization techniques for analyzing such target beams. The result for the butadiene-sulfur dioxide system is shown in Fig. 1. An example of its application is shown in Fig. 2, in which the nozzle-pressure dependence of the formation probability of the highly endoergic product $C_4H_6SO^+$ is compared with the target beam analysis. It is clear that this product is made almost entirely from trimers and larger clusters, but at nozzle pressures of 400 and 500 torr its formation from heterodimers is revealed. This result is highly unexpected, very difficult to explain, and therefore important. From carefully measured spectra at 500 and 800 torr and the application of the analysis of Fig. 1 the relative cross sections for the production of $C_4H_6SO^+$ from dimers and trimers were obtained and are shown in Fig. 3.
(Supported by the U.S. Dept. of Energy.)

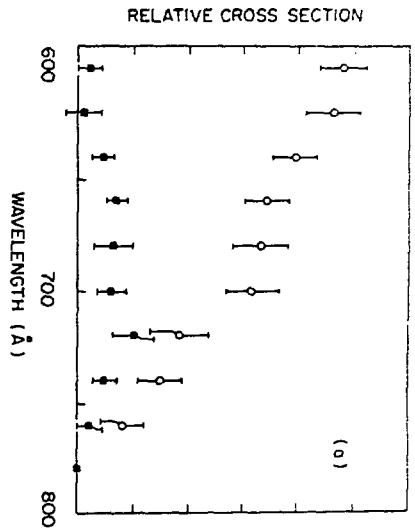

Fig. 3. Efficiency functions for producing $C_4H_6SO^+$ from $C_4H_6 \cdot SO_2$ (black squares) and trimers (open circles).

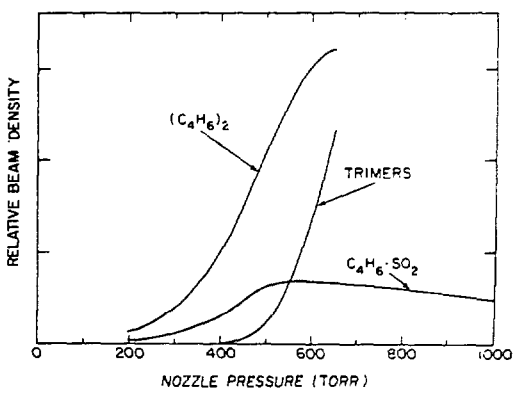

Fig. 1. Analysis of the products of the jet expansion of 1:4 1,3-butadiene:sulfur dioxide.

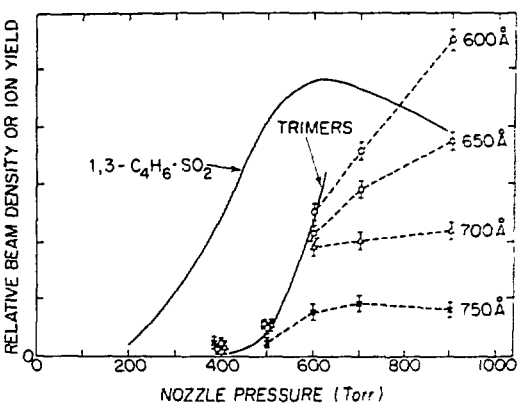

Fig. 2. Comparison of the production of $C_4H_6SO^+$ (points) with target beam composition.

PHOTOIONIZATION STUDIES OF THE HOMODIMER (ALLYL BROMIDE)$_2$

J. R. Grover (BNL), E. A. Walters, T. J. Schwartz and D. L. Arneberg
(U. New Mexico)

Photoionization efficiency-mass spectrometry studies were carried out on molecular beams of the title complex in the wavelength region 400 to 1400 angstroms. The target beams were made by recollimation of the free jet expansion of 1:9 mixtures of allyl bromide vapor and argon at room temperature. We were surprised to find that $C_6H_9^+$ is the principle product of the photoionization of (allyl bromide)$_2$ at 584 Å (21 eV). Threshold measurements established the following ionization or appearance potentials: $C_3H_5Br^+$ from C_3H_5Br, 9.68±0.01 eV; $(C_3H_5Br)_2^+$, 9.40 eV; $C_6H_9^+$, 9.55 eV; $C_3H_5^+$ from C_3H_5Br, 10.08 eV. A principal goal of this work is to establish whether the important bihalide radical HBr_2 exists, and if it does, to measure its heat of formation. The above measurements show that the heat of formation of $C_6H_9^+$ is 223+D(HBr·Br) kcal mol^{-1}, where D(HBr·Br) is the dissociation energy of HBr_2. Thus, if the heat of formation of $C_6H_9^+$ is known, D(HBr·Br) can be calculated. Unfortunately, not enough information is available, and in particular, the structure of $C_6H_9^+$ is unknown. It should be recognized that because of its very gentle formation at threshold, this ion is not necessarily the most stable possible isomer, unlike what might be expected with ionization by high energy electron impact. To provide guidance for the identification of the correct isomer of $C_6H_9^+$, semi-empirical calculations of the heats of formation of many of its isomers were made, using MINDO/3 (for which a mean uncertainty of ±8 kcal mol^{-1} is to be expected). Only sixteen isomers have calculated heats of formation in the sensible range 215-236 kcal mol^{-1} (there are several hundred possible isomers of $C_6H_9^+$), and of these only seven represent simple links between two allyl radicals with loss of hydride, which structural feature we believe to be the most likely. Further experiments to identifiy the pertinent isomer, guided by the calculations, are planned. This work illustrates the promise of dissociative photoionization of van der Waals dimers for the synthesis of metastable species.

This research was carried out at Brookhaven National Laboratory under contract DE-AC02-76CH00016 with the U. S. Department of Energy and supported by its Division of Chemical Sciences, Office of Basic Energy Sciences.

PHOTOIONIZATION OF BARIUM ATOMS AT ENERGIES IN EXCESS OF THE SECOND IONIZATION POTENTIAL

J. M. Preses, Department of Chemistry, Brookhaven National Laboratory

C. E. Burkhardt, M. Ciocca, W. P. Garver, M. J. Kernan, J. L. Libbert, J. J. Leventhal, Xian Liu, P. H. Schmidt, Department of Physics, University of Missouri - St. Louis

We have investigated photoionization of barium atoms in the wavelength range 500-800 Å. All photons in this range have sufficient energy to effect double photoionization of Ba. Using a novel detection scheme which permits discrimination between singly and doubly charged ions we have, for the first time, been able to isolate these separate contributions to the total absorption spectrum.

There are several possible ionization paths. Single ionization with the resulting Ba^+ in the ground state may occur. Double ionization leaving the Ba^{++} in the ground state may take place. Both of these processes would lead to nearly structureless spectra with no features indicative of the quantum states of Ba *I*, Ba *II* or Ba *III*. Other paths would however reflect the complicated nature of the quantum states of Ba *I* and Ba *II*. For example, removal of a 6s electron accompanied by excitation of a 5p electron produces an excited Ba^+. The excited state is embedded in $Ba^+ + e$ and the $Ba^{++} + 2e$ continua. Thus, the Ba *I* absorption spectrum will be composed of features that result from a complicated superposition of these processes[1].

Figure 1 shows a small portion of our Ba^{++} spectrum together with the corresponding Ba *I*

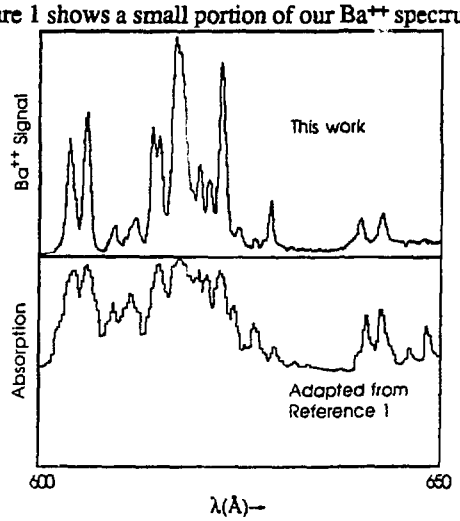

Fig. 1. Portion of the Ba^{++} spectrum acquired in this work. The lower panel is the total absorption spectrum for the same wavelength range and is shown for comparison.

absorption spectrum in a wavelength range described as the "complex central region". Comparison of these spectra immediately permits assignment of those features of the absorption spectra that are due to autoionization of excited Ba^+ produced in the photoionization. Note that the relatively large continuum background in the absorption spectrum is absent in our Ba^{++} spectrum.

Additional experiments have been performed in which synchrotron light in the same wavelength range irradiated *laser-excited* barium atoms. We were thus able to observe photoionization of ground state barium, as described above, with the effects of photoionization of excited atoms superposed. Because the laser-excited resonance level of Ba, the 6p $^1P_1$ state, is not the lowest-lying singlet state, the excited atoms are in both this state and the lower-lying metastable 5d $^1D_2$ state. The data show enhancement of some of the features present in the spectra acquired with only ground state atoms as well as some new features, the origins of which are currently under investigation.

References

1. J. P. Connerade, M. W. D. Mansfield, G. H. Newsom, D. H. Tracy, M. A. Baig and K. Thimm, Phil. Trans. R. Soc. A **290**, 327 (1978).

RESONANT PHOTOIONIZATION OF H_2S

M. G. White (BNL) and P. Miller (Yale)

Vibrationally-resolved photoelectron spectroscopy was used to study the non-radiative decay dynamics of the $5a_1$-$6sa_1$ Rydberg state transition near 12.5 eV in H_2S. Dispersed radiation in the range 930-1050 Å from the U11 NIM monochromator was used to selectively excite vibronic levels of the 6s Rydberg state which decays via autoionization to vibrational levels of the X^2B_1 ground ionic state of H_2S^+. The resulting H_2S^+ ions were found to be very vibrationally "hot" with most of the vibrational excitation in the ν_2 bending mode. These results suggest strong mode selectivity in the autoionization process.

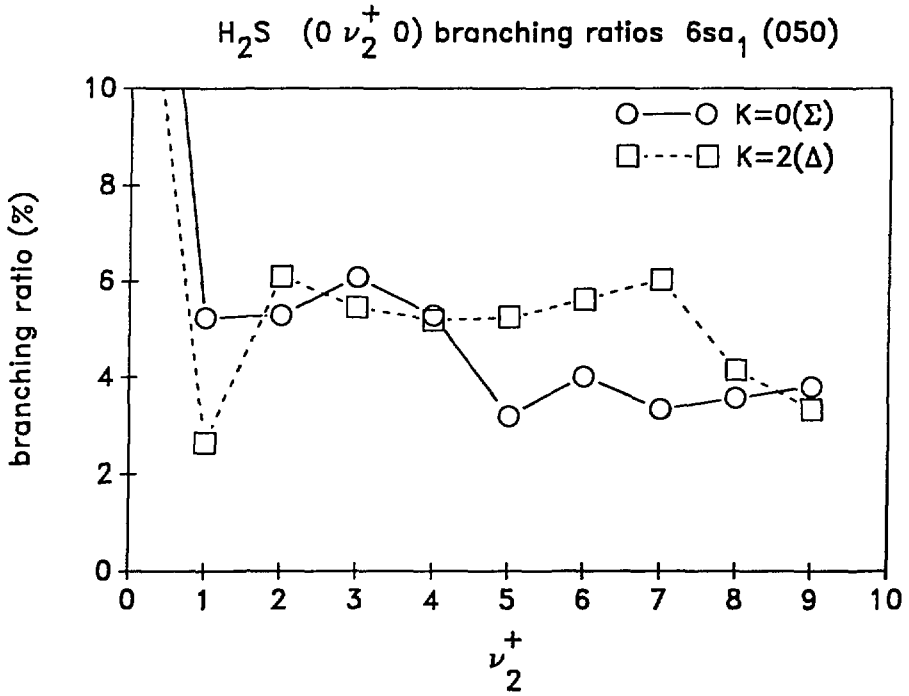

Figure Caption: Vibrational state branching ratios for the X^2B_1 state of H_2S^+ following resonant excitation of the ν_2 = 5 (K = 0 and k = 2) vibronic modes of the $6sa_1$ Rydberg state.

This research was carried out at Brookhaven National Laboratory under contract DE-AC02-76CH00016 with the U. S. Department of Energy and supported by its Division of Chemical Sciences, Office of Basic Energy Sciences.

Defect generation in silicon dioxide from synchrotron radiation below 41 eV

C.K. Williams, A. Reisman,† P. Bhattacharya
Microelectronics Center of North Carolina, P.O. Box 12889, Research Triangle Park, NC 27709

Synchrotron radiation is currently being explored as a source of X rays for X-ray lithography in semiconductor device fabrication because it produces a very intense collimated beam, reducing exposure time and undercutting of the mask. One of the concerns with X-ray lithography that has to be contended with is the extensive damage to gate and field insulators in Insulated Gate Field Effect Transistors (IGFETs)[1-7] that exposure to X rays can generate. A possible solution to the problem of radiation induced damage is to work in a photon energy range that produces no (or very little) damage, provided such a range exist, and that X-ray mask material for this range exist. In earlier work[1] the authors investigated the photon energy range from 300 to 1000 eV and found extensive damage was done to the gate insulators of the monitoring devices, and that the amount of damage measured was essentially independent of the photon energy for a constant radiation absorbed dose. This damage was in the form of fixed positive charge, neutral electron traps, and fixed negative charge. The purpose of this work was to investigate photon energy range below 41 eV using beamline U-11 of the National Synchrotron Light Source located at Brookhaven National Laboratory. It was found that incident X-ray exposures of 120 mJ/cm^2 in this photon energy range do little or no damage to the gate oxide of monitoring devices used. Since the mass absorption coefficients of the overlying SiO_2 and polycrystaline silicon layers are not available in this energy range, it cannot be determined whether the reason for the lack of damage is due to absorption in overlying layers, preventing the X rays from reaching the gate oxide, or if the X rays are simply not energetic enough to create any damage. These results suggest that X-ray lithography may be able to overcome the problem of X-ray induced insulator damage by tailoring the photon energy used for the exposures.

References

1. C.K. Williams, A. Reisman, P.K. Bhattacharya, and W. Ng, J. Appl. Phys. **64**, 1145 (1988).
2. E.H. Snow, A.S. Grove, and D.J. Fitzgerald, Proc. IEEE **55**, 1168 (1967).
3. B.E. Deal, IEEE Trans. on Electron Dev. **ED-27**, 606 (1980).
4. A. Reisman, C.J. Merz, J.R. Maldonado, and W.W. Molzen, Jr., J. Electrochem. Soc. **131**, 1404 (1984).
5. A. Reisman, C.K. Williams, and J.R. Maldonado, J. Appl. Phys. **62**, 868 (1987).
6. J.M. Aitken and D.R. Young, J. Appl. Phys. **47**, 1196 (1976).
7. J.M. Aitken, D.J. DiMaria, and D.R. Young, IEEE Trans. Nucl. Sci. **NS-23**, 1526 (1976).

†Also at Department of Electrical and Computer Engineering, Box 7911, North Carolina State University, Raleigh, NC 27695-7911

Photoelectron Diffraction Study of Ta(100)

R.A. Bartynski[a*], D. Heskett[b†], K. Garrison[a], G.M. Watson[b], D.M. Zehner[c], W.N. Mei[d], S.Y. Tong[e], and X. Pan[b]

a) Department of Physics, Rutgers University, Piscataway, New Jersey 08855
b) Department of Physics, University of Pennsylvania, Philadelphia, Pennsylvania 19104
c) Solid State Division, Oak Ridge National Laboratory, Oak Ridge, Tennessee 37831
d) Department of Physics, University of Nebraska, Omaha, Nebraska 68182
e) Department of Physics and Laboratory for Surface Studies, University of Wisconsin, Milwaukee, Wisconsin 53201

Using the surface shifted 4f core levels, a photoelectron diffraction study of Ta(100) was performed to determine the first interlayer spacing of this surface. Photoemission intensities of the bulk and surface shifted core levels of Ta(100) were measured as a function of photon energy at normal emission and near the <111> direction of the crystal. In addition, the intensities were measured as a function of polar angle near the <011> azimuth at a photon energy of 65 eV. To eliminate the necessity of extensive normalization, the ratios of photoemission intensities from the bulk and surface shifted 4f core levels were measured in each of these experimental modes. We have also performed a multiple scattering photoemission calculation for several first interlayer spacings ranging from the bulk value (d_{12} = 1.6550Å) to a 15% contraction (d_{12} = 1.4089 Å) in 5% increments.

Panel (a) of the figure below shows the measured surface/bulk intensity ratios (open squares) as a function of photon energy at normal emission. The solid curves are the results of the multiple scattering calculation assuming different first interplanar spacings. The best agreement with experiment is obtained for the d_{12} = 1.4894 Å curve. The considerable disagreement with calculations for 5% and 15% contractions indicates a contraction of 10 ± 3%. The intensity ratios obtained away from normal emission are shown in panel (b). Considerably less intensity modulation than the normal emission results is seen for the off normal data and the calculations for those geometries are not as sensitive to changes in the first interplanar spacing. Nevertheless, best agreement between theory and experiment is also obtained for the calculation for a 10% contracted surface.

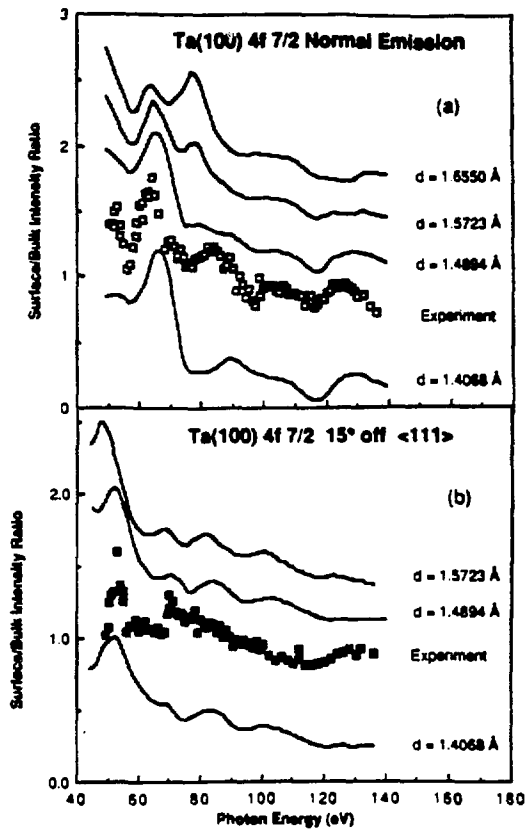

R.A. Bartynski (Rutgers U.), E. Jensen (Brandeis U.), K.C. Garrison (Rutgers U.), S.L. Hulbert, E. Johnson, and R. Garrett (NSLS)

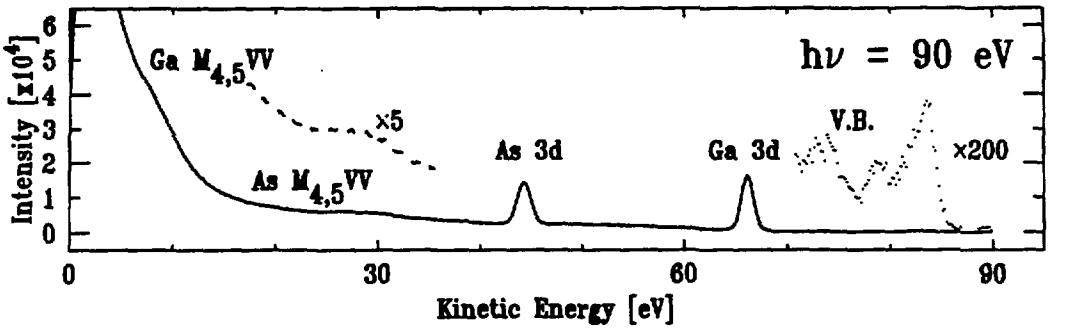

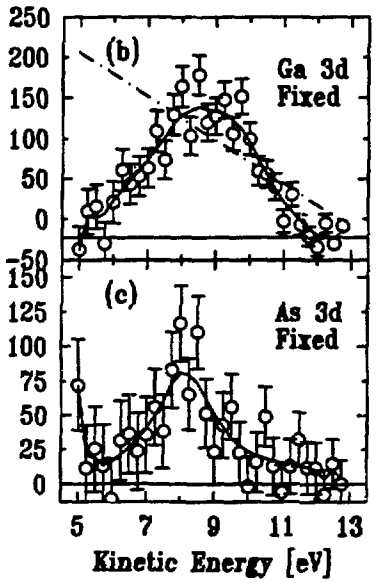

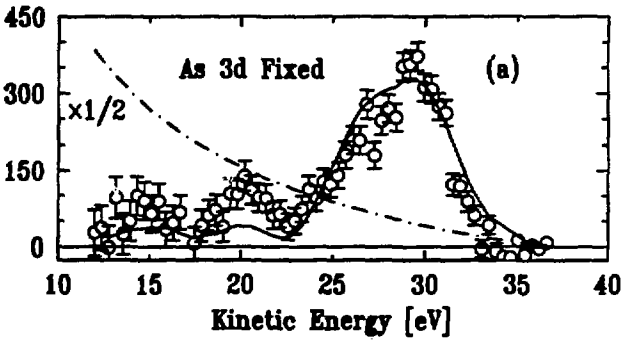

We present core-valence-valence (CVV) Auger spectra from the GaAs(110) surface obtained in coincidence with Ga and As 3d core photoelectrons. These data were taken at a photon energy of 90 eV on the 15° TGM beamline on U12. In APECS, two electron analyzers are focused on the same sample illuminated by synchrotron radiation. For these data, the kinetic energy of one analyzer was fixed to accept photoelectrons from a core level while the other swept the kinetic energy region of the CVV Auger spectrum. When an electron is simultaneously detected in both analyzers, an event is counted. The resolution in each analyzer was ~0.8 eV. Total resolution (electrons + photons) was ~1 eV.

The upper panel shows an ordinary photoemission (singles) spectrum taken at 90 eV photon energy. The As $M_{4,5}VV$ Auger spectrum, starting near 33 eV kinetic energy, is barely visible in the ×5 inset while the Ga $M_{4,5}VV$ Auger spectrum, with a kinetic energy threshold of 12 eV, cannot be distinguished from the background. The ×200 inset shows the valence band.

The open circles in panel (a) show the As $M_{4,5}VV$ Auger spectrum obtained in coincidence with As 3d core photoelectrons at 44.2 eV. A smooth background (dot-dashed line) was subtracted from the coincidence spectrum to remove the contribution from correlated secondary Auger emission. The solid line is a scaled, background subtracted singles spectrum obtained along with the coincidence data. The coincidence spectrum shows an increase in the relative intensity of the 20 eV features compared the 28 eV peak. This enhancement of the 20 eV features may be due to the greater surface sensitivity of the coincidence measurement reflecting a change in the local surface valence band density of states.

Panels (b) and (c) show the kinetic energy range of the Ga $M_{4,5}VV$ Auger spectrum taken in coincidence with the Ga and As 3d photoelectrons, respectively. A linear background (dot-dashed line) has been subtracted from each coincidence spectrum. The peak in panel (b) is attributed to Ga $M_{4,5}VV$ Auger transitions while the peak in the lower panel is associated with the As $M_{4,5}VV$ transition originating from As 4s DOS in the valence band. These transitions overlap the Ga Auger spectrum and are not observable with conventional spectroscopic techniques.

This work was supported by New Jersey Comm. on Science and Technology Grant 87-240040-7 (Bartynski), and Analog Devices Career Development Grant (Jensen), and the Division of Material Sciences U. S. Department of Energy under Contract No. DE-AC02-76CH00016.

AUGER PHOTOELECTRON COINCIDENCE SPECTROSCOPY (APECS) OF Al(111)+O U12

S. Hulbert, E. Johnson, and R. Garrett (NSLS), E. Jensen (Brandeis U.), and R. Bartynski (Rutgers U.)

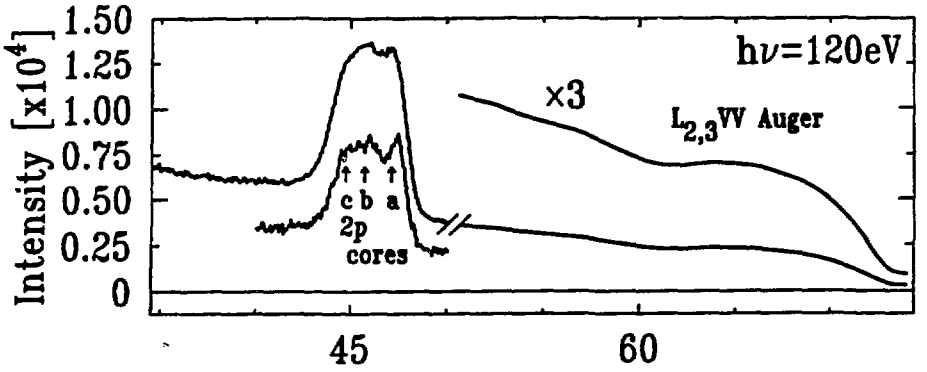

We present APEC spectra taken at 120 eV photon energy with the 15° monochromator on beamline U12 at the NSLS. The top panel shows an ordinary photoemission scan, subsequently called singles, through the Al 2p ($L_{2,3}$) unshifted (47.2 eV)[1] and oxide-shifted core lines (45.8 and 44.8 eV) and the broad Al $L_{2,3}VV$ Auger lines (50-74 eV). All kinetic energies are measured with respect to $E_F = 0$.

The APEC spectra, shown in the side panels, were taken with one analyzer fixed at 47.2 eV (a), 45.8 eV (b), and 44.8 eV (c), which correspond to the core lines of unshifted Al metal, the chemisorbed-oxygen phase[1], and the oxide phase, respectively (see arrows in the singles spectrum). A second analyzer was scanned through the $L_{2,3}VV$ Auger region. Coincidence events were counted only when electrons were received in each analyzer simultaneously. The coincidence data are shown as open circles with error bars. The solid lines are digital smooths to the data (ΔE=1.0 eV fwhm) and the dashed line in panel (a) shows the corresponding singles spectrum. The energy resolution — electron plus photon — is ~1.0 eV (60 eV pass, large aperture) in each analyzer.

The Auger spectra associated with the three Al 2p core lines are distinctly different from one another:

Panel (a): The Auger spectrum of the unshifted Al 2p line is broad, featureless, and extends up to 74eV kinetic energy. This is characteristic of decay involving the Al 3sp valence band, which is broad, featureless, and extends to E_F. This spectrum is very similar to that of clean Al.

Panel (c): The Auger spectrum of the oxide-shifted core level is peaked in the 54-60eV kinetic energy region and has very low intensity in the 65-74eV region. This is characteristic of decay involving the O 2p levels. The fact that this is the dominant structure in decay from an Al core level indicates that nearly all of the Al valence band electrons have been transferred to the O orbitals. This spectrum is very similar to that of bulk aluminum oxide.

Panel (b): The Auger spectrum of the chemisorbed peak is different from either of the other spectra. This is at first somewhat surprising, since calculations predict very similar densities of states for oxide and for chemisorbed oxygen layers.[2,3] The resolution comes from the fact that this decay preferentially samples the aluminum site. The fact that both deep (54-60eV) and shallow (65-74eV) features are seen is direct evidence that both the Al 3sp and O 2p levels are occupied and participate in the Al 2p decay. Further analysis may allow us to make quantitative statements about the Al site-projected density of states for this chemisorbed-oxygen state (e.g. the relative occupation of the O 2p and Al 3sp levels). Note that this spectrum cannot be measured by conventional Auger spectroscopy because of interference from the unshifted and oxide-shifted lines, and requires the APECS technique.

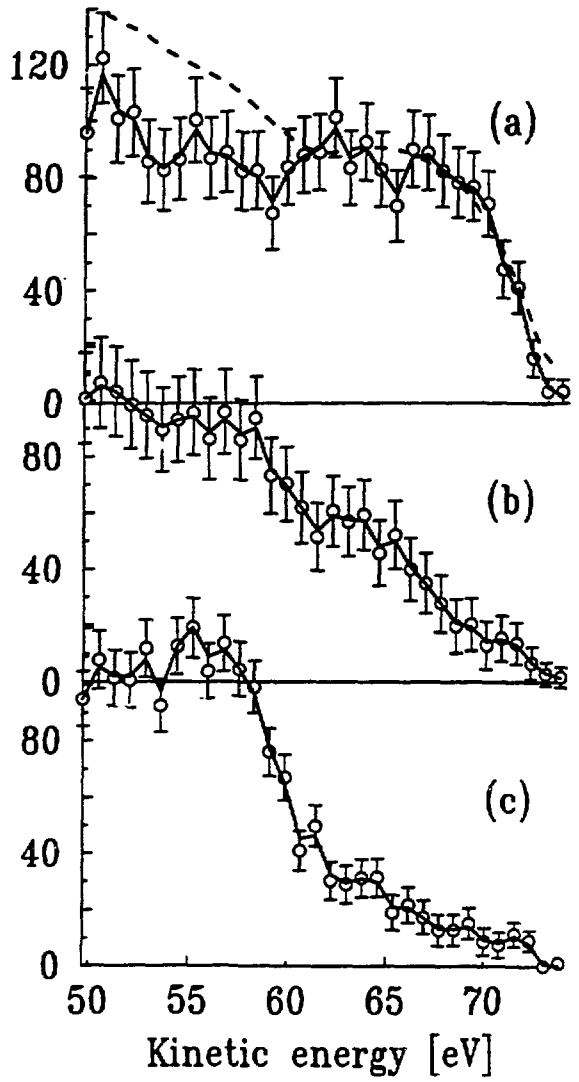

[1] S. A. Flodstrom, C. W. B. Martinson, R. Z. Bachrach, S. B. Hagstrom, and R. S. Bauer, Phys. Rev. Lett. 40, 907 (1978).

[2] S. Ciraci and I. P. Batra, Phys. Rev. B 28, 982 (1983).

[3] D. S. Wang, A. J. Freeman, and H. Krakauer, Phys. Rev. B 24, 3092 (1981).

This work was supported by Analog Devices Career Development Grant (Jensen), Rutgers Research Council (Bartynski), and the Division of Material Sciences U. S. Department of Energy under Contract No. DE-AC02-76CH00016.

Surface States on NiAl(110)

S. C. Lui[+], D. M. Zehner* and E. W. Plummer[+]

[+]University of Pennsylvania, Philadelphia, PA 19104

*Solid State Division, Oak Ridge National Lab, Oak Ridge, TN 37831

Surface states on NiAl(110) have been investigated experimentally using angle-resolved photoemission. The primilary interest in studying surface electronic structure of NiAl(110) is to find out the relationships in electronic structure between surfaces of this alloy to that of the bulk, which is characterized by filled Ni *d*-bands. The NiAl(110) crystal can be cleaned in situ by Ne^+ sputtering and subsequently annealed to 850°C. Using both s- and p-polarization of the incident radiation and collecting photoelectrons emitted normal to the surface, three surface states are observed and the symmetry of these states are Σ_1 , Σ_3 and Σ_4. The dispersions of these surface states were measured along $\overline{\Gamma Y}$ and $\overline{\Gamma X}$ of the surface Brillouin zone. Theoretically, the NiAl(110) surface is simulated by a 5- layer slab and the surface state dispersions were calculated self-consistently by Kang and Mele using a first principle pseudopotential scheme within the local-density approximation(LDA)[1].

Figures 1 *a*-d showed even and odd bulk projections along the $\bar{X}$–$\bar{\Gamma}$–$\bar{Y}$ directions. Due to diff rences between the measured and calculated bulk bands, the bulk projections are plotted in different figures. Figures 1b and 1d show the projections of bulk bands and surface states from theory and Figures 1a and 1c show those from our experiment. In Figures 1b and 1d, surface(resonance) bands are indicated by solid(dashed) lines and are labelled as $A_n(a_n)$,$B_n(b_n)$,etc. for even(odd) states with n being the band index.

In general the energy position, symmetry and dispersion of the surface state bands observed experimentally are reproduced by the theoretical calculation. A detailed discussion between theory and experiment is reported elsewhere[2]. An interesting aspect of this study is that the first moment of the surface density of states (DOS) is shifted towards the Fermi level by ≈ 0.5 eV. Since the bulk Ni *d*-bands are filled and the bonding is primilarly through hybridization, the shift in surface DOS suggest that the surface Ni and Al atoms in the alloy have recovered some of their individual bonding behavior, i.e. a loss of bulk hybridization at the surface. However, the magnitude of the shift in the surface DOS is not large enough to affect the DOS at the Fermi level. Therefore, the magnetic property of NiAl(110) is expected to be the same as the bulk, i.e., non-magnetic.

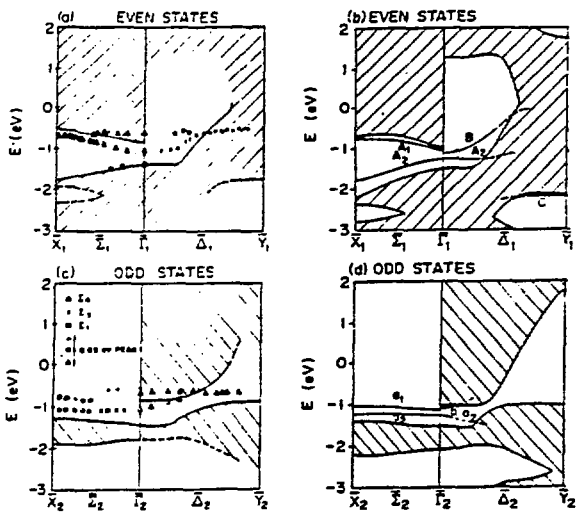

fig.1

References:

1. M. H. Kang, Ph.D. thesis, University of Pennsylvania,1988.
2. S. -C. Lui, M. H. Kang, E. J. Mele, E. W. Plummer and D. M. Zehner, submitted to Phys. Rev. B.

Acknowledgements

The synchrotron beam line was funded and supported by NSF/MRL program DMR-8519059, and by the Division of Materials Science, U.S. Department of Energy under contract DE-ACO5-840R21400 with Martin Marietta Energy Systems, Inc.

QUASIPARTICLE BAND STRUCTURE OF NA*

In-Whan Lyo and E.W. Plummer (U of Pennsylvania)

We have measured the quasiparticle band structure of Na(110) using angle resolved photoemission and an extremum search procedure[1]. This procedure though tedius allows for a direct determination of the band structure to be made, without any assumptions or theoretical input. The experimental results for the simple metal Na show conclusively that there are large differences between the calculated single particle band structure and the measured quasiparticle band structure due to many-body interactions in the electron gas. For example the quasiparticle occupied band is 18% narrower than the calculated single particle band. The experimental data can be used to generate directly the k dependence of the electron self energy $\Sigma(k)$, where simply put the self energy is the correction to the single particle band structure due to the many body electron-electron interaction. The figure plots our measured self energy and compares it to two different calculations of the self energy for an electron gas of the density of Na. The dashed curve is calculated in the Random Phase Approximation (RPA), which underestimates the self energy. The solid curve is our calculation where the exchange-correlation hole is included (beyond RPA) in the calculation[1].

*This work was supported by NSF-DMR-8610491.

[1]I.-W. Lyo and E.W. Plummer, Phys. Rev. Letters 60, 1558 (1988).

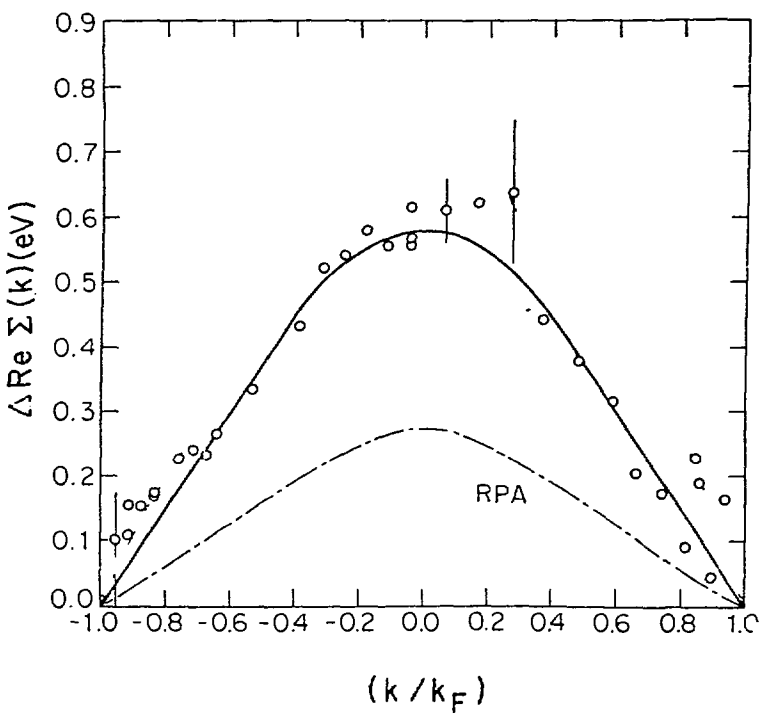

NON-METALLIC BEHAVIOR OF CESIUM ON GaAs(110)

T. Maeda Wong, D. Heskett*, N. J. DiNardo+, E. W. Plummer
University of Pennsylvania, Philadelphia, PA
+Drexel University, Philadelphia, PA

The valence states of Cs on GaAs(110) as a function of Cs coverage was examined by angle-resolved photoemission and work function change ($\Delta\phi$) measurements in an effort to establish the nature of the interface. The photoemission spectra show that the interface formed at room temperature(300K) is not metallic. A measure of the work function, ϕ, at saturation (one Cs layer) showed a reduction from the clean surface value by 3.6 eV; a minimum in ϕ is not observed, in contrast to the case of Cs on metals [1,2].

In order to assess the sensitivity of uv-photoemission to metallic Cs states at the Fermi level(E_f), a second Cs layer at low temperature(190K) was subsequently grown. In this case, the resulting overlayer was found to be metallic. The non-metallic nature of the ~300K interface is quantitatively assessed by comparing the expanded intensity scales from our data.

Valence band spectra($h\upsilon$ = 25 eV, normal emission) for various Cs coverages are presented in Figure 1. The energy scale is referenced to E_f as determined by photoemission from the metal sample holder. A Cs-induced band-bending shift of ~100 meV at saturation was determined by the analysis of the Ga 3*p* core level and the spectra are shifted accordingly. Clean GaAs (fig. 1a) shows a surface state ~1.2 eV below E_f [3]. Low Cs coverages attenuate the surface state emission (fig. 1b) and no emission at E_f is observed. Saturation coverage at ~300K (fig. 1c) produces further attenuation of the GaAs features, with no emission within ~0.4 eV of E_f. The metallic nature of the interface is indicated by the Cs-induced emission at E_f after 2 layers of Cs (fig. 1d) and is accompanied by an increase in ϕ by ~0.3 eV, close to that of bulk, metallic Cs. Spectra were also recorded at various critical points and high symmetry lines of the surface Brillouin zone with similar results.

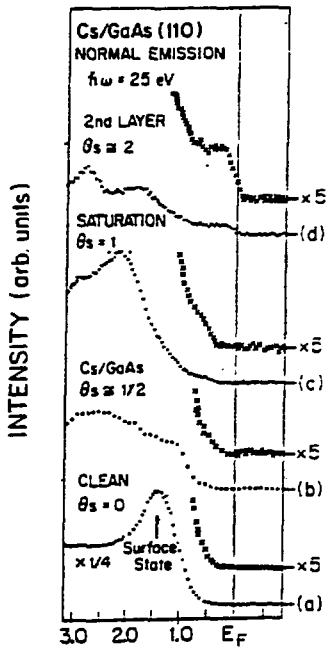

fig.1

From this study, we come to the conclusion that the Cs/GaAs(110) interface at room temperature is not metallic. This result suggests that the nature of this interface should be described by a model where the Cs-GaAs interaction is much stronger than the Cs-Cs interaction. Cs/GaAs need not behave like Cs on metal substrates. Further details of the bonding interaction, bonding site(s), and absolute Cs coverages are presently under further investigation[4].

References:

* Present Address: Dept. of Physics, University of Rhode Island, Kingston, RI 02881

1. A. Hohlfeld, M. Sunjic, and K. Horn, J. Vac. Sci. Tech. A5 (1987) 679.
2. S. A. Lindgren and L. Walden, Solid State Comm. 25 (1978) 13; Phys. Rev. B22 (1980) 5967.
3. J. A. Knapp and G. J. Lapeyre, J. Vac. Sci. Technol. 13 (1976) 757; A. Huijser, J. van Laar, and T. L. van Rooy, Phys. Lett. 65A(1978) 337; J. A. Knapp, D. E. Eastman, K. C. Pandey, and F. Patella, J. Vac. Sci. Technol. 15 (1978) 1252; T.-C. Chiang, J. A. Knapp, M. Aono, and D. E. Eastman, Phys. Rev. B21 (1980) 3513.
4. T. Maeda Wong, D. Heskett, N. J. DiNardo, E. W. Plummer, to be published.

Acknowledgements

This project is supported by Office of Naval Research, #N00014-86-K-0304.

Study of the Surface Resonances on Ta(001)

Xiaohe Pan, M. Weinert †, G. Watson, D. Heskett, and E. Ward Plummer

Department of Physics and LRSM, University of Pennsylvania

We have studied the electronic structure of the surface states on Ta(001) by synchrotron radiation angle-resolved photoemission in the photon energy range of 10 eV to 100 eV. Three occupied surface resonances states are identified at the $\bar{\Gamma}$ point. They are located at about 0.3 eV, 2.9 eV and 3.6 eV below the Fermi level. The dispersion of the surface resonance states have been measured along both $\bar{\Sigma}$ and $\bar{\Delta}$ direction. The resonances located at 0.3 eV and 3.6 eV binding energy are mainly d_{z^2} in orbital character, and the one at 2.9 eV is primarily $d_{x^2-y^2}$. The experimental data are compared to our self-consistent local density calculations on nine-layer relaxed Ta(100) film. Inclusion of spin-orbit interactions does not significantly change the occupied bands and thus the position of the resonances are associated with the symmetry gaps along the $\bar{\Sigma}$ and $\bar{\Delta}$ direction.

†*Physics Department, Brookhaven National Laboratory.*

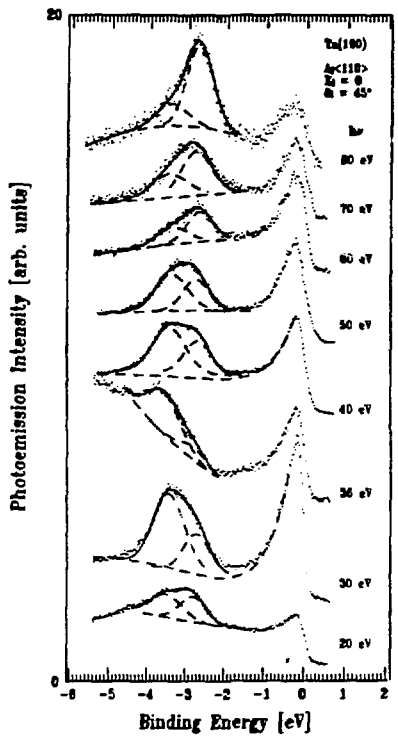

Figure 1. Normal emission angle-resolved photoelectron spectra from the Ta(001) surface taken at various energies and 45 ° incidence angle.

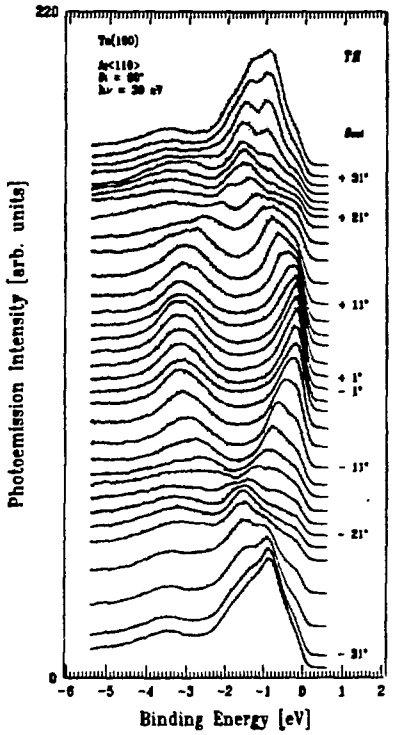

Figure 2. Angle-resolved photoelectron spectra from Ta(001) taken at various polar angles along the [11] direction.

The Orientational Behavior of Hexadecyl-pyrrole Langmuir-Blodgett Films

J. M. Chen, X. Q. Yang, T. Inagaki, T. A. Skotheim (BNL), M. L. denBoer (CUNY), Y. Okamoto (Polytech. U), L. Samuelson, S. Tripathy (U Lowell).

Near edge X-ray absorption fine structure (NEXAFS) spectroscopy has been widely used to study the orientational behavior and bond-length of low-Z molecules and Langmuir-Blodgett (LB) films. We have used NEXAFS to determine the orientation of Hexadecyl-pyrrole (HDP) LB films on platinum substrate. We also observed a charge transfer interaction between the LB film and the Pt substrate. The work was performed on beam line U14..

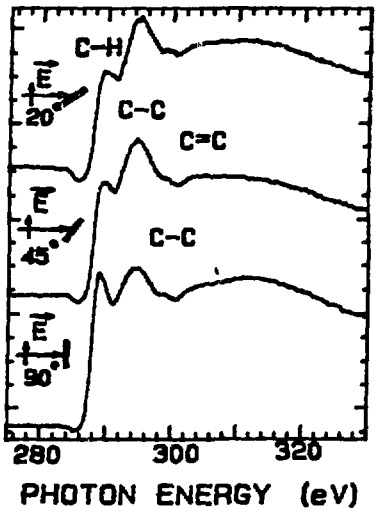

Fig. 1. C *K*-edge NEXAFS of a single layer HDP monomer LB film with three incident angles.

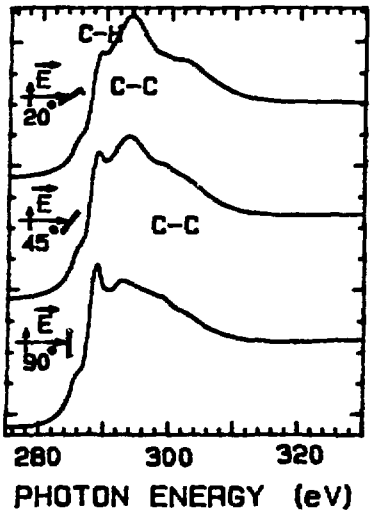

Fig. 2. C *K*-edge NEXAFS of a 7 layer HDP monomer LB film at three incident angles.

Figure 1 shows the carbon *K*-edge NEXAFS spectra of a single layer HDP monomer LB film with the incident x-ray beam at 90°(normal incidence), 45° and 20°(grazing incidence). The dipole transition rule implies that the probability of photoexcited transitions from the C 1*s* state to unoccupied molecular states depends on the symmetry (σ or π) of the final state, so that the transition rate depends of the orientation of the electric field E of the photon with respect to the molecular axis[1]. This phenomenon has been widely used to study the orientational behavior of low-Z organic molecules taking advantage of the high degree of polarization of synchrotron radiation. In figure 1, the intensity of the 288.5 eV peak which corresponds to transitions to the C-H bonding state, increases while the intensity of the 293.5 eV peak corresponding to transitions to the σ^* C-C decreases with increasing incident angle of the X-ray beam. The C-H bond is perpendicular to the hydrocarbon tail, while C-C bonds are oriented along the tail. The observed intensity changes clearly indicate that the hydrocarbon tails are highly ordered normal to the sample substrate.

Figure 2 shows the C *K*-edge NEXAFS spectra of a 7 layer HDP monomer LB film. The orientational dependence of this multilayer film is essentially identical to that of the single layer film, indicating that the multilayer film is also well-ordered. However, the 286 eV shoulder before the main edge present in this film is absent from the single-layer film in Fig. 1. This shoulder corresponds to a transition to the π^* C=C bond of the pyrrole headgroup. The absence of this feature in the single monolayer is indicative of charge transfer interactions between the pyrrole head group to the Pt substrate with which it is in close contact, as further described in Ref 2.

References

1. J. Stöhr and R. Jaeger, Phys. Rev. B.26,4111 (1985).
2. T. Skotheim, X. Yang, J. Chen, P. D. Hale, T. Inagaki, L. Samuelson, S. Tripathy, K. Hong, M. F. Rubner, M. L. denBoer and Y. Okamoto, Synth. Met. (to be published).

Acknowledgement: This work was supported by the Division of Materials Science, U. S. Dept. of Energy under contract No. DE-AC02-76CH00016.

A Resonance Photoemission Study of CO Adsorbed on Ni_3Al (111)

R. Garrett (NSLS BNL) and C. Loxton and A-M. Venezia (U. Ill).

We have used resonance photoemission to study the adsorption of CO on Ni_3Al (111). The crystal was exposed to saturation doses (4L) and NEXAFS measurements were used to confirm that, as for most metal surfaces, CO adsorbes "standing up" on Ni_3Al (111).

Figure 1 shows valence band photoemission spectra as the photon energy was varied through the Ni 3p threshold (66 and 68 eV). On pure Ni,[1] and on clean Ni_3Al[2] it is well known that the Ni "shake up" satellite exhibits a pronounced resonance at the 3p threshold. The valence band spectra exhibit three main features away from resonance (eg photon energy of 63 eV): The large Ni 3d valence band; and two CO derived features being the 4σ at a binding energy of 11 eV, and the superimposed 5σ and 1π molecular levels at 8.5 eV. The accepted picture of CO-metal bonding has the 5σ as the bonding level, and indeed this level can be seen undergoing a resonant enhancement at the 3p threshold, due presumably to a mixing with Ni d states in forming the CO-metal bond.

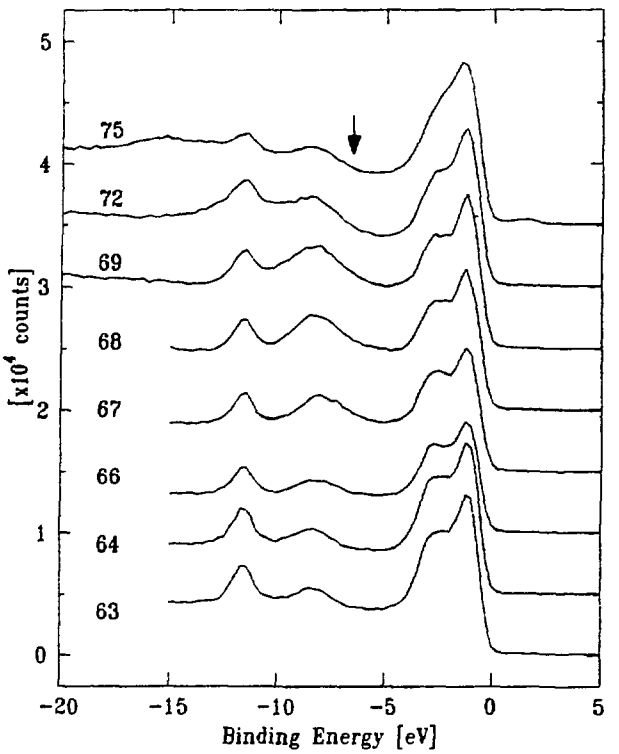

Figure 1. Valence band photoemission spectra of 4L CO on Ni_3Al (111) at photon energies between 63 and 75 eV. The arrow marks the position of the Ni "shake up" satellite on clean Ni_3Al.

References

1. C. Guillot, Y. Ballu, J.Paigne, J. Lecante, K. Jain, P, Thiry, R. Pinchaux, Y. Petroff and L. Falicov, Phys. Rev. Lett. **39**, 1632 (1972).
2. S. Wu, Z. Wang, R. Garrett, D. Sondericker, J. Sokolov and F. Jona, Europhys. Lett., **1**, 655 (1986).

Supported by the US DoE under contract number DE-AC02-76CH00016

Electronic State of Sm on Tantalum

U14A

S. Horn,[1] L. Tao,[1] and M.L. denBoer[2]

1. Department of Physics, New York University, 4 Washington Place, New York, N.Y. 10003
2. Department of Physics, Hunter College of CUNY, 695 Park Ave, New York, N.Y. 10021

The objective of our measurements is to investigate the electronic state of rare earth atom overlayers on transition metal (TM) surfaces as a function of coverage and transition metal substrate. At the same time possible changes of the surface electronic structure of the transition metal substrates are examined. Although ultimately TM single crystalline surfaces will be used as substrates, it appeared practical to study RE atoms on polycrystalline TM substrates in the beginning to find systems providing interesting physical effects which later can be studied in greater detail using TM single crystals as substrate for ordered RE overlayers. In this report we describe briefly the results of measurements on a Ta-Sm substrate-overlayer system.

Ta foil was used as a substrate. A clean Ta surface was obtained by repeatedly heating the foil close to the melting point. After many cleaning cycles no traces of oxygen were found, and from oxidation studies we estimate the residual oxygen coverage was less than 1/1000 of a monolayer. On this clean substrate, Sm overlayers at a range of coverages from as low as 1% of a monolayer to several monolayers of Sm were measured. It was found that at the lowest coverage both a Sm^{2+} and a Sm^{3+} component is present. When the coverage is increased, the 3+ component initially increases with increasing Sm coverage with respect to the 2+ component. However, at high coverage the 3+ component decreases again, probably when the coverage exceeds one monolayer, and a divalent surface layer is formed. The figure shows spectra taken at the resonace energy of Sm^{3+} for four different coverages, with *a* the lowest coverage and *d* the highest, highlighting the increase in the trivalent Sm contribution with increasing coverage.

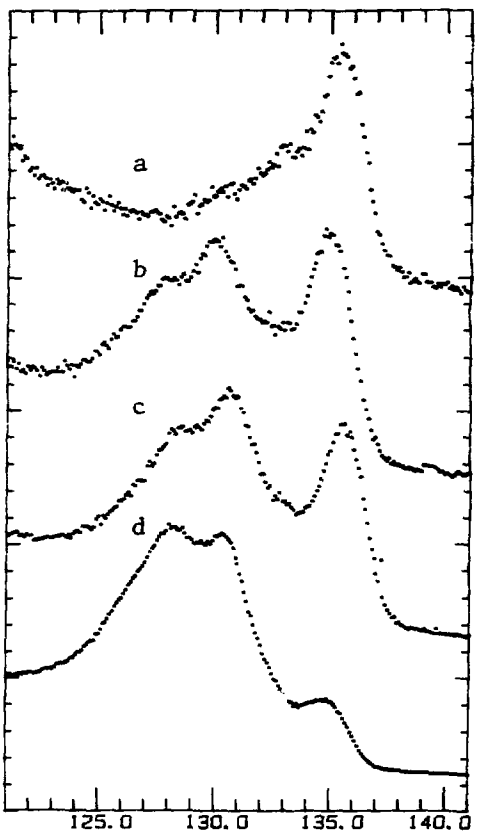

The clean Ta sample showed three distinct valence band contributions, which have been interpreted earlier as surface states. We investigated the energy dependent cross section of these three contributions and found significant differences. Surprisingly for surface states, none of the contributions was very sensitive to oxidation. The effect of the Sm deposition on the surface states has not yet been investigated.

Photoemission from Alkali metals coadsorbed with oxygen on Ru(001) U14

DATE OF EXPERIMENT: from: 1/22 to: 2/18

EXPERIMENTER(S):	AFFILIATION:
J. Hrbek, G. O. Xu	Chemistry, BNL
T. K. Sham	SRC, Wisconsin
M. L. Shek	Hunter College

WORK SPONSORED BY: DOE

Four alkali metals (Li, Na, K and Cs) in submonolayer, monolayer and multilayer coverage range and their interactions with oxygen were studied. Using photons with energy from 40 to 100 eV we measured valence band spectra and alkali metals' core levels (Li 1s, Na 2p, K 3p, Cs 4d and 5p).

Main findings of the study of clean alkali metals are summarized in the following:

- o Surface-core level binding energy shift is observed at multilayer coverages for all four metals.
- o Core levels in monolayer coverage range have lower binding energy and broader peak than in the multilayer range. In the following figure the EDC of the K multilayer on Ru (001) shows the surface and bulk K $3p_{3/2,1/2}$ levels together with the K 3p level at higher K.E., derived from potassium layer adsorbed directly at the Ru (001) surface. Notice the spin-orbit splitting observed for the first time for the K 3p level in the solid state.

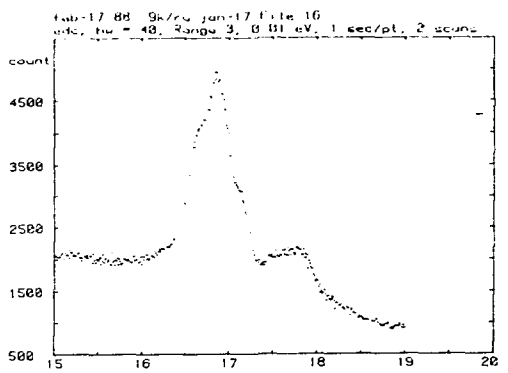

Coadsorption of oxygen was carried out for all four alkali metals at different metal coverages and metal/oxygen stoichiometries.

- o Negative shifts of B.E. of the alkali metals' core levels and changes in the peak shape are observed during oxygen coadsorption.
- o Large increase in photoemission intensity of core levels was noticed for all four alkali metals.

PHOTOEMISSION FROM ALKALI METALS COADSORBED WITH OXYGEN ON Ru(001)

J. Hrbek and G.-Q. Xu (Brookhaven National Laboratory), T. K. Sham (University of Western Ontario), M.-L. Shek (Hunter College).

Photoemission from alkali metal core levels (Li 1s, Na 2s, K 3p, Cs 5p and 4d) has been studied for different alkali metal coverages on Ru(001). The alkali atoms interacting directly with the Ru substrate show coverage dependent binding energy shifts towards the Fermi level, with the largest shift for Li (1.1 eV) (Fig.) and the smallest ones for K and Cs. At coverages > 1 ML, the core level shift between the second (surface) and the first (interface) layer is observed in all alkali overlayers. At "thin" multilayer coverages (~ 3 mL), all alkali overlayers exhibit 3 sets of core-level photoemission bands which are assigned to the interface, the immediate "bulk" and the surface in increasing binding energy. At coverages > 5 ML ("thick" multilayer) all alkali metals exhibit bulk-like properties and surface-atom core-level binding energy shifts are observed in all cases.[1,2]

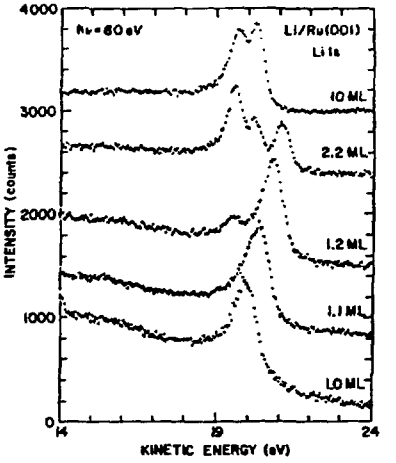

Fig. 1. Li 1s core level photoemission spectra of Li/Ru(001) surface as a function of Li coverage.

The interaction of oxygen with alkali metals (Li, NA, K and Cs) was studied with valence and core-level photoemission. During the stepwise coadsorption of oxygen at 80 K an increase in the emission intensity, line-width broadening and negative binding energy shift of alkali metal core-levels is observed. Two stages of oxygen adsorption are identified in PE. In the low O_2 exposure range an oxide species is formed; at higher exposures, peroxide and superoxide species are observed in Na, K and Cs.[3]

1. T. K. Sham, G.-Q. Xu, J. Hrbek and M.-L. Shek, Surface Sci., submitted.
2. T. K. Sham, M.-L. Shek, G.-Q. Xu, J. Hrbek, J. Vac. Sci. Technology, submitted.
3. J. Hrbek, G.-Q. Xu, T. K. Sham and M.-L. Shek, J. Vac. Sci. Technology, submitted.

This research was carried out at Brookhaven National Laboratory under contract DE-AC02-76CH00016 with the U.S. Department of Energy and supported by its Division of Chemical Sciences, Office of Basic Energy Sciences.

E. Jensen (Brandeis U.), R. Bartynski (Rutgers U.), and S. Hulbert, E. Johnson, and R. Garrett (NSLS)

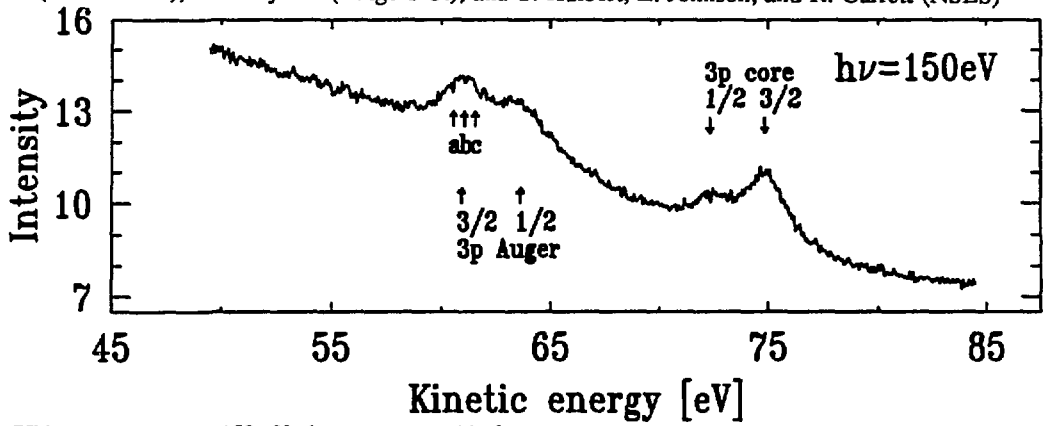

We present APEC spectra taken at 150 eV photon energy with the PGM monochromator on beamline U14 at the NSLS. The top panel shows an ordinary photoemission scan, subsequently called singles, through the Cu 3p core lines (72.4 and 74.9 eV) and the Cu $M_{2,3}VV$ (3p3d3d) Auger lines (61.0 and 63.7 eV). All kinetic energies are measured with respect to $E_F = 0$. The APEC spectra, shown in the side panels, were taken with one analyzer fixed at 60.6 (a), 61.1 (b), and 61.6 (c) eV, in the $3p_{3/2}$ part of the Auger spectrum (see arrows in the singles spectrum). A second analyzer was scanned through the 3p core region. Coincidence events were counted only when electrons were received in each analyzer simultaneously. The coincidence data are shown as open circles with error bars. The solid line is a digital smooth to the data (ΔE=0.5 eV fwhm) and the dashed line is the corresponding background-subtracted singles spectrum. The energy resolution — electron plus photon — is ~0.5 eV in each analyzer.

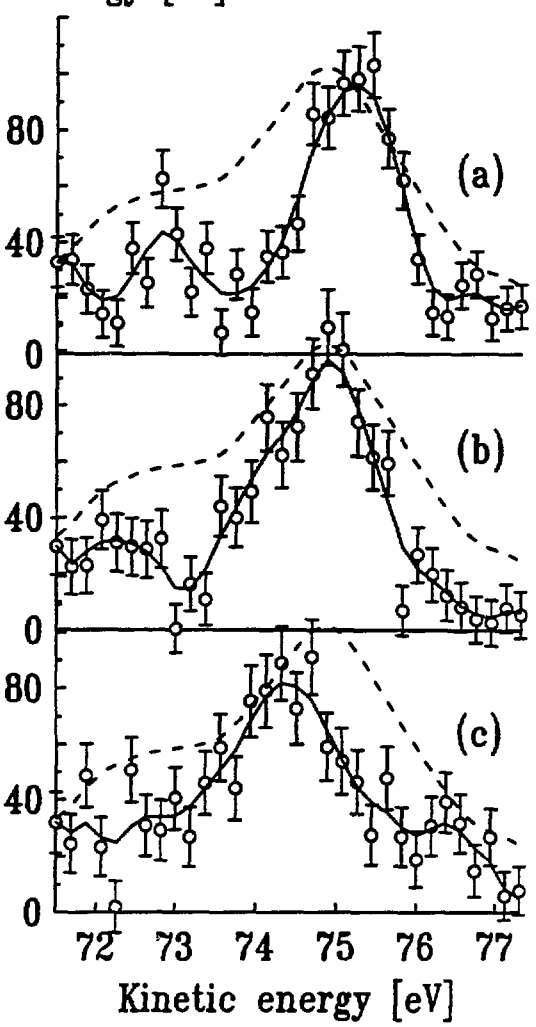

Three significant effects are seen in the APECS data.

1. The large background under the singles spectrum is eliminated.
2. The $3p_{1/2}$ component of the core spectrum is eliminated. The small remainder is due to Coster-Kronig decay of the $3p_{1/2}$ core hole into the $3p_{3/2}$.
3. The large (~2 eV) core lifetime broadening of the photoelectron spectrum is eliminated and the energies of the photoelectron peaks in the coincidence spectra track the energies of the fixed (Auger) analyzer due to the requirement of energy conservation between the Auger- and photo-electrons.[2] The remaining width is partly instrumental. We estimate that the intrinsic width of the main peak in panel (a) is ~ 1.0 eV. This is the intrinsic width of the Auger final state, which has been calculated to be 0.2 eV[3]. The extra structure and increased widths in panels (b) and (c) are attributed to transitions to other Auger final states.

[1]E. Jensen, R. A. Bartynski, S. L. Hulbert, E. D. Johnson, and R. F. Garrett, PRL *62*, 71 (1989),
[2]H. W. Haak, et.al., PRL *41*, 1825 (1978),
[3]G. A. Sawatzky and A. Lenselink, PRB *21*, 1790 (1980).

This work was supported by Analog Devices Career Development Grant (Jensen), New Jersey Comm. on Science and Technology Grant 87-240040-7 (Bartynski), and the Division of Material Sciences U. S. Department of Energy under Contract No. DE-AC02-76CH00016.

E. Jensen (Brandeis U.), R. Bartynski (Rutgers U.), and S. Hulbert, E. Johnson, and R. Garrett (NSLS)

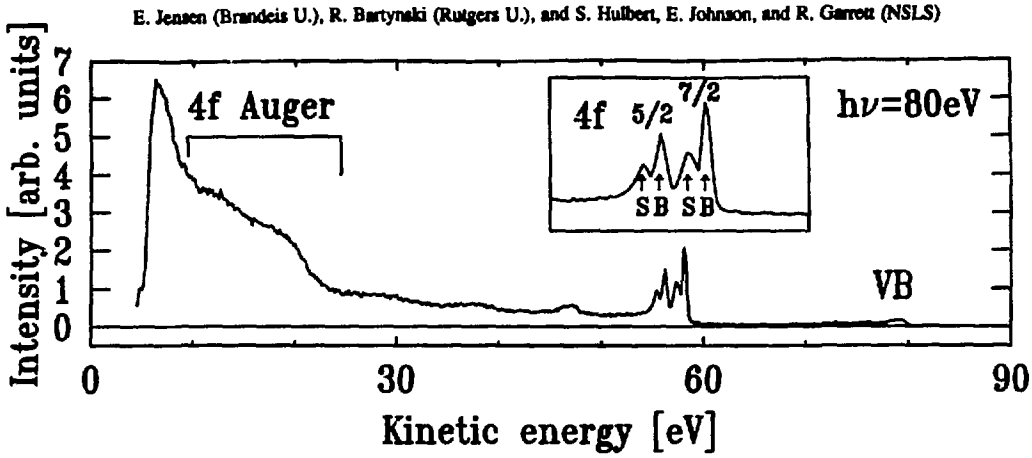

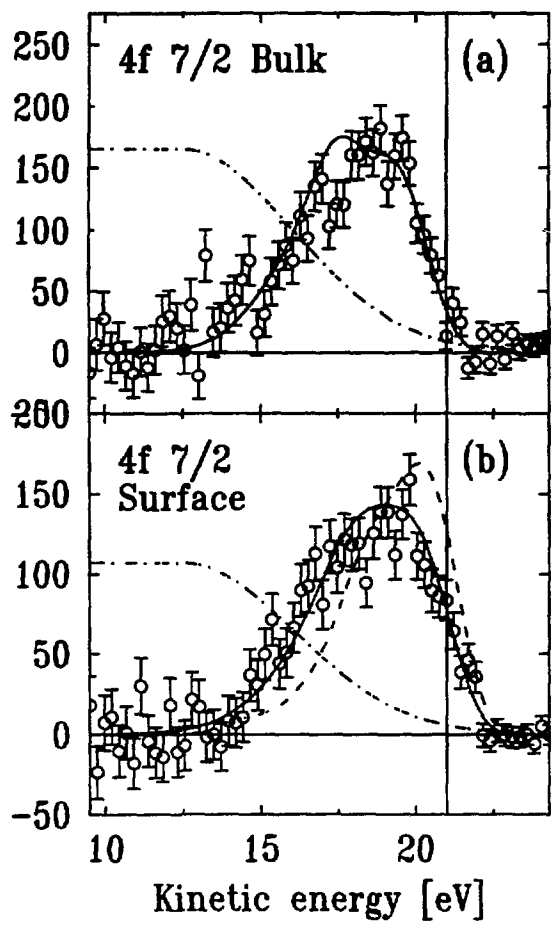

The top panel is a wide ordinary photoemission (singles) scan showing the Ta 4f core lines, the Ta $N_{6,7}VV$ (4f5d5d) Auger peaks, and the valence band region. We present hν=80eV APEC spectra, shown in the side panels, with one analyzer fixed either at the peak of the bulk (58.1 eV (E_F=0), panel a) or surface-shifted (57.4 eV, panel b) $4f_{7/2}$ core line. A second analyzer was scanned through the $N_{6,7}VV$ Auger region. Coincidence events were counted only when electrons were received in each analyzer simultaneously. A smoothly-varying background (dash-dot line) resulting from correlated Auger secondary emission has been subtracted from the measured APEC spectra. The background-removed coincidence data are shown as open circles with error bars. The remaining lines (solid and dashed, identified below) are self-convolutions of layer-resolved valence band DOS (SCDOS) calculated by Krakauer[1]. The energy resolution — electron plus photon — is ≤0.5 eV in the fixed core-level analyzer and ≤1.0 eV in the swept Auger-region analyzer. Four significant effects are seen in the APECS data.

1. The large background under the singles spectra is removed. The secondary background subtracted from the surface spectrum is ~2/3 that of the bulk, because an Auger electron produced at the surface can more easily escape without inelastic scattering.
2. The maximum bulk $4f_{7/2}$ Auger kinetic energy (panel a) is lower than that for the surface (panel b) by the Ta(001) $4f_{7/2}$ surface core level shift (0.7eV).
3. The bulk $4f_{7/2}$ APEC spectrum (panel a) is similar in threshold behavior and overall width to the SCDOS (solid line), except for the discrepancy at 17.5 eV which is attributed to matrix element effects.
4. The surface $4f_{7/2}$ APEC spectrum (panel b) is very different in position, width and shape from the SCDOS for the surface layer (dashed line). The agreement is much better between the APEC spectrum and the average of the SCDOS for the surface and second layers (solid line). We speculate that this is due to core hole migration from surface to bulk, with subsequent bulk Auger decay. This extra decay mode could also explain the previously observed anomalously large width of the surface-shifted $4f_{7/2}$ core level.[2]

[1] H. Krakauer, Phys. Rev. B *30*, 6834 (1984)
[2] D. Spanjaard, et. al., Surf. Sci. Repts. *5*, 1 (1985)

This work was supported by Analog Devices Career Development Grant (Jensen), New Jersey Comm. on Science and Technology Grant 87-240040-7 (Bartynski), and the Division of Material Sciences U. S. Department of Energy under Contract No. DE-AC02-76CH00016.

VALENCE BAND ELECTRONIC STRUCTURE MEASUREMENTS FROM IRON OXIDE SINGLE CRYSTALS

Robert J. Lad and Victor E. Henrich

Applied Physics, Yale University, New Haven, CT 06520

The interpretation of valence band photoemission spectra from iron compounds containing ferrous (Fe^{2+}) and ferric (Fe^{3+}) cations has been a long-standing challenge in surface science. Early analyses assumed the presence of localized 3d cation levels, and the photoemission features were correlated to the calculated multiplet and crystal-field split final states. However, recent calculations of the electronic structure for transition-metal compounds have suggested that cation-ligand hybridization must also be taken into account to correctly describe the valence band electronic structure.

To further investigate this issue, we have performed resonant photoemission measurements across the 3p→3d photoabsorption threshold from cleaved $Fe_{0.94}O$, Fe_3O_4, and α-Fe_2O_3 single crystals, using synchrotron radiation. Using well-characterized single crystals, we have been able to identify the 3d-derived states associated with Fe^{2+} cations (in $Fe_{0.94}O$) and Fe^{3+} cations (in α-Fe_2O_3) that are octahedrally coordinated to oxygen ligands, and we have distinguished this 3d-derived emission from the overlapping unhybridized O 2p states. In Fe_3O_4, a complex valence band structure results from the presence of both octahedrally coordinated Fe^{2+} and Fe^{3+} cations and tetrahedrally coordinated Fe^{3+} cations. By comparing the photoemission spectrum from Fe_3O_4 to the spectra from the other iron oxides, the 3d-derived states associated with each cation environment can be determined.

An important result that we find is that the 3d-derived states extend to about 18 eV below the Fermi level in each of the iron oxides. The degree of hybridization between the cation and ligand states which causes this wide valence band was inferred from constant-initial-state (CIS) spectra measured across the 3p→3d threshold. States near the top of the valence band were found to exhibit antiresonant CIS spectra, characteristic of final states involving ligand charge transfer ($3d^n\underline{L}$, where $\underline{L}$ is a ligand hole). At higher binding energies, the CIS spectra displayed the Fano-like resonances expected for $3d^{n-1}$ final states. However, in these materials, the $3d^n\underline{L}$ and $3d^{n-1}$ final states cannot be referred to as the main line and satellite (e.g. as in NiO), since they overlap considerably. Good agreement is obtained when comparing our data to the available configuration interaction cluster calculations for these materials.

This work was supported in part by NSF Solid State Chemistry Grant # DMR-87-11423 and was carried out at the National Synchrotron Light Source at Brookhaven National Laboratory using beamline U14.

PHOTOEMISSION FROM ALKALI METALS COADSORBED WITH OXYGEN ON Ru(001)

M. L. Shek (CUNY), T. K. Sham (CSRF), G. Q. Xu (BNL) and J. Hrbek (BNL)

Photoemission spectra of four alkali metals (Li, N, K, Cs) of varying coverages adsorbed on Ru(001) surface were measured using soft X-ray synchrotron radiation. We have investigated the changes of semicore and core levels Li 1s, Na 2p, K 3p, Cs 5p and 4d, and valence band upon interaction with oxygen at 80 K. This is part of our effort to characterize the alkali oxides which are used in several industrial processes for catalyst promotion. Here we specifically address the striking behavior of the core levels: i) increase in the emission intensity during the oxygen coadsorption which can be as large as a three-fold increase upon saturation; ii) negative binding energy shifts. Some of these effects were previously noticed in passing in several isolated studies. However, this work examines, for the alkali metals series, the coverage, stoichiometry and photon energy dependencies of the core levels photoemission.

In initial stages of oxygen coadsorption (<0.25 L) on potassium covered Ru surface (θ_K = ~4 monolayers) oxygen penetrates the top layers and interacts with K at the K-Ru interface. For higher oxygen exposures (>0.5 L) the K 3p level broadens, shifts to lower B.E. and increases in intensity. At saturation the B.E. of the K 3p is 17.38 eV, down from 18.73 eV for a clean K overlayer, the line width is 1.9 eV (only 0.3 eV for a clean one) and the integrated intensity 2.7 times higher.

For a thick alkali overlayers, part of the core emission increase can arise from the disappearance of the associated plasma excitations upon oxidation. However, for (2 x 2) and ($\sqrt{3}$ x $\sqrt{3}$)R30 Na submonolayers, neither plasma excitations nor escape depth effects should play a role in the observed photoemission intensity. At hv = 50 eV, oxygen saturation leads to at least a three-fold increase, while at higher photon energies (55 and 75 eV), the intensity is less than twice the original value.

Increase in intensity of photoemission of core level and their negative binding energy shifts are general phenomena of oxidized alkali metals. Theoretical work is needed to understand the intensity increase and its implications for the use of photoemission for the determination of composition.

This research was carried out at Brookhaven National Laboratory under contract DE-AC02-76CH00016 with the U. S. Department of Energy and supported by its Division of Chemical Sciences, Office of Basic Energy Sciences.

THE INTERACTION OF S WITH CU AND WITH FE* U14

M.L. Shek (Hunter College) and P.M. Stefan (Brookhaven National Lab)

We made the following measurements on c(2x2)S on Fe(100) and S on evaporated Cu: S $L_{23}VV$ Auger, S 2p core level and Fe(Cu)+S 3p valence band, with photon energies between 40 and 320 eV (P3 and P2 ranges). Fig. 1 shows that Fe-S and Cu-S result in differences in the high kinetic energy sides of the S Auger spectra. The similarity in the $L_{23}M_{23}M_{23}$ energies (main peak at 145.8 eV), in spite of a larger energy separation between 2p and 3p for S on Cu, might be due to a larger effective hole-hole interaction in S 3p on Cu.

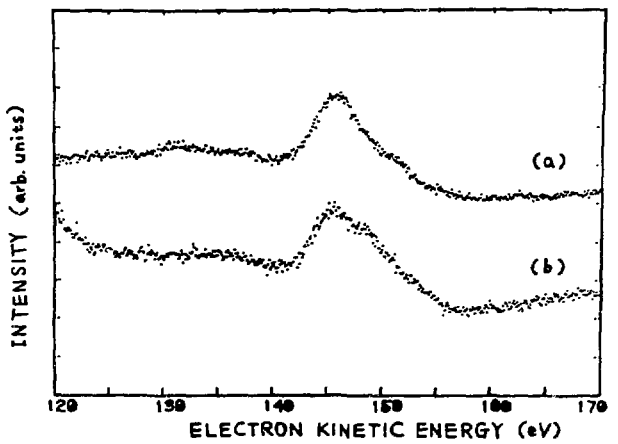

Fig. 1
S $L_{23}VV$ Auger spectra obtained with a double-pass CMA:
(a) c(2x2)S on Fe(100)
(b) S on evaporated Cu
-5.1 eV should be added to reference the kinetic energies to the Fermi level.

* Proposal #88-V-30/1, Expt. U14-88-GU63, 1988 Aug. 29 - Sept. 9
Acknowledgements: We acknowledge J. Hrbek, G.-Q. Xu, F. Loeb for their help; and PSC-CUNY award no. 668359.

RESONANT PHOTOEMISSION FROM Ti_2O_3 AND V_2O_3: HYBRIDISATION AND LOCALISATION OF CATION d-STATES

Kevin E. Smith and Victor E. Henrich, Applied Physics, Yale U., 15 Prospect St., New Haven, CT 06520.

The phenomenon of resonant photoemission, whereby the number of cation d-electrons photoemitted is seen to increase dramatically when the photon energy is swept through a cation core level optical absorbtion edge, has been the subject of much investigation recently and is being used increasingly as a spectroscopic tool to isolate the cation d-state contribution to complex hybridised ligand states. We have investigated the 3p → 3d resonance in single crystal oxides of Ti and V as observed in both angle integrated and angle resolved photoemission spectra taken from cleaved surfaces. Large differences exist between the resonance profiles (emission intensity vs. photon energy plots) measured in these two modes. Specifically, for either $Ti_2O_3(10\bar{1}2)$ or $V_2O_3(10\bar{1}2)$ the resonance maximises at a photon energy ≈ 10 eV higher when the spectra are taken in an angle resolved normal emission mode than in an angle integrated mode. The angle resolved data can be explained by a localised molecular orbital picture of the d-state electronic structure, with the resonance at threshold displaying great sensitivity to the local nature of the occupied orbitals. However, we have observed dispersing d-bands from these oxides, and their transport properties are well described by a delocalised band model for the d-state electronic structure. Thus the data leads to the apparent paradoxical situation of requiring simultaneously the use of both local and non-local models of the electronic structure of these materials to explain their observed photoemission properties. We interpret our results in the context of the accepted localised picture of the resonance. However, we also obtained data on the resonance in these materials which is more difficult to explain using this localised picture. We have observed that in Ti_2O_3, which has one d-electron per cation (a $3d^1$ configuration), the integrated area under the O 2p emission feature in the photoemission spectra increases by over 100% as the photon energy is swept through the Ti 3p → 3d optical absorption edge. In contrast, for V_2O_3, which has two d-electrons per cation (a $3d^2$ configuration), the emission from the O 2p band is seen to increase by only 25% as the photon energy is swept through the V 3p → 3d absorption edge. Thus if only d-state hybridisation is considered as a source for the enhanced emission, this data indicates that there is considerably more d-state character in the O 2p band in Ti_2O_3 than in V_2O_3. This is a surprising conclusion since the O 2p band lies almost 2 eV closer to the cation d-band in V_2O_3 than it does in Ti_2O_3, which is indicative of greater d-character in the O 2p band of V_2O_3. Thus in these compounds a mechanism other than conventional resonant photoemission from hybridised d-states may be responsible for the enhancement of the O 2p emission.

This work was partially supported by NSF Solid State Chemistry Grants DMR-82-02727 and DMR-87-11423.

A NEXAFS Study of the Effect of Annealing Treatment on the Structure of Thin Polyacrylonitrile Films Deposited on Ni.

G. Tourillon (LURE, Orsay, France), M. Raynaud, C. Reynaud, G. Lecayon, and P. Viel (CEN-Saclay, Gif-sur-Yvette, France) and R. Garrett and N. Lazarz (NSLS, BNL).

Bulk polyacrylonitrile is an important polymer because its chemical structure and its electrical properties can be varied with the annealing treatment used in preparing the polymer. We have used the NEXAFS technique to investigate the effects of annealing treatments on the structure and chemistry of the polymer, for thin films of polyacrylonitrile deposited on polycrystalline Ni.

NEXAFS spectra after different annealing treatments are shown in Figure 1, and reveal a dramatic evolution of the polymer structure and composition. After annealing to 300°C much of the N component of the polymer is removed, and features associated with C≡N bonds (peaks 1,3 and 9) are reduced. Also resonances due to the formation of C=N and C=C bonds appear (peaks 2 and 8). After annealing to 500°C the film is composed essentially of C=C and C-H bonds, with some residual C=N and C-N groups.

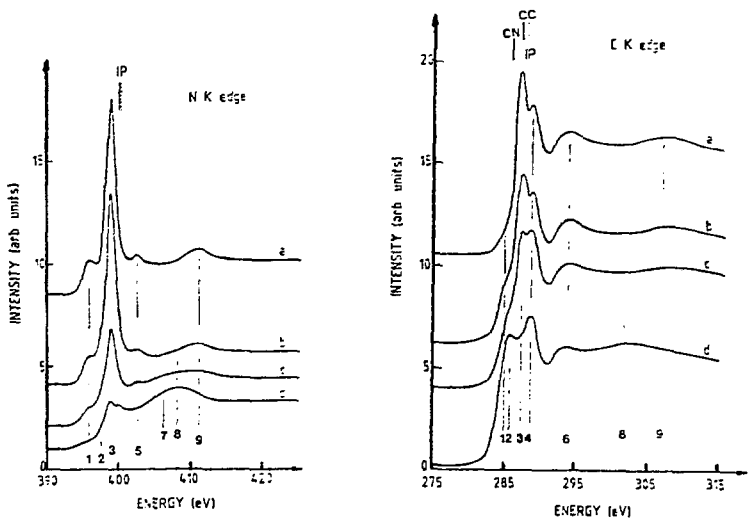

Figure 1. Polyacrylonitrile NEXAFS spectra from: a) 140 Å unannealed film; b) 500 Å unannealed film; c) film annealed at 300°C; d) film annealed at 500°C.

Supported by the US DoE under contract number DE-AC02-76CH00016

A NEXAFS Study of the Effect of Film Thickness on the Structure of Thin Polyacrylonitrile Films Deposited on Ni.

G. Tourillon (LURE, Orsay, France), M. Raynaud, C. Reynaud, G. Lecayon, and P. Viel (CEN-Saclay, Gif-sur-Yvette, France) and R. Garrett and N. Lazarz (NSLS, BNL).

We have used the NEXAFS technique to investigate the effects of film thickness on the structure of polyacrylonitrile, and of the polymer/substrate interface, for thin films of polyacrylonitrile deposited on polycrystalline Ni.

Our NEXAFS data reveal that the electronic and structural properties of thin polyacrylonitrile films depend strongly on the thickness of the polymer film. From the polarization dependence, three regimes are observed as a function of film thickness: i) the first layer has a "monomer like" structure, with the molecules oriented normal to the surface and the C≡N triple bonds replaced by C=N groups due to a strong interaction with the Ni substrate; ii) for thicknesses up to 50 Å (Figure 1) the polymer chains are well ordered with the aliphatic backbone normal to the surface and the C≡N groups parallel to it. The split π^* resonance (Fig. 1 peaks 1 and 3) is a consequence of lifting the orbital degeneracy of the antibonding π levels due to intramolecular C≡N interactions; and iii) for thicker films the polymer chains become randomly oriented, and structural defects, eg C=C bonds, appear.

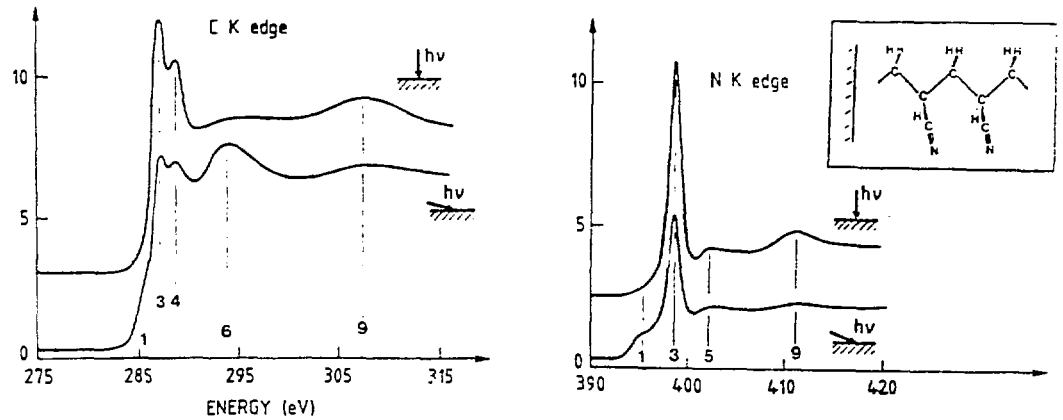

Figure 1. NEXAFS spectra from a 20 Å polyacrylonitrile film at both the C and N K-edges, showing the polarization dependence obtained.

Supported by the US DoE under contract number DE-AC02-76CH00016

NEXAFS STUDY OF POLYPYRROLE AND POLYTHIOPHENE LANGMUIR-BLODGETT FILMS.

X. Q. Yang, J. Chen, T. Inagaki*, P. Hale, T. A. Skotheim, BNL; Y. Okamoto, Polytechnic University; M. denBoer, Hunter College (CUNY); L. Samuelson, S. Tripathy, U of Lowell; K. Hong, M. Rubner, MIT.

Langmuir-Blodgett films of hexadecylpyrrole, octadecylpyrrole and Polythiophene/Stearic Acid have been studied by NEXAFS Spectroscopy using sample current total yield detection. The polarization dependant Carbon K edge and Sulphur L edge NEXAFS spectra show a high degree of ordering with the hydrocarbon tails normal to the substrate for the multi-layer LB films. The ordered but tilted hydrocarbon tails in the monolayer LB films were attributed to the strong interaction between the heterocyclic head groups and the Pt substrate.

Energies and proposed assignment of features in the C 1s spectrum of Hexadecylpyrrole (HDP) LB films

	HDP monolayer			HDP multi-layer			Assignment (final orbital)	
#	E (eV)	Intensity 90°	20°	E (eV)	Intensity 90°	20°	Ring	Hydrocarbon tail
1	285.5			285.5	sh	sh	π^* $3b_1$(C=C)	
2	288.5	s	m	288.5	s	m	[π^* $2a_2$(C=C)]	π^* (CH_2)
3	294	s	s	294	m	s	σ^* (C-C)	σ^* (C-C)
4	298.5	w	w	298.5	w	w	σ^* (C-C)	σ^* (C-C)
5	303	wm	m	303	wm	m	σ^* (C=C)	

s strong; m medium; wm weak medium; w weak; sh shoulder

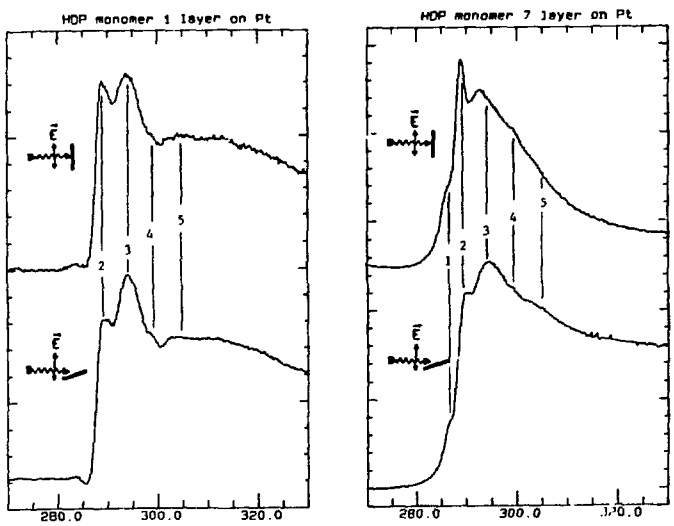

Work supported by the U.S. Department of Energy Division of Materials Science under Contract No. DE-AC02-76CH00016.

* UBE Industries Fellowship Recipient

BEAM LINE U14

ORIENTATIONAL BEHAVIOR OF THIN FILMS OF POLY(3-METHYLTHIOPHENE) ON PLATINUM SURFACE STUDIED BY NEXAFS SPECTROSCOPY.

X. Q. Yang, J. Chen, T. Inagaki*, P. Hale. T. A. Skotheim, BNL; M. denBoer, Hunter College (CUNY).

Carbon K edge and sulphur L edge NEXAFS spectroscopy have been used to study the orientational effects for thin films of poly(3-methylthiophene) electrochemically grown on a platinum surface. The polarization dependence of the Carbon K edge spectra for 230 Å films show a higher degree of ordering for higher polymerization potentials, this is consistent with the nucleation-growth models where disorder is introduced by rapid growth. The figures shows the Carbon K edge spectra for 230 Å films grown at 1.4 V and 1.8 V vs a saturated calomel electrode.

Energies and proposed assignment of features in the C 1s spectrum of Poly(3-methylthiophene) (PMET) thin films

	PMET 1.8 V 230 Å			PMET 1.4 V 230 Å			Assignment (final orbital)
#	E (eV)	Intensity 90°	20°	E (eV)	Intensity 90°	20°	Ring
1	285.5	sh	sh	285.5	sh	sh	π^* 3b$_1$ (C=C)
2	288.5	m	m	288.5	m	s	[π^* 2a$_2$ (C=C)]
3	295	s	s	295	s	s	σ^* (C-C)
4	298.5	w	w	298.5	w	w	σ^* (C-C)
5	304	m	m	304	m	m	σ^* (C=C)

s strong; m medium; wm weak medium; w weak; sh shoulder

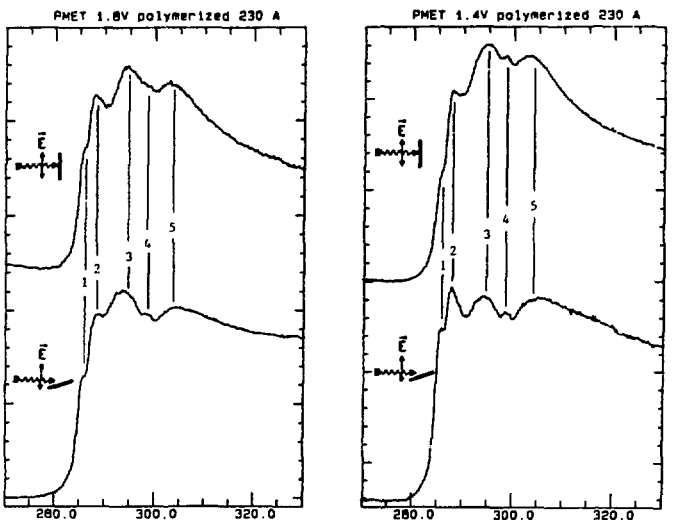

Work supported by the U.S. Department of Energy Division of Materials Science under Contract No. DE-AC02-76CH00016.

* UBE Industries Fellowship Recipient.

Compact Photon Beam Position Monitor

E.D. Johnson and T. Oversluizen (NSLS)

We have developed a new compact water-cooled beam position monitor for use at the NSLS X-13 Insertion Device Development beamline. To study the impact of this devices novel geometry on its sensitivity, stability and linearity we constructed a prototype which incorporated all of the new design features except the water cooling. The monitor is based on a copper monolith which is positioned by a stepper-motor controlled x-y stage. The beam passes through the center of the monolith intercepting the edges of four tungsten blades which are mounted 90 degrees apart via beryllia shims. The blades are thus well cooled, but electrically isolated from the monolith, which is itself, isolated from ground. The monolith can then be biased with respect to the blades and act as a collector of the photo-current produced at their edges. This has the effect of reducing cross-talk between blades. The position of the beam relative to the center of the monitor is then recorded as the ratio of the difference of the blade currents to their sum. By moving the monitor through the beam in known increments, we have established a position sensitivity better than 0.1 microns, and a linear response over a range of 1.7 mm. By positioning a second detector with a slit behind the photoelectron monitor, we have demonstrated a long term stability of better than 10 microns, our current experimental resolution limit. It is worth remembering that the vertical source sigma in the NSLS VUV ring is typically 200 microns, and that the design value is 60 microns. It is expected that monitors of this type will be useful for stabilizing the beam position in insertion devices at synchrotrons of this, and future generations.

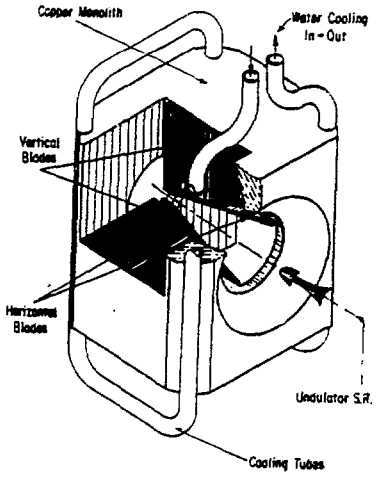

This work supported under the auspices of the U.S. Department of Energy, contract # DE-AC02-76CH00016.

SOFT X-RAY REFLECTION-EXAFS AT THE CARBON K-EDGE. D. R. Black (NIST, formerly NBS) and G. G. Long (NIST, formerly NBS).

The structure of glassy carbon has been a subject of much interest because its properties are different from those of other carbons, leading to a variety of new applications. Various experimental studies concerning the glassy carbon structure have been made, in particular concerning the likely contribution of tetrahedral bonding together with trigonal bonding in the construction of an apparently isotropic carbon structure.

The present study involves measurements of the soft x-ray absorption spectrum at the carbon K-edge by means of the method of external reflection below the critical angle. Model materials which were measured include highly oriented pyrolytic graphite (where measurements were made with the polarization vector parallel and perpendicular to the c-axis) and single crystal diamond. It is of interest to compare diamond and graphite because of the different coordinations (trigonal in graphite and tetrahedral in diamond) leading to substantial differences in bonding and properties, each contributing to some fraction of glassy carbon bonding.

Examples of reflectivity spectra for glassy carbon, diamond, graphite ($\hat{\epsilon} \perp c$) and graphite (with $\hat{\epsilon} \parallel c$) are shown in Fig. 1. These spectra were taken from families of reflectivity curves with reflection angles between 0.5^{o} and 3.5^{o}. The spectra shown here all were taken with reflection angles near 1.5^{o}.

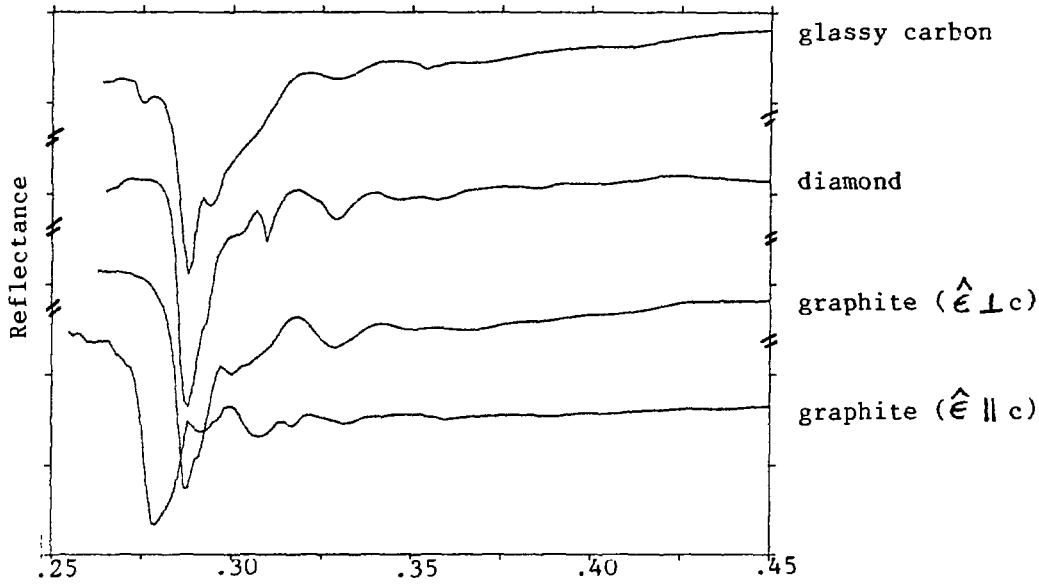

Fig. 1.

The reflectance spectra are being analyzed to derive the optical constants as a function of energy for these materials, and from the imaginary part, the absorption spectra are obtained. Similar spectra were obtained from x-ray Raman data, where those results are the mirror image of the absorption spectra.

VALENCE HOLE LOCALIZATION IN MOLECULAR AUGER DECAY

D.M. Hanson, D.A. Lapiano-Smith, C.I. Ma, and K.T. Wu (SUNY at Stony Brook)

Studies of the unimolecular decay of carbon tetrafluoride and silicon tetrafluoride following the excitation of core electons provided evidence for a "valence bond depopulation" fragmentation mechanism. This term refers to an Auger final state in which the two valence holes produced by the Auger decay are highly correlated and localized on the atomic site of the core hole. The observation of F^{2+} ions in time-of-flight mass spectra following excitation of a fluorine 1s electron in silicon tetrafluoride is significant because it provides direct evidence for the formation of this localized two hole state and its persistence over the time of fragmentation. In contrast, the lack of F^{2+} ions from carbon tetrafluoride indicates that the fragmentation occurs through a delocalized two hole state in this compound. This difference in these two molecules indicates smaller intramolecular interactions in the silicon analog, which is consistent with its increased ionicity and larger fluorine - fluorine distances.

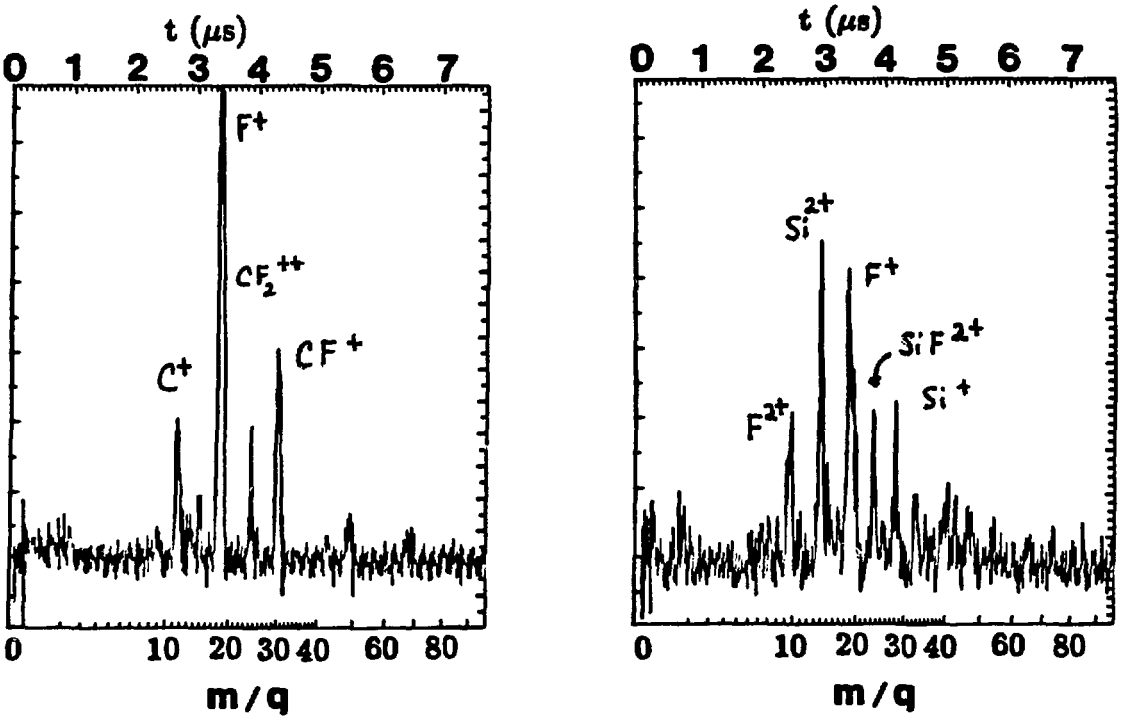

This research was supported by the National Science Foundation (CHE-8703340).

Magnetic Scattering at the Iron L2,3 Edge

U15

J.B. Hastings, E.D. Johnson and D.P. Siddons (NSLS)

The data we present here were obtained from an iron film 388 Å thick grown epitaxially on a (110) gallium arsinide substrate. The measurements were made in a vacuum diffractometer with the axes of rotation perpendicular to the plane of polarization of the incident radiation. The (100) direction of the crystal was along the axis of rotation, and clamped in the pole pieces of an electromagnet. This instrument then allowed us to study the scattered intensity as a function of angle, photon energy, and sample magnetization. A resonant enhancement for the magnetic scattering had been theroretically predicted at the L 2,3 edge of iron*, so this work was done at photon energies of 700 to 740 eV.

The first figure shows spectra in the absence of magnetic field. The absorption data shows lines for the 2p 3/2 and 2p 1/2 in the ratio of 2:1 integrated intensity, with a gaussian sigma of 5 eV dominated by the monochromator resolution. The off specular scattering is primarily fluorescence, and has very little intensity below the edge. The specular reflection is the difference between the specular and offspecular scattering and is relativly high below the edge as expected. In second figure we show the so called "flipping ratio". This is the ratio of the difference in intensities when the sample is magnitized in opposite directions, to the average intensity. We find that it can be fitted with two broad lorentzians of different sign, with energies and relative intensities which correspond to scattering from the 2p 3/2 and 1/2 spin orbits. Still to be understood is why these peaks are almost an order of magnitude broader than the unoccupied d-band. We are encouraged by these results and are hopeful that this technique may provide insight into the magnetic properties of very thin layers.

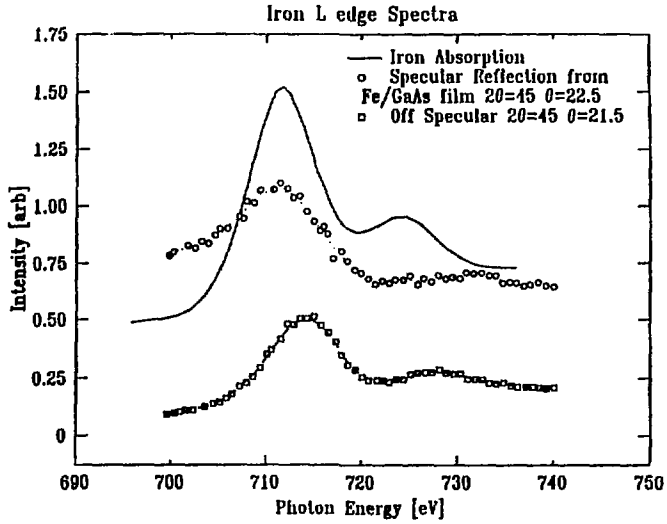

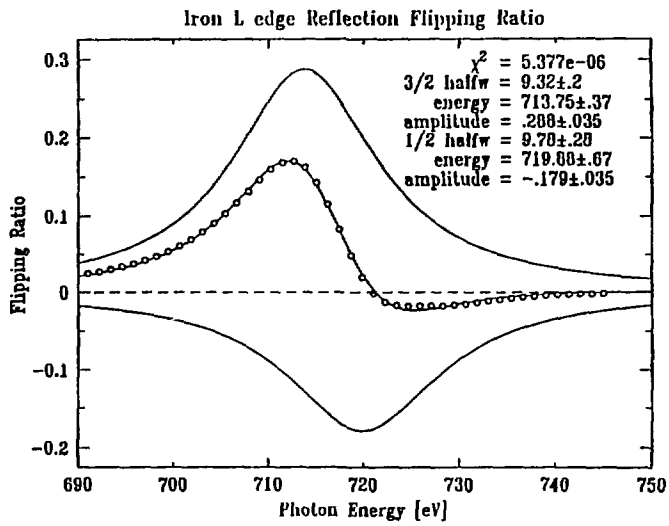

*J P. Hannon, G.T. Trammel, M. Blume and Doon Gibbs, PRL 61(1988)1245

This work supported by the US Dept. of Energy, contract #DE-AC02-76CH00016.

FLUORESCENCE OF AUGER DECAY PRODUCTS

L.A. Kelly and E.D. Poliakoff (Boston University)* and
D.M. Hanson, C.I. Ma, D.A. Lapiano-Smith, and K.T. Wu (SUNY at Stony Brook)**

Auger decay and autoionization following selective excitation of core electrons in molecules can produce sufficient quantities of doubly charged ions to allow luminescence spectra to be observed. Vibrational structure in the luminescence spectra provides significant information about excited state properties of these ions and about the dynamics of core electron excitation and relaxation. The figure below shows the vibrationally resolved fluorescence spectrum of O_2^{2+} following oxygen 1s to σ^* excitation. The core hole excited state electronically autoionizes and then the resulting doubly charged ion fluoresces. The vibronic spacings and intensities are being analyzed in terms of the electronic potentials and the level populations of the states that are involved.

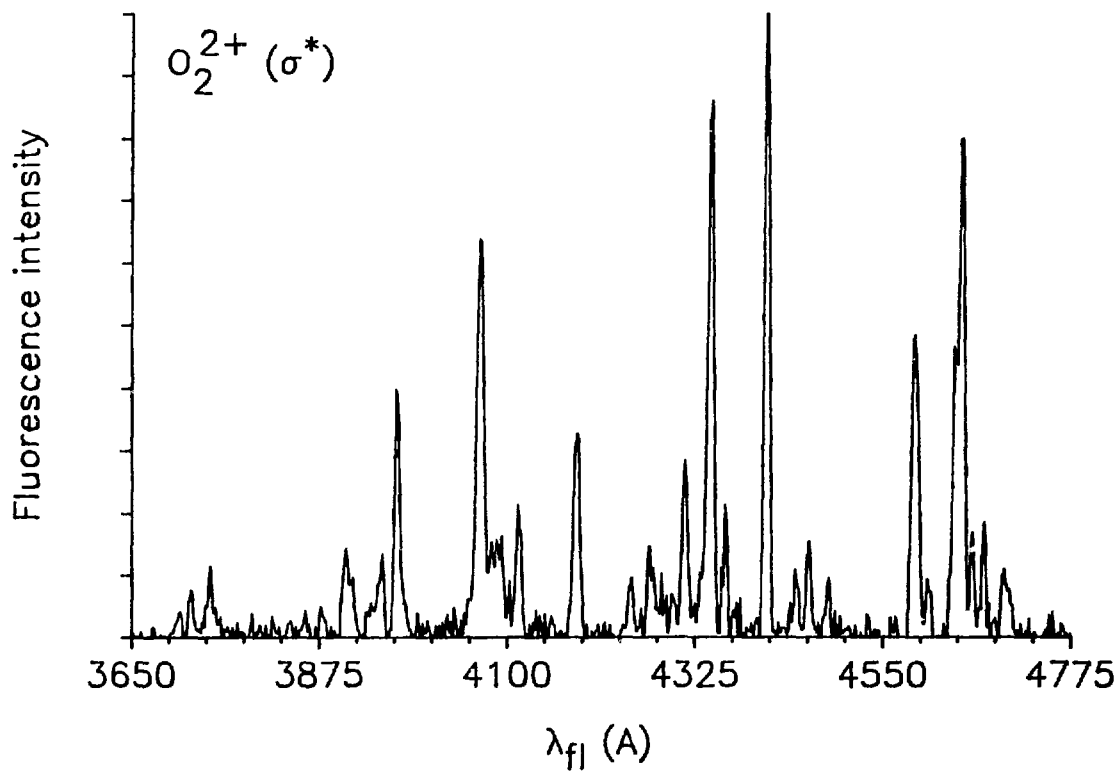

*Support from the Air Force Office of Scientific Research (Physics and Geophysics 840261) and the National Science Foundation (CHE-8613428) and from **the National Science Foundation (CHE-8703340) is gratefully acknowledged.

STUDIES OF AN AlAs/GaAs and GaAs/AlAs HETEROJUNCTIONS BY TOTAL ELECTRON YIELD

A. Krol, C. J. Sher, S. C. Woronick, H. Resat, L. Krebs, Y. H. Kao, (SUNY at Stony Brook), and L. L. Chang (IBM Thomas J. Watson Research Center, Yorktown Heights, NY 10598).

Total electron yield (TEY) by means of soft x-ray excitation of AlAs/GaAs and GaAs/AlAs heterojunctions has been studied. These heterojunctions were prepared by an overgrowth of a 250 Å AlAs (GaAs) layer on a GaAs (AlAs) substrate using Molecular Beam Epitaxy. The AlAs/GaAs heterojunction was capped with a 25 Å layer of GaAs. TEY spectra were recorded by measuring both the photoemission with an electron collector and the neutralizing current with an electrometer vs grazing angle of incidence at fixed incoming photon energies (400-800 eV), see Fig. 1 and 2. X-ray scattering was also measured simultaniously. Experimental data are compared with theoretical analysis, based on a modified Fresnel formulation, to calculate the wave field distribution in stratified media with interfacial roughness. The TEY angular profiles and their derivatives, which were obtained at a given x-ray energy, reveal information on the interfacial roughness, electron mean-free-path, and optical constants of the epilayer in the soft x-ray regime. It has been proven that the information depth is larger than the electron mean-free-path.

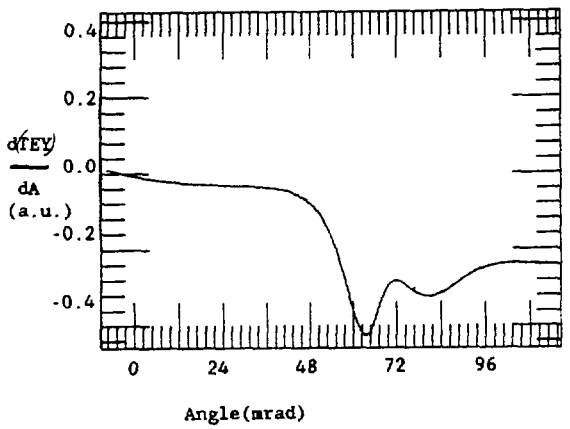

Fig. 1. The derivative of TEY with respect to angle vs angle for GaAs/AlAs. Experiment···; theory——; cut-off angle 40 mrad; energy 600 eV.

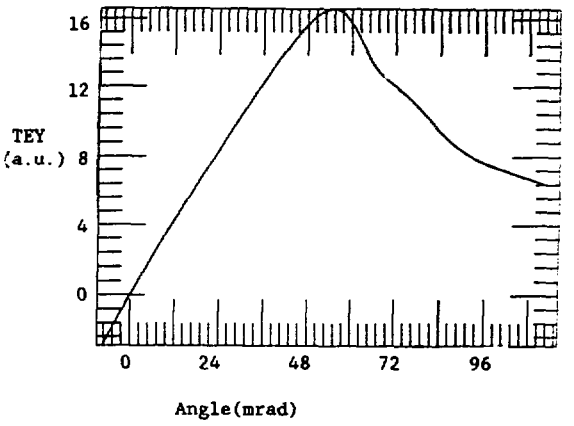

Fig. 2. As Fig. 1 but TEY vs angle.

This research is supported by ONR under grant No. N0001483K0675, and by DOE under grant No. DE-FG02-87ER45283.

CHARACTERIZATION OF $In_{.53}Ga_{.47}As/InP$ AND $In_{.53}Ga_{.47}As/GaAs$ EPITAXIAL STRUCTURES BY SOFT X-RAY REFLECTIVITY

A. Krol, C. J. Sher, S. C. Woronick, H. Resat, W. Ng, and Y. H. Kao (SUNY at Stony Brook), A. Green, and V. Rehn (Michelson Laboratory, China Lake, Ca 93555).

Total external x-ray reflectivity and scattering in the soft x-ray regime (550-700 eV) is a nondestructive and very sensitive technique for probing the electron density profile vs depth in layered structures. This method has been utilized to determine the roughness of interfaces, the epilayer thickness and the density in $In_{.53}Ga_{.47}As/InP$ and $In_{.53}Ga_{.47}As/GaAs$ heterostructures, with 300 Å of epilayer thickness, grown by molecular beam epitaxy. A general Fresnel matrix formulation of the electromagnetic field in stratified media with uncorrelated interfacial roughness has been applied. By fitting the experimental results to our calculation (see Fig.1 and 2), we conclude that surface rms roughness of the GaAs epilayer does not depend on the type of the substrate and is 9±4 Å in both cases. This is similar to the value 7±4 Å observed for bulk the GaAs crystal surface (1 u thick MBE layer grown on GaAs substrate). This seems to indicate the existence of a smoothing process during the crystal growth. The epilayer strain in $In_{.53}Ga_{.47}As/GaAs$ is very large (3.7%), but the observed fluctuations of electron density profile at the interface, rms 10±5 Å, are comparable with those measured on the surface of bulk GaAs. Similar phenomena are observed in a strain-free $In_{.53}Ga_{.47}As/InP$ heterostructure, where the measured interfacial rms roughness, 15±5 Å, is the same as that measured on the surface of the bulk InP used as the substrate. Thus we conclude that overgrowing a thin epilayer of GaAs does not change significantly the substrate roughness.

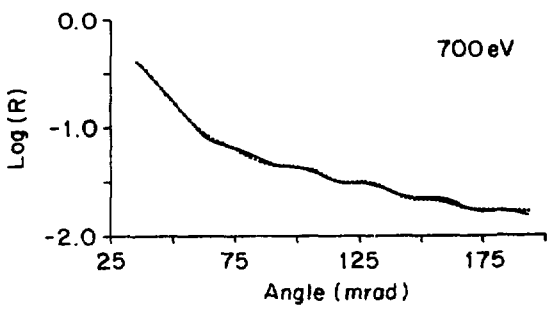

Fig. 1. $In_{.53}Ga_{.47}As/InP$ Experiment··· ; theory ——

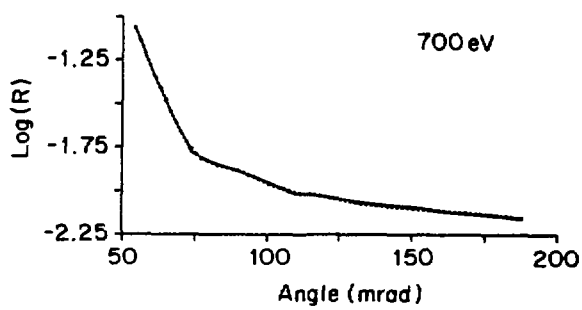

Fig. 2. $In_{.53}Ga_{.47}As/GaAs$ Experiment··· ; theory ——

This research is supported by the Office of Naval Research under grant No. N0001483K0675, and by the Department of Energy under grant No. DE-FG02-87ER45283.

Anisotropic Dissociation of Oxygen Following Core Electron Excitation

D.A. Lapiano-Smith, C.I. Ma, K.T. Wu, K. Lee, and D.M. Hanson (SUNY at Stony Brook)

Gas phase fragmentation processes can be studied by using tunable, soft x-rays to excite the core electrons of specific atoms. Total ion yield spectra show the production of fragment ions as a function of the excitation energy. Total ion yield spectra of molecular oxygen in the region of the oxygen K edge are shown.

The spectrum in Fig. 1 exhibits strong π^* and σ^* resonance peaks. The data were obtained by applying a high extraction field of 220 V/cm across the ionization region. In contrast, Fig. 2 reveals a substantial decrease in the σ^* resonance and continuum. This yield spectrum was obtained with a very low extraction field, 8 V/cm. The loss of intensity is attributed to an anisotropic angular distribution of fragments. Because the incident radiation is polarized, the core hole excited molecules are aligned preferentially with the internuclear axis perpendicular, at the σ^* resonance, or parallel, at the π^* resonance, to the axis of the mass spectrometer. With a small extraction field, the large velocity components along the direction of the internuclear axis carry the fragment ions away from the detector for σ^* excitation or into the detector for π^* excitation.

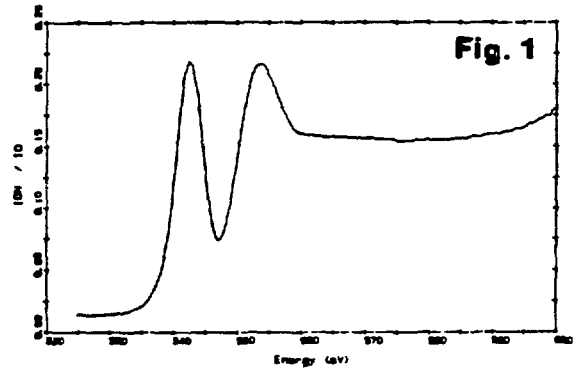

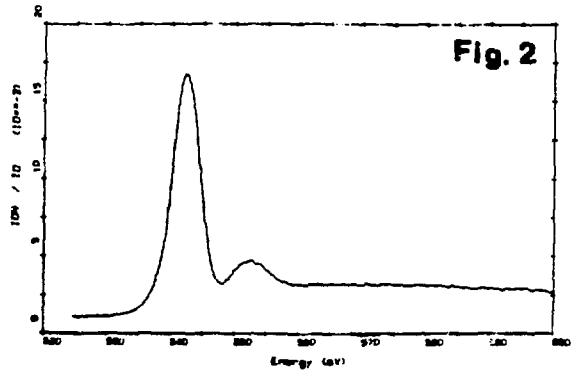

This research was supported by the National Science Foundation (CHE-87 03340).

AUTOIONIZATION AND AUGER DECAY OF OXYGEN CORE HOLE EXCITED STATES

K. Lee, D.A. Lapiano-Smith, C.I. Ma, K.T. Wu and D.M. Hanson (SUNY at Stony Brook)

Electron energy spectra associated with relaxation of core hole excited states in oxygen molecules in a molecular beam have been obtained. Fig. 1 and 2 show the Auger-like autoionization spectra following excitation of a 1s core electron to the $1\pi_g$ and $3\sigma_u$ valence orbitals, respectively. Fig 3 shows the Auger spectrum resulting from ionization of a 1s electron. The apparent differences among these spectra reflect not only the initial states achieved after photoabsorption, which determine the total energy that must be dissipated, but also the transition probabilities governed by the wave functions of the initial and final states. Initial analysis indicates that ground state O_2^+ ions, which have a binding energy of 12.07 eV, are generated after autoionization following excitation at the π resonance (519 eV peak in Fig. 1, excitation energy: 531 eV), but not at the σ resonance (lack of 530 eV peak in Fig. 2, excitation energy: 542 eV). Comparisons with O_2 Auger spectra obtained from eletron impact excitation (5kV) reveal states that are enhanced using synchrotron photon excitation at the resonances.

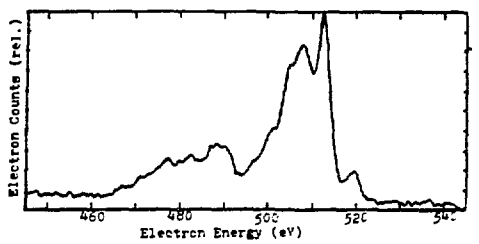

Fig. 1
Pi Resonance
(E_{ex} 531 eV)

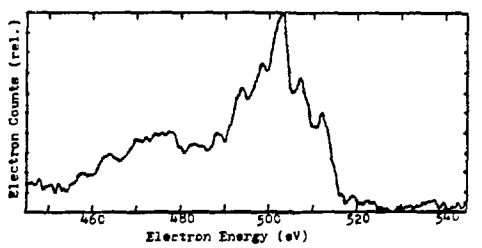

Fig. 2
Sigma Resonance
(E_{ex} 542 eV)

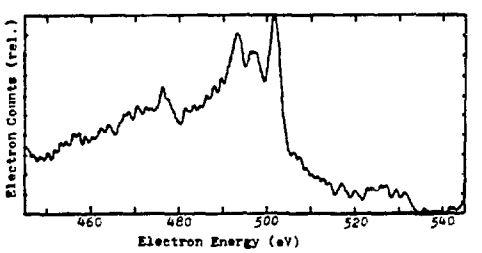

Fig. 3
1s Continuum
(E_{ex} 700 eV)

Support from the National Science Foundation (CHE-8703340) is gratefully acknowledged.

REFLECTION-EXAFS EXPERIMENTS TO INVESTIGATE THE STRUCTURAL INFLUENCE OF MOLYBDENUM ON THE CORROSION BEHAVIOR OF ALUMINUM FILMS.

G. G. Long (NIST, formerly NBS), W. C. Moshier (Martin Marietta Labs), G. D. Davis (Martin Marietta Labs) and D. R. Black (NIST, formerly NBS).

Aluminum and aluminum-alloys exhibit limited resistance against localized attack in air-saturated chloride-containing solutions. Recently, aluminum-(6%)molybdenum alloy films[1] were produced by RF magnetron sputtering to create surfaces with improved resistance to localized attack. The rate of corrosion of aluminum can alternatively be diminished by anodization in the presence of pitting inhibiting compounds such as molybdates. Examples of thin films were studied from each of these systems to investigate the mechanisms by which molybdenum influences the corrosion behavior of aluminum. These systems have been studied extensively by means of XPS, and the data from these complementary techniques will ultimately be combined.

The films that were used in the soft-xray reflection-EXAFS study were formed on highly polished single crystal silicon wafers. A 100 nm film of aluminum was deposited onto the silicon surface, and then the surface was anodized in the presence of molybdates. For the other set of samples, the Al-(6%)Mo alloy was deposited directly onto the silicon wafer. Samples of polished single crystal sapphire were used as standards.

An example of a family of refl-EXAFS spectra for one of the Al-(6%)Mo films is shown in Fig. 1.

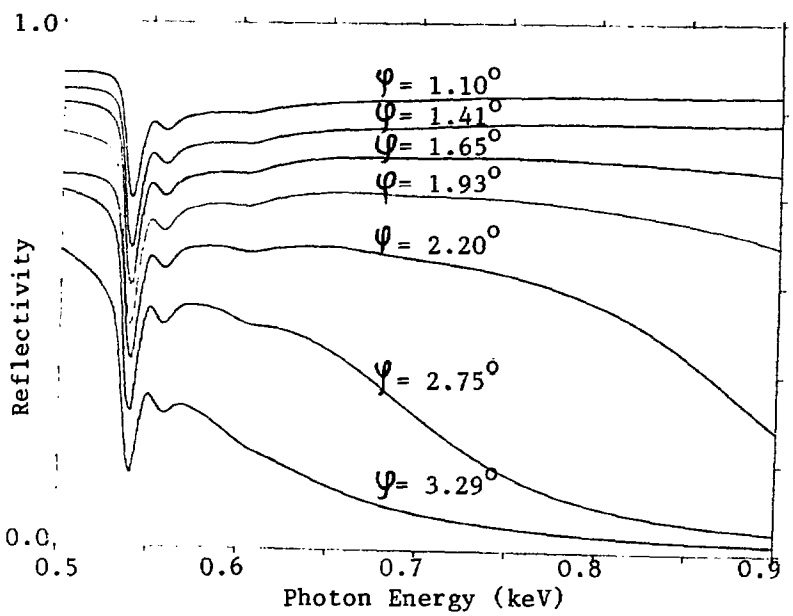

Fig. 1.

These curves were used to derive the optical constants, and thus the absorption coefficient for the sample. The structures are being analyzed to understand the changes that take place in the amorphous oxide/hydroxide lattice.

1. W. C. Moshier, G. D. Davis, J. S. Ahearn and H. F. Hough, J. Electrochem. Soc., 133, 1063 (1986). This work supported, in part, by the N.S.F.

Resonance Auger Electron - Ion Coincidence Studies of Oxygen

C.I. Ma, D.A. Lapiano-Smith, K.T. Wu, K. Lee, and D.M. Hanson (SUNY at Stony Brook)

Monochromatic, synchrotron radiation has been used to excite selectively the 1s core electrons of oxygen at the π^* resonance and the electronic relaxation (Fig. 1) and concomitant fragmentation processes were examined. Time-of-flight mass spectra show the distribution of ions collected in coincidence with energy selected electrons that correspond to features observed in the autoionization spectrum.

The TOF spectra show the simultaneous disappearance of O^+ (m/q = 16) and the appearance of O_2^+ (m/q = 32) as the electron energy increases from 189 (2), 202 (3), 212 (4) to 222 eV (5). Information about the kinetic energy released in the fragmentation can be obtained from the lineshape of the mass spectra.

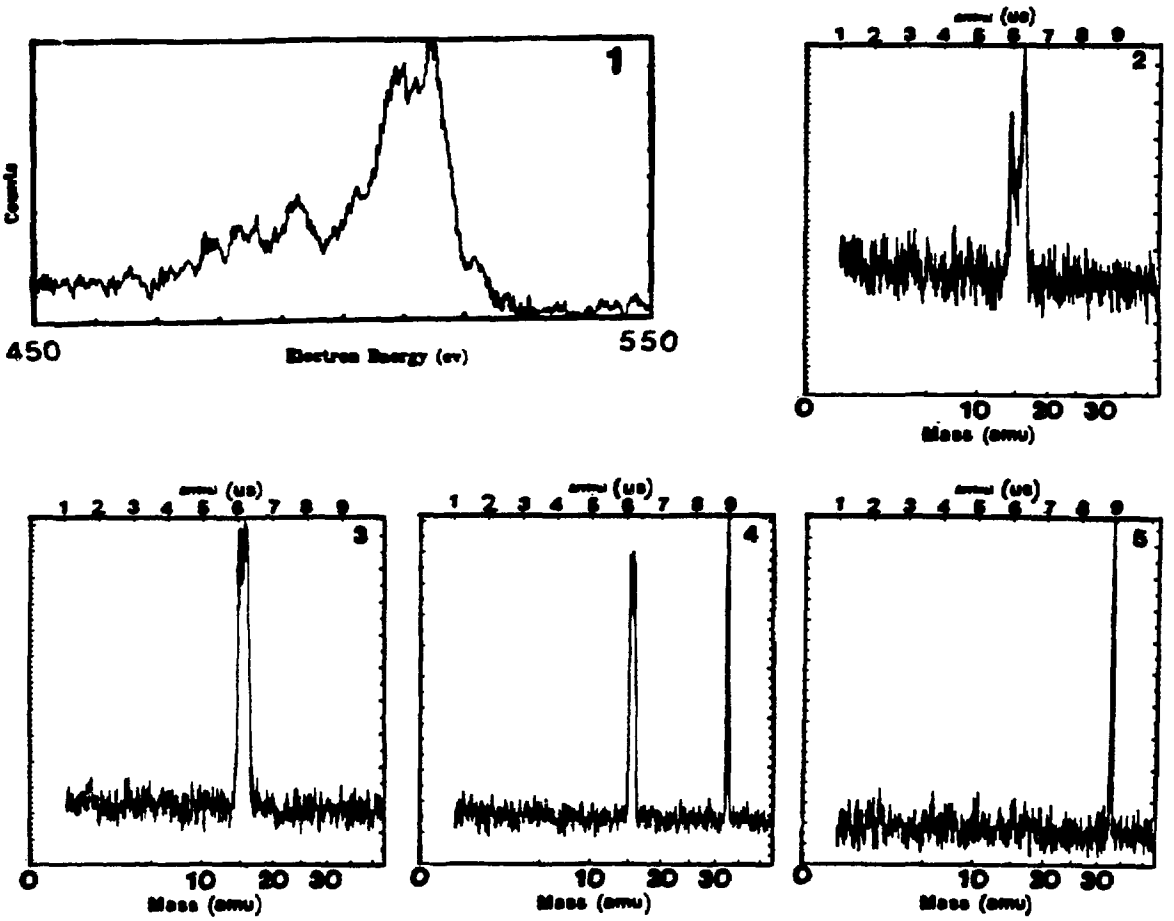

This research was supported by the National Science Foundation (CHE-87 03340).

October 12 1988
U-15

A COMPACT PROPORTIONAL COUNTER FOR SOFT X-RAY MICROSCOPY

E.Tang*, H.Ade, C.Buckley, J.Kirz (SUNY at Stony Brook)
G.C.Smith, (BNL)

The soft X-ray imaging beamline X1A at the NSLS will make use of the world's brightest soft X-ray source. In the case of the STXM (Scanning Transmission X-ray Microscope) the photon flux in a zone plate focused spot of 500A will be 10**7 p/s . A proportional counter is quite suitable for soft X-ray detection due to its high quantum efficiency and low noise. However these detectors have an upper counting limit due to space charge effects and the time resolution of the electronics. We have designed and made a compact proportional counter to fit the physical restrictions of the STXM and implemented a fast, low noise electronic counting chain with an output pulse width of about 20 ns.

The counter with an entrance window of 0.25*0.25 mm was tested at U-15 at a wavelength of 32 A. An air-path length versus counting rate experiment was performed. The results show that the counting system has good lineality and the slope is consistent with air absorbtion calculations. The maximum counting rate now is 6.8*10**6 c/s, about one order of magnitude higher than for the previous system.

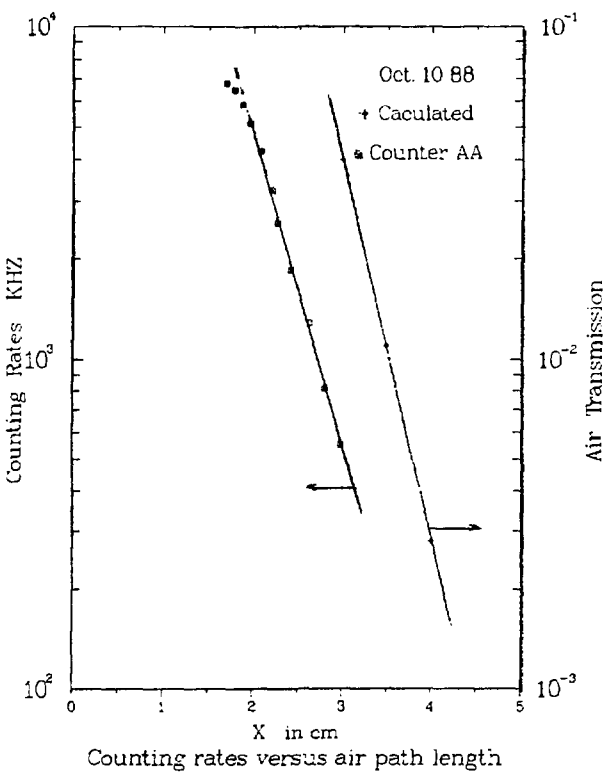

Fig.1: Countrate versus airpath of the high count rate proportional counter, showing good linearity up to 6*10**6 c/s.

* Supported by Lee Hysan Fellowship through the Committee for Education Exchange with China.

HIGH PERFORMANCE BEAMLINE FOR SURFACE AND FILM STUDIES IN THE ENERGY RANGE 100-1200 eV

U16A

The Extended Range Grasshopper (ERG) U16A beamline was built by Cornell University (c/o Prof. R. P. Merrill and Prof. T. N. Rhodin) and Sandia National Laboratories (Dr. N. Shinn) and is managed by Dr. King Tsang.

The most significant achievement on beamline (U16A) is that the first light was monitored on November 16, 1988 (see enclosed preliminary calibration) and that it expected to transmit full current by December 31, 1988.

The performance is designed to deliver an estimated maximum flux of 1.0×10^{10} photons/sec mm^2, mn^2 (0.1% B.W.) at the exit slit and operate over the predicted working energy range of 100 to 1200 eV. The resolution will vary from 50 to 200 mV depending on the energy range and the setting of the entrance and exit slits.

Effort will be focussed on optimizing the performance of the beamline, on improving the computer interfacing and of completing the construction and installation of the end-stations. One end-station will be optimized for precise band mapping under UHV conditions using *in situ* surface preparation and characterization. The second end-station will be optimized for pulsed molecular beam studies of time resolved photoemission of surface processes in ultrahigh vacuum. A third end-station will be used to do core-level spectroscopy and related UHV surface studies.

A major anticipated innovation will be the retrofitting of a SEYA-NAMIOKA monochromater to be used in combination with the ERG beamline for which it has been designed. This will add the important energy band of 1-100 eV and provide high flux, polarized photons over the energy range from 1-1200 eV. The lower end of this range is ideally suitable for band structure-mapping and for overlapping in energy with currently available tunable dye lasers operating in the vacuum ultraviolet. Combined with the high beam currents now available in the NSLS-UV storage ring, performance in the beamline at NSLS in the low electron energy range will be comparable to or superior to that of any comparable monochromators at other storage ring facilities to our knowledge.

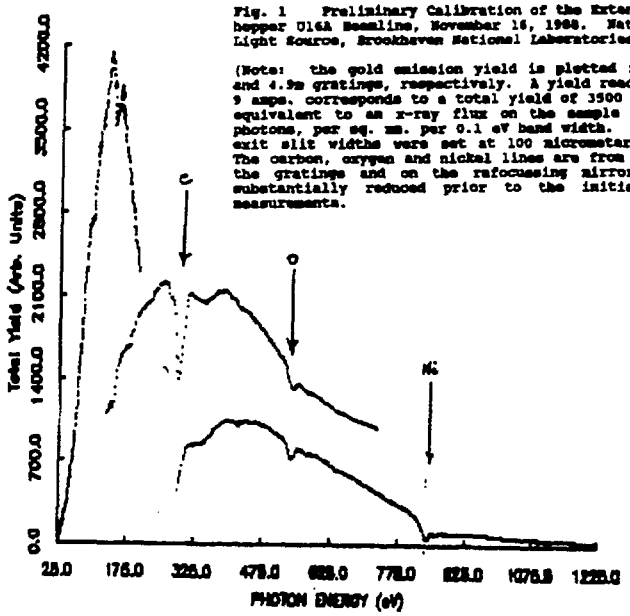

Fig. 1 Preliminary Calibration of the Extended Range Grasshopper U16A Beamline, November 16, 1988. National Synchroton Light Source, Brookhaven National Laboratories.

(Note: the gold emission yield is plotted for the 2m, 3.6m and 4.9m gratings, respectively. A yield reading of 1x10 exp-9 amps. corresponds to a total yield of 3500 which is equivalent to an x-ray flux on the sample of 10x10 exp 10 photons, per sq. mm. per 0.1 eV band width. The entrance and exit slit widths were set at 100 micrometers, respectively. The carbon, oxygen and nickel lines are from contamination on the gratings and on the refocussing mirror which will be substantially reduced prior to the initiation of actual measurements.

Research Reports For The X-Ray Beamlines

Beamline X1A

Beamline X3

Beamline X7A

Beamline X9A

Beamline X11

Beamline X12C

Beamline X14

Beamline X15B

Beamline X16A

Beamline X16B

Beamline X16C

Beamline X18B

Beamline X19C

Beamline X20

Beamline X22C

Beamline X23

Beamline X23 A2, A3

Beamline X23B

Beamline X24A

Beamline X26C

CHARACTERIZATION OF THE SOFT X-RAY UNDULATOR

H. Rarback, C. Buckley, R. Alforque, D. Shu (NSLS)

J. Kirz, H. Ade, S. Hellman, N. Iskander, S. Lindaas, I. McNulty, M. Oversluizen, E. Tang (Stony Brook)

D. Attwood, R. DiGennaro, M. Howells, C. Jacobsen (LBL)

We have measured the central intensity of the NSLS Soft X-Ray Undulator (1). The figure shows measured and calculated intensities for a K value of 1.50 and indicates both the undulator performance and x-ray ring emittance are within a factor of two of design values.

This work was supported by the DOE (NSLS) and NSF (Stony Brook, LBL).

1. C. Buckley et. al., SRI-88, in press.

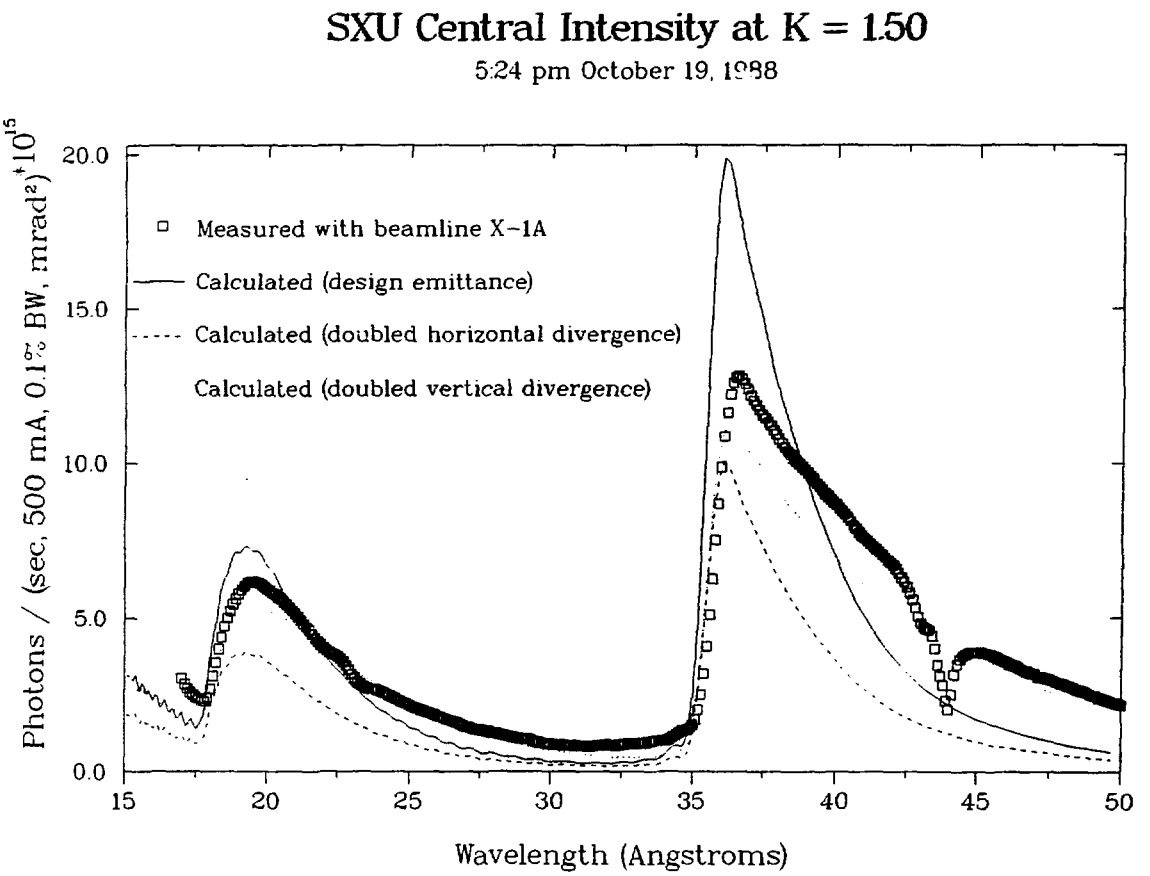

PERFORMANCE OF AN SGM WITH UNDULATOR RADIATION

H. Rarback, C. Buckley, R. Alforque, D. Snu (NSLS)

J. Kirz, H. Ade, S. Hellman, N. Iskander, S. Lindaas, I. McNulty, M. Oversluizen, E. Tang (Stony Brook)

D. Attwood, R. DiGennaro, M. Howells, C. Jacobsen (LBL)

We have commissioned an sgm monochromator (1) optimized for high spatially coherent output of soft x-rays to be used in imaging experiments. We have characterized its resolving power using the x-ray absorption near edge structure (XANES) of calcium fluoride. The figure indicates the sgm has achieved its design resolving power of 1800.

This work was supported by the DOE (NSLS) and NSF (Stony Brook, LBL).

1. C. Buckley et. al., SRI-88, in press.

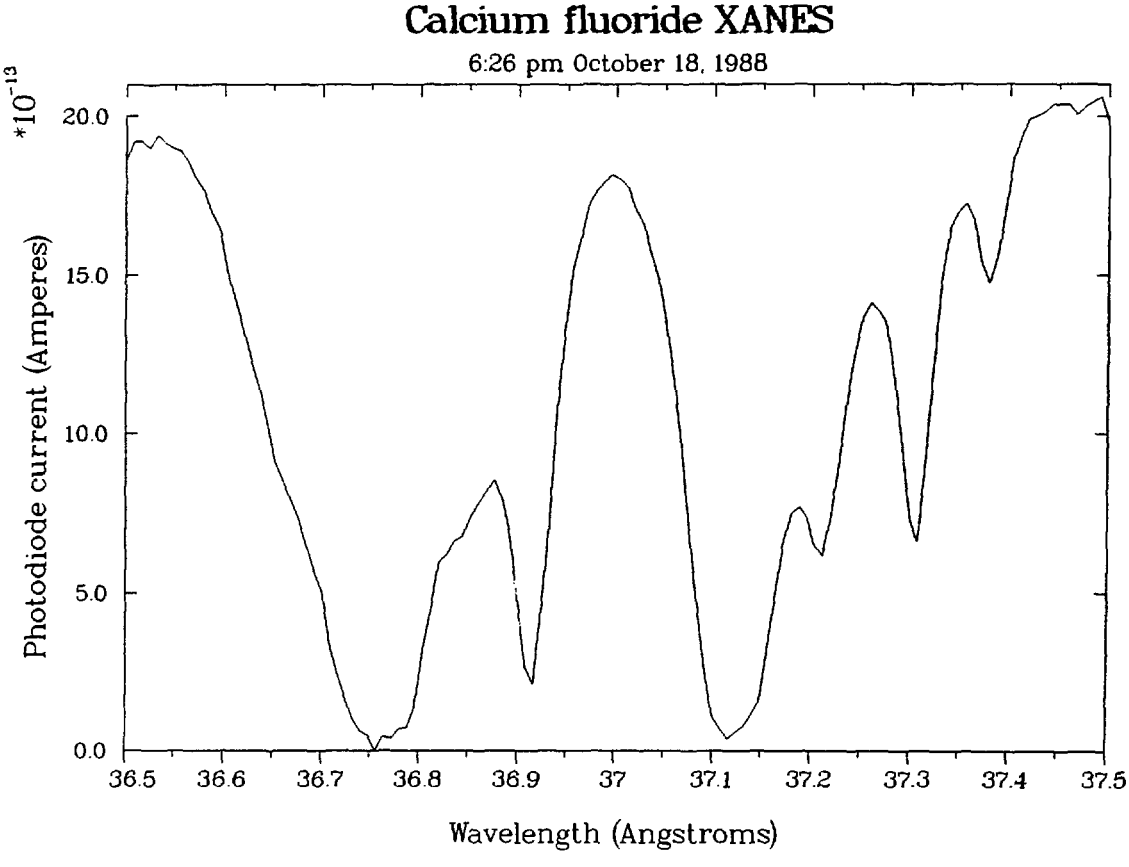

X-ray Diffraction of A Single PPTA (Kevlar) Fiber

Benjamin Chu, Yingjie Li and Chi Wu, SUNY at Stony Brook
Eric Roche, CR&D, DuPont Experimental Station
James Phillips, SUNY at Buffalo and Beamline

We successfully measured single poly(p-phenylene terephthalamide) (PPTA or Kevlar, a trademark of Dupont) fiber equatorial diffraction patterns by using the SUNY X-3 Beamline at NSLS/BNL. PPTA fiber has exceptional mechanical properties and its tensile strength can be related to local anisotropic structure. All previous x-ray diffraction experiments have been done with bundle PPTA fibers because conventional x-ray sources are not able to provide enough intensity for a single PPTA fiber diffraction. Thus, the literature x-ray diffraction patterns represent some average properties of the fiber bundle, including broadening of the diffraction peaks caused by oriented amorphous components or simply by misalignement of the fibers in the bundle.

Our experiments were designed to measure equatorial 200, 110 and 211 diffraction patterns of a single PPTA fiber under different stress. One specially made PPTA fiber (diameter $\simeq$ 25 μm) and two commercial PPTA fiber K49 and K29 (diameter $\simeq$ 12.5 μm) were used for the experiments. The stress was induced by putting a known weight on one end of the fiber. The weight on the fiber was increased in steps of about 7 grams until the fiber was broken. The final weights were about 70 grams and 20 grams for the specially made fiber and K49 (K29), respectively. Typical measurment time under normal beam condition (2528 Mev and 90 mA) without strong focusing and by using a Braun linear position sensitive detector was 2000 seconds. We estimated that the same experiment would take 20 days using a conventional x-ray source, which is practically impossible. Except for the single fibers, we also measured the diffraction from a bundle PPTA fibers for comparision purposes.

A typical x-ray diffraction pattern is shown in the following figure, where the solid line represents the diffraction from a single specially made PPTA fiber without stress and dot-points represent the diffraction under a weight of 56 grams. We observed that both the 200 and the 110 peaks shift to higher scattering angles with increasing stress. We aslo observed that the ratio of the 200 peak height to the 110 peak height increases with increasing stress. It is difficult to obtain useful information from the weaker 211 diffraction peak at this time. More detailed data analysis is in progress.

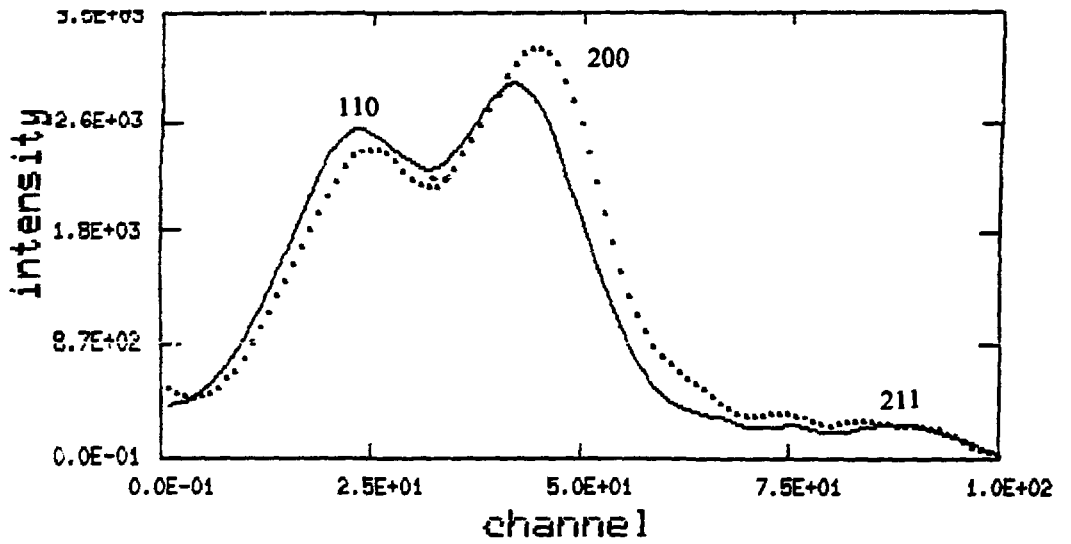

Morphology of Poly(ethylene-methacrylic acid)/Pb^{2+} Ionomers

Benjamin Chu[1], Dan Q. Wu[1], Walter Mahler[2], and James C. Phillips[3]
1. Dept of Chemistry SUNY at Stony Brook, Long Island, NY 11794-3400
2. Central Research & Development Dept., E.I. du Pont de Nemours & Company Wilmington, Delaware 19898
3. The SUNY Beamline, X3A, NSLS, BNL, Upton, NY 11973

Poly(ethylene (85 wt%)-methacrylic acid (15 wt%)) copolymer (MEA) neutralized partially or completely by lead acetate (EMA/Pb^{2+}) is a very interesting ionomer which possesses the unique mechanical and electric properties because of the dispersion of ionic clusters in a crystalline matrix formed by ethylene segments[1].

This work is intended to study the morphology of EMA/Pb^{2+} ionomers. It is desirable to measure the structures of the crystalline copolymer and of the ionic clusters of lead salts simultaneously using a small angle x-ray diffractomater[2] at X3A, SUNY Beam Line, NSLS. The SAXS studies of the ionomers with different Pb^{2+} contents (from 0 to 20 wt%) show a variation of two characteristic diffraction peaks: one located at q_l~0.6 nm^{-1}, due to a lamellar structure formed by the ethylene segments, another at q_i~2.5-3.5 nm^{-1}, due to ionic aggregations of the Pb salt groups. Typical SAXS patterns of EMA/Pb^{2+} ionomers are shown in Fig. 1. For the lead-free acid form, only a lamellar peak, corresponding to a Bragg spacing of 10 nm, was observed. With increases of Pb^{2+} content, the lamellar peak retains its peak position but becomes less sharp and eventually vanishes while the ionic peak grows and shifts to a lower q. Differential scanning calorimetry (DSC) measurements showed the existence of a crystalline phase for EMA/Pb^{2+} samples of all Pb contents and the crystallinity decreases as the Pb^{2+} content increases. By combining the results of SAXS and DSC, we could conclude that (1) the ionic groups aggregate in the amorphous regions of the copolymer matrix; (2) the inter-lamellar spacing is insensitive to the degree of neutralization; (3) The increasing Pb^{2+} content reduces the crystallinity of the copolymer therefore possibly the size of the spherulites; (4) the average size of the ionic clusters tends to increase with increasing Pb^{2+} content.

References:

1. Mahler, W. *Inorg. Chem.*, **1988**, *27(3)*, 435
2. Chu, B.; Wu, D.Q.; Wu Chi; *Rev. Sci. Instr.*, 1987, *58*, 1158

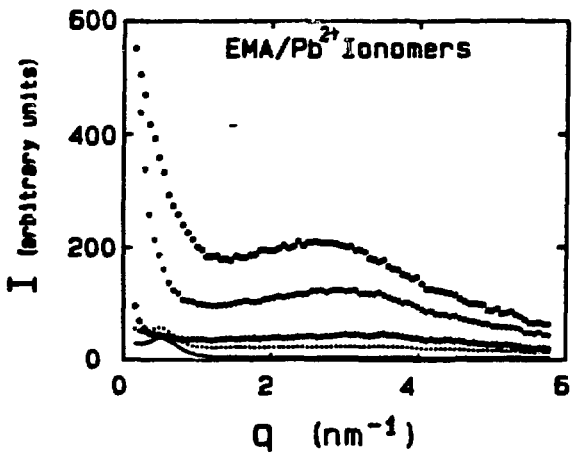

Figure 1. SAXS pattern of EMA/Pb^{2+} ionomers. All curves are corrected for x-ray intensity fluctuation, background scattering, sample attenuation, and normalized to 1 sec. $q=(4\pi/\lambda)\sin(\theta/2)$, with λ=0.15 nm^{-1}, the wavelength of x-ray; θ being the scattering angle. Two diffraction peaks, due to lamellar structure and ionic clusters are shown at q~0.6 and 2.5-3.5 nm^{-1}, respectively. The curves (from the top) contain 20, 10, 5, 2, and 0 wt% Pb, respectively.

High Flux X-ray Scattering of Polydiacetylene (P4BCMU) in Dilute Solution

Benjamin Chu,[1,2] Renliang Xu,[1] Yingjie Li,[1] and Danqing Wu[1]
Department of Chemistry[1] and Materials Science,[2]
State University of New York at Stony Brook, Long Island, NY 11794

Polydiacetylenes, $(=CR-C\equiv C-CR=)_n$, are novel conducting polymers. Their peculiar electric and optical properties have revealed potentially industrial applications. Polydiacetylene molecules in solution could exist in different conformations depending on the solvent quality, temperature and solution concentration. Various techniques have been employed in studies of polydiacetylene dilute solution in good solvent, e.g. chloroform, and in poor solvent, e.g. toluene, to clarify the macromolecular states in solution.

It has been found that P4BCMU ($R = (CH_2)_4O\text{-}CO\text{-}NHCH_2\text{-}CO\text{-}OC_4H_9$) in dilute toluene solution at room temperatures form large rod-aggregates with the radius of gyration (R_g) being up to 0.2 μm by using small angle laser light scattering and transient electric birefringence [1]. Small angle X-ray scattering (SAXS) could provid a better approach to study the local structure of such large particles. In the present study, high flux x-ray from synchrotron radiation at the National Synchrotron Light Source (NSLS), BNL, has been used to study P4BCMU in dilute toluene solution at an angular range of 1.2-32 mrad, corresponding to q values of 0.005-0.13 $Å^{-1}$ by using a Braun linear position sensitive detector [2].

The preliminary results show that by using the synchrotron radiation the polydiacetylene solution could yield a SAXS curve for P4BCMU even at very dilute concentrations ($C \sim 6.2\times10^{-6}$ g/mL $< C^*$, overlap concentration) after only a few hours of accumulation. The following figure shows the scattered signals from toluene (lower curve) and from the P4BCMU solution (upper curve).

References

1. R. Xu, **Ph.D. Dissertation**, SUNY at Stony Brook, (in preparation)
2. B. Chu, D. Wu, C. Wu, **Rev. Sci. Instrum.**, 58, 1158 (1987)

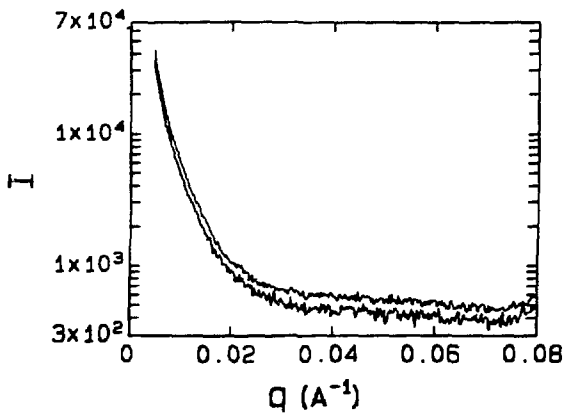

LAYER OCCUPANCY IN HIGH T_c SUPERCONDUCTORS BY ANOMALOUS CONTRAST CRYSTALLOGRAPHY

P. Coppens, P. Lee, H.S. Sheu, R. Restori, Y. Gao, and A. Darovskikh (Chemistry Department, SUNY/Buffalo).

The non-stochiometry of the high-T_c superconductors is accompanied by mixed occupancy of many of the metal sites in the crystals. In general, the nature of the minority occupants of a particular layer or site cannot be established with confidence by conventional crystallographic methods. With synchrotron radiation, selective contrast can be obtained by using the variation of the atomic scattering factors near absorption edges.

Using a single crystal of the 2212 phase of Bi-Sr-Ca-Cu-O, we have measured a set of main reflections at wavelengths of 1.38 and 1.42Å, at and below the Cu absorption edge. The f ' contribution to the Cu scattering factor varies by almost 5 electrons between these two wavelengths. An even larger variation of about 11 electrons occurs for bismuth at the wavelengths of 0.924 and 0.950Å. Test calculations have been done to identify the subset of reflections most sensitive to delocalization of the Bi atoms. The experiment is to be continued in November.

Small Angle X-Ray Scattering of Blockcopolymer Aggregates

R. Hilfiker, B. Chu and H. Fuchs
S.U.N.Y. @ Stony Brook

Polystyrene-polyisoprene blockcopolymers form aggregates in aniline, which is a selective solvent for polystyrene, is isorefractive with polystyrene and has the same electron density as polystyrene. Three different blockcopolymers with a polyisoprene block having a molecular weight of 19 kg/mol and a polystyrene block with a molecular weight of 28, 41 and 61 kg/mol were investigated by static and dynamic light scattering and viscosity measurements.
From the data it was clear that the two blockcopolymers with the bigger polystyrene blocks form micelles with a liquid-like polyisoprene core. However, from the results of the light scattering experiment it was not possible to decide whether the copolymer with the short polystyrene block forms a micelle with a polyisoprene core of low density (penetrated by aniline) or a vesicle.
The aim of the SAXS experiment was to find out whether the form factor of the aggregate corresponds better to a solid or a hollow sphere. The radius of the micelle or vesicle was determined by light scattering to be 60 nm. As can be seen in the figure, the form factor for a solid sphere (r=60 nm) and a hollow sphere (r = 60nm; shell thickness = 10 nm) differ considerably at large Kr, which are inaccessible in light scattering but lie within the range of SAXS.
A distinction between solid and hollow sphere should therefore be possible. SAXS experiments were carried out for solutions with different concentrations of the blockcopolymer and for the solvent. The treatment of the data is still under way.

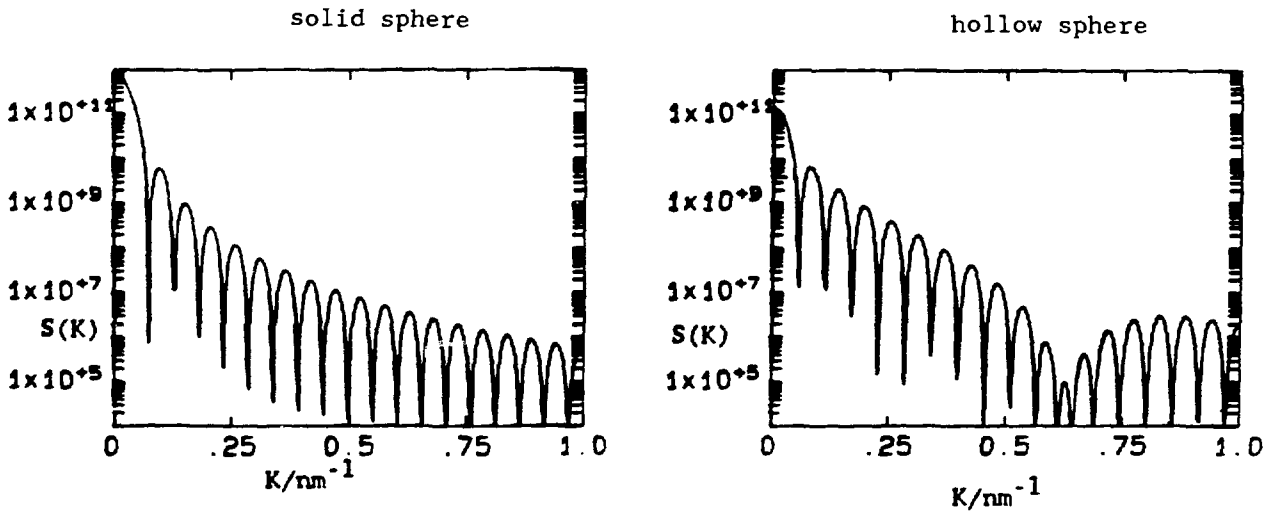

X-RAY FLUORESCENCE YIELD STUDIES OF $CoSi_2$/Si HETEROJUNCTIONS

A. Krol, S. C. Woronick, C. J. Sher, Y. H. Kao, (SUNY at Stony Brook), J. C. Phillips (SUNY X3 beam line and SUNY at Buffalo) Y. C. Kao, and K. L. Wang (UCLA, Los Angeles).

Measurements of x-ray fluorescence vs. grazing incidence angle at fixed incoming photon energy can provide useful information about surface and interfacial microstructure. This method has been utilized to determine the roughness of the surface and interfaces, the concentration profile of fluorescent atomic species vs. depth, and the epilayer thickness. The heterojunctions studied were $CoSi_2$/Si(111) heterostructures obtained by Molecular Beam Epitaxy (MBE) and Solid Phase Epitaxy (SPE), with a 220 Å nominal epilayer thickness. The samples were positioned on a goniometer driven by stepping motors with 0.01 mrad angular resolution. A two-crystal Si(111) monochromator with very narrow slits was used in order to provide highly collimated and monochromatized radiation. The intensities of the incoming and scattered beams were measured using ion chambers while the fluorescence emission was detected using scintillation counters equipped with filters. An example of our results, shown in Fig. 1, is the measured fluorescence yield obtained at an incident photon energy of 7.72 keV, as compared to the theoretical analysis. A matrix formulation of radiant energy flow inside a layered material, and hence angular fluorescence emission, with a vector scattering model to account for the effect of interfacial roughness, has been applied in order to model obtained results. By fitting the experimental Co angular fluorescence yield curves we concluded that Co exhibits uniform concentration profile in the investigated $CoSi_2$ epilayers, with surface and interfacial rms roughness parameters which are smaller than 10 Å in the MBE sample, as compared to the surface roughness which is much larger (rms of order of 20 Å) in the SPE sample.

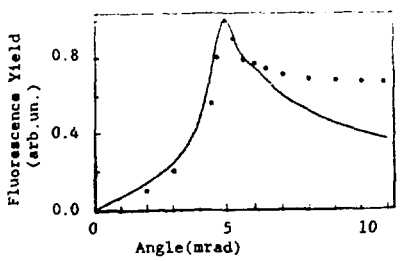

Fig. 1. The fluorescence yield vs angle for $CoSi_2$/Si(111). Experiment···; theory—; energy of incoming photons 7.72 keV.

This research is supported by ONR under grant No. N0001483K0675, and by DOE under grant No. DE-FG02-87ER45283.

DETERMINATION OF NUCLEIC ACID STRUCTURE IN SOLUTION BY MEANS OF X-RAY SCATTERING IN SOLUTION

N.C. Seeman (New York University), R. Sheardy (Pennsylvania State University), J.E. Mueller (SUNY/Albany), A. Darovskikh (SUNY X3 Beam Line and SUNY/Buffalo), and J. C. Phillips (SUNY X3 Beamline and SUNY/Buffalo).

Nucleic acids constitute a particularly favorable case for the determination of structure in solution by means of heavy atom labels. The basic features of nucleic acid structure have been determined at high resolution by single crystal and fiber-diffraction techniques. The details of double helical B-DNA structures of more complicated complexes, such as Holliday recombination intermediates, in which 4 double helices eminate from a single junction. The first interesting structural question about this system is the relative disposition of the 4 double helical arms.

We seek to answer this question by the substitution of an iodine label for a methyl group at two sites on the 4-stranded complex. The iodine-iodine distance is available by comparison of the substituted complex with the unsubstituted complex. In principle, a number of pairwise substitutions of this sort must be made in order to determine the structure in the absence of information other than the structure of the double helix. We have worked out the chemistry to perform this substitution [1], and have prepared a Holliday junction analog containing two internal iodine labels, as well as the complex made from uniodinated DNA. The complex contains 32 nucleotide pairs, eight on each of four individual arms. The scattering difference between the two complexes is estimated to be about 2%, which is why the high counting rates available from synchrotron radiation are necessary in order to obtain the necessary counting statistics. As a control experiment, the same strand that contains the two iodine labels is paired with its double helical complement, in order to establish the detectability of the effect we seek. The double helical structure should have a well-defined distance between the two iodine atoms.

Data from hydroxyl radical susceptibility suggest that the four double helical arms of the Holliday junction arrange themselves in two helical domains. Two different structures can accomplish this, and the equilibrium constant for isomerization between the two different structures appears to be significantly different from unity, perhaps as large as 10. Iodine substitution at different sites from the ones for structural determination will provide signatures for the two conformational isomers. The estimate of the equilibrium constant derived in this fashion ought to be far superior to those obtained from chemical attack or enzymatic digestion, because a much smaller perturbation of the molecule is involved. These experiments require even better counting statistics than those involving structure determination, since the sample is partitioned between two states, and both must be observed to get the ratio.

Reference

1. R. Sheardy and N.C. Seeman, J. Org. Chem. 51 (1986) 4301.

SAXS on Sulfonated Polystyrene Ionomers

D.Q. Wu[1], B. Chu[1], R.D. Lundberg[2], W.J. MacKnight[3] and J.C. Phillips[4]

1. Dept of Chemistry, SUNY at Stony Brook, Long Island, NY 11794-3400
2. Paramins Division, Exxon Chemical Company, Linden, NJ, 07036
3. Dept of Polymer Science and Engineering, Univ. of Massachusetts, Amherst, Mass. 01003
4. SUNY X3 Beamline, NSLS, BNL, Upton, NY 11973

The field of ion-containing polymers, with its many industrial applications, has undergone explosive growth in recent years[1]. The ion aggregation in ionomers is known to achieve many excellent material properties. Nevertheless, a fundamental understanding of ionomer morphology, the spatial arrangement of ionic groups in ionomers, has remained elusive. In this work, model systems, containing cesium, sodium, and zinc salts of slightly sulfonated polystyrene (SPS) were studied by small angle x-ray scattering (SAXS) at the SUNY Beamline, X3A. SAXS intensity profiles with a wide angular range and a high spatial resolution were achieved[2]. The profiles showed not only a broad "ionic peak", but also a strong small angle upturn that was attributed to the long range inhomogeneities of the ions[3]. Although the ionic peak position was insensitive to the type of metal ions, its shape was: the cesium and sodium salts showed narrower and sharper peak than that of zinc salts. Obviously mono-valent metal ions formed more uniform ion clusters than bi-valent ions. One of many excellent properties of ionomer materials is an increase of the glass transition temperature and modulus. Fig. 1 shows the SAXS intensity profiles of a sodium salt of SPS (4.5 mole% of sulfur, 100% neutralized) at different temperatures. The ionic peak grew slightly, reached a maximum in height at ~200°C suggesting a further ion aggregation. The peak was retained even at 250°C though thermal energy eventually broke down some of the clusters and reduced the peak height. The spatial arrangement of the ions in ionomers can best be demonstrated by the electron density-density correlation function which will soon be obtained by using a new, least-biased Fourier transform: the maximum entropy method.

References:

1. MacKnight, W.J.; Earnest, T.R., Jr. *J. Polym. Sci., Macromol. Rev.*, **1981**, *16*, 41
2. Chu, B.; Wu. D.Q.; MacKnight, W.J.; Wu, C.; Phillips, J.C.; LeGrand, A.; Lantman, C.W.; Lundberg, R.D.; *Macromolecules*, **1988**, *21*, 523
3. Wu, D.Q.; Phillips, J.C.; Lunberg, R.D.; MacKnight, W.J.; Chu, B.; *Macromolecules*, to be published.

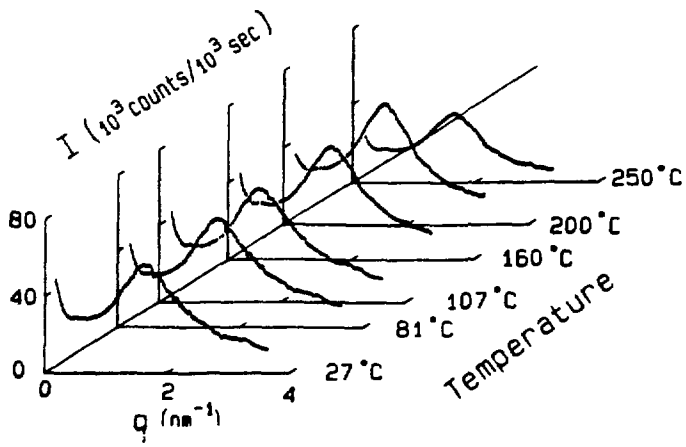

Time-resolved SAXS and WAXS Studies of Polyethylene HD/LD and LLD/LD Blends

D.Q. Wu[1], H.H. Song[1], M. Satkowski[2], S. McGuire[2], R.S. Stein[2], J.C. Phillips[3], B. Chu[1]

1. Dept of Chemistry, SUNY at Stony Brook, Long Island, NY 11794-3400
2. Polymer Research Institute, Univ. of Massachusetts, Amherst, Mass. 01003
3. SUNY Beamline X3A, NSLS, BNL, Upton, NY 11973

For the first time, the time-resolved small angle x-ray scattering (SAXS) and wide angle x-ray scattering (WAXS) were used simultaneously to measure the crystallization process of polyethylene blends, respectively in the lamellar scale, and in the crystalline level. An electrospatial image intensifier photo-diode-array position sensitive detector covered an angular range of $0.05^0 \leq \theta \leq 2.3^0$ where a diffraction peak due to the lamellar structure was recorded, while a Braun position sensitive detector monitors the polyethy-lene crystalline 110 and 200 peaks, at $\sim 12^0 \leq \theta \leq \sim 30^0$. Two blends: a blend of high density (HD) and low density (LD) polyethylene and a blend of linear low density (LLD) and low density polyethylene were studied at various HD/LD and LLD/LD ratios. The crystallization process was carried out by: (1) fast quenching, (2) slow cooling, and (3) isothermal crystallization.

Typical time-resolved SAXS intensity profiles of HD polyethylene during a temperature jump from 135 to 65°C are shown in Fig. 1. Upon cooling, the lamellar peak increases in height then subsequently changes its position to a lower q. It suggests that a disordered lamella structure with a very broad distribution of lamellar spacing and large amounts of amorphous gap in the early stage of the crystallization, changes to more well-defined lamella stacks. More studies on HD/LD blends during quenching as well as during slow cooling and isothermal crystallization, show that the HD component dominates the crystallization process during the early stage and the LD component crystallizes from the amorphous region between the lamellar stacks formed mainly by the HDPE.

The crystallization kinetics on LLD/LD polyethylene blends is very different from that of HD/LD PE blends. During quenching, similar kinetics was observed. However during slow cooling and isothermal crystallization, no apparent lamellar peak was detected, and less crystallinity than LDPE was measured by WAXS. Although small angle light scattering showed the spherulites, apparently no well-defined lamella structure is present in LLD/LD polyethylene blends during slow cooling and isothermal crystallization processes.

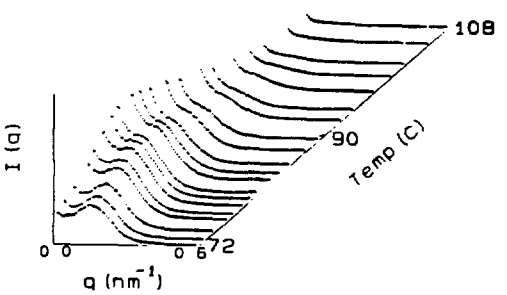

Figure 1. Typical time-resolved SAXS intensity profiles of HDPE during a temperature jump from 135 to 65 °C (ΔT = 70 °C). Each curve has been collected for 0.5 s and corrected for detector nonuniformity, background, and absorption.

EXAFS STUDIES OF Ag-DOPED Y-Ba-Cu-O HIGH-T_C SUPERCONDUCTORS

F.Xu, Y. D. Yao, A. Krol, C. J. Sher, L. W. Song, Y. H. Kao (SUNY at Stony Brook), A. Darovsky (SUNY X3 beam line), and J. C. Phillips (SUNY X3 beam line and SUNY at Buffalo).

EXAFS measurements above the Ag K absorption edge were made to explore the local structure around Ag dopants in the high-T_C superconductor $YBa_2Cu_3O_{7-y}$. The samples used in this experiment were prepared by a solid state reaction technique using high purity powders of Y_2O_3, $BaCO_3$, CuO, and Ag_2O. The structure of samples was characterized by x-ray powder diffraction and $YBa_2Cu_3O_{7-y}$ was identified as the major phase. EXAFS data were obtained by measuring x-ray transmission, through layers of fine powder of the Ag doped samples on plastic tape at room temperature. A typical absorption spectrum around the Ag K edge obtained with a sample of nominal composition $YBa_2(Cu_{0.9}Ag_{0.1})_3O_{7-y}$ is shown in Fig. 1. The oscillatory EXAFS component was extracted by a standard background removal procedure and analyzed by a Fourier transform method. A similar EXAFS obtained with Ag_2O powder was used as reference for phase-amplitude analysis. The magnitude of Fourier transform of the EXAFS spectrum obtained from the experimental curve shown in Fig. 1 is presented in Fig. 2. The first and second peak at lower values of R are identified as due to Ag-O bonds, and the third peak is identified as due to Ag-Ag bonds with an interatomic distance 2.85±0.04 Å arising from some Ag clusters in the sample. Similar EXAFS spectra with 20% nominal Ag doping where also measured. Our data indicate that as the Ag content is increased, the local environment surrounding the Ag impurity atoms changes. The second peak in Fig. 2 with Ag-O bond length equal to 2.26±0.04 Å is believed to arise mainly from atoms taking Cu sites in the CuO planes. Its coordination number increases with addition of Ag. This result suggests that as the Ag content is increased from 10 to 20%, the additional Ag atom mainly occupy Cu(2) sites in the basal plane.

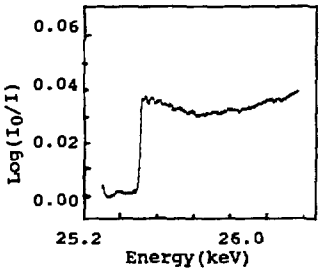

Fig. 1. Absorption spectrum of $YBa_2(Cu_{0.9}Ag_{0.1})_3O_{7-y}$.

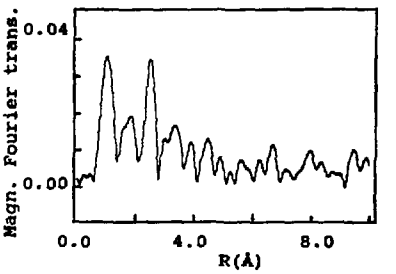

Fig. 2. Magnitude of Fourier transform of EXAFS spectrum.

This research is supported by ONR under grant No. N0001483K0675, and by DOE under grant No. DE-FG02-87ER45283.

HIGH RESOLUTION SYNCHROTRON X-RAY POWDER DIFFRACTION OF CALCIUM SULFATE HYDRATES

C. Bezou (U. Dijon, France), A.N. Christensen (Aarhus U., Denmark), and D.E. Cox* (BNL).

X-Ray synchrotron powder data were collected from 0.7 mm diameter capillary samples of the calcium sulfate hydrates $CaSO_4.0.5\ H_2O$ and $CaSO_4.0.6\ H_2O$. The first compound is monoclinic with a = 12.028, b = 12.678, c = 6.927, $\gamma = 90.21^{o}$, and space group I2, the second compound has a higher symmetry, and the pattern can be indexed with an orthorhombic cell with a = 12.005, b = 12.735, c = 6.931 Å, or possibly with a hexagonal cell derived from this orthorhombic cell. The powder data will be used in least squares profile refinements of the structures to determine the differences between the structure of $CaSO_4.0.5\ H_2O$ and that of $CaSO_4.0.6\ H_2O$.

* Work supported by Div. of Materials Sciences. U.S. Dept. of Energy under contract DE-AC02-76CH00016.

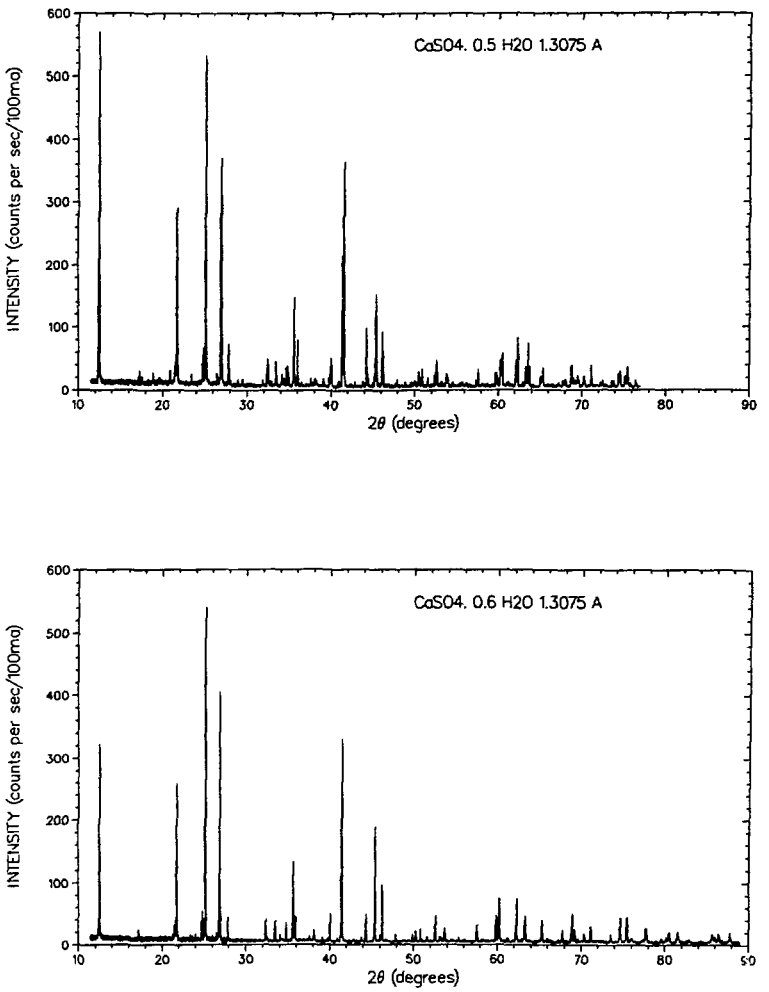

Observed powder profiles of $CaSO_4.0.5\ H_2O$ and $CaSO_4.0.6\ H_2O$.

A CRYSTAL STRUCTURE DETERMINATION OF PbC_2O_4 FROM SYNCHROTON X-RAY AND NEUTRON POWDER DIFFRACION DATA

A. N. Christensen (Aarhus U., Denmark), M. S. Lehmann (ILL, Grenoble), and D. E. Cox* (BNL)

The crystal structure of lead oxalate, PbC_2O_4, was solved *ab initio* from synchrotron x–ray and neutron diffraction powder patterns. The unit cell was obtained by auto–indexing of Guinier film data, the basic features of the structure were solved using direct methods and integrated intensities obtained from high resolution synchrotron x–ray data, and the structure was refined by Rietveld analysis of these and high resolution neutron data. Although there were serious discrepancies in the overall profile fit of the x–ray data because of pronounced anisotropic peak broadening, the two sets of positional coordinates were in good agreement.

The unit cell is triclinic, space group $P\bar{1}$ (no. 2) with lattice parameters from the synchrotron refinement, $a = 555.70(1)$, $b = 697.72(1)$, $c = 557.26(1)$ pm, $\alpha = 109.554(1)$, $\beta = 113.610(1)$, $\gamma = 88.802(1)$ deg., $Z = 2$. The structure has two crystallographically independent oxalate ions stacked in layers alternating with layers of lead ions in the [001] direction. The oxalate ions form channels along the b–axis in which the lead ions are situated in highly asymmetric coordination with seven oxygen atoms.

Individual peak fits of the synchrotron data revealed all of the reflections to be broadened appreciably compared to the instrumental resolution. Those with scattering vectors close to the [001] axis showed an additional systematic broadening consistent with stacking faults in this direction.

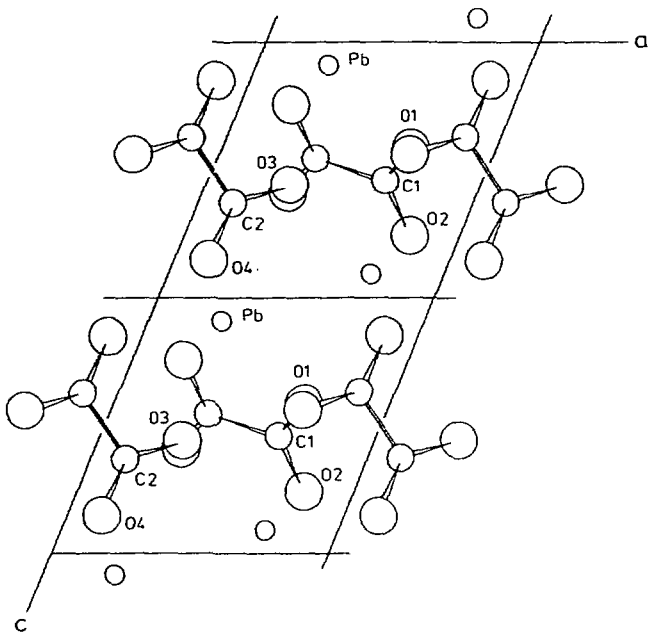

Structure of PbC_2O_4 viewed along the b–axis. Layers of lead and oxalate ions alternate along the c^* direction.

*Work supported by Div. of Materials Sciences, U. S. Dept. of Energy under contract DE-AC02-76CH00016.

STRUCTURAL CHARACTERIZATION OF $La_{2-x}M_xCuO_4$ (M=Sr, Ba) SAMPLES BY SYNCHROTRON X-RAY AND NEUTRON POWDER DIFFRACTION TECHNIQUES

D.E. Cox (BNL), S.C.Moss, R.L. Meng, P.H. Hor and C.W. Chu (U. of Houston)

High resolution synchrotron x-ray powder diffraction studies on samples of $La_{2-x}M_xCuO_4$ (M=Sr, Ba) prepared by standard ceramic techniques show that macroscopic compositional inhomgeneities may exist which are unlikely to be revealed by conventional x-ray diffraction methods. Fig. 1 shows some data collected at 1.3154A from a sample of nominal composition $La_{1.8}Sr_{0.2}CuO_4$ which can be analyzed in terms of two tetragonal phases with closely similar tetragonal lattice parameters (a_1=3.7707(1), c_1=13.2505(2); a_2=3.7743(2), c_2=13.245(1)Å) indicative of slightly different Sr contents. Rietveld refinement of neutron data collected at 200, 50 and 11K from this sample gave satisfactory fits to a tetragonal structure of K_2NiF_4-type at all three temperatures. However careful individual peak fits revealed that part of the sample transforms to orthorhombic between 200 and 50K, corresponding to the phase with the lower Sr content. It is suggested that this multiphase character has an important influence on the superconducting properties.

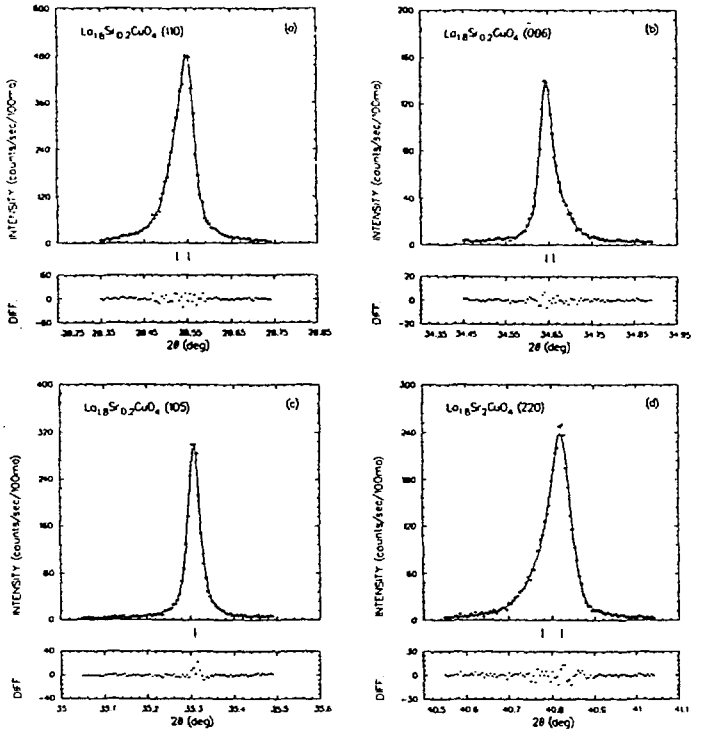

Fig. 1 (a)-(d) Least-squares fits to synchrotron x-ray data from $La_{1.8}Sr_{0.2}CuO_4$. Points represent observed values, solid lines the calculated profile. Difference plots are below. Short vertical markers represent peak positions for the two components.

Work at Brookhaven supported by the Div. of Mater. Sci., US Dept. of Energy, under Contract No. DE-AC02-76CH00016 (DEC). Work at Houston supported by the National Science Foundation, Grant No. DMR-8603662 (SCM), and DMR-8616539 and the Texas Center for Superconductivity (RLM, PHH and CWC).

THE SYNTHESIS AND STRUCTURE DETERMINATION FROM POWDER DIFFRACTION DATA OF $LaMo_5O_8$, A NEW OXOMOLYBDATE CONTAINING Mo_{10} CLUSTERS.

S. J. Hibble, A. K. Cheetham, A. R. L. Bogle, and H. R. Wakerley (Oxford U.), and D. E. Cox* (BNL)

The synthesis of transition metal cluster compounds and the structural characterization of polycrystalline powders are both subjects of considerable current interest. In our exploration of the La–Mo–O phase diagram we have prepared a new phase, $LaMo_5O_8$, the most highly reduced compound yet reported in this system. It contains M–M bonded $Mo_{10}O_{16}$ units, consisting of pairs of edge–sharing Mo_6 octahedra. The new compound was first observed in an analytical electron microscope study of a polyphasic mixture, and the structure was subsequently determined from a study of a polycrystalline sample by selected area electron diffraction, synchrotron x–ray diffraction and neutron diffraction. The success of this work demonstrates the feasibility of identifying and characterizing new compounds with previously unknown structures, even when single crystals are not available.

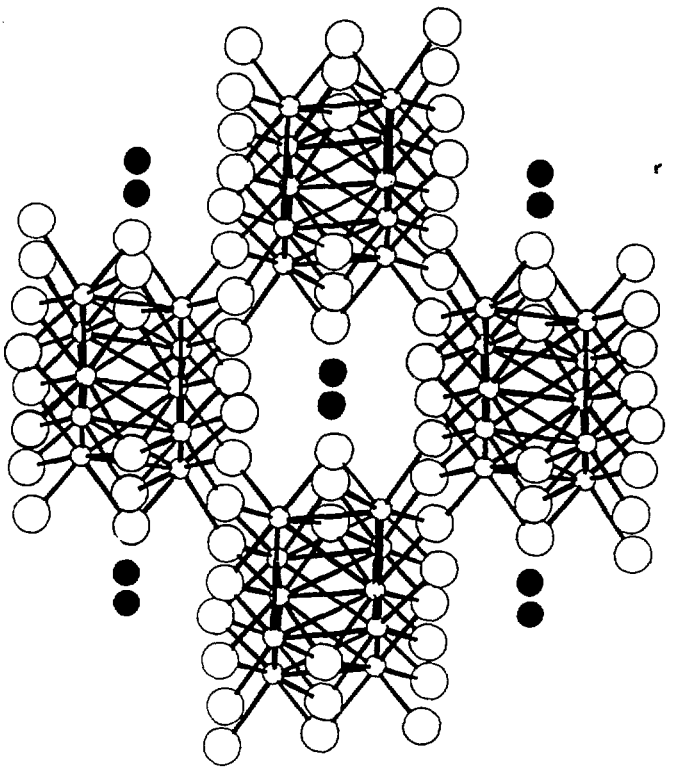

The $LaMo_5O_8$ structure viewed down the c–axis La (solid circles); Mo (small open circles); O (large open circles).

*Work supported by Div. of Materials Sciences, U. S. Dept. of Energy under contract DE-AC02-76CH00016.

SYNCHROTRON X-RAY DIFFRACTION DATA FOR MONOCLINIC ZSM-5

J. B. Higgins, R. von Ballmoos, and J. L. Schlenker
Mobil Research and Development Corporation

ZSM-5 is a synthetic zeolite catalyst which is used in the petroleum process industry. Previous studies of ZSM-5 materials include structural characterization of orthorhombic materials [1,2,3,4] and a study of factors affecting crystal symmetry [5]. Synchrotron x-ray powder diffraction data has been used to characterize a high silica (Si/Al > 50,000), monoclinic NH_4 ZSM-5.

The crystals were synthesized with high purity SiO_2, air calcined and ammonia exchanged. The crystals are highly twinned and approximately 10-15μm on edge. X-ray data was obtained on the X-13A powder diffraction beamline with a Ge (220) incident beam monochromator (1.3186 A). A flat plate sample was step scanned 4.0-43.0 degrees 2θ at 0.01 degree steps with 3.0 second counts. The x-ray wavelength and 2θ zero were calibrated with an NBS Si standard.

Intercrystalline d-spaces were measured with a second derivative peak search algorithm. The data were indexed on a monoclinic unit cell and lattice parameters were calculated from 96 measured d-spacings and their assigned indices. Only reflections for which a unique index could be assigned were used in the least-squares lattice parameter refinement. Refined lattice parameters are: a=19.8846(6), b=20.1165(6), c=13.3728(4), α=90.000, β=90.644(3), γ=90.000.

The maximum topological symmetry of the ZSM-5 framework is Pmna. A reduction to monoclinic symmetry may result in a framework with symmetry $P2_1/n$ or $P2_1/m$. An examination of h01 and 0k0 reflections with unique indices revealed that for h01 reflections either h or l may be odd or even and that h+l=2n, and for 0k0 reflections k=2n. These conditions are consistent with space group $P12_1/n1$.

1. Olson, D.H., Kokotailo, G.T. and Lawton, S.L., "Crystal Structure and Structure-Related Properties of ZSM-5", J. Phys. Chem. 85, 2238-43 (1981).

2. Kokotailo, G.T., Lawton, S.L. and Olson, D.H., "The Structure of Synthetic Zeolite ZSM-5",Nature 272, 431 (1978).

3. Flanigen, E.M., Bennett, J.M., Grose, R.W., Cohen, J.P., Patton, R.L., Kirchner, R.M. and Smith, J.V., "Silicalite, a New Hydrophobic Crystalline Silica Molecular Sieve", Nature 271, 512-516 (1978).

4. Baerlocher, Ch., "The Possibilities and Limitations of the Powder Method in Zeolite Structure Analysis. The Refinement of ZSM-5", Proceedings of the Sixth International Zeolite Conference, D. Olson and A. Bisio editors. Butterworths, Guildford, UK, 823-833 (1984).

5. Wu, E.L., Lawton, S.L., Olson, D.H., Rohrman, A.C. and Kokotailo, G.T., "ZSM-5-Type Materials. Factors Affecting Crystal Symmetry", J. Phys. Chem. 83, 2777-2781 (1979).

HIGH RESOLUTION SYNCHROTRON X-RAY POWDER DIFFRACTION WITH A LINEAR POSITION-SENSITIVE DETECTOR

M. S. Lehmann (ILL, Grenoble), A. N . Christensen (Aarhus U., Denmark), M. Nielsen and R. Feidenhans'l (Riso National Laboratory, Denmark), and D. E. Cox* (BNL)

X-ray synchrotron powder data were collected from a capillary sample of a small-molecule organic peptide compound, glycyl-glycine ($NH_2CH_2CONHCH_2$) by step-scanning at 1° intervals with a linear position sensitive detector covering an angular range of 2.7° in order to test the feasibility of recording a high resolution pattern and using the data for Rietveld analysis. Appropriate corrections for detector linearity and position were implemented, and comparison with a diagram recorded with a single scintillation detector and a crystal analyser system showed similar quality for the two sets of data. A detailed comparison of the refined atomic coordinates and those of an earlier x-ray single crystal study showed the estimated standard deviations to be significantly underestimated in both refinements. A linear detector should be particularly useful for small samples and capillary specimens of moderately absorbing materials.

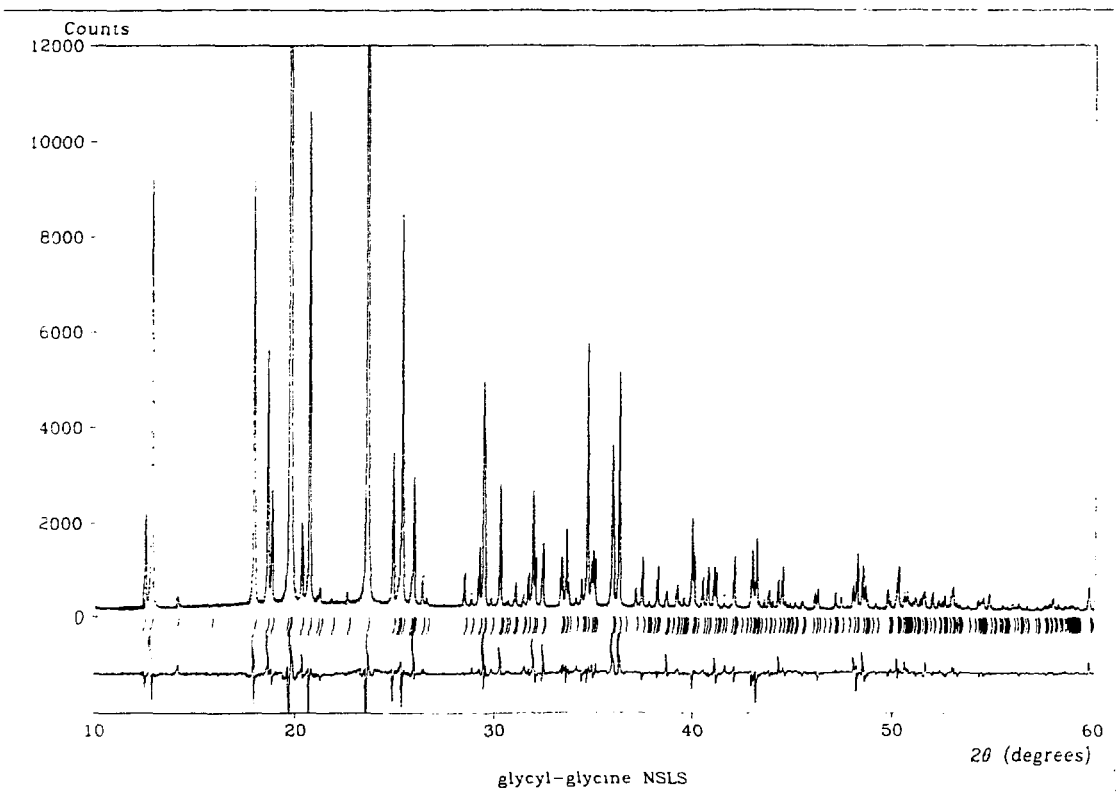

Profile fit and difference plot for glycyl-glycine. Short vertical markers denote allowed reflections.

*Work supported by Div. of Materials Sciences, U. S. Dept. of Energy under contract DE-AC02-76CH00016.

THE *AB-INITIO* CRYSTAL STRUCTURE DETERMINATION OF UPd_2Sn BY SYNCHROTRON X-RAY RADIATION POWDER DIFFRACTION

M. Marezio and C. Rossel (CNRS, Grenoble), and D. E. Cox* (BNL)

The structure of the heavy-fermion compound UPd_2Sn has been determined by *ab initio* synchrotron x-ray radiation powder diffraction techniques. It is orthorhombic, space group Pnma, with lattice parameters $a = 9.97871(12)$, $b = 4.58843(5)$, $c = 6.89166(8)$Å, and $Z = 4$. All atoms, one U, one Sn, and two Pd are in 4(*d*) special positions at $(x, 1/4, z)$. The refinements were carried out by the Rietveld method with a pseudo-Voigt peak shape function. The final conventional R factors were: $R_{wp} = 21.3$ and $R_E = 14.3$. The U positions in the unit cell were unequivocally located, but because of the similarity in x-ray scattering factors it was not possible to determine whether the Pd and the Sn atoms are ordered or disordered on the other three sites. The structural arrangement of UPd_2Sn is of either $MnCu_2Al$, or ordered NaTl or disordered Fe_3Al type, all these structures being cubic and b.c.c. related. The orthorhombic distortion is large, but no evident single driving factor (size, 5(f) electrons, electronegativity) could be found to explain it.

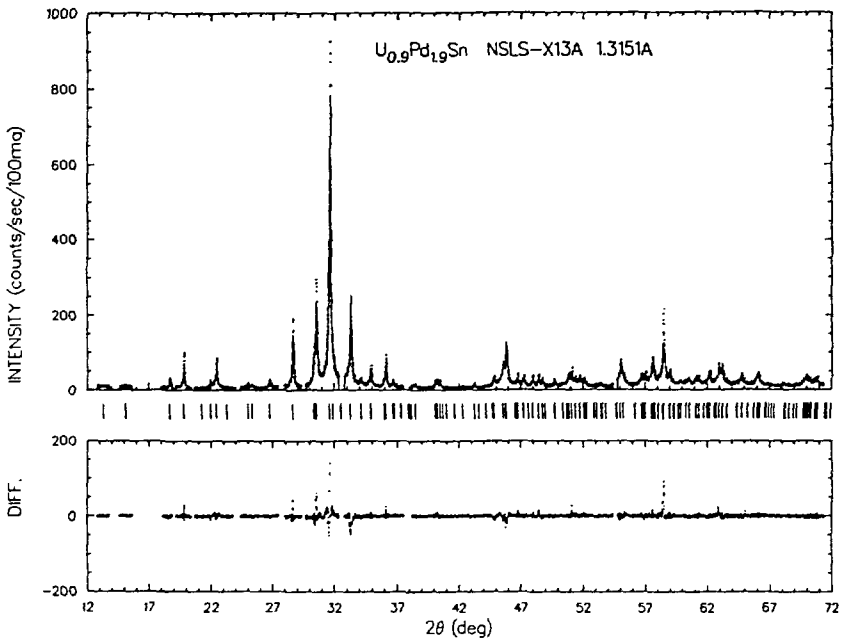

Profile fit and difference plot for UPd_2Sn. Short vertical markers denote allowed reflections.

*Work supported by Div. of Materials Sciences, U. S. Dept. of Energy under contract DE-AC02-76CH00016.

A SYNCHROTRON X-RAY POWDER DIFFRACTION STUDY OF $Li_{1.15}Ti_{1.85}In_{0.15}P_3O_{12}$

D. Tran Qui (CNRS, Grenoble), E. Prince (NBS), and D. E. Cox* (BNL)

A parasitic phase coexisting with the rhombohedral ionic conductor compound $Li_{1+x}Ti_{2-x}In_x P_3O_{12}$ of nominal composition $x = 0.25$, has been observed and identified as $LiInP_2O_7$ by profile analysis of a synchrotron x-ray powder pattern. Subsequent refinements using those regions of data associated with the $Li_{1.25}Ti_{1.75}In_{0.25}P_3O_{12}$ phase confirmed the previous neutron results that the arrangement of the $[Ti_{2-x}In_xP_3O_{12}]$ framework in the conducting phase is of Nasicon-type in the range $0.0 < x < 0.4$.

Synchrotron x-ray powder diffraction data were collected at room temperature at beamline X 13A at the Brookhaven National Synchrotron Light Source. A perfect crystal Ge(111) monochromator and a narrow-mosaic LiF(400) analyzer crystal were used at a wavelength of 1.3233 Å. With this arrangement, the instrumental resolution function has a minimum at 2Θ at $\approx 50°$ where the full width at half-maximum is about 0.025°. Data were collected from a flat-plate sample over the 2Θ range $12 - 86°$ at step-intervals of 0.01°. The sample was oscillated over a few degrees at each point so as to average over a sufficient number of crystallites.

Because of the high resolution of the x-ray pattern, 33 reflections from the parasitic phase well-resolved from the expected lines (compared to six in the neutron patterns) were observed and successfully indexed on the basis of the monoclinic unit cell parameters; $a = 4.9154\,(7)$, $b = 8.4345\,(26)$, $c = 7.0493\,(25)$ Å, $\beta = 110.85\,(18)$ deg., space group $P2_1$.

The presence of this indium-rich parasitic phase, $Li\,In\,P_2O_7$, explains the systematic disagreement between the In concentration given by structure refinement, $x = 0.15$, and by chemical analysis, $x = 0.25$. This latter method determines the total In content and hence overestimates the actual In/Ti ratio in the main phase, $Li_{1+x}Ti_{2-x}In_xP_3O_{12}$. Full details of the structure determination will be given in a subsequent publication.

*Work supported by Div. of Materials Sciences, U. S. Dept. of Energy under contract DE-AC02-76CH00016.

THE CRYSTAL AND MOLECULAR STRUCTURE OF BERYLLIUM HYDRIDE

G.S. Smith and Q.C. Johnson (LLNL), D.K. Smith (Penn State U.), D.E. Cox (BNL), R.L. Snyder and R-S. Zhou (Alfred U.), and A. Zalkin (LBL)

The crystal and molecular structure of BeH_2 has been determined from high-resolution powder diffraction data obtained at a synchrotron radiation source. Computer indexing methods gave the unit cell as body-centered orthorhombic with a=9.082(4), b=4.160(2), c=7.707(3)Å; V=291.2(2)Å^3, with systematic absences corresponding to space groups, Ibam or Iba2. Essentially, single crystal methods were used for the structure determination: Patterson synthesis to locate the Be atoms and a "heavy-atom" electron-density synthesis to confirm the location of the H atoms. The crystal structure is based on a network of corner-sharing BeH_4 tetrahedra rather than flat infinite chains containing hydrogen brides previously assumed (see Fig. 1). The Be-H bond distances are 1.38(2) Å around Be(1) and 1.41(2)Å around Be(2). The H-Be-H tetrahedral bond angles range from 107° to 113° and the Be-H-Be bond angle is approximately 128°. The space group in Ibam, and there are 12 BeH_2 molecules in the unit cell. The theoretical density is 0.755 g/cm^3. Atomic positions are listed in Table 1 and bond distances and angles in Table 2.

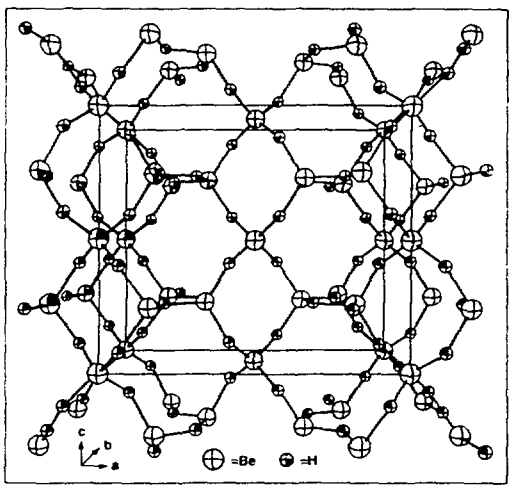

Fig. 2. Crystal structure of BeH_2 showing a network of corner-sharing BeH_4 tetrahedra. The origin of this figure is shifted by 0,0,1/4 from the customary Ibam center of symmetry for clarity.

Work performed under the auspices of the U.S. Dept. of Energy by Lawrence Livermore National Laboratory under contract No. W-7405-Eng-48, by Brookhaven National Laboratory under contract No. DE-AC02-76CH00016, and by Lawrence Berkeley Laboratory under contract No. DE-AC03-76SF00098.

Table 1. Atomic parameters of BeH_2. Standard deviations in last significant figures are shown in parenthesis.

Atom	x	y	z	B, Å^2
Be(1)	0.0	0.0	0.25	2.9(2)
Be(2)	0.1699(6)	0.1253(11)	0.0	1.8(1)
H(1)	0.0895(15)	0.1949(14)	0.1515(9)	-0.8(4)
H(2)	0.3055(21)	0.2823(32)	0.0	-0.2(5)

Table 2. Bond distances and angles with standard deviations for BeH_2.

Be(1) - 4H(1)	1.38(2)Å
Be(2) - 2H(1)	1.41(2)
Be(2) - H(2)	1.39(2)
Be(2) - H(2)	1.44(2)
H(1) - Be(1) - H(1)	113.0(5)°
H(1) - Be(1) - H(1)	107.7(5)
H(1) - Be(2) - H(1)	112.1(5)
H(1) - Be(2) - H(2)	111.2(5)
H(1) - Be(2) - H(2)	106.5(5)
H(2) - Be(2) - H(2)	109.1(5)
Be(1) - H(1) - Be(2)	130(1)
Be(2) - H(2) - Be(2)	127(1)

EFFECT OF SYNCHROTRON IRRADIATION ON CYTOCHROME C OXIDASE X9A

I. Ayene, B. Chance (Univ. of PA, UCSC/ISFS)

EXAFS study of cytochrome c oxidase at room temperature leads to an altered edge feature of copper which subsequent workers identified with reduction to copper (1). The first on-line optical monitoring of cytochrome oxidase at room temperature showed the kinetics of reduction during irradiation and reoxidation after irradiation (2). Hence, the present study was carried out to quantitate both spectroscopically and polarographically the radiobiological damage and its significance in EXAFS. Experiments were also carried out to protect the samples against irradiation by radioprotectors.

a) Aqueous Samples: Cytochrome oxidase of different concentrations (80,100 μM) in phosphate buffer (0.1 M, pH 7.0)was exposed to synchrotron radiation (NSLS, BNL) for two and a half hours at 40-45 mA (Table I). The radiation damage was determined by measuring the ratio of the absorption at 605/655 nm. The ratio was found to be increased after irradiation.

b) Dry Film Mounted Samples: The radiation damage of the enzyme was determined by measuring the absorption at 605/655 nm. In dry PVA film mounted samples (Table II), the ratio decreases after irradiation. The unusual behavior of the enzyme in dry film mounted samples cannot be easily explained. However, these results indicated that the redox effects of hydrated electrons is predominant in aqueous samples whereas no such effect is implicated in dry film mounted samples.

c) The activity of the enzyme was studied polarographically. The activity was decreased by about 20% after the sample was exposed to 1.73×10^{15} photons. However, the damage was decreased by about 75% after the addition of cystamine (Table III).

Thus these experiments have confirmed that cytochrome oxidase gets reduced at room temperature by synchrotron radiation. In addition to the reduction of the heme, the activity was also found to be reduced due to prolonged exposure (~ 8 hrs.). However, these damages can be reduced by cystamine which was found to be more effective than the other radical scavengers (DMSO, HCOONa, t-butanol, ethanol, cysteamine, WR-2721) tested in this laboratory.

Further experiments will be carried out to study the effect of synchrotron irradiation on enzymes and proteins at low temperatures (-70 c). Such exposed and unexposed samples will be used to study the difference in their EXAFS.

TABLE I:

Effect of Synchrotron Radiation on Cytochrome Oxidase of Different Concentrations
BNL-NSLS Line X9A, 0.1 M Phosphate Buffer pH 7.0
1×10^{10} photons/sec, 7.64 KeV
Dose: 4.82×10^{13} photons

Concentration of Enzyme (μm)	Ratio of the Peak 605/655 % Increase
83 C	0
R	45
100 C	0
R	33

Supported by NIH-RR01633,GM31992,GM33165;NSF-DMR85190959

FREEZE TRAPPING EXPERIMENTAL REPORT--BEAM LINE X9A X9A

B. Chance and A. Blaglow (U. of PA/U. City Sci. Ctr.)

Of the many approaches to time resolved X-ray absorption spectroscopy, freeze trapping or freeze quenching offers the greatest possibilities for acquisition of data at a high signal-to-noise ratio from dilute reactants; the duty ratio is 100% while many other devices have fractional duty ratios and therefore require corresponding longer integration times.

The problems of rapid freeze trapping that are special to the EXAFS study are the acquisition of sample in an adequate configuration to take advantage of the large beam size at X9A and avoidance of "freeze marks" that may seriously interfere with data analysis.

Activity on the development of an appropriate freeze-trapping device for NSLS has proceeded during the current year and a new design of the apparatus has been completed. Tests show the trapping of a model compound and acceptable EXAFS spectrum taken at NSLS. The freeze trapping apparatus is available to the X9A PRT and qualified general users.

Description of freeze-trap apparatus. Figure 1 illustrates the principle of the freeze-trapping apparatus which has been under construction and test in the current year. It can be seen that this differs significantly from the Bray apparatus in that the coolant is continuously circulated through the cold chamber at a high velocity. This assures uniform temperature distribution and temperatures very near the freezing point of isopentane.

The freeze-trapped material accumulates in a thin mesh at the observation point. The mesh is usually made of nylon. It is of small enough mesh so that most of the frozen droplets are caught on the first pass; however, continuous circulation of the smaller frozen droplets will eventually cause their accumulation in the observation area.

The injection of the unstable intermediate is into a rapidly flowing portion of the coolant. Turbulent flow is assured here and small droplets are rapidly frozen, under conditions of optimal mixing. The observation chamber is especially designed to be compatible with the wide beam of Beam Line X9A, i.e., 150 mm long. Thus, a high signal-to-noise ratio from a dilute sample is assured.

Experimental studies. A number of optical studies on the uniformity of the "freeze" and its accumulation in the nylon net have been made. It was thought that X-ray absorption spectroscopy was the sole arbiter of the adequacy of the freeze and the homogeneity of the signal and Figure 2 gives the EXAFS of zinc oxide freezed trapped in this way. The spectrum was recorded especially to determine whether diffraction effects, i.e., freeze marks, predominated. They do not, the edge and near-edge features are determined.

Future plans include a replaceable observation chamber so that minimal downtime between EXAFS studies intervenes.

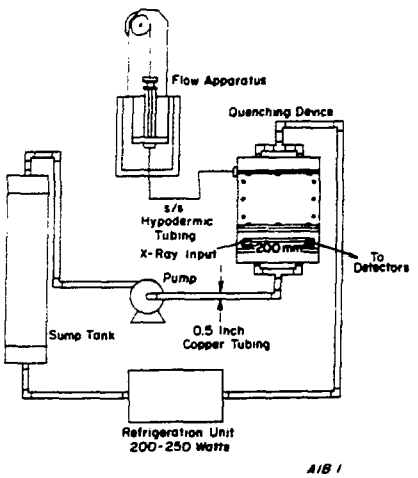

Figure 1. Functional diagram of 200 mm freeze quench apparatus for intermediate state of dilute metalloproteins.

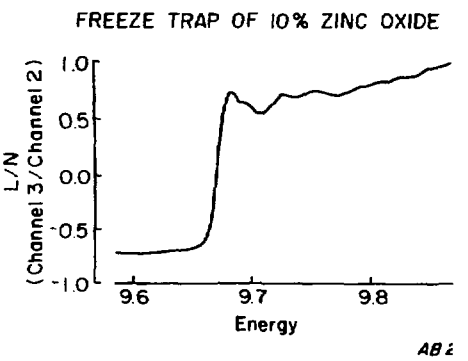

Figure 2. ZnO EXAFS trapped in apparatus.

This work is supported by NIH through RR-01633, GM-33165 and GM-31992; and by NSF through DMR-85190959

RATIOING THE 13-ELEMENT Ge-DETECTOR FOR IMPROVED SIGNAL/NOISE RATIO FOR XAFS SPECTROSCOPY B. Chance, S. Khalid, (Univ. City Science Ctr., PA) X9A

The 13-element Ge-detector has a large surface area and is capable of high count rates with energy dispersion and, therefore, it could be an ideal detector for X-ray absorption spectroscopic studies of dilute samples.

In this experiment, the scattering peak from a single element of the Ge-detector was used as reference, and its ratio was taken with the fluorescent signal peak. The idea was to improve the signal-to-noise ratio by minimum non-linearities of the single detectors as compared with ratioing the signals from two different detectors, i.e. an ionization chamber versus a Ge-detector. In this study the sample scattering at the fluorescence excitation energy was employed, it is also possible to ratio the signal from two fluorescent signals, one from the iron signal as here employed, the other from the fluorescent signal from the guard filter of Mn, in the case of Fe studies, with the advantage that the energy of the fluorescence is constant, that of the excitation is variable.

We used a highly attenuated iron signal at 6.9 KeV incident X-ray energy and resolved the 6.4 KeV, Fe, Kα and 6.9 KeV scatter peaks on two MCAs. A total internal count rate of 100 K was observed, the shaping time of Canberra 2020 amplifier was set at 0.5 μs. An integrated count rate of 38 K and 40 K was observed for the fluorescent and scattering peak respectively. The positive logic pulse output of the Single Channel Analyzer was converted to analog signals and the wide band ratio of the reference and sample signal was measured. A signal generator at 13 KHz was also used for performance evaluation and the noise fluctuations of the ratio were observed at a bandwidth of the ratio circuit of about 200 Hz On the slow time base, the fine structure of the noise disappeared, however, it was apparent in the amplitude of that trace. With two equal inputs, the noise was greater by the sq. root of 2 as expected, but the peak noise was decreased. The data showed the diminution of these non-white fast fluctuations. The goal of a completely linear compensation circuit is achieved.

WIDE BAND RATIO DETECTOR
Sample is Fe shielded by
12 thicknesses of aluminium foil

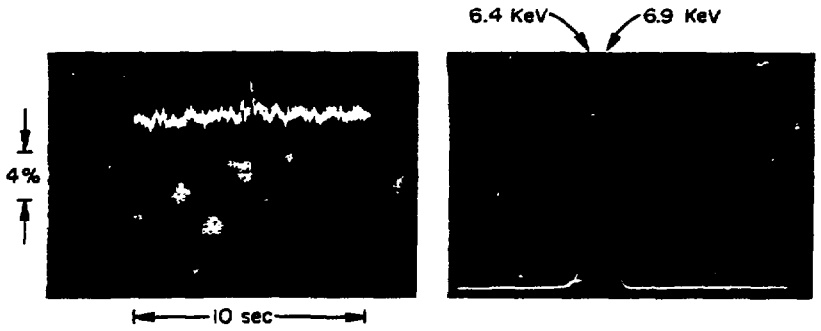

Analog output of ratio detector

MCA trace

A. 270 mV / 92 mV window
B. 223 mV / 55 mV window
5000 cts/sec

MZ 26

Supported by NIH-RR03990;RR01633; NSF-DMR85190959

TABLE II:

Effect of Different Exposures of Synchrotron Radiaton on Cytochrome Oxidase (PVA FILM MOUNTED SAMPLE: 0.166 mM)--SSRL Beam Line II-2, 1 x 10^{10} photons/sec, 7 KeV

Dose X 10^{13} Photons	Ratio of the Peak 605/655 % Decrease
0	0
2.3	15
3.8	33
6.4	33
13.6	33

TABLE III:

Effect of Synchrotron Radiation on Cytochrome Oxidase and Myoglobin

Beam Line X9-A, NSLS

Dose Rate: 3 x 10^{9} Photons/sq. mm., 7.6 KeV

Dose: 1.73 x 10^{15} Photons/20 sq. mm.

Dose	Samples	Activity
0	Cytochrome Oxidase (189μM)	100 ± 1
1.73 x 10^{15}	-do-	80 ± 3
0	+cystamine (300μM)	100 ± 5
1.73x10^{15}	-do-	95 ± 4

Beam Line II-2, SSRL, 7-8 KeV, ~ 10^{13} Photons

Dose	Samples	%MbO_2 Formation
0	Myoglobin(1.57 mM)	0
2 hrs.	-do-	20 ± 4
2hrs.	+cystamine	2

13-ELEMENT Ge-DETECTOR FOR XAFS AT BEAM LINE X9 X9A

S. Khalid, B. Chance (Univ. City Science Center, PA)

A single element Ge-detector provides energy dispersion while collecting data of dilute samples in fluorescent mode. However, this device is count-rate limited and because of its small area does not improve the signal-to-noise ratio when compared with the conventional detection techniques through ion chambers or large area ZnS(Ag) detectors.

The Canberra intrinsic Ge-detector model GL0110 with 13 elements improved the signal-to-noise ratio and the count rates. Each element has an active diameter of 11.3 mm, with a total active area of 13 cm^2. The elements are arranged in an array and enclosed to give a large circular area of diameter 64.5 mm. Each element has its own pre-amplifier. The output is connected to a linear amplifier Model 2020 and to a single channel analyzer where an upper and lower threshold can be set, the pulses can be separately counted using a HEX scaler or a latching scaler (Fig. 1). This way we can pick up the fluorescence from the element that we are interested in, and we can reject the harmonics, filter fluorescence and scattering, the main sources of noise in the spectra.

The detector has an outer and an inner Be window of thickness 250 and 25 microns respectively. The outer window can be removed for low energy XAFS work.

The detector has a resolution of about 200 eV at 5.9 KeV and each element is capable of counting up to 30,000 photons/s with pile up rejection. This limit can be increased to 100,000 cps if appropriate corrections for dead time losses are introduced.

Fig. 2 gives the XAFS spectrum of a cytochrome aa_3 sample collected from an area of 5 mm x 2 mm and using 5 of the 13 channels. The I_f/I_O ratio exhibits an edge jump of about 1 to 4.5 below and above the edge, without filters. Improvement by the square root of 13/5 is expected as soon as computer hardware/software becomes available.

Fig. 1

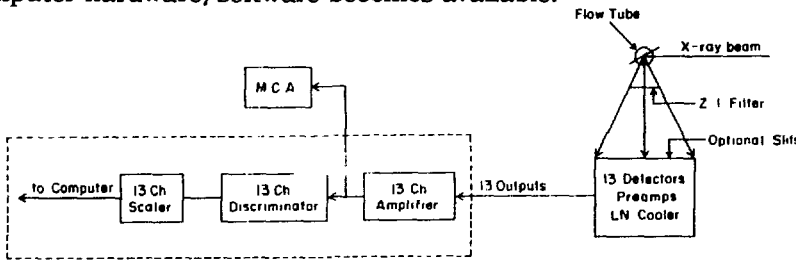

13 ELEMENT Ge-DETECTOR AND ANCILLARY EQUIPMENT

SK 2i

Fig. 2

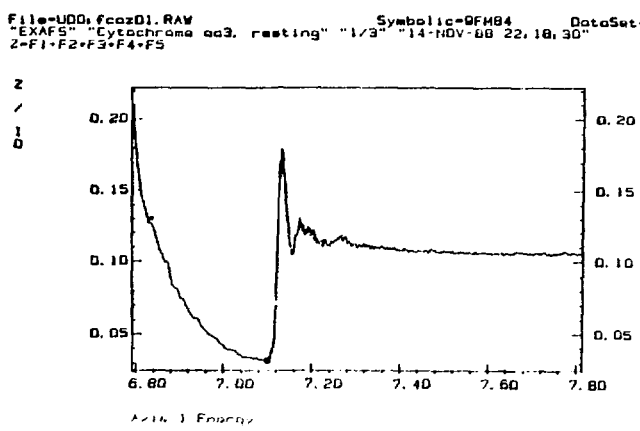

Supported by NIH-RR03990;RR01633; NSF-DMR85190959

X-RAY ABSORPTION SPECTROSCOPIC INVESTIGATIONS OF METALLOENZYMES

M. J. Maroney, G. J. Colpas, M. Kumar, U. of Massachusetts at Amherst

Our use of x-ray absorption spectroscopy is focused on the use of the technique to probe the structure of transition metal sites in metalloenzymes. Typically, this involves the use of EXAFS to obtain information regarding the nature and number of scattering atoms surrounding the absorbing metal atom and the distances between the absorber and scattering atoms. More recently, many investigators in the field have begun to explore the analysis of XANES, which includes discrete electronic transitions that are expected to obey electronic absorption selection rules, to obtain information regarding coordination geometries and infer information concerning oxidation state changes. Scott et al.[1,2] have employed edge analysis for a number of Ni-containing proteins, including hydrogenases, carbon monoxide dehydrogenase, and S-methyl coenzyme M methyl reductase. The analyses carried out on homoleptic (or nearly so) model compounds in ideal geometries has indicated that small shifts in the edge energy (ca. 1-2 eV) are associated with the formal oxidation of Ni(II) to Ni(III) in the enzymes, and that 1s → 3d transitions are strong for noncentrosymmetric complexes and weak for centrosymmetric complexes. A transition assigned to 1s → $4p_z$ (with shakedown contributions) has been shown to be characteristic of planar and pyramidal complexes. We have recently completed experiments designed to explore the effects of geometric distortion and mixed donor sets on these Ni K-edge features. Some of our data are summarized by Figures 1-2.

Figure 1. Effects of oxidation and axial ligation on the Ni K-edge structure of a planar $Ni(N_2O_2)^{2-}$ complex.

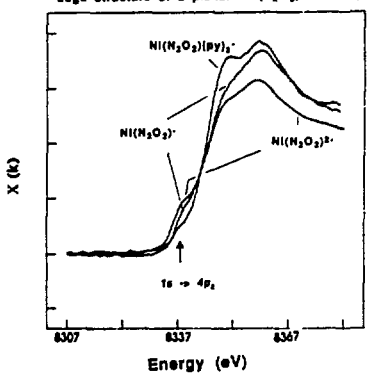

Figure 2. A Comparison of Ni K-edge Structure in 5-coordinate geometries.

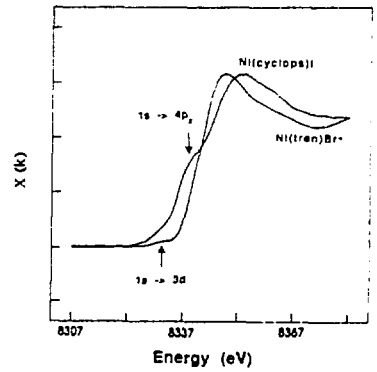

Figure 1 shows edge data for the $N_2O_2^{4-}$ donor set of N,N'-ethylenebis (o-hydroxybenzamide) as the Ni atom in the four-coordinate (C_s) complex is formally oxidized from +2 to +3 and then ligated by two axial pyridine ligands, as demonstrated by epr investigations.[3] This edge data indicates that the starting Ni(II) complex is planar (no 1s → 3d transition, shoulder is 1s → $4p_z$) and remains so in the formally Ni(III) complex. However, no shift in the edge energy is apparent in the spectra. Addition of axial pyridine ligands greatly reduces the 1s → $4p_z$ transition, consistent with six-coordination, but also does not affect the edge energy; all three spectra

cross at a single point. Similar results are obtained for an analogous $N_2S_2^{4-}$ ligand with thiophenolate donor atoms. This data indicates that a significant change in edge energy is not required upon formal oxidation where the ligands act to stabilize the higher formal oxidation state by preventing a change of electron density on the Ni center.

Figure 2 compares the edge data obtained for two five-coordinate geometries, pyramidal pseudo-C_{2v} Ni(cyclops)I and C_{3v} Ni(tren)Br^+. Small 1s → 3d transitions are visible in both cases, while only the pyramidal complex displays a 1s → $4p_z$ transition. The 1s → 3d transition obtained for the C_{3v} complex is considerably weaker than expected; it is essentially indistinguishable from that obtained for six-coordinate $Ni(Im)_6^{2+}$. Thus, it will be difficult to choose between a pseudo-trigonal bipyramidal geometry and six-coordinate geometries on the basis of solution state or powder XANES data.

References

1. R. A. Scott, S. A. Wallin, M. Czechowski, D. V. DerVartanian, J. LeGall, H. D. Peck, Jr., I. Moura, J. Am. Chem. Soc. **1984**, 106, 6864.
2. S. P. Cramer, M. K. Eidsness, W.-H. Pan, T. A. Morton, S. W. Ragsdale, D. V. DerVartanian, L. G. Ljungdahl, R. A. Scott, Inorg. Chem. **1987**, 26, 2477.
3. H.-J. Krüger, R. H. Holm, Inorg. Chem. **1987**, 26, 3647.

Acknowledgement. This work is supported by NIH GM-38829 (M.J.M.) and by the National Biostructures PRT and its supporting agencies; NIH RR-01633 and NSF DMR-85190959. We are also grateful for funds from the NSLS/HFBR Faculty-Student Support Program.

RECOMMISSIONING OF BEAM LINE X9A

G. Rosenbaum and S. Khalid, Univ. City Sci. Ctr./Inst. for Struct. & Funct. Studies, PA

After the resumption of production of X-rays by NSLS in June, 1988, Beam Line X9A has been recommissioned for operation. The basic hardware of the beam line was unchanged from the state in March, 1987.

Beam observation conducted in April, 1988 had shown that 16.9 mrad horizontal divergence out of 18 mrad (nominal) is available at the front of Beam Line X9A. (On port X9B, 17.7 mrad is available). Some alignment of the front end may be necessary at a later time.

The measured flux was 2.5 x 10^9 photons/sec/mm^2/100 mA which is in reasonable agreement (30%) with the flux measured before the shutdown. The vertical beam profile was as expected. The horizontal beam profile over the 135 mm width of the monochromatic beam showed an improvement in flatness compared to 1986 due to improved flatness of the crystal carrier blocks. Still, the remaining twist in one of the crystals produces a significant decrease in flux at one end. However, a region of 50 mm width can be selected which has a flux which is constant within 5%.

An oscillation of the flux of the monochromatic beam with a period of 190 sec has been observed when the second crystal is detuned. For 15% detune ($I=0.85\ I_{max}$), the amplitude of the oscillation was 5% peak-peak. The period and phase of the oscillations closely tracked the oscillations of the NSLS cooling water temperature of about 0.65°C peak-peak. No flux oscillations are observed when the second crystal is tuned to maximum flux.

The 800 mm long Ni-plated mirror is used for rejection of harmonics. The mirror is set to a grazing angle of 3.25 mrad and to focus at infinity, providing a beam of 2.5 mm height in the hutch. In this setting, photons up to 15 keV are reflected and rejection of the third harmonic is provided for photon energies above 7 keV.

This configuration of the beam line has been used through September 6, 1988.

The National Biostructures PRT is supported by NIH through RR-01633 and NSF through DMR-85190959

INSTALLATION OF THE NEW CONSTANT EXIT HEIGHT MONOCHROMATOR AT BEAM LINE X9A G. Rosenbaum, M. Sullivan, J. Schug (Univ. City Science Center, PA)

Between September 7 and October 16, 1988 the old monochromator was removed from beam line X9A and a new monochromator with constant height of the exit beam has been installed.

The new monochromator is a scanning double crystal monochromator for EXAFS experiments and has several novel features. We have designed a double parallelogram linkage between the first and second crystal axes for extremely precise angular tracking. The second crystal axis is supported by a trolley which is positioned by a separate linear drive to maintain the constant height of the exit beam. A sagittal focusing stage for the second crystal is in construction. The first crystal axis is driven by a precision rotary table via a rotary vacuum feedthrough. Cooling water is supplied into the vacuum tank very close to the crystal surface via flexible hoses enclosed by bellows. The monochromator is designed to accept up to 17 mrad of horizontal divergence. A vibration isolation system consisting of 2500 lb inertia based on springs is supporting the monochromator which is separated from the vacuum enclosure by flexible bellows.

Fig. 1 shows an EXAFS-spectrum of a 10 mM Ferric EDTA-solution obtained with the new monochromator. The dotted curve represents the incident flux of three different scans. No closed-loop feedback or any other correction is applied to the piezo-translator used for fine tuning of the second crystal after the initial tuning to maximum intensity before the start of the scan. The drop in flux indicates that the parallelograms of the linkage are not perfect. However, the deviations are reproducible and are changing very smoothly with the Bragg-angle.

In order to correct the drop in flux, a program has been added to the data accumulation software which performs a peak scan within 0.5 sec at every new energy position. Fig. 2 shows an EXAFS spectrum and the incident flux (dots) obtained in this mode. The total change of I_0 is 3%. The change of I_0 between energy points is typically less than 0.5%.

Because of the problems with hysteresis and relaxation of the piezo-translator, the parameters of the peak-tuning software need to be precisely trimmed for stable performance. As the deviation of the parallelogram linkage from exact tracking seems to be a simple, smooth and reproducible function of angle, we intend to implement a software that calculates the corrective voltage to the piezo-translator as a function of energy.

The vibration isolation system is very effective. A Fourier-analysis of I_0 does not show any peaks below 22 Hz except for a very low and broad bump at 11.9 Hz. The resonance frequency of the inertia base of about 2.7 Hz is not present in I_0. The 22 Hz-peak is the resonance frequency of the linkage. Above 22 Hz are peaks around 60 Hz which are probably due to the electronics.

The National Biostructures PRT is supported by NIH Grant RR01633 and NSF Grant DMR85190959

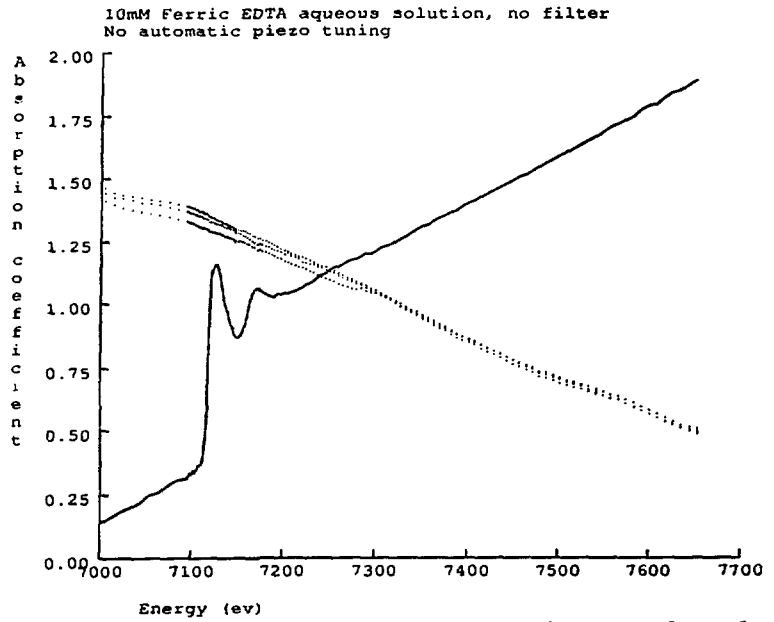

Fig. 1: Absorption coefficient of a 10 mM Ferric EDTA solution and incident flux (dots) as a function of energy. Angular tracking of the second crystal is provided by the double parallelogram linkage only.

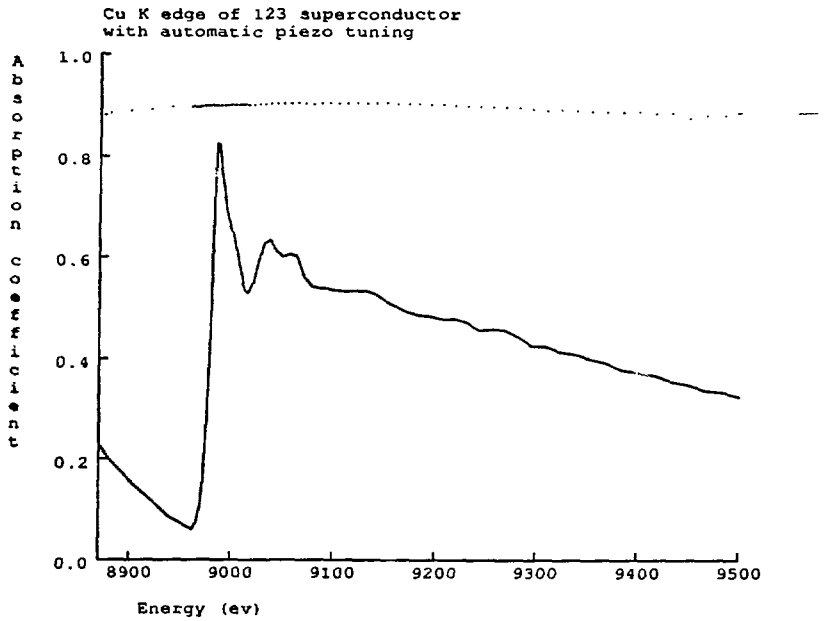

Fig. 2: Absorption coefficient of a superconductor compound and incident flux (dots) as a function of energy at the Cu K-edge. The incident flux is maximized at each scan point by a peak-finding program in the control software.

Reflection EXAFS Study of Metal-Semiconductor Interfaces.

Pathikrit Bandyopadhyay and Bruce A. Bunker, Notre Dame

Reflection-mode EXAFS with fluorescence detection has been used to probe the Al/GaAs buried interface to directly determine interdiffusion, compound formation, and phase segregation near the interface. Two sets of samples were prepared by *in situ* deposition of 500Å of Al on MBE-grown GaAs at (a) ambient growth temperature, approximately 500C, and (b) 90C. Preliminary results of both the A_ and Ga edges show clear interdiffusion of Al into the GaAs, with clearly more interdiffusion in the higher-temperature sample. No evidence is seen for large As phase separation near the interface.

Supported by Office of Naval Research under contract N00014-85K-0614.

INCLUSION OF ORGANOMETALLICS IN ZEOLITE HOST STRUCTURES. EXAFS AND IN-SITU VIBRATIONAL STUDIES.

Thomas Bein*, Karin Moller, and Aticha Borvornwattananont,
Department of Chemistry, University of New Mexico,
Albuquerque, New Mexico 87131 (U. S. A.)

Attempts to immobilize organometallic catalysts on solid supports are motivated by the notion that it should be possible to combine the advantages of homogeneous catalysts, such as high selectivity, mild reaction conditions, or the potential utilization of all metal atoms, with those of heterogeneous systems, i. e. facile product separation, facile recovery of the expensive catalyst, and inherent stability. In contrast to their amorphous counterparts, zeolite molecular sieve supports are highly crystalline oxides with well-defined pore sizes of typical molecular dimensions, and intrazeolite catalysts can offer diffusional shape selectivity for substrate and product molecules, selectivity of polar vs. nonpolar substrates, and other advantages. We explore intrazeolite anchoring concepts for organometallic species which utilize the bridged hydroxyl groups present in the acid forms of many zeolite structure types. We study the different relative reactivities and stabilities of ligands at a metal center with respect to the bridged intrazeolite hydroxyls as a basis for the rational design of zeolite-based hybrid catalysts. To date, intrazeolite reactions of $[CpFe(CO)_2]_2$ [1] (Fp2), $COTFe(CO)_3$ [2] (COT), $CpFe(CO)2CH_3$ (FpMe) and ferrocene, diffused into different acid forms of dehydrated zeolite Y under inert conditions, have been examined.

EXAFS measurements of sealed samples were performed at NSLS, Beamline X-11A, with a stored electron energy of 2.5 GeV and ring currents between 60-110 mA. Fe K-edge data at 7112 eV were collected at about 100 K in transmission using a Si(400) monochromator. The EXAFS data were analyzed following standard procedures[3]. Additional characterization of the samples included in-situ FT-IR experiments coupled with Temperature-Programmed -Desorption/MS studies.

As an example, the intrazeolite chemistry of the dimer Fp2 is discussed. We have found that the tricarbonyl cation $CpFe(CO)_3^+$ forms in the pores of the acid zeolite hosts H2Y and H6Y (2 and 6 protons per supercage, respectively) via oxidation of Fp2 at room temperature. The intensity of the iron-iron scatterer pair observed in the EXAFS spectrum of the unsupported complex is reduced to 20% after adsorption into the zeolite, indicating cleavage of the metal-metal bonds of the dimer. The fitted EXAFS data are consistent with the presence of about 40% $CpFe(CO)_3^+$, 40% $CpFe(OZ)_2$, and a remainder of 20% of the dimer (OZ: zeolite oxygen atoms). An increasing relative amount of intrazeolite protons favors the oxidation of the dimer to the monomeric cation. The zeolite host H6Y with even higher proton activity opens a reaction path to form the protonated dimer $[Cp(CO)_2Fe]_2H^+$. If sample H2YFp2 is heated at 473 K for 10 hours, striking changes of the EXAFS data can be observed (Figure 1a,b). The small Fe-Fe backscattering contribution and that from linear CO ligands present at room temperature are eliminated. Two peaks near the position of the original Fe-Cp shell are now dominant (Figure 1.b). The fitting routine deconvolutes these peaks, revealing as the major contribution an Fe-Cp fragment at 2.07 Å. An optimum fit indicates the presence of two Fe-O species, i.e. bare iron ions at 1.93 Å plus CpFe(OZ)n at 2.16 Å. A smaller peak at about 2.8 Å is clearly visible at this temperature and is assigned to backscattering from the zeolite framework metals Si or Al. The combined appearance of these new peaks is a strong indication for coordination of the resulting complex fragments to zeolite cation sites[4]. As confirmed by FTIR measurements, the

tricarbonyl cation thus splits off all CO ligands at higher temperatures. However, no Cp fragments are detected in the vapor phase, and the EXAFS analysis shows that the Cp ligands are still coordinated to the iron metal to form the "half-sandwich" $CpFe^{+}(OZ)_n^{-}$, (2 n 3), anchored to the oxygen rings present in the zeolite supercage.

In conclusion, the stability of these and the other complexes is influenced by the intracavity concentration of the zeolite bridged hydroxyl groups. Upon treatment at higher temperatures under vacuum, carbonyl and other ligands split off from the complexes and the remaining fragments attach to the zeolite host structure via oxygen coordination. These fragments are stabilized against migration and agglomeration. The judicious choice of intrazeolite ligand chemistry allows us to control the 'anchoring chemistry' aimed at the rational design of zeolite hybrid catalysts.

Acknowledgement is made to the Donors of the Petroleum Research Fund, administered by the American Chemical Society, and to the Sandia-University Research Program (DOE), for partial support of this research. The operational funds for NSLS beamline X-11A are supported by DOE grant DE-AS0580ER10742.

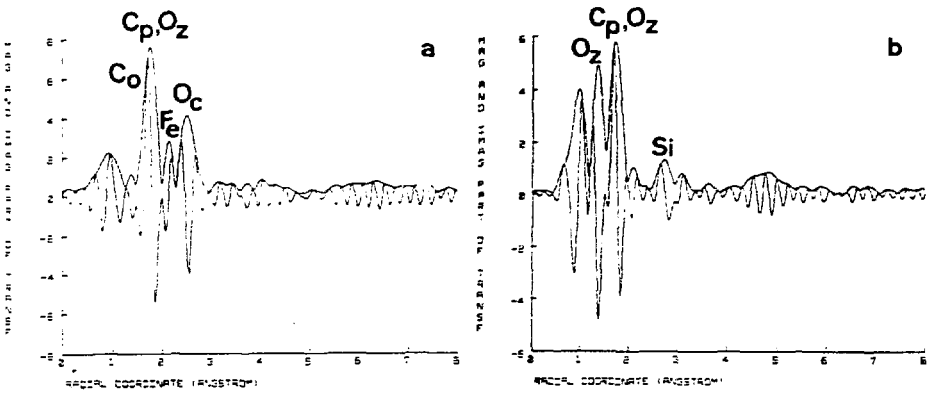

Figure 1. Iron EXAFS spectra of a,b) $[CpFe(CO)_2]_2$ at room temperature and 473 K, and c,d) ferrocene at room temperature and 573 K, in acid support HY. The magnitudes and imaginary parts of the k^3 weighted Fourier transformations are shown. The spectra are uncorrected for phase shifts. Labels indicate the following backscatterers: Co = Fe-CO, Cp = Fe-Cp, Fe = Fe-Fe, Oz = Fe-O(zeolite), Oc = Fe-CO, Si = Fe-Si/Al. Some peaks are convoluted and labels indicate the positions obtained from the EXAFS analysis.

1 Moller, K.; Borvornwattananont, A.; Bein, T. submitted to J. Phys. Chem.
2 Borvornwattananont, A.; Moller, K.; Bein, T. J. Phys. Chem., in press
3 Lee, P. A.; Citrin, P. H.; Eisenberger, P.; Kincaid, B. M. Rev. Mod. Phys. 1981, 53, 769
4 Woolery, G.; Kuehl, G.; Chester, A.; Bein, T.; Stucky, G. D., Sayers, D. E. J. Physique 1986, 47, C8-281

EXAFS STUDY OF BOND STRENGTHS IN β-PHASE ALLOYS.*

D.L. Brewe, D.M. Pease, J.I. Budnick, and Z. Tan, (U. of Conn.), C. Law, United Technologies-Pratt&Whitney), M.H. Choi, (Catholic Med. College, Seoul, Korea.

We have measured temperature-dependent EXAFS of TM-Aluminum (TM = Co,Ni,Fe) alloys possessing the cesium chloride structure. From a plot of σ^2_{EXAFS} vs. temperature, information on bonding is obtained. We have used these results to investigate correlations between brittleness and bond strength. We find that the TM-TM bond strength is largest in CoAl, which is the most brittle member of the group.

We have also investigated temperature dependent EXAFS of CoFe and CuZn alloys, which are also cesium chloride structures. CuZn exhibits the greatest temperature dependence of σ^2_{EXAFS} of all these systems, and is the most ductile of these alloys. We have found that cold work disorder from grinding of sample powder produces a distinct damping of the EXAFS oscillations in FeAl and NiAl, with the effect being largest for FeAl. We find that $CoSi_2$ is a good standard material for analyzing TM-Al EXAFS.

*Supported by US DOE under contract DE-A505-80ER10742 and United Technologies and the US Air Force under contract F33615-86-C-5037.

THE THERMAL VARIATION OF THE MSRD^{+}FOR THE Pt-Pt PAIR IN THE $Ni_{10}Pt_{90}$ RANDOM SOLID SOLUTION ALLOY.

*M. Choi, J.I. Budnick, D.M. Pease, (U. of Conn.), S.M. Heald, (BNL).

To investigate the disorder of the Pt-Pt pair in $Ni_{10}Pt_{90}$, the Pt L_3 EXAFS data taken at four different temperatures ($7K \lesssim T \lesssim 300K$) have been analyzed with the ratio fit. The relative disorder squared of the Pt-Pt pair at each of the four different temperatures with respect to that of the Pt-Pt pair in pure Pt at 7K was obtained. Only a high k region above ~12$\AA^{-1}$ was used for the ratio fit. Since about 90% of the near neighbors are Pt atoms, in a high k region where the Pt backscattering overwhelms the Ni backscattering, the contribution of Ni neighbor backscattering is assumed to be negligibly small. Subsequently the MSRD values were determined by Einstein model fits. The results are in good agreement with those of two shell fits.

+Mean square relative displacement between the absorbing atom and the backscattering atom.

*present address: Catholic Univ. Med. College, Seoul, Korea.

Supported by USDOE under contract numbers, DE-AS05-80ER10742 and DE-AC02-76CH00016. M. Choi was also supported by KOSEF.

XAFS STUDIES OF $Tl_2CaBa_2Cu_2O_x$ THIN FILMS

D. Di Marzio, D. H. Chen, S. M. Heald, R. L. Sabatini, and H. Wiesmann, and (BNL-DAS)

Cu K-edge x-ray absorption fine structure measurements (XAFS) were made on thin films of superconducting (T_c~105 K) $Tl_2CaBa_2Cu_2O_x$. The films were prepared by reactive co-sputtering using Tl, Ca/Ba, and Cu targets. XAFS measurements were taken at the X-11A beam line at NSLS.

The Tl-Ca-Ba-Cu films (~1 μm thick) were positioned with the substrate (cubic zirconia) parallel to the polarization of the x-ray beam. The angle of incidence of the x-ray beam with the substrate surface was 30°, and the x-ray fluorescence signal was measured with a detector placed above the sample. The 30° angle of incidence gave a reasonably good x-ray energy window (around and above the Cu K-edge) free from Bragg peaks from the underlying ZrO_2 substrate.

Both the Cu K near edge (XANES) and extended fine structure (EXAFS) of the Tl-Ca-Ba-Cu film exhibits diminished oscillations which is characteristic of reduced long range order. The near edge shows a small $1s \rightarrow 3d_{x^2-y^2}$ pre-edge feature, a weak shoulder representing the $1s \rightarrow 4p\sigma$ transition with a charge screening shake down from the O 2p orbital, and a sharp $1s \rightarrow 4p$ main peak. In comparison with XANES results for oriented $Tl_2CaBa_2Cu_2O_x$ powders taken by Heald et al.,[1] our near-edge structure indicates that the Tl-Ca- Ba-Cu films are oriented preferentially with the C axis perpendicular to the substrate surface. This observation is also supported by our EXAFS measurements. Preliminary EXAFS bond length calculations are consistent with previous results.

This work was performed under the auspices of the U.S. Department of Energy, Division of Materials Sciences, Office of Basic Energy Sciences under Contract No. DE-AC02-76CH00016.

1. S. M. Heald, J. M. Tranquada, C. Y. Yang, Y. Xu, A. R. Moodenbaugh, M. A. Subramanian, and A. W. Sleight, Proc. Intern. Conf. XAFS, Seattle, WA, Aug. 1988.

ORIENTATION DEPENDENT X-RAY ABSORPTION IN HIGH Tc SUPERCONDUCTORS

S.M. Heald, J.M. Tranquada, A.R. Moodenbaugh, Y. Xu (BNL) and
M.A. Suramenian, A.W. Sleight (DuPont)

Oriented high T_c superconductors were prepared by casting 400 mesh powders in epoxy in an 8 tesla magnetic field. Figure 1 compares the Cu K edge absorption for all four classes of high T_c materials. Measurements were made with the X-Ray polarization $\hat{e}$ vector parallel and perpendicular to the c axis of the materials. For the perpendicular case all of the edges are very similar as expected, since the X rays are probing the Cu-O planes which are common to all the materials. For the parallel case the differing structures give rise to differing features, but all edges show a weak 1s-4pπ shakedown feature. This is much weaker than typically found in planar Cu-O materials, and may indicate the presence of holes in the O p bands.

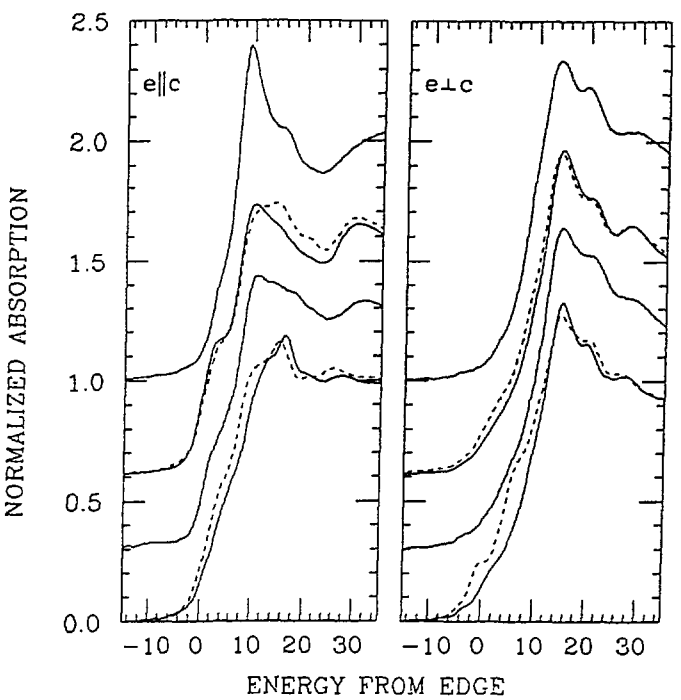

Figure 1: Orientation dependent near edge absorption for, from bottom: $YBa_2Cu_3O_{7-x}$ with x=0(solid) and x=0.77(dashed), $Bi_2Sr_{1.75}Ca_{1.25}Cu_2O_{8+x}$, $Tl_2Ba_2CaCu_2O_x$(dashed) and $Tl_2Ba_2Ca_2Cu_3O_x$(solid),and $La_{1.85}Sr0.15Cu_2O_4$.

EXAFS Study of the Ge Site in $Ge_xSn_{1-x}Te$ Ferroelectric Alloys.

Quazi T. Islam[+] and Bruce A. Bunker, Notre Dame

The role of the Ge site on the structural phase transition of $Ge_xSn_{1-x}Te$ alloys has been investigated using the EXAFS technique. The Ge appears to be displaced along the <111> direction from the Sn site both above and below the transition temperature T_c. The magnitude of the displacement is such that the Ge-Te near-neighbor bond length is approximately independent of x and T, both above and below T_c, and is comparable to the Ge-Te bond length in $Ge_xPb_{1-x}Te$ alloys.[1] As in the $Ge_xPb_{1-x}Te$ alloys, there is evidence that the interaction between nearby off-center ions strongly influences the ferroelectric transition of the $Sn_{1-x}Ge_xTe$ alloys.

[+] Current Address: North Carolina State University.

[1] Q. T. Islam and B. A. Bunker, Phys. Rev. Lett. 59, 2701 (1987).

Supported by Office of Naval Research under contract N00014-85K-0614.

Glancing Angle EXAFS of Tungsten-Carbon Multilayers

G.M. Lamble,* S.M. Heald† D.E. Sayers,* E. Ziegler‡ and P.J. Viccaro* X11A

* North Carolina State University, † Brookhaven National Laboratory, ‡ E.S.R.F,
* Argonne National Laboratory.

The glancing angle EXAFS technique has been applied to investigate the structure of W/C multilayers and the effects of moderate annealing. There is evidence of considerable interlayer mixing prior to any heat treatment. It is found that after annealing to 350°C for several hours, drastic changes can occur in the structural environment of the W atoms, with minimal changes in the reflectivity of the sample. There is extensive formation of W_2C depending on the W thickness and the W/C ratio. Identification of this carbide as the product of annealing is unambiguous. Above a critical thickness, W begins to grow in its bcc form within the W layer, as it is prepared. This bcc layer is unaffected by the annealing process. The presence of carbon is shown to stabilise the amorphous state of W and inhibits any formation of W_2C when the W thickness and the W/C ratio is small.

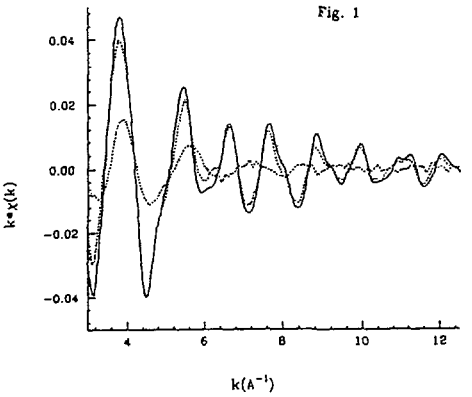

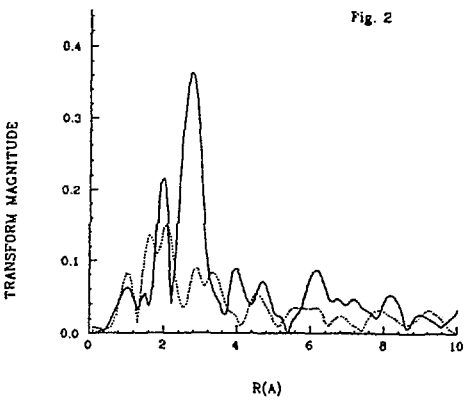

Fig.1 Broken curves show EXAFS from multilayer A, 43Å W/ 40Å C, before annealing (small amplitude) and after annealing (large amplitude). The latter shows distinct similarities to the EXAFS from W_2C (full line).

Fig. 2 Comparison of Fourier transforms from unannealed samples A, 43Å W/ 40Å C, (broken line) and sample B, 65Å W/ 18Å C, (full line). Sample B shows significant contribution from b.c.c. W components at around 3.0Å

This work was supported by the U.S. Department of Energy under contract Nos. DE-AS05-80-ER10742 and DE-AC02-76CH00016 and by the Argonne National Laboratory Advanced Photon Source R&D funds.

STABILIZATION OF CADMIUM SULFIDE AND CADMIUM SELENIDE MOLECULAR CLUSTERS IN ZEOLITE Y: EXAFS AND X-RAY DIFFRACTION STUDIES.

Karin Moller[a], Thomas Bein[a]*, Mike Eddy[b], Galen D. Stucky[b]*, Norman Herron[c] , Ying Wang[c], and Dave E. Cox[d]

Department of Chemistry, University of New Mexico[a], Albuquerque, NM 87131; Department of Chemistry, University of California[b], Santa Barbara, CA 93106; Central Research and Development Department[c], E.I. DuPont de Nemours & Co.,Wilmington, DE 19898; and Department of Physics[d], Brookhaven National Laboratory, Upton, Long Island, NY 11973

Semiconductor clusters are of interest due to the dramatic changes of optical properties and other 'quantum-size effects' with decreasing cluster size. Classical preparation methods for semiconductor clusters include wet colloidal techniques[1], growth in dielectric glassy matrices[2], or in polymers.[3] However, particle sizes are usually non-uniform and agglomeration of individual particles often occurs.[4] Thus, the effect of particle size on optical and other properties is obscured. We have recently reported an alternative method to stabilize well-defined semiconductor clusters which are much smaller than those typically formed by classical colloidal techniques. Selenium species, cadmium sulfide and cadmium selenide ensembles were encapsulated in the crystalline pore structure of zeolite matrices.[5,6,7] We discuss EXAFS and synchroton x-ray diffraction studies of the latter two systems. The intrazeolite CdS/CdSe clusters are composed of a few atoms only which strongly interact with the zeolite host such that their bonding must be considered completely distinct from that of the bulk solid and typical semiconductor clusters. The interaction with the zeolite allows us to stabilize these species in condensed phase at ambient conditions. We illustrate the complimentarity of powder X-ray diffraction (XRD) and X-ray absorption spectroscopy (EXAFS). Both techniques have been applied to the elucidation of the structure of CdS/Se loaded into zeolite Y. In combination, Rietveld refinement of powder diffraction data determines the statistical occupancy of the atoms in crystallographically defined positions, while EXAFS yields crucial information on bond formation by monitoring the local environment of the absorber atoms.

Small ensembles of CdSe and CdS have been synthesized within the cage system of zeolite Y via ion exchange with Cd(II) and subsequent treatment with H_2Se and H_2S. EXAFS experiments were carried out at the X-11A beamline at the Brookhaven National Synchroton Light Source with a stored electron energy of 2.5 GeV and ring currents between 40-130 mA. Data of the Cd K-edge (26,711 eV) and Se K-edge (12,657.8 eV) were collected in transmission using a Si(400) crystal monochromator. High resolution x-ray powder data were collected on the powder diffractometer at beam line X13A at the Brookhaven National Synchroton Light Source. A perfect Ge(111) crystal scattering in the horizontal plane was used to monochromate the incident x-ray beam. The wavelength was determined to be 1.53668 Å by calibration with a Si standard and data were collected by step-scanning from 5^o to 73^o in intervals of 0.01^o for periods of 2 to 10 seconds. The intensity at the sample position was 10^{10} photons/sec for a storage ring current of 100 mA.

The uptake of Se by the Cd(II)-exchanged zeolite and bond formation to cadmium ions with a bond length of 2.60 Å is clearly evident from EXAFS data of both Cd- and Se-absorption edges. For example, a comparison between the EXAFS data of cadmium-exchanged zeolite CdY (Figure 1a) and the sample treated with hydrogen selenide gas shows that major changes occur in this sample (Figure 1b). The CdSe molecular clusters are stabilized at ambient conditions through strong interactions with the zeolite host. Rietveld analysis and EXAFS results indicate the

presence of 70% of the cadmium ions at SI' and 30 % at SIII. Se,O bridged cadmium dimers and Cd_4O_4 cubes are formed in the sodalite unit. Cadmium ions present in twelve ring windows are coordinated to one Se and additional oxygen atoms. Small amounts of Se helical chains and CdSe clusters are also detected.

In contrast to the CdSe samples, the intrazeolite synthesis of CdS leads to a novel supercluster with a structural geometry superimposed by the host framework. The structural characterization reveals discrete $(CdS)_4$ cubes located within the small sodalite units of the structure which begin to interconnect as the loading density within the zeolite rises. As this three-dimensional interconnection proceeds, the corresponding changes in optical properties indicate a transformation to a semiconductor supercluster with behavior intermediate between that of the discrete CdS cubes and bulk semiconductor.

Acknowledgement:
Support provided by the Sandia-University Research Program (DOE; T. B.) and ONR (G. D. S.) is gratefully acknowledged. The operational funds for NSLS beamline X-11A are supported by DOE grant # DE-ASO580ER10742.

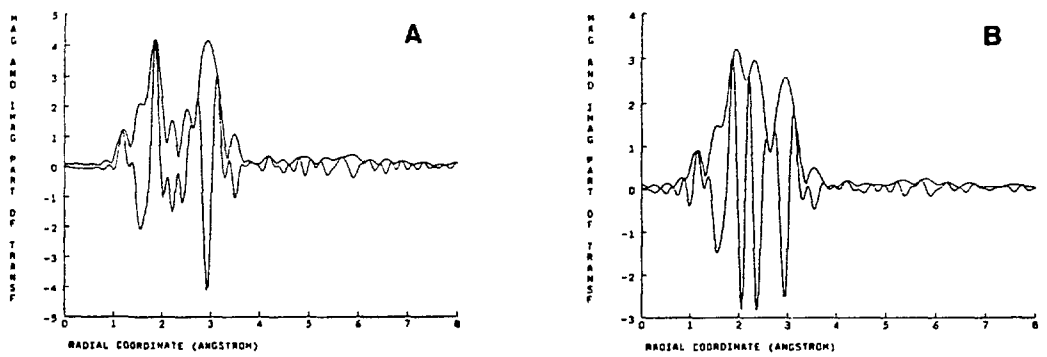

Figure 1. Cd-edge normalized, Fourier transformed EXAFS data of (a) Cd(II)Y zeolite, and (b) Cd(II *treated with* H_2Se.

1 Henglein, A. Ber. Bunsen Ges. Phys. Chem. 1984, 88, 969

2 Ekimov, A. I.;Efros, Al. L.; Onushchenko, A. A. Solid State Comm. 1985, 921

3 Wang, Y.; Mahler, W. Opt. Comm. 1987, 61, 233

4 Chestnoy, N.; Hull, R.; Brus, L. E. J. Chem. Phys. 1986, 85, 2237

5 Parise, J. B.; MacDougall, J. E.; Herron, N.; Farlee, R.; Sleight, A. W.; Wang, Y.; Bein, T.; Moller, K.; Moroney, L. M. Inorg. Chem. 1988, 27, 221

6 Herron, N.; Wang, Y.; Eddy, M.; Stucky, G. D.; Moller, K.; Bein, T.; Cox, D. E. J. Am. Chem. Soc., in press

7 Moller, K.; Eddy, M.; Stucky, G. D.; Herron, N.; Bein, T. J. Am. Chem. Soc., in press

STABILIZATION OF METAL ENSEMBLES AT ROOM TEMPERATURE: EXAFS STUDIES OF PALLADIUM CLUSTERS IN ZEOLITES

Karin Moller*, Diek C. Koningsberger+, Thomas Bein**

*Department of Chemistry, University of New Mexico, Albuquerque NM 87131
+Laboratory for Inorganic Chemistry and Catalysis, Eindhoven University of Technology, 5600 MB Eindhoven, The Netherlands

Small metal particles or clusters have attracted great interest during the last decade. Optical, electronic and catalytic characteristics of clusters are expected to change from 'bulk' properties to 'molecular' properties within a certain size-range. Based upon their unique, crystalline pore structure with dimensions at the molecular level (pore sizes between 3 and 12 Å are common) *molecular sieves* appear to be promising supports for the room-temperature stabilization of small metal clusters. We report the synthesis and characterization of *Pd ensembles, consisting of 2 to 4 correlated atoms, which are stabilized at room temperature in an open, chemically accessible zeolite matrix* [1,2]. These ensembles are ideal model systems to study physical, chemical and catalytic characteristics of small metal systems at ambient conditions. Characterization of the clusters was done by means of x-ray absorption spectroscopy (EXAFS) at the X11A beamline. A detailed data analysis, utilizing phase- and amplitude corrected Fourier transformations (FT) of the EXAFS data combined with a difference-file and iterative fitting technique provided insight in the structure and local environment of these clusters.

The palladium clusters of low nuclearity were prepared in the cavities of X and Y zeolites via ion exchange with $Pd(NH_3)_4Cl_2$, oxidative dehydration, and subsequent reduction of the dry Pd(II)zeolites with hydrogen at 295 and 425 K. EXAFS measurements were done at the X-11A beamline with an electron energy of 2.5 GeV and ring currents between 40-120 mA. Data were collected with a Si(400) crystal pair monochromator at the Pd K-edge (24,350 eV) at ca. 100 K.

Experimental EXAFS data and Fourier transformations of PdX zeolite samples after two different treatments are shown in Figure 1: after oxygen pretreatment at 625 K (PDXO, Figure 1.A,B); after H_2 exposure at room temperature (PDX, Figure 1.C,D). In sample PDXO, the coordination of Pd^{2+} to oxygen with a Pd-O distance of 2.07 Å (1.5 Å uncorrected) is detected as the main peak (Figure 1.B). From x-ray crystallographic studies of palladium exchanged zeolites, this was found to be a typical value for Pd^{2+}-O when coordinated to the framework via three oxygens in the hexagonal windows of the sodalite subunit (SI'). A coordination of Pd to the zeolite is further indicated by the concomitant appearence of a peak at about 3.0 Å (uncorrected), typical for Si/Al scatterer of the zeolite framework.

If the sample PDXO is exposed to hydrogen at 295 K (PDX), drastic changes are visible in the corresponding EXAFS data (Figure 1.D). The unsmoothed, low-noise data do not show <u>any</u> sign of remaining cationic Pd-zeolite-oxygen coordination as in the precursor sample PDXO, but instead a small, well resolved contribution from Pd-Pd scattering. <u>No</u> outer palladium shells are visible, indicating an extremely small cluster size.

Detailed analysis of the Pd K-edge data shows that the average first shell Pd-Pd coordination number of the reduced system is only about N = 1.5 at a distance of 2.78 Å. A long, relatively

disordered coordination of the reduced Pd to framework oxygen and silicon indicates the stabilizing, templating function of the zeolite matrix. Geometric models based upon the EXAFS results show that intrazeolite Pd_2, Pd_3, and Pd_4 clusters are formed by partial occupation of SI' and SII' positions of the sodalite subunits of the zeolite. This study presents evidence for the formation of 'molecular' metal ensembles stabilized in an open-framework matrix to at least 425 K.

Acknowledgement:
T.B. is grateful for funding from the Sandia University Research Program (DOE). The operational funds for NSLS beamline X11A are supported by DOE grant # DE-AS0580ER10742.

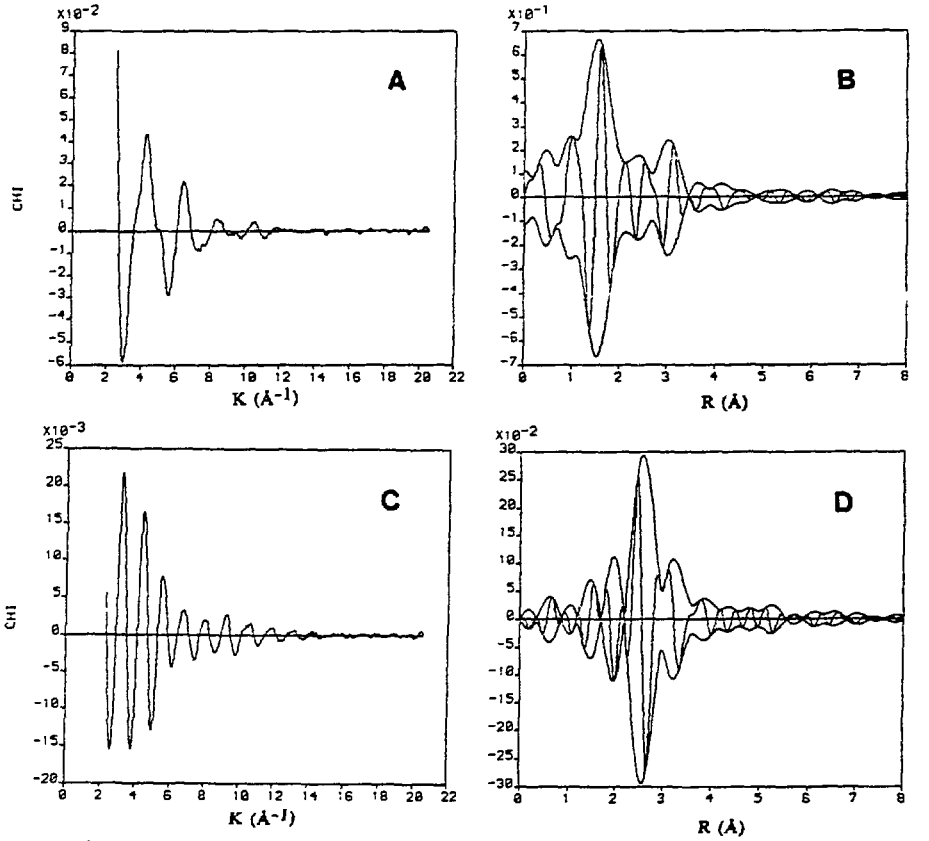

Figure 1. A,C Pd K-edge normalized EXAFS data and B,D their Fourier transformations over a range of k = 3.5-10.8 Å $^{-1}$ using a k^2 weight and phase correction with PdO (B), phase and amplitude correction with Pd foil (D). A,B: Sample PDXO; C,D: Sample PDX.

1 K. Moller, D. C. Koningsberger and T. Bein, J. Phys. Chem., submitted
2 K. Moller and T. Bein, J. Physique, 47 (1986) C8-231

EXAFS Study of Bond Lengths in $Hg_{1-x}Cd_xTe$.

Way-Faung Pong, Robert Mayonovic, and Bruce A. Bunker, Notre Dame

The narrow-gap disordered alloy $Hg_{1-x}Cd_xTe$ exhibits a number of anomalies, including unusual charge-transfer effects. Recent calculations[1] of the Hg-Te and Cd-Te bond lengths in the alloy series indicate that charge-transfer effects cause the bond lengths to *increase* even though the lattice constant slightly *decreases* with x. EXAFS results for both the Hg and Cd edges show the bond lengths remaining constant within 0.005A between x = 1.0 and x = 0.15 of the alloys, clearly conflicting with the predictions.

---

[1] A. Sher, A. B. Chen, W. E. Spicer, and C. K. Shih, J. Vac. Sci. Technol. 3, 105 (1985); K. C. Hass and D. Vanderbilt, J. Vac. Sci. Technol. 5, 3019 (1987).

Supported by Office of Naval Research under contract N00014-85K-0614.

EXAFS STUDY OF THE MODIFICATION OF $YBa_2Cu_3O_{7-x}$ BY WATER

M. W. Ruckman, S. M. Heald, D. Di Marzio, and A. R. Moodenbaugh (BNL-DAS)

The chemical and structural modification of the 1-2-3 high T_c superconductor by water is examined using extended x-ray absorption fine structure (EXAFS). A ten-minute exposure to water at 80°C destroys the oxygen deficient samples and produces a disordered reaction product consisting of $BaCO_3$, CuO and at least one other Cu^{2+} containing phase. $YBa_2Cu_3O_7$ retains the orthorhombic structure, but small changes in the EXAFS signal suggest that the bulk structure changes. Examination of the Cu k-edge (Fig. 1) shows that some of the copper is reduced from the 2^+ to 1^+ oxidation state. Comparison of our data with those reported for $H_xYBa_2Cu_3O_7$ and TEM studies of the 1-2-3 material exposed to atmospheric moisture suggest that the diffusion of hydrogen or water into the bulk is a likely explanation.

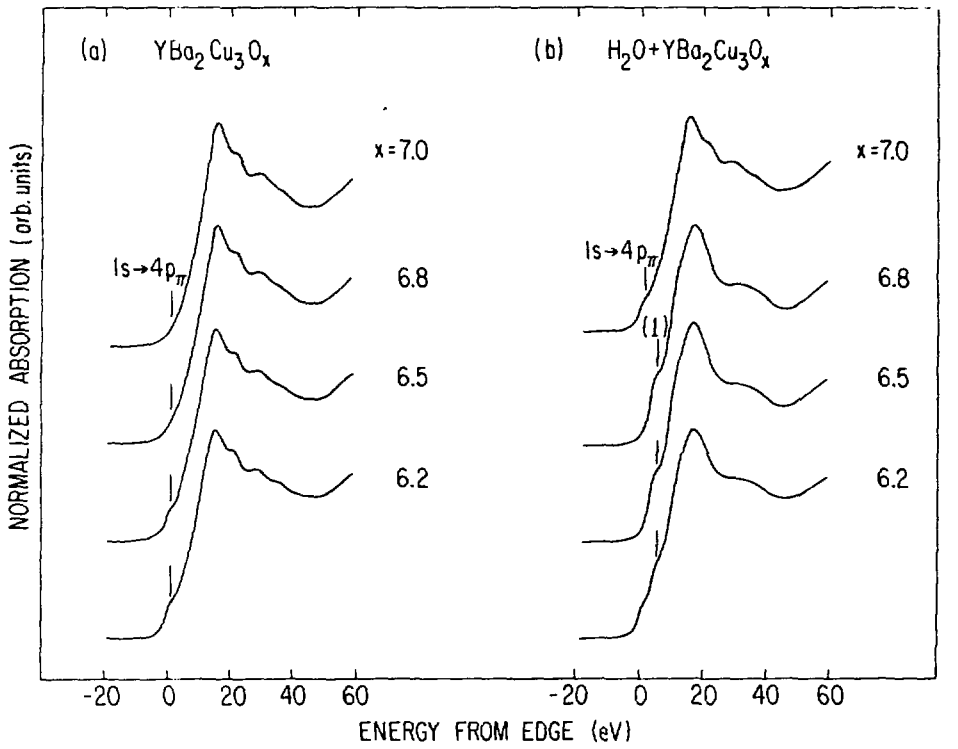

Fig. 1. Cu k-edge data for the 1-2-3 material before and after exposure to water.

This work was supported by the U.S. Department of Energy under Contract No. DE-AC02-76CH00016.

GLANCING ANGLE EXAFS STUDY OF Al/Nb INTERFACE REACTION.

Zhengquan Tan, J.I. Budnick, (U. of Conn.,) Y. Bruynserade, W. Sevenhans, (Katholieke Univeriteit Leuven, Belgium,)S.M. Heald, J.M. Tranquada, (BNL).

We have carried out fluorescence and reflection glancing angle EXAFS studies of reactions at the as sputtered and ion beam irradiated 700Å Al/2000Å Nb interface over float glass. Very little compound formation was observed at the as sputtered interface Al^+ ion beam irradiation tends to induce disordered or short-range-only ordered phases which depend strongly on the irradiation condition. Structural inhomogeneity generally exists in the irradiated interface region. For a sample irradiated with 50 kev Al^+ to a total dose of $1x10^{16}$ Al^+/cm^2, we found two different interfacial regions. One region immediately underneath the Al overlay is Nb rich with Al near neighbors only at 5.8 Å and beyond. The other region is more closer to the Nb buried layer with Nb and Al near neighbors at 2.75 Å and 2.76 Å respectively. The EXAFS amplitude distortion due to dispersion of optical constants and its effect on the structural parameter determination are analyzed. The amplitude distortion is more severe and more dependent on incident angle in fluor-EXAFS than in refl-EXAFS. In most cases of interest to interface study, the distortion can be treated as a constant reduction such that only the coordination number is affected significantly.

This work is supported by the Division of Materials Science of DOE under contract No. DE-AS05-80-ER10742.

DETERMINATION OF BOND STRENGTHS OF ARSENIC AND ARSENIC CHALCOGEN COMPOUNDS USING THE TEMPERATURE DEPENDENCE OF EXAFS

C.Y. Yang, M.A. Paesler and D.E. Sayers
Department of Physics, North Carolina State University, Raleigh, NC 27695-8202
and
J.M. Tranquada
Physics Department, Brookhaven National Laboratory, Upton, NY 11973

We present an EXAFS study of the temperature dependence of crystalline (c-) As, As_2S_3, and As_4S_4, amorphous (a-) As, and glassy (g-) As_2S_3. Based on an Einstein model, we find that the mean-square relative displacement of the materials in the first shell is primarily attributable to bond stretching forces of vibration. From a comparison with Raman spectra, it is evident that the Einstein vibrational frequencies derived from EXAFS measurements are related to the effect bond-stretching force constants. Our results indicate that As-As bonds in c-As are about 17% weaker than those in a-As. Bond stretching forces of the As-S bonds in c- and g-As_2S_3 are quite similar. The calculations of bond strengths in c-As_4S_4 shows that As-S bonds are about 30% stronger than As-As bonds. This work underscores the fact that temperature-dependent EXAFS data may be used to provide information about the nature - i.e., the strength - of local bonding.

This work has been supported, in part, by the Department of Energy, Office of Basic Energy Sciences under contract # DE-AS05-80ER10742.

MEASUREMENT OF LOCAL STRUCTURAL CONFIGURATIONS ASSOCIATEDWITH REVERSIBLE PHOTOSTRUCTURAL CHANGES IN ARSENIC TRISULFIDE FILMS

C.Y. Yang, M.A. Paesler and D.E. Sayers
Department of Physics, North Carolina State University, Raleigh, NC 27695-8202

Extended x-ray absorption fine-structure measurements have been made on three reversible and reproducible cycles of thermally annealed and light-soaked amorphous As_2S_3 films. Associated with the light-soaked material are (1) a very small increase in the population of wrong bonds in the first shell, (2) an enlarged As-S-As bond angle with an expansion of the As-As distance in the second shell, (3) a larger spread in the distribution of the As-S-As bond angles, and (4) an absence of any change in the third As-S shell. From these data we present the first quantitative correlation between observed local atomic structural changes and measured macroscopic properties that are associated with photodarkening. Our data demonstrate that the photoinduced structural changes mainly involve bonding alterations at S atoms as well as a change in the dihedral angle relationship between AsS_3 pyramids joined at S atoms.

This work has been supported, in part, by the Department of Energy, Office of Basic Energy Sciences under contract # DE-AS05-80ER10742.

X-RAY ABSORPTION SPECTROSCOPY STUDIES OF GLASSY AS_XS_{1-X}: THE ROLE OF COMPOSITION

C.Y. Yang, M.A. Paesler and D.E. Sayers
Department of Physics, North Carolina State University, Raleigh, NC 27695-8202

We have examined the effect of the composition on the local structure of chalcogenide glasses in the As-S system using x-ray absorption spectroscopy. Structural differences among glasses are discussed on the basis of results of extended x-ray absorption fine structure measurements. Structural changes associated with composition indicate that with increasing S content the S-rich glasses on the As site have a similar local structure to crystalline As_2S_3 (orpiment), but the As-S-As linkages are replaced by As-S-S linkages at higher concentration. In As-rich glasses a breakdown of the local AsS_3 configuration is evident and the formation of As-As bonds is observed. Further comparison between As-rich alloys and crystalline As_4S_4 (realgar) suggests that a significant fraction of disordered As_4S_4 molecular fragments are contained in the As-Rich region.

This work has been supported, in part, by the Department of Energy, Office of Basic Energy Sciences under contract # DE-AS05-80ER10742.

X-RAY ABSORPTION SPECTROSCOPY STUDIES OF GLASSY AS_2S_3: THE ROLE OF RAPID QUENCHING

C.Y. Yang, M.A. Paesler and D.E. Sayers
Department of Physics, North Carolina State University, Raleigh, NC 27695-8202

We have examined the effect of the thermal quenching rate on the structure of As_2S_3 chalcogenide glasses. Structural differences among glasses are discussed on the basis of results of x-ray absorption measurements. We find that small structural differences are seen among glassy As_2S_3 samples bulk quenched from various temperatures between 350 and 800°C. Comparatively large changes are observed, however, among samples quenched from annealing temperatures between 200 and 300°C with the structural disorder decreasing with increasing annealing temperature. Material quenched at 300°C shows a strong tendency toward ordering. Structural differences among samples are discussed in terms of (1) distortions in the As-S-As bond angles between helices and within a helix and (2) deviations of the As apex angle.

This work has been supported, in part, by the Department of Energy, Office of Basic Energy Sciences under contract # DE-AS05-80ER10742.

STRUCTURAL ANALYSIS OF A SERIES OF ANTIVIRAL AGENTS COMPLEXED WITH HUMAN RHINOVIRUS 14.

J. Badger (Purdue U.), I. Minor (Purdue U.), M. J. Kremer (Purdue U.), M. A. Oliveira (Purdue U.), T. J. Smith (Purdue U.), J. P. Griffith (Purdue U.), D. M. A. Guerin (Purdue U.), S. Krishnaswamy (Purdue U.), M. Luo (Purdue U.), M. G. Rossmann (Purdue U.), M. A. McKinlay (Sterling-Winthrop Res. Inst.), G. D. Diana (Sterling-Winthrop Res. Inst.), F. J. Dutko (Sterling-Winthrop Res. Inst.), M. Fancher (Sterling-Winthrop Res. Inst.), R. R. Rueckert and B. A. Heinz (Institute for Molec. Virol.)

The binding to human rhinovirus 14 of a series of eight antiviral agents that inhibit picornaviral uncoating after entry into host cells has been characterized crystallographically. All of these bind into the same hydrophobic pocket within the viral protein VP1 β-barrel structure, although the orientation and position of each compound within the pocket was found to differ. The compounds cause the protein shell to be less flexible, thereby inhibiting disassembly. Although the antiviral potency of these compounds varies by 120-fold, they all induce the same conformational changes on the virion. The interactions of these compounds with the viral capsid are consistent with their observed antiviral activities against human rhinovirus 14 drug-resistant mutants and other rhinovirus serotypes. Crystallographic studies of one of these mutants confirm the partial sequencing data and support the finding that this is a single mutation that occurs within the binding pocket.

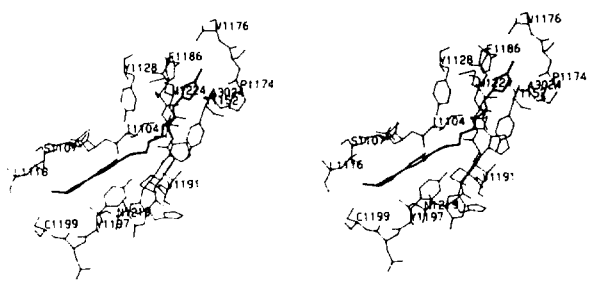

Fig. 4. Stereo view of the protein environment of antiviral compound II. The binding of this molecule to rhinovirus was studied at the NSLS.

(The work was supported by grants from the National Institutes of Health and the National Science Foundation as well as from the Sterling-Winthrop Research Institute.)

SUBUNIT SYMMETRY OF CRYSTALLINE AMP NUCLEOSIDASES FROM *ESCHERICHIA COLI* AND *AZOTOBACTER VINELANDII*.

V. L. Giranda and H. M. Berman (Fox Chase Cancer Center, Phila., PA), V. L. Schramm (Albert Einstein College of Medicine, Bronx, NY)

AMP nucleosidases are procaryotic enzymes which catalyze the hydrolysis of AMP to adenine and ribose 5′-phosphate. The enzymes are allosterically activated by ATP. Formycin monophosphate (FMP) is a strong competitive inhibitor of AMP nucleosidases.

Enzyme from both sources has been crystallized in the presence of saturating ATP and FMP. AMP nucleosidase crystals from *E. coli* belong to the space group $P4_12_12_1$ with a = 120.1 Å and c = 243.7 Å. AMP Nucleosidase crystals from *A. vinelandii* crystallize in the space group C2 with a = 347 Å, b = 204 Å and c = 114 Å, $\beta = 91.7^{o}$. These crystals are hexagonal plates which grow to maximum dimensions of 0.7 x 0.7 x 0.2 mm, are stable to X-irradiation, and diffract X-rays to at least 2.9 Å.

Both crystal types have multiple subunits in the asymmetric unit, probably three for *E. coli* and twelve for *A. vinelandii*. Two data sets have been collected for the native *E. coli* crystals. The first data set, to 3.0 Å, was collected at the National Synchrotron Light Source at the Brookhaven National Laboratory. A second low-resolution data set was also collected for the *A. vinelandii* AMP nucleosidase crystals using an area detector.

These data sets have been used in self-rotation functions to determine the local subunit symmetry that exists in these crystals. These results suggest that enzyme from both sources crystallize as hexamers with point symmetry 32. The subunits of the four hexamers have orientations consistent with point group O 432. However, translational elements required by crystal packing considerations preclude formation of the closed point group O 432. For the *E. coli* crystals, the local four-fold axes are parallel to the a, b and c axes and the local three-fold axes are oriented 55^{o} from the local four-fold axes. In the *A. vinelandii* crystals a local three-fold axis is parallel or nearly parallel to the c^{*} axis, and a local two-fold is parallel to a crystallographic two-fold axis. Local four-fold axes are 55^{o} from the three-fold axes with one of these axes in the ac plane. This elucidation of these noncrystallographic symmetries will greatly facilitate the determination of the crystal structures.

Support was provided by for H. M. B. by grants from NIH, GM21589, CA06927, RR0559, for V. L. S. by a grant from NIH, GM 21083 and for V. L. G. by a training grant from NIH, AM07163.

STRUCTURAL DIFFERENCES DETECTED BETWEEN WILD TYPE AND ASP-43 STAPHYLOCOCCAL NUCLEASE.

P. J. Loll and E. E. Lattman (Johns Hopkins U. Med. School)

Using oscillation data collected at the protein crystallography beamline at NSLS, the structure of the Asp-43 mutant of staphylococcal nuclease has been determined and refined at a resolution of 1.65 angstrom to a crystallographic residual of 0.185. In comparing the mutant structure to that of the wild type enzyme, we observe that while the backbone conformations of the two proteins are virtually identical, substantial side chain and water rearrangements are seen in the vicinity of the amino acid substitution (which is in the enzyme's active site). Perhaps more surprisingly, we also see small but significant differences in side chain packing in areas remote from the site of mutation. The solution structure of the mutant has been observed to differ from that of the wild type protein; however, the specific differences inferred from NMR measurements are not seen in the crystal structure.

This work has been supported by NIH grant GM-36358-03.

CRYSTAL STRUCTURE OF PHOTOSYNTHETIC REACTION CENTER FROM *RHODOBACTER SPHAEROIDES*

D.C. Rees (UCLA), T.O. Yeates (UCLA), H. Komiya (UCLA),
J.P. Allen (UCSD), G. Feher (UCSD)

Photosynthetic reaction centers (RCs) are integral membrane protein-pigment complexes which carry out the primary processes of photosynthesis: the light induced electron transfers from a donor to a series of acceptor species. Crystals of the RC from the purple bacteria *R. sphaeroides* grow in space group $P2_12_12_1$, with cell constants a=138.0Å, b=77.5Å, c=141.8Å, and diffract to about 2.8Å resolution on stills. During data collection on rotating anode generators in our laboratory, however, we had only achieved a practical resolution limit of 3.3Å resolution. We had obtained an initial structural model to this resolution, and needed the high resolution data to more reliably characterize the protein and cofactor structures. At the light source, we collected 172 film packs, using a 0.6^o range for the oscillation photographs. 128 film packs were processed to yield 23,349 unique reflections with an intensity exceeding twice the standard deviation. This is 62% of the total number of reflections to 2.8Å (25% of the possible reflections were observed between 2.8 - 2.9Å resolution) . R factors for scaling front and back films in a pack ranged between 3-5%, while the overall merging R factor (on intensities) was 8.9%. Each recorded reflection was measured on an average of 4 times. Scanning was complicated by the large mosaic spread of the crystals, which was approximately 0.5^o, so that essential no whole spots were recorded on films. Nevertheless, the data processing went smoothly, and the final data set agreed well with earlier detector data. Structure refinement (Hendrickson-Konnert) has proceeded to an R factor of 24% with data from 8-2.8Å resolution. A stereoview of the Cα backbone and the cofactor arrangement in the RC is illustrated below. A description of this work has been published (Allen, J.P., Feher, G., Yeates, T.O., Komiya, H., Rees, D.C. (1987) *Proc. Natl. Acad. Sci. USA* **84**, 5730-5734).

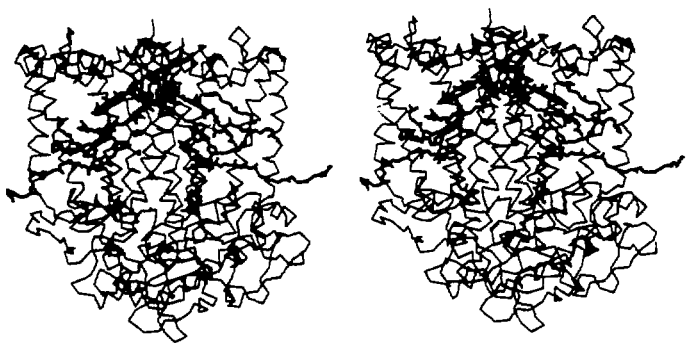

This work was supported by grants from the National Institutes of Health, the National Science Foundation, and the Chicago Community Trust/Searle Scholars Program.

X-RAY DIFFRACTION STUDY OF A THIN GaAs FILM ON Si(100)[1]

A. S. Bommannavar, C. J. Sparks, A. Habenschuss, G. E. Ice, A. Dhere (ORNL), H. Morkoc and H. Zabel (U. Illinois)

Thin GaAs films grown on single crystal silicon substrates are shown to have a nearly linear strain gradient through their thickness because of lattice mismatch. The GaAs films, ~900 Å thick grown by MBE, are strained to accommodate the 4% smaller Si lattice. Previous studies showed a small change in the average lattice spacing of the GaAs films, but ours is the first to analyze the broadening of the Bragg reflections to show that a strain gradient exists between the surface and interface of the GaAs film. Only 10% of the lattice mismatch is accommodated by strain in the bulk of the GaAs film. The remaining 90% is dissipated in the first few GaAs planes at the silicon interface. The mosaic spread in the GaAs film is slightly larger in the direction up-down the stepped surface than at 90° for the Si surface cut 4.1° from the (001) plane. An interfacial dislocation about every 25 atomic rows would accommodate the 4% mismatch as shown in the figure below.

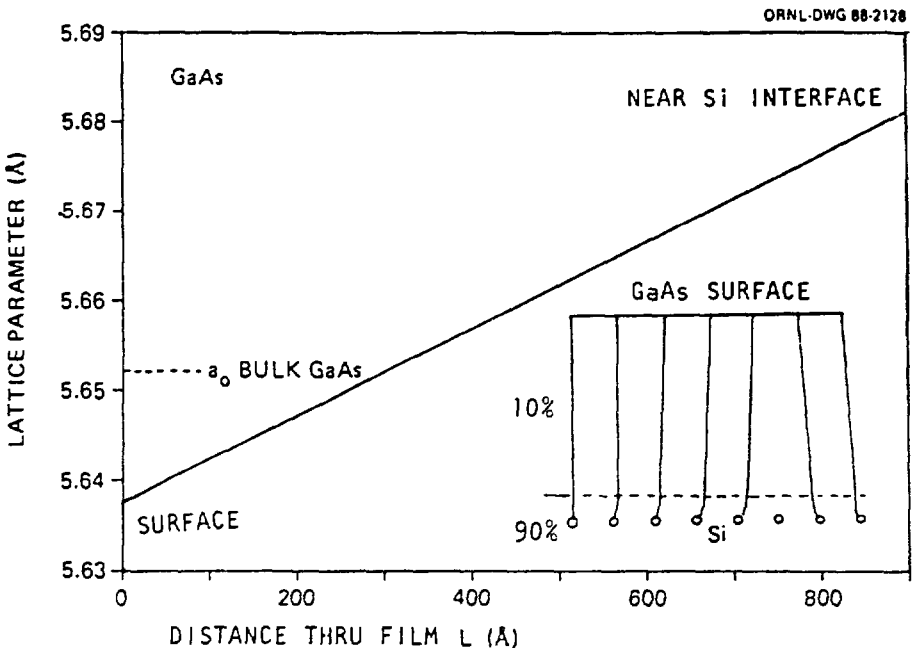

[1]MRS Symp. Proc., Epitaxy of Semiconductor Layered Structures, Vol. 102, 223 (1988)
Research sponsored by the Divisions of Materials and Chemical Sciences, DOE.

RESIDUAL STRAIN GRADIENTS IN A FULLY STABILIZED ZIRCONIA SAMPLE[1]

B. Hwang and C. Houska (Virginia Tech.), G. Ice and A. Habenschuss (ORNL)

Diffraction profiles of polished and severly ground fully stabilized zirconia (FSZ) samples are examined for the asymmetry that results from a d-spacing gradient extending from the free surface into undisturbed bulk material. Variations in residual strain or chemical composition could account for this depth gradient. The latter is eliminated by X-ray photoelectron spectroscopy (XPS). A maximum compressive strain of approximately 4% is obtained at the surface of the ground sample which decreases gradually to zero at greater depths. The overall compressive zone is approximately 1 μm. A similar but smaller compressive zone is found in the polished sample.

Although the maximum strains are large, they are reasonable for ceramic materials in compression. Such large residual elastic strains would be relaxed by plastic deformation in metals. Understanding residual stress is an important step toward designing ceramics toughened against crack propagation initiated by large elastic stresses.

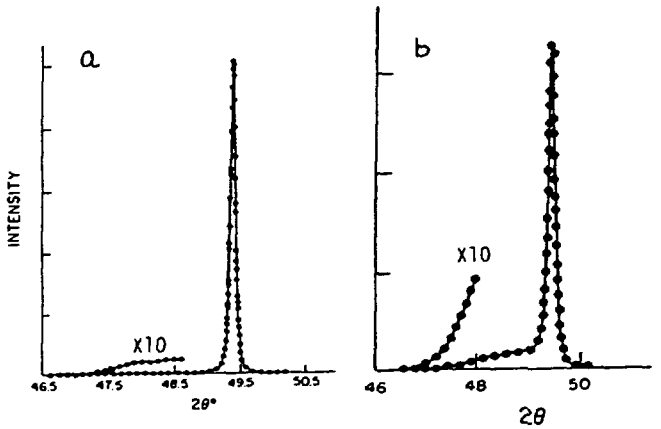

Fig. 1. X-ray diffraction line shapes of a ZrO_2 sample show low-angle tails caused by compressive strains in the plane of the polished surface which expand the d-spacing normal to the surface. Here, λ is 2.48 Å. In (a) the incident and diffracted beams make equal angles near 25° to the surface. In (b) the incident beam at a low angle of 3° enhances the near-surface contribution .

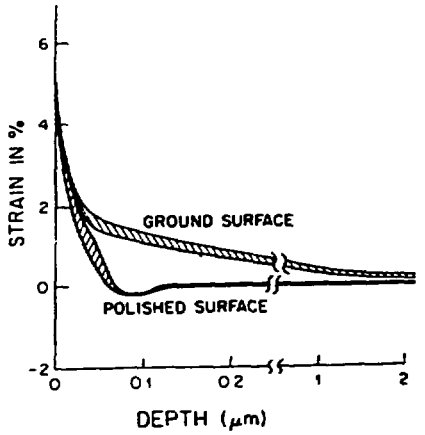

Fig. 2. The strain profiles for a polished and more heavily damaged ground surface are derived by trial and error fitting to the diffraction profiles in Fig. 1. (The solid lines in Fig. 1 are the profile fit to the data points.)

[1]*J. Appl. Phys.* **63**, 11 (1988).

Research sponsored by the Division of Materials and Chemical Sciences, DOE.

X-RAY ANALYSIS OF THE NEAR SURFACE PHASE DISTRIBUTION APPLIED TO WEAR ON A PSZ DISK[1]

B. Hwang and C. Houska (Virginia Tech.), G. Ice and A. Habenschuss (ORNL)

X-ray diffraction methods were used to determine the depth distribution of any phase in a multiphase sample by using either different wavelengths or symmetrical and asymmetrical diffraction optics or a combination of the two. Measurement of X-ray intensity ratios from different phases as a function of the known wavelength or diffraction geometry reveals the unknown depth distributions of the phases. The depth distribution of phases is demonstrated on a partially stabilized zirconia (PSZ) sample subjected to a pin-on-disk wear tester to induce a near-surface phase transformation. In an earlier study,[2] the debris collected from a prolonged pin-on-disk test of this MgO-PSZ was found to be highly defective with only the high-temperature cubic form. Typical diffraction patterns made with 2.48 Å X rays, as shown in Fig. 1, were unscrambled into symmetrical peaks with Pearson-VII functions.

The distribution of the high-temperature cubic and tetragonal phases (H_{ct}) is plotted in Fig. 2. The lower curve (a) shows that even the preliminary polishing process may produce surface heating and somewhat rapid cooling enhancing the high-temperature cubic and tetragonal phases near the surface. Further enhancement to greater depth of the high-temperature phases of ZrO_2 is found after wear testing, Fig. 2(b).

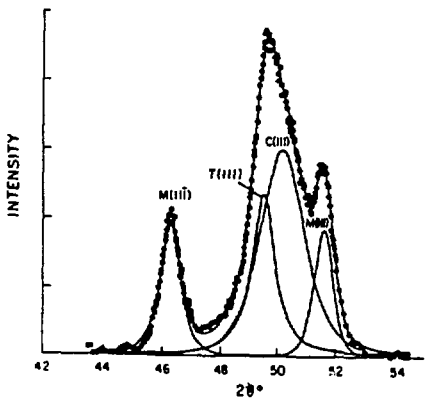

Fig. 1. The monoclinic (M), tetragonal (T), and cubic (C) phases of ZrO_2 are identified from peak positions and their relative amounts determined from the areas under the curves.

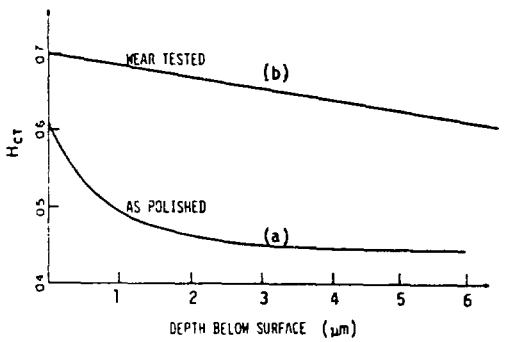

Fig. 2. The high-temperature forms of stabilized ZrO_2 are enhanced near the surface by both polishing (a) and by wear testing (b) which effects the transformation to a much larger depth.

[1] *Advanced Ceramic Mater.* 3, 180 (1988).
[2] S. Rao and C. R. Houska, *Acta Crystallogr. A* **42**, 14 (1986).
Research sponsored by the Division of Materials and Chemical Sciences, DOE.

MICRODIFFRACTION WITH SYNCHROTRON RADIATION[1]

X14

G. E. Ice, Metals and Ceramics Div., ORNL, Oak Ridge, TN 37830

In preliminary microdiffraction experiments using synchrotron radiation, x-ray beams were passed through specially prepared heavy metal pinholes to achieve probes as small as 10 microns. Both white beam and monochromatic beam techniques were tried and the relative merits compared. In the first experiment, 8 keV focused monochromatic radiation from the Oak Ridge National Laboratory beam line X14 was used to measure the strain field near a niobium hydride precipitate in a niobium single crystal. Laser drilled pinholes in 100 to 200 micron thick platinum foils were used to define the beam size on the sample. Data was taken with a 25 micron diameter pinhole because of difficulty in determining the starting position on the specimen with smaller apertures. Rocking curve measurements were made in the Bragg geometry on a point by point grid near the precipitate (Fig. 1). With the 25 micron pinhole, the beam line optics had to be detuned to keep from paralyzing the detector. Based on the count rate with 10 and 25 micron pinholes it appears that submicron resolution can be obtained.

In a second experiment, unfocused white radiation from the SUNY topography beam line X19C was used to study the strain field near notches in 250 and 500 micron thick single crystals of molybdenum. The specimen was oriented in the Laue geometry with its surface normal to the incident beam (Fig. 2). The diffraction angles of several reflections with x-ray energies between 30 and 50 keV were located using a computer controlled L-shaped block of tantalum. The energy of the reflection was determined using a Si(Li) solid state detector with a 1 cm diameter active area. From the position and energy shifts observed, the dilation and rotation of the lattice was calculated. The strain field was studied as the samples were stressed. The present limitation to this technique was found to be the limited thickness of existing pinholes. The ratio of x-rays transmitted through a pinhole foil, to the x-rays passed through the hole scales like the inverse of the pinhole diameter squared. It was found necessary with the present foils to use a 25 micron diameter pinhole to maintain a good signal to background ratio. This limitation can be improved by using thicker foils, or by using a bandpass filter to reduce background radiation. Again, sufficient x-ray intensity exists to achieve submicron resolution.

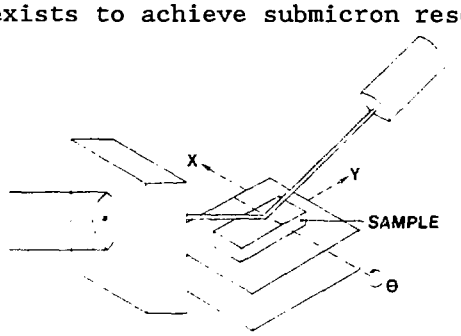

Fig. 1

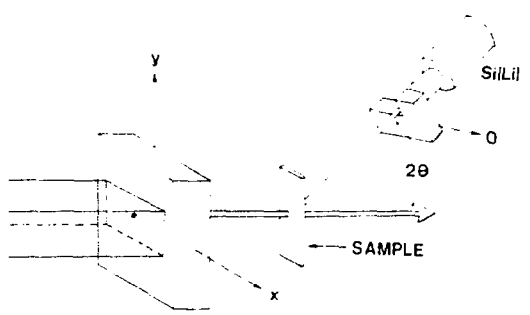

Fig. 2

[1]Nucl. Inst. and Methods, B24/25 (1987) 397-399.
Research sponsored by the Division of Materials and Chemical Sciences, DOE.

X-RAY RESONANCE EXCHANGE SCATTERING IN URANIUM ARSENIDE

E. D. Isaacs and D. B. McWhan (AT&T Bell Laboratories); C. Peters and G. E. Ice (ORNL); D. P. Siddons and J. B. Hastings (NSLS); C. Vettier (ILL, Grenoble); O. Vogt (ETH, Zurich)

A resonant enhancement of magnetic scattering was found on tuning through the L_{III} absorption edge,[1] and much larger enhancements have been predicted for the M_{IV} and M_V edges in 4f and 5f materials.[2] The magnetic scattering in UAs was measured. The intensity at the M_{IV} edge is 1% of the charge scattering and the amplitude approaches $10r_e$ in qualitative agreement with the prediction. The intensity at the M_V edge is 75 times weaker than at the M_{IV} edge and no magnetic scattering was observed at the M_{II} and M_{III} edges.

The measurements were made using a beamline with minimum windows and either helium or vacuum flight paths from source to detector. A neon-carbon dioxide filled proportional counter was used in conjunction with a Al(111) analyzer crystal for polarization analysis.

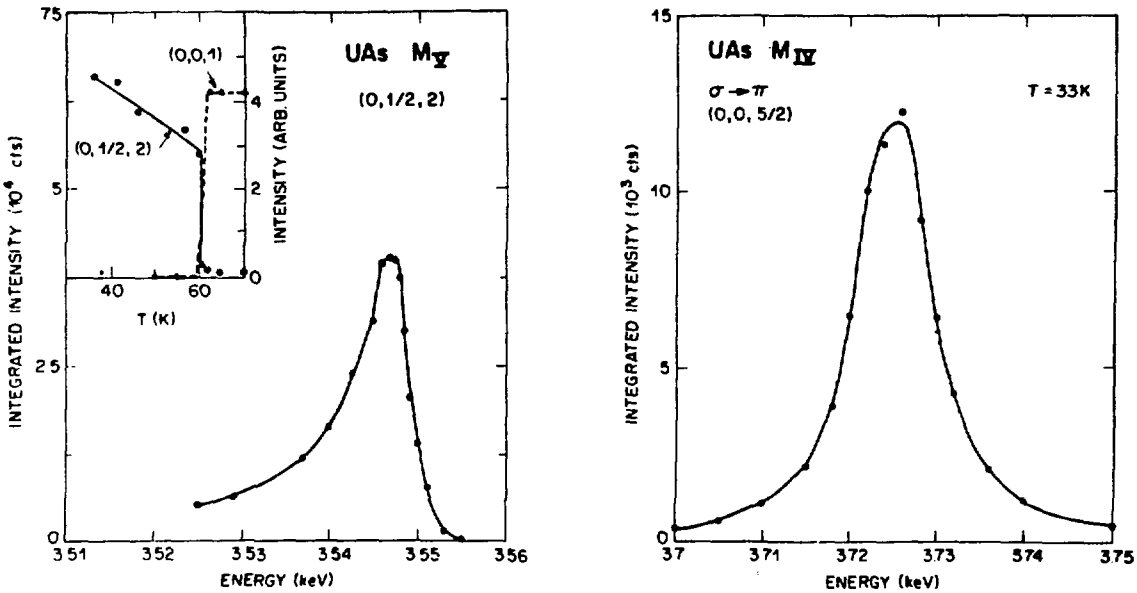

Figure: (left) Inset shows transition from type 1 to type 1a structure as measured by (001) of former and (0,0.5,2) of latter, and intensity versus energy at M_V edge. (right) Intensity of rotated component of linear polarization versus energy for M_{IV} edge.

[1]Doon Gibbs, D. R. Harshman, E. D. Isaacs, D. B. McWhan, D. Mills, and C. Vettier, Phys. Rev. Letts. 61, 1241 (1988).
[2]J. P. Hannon, G. T. Trammell, M. Blume, and Doon Gibbs, Phys. Rev. Letts. 61, 1245 (1988).

Work at BNL supported by Div. of Materials and Chemical Sciences, D.O.E.

A NOVEL FEEDBACK SYSTEM FOR FIXED-EXIT DOUBLE-CRYSTAL MONOCHROMATORS

A. A. MacDowell,† T. Hashizume,* and P.H. Citrin, AT&T Bell Labs

Good monochromatic beam stability on the sample during an energy scan is essential for low noise SEXAFS or dilute EXAFS measurements. This is especially so when working in the soft x-ray region, $\lesssim$3 keV, where poor thermally conducting monochromator crystals, large Bragg angles, and large angular scans are used. The latter effect gives rise to significant variations in heat loading on the first crystal, which in turn slightly alters the 2d lattice spacing near the surface of the crystal and causes the monochromator output beam of the "fixed-exit" monochromator to move vertically while scanning. This situation is found to occur when the monochromator feedback servo system locks onto a specific point on the crystal rocking curve. The advantage of placing the monochromator in front of the focusing mirror to achieve high energy resolution, as done on X15B, costs the price of making the distance between the monochromator output and the sample particularly long. This means that any small beam movement at the output end of the monochromator becomes greatly amplified near the sample, rendering the conventional method of monochromator feedback unacceptable. For this reason, a novel servo system was developed which looks not at a point on the rocking curve but rather at the vertical position of the monochromatic beam. Two photodiodes mounted $\sim$1 m in front of the focus, see Fig. 1, sample top and bottom portions of the beam. These two signals are fed into an analogue divider circuit, and the output is held at a constant value by using it as input for the feedback loop controlling the monochromator servo system. The servo system consists of fine tuning the top crystal by means of a solenoid. With this arrangement, vertical beam stability at the sample of $<$10 μm, corresponding to an angular displacement of $<$1 μrad ($<$0.2 arc sec), has been achieved.

Setting up an EXAFS scan involves selecting a suitable point on the rocking curve (usually the maximum) at some given photon energy and then locking the servo system onto the vertical output position of the monochromatic beam. As the energy is scanned and the heat load on the first crystal is altered, the constant-output-position feedback system moves the first crystal (via the solenoid) and thus changes the initial setting point on the rocking curve. Fortunately, this detuning turns out to be very small, resulting in only a minor reduction in flux. Were there no premirror in the beamline, this movement on the rocking curve would have the additional effect of varying the harmonic content of the output beam. However, the use of a premirror on X15B with suitable grazing angle to remove the higher harmonics eliminates this problem completely.

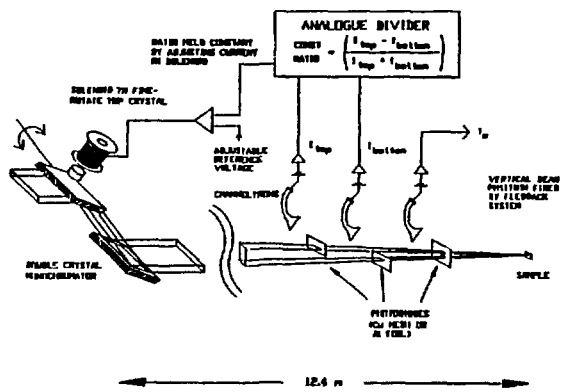

Fig. 1 Schematic layout of new monochromator feedback system.

† Mailing address: NSLS, Brookhaven Nat. Lab, Upton, NY 11973
* Present address: Institute for Solid State Physics, U. of Tokyo.

A SURFACE EXAFS BEAMLINE FOR STUDIES IN THE RANGE 0.8-15 keV

A. A. MacDowell,† T. Hashizume,* and P.H. Citrin, AT&T Bell Labs

A SEXAFS beamline has been commissioned on X15B, providing very high intensity, brightness, resolution, and beam stability over an extremely wide range of energy. The beamline's features, some of which exist on selected soft x-ray lines, some on selected hard x-ray lines, and some found nowhere else in the world, open up a number of new, previously inaccessible experiments.

In the design, see Fig. 1, both mirrors (Pt-coated electroless Ni-plated Aℓ) are vibrationally isolated from the beamline and have independently adjustable meridonal radii. The collimating mirror is rotatable, making it a low-pass filter (see Fig. 2) for removing higher harmonics and for protecting the radiation-sensitive alumina, beryl, and silica crystals used to cover the 0.8-1.8 keV range. The rest of the beamline pivots about the mirror to follow the reflected beam and is positioned easily and reproducibly by synchronous computer control of stepping motors. The second mirror focuses the beam into a spot $\lesssim 1\text{mm}^2$ for radiation $\lesssim 3$ keV (at higher energies the vertical size increases due to the mirror's 22 Å rms surface roughness). A small decrease ($<0.1°$) from 0.4° incidence angle on both mirrors moves the reflectivity cutoff to ~ 15 keV and repositions the focal point without need to adjust the monochromator. This latter feature allows multiple "end-of-line" stations to be set up in series along the beamline with ease and minimal degradation in focus. Differential pumping of the ~ 10 m-long drift tube following the focusing mirror allows true UHV, i.e., $\lesssim 10^{-10}$ Torr, to be realized at the sample. High beam stability of <10 μm is achieved with a novel monochromator feedback system described in the accompanying abstract. Heat loading from the white beam is minimized by directly cooling the metal premirror using convection heat pipes, and the first monochromator crystal using a water-cooled Cu backplate thermally coupled to the crystal with Ga metal.

The fixed-exit monochromator is an upgraded version of a Daresbury instrument which relies on a unique translation ↔ rotation linkage mechanism. The energy range of 0.8-15 keV is covered by venting the monochromator and changing premounted crystal pairs with different 2d spacings (8 pairs in total). Differential pressures of $\sim 10^3$ Torr between the monochromator and beamline vacuums, achieved by 0.2 μ-thick carbon foils mounted in window gate valves, allows crystal changing and pumpdown in as little as 30 minutes.

Energy resolution is determined only by the electron source size and the rocking curve of the crystals, not by the photon beam size or focusing optics. This is the result of adjustably bending the collimating mirror, thereby minimizing photon beam divergence in the working energy range, and placing the monochromator in front of the focusing mirror, thereby avoiding aberrations in the vertical (dispersive) direction.

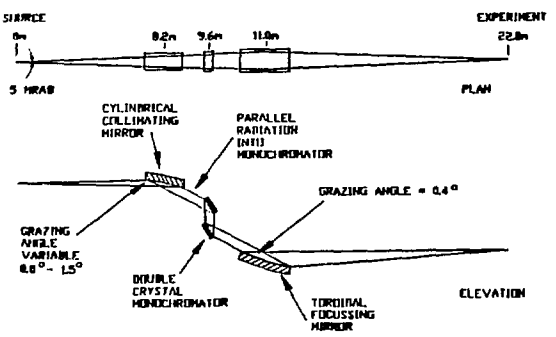

Fig. 1 Schematic layout of the beamline.

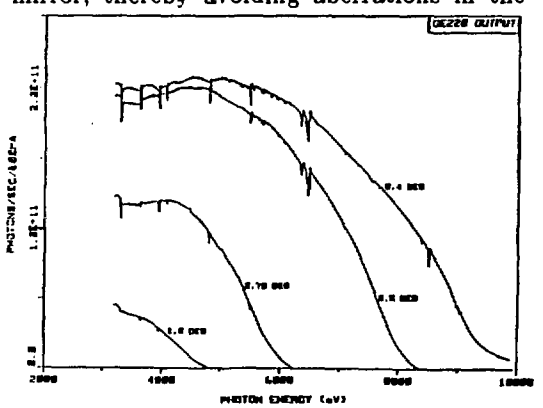

Fig. 2 Output from Ge(220) crystals for various grazing angles on the collimating mirror.

† Mailing address: NSLS, Brookhaven Nat. Lab, Upton, NY 11973
* Present address: Institute for Solid State Physics, U. of Tokyo.

THE FIRST SEXAFS EXPERIMENTS ON X15B

R. McGrath, A. A. MacDowell,† T. Hashizume,* F. Sette, and P.H. Citrin, AT&T Bell Labs

As the concentration of absorbing atoms in an EXAFS experiment decreases and the sophistication of measuring the signal increases, e.g., use of multiple fluorescence detectors in biological studies, the demands of the experiment go beyond obvious increases in data accumulation time and equipment cost. Sample inhomogeneities, detector nonlinearities, and small beam movements – all of negligible size in most bulk measurements – take on new meaning in dilute systems: they introduce systemic, i.e., nonstatistical errors whose magnitudes ultimately determine the success of the study. It is for these reasons that SEXAFS measurements from submonolayer surface concentrations (as much as 10^6-10^7 lower than in bulk systems) are among the most difficult experiments to perform with synchrotron radiation. Added to these inherent systematic factors has been, historically, the limited availability of dedicated synchrotron radiation during the time in which the SEXAFS methodology was being developed. This background, along with the recent commissioning of the upgraded NSLS x-ray ring, serves to underscore the enthusiasm with which the present SEXAFS data are reported.

Figure 1 shows some of the first results obtained on X15B from a 0.5 monolayer coverage of S adsorbed on Ni(001). This system was chosen, among other reasons, for comparison with S *K*-edge SEXAFS measurements performed last year at SSRL using the same coverage, crystal, and fluorescence detector.[1] The strong features in the incident intensity, I_o, and raw SEXAFS data, I, corresponding to the Pt *M*-edge absorption from the Pt-coated collimating and focusing mirrors, are perfectly cancelled in the normalized SEXAFS data, I/I_o. This is one of the clearest demonstrations that systematic errors have been eliminated. The quality of the data is state-of-the-art, with a signal/noise level (normalized to beam current and counting time) at least a factor two greater than that previously obtained.[1] Additional optimization of beamline parameters, currently underway, should increase this factor further.

Finally, with a look to the future, we note that the features of high energy resolution and beam stability, already incorporated in the design of X15B (see accompanying abstracts), open up a number of measurements complementary to SEXAFS, e.g., x-ray photoemission x-ray standing waves, and near-edge x-ray absorption. Studies of interface and surface electronic, dynamic, and geometric properties, all performed on the same sample, should therefore be possible.

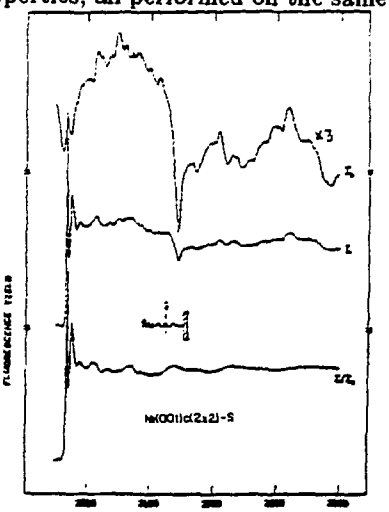

Fig. 1 Incident intensity (top), raw SEXAFS data (middle), and normalized data (bottom) from 0.5 monolayers of S. Note the very high statistical quality of the data and the excellent cancellation of the Pt *M*-edge absorption features (from the Pt-coated beamline optics).

1. F. Sette, T.Hashizume, F. Comin, A. A. MacDowell, and P. H. Citrin, Phys. Rev. Lett. *61*, 1384 (1988).

† Mailing address: NSLS, Brookhaven Nat. Lab, Upton, NY 11973.
* Present address: Institute for Solid State Physics, U. of Tokyo.

FOUR-STATE MODEL FOR THE PHASE TRANSITION OF THE Pt(110) 1×2 SURFACE

I. K. Robinson (AT&T Bell Labs) and K. Kern (KFA, Julich, FRG)

The Au(110) 1×2 and Pt(110) 1×2 surfaces have attracted much attention in recent times because they have a simple reconstruction that undergoes a structural phase transition at high temperature. A Low Energy Electron Diffraction (LEED) study of Au(110) concluded that the transition could be classified as an Ising model and found the experimental critical exponents to be in good agreement[1]. More recently, a Monte Carlo simulation of both surfaces also claimed an Ising model and showed agreement in the calculated divergence of the correlation length above the transition[2]. As stated in that work, the Ising model predicts a broadening of the diffraction peaks above the phase transition that is symmetric about the half-order position [2], and this agrees with the LEED result for Au(110)[1]. However, x-ray work previously reported for Au(110)[3] and seen in this work for Pt(110) shows a clear and systematic shift of the peaks from the half-order positions that is directly related to monatomic steps in the surface, whereas this was not detected in the LEED experiments[1].

Figure 1 compares the temperature dependence of the 3/2 00 x-ray diffraction peak intensity for Pt(110) with that of Au(110), showing the similarity between them. This is also consistent with the dependence of the LEED peak height[1]. The lineshape was broadened and shifted at low temperature in much the same way as

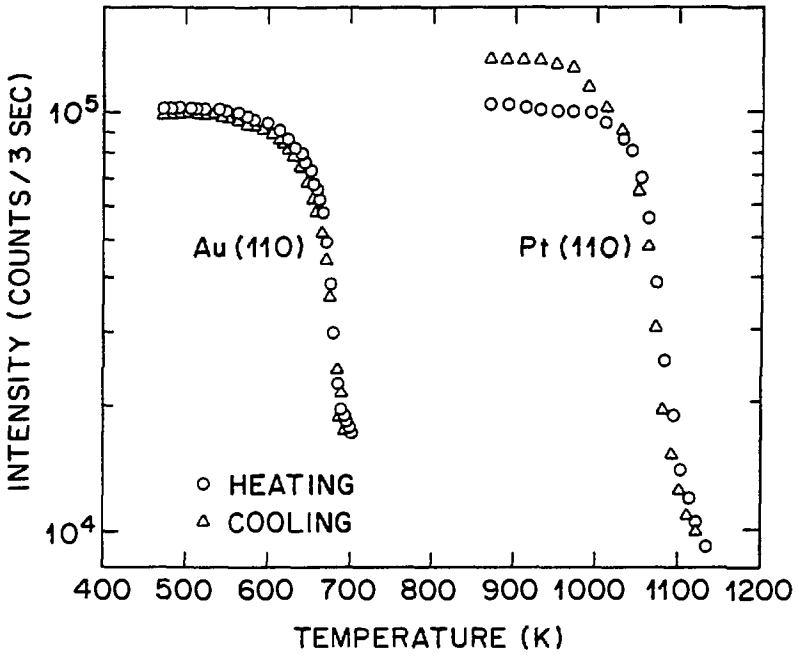

Figure 1

Au(110)[3]; this was found to evolve with surface preparation but stabilized to a constant shape that was used as a reference. Heating through the transition caused the shape to vary in both parallel and perpendicular directions. Scans taken at various temperatures were fit to a 2D Lorenzian form convolved with the low-T reference lineshape. Six parameters were allowed to vary: two widths, two peak positional coordinates, a height and a background. The results of this analysis are plotted in Fig. 2.

The new aspect of these results is that the shift of the peaks *changes with temperature* above the transition and hence that the steps must be an intimate and essential constituent of the phase transition model. For Pt(110), at least, the simple Ising model cannot be the complete picture and a four-state model may be more appropriate to describe the transition. Because the density of steps changes through the transition the surface roughness must also change, and the phase transition must be considered to be a kind of roughening transition, as has been suggested by Monte Carlo calculations.[4]

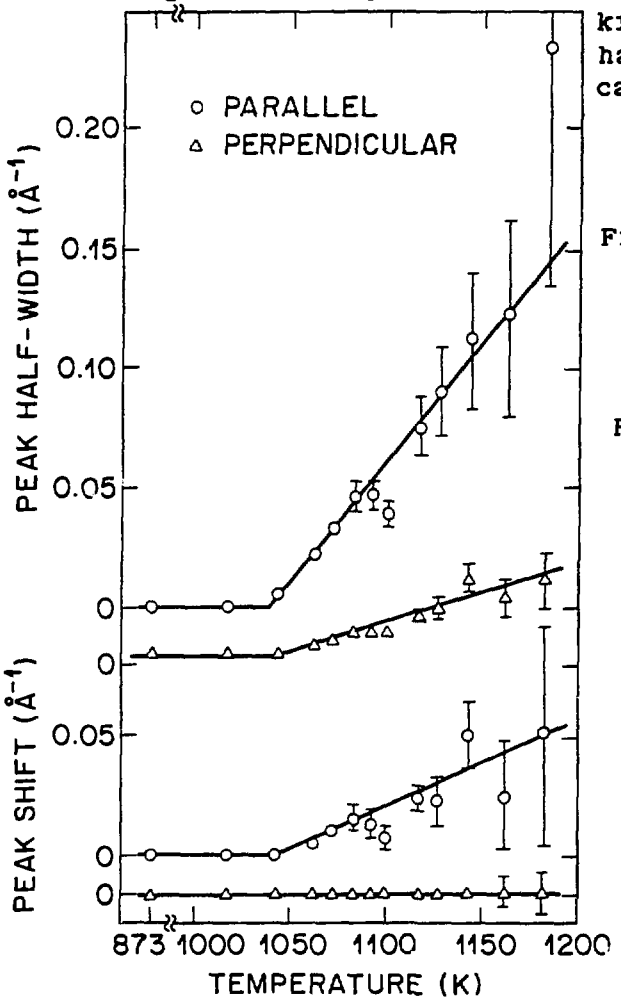

Figure 2

References

1. J-C Campuzano et al, Phys. Rev. Lett. *54*, 2684 (1985)
2. M.S. Daw, S.M. Foiles, Phys. Rev. Lett. *59*, 2756 (1987)
3. I.K. Robinson in "Structure of Surfaces", p. 60, ed M.A. van Hove, S.Y. Tong (Springer, 1985); Phys. Rev. Lett. *50*, 1145 (1983)
4. F. Ercolessi, E. Tosatti, Surf. Sci. *189* 636 (1987).

ROUGHENING TRANSITION OF THE Ni(113) SURFACE

I. K. Robinson (AT&T Bell Labs) and E. H. Conrad (Dept. of Physics and Astronomy, Univ. of Missouri)

Recent work at the NSLS[1-3] has shown that x-ray diffraction is sensitive to the transition of certain surfaces from smooth to rough as temperature is raised, and thus confirmed the existence of a "roughening transition". Previous work with atom scattering from the Ni(113) surface has confirmed its existence as well.[4] In this study, we have established that there is a change of diffraction lineshape associated with the Ni(113) transition and that it can be satisfactorily explained as a superposition of a sharp Bragg peak and a diffuse critical scattering peak over the entire transition region. Thus it is a classical second order phase transition.

Figure 1 shows a typical diffraction profile measured at the reciprocal space point (6/11 6/11 -4/11) which is the intersection of the truncation rod linking the (11$\bar{1}$) to the (002) bulk Bragg peak, with the surface plane (perpendicular to (113)). The lineshape has been fit to a narrow Gaussian, constrained to the width (0.025 $\AA^{-1}$ fwhm) measured at low temperature and the sum of a broad Lorenzian lineshape. Below 600K the diffraction is described well by just this sharp component of constant width; the temperature dependence follows closely that of Liang et al. for Cu(113)[3], although our peak was 10 times narrower in both directions and 100 times more intense. This dependence in the pre-roughening regime is adequately explained by the statistical-mechanical theory of Villain[5].

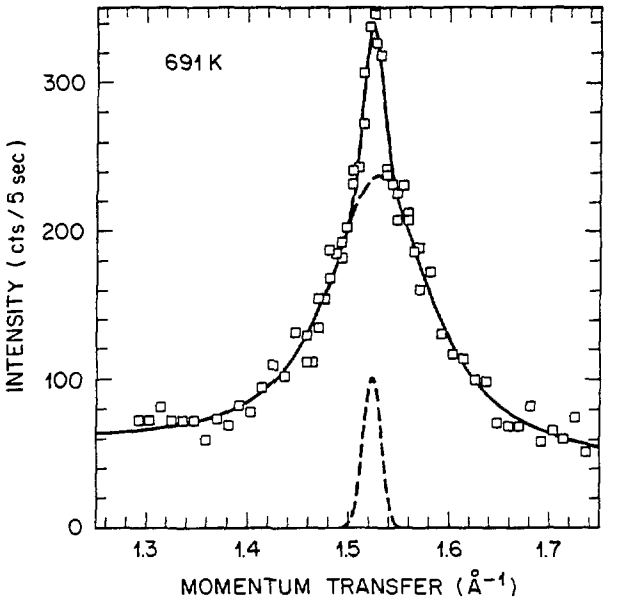

Figure 1. Diffraction lineshape of the first-order crystal truncation rod of Ni(113) at 691K. The scan is approximately radial, keeping the angle of the incident and exit beams with respect to the surface constant and approximately equal to the critical angle. The full curve is the two component fit; the dashed curves are decomposed into the separate Gaussian and (Lorenzian + background) components.

The temperature dependence of the two components near to the transition of 670K is shown in fig 2(a). The sharp component decreases continuously with higher temperatures. Figure 2(b) shows the decomposition of the broad component into peak height and width, which pass through a broad maximum and minimum respectively, just as would be expected for a classical second-order phase transition. The maximum in diffuse intensity falls a little below the disappearance of the Bragg peak.

Proof of uniqueness in lineshape fitting is a notoriously difficult problem, however. We have found that reasonable fits to finite-size-broadened $|q|^{-\eta}$ lineshapes are also possible with appropriate variation of η with temperature, as others claim to have seen in roughening transitions[2]. Which of the descriptions is better requires further work and is in progress.

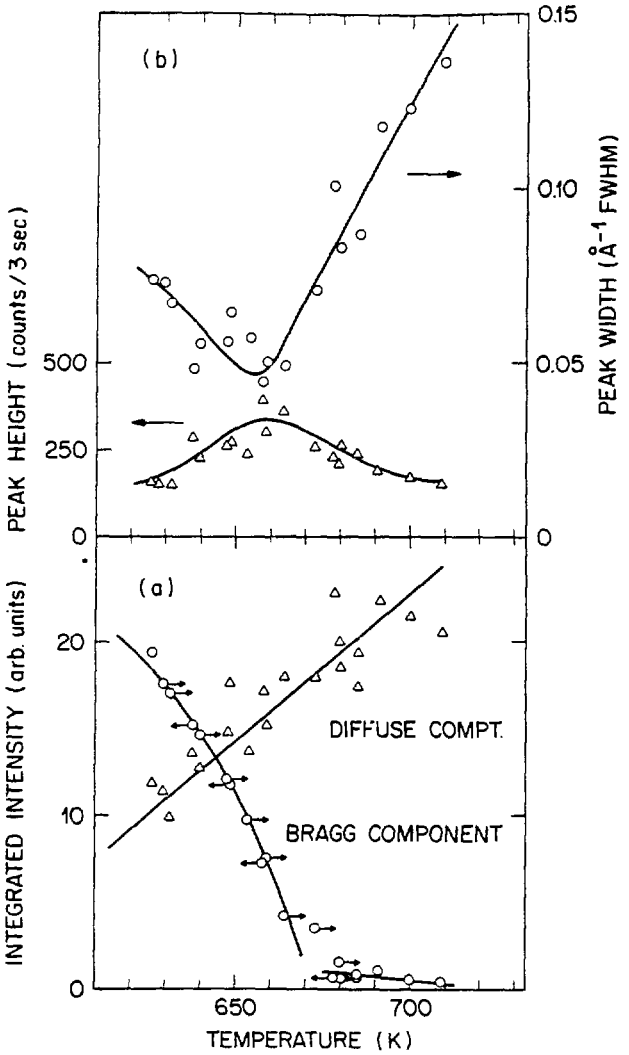

Figure 2. (a) Temperature dependence of the Gaussian, (Bragg) component and Lorenzian (diffuse) component, integrated over the momentum transfer, Q. The integration does *not* include the transverse lineshape which also broadens. (b) Temperature dependence of the width and height of the diffuse component. All lines are guides to the eye.

References

1. S.G.J. Mochrie, Phys. Rev. Lett. *59* 304 (1987)
2. G. A. Held et al, Phys Rev. Lett. *59* 2075 (1987)
3. K.S. Liang et al. Phys. Rev. Lett. *590* 2447 (1987)
4. M. den Nijs et al, Phys. Rev. Lett. *57*, 1279 (1986)
5. J. Villain et al, J. Phys. F. *15*, 809 (1985)

X-RAY RESONANCE EXCHANGE SCATTERING IN DYSPROSIUM

E. D. Isaacs and D. B. McWhan (AT&T Bell Laboratories); D. P. Siddons and J. B. Hastings (NSLS); and Doon Gibbs (Physics, BNL)

The separation of the orbital and spin angular momentum densities in the spiral antiferromagnet Holmium has been demonstrated.[1,2] During these studies a fiftyfold enhancement of the intensity of the magnetic scattering was observed when the energy of the incident x-ray beam was tuned through the L_{III} absorption edge. Polarization analysis of the intensity of the various harmonics showed that there were two peaks displaced in energy by 6 eV. A similar enhancement and polarization dependence has been found in Dy (see Fig.)

Beamline X16B has a horizontal monochromator but the energy can be scanned over a range of 100 eV in the region from 7 to 9 keV by rotating the monochromator and rotating and translating the diffractometer. Measurements of the absorption coefficient of Dy versus energy are shown in the figure. To improve the efficiency of the polarization analysis the Be (11.0) was used instead of the graphite (00.6) because the former had a reflectivity of 30%. In addition, an intrinsic Ge detector was used to improve signal to noise and energy resolution.

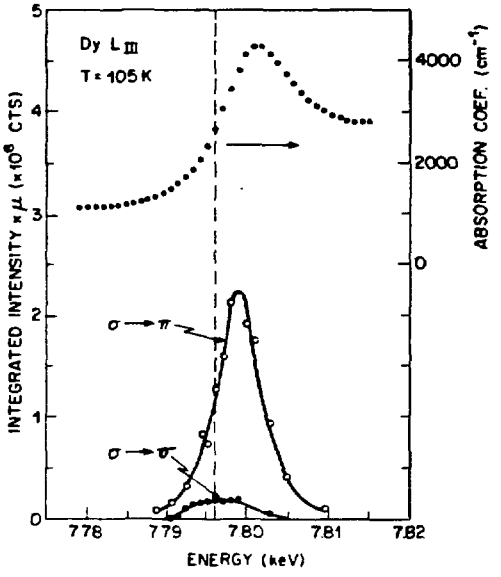

Figure: Absorption coefficient vs energy and intensity of the (0,0,2.183) of Dy vs energy for the linear components of polarization rotated or unrotated during scattering.

[1]D. R. Harshman, D. B. McWhan and Doon Gibbs, NSLS Annual Report (1987) pg. 3-116.

[2]Doon Gibbs, D. R. Harshman, E. D. Isaacs, D. B. McWhan, D. Mills, and C. Vettier, Phys. Rev. Lett. 61, 1241 (1988).

Work at BNL supported by the U.S. Dept. of Energy under Contract No. DE-AC02-76CH00016.

RENNINGER SCANS OF [222] Si FOR σ- AND π-POLARIZATION

N. G. Alexandropoulos* and D. McWhan, AT&T Bell Laboratories, and
H. J. Juretschke, Polytechnic University.
*Visiting Research Professor, Polytechnic Univ.; permanent location
U. of Ioannia, Greece.

The asymmetries in the shoulders of multiple interaction peaks in Renninger scans have been measured for σ- and π-polarization, at several wavelengths. The purpose of the study was to compare the profiles for the two polarizations, in particular with respect to the shape, or even the reversal, of the characteristic asymmetry, in their effectiveness in bringing out information about the invariant phase of the relevant structure factor combination. Such an experiment is needed because most of the experimental work to date on n-beam interactions has been carried out with unpolarized incident radiation that may wash out specific features of a single polarization mode. The study has been supplemented by measuring the rocking curves at a series of angular distances from some major n-beam interactions.

In this investigation the [222] n-beam assymetric unit pattern of Si has been recorded making use of a biaxial diffractometer with the two rotation axes mutually orthogonal, in conjunction with a highly collimated monochromatic and polarized incident beam. The scanning step size around the azimuthal axis [222] was 0.005°, or 18", while around the axis normal to [222] it was 0.0005°. Hence the rocking curve could be scanned with steps of 1.8".

Fig. 1 shows two prominent interaction peaks at λ=1.28Å, σ-polarization, near 5° from the 211 direction. Fig. 2 shows the rocking curve of the main peak in Fig. 1 at an angular distance of 27" from its peak position.

The extensive collection of data during the period July-August 1988 is now being analyzed.

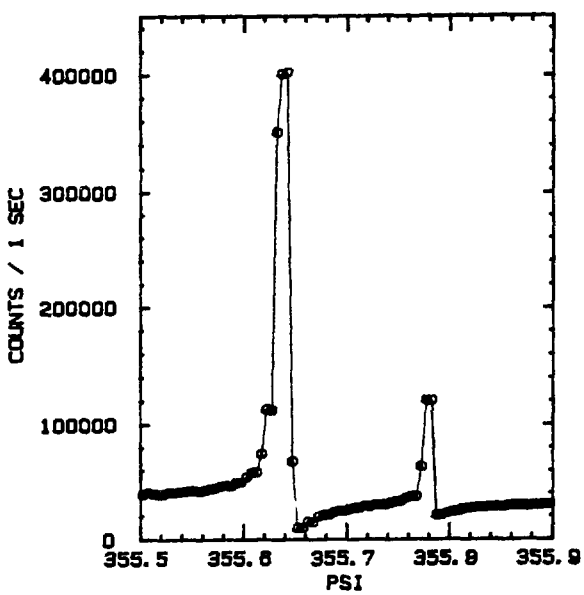

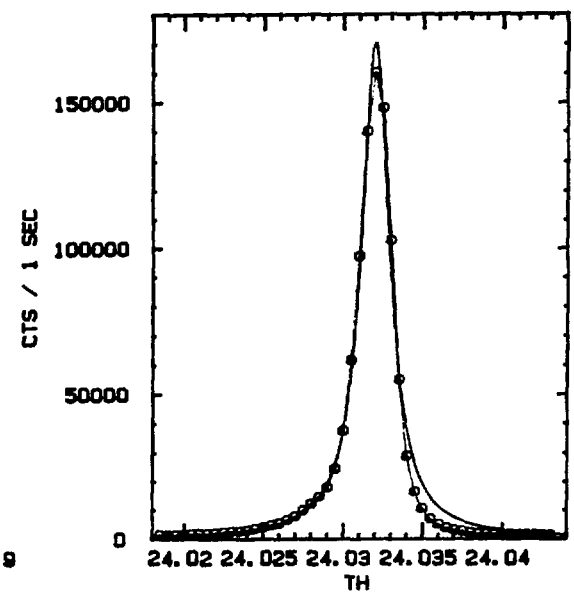

A NEW APPROACH TO DETERMINING THE CHARGE DISTRIBUTION IN COPPER COMPOUNDS (*) X-18B

E.E. Alp, G. L. Goodman, L. Soderholm, S. M. Mini, M. Ramanathan, G.K. Shenoy,
Argonne National Laboratory, Argonne, Illinois 60439
A. S. Bommannavar, *Brooklyn College of CUNY, Brooklyn, NY 11210*

We have developed a new empirical approach to the relationship between charge distribution and the onset of X-ray absorption in copper compounds. We have measured the x-ray absorption spectra at the Cu K-edge of a series of 17 copper compounds with formal valences of +1, +2, and +3, and then analyzed the location of the edge features in terms of energy moment analysis. In this way we obtain a characteristic energy that correlates with formal valence in a semiquantitative way. There is a consistent shift towards higher energy positions with increasing Cu valency. We believe this procedure can also be extended to other X-ray absorption edges and to other absorbing atoms. In this way we hope to have made possible better and more reliable correlations between XANES features and the valence of the absorbing atoms.

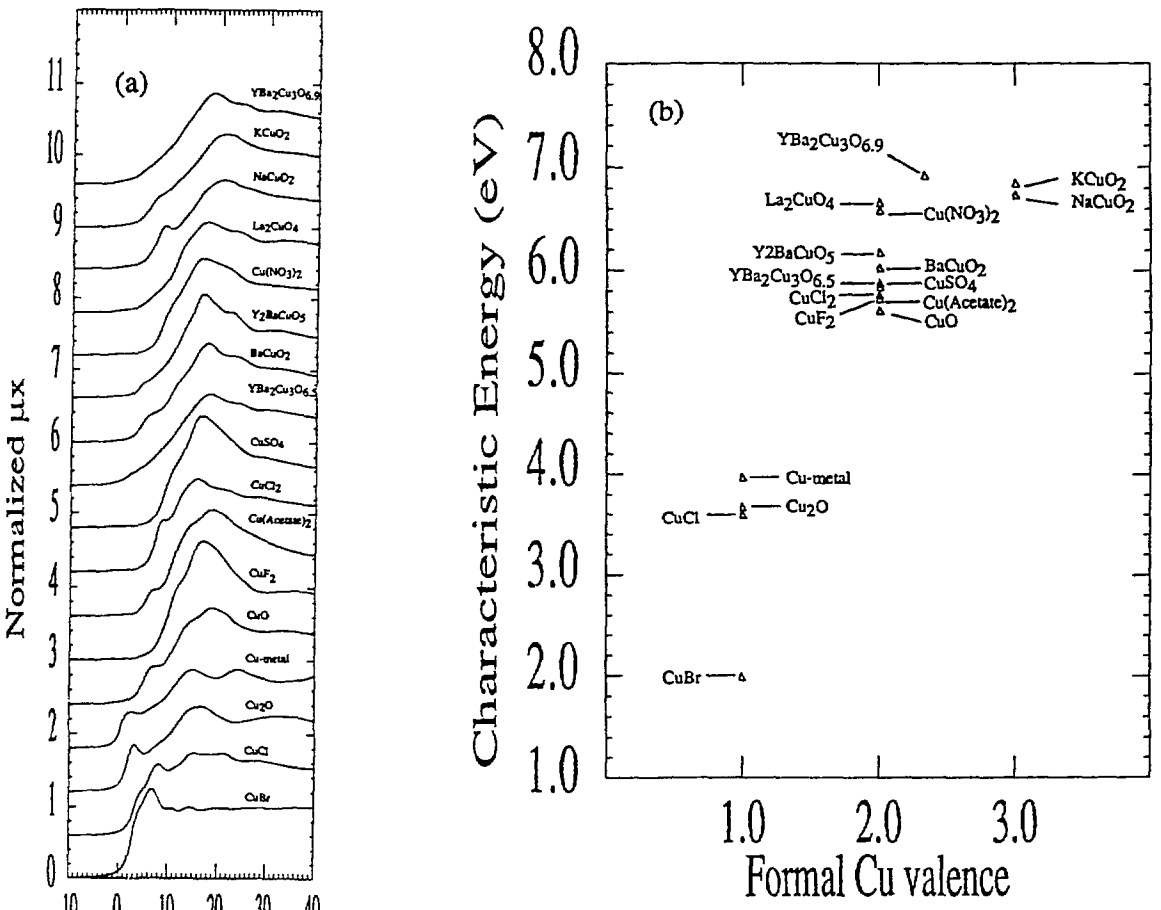

Fig. 1. (a) The XANES of 17 copper compounds studied, and (b) characteristic energies of these compounds determined with the new procedure.

(*) Work Supported by US-DOE, BES Materials and Chemical Sciences, under contract # W-31-109-ENG-38.

X-RAY ABSORPTION STUDIES OF BA-K-BI-O SUPERCONDUCTORS (*)X-18B

E.E. Alp, S. M. Mini, L. Soderholm, G.K. Shenoy , M. Ramanathan,B.Dabrowski, D.G.Hinks
Argonne National Laboratory, Argonne, Illinois 60439
A. S. Bommannavar, *Brooklyn College of CUNY, Brooklyn, NY 11210*

A series of Bi compounds have been studied at the L_3, L_2, and L_1 absorption edges, in an effort to establish the difference between formally +3,+4, and +5 Bismuth oxides. The standard compounds measured are shown in Fig. 1. There is a consistent shift towards higher energies at the L_3 -edge for Bi_2O_3, $BaBiO_3$, and $KBiO_3$. The last two compounds are the end points of a series of compounds in which K is substituted at the Bi site. This series of $Ba_{1-x}K_xBiO_3$ is superconducting at 30 K range for $0.30 < x < 0.45$. However, as shown in Fig. 2., there is very little change in the Bi L_3 -edge spectra for $0.1 < x < 0.4$. This may support the view that the charge compensation for K-doping may predominantly come from Oxygen atoms rather than Bi atoms directly.

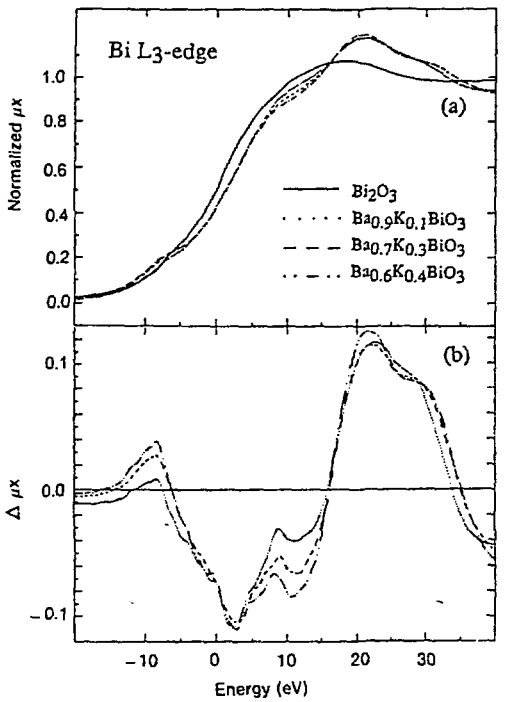

Fig. 1. (a) XANES of Bi_2O_3, $BaBiO_3$, $KBiO_3$,and the superconducting compound $Ba_{0.6}K_{0.4}BiO_3$; (b) The difference spectra in which Bi_2O_3 spectrum is subtracted from the others.

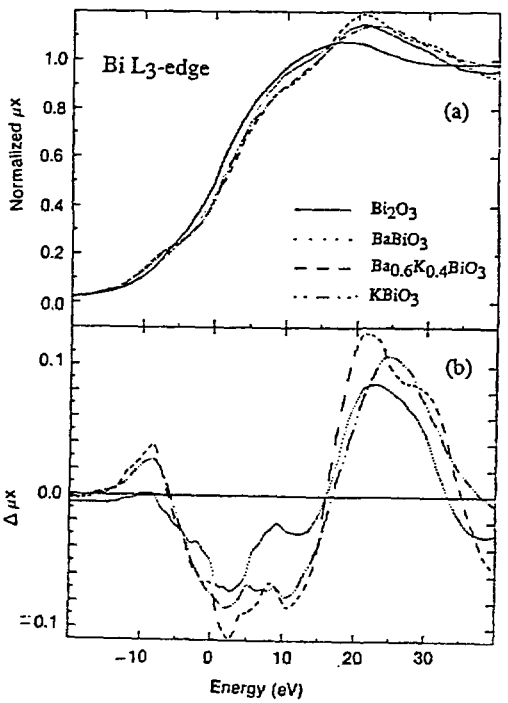

Fig. 2. (a) XANES of Bi_2O_3 and the series of $Ba_{1-x}K_xBiO_3$ compounds to indicate the effect of K doping ; (b) The difference spectra in which Bi_2O_3 spectrum is subtracted from the others.

(*) Work Supported by US-DOE, BES Materials and Chemical Sciences, under contract # W-31-109-ENG-38.

POLARIZED EXAFS STUDIES OF $YBa_2Cu_3O_x$ AND $La_{2-x}Sr_xCuO_4$(*)

S.M. Mini, E.E. Alp, M. Ramanathan, B.W. Veal
Argonne National Laboratory, Argonne, Illinois 60439
A.S. Bommannavar, *Brooklyn College of CUNY, Brooklyn, NY 11210,* and
O.B. Hyun, *Iowa State University, Ames, IA, 50011-3020*

Polarized EXAFS studies were carried out at the Cu K-edge of magnetically oriented $YBa_2Cu_3O_x$ for x=6.1,6.5, and 6.9 and $La_{2-x}Sr_xCuO_4$ for x=0.0 and 0.15. Figures 1 and 2 show the angular dependence of the Fourier transform of $k^3\chi(k)$ of $YBa_2Cu_3O_{6.1}$ and $YBa_2Cu_3O_{6.9}$ respectively. The bond lengths (specifically Cu-O1 and Cu-O2) calculated from the spectrum are in good agreement with those determined by x-ray and neutron diffraction[1,2]. A procedure is being developed to analyze the angle dependent polarized EXAFS spectra.

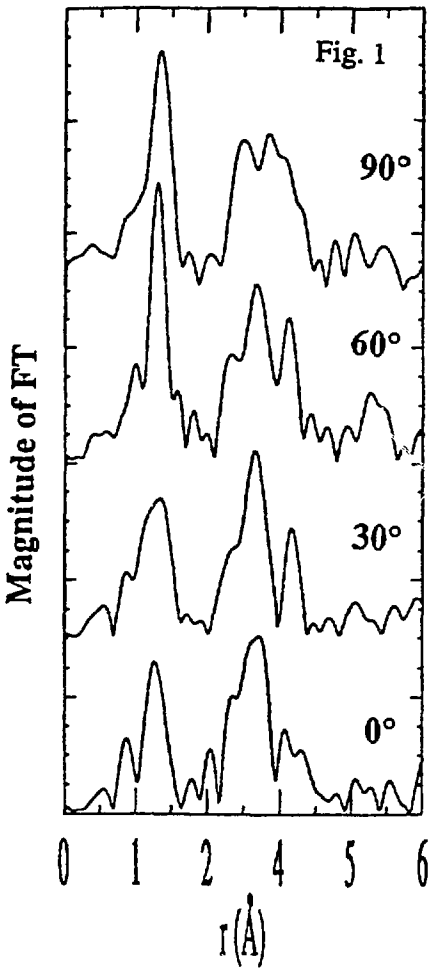

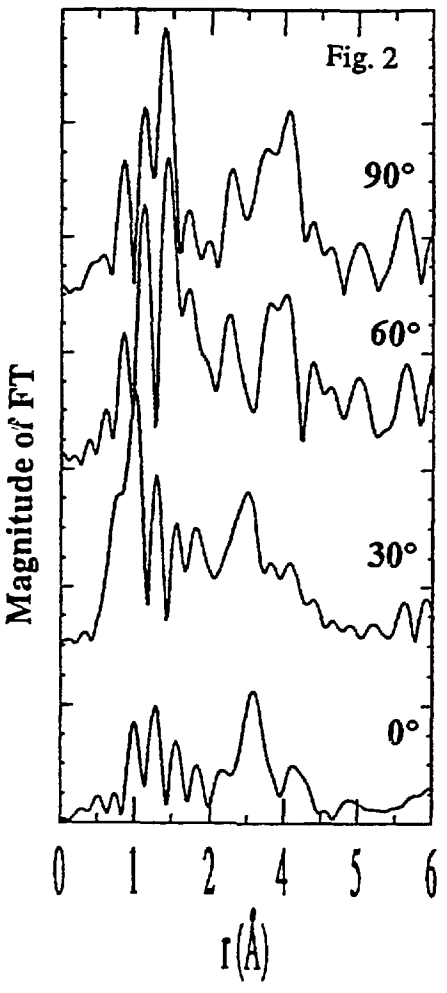

(*)Work supported by US DOE-BES Materials Sciences, under contract # W-31-109-ENG-38
(1) A. Hewat et.al., Solid State Comm. 64 (1987) 301.
(2) M. Beno et.al., Appl.Phys. Lett. 51 (1987) 57.

CONTROLLED ATMOSPHERE CATALYST SAMPLE CELL AND ITS USE IN X-RAY ABSORPTION STUDIES OF CATALYSTS

Guang Zhang and Gary S. Mondo (Chevron Research Company)

Chevron has completed two beam-time assignments since we joined the X18B PRT. Our first feasibility tests of the beam line and the controlled atmosphere catalyst sample cell were performed in mid-August, 1988. This sample cell was designed to treat the catalyst samples under vacuum or with various gases at elevated temperatures and to do in-situ X-ray absorption experiments at room or low temperatures. The current design of the sample cell is illustrated in the following figure:

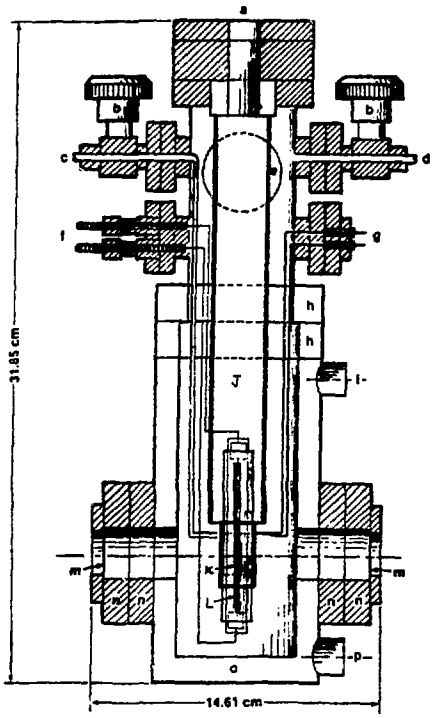

A. Liquid Nitrogen Dewar Opening
B. Nupro Vacuum Valves
C. Gas Inlet
D. Gas Outlet
E. High Vacuum Port
F. Power Feedthrough for the heating lamps
G. Thermocouple Feedthrough
H. Sample Chamber Connecting Flange
I. Cooling Water Outlet
J. Liquid Nitrogen Dewar
K. Sample Holder
L. Quartz Heating Lamp
M. Mylar/Kapton Window
N. Window Attachment Flange
O. Water Jacket
P. Water Outlet

With this sample cell, catalyst wafers could be heated up to 650 C at user's desired heating rate and cooled to -120 C for X-ray data collection. Our test indicates that the design of this sample cell is appropriate for X-ray absorption studies of catalysts.

Transmission X-ray absorption experiments were conducted on catalysts containing platinum, cobalt, zinc, and iron. The data analysis is in progress.

This work was supported by Chevron Corporation.

MICRORADIOGRAPHY OF CREEP DAMAGE IN COPPER

J.E. Benci and D.P. Pope, Department of Materials Science and Engineering, University of Pennsylvania.

There has been a great deal of work done in the last several years using constitutive equations and continuum mechanics to model the development of damage and fracture of materials under slow strain rate, high temperature service conditions. Unfortunately,there has been no good experimental check on the accuracy of these models. Most investigators did not even compare their computer predictions with experimental results while a few compared their models to micrographs from polished surfaces of creep damaged samples. Examining a polished surface has the limitation that the surface may not be representative of the bulk sample. Additionally, artifacts may be introduced while other features are concealed during the polishing process. A technique which can reveal information on the size and spatial distribution of creep damage in a bulk sample would be an excellent test for the damage models. Microradiography is such a technique.

A high purity copper alloy which had been heavily doped with oxygen was chosen as the material for this study. This material exhibited a ductility minimum at about 500°C, with a resultant reduction of area of about 3.1%. The fracture at 500°C was totally intergranular due to cavity coalescence. Axisymmetric notched tensile samples were machined from this material. Nearly identical specimens were tested at 500°C at a constant displacement rate of 2.11×10^{-5} mm/sec. Different specimens were interrupted at various fractions of the samples lifetime. Longitudinal cuts were made in the samples using EDM to remove the center sections of each specimen. These 1.5 mm thick slices were then mounted and prepared for microradiographic analysis by polishing both faces.

The development of creep damage as a function of time was observed as well as the spatial distribution of the damage for this material. Fig. 1 is a radiograph from a sample which was interrupted relatively early in its creep life. The small white features, about 150 μm long, emanating from both notches are microcracks, failed grain boundary facets. Fig. 2 is a radiograph from a nearly identical sample interrupted much later in its creep life. A macroscopic creep crack extends most of the way across the sample. It can be seen from both figs. 1 and 2 that all of the creep damage is located in a fairly narrow band around the minimum cross-section in these samples. This is in marked contrast to previous results from high purity iron samples. The damage in iron developed at fairly sharp angles to the notch or crack plane. This would imply that the damage process in iron is controlled by the effective stress while the formation of damage in this copper alloy is controlled by the maximum principal or hydrostatic stress. The finite element modelling to confirm this hypothesis is currently being performed.

ACKNOWLEDGEMENTS

Part of this work was performed at SSRL which is supported by the Department of Energy, Office of Basic Energy Sciences. This work was funded through the Synchrotron Topography Project of the National Synchrotron Light Source, Brookhaven National Laboratory, which is supported by the Department of Energy under grant DE-FG02-84ER45098.

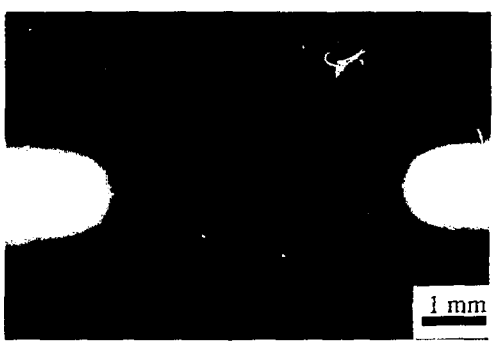

Figure 1. Radiograph of an axisymmetric notched copper sample tested at 500°C and interrupted at 0.75 x (max. stress) while the stress was still increasing.

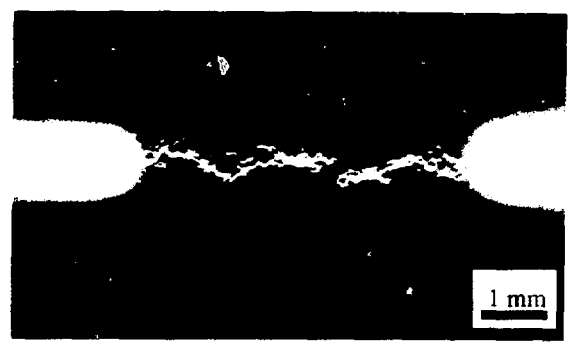

Figure 2. Radiograph of a nearly identical sample as the one from fig. 1 tested at 500°C and interrupted at 0.4 x (max. stress) after the sample had already passed the max. stress.

COMPARISON OF NEUTRON TOPOGRAPHS AND SYNCHROTRON X-RAY TOPOGRAPHS RECORDED FROM ORGANIC CRYSTALS.

M.Dudley (SUNY SB).

One of the potential drawbacks of the use of white beam X-ray topographic techniques for the investigation of the influence of microstructure on single crystal reactivity, is beam induced reaction or damage. In many systems the susceptibility to such damage can be reduced to tolerable levels via filtering of the incident white beam, although in others it can be so large as to make it impossible to record X-ray topographs in a non-destructive fashion. In this latter case, an alternative non-destructive technique must be found. Such a technique might also be used to verify the non-destructive nature of the filtered white beam technique. A technique that would seem ideally suited for such studies is neutron topography. This research was performed to test the feasibility of using neutron topography as an ally technique to synchrotron X-ray topography for the study of reactive crystals. Examples of each type of image, recorded from a crystal of deuterated pyrene, are shown in figure 1. In the synchrotron topograph, images of dislocations propagating from the seed to a growth face, as well as a growth sector boundary, can clearly be seen. However, on the neutron image, which was recorded at ILL, Grenoble, using a Barth-Hosemann geometry, the quality of the image is clearly inferior, although the main microstructural features can still be discerned. A full analysis of all factors influencing the differences in effective resolution on these topographs has been performed. Results indicate the potential applicability of neutron topography in such studies, particularly when used as an ally technique to synchrotron topography.

Figure 1. Comparison of neutron (a)(λ =1.7Å, g=$\bar{3}$21) and white beam X-ray (b) (λ=0.9A, g=220) topographs, respectively.

Acknowledgement: Work performed in part on the Synchrotron Topography Project Beamline X-19C, which is supported by the U.S. Department of Energy under Grant No. DE-FG02-84ER45098. The neutron work was supported by the Rutherford Lab.,(UK).

WHITE BEAM SYNCHROTRON TOPOGRAPHIC STUDIES OF THE LONG RANGE INFLUENCE OF REACTION INDUCED STRESS ON LOCAL REACTION KINETICS IN THE SINGLE CRYSTAL TO SINGLE CRYSTAL POLYMERIZATION OF PTS.

M. Dudley (SUNY SB).

The influence of reaction induced stress on single crystal reactivity is important from several different points of view. For example, reaction induced stress can potentially control the kinetics and/or mechanism of the reaction. It is also intimately involved with the potential for preferential reactivity at defects. Previous studies of the influence of reaction induced stress on reactivity, conducted by McBride et al[1] on acyl peroxide photolysis using FTIR and EPR, seem to indicate that this influence is suprisingly long range in nature. This research was conducted to investigate such influence in the single crystal to single crystal polymerization of PTS. Experiments consisted of inducing localized reaction in a crystal by irradiation through a pinhole and observing the response of the surrounding matrix in a dynamic fashion by filtered white beam synchrotron X-ray topography. Analysis of contrast enables some characterization of the induced strain field. The strain field changes as a function of time as a result of two effects, (1) stress induced reaction, and (2) plastic relaxation (via microcrack formation). Observations indicate that the influence of the reaction induced stress can be long range in nature. The sequence below shows representative topographs illustrating the development of strain as a function of time, λ = 0.8 Å, (a), (c) g=$\bar{1}04$, (b), g=$10\bar{4}$.

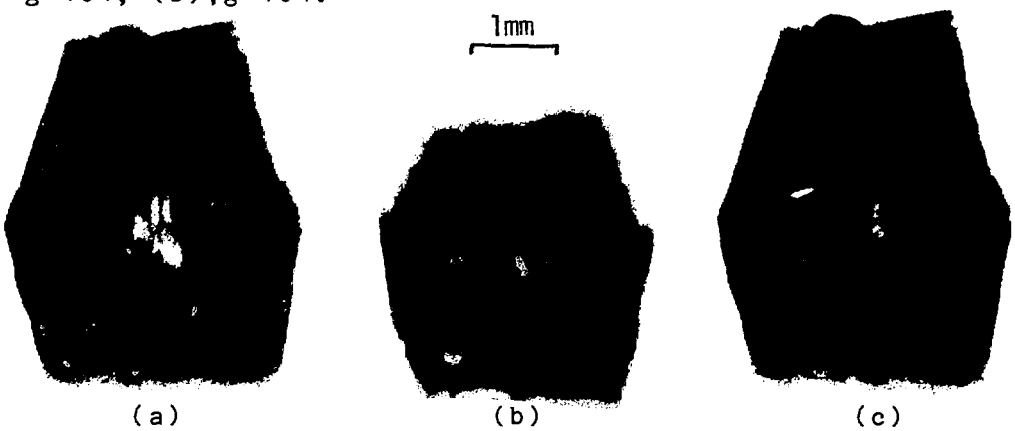

(a) (b) (c)

Reference. 1. M.D. Hollingsworth and J.M. McBride, Mol. Cryst. Liq. Cryst., 161, 25, (1988).

Acknowledgements: Work performed in part on the Synchrotron Topography Project Beamline X-19C, which is supported by the U.S. Department of Energy under Grant No. DE-FG02-84ER45098.

WHITE BEAM SYNCHROTRON TOPOGRAPHIC STUDIES OF THE PERFECTION OF $Zn(H_2O)_4(HC{\equiv}CCOO)_2$ SINGLE CRYSTALS.

M. Dudley (SUNY SB) and B.M. Foxman (BRANDEIS U).

Single crystals of $Zn(H_2O)_4(HC{\equiv}CCOO)_2$ undergo solid state polymerization, which can be induced by UV, X-ray or Gamma irradiation. These materials, and others related, have potential application as radiation detectors and as resists for lithography. Work reported here constitutes an examination of the feasibility of using white beam synchrotron X-ray topography to study the influence of lattice strain and defects on the reactivity of this class of material. Understanding such influences can contribute toward the future design and development of similar materials with potentially improved properties. To this end, the defect structures of large single crystals of $Zn(H_2O)_4(HC{\equiv}CCOO)_2$, grown via solvent evaporation from aqueous solution, were examined by filtered white beam X-ray topography. Figure 1 shows a white beam topograph ($g=\bar{3}12$, $\lambda = 0.6$Å) recorded from a typical as grown crystal. No dislocations are evident, the only visible defect being the inclusion denoted by the letter I. The Pendellosung fringes visible in the lower part of the image (denoted by the letter P), which arise as a result of the wedge shape of the crystal (two of the main habit faces, (010) and (011), are mutually inclined at an angle of ~52°), also attest to high perfection. Observed fringe spacing agrees with that calculated from dynamical theory. Further observations indicated that deleterious X-ray induced effects (either reaction or damage) do not become apparent until cumulative exposures exceed several tens of minutes. It was concluded that (1) large single crystals of $Zn(H_2O)_4(HC{\equiv}CCOO)_2$ of sufficient quality for topographic study can be readily grown, and (2) filtered white beam topographic techniques are well suited to the study of the influence of lattice strain and defects on the reactivity of this class of material. Further studies are in progress.

Figure 1.

Acknowledgements: Work performed in part on the Synchrotron Topography Project Beamline X-19C, which is supported by the U.S. Department of Energy under Grant No. DE-FG02-84ER45098.

WHITE BEAM TOPOGRAPHIC IMAGING IN GRAZING BRAGG-LAUE GEOMETRIES.

M.Dudley, J. Wu and G.-D. Yao, (SUNY SB).

It has recently been shown[1] that penetration depths in grazing Bragg-Laue geometries are a function of the local distortion, with kinematical theory being the determining factor in disorted regions, and dynamical theory being the determining factor in more perfect regions. In the more perfect regions, defect structures in subsurface layers of thickness ~1000Å and greater can be imaged. Detailed studies have been undertaken of the feasibility of conducting imaging in such geometries. Figure 1 shows a typical plot of dynamical penetration depth as a function of both the glancing angle Φ_o, and wavelength λ. Figure 2 shows the same plot truncated at a penetration depth of 1 μm. Clearly the use of long wavelength X-rays enables such narrow penetration depths to be achieved without the need for very small glancing angles, which can be difficult to attain in practice. Small glancing angles also lead to large degrees of geometric distortion, which can complicate image interpretation. Generally, the tunability of the source allows ready optimization of these geometric conditions, while at the same time enabling penetration depths to be conveniently varied in the range <0.1 μm - ~ 3 μm. This range is particularly well suited for the depth profiling of defect structures in thin layer semiconductor devices. It is concluded that this technique is far more versatile than the previously reported conventional monochromatic technique,[2] wherein the desire for large area coverage necessitates the use of scanning mechanisms, which are complicated by the fact that scanning must be performed in planes inclined to the plane of diffraction (defined by the incident and diffracted beam directions).

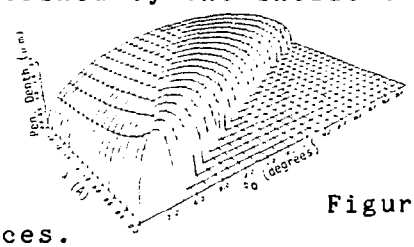

Figure 1

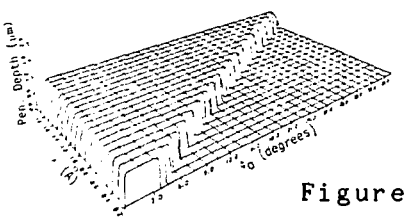

Figure 2

References.

1. M. Dudley, G.-D. Yao, Submitted to Nucl. Inst. and Meth.
2. A.M. Afanasev,P.A. Aleksandrov, R.M. Imamov, E.M. Pashaev and V.I. Polovinkina, Phys. Stat. Sol. (a) 90, 419, (1985).

Acknowledgements: Work supported by the NSF under Grant No. DMR-8506948, and performed in part on the Synchrotron Topography Project Beamline X-19C, which is supported by the U.S. Department of Energy under Grant No. DE-FG02-84ER45098.

DETERMINATION OF SIZE SHAPE AND POSITION OF CRYSTALLITES IN LOW ABSORPTION CONTRAST COMPOSITES BY WHITE BEAM SYNCHROTRON MICRO-TOPOGRAPHY.

M. Dudley, D. Yuan (SUNY SB), and S. Trivedi (BRIMROSE CORP.)

Non-destructive and non-intrusive determination of the positions, size and shape of crystalline inclusions of NH_4ClO_4 in an amorphous organic matrix is a task that eludes study by conventional means. Optical techniques are not applicable due to the opacity of the organic matrix. Similarly, techniques based upon X-ray absorption, such as tomography, can be effectively ruled out due to the low absorption contrast of the composite. A logical alternative, would be to consider diffraction based techniques. This research was concerned with the development of such a technique enabling the solution of this problem. The technique basically consists of recording filtered white beam transmission Laue patterns from the sample, with several specimen detector distances and orientations. The preliminary studies reported here were undertaken with the crystallites mounted alone on thin glass slides, which enabled ready comparison of X-ray data with optical microscopic data. Analysis then consisted of quantitative ray tracing, performed with the aid of an algorithm developed for this purpose, enabling the determination of the positions, size and shape of the individual crystallites. This ray tracing effectively eliminates any errors arising from crystallite distortion. Accuracy is currently limited by the nature of the film cassettes utilized, and the measurement of the diffraction spot shapes and sizes. Improved cassette design should alleviate the first source of inaccuracy, and digitizing the X-ray images should largely eliminate the second. Current accuracies in particle size determination are within 10 μm, and accuracies in position determination can be within 20 μm. An example of the comparison between particle size distribution obtained by this technique with that obtained optically is shown below.

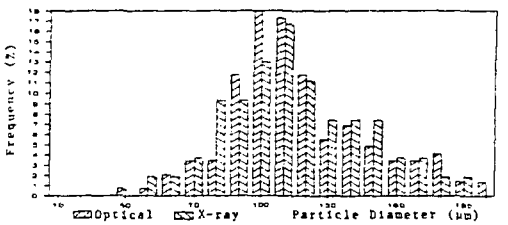

Acknowledgements: Work performed in part on the Synchrotron Topography Project Beamline X-19C, which is supported by the U.S. Department of Energy under Grant No. DE-FG02-84ER45098. The interest of Dr R.G. Rosemeier of Brimrose Corp. and Dr C. Lowe-Ma of NWC is acknowledged.

ROCKING CURVE MEASUREMENTS OF COMPOUND SEMICONDUCTOR THIN FILMS GROWN ON SILICON

H.-Y. Lee and Haydn Chen, University of Illinois, Urbana, IL

Today's thin film fabrication technologies are advanced to a stage that the heteroepitaxial growth of a single layer or hybrid assembly of III-V or II-VI compound semiconductors on silicon or other substrates can be accomplished. Regardless of the applications, a high degree of perfection is required for those grown films in order to achieve the most desirable performance. High yields of reliable devices can be more reasonably assured if substrate-treading dislocation densities are low, interfaces are sharp and contain few misfit dislocations, stresses and strains are small and thus warpage and cracking are prevented, and epitaxial structures are uniform over large areas. Double crystal rocking curve measurements and x-ray diffraction topographic methods are powerful techniques that are very well suited to the determination of crystalline perfection. The attributes of high flux, high resolution and wavelength tuneability of a synchrotron radiation source make such analysis simpler and more flexible. Some examples are illustrated as follows.

Epitaxial layers of InSb have been grown on Si substrates by Morkoc and his colleages using the Molecular Beam Epitaxy method.* These films were grown with and without a thin GaAs buffer layer. Electrical measurements, van der Pauw Hall, and optical transmission measurements were carried out to assess the electrical and optical properties of the InSb layers. Structural qualities were examined using double-crystal rocking curve apparatus. Results are shown in Table 1. It can be concluded that thicker InSb layers (8 μm) show higher electron mobilities, narrower rocking curve widths and sharper band edge transmission curve. These results are encouraging as relatively high quality InSb epilayers can be grown on Si in spite of the large 19% lattice mismatch.

Table 1

Specifications of InSb Epilayers on Si(100)

Layer	d_{InSb} (μm)	d_{GaAs} (μm)	μ_{300} ($cm^2/V\cdot s$)	n_{300} (cm^{-3})	μ_{77} ($cm^2/V\cdot s$)	n_{77} (cm^{-3})	RCW (sec)
A	3.2	0.3	48000	2.2×10^{16}	3700	5.8×10^{15}	575
B	3.2	0.05	46000	2.2×10^{16}	2600	5.6×10^{15}	---
C	3.2	0.0	39000	2.7×10^{16}	700	2.4×10^{16}	510
D	8.0	0.3	55000	2.0×10^{16}	1700	6.0×10^{15}	410

μ = mobility, n = electron carrier density, RCW = rocking curve width

*J.-I. Chyi, D. Biswas, S.V. Iyer, N.S. Kumar, H. Morkoc, R. Bean, K. Zanio, H.-Y. Lee and and Haydn Chen, Appl. Phys. Lett. (1988) submitted.

A STUDY OF THE DEFORMATION BEHAVIOUR IN RECRYSTALLIZED MOLYBDENUM CRYSTALS VIA IN-SITU SYNCHROTRON TOPOGRAPHY

V. Wakharkar (SUNY SB), J. C. Bilello (CSUF)

In the present investigations Synchrotron X-ray Topography (SXRT) is being used as an in-situ probe to study the evolution of the deformation substructure in recrystalized Mo single crystals under controlled stress conditions. The typical characteristics of the substructure in recrystalized Mo crystals as revealed by Double Crystal X-ray Topography is the presence of (a)misoriented domains and subgrain boundaries (b)embedded misoriented regions of slightly different orientations i.e. "island grains". Room temperature tensile tests were carried out using a miniature tensile stage and the time dependent change in substructure was followed in the transmission Laue geometry using the white beam from the Synchrotron. A low resolution real-time image can be viewed directly on a monitor using a X-ray TV camera. The use of the white beam allowed the imaging of the misoriented "island grains" and it also permitted imaging of heavily strained samples. In specimens that were continuously pulled at a strain rate of the order of 10 (-4)/sec the evolution of the deformation structure could be followed on film plates taken in rapid sequence. Several stages in the evolution of the deformation structure could be distinguished including source activation, slip initiation and propagation. Interesting observations were also made related to the presence of "island-grains" in the bulk single matrix. The "island-grains" had a pronounced effect on the deformation characteristics of these crystals. The single crystal - "island-grain" interfaces imposed severe constraints on the plastic deformation process by providing effective barriers to dislocation motion. The discontinuous nature of slip occurring in slip bands gave rise to microplastic incompatibility effects when these slip bands impinged on the interface. In such cases it was observed that the deformation was principally associated with lattice regions in the vicinity of the interface and to a lesser degree with other regions in the specimen. The net result of the barrier effect and plane bending was that these regions were now suspect sites for microcrack nucleation. With increasing applied stress, the stress concentration at the end of a slip band impinging on the interface continued to increase and in some cases this indeed lead to nucleation of microcracks near the interface.

This work was performed on the Synchrotron Topography Project Beamline X-19C which is supported by the U.S. Department of Energy under Grant No. DE-FG02-84ER45098.

X-ray Scattering Study of Crystalline Order in Thin Liquid Crystal Films

D. Y. Noh, J. D. Brock, J. O. Fossum, W. J. Nuttall, J. D. Litster and R. J. Birgeneau
Department of Physics, Massachusetts Institute of Technology
Cambridge, Massachusetts 02139

In two-dimensional systems, the density-density correlation function decays algebraically due to the large thermal fluctuations. The absence of true long-range order and the theoretical prediction of a continuous melting transition initiated a lot of experimental and theoretical work on quasi two-dimensional systems.

Freely suspended thin films of smectic liquid crystal are ideal for the study of ordering in two dimensions. Unlike adsorbed systems or surfaces of a bulk sample, they are free from the effects of a substrate potential or the bulk part of the sample. By systematically varying the number of smectic layers one can study the crossover from two-dimensional to three-dimensional behavior. We report an x-ray scattering study of of thin films of liquid crystal 8OSI (4-(2-methybutyl)phenyl4'-(octyloxy)-(1,1')-biphenyl-4-carboxylate) in the crystalline Smectic J phase. Single domain samples of 8OSI provided by the freely suspended film technique were used.

The thickness of a film was measured by the width of the peak in a scan perpendicular to the smectic layer through the in-plane peak. Thin films of 8OSI have AAA type stacking order in the Smectic J phase. To get meaningful information about the algebraically decaying correlation function, the resolution function in all directions and the mosaicity of the sample need to be considered carefully. Assuming that the out of plane dependence of the structure factor can be separated from the in-plane dependence, the structure factor can be written as,

$$S(\vec{q}) = I_0\, F(q_z)\frac{1}{(\vec{q}_\perp - \vec{\tau}_\perp)^{2-\eta}}. \qquad (1)$$

The measured longitudinal line shapes were fitted to Eq. (1) convolved with the resolution function. Two representative scans are illustrated in figure 1. The value of η for the 5-layer film is 0.4±.05 which is slightly greater than the theoretically predicted upper limit, $\frac{1}{3}$. η for the 14-layer film is about 0.27. It is observed that the value of η is decreasing with increasing thickness. This is consistent with the fact that η is zero for a true 3D system.

The contributions to the beam lines at the NSLS are supported by the NSF-Material Research Laboratory under Grant No. DMR 84-18718 . The liquid crystal research at MIT is supported by the NSF grant DMR 84-18718 and DMR 86-19234.

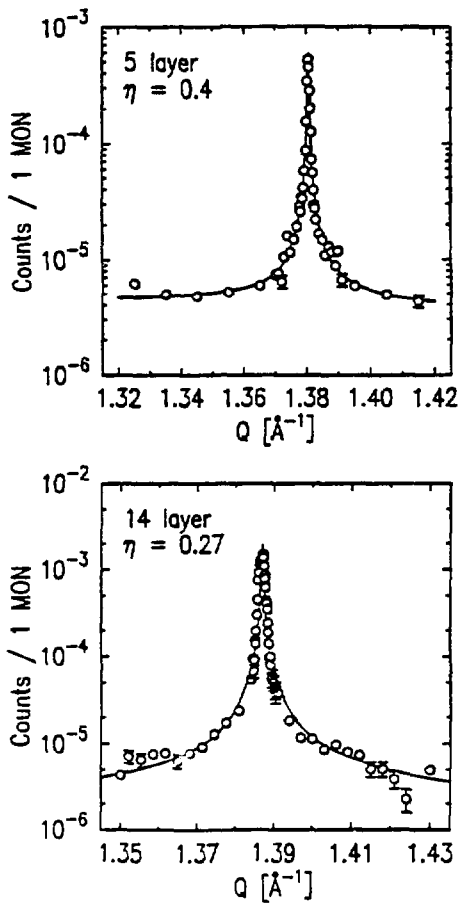

Figure 1

X-RAY SCATTERING STUDIES OF Au(001) SURFACE STRUCTURE AND PHASE TRANSFORMATIONS

D. Gibbs, B. Ocko (BNL†); S.G.J. Mochrie (MIT); and D.M. Zehner (ORNL)

A new apparatus for UHV surface x-ray scattering studies has been developed at X22C. The instrument consists of a high-resolution 4-circle spectrometer and a UHV surface chamber supporting a 210° Be window and standard surface diagnostics (including LEED, AES, ion sputtering, variable temperature control, etc.). The first measurements have been concerned with the structure of the clean Au(001) surface. They are performed using the glancing incidence geometry, in contrast to earlier studies of the specular and non-specular reflectivities carried out in the BNL rotating anode lab and at CHESS.[1] At room temperature we observe a complex, incommensurate diffraction pattern of hexagonal symmetry. Regularly spaced satellites are observed surrounding the principal hexagonal positions along directions parallel to (11ℓ). Contour scans of the principal hexagonal position reveal a cluster of rods mutually separated by distances of order 0.01 a*. Detailed studies of the diffraction pattern at room temperature and at temperatures up to bulk meeting (≈1050C) are continuing.

1. D. Gibbs, B. Ocko, D.M. Zehner, S.G.J. Mochrie, Phys. Rev. B38, 7303 (1988).

† This work was supported by the Division of Materials Sciences, U.S. Dept. of Energy under Contract DE-AC02-76CH00016.

HIGH RESOLUTION STUDY OF STRUCTURAL PHASE TRANSFORMATIONS IN SUPERCONDUCTING $La_{2-x}Ba_xCuO_4$

D. Hohlwein (U. Tübingen); H. Moudden, D.E. Cox, D. Gibbs, A. Moodenbaugh, J.D. Axe (BNL*).

$La_{1.9}Ba_{0.1}CuO_4$ has been observed[1] to undergo the following sequence of transformations upon cooling from 300K--

$$\text{tetr.}(14/mmm) \xrightarrow{T_0=270K} \text{ortho.}(Cmca) \xrightarrow{T_1=52K} \text{tetr.}(P4_2/ncm).$$

The newly discovered low temperature tetragonal structure can be understood geometrically as arising from a coherent superposition of the two domain modifications of the orthorhombic structure. Dynamically, it results from a second instability in the two-fold degenerate soft modes of the high temperature tetragonal phase. Energetically, the system can be modelled as a XY-spin system with temperature dependent quartic anisotropy, v(T), and the low temperature transformation coincides with an isotropic point, $v(T_1)=0$. We have performed further studies of the phase stability of this new phase vs. Ba concentration using high resolution x-ray powder diffraction. We find that the phase is most stable near x=0.1, with the transformation temperature dropping to zero near x=0.05 and x=0.20. It is possible that the anomalous behavior of superconducting T_c vs. temperature[2] is correlated with the amount of tetragonal phase present at low temperature.

(1) J.D. Axe, D.E. Cox, K. Mohanty, H. Moudden, A.R. Moodenbaugh, and Y. Xu, IBM J. Res. and Development (to be published).
(2) A.R. Moodenbaugh, Y. Xu, and M. Suenaga, Proc. Matl. Res. Soc., 99, 427 (1987).

* This work was supported by the Division of Materials Sciences, U.S. Dept. of Energy under Contract DE-AC02-76CH00016.

NOVEL DISRUPTIVE X-RAY INTERACTION WITH LIQUID-ENCAPSULATED-CZOCHRALSKI-GROWN CRYSTALS OF UNDOPED GALLIUM ARSENIDE

Masao Kuriyama, Bruce Steiner, Ronald C. Dobbyn (National Bureau of Standards), Margaret Brown and David Larson (Grumman Aerospace Corporation)

A novel disruptive interaction has been observed in the transmission of highly parallel monochromatic x-rays through two undoped gallium arsenide crystals grown by liquid encapsulated Czochralski methods. The novel features appear in beams with a divergence of 1 arcsecond and 0.1 arcsecond, respectively, but are more prominent in the latter beams. The phenomenon appears as purely disruption "shadows," aligned in the direction of the incident radiation. They are therefore traceable to features in the interior of the crystals rather than on the surface. These disruption images appear to be identical in both H and O image pairs, but to vary in visibility with diffraction direction, as illustrated in Figures 1 and 2. The source of these observations appears to be <110> platelets embedded in the crystals, which interact with the diffracting x-rays in a manner similar to magnetic domain walls previously observed[1]. These images are in addition to the cellular structure, which is observed here also to vary with the diffraction, in contrast to previous observation by Lang topography[2].

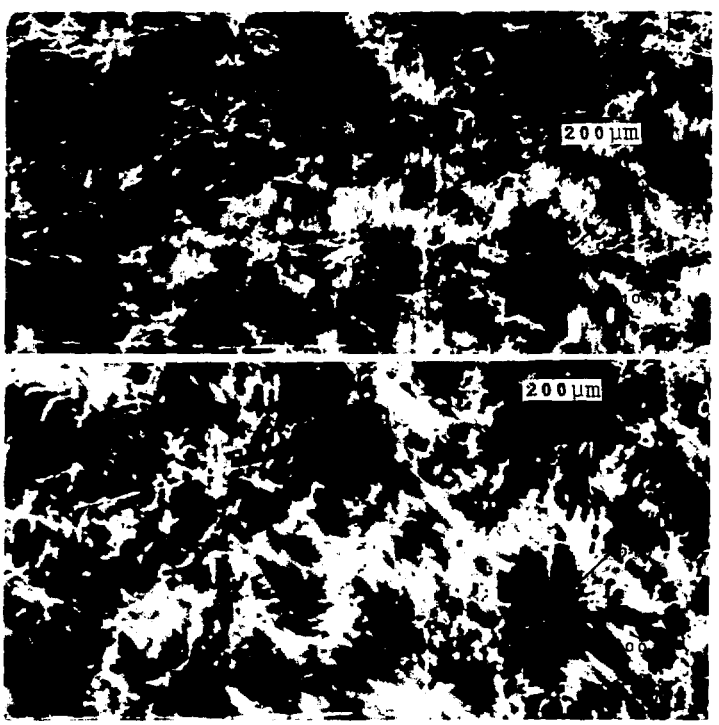

Fig. 1. Image of $(2\bar{2}0)$ O beam diffraction from undoped gallium arsenide in monochromatic 8 keV radiation.

Fig. 2. Image of (400) O beam diffraction from undoped gallium arsenide in monochromatic 10 keV radiation.

[1] W. J. Boettinger, H. E. Burdette, and M. Kuriyama Phil. Mag. 36, 763-776 (1977).

[2] E. Zielińska-Rhoozińska J. Crystal Growth 87, 154-156 (1988).

"OUT STATE" ANALYSIS OF STRAINS DISPLAYED IN HIGH ANGULAR RESOLUTION DIFFRACTION IMAGES OF LIQUID-ENCAPSULATED-CZOCHRALSKI-GROWN INDIUM DOPED GALLIUM ARSENIDE

Masao Kuriyama, Bruce Steiner, Ronald C. Dobbyn (National Bureau of Standards), and Hidehiko Kuwamoto (Rockwell International Science Center)

"Out state" diffraction analysis of monochromatic 8 keV (004) diffraction images of liquid-encapsulated-Czochralski-grown indium doped gallium arsenide in Laue geometry (Figures 1 and 2) has shown that strains associated with the circumferential growth striations are substantially greater than the strains associated with the central faceted growth region. The relative degree of strain is shown in the variation of the central strain patterns with small changes in observation angle (momentum transfer), while the appearance of the striated strains does not change substantially over this range.

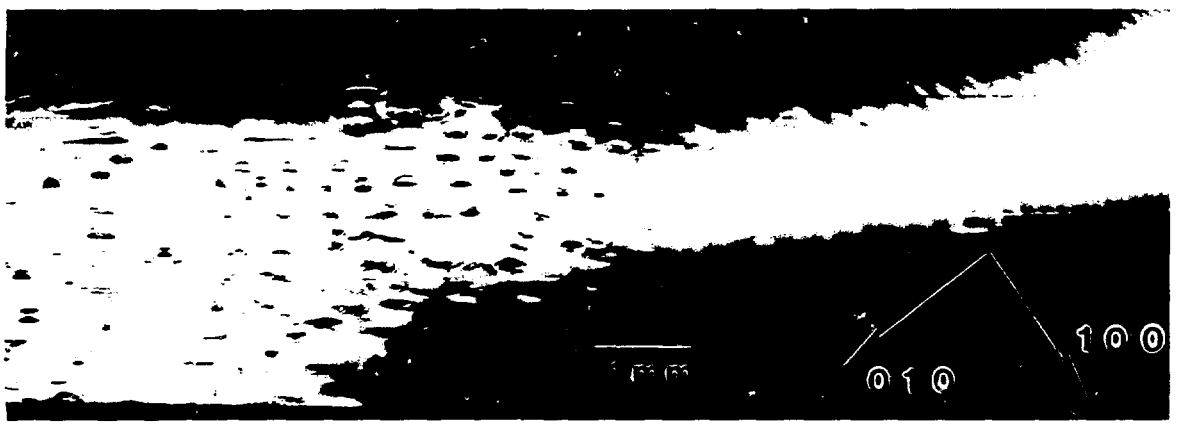

Fig. 1. Image of indium doped gallium arsenide in monochromatic 8 kev radiation taken in the vicinity of the peak of the (004) diffraction.

Fig. 2 Image of indium doped gallium arsenide in monochromatic 8 keV radiation taken off of the peak of the (004) diffraction.

INDIVIDUAL DISLOCATIONS IN HIGH RESOLUTION MONOCHROMATIC DIFFRACTION IMAGES OF LIQUID-ENCAPSULATED-CZOCHRALSKI-GROWN INDIUM DOPED GALLIUM ARSENIDE

Bruce Steiner, Masao Kuriyama, and Ronald C. Dobbyn (National Bureau of Standards), and Hidehiko Kuwamoto (Rockwell International Science Center)

Individual dislocations have been clearly resolved in monochromatic 10 keV (040) diffraction images (topographs) of liquid-encapsulated-Czochralski grown indium doped gallium arsenide in Laue geometry. Dislocations observed around the edge of the boule, associated with the outermost circumferential growth striations, tend to be grouped in linear arrays of "slip planes" along [110] directions (Figure 1). Elsewhere in the boule, that is, in the central region characterized by faceted growth and among the innermost circumferential growth striations, the dislocations are more isolated from one another (Figure 2). The character of these images is clearly distinguishable from precipitates or other imperfections.

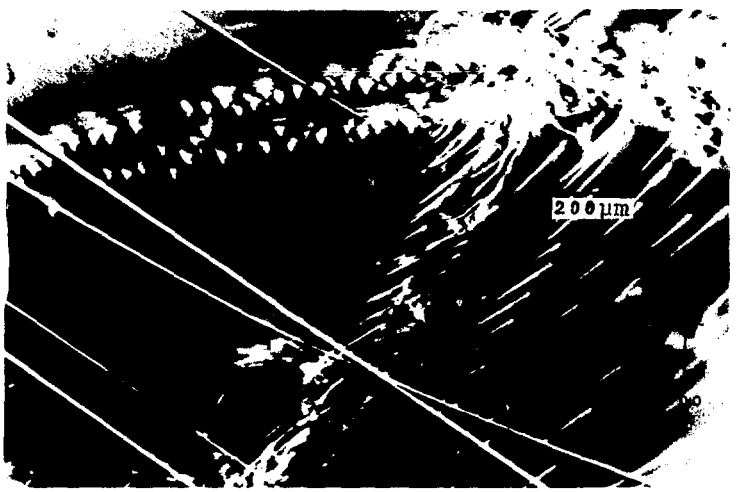

Fig. 1. Arrays of dislocations observed in (040) diffraction of monochromatic 10 keV radiation through the outer regions of an indium doped gallium arsenide crystal.

Fig. 2. Isolated dislocations observed in (040) diffraction of monochromatic 10 keV radiation through the central area of an indium doped gallium arsenide crystal displaying faceted growth.

INITIAL STUDY BY MONOCHROMATIC DIFFRACTION IMAGING (TOPOGRAPHY) OF VAPOR GROWTH OF MERCURIC IODIDE

Bruce Steiner, Masao Kuriyama, and Ronald C. Dobbyn (National Bureau of Standards), and Lodewijk van den Berg (EG&G)

Individual grains, crystallographically oriented with respect to one another, have been identified in a series of diffraction images from a set of vapor grown mercuric iodide crystals taken from a single boule. The presence of these grains in various crystals indicates that the grains are associated with the growth of the crystal rather than subsequent handling. The grains, observed in diffraction from (006), (008), (107), (108), (109), (1 0 10), (1 0 11), (1 0 12), (208), (1 1 10), and (1 1 12) planes in monochromatic 8 keV radiation, are mutually rotated by 1 ~ 2 arc minutes around the [110] axis. An enlarged image of the (1 1 12) diffraction is shown in Figure 2, which displays dendritic features not previously observed in mercuric iodide. The correlation of these features among the various grains confirms the growth origin of the individual grains.

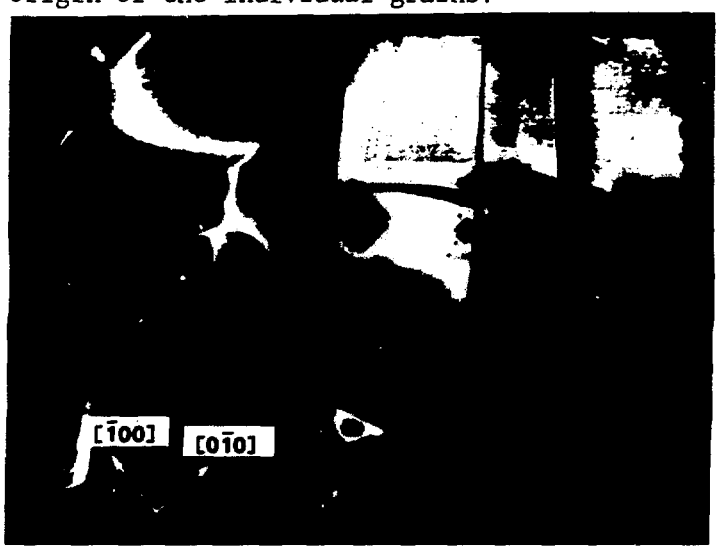

Fig. 1. 8 keV (1 1 12) diffraction image of vapor grown mercuric iodide in Bragg geometry.

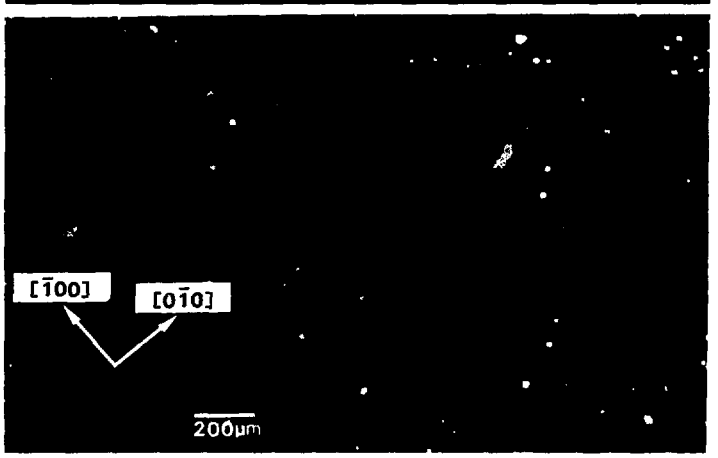

Fig. 2. Enlargement of portion of 8 keV (1 1 12) diffraction image shown in Figure 1.

STRAINS IN THE LAYERING IN THE CZOCHRALSKI GROWTH OF BISMUTH SILICON OXIDE

Bruce Steiner, Masao Kuriyama, and Ronald C. Dobbyn (National Bureau of Standards)

In the faceted Czochralski growth of bismuth silicon oxide, layered strains from periodic growth fluctuations have been shown to be restricted to the direction perpendicular to the layering[1]. This conclusion follows from comparison of the image of the $(0\bar{6}0)$ diffraction, Figure 1, with the image of the $(\bar{6}00)$ diffraction, Figure 2. Those segments of the crystals in which layering is oblique to the diffraction vector interrupt transmission while those segments in which layering is parallel to the diffraction vector transmit. Thus, the strains parallel to the layering are negligible in comparison with the strains oblique to it. Similar conclusions follow from a detailed analysis of the fringes in the central portion of the crystal.

Fig. 1. Image of $(0\bar{6}0)$ diffraction from bismuth silicon oxide crystal displaying faceted growth

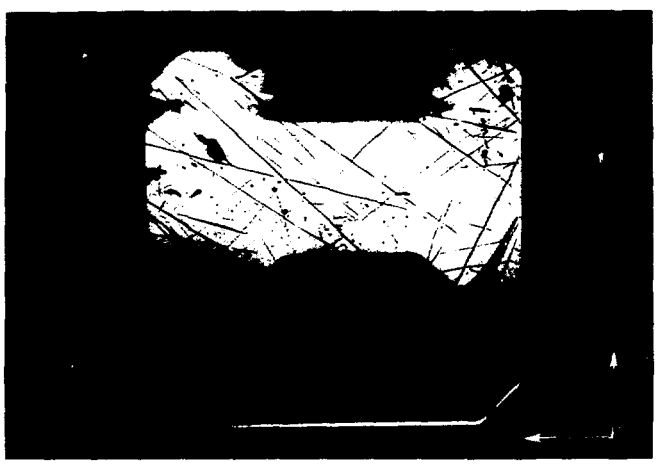

Fig. 2. Image of $(\bar{6}00)$ diffraction from the bismuth silicon oxide crystal displaying faceted growth shown in Figure 1.

[1] Bruce Steiner, Uri Laor, Masao Kuriyama, Gabrielle G. Long, and Ronald C. Dobbyn, J. Crystal Growth 87, 79-100, 198[9]

NOVEL SURFACE FEATURES OBSERVED IN LIQUID-ENCAPSULATED-CZOCHRALSKI-GROWN CRYSTALS OF UNDOPED GALLIUM ARSENIDE

Bruce Steiner, Masao Kuriyama, Ronald C. Dobbyn (National Bureau of Standards), Margaret Brown and David Larson (Grumman Aerospace Corporation)

Stripes that alternate in visibility between H and O image pairs in diffraction through undoped gallium arsenide grown by liquid encapsulated Czochralski have been observed in monochromatic 8 and 10 keV radiation. These stripes in the [110] direction are caused by diffraction by the crystal surface over relatively large areas alternately into the H and O images, as shown in Figures 1 and 2. Such diffraction over relatively large areas has not been previously observed. The observation of correlated features in (004) and (444) diffraction in Bragg geometry confirms that the features causing the stripes are close to the surface being viewed.

Fig. 1. $(2\bar{2}0)$ diffraction image of the H beam from undoped gallium arsenide in monochromatic 10 keV radiation

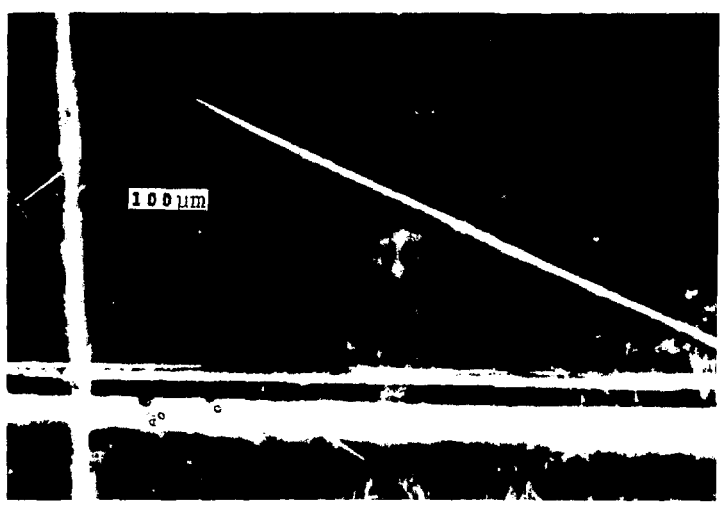

Fig. 2. $(2\bar{2}0)$ diffraction image of the O beam from undoped gallium arsenide in monochromatic 10 keV radiation

X23

INITIAL STUDY BY MONOCHROMATIC DIFFRACTION IMAGING (TOPOGRAPHY) OF CADMIUM TELLURIDE GROWN IN A BRIDGEMAN FURNACE DESIGNED FOR USE IN SPACE

Bruce Steiner, Masao Kuriyama, and Ronald C. Dobbyn (National Bureau of Standards), G. Bostrup, J. Viola, and E. Gertner (Rockwell International Science Center), and W. Aldrich (NASA Marshall Space Flight Center)

The principal long range imperfection in cadmium telluride grown in a furnace designed for space use has been observed in video recorded monochromatic 8 keV radiation imaging of the (444) diffraction as gradual warping or variation in the lattice parameter. No high contrast boundaries delineating major subgrains, which had been postulated on the basis of rocking curve measurements, are observed. The microstructure of the image, Figure 1, is observed to consist of cells defined by arrays of dots at the limit of resolution of the observations, 1 micrometer. These dots are extended in the direction of diffraction by the trajectory of the x-rays through the photographic emulsion, Figure 2. Since these features are observed as regions of maximum diffraction, they are located at the surface of the crystal rather than in the interior.

Fig. 1. (444) diffraction in monochromatic 8 keV radiation from cadmium telluride in Bragg geometry.

Fig. 2. Enlarged portion of (444) diffraction in monochromatic 8 keV radiation from cadmium telluride in Bragg geometry.

NOVEL DIFFRACTION IMAGING ANALYSIS OF INDIVIDUAL PARTICLES IN POLYCRYSTALLINE MATERIALS

David R. Black, Richard Spal, and Masao Kuriyama

The determination of particle size, shape, strain, crystallographic orientation, and distribution normally has required analyses of x-ray diffraction data obtained from line profiles or small angle scattering (SAXS). Such analyses are dependent entirely on the mathematical models chosen by the investigators. With a highly parallel monochromatic beam prepared from synchrotron radiation with a few arc-second divergence, we have performed an analysis that is independent of mathematical models.

Polycrystalline diffraction produces numerous small spots, grouped to form a ring, historically called a "Debye-Scherrer" ring. We have resolved individual spots, diffracted from single grains and particles, with 10 μm spatial resolution as shown in Figure 1. The relative crystallographic orientation of individual particles has been determined, as shown in Figure 2. The beam used in this work was 2 arc-seconds wide in the vertical direction and 30 arc-seconds in the horizontal direction, and had a 1 mm X 0.2 mm cross section. These conditions can be adjusted for each measurement as required. The acquisition of the profile for all particles in one diffraction line can be achieved within 20 minutes. The relative orientation of particles can be recorded within 5 minutes by rotating the sample while a detector remains in a fixed position. In demonstration experiments on a silicon standard sample and an alumina disk with 8.048 keV radiation, particles of slightly less than 10 μm are clearly separated. This resolution is not limited in fundamental factors, and can be improved. Within each particle, at the current resolution one can see fine structure such as crystal imperfections, subgrain boundaries and inhomogenous strains.

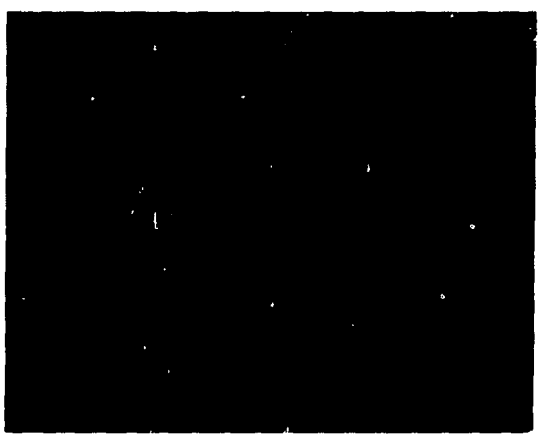

Figure 1. Diffraction rings, magnified 2.5 times, from α-Al_2O_3, indicating individual particle diffraction, taken at 8.048 keV.

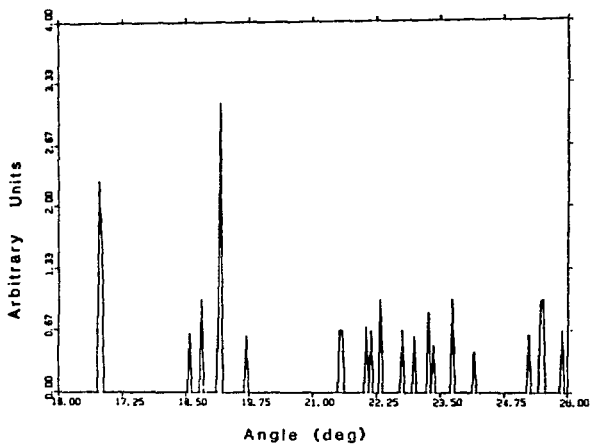

Figure 2. The relative angular orientation of individual particles is shown as the sample is rotated. The detector is set to receive the (113) diffraction line of αAl_2O_3.

LIMITING RESOLUTION IN X-RAY IMAGE MAGNIFICATION OF DIFFRACTION IMAGES

Ronald C. Dobbyn, Bruce Steiner, and Masao Kuriyama

There have recently been many advances in real-time direct diffraction imaging. An important question now is: "What is the limiting spatial resolution?" Is resolution limited by diffraction effects within samples or by x-ray optical elements that prepare the beam and produce images? An x-ray image magnifier of 30 X to 40 X has now been demonstrated for images of an electronic device on gallium arsenide. The device was set for 004 symmetrical diffraction in Bragg (surface reflection) geometry. The magnifier was aligned in non-dispersive geometry with 9.3 keV radiation. As shown in Figures 1 and 2, the details of the device down to approximately 2.5 micrometers are clearly visible. Crystalline imperfections are also evident. The present result indicates that the resolution to date has not been limited by material diffraction effects, and thus that increase in magnification can be used to achieve real-time imaging with submicron resolution aided by efforts to develop high sensitivity 2D detectors. Moreover, for the evaluation of devices, these diffraction images demonstrate that crystal imperfections can be distinguished from device detail.

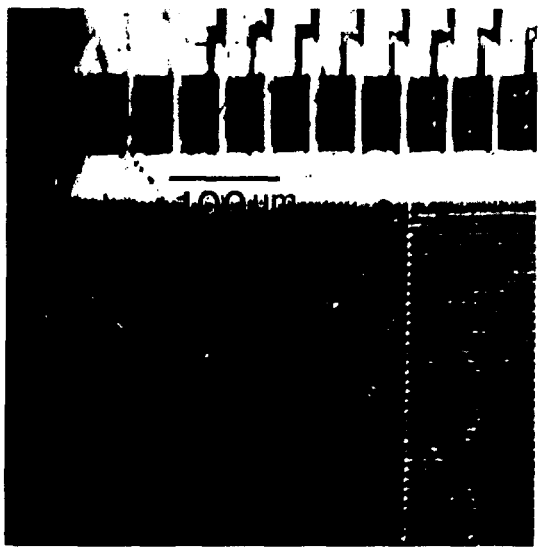

Figure 1. (400) diffraction image in the surface reflection geometry taken from a device on a gallium arsenide (100) substrate at 9.3 keV, using an x-ray image magnifier, 30X.

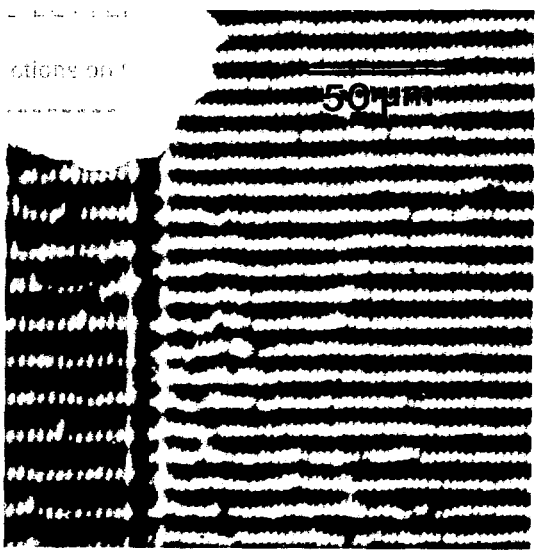

Figure 2. Enlarged portion of the device of Figure 3a, showing details of approximately 2.5 μm.

A TWO-DIMENSIONAL POSITION SENSITIVE IONIZATION CHAMBER

Richard D. Spal

A two-dimensional position sensitive ionization chamber with a square aperture of 6 cm has been demonstrated to have a resolution of 35 microns. It relies on current division between four electrodes to locate the centroid of an x-ray beam. Two such chambers have been built into the tunable double crystal monochromator on NIST beamline X23A at NSLS. They are used to align the monochromator, and to monitor the position and intensity of the white beam at the entrance to the monochromator and the characteristics of the monochromatic beam at the exit. Because the chamber has a large aperture and operates with helium, it may be stationed permanently in the beam without degrading it.

The chamber design, shown in Fig. 1, is similar to the one-dimensional position sensitive ionization chamber developed by Tischler and Hartman[1]. The chamber aperture is square, rather than rectangular as in Ref. 1, to increase the electric field gradient $\partial E_x/\partial x$ at the center, thereby making x coordinate measurement practical. Electrodes 1 through 4 and the housing are grounded, while electrodes 5 and 6 are held at a positive potential shown in Fig. 2. Four single pole double throw coaxial relays independently connect electrodes 1 through 4 either to ground or to the virtually grounded input of a picoammeter. Any combination of currents from electrodes 1 through 4 may be summed and routed through the picoammeter by actuating the corresponding relays. The current sum $I=I_1+I_2+I_3+I_4$, where I_i is the current through electrode i, indicates beam intensity. The ratio of current sums $R_{34} = (I_3+I_4)/I$ indicates the x coordinate of the beam, while $R_{13} = (I_1+I_3)/I$ indicates the y coordinate.

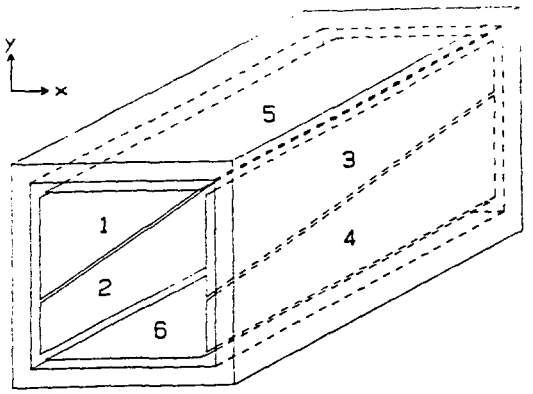

Fig. 1. Isometric drawing.

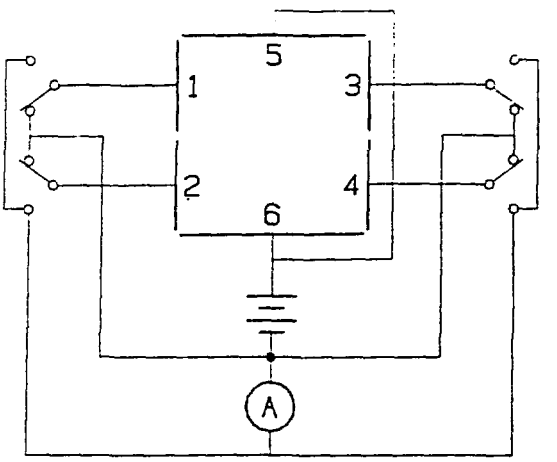

Fig. 2. Electrical schematic drawing.

1. J. Tischler and P. L. Hartman, Nucl. Instr. and Meth. 172 67 (1980).

DISCOVERY OF PERVASIVE ANTIPHASE BOUNDARIES IN LIQUID ENCAPSULATED CZOCHRALSKI-GROWN SEMI-INSULATING UNDOPED GALLIUM ARSENIDE

Bruce Steiner, Masao Kuriyama, Ronald C. Dobbyn, Uri Laor, David Larson, and Margaret Brown

The novel, pervasive, streak-like features observed only in the direction of the scattering vector in diffraction images of monochromatic synchrotron radiation (8-10 keV) transmitted through LEC semi-insulating undoped gallium arsenide (accompanying Experimental Abstract) have been shown to be due to antiphase boundaries characterized by lattice coherence but incorporating a phase (atomic) shift[1].

These boundaries have been observed moreover to align themselves to form cellular structure (Figure 1) and linear and very low-angle subgrain boundaries in <110> directions (Figure 2), as well as surface stripes in a <110> direction observed in one sample (accompanying Experimental Abstract) and systematic differences in the acceptance angle for images involving various diffraction vectors. We thus have arrived at the first comprehensive model for LEC defect structure with a unified interpretation.

Fig. 1. Cellular structure in (040) **0** beam diffracted 10 keV synchrotron radiation of undoped gallium arsenide crystal in Laue geometry.

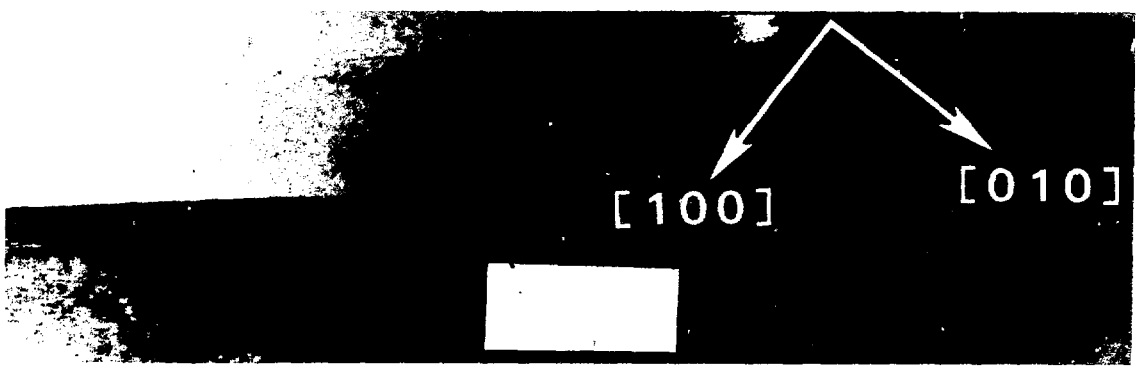

Fig. 2. Linear very low-angle subgrain boundary in $(\bar{2}\bar{2}4)$ 8 keV.

1. Kuriyama, M., Steiner, B., Dobbyn, R. C., Laor, U., Larson, D., Brown, M. Physical Review B (in press, 1988).

Oxidation State of Cr Complexes adsorbed on Carbon

W. T. Elam and E. F. Skelton (NRL), R. Gibbs (NSWC)

Studies have been undertaken to determine if X-ray Absorption Spectroscopy can determine the oxidation state of chromium compounds in chemical complexes absorbed on high-surface-area carbons. The first phase of such studies involved measuring the shift in the Cr K absorption edge for standard compounds of known oxidation state. The figure shows the results of these experiments. The shift is readily apparent for all of the known oxidation states of Cr. Note particularly the peak below the edge for the +6 oxidation state.

The next step was to measure samples with a mixture of oxidation states to see if the relative proportions could be determined. Unfortunately, the resolution of our beamline (about 2.6eV) was not sufficient to distinguish a mixture of +3 and +6 oxidation states from a pure +4 oxidation state. More sophisticated modeling of the edge shape (possible with molecular orbital programs) and/or better energy resolution will be required.

A more promising approach is to consider the amplitude of the peak which appears below the edge for the +6 oxidation state. The amplitude of this peak decreases in relation to the amount of Cr present in the +6 state. It remains well separated from the main edge for all conditions and, when calibrated, may serve as a reliable indicator of the proportion of Cr atoms in this state.

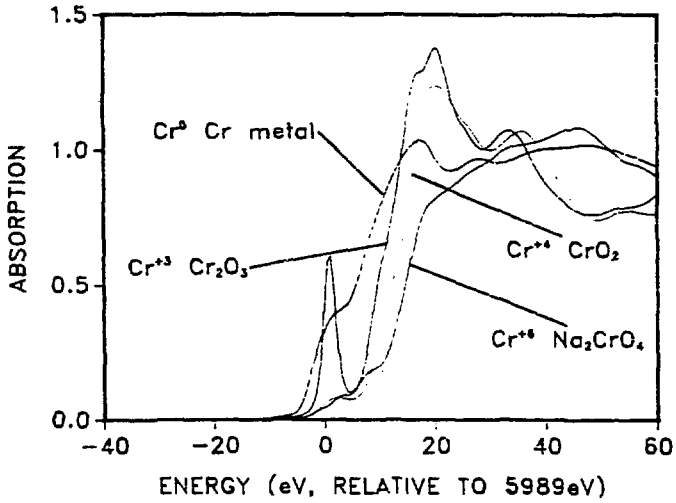

Y. U. Idzerda, W. T. Elam, B. T. Jonker, and G. A. Prinz (Naval Res. Lab)

These experiments are aimed at verifying the bulk atomic structure of thin films of cobalt grown epitaxially on GaAs single crystals. The equilibrium structure of cobalt is hcp, but a bcc metastable phase is predicted theoretically. Such a phase has been synthesized[1] by epitaxial growth on (110) GaAs, which very closely matches the predicted lattice constant. Magnetic and diffraction measurements both indicate the presence of the desired bcc phase, but the diffraction results are inconclusive because of the presence of the strong substrate peaks at the same d-spacings.

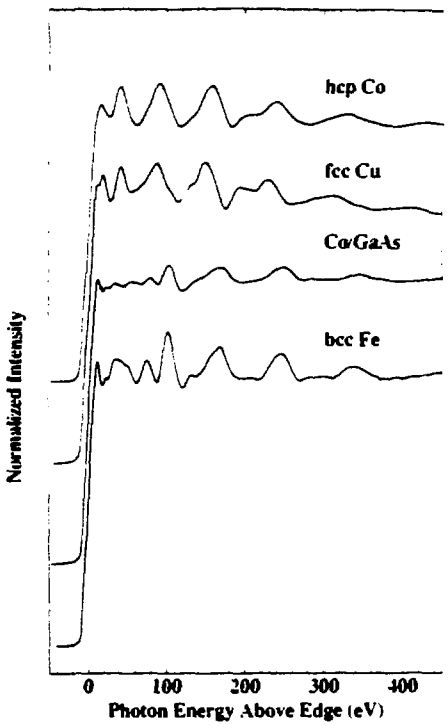

We have undertaken to measure the bulk atomic geometry by making EXAFS measurements above the cobalt K-edge, thus eliminating interference from the substrate. The EXAFS data can be compared with normal hcp cobalt as well as bcc iron and fcc copper to unambiguously determine the structure.

Shown at left is the data obtained thus far in the project. All of the data, including the standards, were collected by measuring the electron yield from the sample surface in a helium gas ionization chamber[2]. Several scans of the single crystal Co on GaAs sample were taken to eliminate glitches from Bragg reflections. The similarity of the epitaxial film to bcc iron is apparent upon inspection. Further analysis, including Fourier transforms and ratios will be performed to obtain lattice constants, etc.

[1]G. A. Prinz, Phys. Rev. Lett. 54, 1051(1985).
[2]W. T. Elam, J. P. Kirkland, R. A. Neiser, and P. D. Wolf, Phys. Rev. B36, 26(1988).

EXAFS ANALYSIS OF AN OXYGEN RICH TETRAGONAL PHASE IN YBCO

R.A. Neiser* (Sachs/Freeman Associates and SUNY Stony Brook)

An unusual, oxygen rich (x=7.3) tetragonal phase was observed in coatings of $YBa_2Cu_3O_x$ prepared by plasma spray processing. The phase is not superconducting and is characterized by lattice parameters a=b=1/3c=3.87 A. The phase can be quickly identified in x-ray diffraction patterns by the lack of the peak splitting commonly observed in the orthorhombic and oxygen deficient tetragonal phases of this material. Peak broadening in the x-ray diffraction patterns suggest that the lattice is highly strained. Simultaneous neutron diffraction, x-ray diffraction and EXAFS studies are being performed to better understand the structure of this oxygen rich phase.

The oxygen rich tetragonal phase can be converted to the desired orthorhombic phase by prolonged anneals at high temperature. The first three transforms shown in the figures below were taken from copper edge EXAFS signals from samples annealed at 930° C for 1) 2 hours; 2) 20 hours; and 3) 100 hours. The 2 hour specimen is the oxygen rich tetragonal phase, the 100 hour sample is orthorhombic, and the 20 hour sample is in an intermediate state. Figure 4 is the transform from a high quality standard pellet. Significant differences are observed in the O and Y+Ba peaks near 1.5 and 3.0 A, respectively, as the anneal time is increased. The structural implications of these changes have yet to be determined.

*This work was performed under contract number N00014-85-C-2628 from the Naval Research Laboratory.

Figure 1. 930 C 2 hours

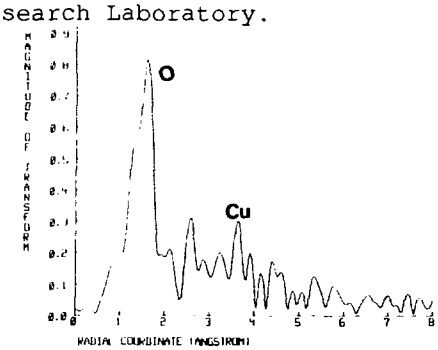

Figure 2. 930 C 20 hours

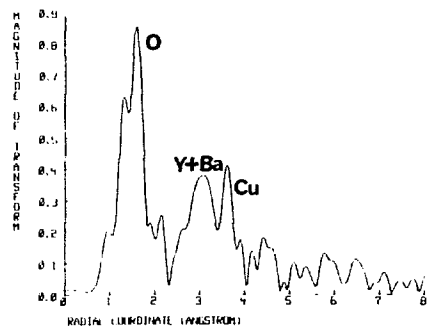

Figure 3. 930 C 100 hours

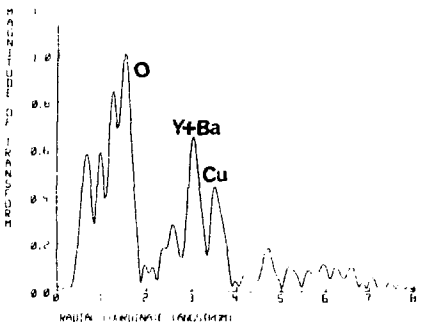

Figure 4. Pellet standard

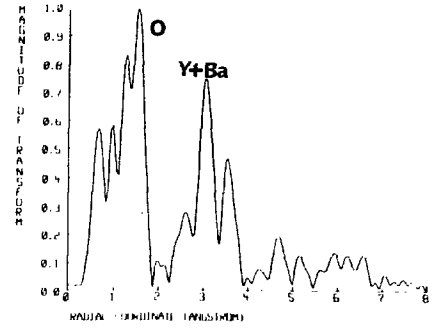

X–RAY DIFFRACTION OF A MONOMOLECULAR FILM SPREAD ON A LIQUID SUBSTRATE. Karl M. Robinson, J. Adin Mann Jr., Dept. of Chemical Engineering, Case Western Reserve University, Cleveland, OH 44106.

The study of thin films on liquid substrates has been limited to macroscopic observations of general film behavior. Synchrtron radiation has provided the means of observing the two–dimensional crystalline properties of thin films. The experiment performed on X–23B was the trial run of a new liquid surface diffractometer. Major emphasis has been placed on vibrational and environmental isolation of the film, in addition to 0.1 micron resolution control of beam positioning. The film is controlled in an ultrapure environment consisting of a fused silica trough, purified N_2 atmosphere, 0.1°C control and chromatography grade surface chemistry. Surface Pressure is monitored by non–destructive surface laser light scattering. The initial data (Figure 1) obtained from the diffractometer shows the reflected beam as well as several scattered peaks of unknown origin. Further analysis of the data will be performed following a more controlled experimental procedure.

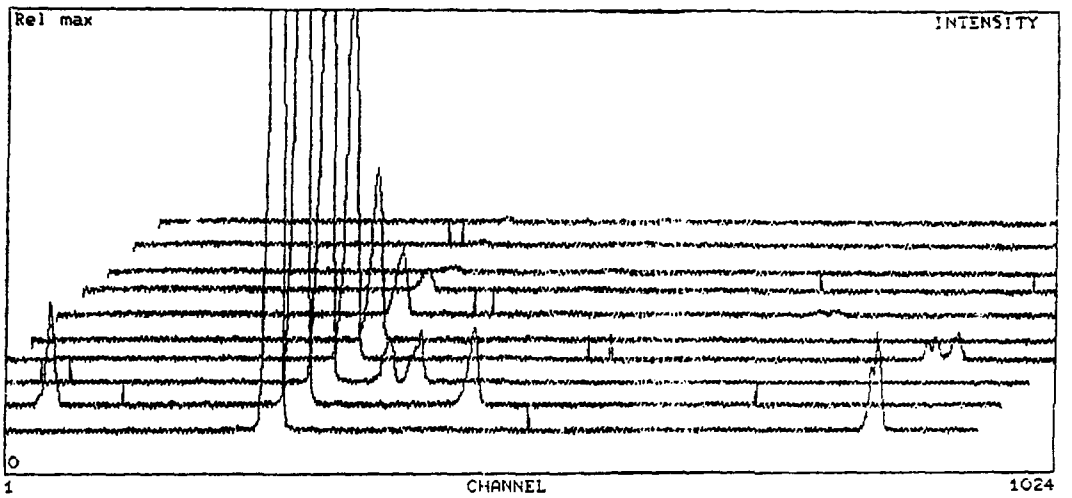

FIGURE 1: Scattered x–ray radiation from a clean water surface. Increasing channel number is an increase in vertical distance above the surface. Each line represents a step of .05° away from the plane of incidence. The profile of the reflected beam is clearly shown as a function of the angular step. Angle of incidence is .310° with an x–ray energy of 7600Ev.

I would like to acknowledge funding by the Office of Naval Research.

PLASMA DEPOSITION OF AMORPHOUS POWDERS - AN EXAFS ANALYSIS

S.Sampath (SUNY-SB), H.Herman (SUNY-SB), R.A.Neiser* (NRL).
* Sachs/Freeman Associates, Landover, MD.

Plasma spraying is a line of sight process which involves the injection of powders into a high temperature plasma jet. This high velocity deposition of plasma melted particles yields highly disordered and metastable structures in many metals, alloys, and ceramics due to rapid solidification on impact. In order to explore this effect, an amorphous powder (Ni-35Mo-9Fe-1.8B) was plasma sprayed onto a steel substrates in air.

Figure 1 shows the Fourier transform of EXAFS for the Ni-edge of the powder The absence of 2nd and higher order shells indicates that the structure is continuously random or amorphous in the true sense. The coating (Fig.2) show a similar structure, with small intensities in the 2nd, 3rd and 4th shells. This indicates a small degree of crystallinity in the coating and correlate well with diffraction data which suggests a similar structure. The amplitudes in Figs. 1 and 2 can be compared to those of a fully crystalline nickel foil standard shown in Fig. 3.

This work sponsored in part by NSF grant number MSM8513038.

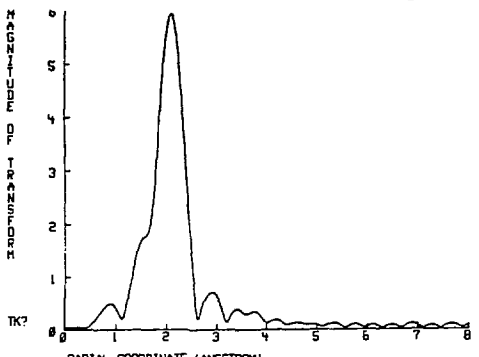

Fig.1 Ni-edge transform (powder)

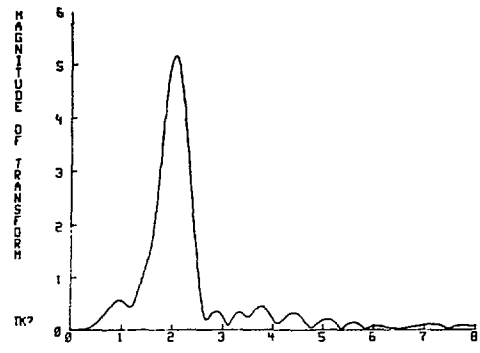

Fig.2 Ni-edge APS coating.

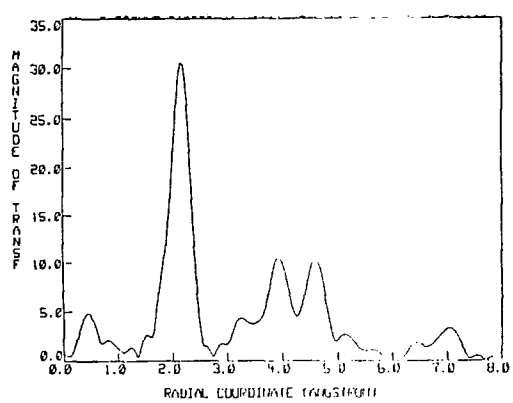

Fig. 3 Transform of Ni-foil standard.

IMPROVEMENTS, CHARACTERIZATION AND RE-COMMISSIONING OF BEAMLINE X-24A.

P.L. Cowan, D.W. Lindle, National Institute of Standards and Technology and B.A. Karlin, Brookhaven National Laboratory.

During the last operations period (May '85 - Feb. 87) beamline X-24A demonstrated unprecedented performance for a synchrotron radiation beamline operating in the photon energy range from 2 to 5 keV. This enhanced performance in flux, focussed intensity and energy resolving power compared to any other bending magnet or insertion device beamline led to a prodigious output of qualitatively new scientific results [1].

The long dark period in 1987-1988 was primarily a time for research activities at other synchrotron radiation facilities. Meanwhile, some improvements were made to the X-24A beamline during this time. These improvements include: a new mechanism for positioning the pre-monochromator x-ray mirror, new viewports for external surveying of beamline optical components, improved computer hardware and software, and re-polishing of the focussing x-ray mirror.

During the irregularly scheduled beamtime in summer 1988, a few tests were conducted using the x-ray beam. Primarily, these tests involved studies of the restricted aperture at port X-24 which has interfered with the reliable delivery of photons to the beamlines at this port. It was established that the effective aperture defined in the NSLS built front-end was significantly smaller than its designed value. Furthermore, it was documented that the established standard orbit is at the limit of this aperture so that orbits within the acceptable tolerance for ring operation can result in a significant obstruction of the photon beam at port X-24 as has repeatedly happened in the past. PRT members were able to improve the size of the effective aperture by purposely displacing front-end components from their specified locations. However, at this writing a corresponding redefinition of the standard orbit has not occurred despite repeated verbal assurances from the NSLS staff that it would.

Beam studies also were performed on the re-polished focussing x-ray mirror. Preliminary observations indicate a substantial improvement in performance of this element. This improvement is consistent with profilometer roughness measurements performed by Peter Tackas that indicate a reduction in surface roughness form ≈8nm r.m.s to less than 1.0nm r.m.s.

Reference:

1. See Beamline X-24A contributions to the NSLS Annual Report 1987.

PRODUCTION AND TRAPPING OF MULTIPLY-CHARGED ATOMS

B.M. Johnson, M. Meron, K.W. Jones (BNL); D.A. Church, S. Kravis (U. Texas A & M); I.A. Sellin, J.C. Levin (U. Tennessee); G. Berry, Y. Azuma (ANL); M. Druetta (U. Lyon).

Studies of ion production and storage in a Penning ion trap were performed using broad-band synchrotron radiation. This work is an extension of previous measurements [1,2], in which it was shown that argon ions in charge states 2 through 8 were confined at mean energies near 40 meV corresponding to room temperature. The most probable charge state was Ar^{4+}.

Enhancements over the previous work included increased photon flux afforded by the use of a 1:1 focussing mirror, data taking with radial (in addition to the previously used axial) detection scheme, and gas-puffing to decrease the background pressure after initial ion production. The focussing mirror delivered more photons through the center of the trap to somewhat localize the ion production and improve the signal to background ratio. The radial detection scheme produced charge-state spectra with considerably higher resolution. The gas puffing allowed for longer storage times for the higher charge-state ions by reducing the density of neutral atoms and thereby diminishing the rate of charge-exchange.

Previously determined [2] rate coefficients for charge exchange were remeasured using (as before) a mechanical chopper to turn the photon beam off for variable delay times before measuring the charge-state distribution. The new results are consistent with the previous work, but are of lower uncertainty. An attempt was made to observe the photoionization of ions by first producing low charge-state ions with electron bombardment, and then turning on the photon beam. Although there were encouraging indications, the results were inconclusive.

Further work is planned to extend and refine the measurements.

1. B. M. Johnson, M. Meron, A. Agagu, and K. W. Jones, Nucl. Instrum. and Meth. in Phys. Res. B24/25 (1987) 391-396

2. D. A. Church, S. D. Kravis, I. A. Sellin, C. S. O, J. C. Levin, R. T. Short, M. Meron, B. M. Johnson, and K. W. Jones, Phys. Rev. A36 (1987) 2487-2490

Research supported by the Division of Chemical Sciences, Office of Basic Energy Sciences, US Department of Energy and the National Science Foundation.

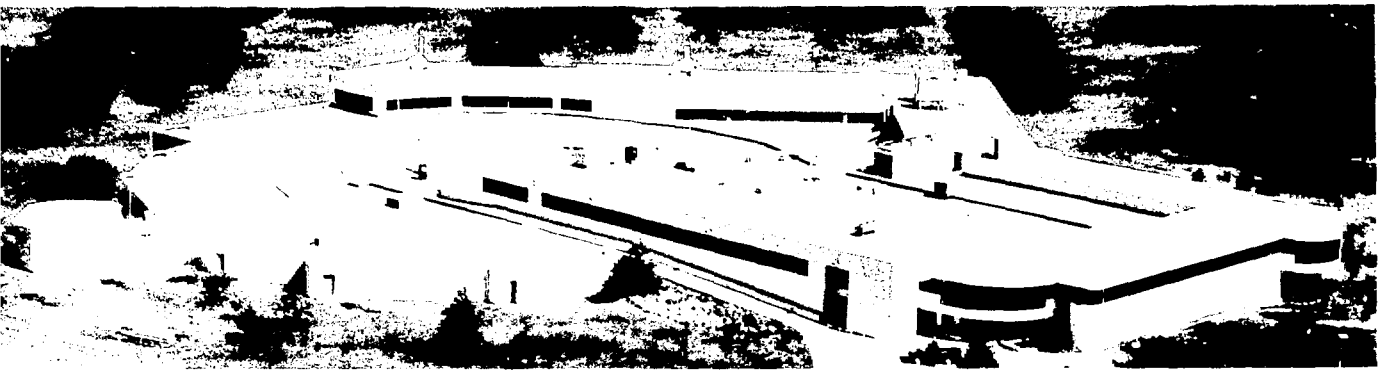

Section VI

Appendices

309/310

NSLS Users Publication List*

Beamline U1

Colbert, J. and Fischer, D.A., "Characterization of Focusing Multilayer Mirrors for Use in Collection of Carbon K Fluorescent Radiation", Symp. on Optical and Optoelectronic Applied Science and Eng., SPIE, **938** (1988).

Eberhardt, W., "Core Electron Excitations and Decay in Molecules", Physica Scripta, **T17**, 28 (1987).

Eberhardt, W., Abeles, B., Yang, L., Stasiewski, H., and Sondericker, D., "Photoemission Study of the a-Si-H/a-SiO_x:H and a-Si:H/a-SiN_x:H Interface Formation", Mat. Res. Soc. Symp. Proc. **77** (1987).

Fischer, D.A., Zaera F., and Gland, J.L., "Fluorescence Yield Near Edge Structures (FYNES): A Novel Technique for In-Situ Surface Chemistry", Proc. of the 14th Int. Conf. on X-ray and Inner-shell Processes, X87, Journal de Physique **48**, C9-1097 (1987).

Gland, J., Fischer, D.A., Zaera, F., and Shen, S., "Displacement of CO by More Weakly Absorbed Hydrogen on the Ni(100) Surface", J. Vac. Sci. Tech. **A6**, 2426 (1988).

Gland, J., Fischer, D.A., Zaera, F., and Shen, S., "Fluorescence Yield Near Edge X-ray Absorption Fine Structure Above the Carbon K Edge: A New Method for Characterizing Adsorbed Intermediates and Surface Reaction Rates in the Presence of Reactive Environments", Catalysis 1987, ed. J. Ward, Elsevier (1988).

Shen, S., Gland, J.L., Fischer, D.A., and Zaera, F., "Hydrogen Displacement of Chemisorbed CO from the Ni(100) Surface", Chinese J. of Mol. Cat. **2**, 137 (1988).

Sondericker, D., Fu, Z., Johnson, D.C., and Eberhardt, W., "Soft X-ray Absorption Studies on High-T_c Superconducting Oxides", Phys. Rev. B **36**, 3983 (1987).

Yang, L., Abeles, B., Eberhardt, W., Sondericker, D., Stasiewski, H., and Fu, Z., "Photoemission Study of a-Si:H/a-SiN_x:H Interface Formation", Journal of Non-Crystalline Solids **97** & **98**, 851 (1987).

Zaera, F., Fischer, D.A., Gland, J.L., and Shen, S., "Fluorescence Yield Near Edge X-ray Absorption Spectroscopy Under Atmospheric Pressures: CO Activation on Ni(100) in the Presence of Hydrogen from 10^{-9} to 0.1 torr", Surf. Sci. **194**, 205 (1988).

Beamline U3C

Bartlett, R.J., Trela, W.J., Michaud, T.D., Southworth, S.H., Alkire, R.W., Roy, P., Rothe, R., Walsh, P.J., and Shinn, N., "Characteristics and Performance of the Los Alamos VUV Beam Line at the NSLS", Nucl. Instr. and Meth. **A266**, 199 (1988).

Beamline U4A

Wertheim, G.K. and Mattheiss, L.F., "Partial Density of States of Ordered Cu_3Au, Phys. Rev. B **38**, 5988 (1988).

Beam Line U4B

Chen, C.T. and Sette, F., Phys. Rev. Lett. **60**, 160 (1988).

Beamline U5U

Johnson, P.D., Clarke, A., Brookes, N.B., Hulbert, S.L., Sinkovic, B., and Smith, N.V., "Exchange-Split Adsorbate Bands: The Role of Substrate Hydridization", Phys. Rev. Lett. **61**, 2257 (1988).

---

* Publications list was compiled from the PRT/IDT progress reports for the reporting period 9/16/87 to 3/15/88 and 3/16/88 to 9/15/88. It contains only published articles, no abstracts, and does not represent a complete listing for the facility.

Beamline U6

Dana, S.S., Maldonado, J.R., Vladimirsky, O., Fair, R., and Viswanathan, R., "Electrical Resistivity and Radiation Damage in Boro-Hydro-Nitride X-Ray Lithography Mask Substrates", Microelectronic Engineering **6**, 233 (1987).

Beamline U7

Chang, C.L., denBoer, M.L., Murgai, V., Horn, S., "Effect of Sm Valence Changes on Low Energy Photomission Spectra", Phys. Rev. B **37**, 6605 (1988).

denBoer, M.L., Chang, C.L., Horn, S., and Murgai, V., "Effect of Sm Valence Changes on Photoemission Spectra", Phys. Rev. B **37**, 6605 (1988).

Murgai, V., Huang, Y.-S., denBoer, M.L., and Horn, S., "5p-5d Resonance in Gd", Solid State Comm. **66**, 329 (1988).

Qiu, S.L., Pan, X., and Strongin, M., Citrin, P.H., "Photoemission from Support Clusters: The Problem of the Support", Phys. Rev. B **36**, 1292 (1987).

Qiu, S.L., Ruckman, M.W., Brookes, N.B., Johnson, P.D., Chen, J., Lin, C.L., and Strongin, M., Sinkovic, B., Crow, J.E., and Jee, C.-S., "Interaction of H_20 with a High-Temperature Superconductor", Phys. Rev. B **37**, 3747 (1988).

Wang, Z.Q., Lok, C.K.C., Quinn, J., Li, Y.S., and Jona, F., "Electronic Structure of Surface Alloy: Cu(001) c(2x2)-Au", J. Phys. C: Solid State Phys., **21**, 653 (1988).

Wu, S.C., Jona, F., et al., "Cu(001) c(2x2)-Pd: An Ordered Surface Alloy", Phys. Rev. B **38**, 5363 (1988).

Beamline U8 A&B

Himpsel, F.J., "Photoemission and Inverse Photoemission from Semiconductor Interfaces", Semiconductor Interfaces: Formation and Properties, Proceedings of the Workshop, Les Houches, G. Le Lay, J. Derrien, and N. Boccara, eds., Springer Proceedings in Physics **22**, 196 (1987).

Himpsel, F.J. Karlsson, U.O., Morar, J.F., Rieger, D., and Yarmoff, J.A., Reply to the Comment by C.T. Chen and F. Sette on "Determination of Interface States for CaF_2/Si(111) from Near-Edge X-ray-Absorption Measurements," Phys. Rev. Lett. **60**, 161 (1988).

Hollinger, G., Bergignat, E., Chermette, H., Himpsel, F.J., Lohez, D., Lannoo, M., and Bensoussan, M., "Anomalous Bonding in SiO_2 at the SiO_2 - Si Interface", Phil. Mag. **B55**, 735 (1987).

Jordan, J.L., Kovac, C.A., Morar, J.F., and Pollak, R.A., "High Resolution Photoemission Studies of the Reactivity of Cr with Polyimide and Model Polymers", Phys. Rev. B **36**, 1369 (1987).

Yarmoff, J.A., Taleb-Ibrahimi, A., McFeely, F.R., and Avouris, Ph., "Chemical Selectivity in Photon Stimulated Desorption from F on Si(111)", Phys. Rev. Lett. **60**, 960 (1988).

Beamline U8 C&D

Spiller, E. and Golub, L., "Fabrication and Testing of Large Area Multilayer Coated X-ray Optics", Topical Meeting on Optical Interference Coatings, April 12-15, 1988, Tucson, Arizona, Techn. Digest, (Opt. Soc. of Am.) **6**, 110 (1988).

Beamline U9A

Holroyd, R.A., Preses, J.M., Woody, C.L., and Johnson, R.A., "Measurement of the Absorption Length and Absolute Quantum Efficiency of TMAE and TEA from Threshold to 120 nm, Nucl. Instr. and Meth. **A261**, 440 (1987).

Preses, J.M., "The Fluorescence Lifetime of Excited Cyclohexane in an Argon Matrix and in Solid State Cyclohexane at Low Temperature," J. Chem. Phys. **89**, 1251 (1988).

Preses, J.M., "New Opportunities in Chemistry: An International Symposium on the Uses of Synchrotron Radiation in Chemistry," Synch. Rad. News **1**, 4 (1988).

Sander, R.K., Tiee, J.J., Quick, C.R., and Romero, R.J., "Quenching of C_2H Emission Produced by Vacuum Ultraviolet Photolysis of Acetylene," J. Chem. Phys. **89**, 3495 (1988).

Sandman, D.J., Valesquez, C.S., Hamill, G.P., Foxman, B.M., Preses, J.M., and Weston, R.E., "The Interaction of Vacuum Ultraviolet Light with Crystalline Monoacetylenes: A Progress Report," Mol. Cryst. Liq. Cryst. Inc., Monlin, Opt. **156**, 103 (1988).

Beamline U9B

Laws, W.R. and Sutherland, J.C., "Synchrotron Radiation as an Excitation Source in Time-Domain and Frequency-Domain Fluorometry", SPIE **99**, 29 (1988).

van Langen, H., "Interpretation of Fluorescence Depolarization Experiments on Lipid Membranes," PhD Thesis, University of Utrecht (1988).

Zinger, D., Geacintov, N.E., and Harvey, R.G., "Conformations and Selective Photodissociation of Heterogeneous Benzo(a)pyrene Diol Epoxide Enantiomer - DNA Adducts", Biophysical Chemistry **27**, 131 (1987).

Beamline U10

Chou, T.S., Foerster, C.L., Halama, H., and Lanni, C., "Proceedings of the Conference on the Vacuum Design of Advanced and Compact Light Sources", American Vacuum Society **5**, *334 (1988).*

Tsang, K.-L., Zhang, C.H., Callcott, T.A., Canfield, L.R., Ederer, D.L., Blendell, E., Clark, C.W., Wassdal, N., Rubensson, J.E., Bray, G., Mortensson, N., Nordgren, J., Nyholm, R., and Cramm, S., "Soft X-ray Absorption and Emission Spectra and the Electronic Structure of the $Ba_2YCu_3O_{7-x}$ Superconductor", Phys. Rev. B **37**, 2293 (1988).

Zhang, C.H., Tsang, K.L., Callcott, T.A., Ederer, D.L., and Arakawa, E.T., "The Al $L_{2,3}$ and Mg Double Ionization Emission Spectra of Dilute Al in Mg Alloys", Phys. Rev. B **37**, 2401 (1988).

Beamline U11

Grover, J.R., Walters, E.A., Arneberg, D.L., and Santandres, C., "Competitive Production of Weakly Bound Heterodimers in Free Jet Expansions", Chem. Phys. Lett. **146**, 305 (1988).

White, M.G., LeRoi, G.E., Ho, M.-H., and Poliakoff, E.D., "Multichannel Interactions in the Resonant Photoionization of HCl", J. Chem. Phys. **87**, 6553 (1987).

Beamline U12

Lui, S.C., Mundenar, J.M., Plummer, E.W., Mostoller, M.E., Nicklow, R.M., Zehner, D.M, Ford, W.K., and Erskine, J., "Electronic and Vibrational Properties of Single Crystal Surfaces of NiAl", Mat. Res. Soc. Symp. Proc. **83**, 47 (1987).

Lyo, I.W. and Plummer, E.W., "Quasiparticle Band Structure of Na and Simple Metals", Phys. Rev. Lett. **60**, 1558 (1988).

Mundenar, J.M., Gaylord, R.H., Lui, S.C., Plummer, E.W., Zehner, D.M., Ford, W.K., and Sneddon, L.G., "Carbon Monoxide Adsorption of (111) and (110) Single Crystal NiAl Surfaces", Mat. Res. Soc. Symp. Proc. **83**, 59 (1987).

Plummer, E.W., "Photoemission from Nearly Free Electron Metals", Physica Scripta **T17**, 186 (1987).

Beamline U13U

Chen, C.T., "Concept and Design Procedure for Cylindrical Element Monochromators for Synchrotron Radiation", Nucl. Instr. and Meth. **A256**, 595 (1987).

Hulbert, S.L. and Sharma, S., "Mirror and Grating Surface Figure Requirements for Grazing Incidence Synchrotron Radiation Beam Lines: Power Loading Effects", Nucl. Instr. and Meth. **A266**, 491 (1988).

Beamline U14

Fulmer, J., Zaera, F., Tysoe, W., "The Orientation and Bonding of CO on Mo(100) using ARUPS and NEXAFS", J. Chem. Phys. **87**, 7265 (1987).

Johnson, E.D. and Garrett, R.F., "In-situ Reactive Cleaning of X-ray Optics by Glow Discharge", Nucl. Inst. and Meth. **A266,** 381 (1988).

Tourillon, G., Fontaine, A., Dartyge, E., Garrett, R., Sagurton, M., Xu, P., and Williams, G., "Chemisorption Geometry of Poly-3Methyl Thiophene Electrochemically Deposited on Pt as Observed by NEXAFS", Europhys. Lett. **4**, 1391 (1987).

Beamline U15

Cinotti, F., Voisin, M.C., Jacobsen, C., Kenney, J.M., Kirz, J., McNulty, I., Rarback, H., Rosser, R., and Shu, D., Proc. International Conf. X-ray Microscopy, Springer-Verlag, Berlin Heidelberg (1987).

Hanson, D., "Atom Selective Photochemistry with Monochromatic Soft X-rays", in *Desorption Induced by Electronic Transitions - DIET III*, Springer Series in Surface Sciences **13**, R.H. Stulen, and M.L. Knotek, eds., Springer-Verlag, Berlin (1988).

Rarback, H., Cinotti, F., Jacobsen, C., Kenney, J.M., Kirz, J., and Rosser, R., "Elemental Analysis Using Differential Absorption Techniques", Biological Trace Element Research **13**, 103 (1987).

Williams, C.K., Reisman, A., Bhattacharya, P., and Ng, W., "Defect Generation in Silicon Dioxide from Soft X-ray Synchrotron Radiation", J. Appl. Phys. **64**, 3 (1988).

Woronick, S.C., Ng, W., Krol, A., Yang, B.X., Kao, Y.H., Meng, R.L., Hor, P.H., Chu, C.W., "Short Range Order Structure Around Oxygen Atoms in the Superconductor Y-Ba-Cu-O", Proc. of High Temperature Superconductor Symp., N.B. Brodsky, et al., eds., Mat. Res. Soc., Pittsburgh (1988).

Woronick, S.C., Yang, B.X., Krol, A., Kao, Y.H., Munekata, H., Chang, L.L., Philips, J.C., "X-ray Reflectivity of InAs/GaAs Heterostructures with Surface and Interfacial Roughness", Proc. 3rd International Conf. on Modulated Semiconductor Structures, J. de Phys. **48**, C5-51 (1987).

Yang, B.X., Kirz, J., and Sham, T.K., "Oxygen K-edge Extended X-ray Absorption Fine-Structure Studies of Molecules Containing Oxygen and Carbon Atoms", Phys. Rev. A **36**, 4298 (1988).

Yang, B.X. and Kirz, J., "Soft X-ray Absorption Cross Section of Argon Determined by a Variable Absorber Technique", Applied Optics **26**, 2823 (1987).

Yang, B.X., Tohji, K., and Hanson, D.M., "Optical Luminescence Excitation Spectra of Molecular Oxygen in the Soft X-ray Region", J. Chem. Phys. **89**, 1215 (1988).

Beamline U16C

Anacker, D. and Erskine, J.L., "Design of NSLS Undulator Beam Line U5 for Spin-Polarized Photoemission Spectroscopy", Nucl. Inst. and Meth. **A266**, 336 (1988).

Beamline X1

DiGennaro, R., Gee, B., Guigli, J., Hogrefe, H., and Howells, M., "A Water-Cooled Mirror System for Synchrotron Radiation", Nucl. Instr. and Meth. **A266,** 498 (1988).

Eberhardt, W. and Murphy, R. "Auger Electron-Ion Coincidence Studies on Free Molecules", *Desorption Induced by Electronic Transitions-DIET III*, Springer Series in Surface Sciences **13**, R.H. Stulen and M.L. Knotek, eds. Springer-Verlag, Berlin (1988).

Eberhardt, W., Plummer, E.W., Lyo, I.-W., Murphy, R., Carr, R., and Ford, W.K., "Core Hole Decay and Fragmentation of Molecules: Electron-ion Coincidence Studies of N_2", J. de Phys. **48**, C9-679 (1987).

Larkins, F.P., Eberhardt, W., Lyo, I.-W., Murphy, R., Plummer, E.W., "The Core Hole Decay of N_2O Following Core to Bound State Excitations", J. Chem. Phys. **88**, 2948 (1988).

Murphy, R., Eberhardt, W., "Site Specific Fragmentation in Molecules: Auger-Electron Ion Coincidence Studies on N_2O", J. Chem. Phys. **89**, 7 (1988)

Murphy, R., Lyo, I.-W., Eberhardt, W., "The Effect of the Nuclear Motion on the Electronic Decay of Core Hole Excited States in Molecules", J. Chem. Phys. **88**, 10 (1988).

Rarback, H., Jacobsen, C., Kirz, J., McNulty, I., "The Performance of the NSLS Mini-Undulator", Nucl. Instr. and Meth. **A266**, 96 (1988).

Shu, D., Siddons, P., Rarback, H., and Kirz, J., "Two-Dimensional Laser Interferometric Encoder for the Soft X-ray Scanning Microscope at the NSLS", Nucl. Instr. and Meth. **A266**, 313 (1988).

Vladinirsky, Y., et al, "Zone Plates for X-ray Microscopy", Nucl. Instr. and Meth. **A266**, 324 (1988).

Beamline X3

Chu, B., Wu, D.-Q., and Wu, C., "A Kratky Block Collimation Small Angle X-ray Diffractometer for Synchrotron Radiation", Rev. Sci. Instr. **58**, 1158 (1987).

Chu, B., Wu, C., Wu, D.-Q., and Phillips, J.C., "Fractal Geometry in Branched Epoxy Polymer Kinetics", Macromolecules, Comm. **20**, 2642 (1987).

Chu, B., Wu, D.-Q., MacKnight, W.J., Wu, C., Phillips, J.C., LeGrand. A.D., Lantman, C.W., and Lundberg, R.D., "Synchrotron Small Angle X-ray Scattering of Sulfonated Polystyrene Ionomers", Macromolecules **21**, 523 (1988).

Coppens, P., Petricek, V., Levendis, D., Larsen, F.K., Paturle, A., Gao, Y., and LeGrand, A.D., "Synchrotron Radiation Study of the Five-Dimensional Modulated Phase of Tetrathiafulvalene-Tetracyanoquinodimethane (TTF-TCNQ) at 15K", Phys. Rev. Lett. **59**, 1695 (1987).

Eng, P.J., Krebs, L.A., Lee, C.-B., Stephens, P W., Woronick, S., Huang, K.-G., Kayed, M.A., Zegenhagen, J., Gibson, W.M., Hansen, D.A., Hudson, J.B., and Phillips, J.C., "The SUNY X21B Beamline at NSLS: Spectroscopy and Versatile Surface Science Facility", Nucl. Instr. and Meth. **A266**, 210 (1988).

Higby, P.L., Shelby, J.E., Phillips, J.C., and LeGrand, A.D., "EXAFS Study of Alkali Galliosilicate Glasses", J. Non Cryst. Sol. **105**, 139 (1988).

LeGrand, A.D., Lehnert, W.F., and Phillips, J.C., "A Time-Resolved Scattering Data Acquisition System at the SUNY X-21A Beam Line at NSLS", Nucl. Instr. and Meth. **A266**, 659 (1988).

Phillips, J.C., LeGrand, A.D., and Lehnert, W.F., "Protein Folding Observed by Time-Resolved Synchrotron X-ray Scattering — A Feasibility Study", Biophys. J. **53**, 461 (1987).

Prewitt, C.T., Coppens, P., Phillips, J.C., and Finger, L.W., "New Opportunities in Synchrotron X-ray Crystallography", Science **238**, 312 (1987).

Song, H.H., Stein, R.S., Wu, D.-Q ., Ree, M., Phillips, J.C., LeGrand, A.D., and Chu, B., "Time-Resolved SAXS on Crystallization of a Low-Density Polyethylene/High-Density Polyethylene Polymer Blend", Macromolecules Comm. **21**, 1180 (1988).

Woronick, S.C., Kao, Y.H., Hills, M.E., Nee, T.W., and Rehn, V., "Short-Range-Order Structure of an InGaAs Compound Superconductor Grown by Liquid-Phase Epitaxy", J. Appl. Phys. **61**, 2836 (1987).

Zegenhagen, J., Huang, K.-G., Hunt, B.D., and Schowalter, L.J., "Interface Structure and Lattice Mismatch of Epitaxial $CoSi_2$ on Si(111)", Appl. Phys. Lett. **51**, 1176 (1987).

Zegenhagen, J., Kayed, M.A., Huang, K.-G., Gibson, W.M., Phillips, J.C., Schowalter, L.J., and Hunt, B.D., "Determination of Lattice Mismatch in $NiSi_2$ Overlayers on Si(111)", Appl. Phys. **A44**, 365 (1987).

Beamline X7A

Cox, D.E., Toby, B.H., and Eddy, M.M., "Acquisition of Powder Diffraction Data with Synchrotron Radiation", Aust. J. Phys. **41**, 117 (1988).

Dmowski, W., Egami, T., Bancel, P.A., Heiney, P.A., Baxter, D.V., and Leake, J.A., "Structure of Quasicrystalline Al-Mn-Ru: X-ray and Neutron Studies", Mat. Sci. Eng. **99**, 345 (1988).

Eddy, M.M., Gier, T.E., Keder, N.L., Stucky, G.D., Cox, D.E., Bierlein, J.D., and Jones, G., "Inclusion Tuning of Non-linear Optical Materials: Sorbates in the KTP Structure", Inorg. Chem. **27**, 1856 (1988).

Egami, T., Graham, C.D., Jr., Dmowski, W., Zhou, P., Flanders, P.J., Marinero, E.E., Notarys, H., and Robinson, C., "Anisotropy and Coercivity of Amorphous Re-TM Films", IEEE Transactions on Magnetics, **Mag-23**, 2269 (1987).

Hibble, S.J., Cheetham, A.K., Bogle, A.R.L., Wakerley, H.R., Cox, D.E., "The Synthesis and Structure Determination from Powder Diffraction Data of $LaMo_5O_8$, a New Oxynolybdate Containing Mo_{10} Clusters", J. Amer. Chem. Soc. **110**, 3295 (1988).

Jephcoat, A.P., Mao, J.-K., Finger, L.W., Cox, D.E., Hamley, R.J., and Zha, C.-S., "Pressure-Induced Structural Phase Transitions in Solid Xenon", Phys. Rev. Lett. **59**, 2670 (1987).

Kohler, J., Simon, A., Hibble, S.J., and Cheetham, A.K., "A Single Crystal and Synchrotron Powder X-ray Refinement of the Structure of $SrNb_8O_{14}$, A New Oxyniobate Containing Nb_6 Octahedra", J. Less. Common Met. **142**, 123 (1988).

Marezio, M., Cox, D.E., Rossel, C., and Maple, M.B., "The Ab-initio Structure Determination of UPd_2Sn by Synchrotron X-ray Powder Diffraction", Solid State Comm. **67**, 831 (1988).

Mao, H.K., Jephcoat, A.P., Hemley, R.J., Finger, L.W., Zha, C.-S., Hazen, R.M., and Cox, D.E., "Synchrotron X-ray Diffraction Measurements of Single-Crystal Hydrogren to 26.5 Gigapascals", Science **239**, 1131 (1988).

McCusker, L., "The Ab-initio Structure Determination of Sigma-2 (a new Clathrasil Phase) from Synchrotron Powder Diffraction Data", J. Appl. Cryst. **21**, 305 (1988).

Moroney, L.M., Thompson, P., and Cox, D.E., "ADPD: A New Approach to Shared-Site Problems in Crystallography", J. Appl. Cryst. **21**, 206 (1988).

Poon, S.J., Dmowski, W., Egami, T., Shen, Y., Shiflet, G.J., "Comparison of Quasicrystalline (T2) and Crystalline (R) Structures in AlCuLI Using High-Resolution X-ray Diffraction", Phil. Mag. Lett. **56**, 259 (1987).

Prewitt, C.T., Coppens, P., Phillips, J.C., and Finger, L.W., Science **238**, 312 (1987).

Smith, G.S., Johnson, Q.C., Smith, D.K., Cox, D.E., Snyder, R.L., Zhou, R.-S., and Zalkin, A., "The Crystal and Molecular Structure of Beryllium Hydride", Solid State Comm. **67**, 491 (1988).

Toby, B.H., Eddy, M.M., Fyfe, C.A., Kokotailo, G.T., Strobl, H., and Cox, D.E., "A High Resolution NMR and Synchrotron X-ray Poser Diffraction Study of Zeolite ZSM-11", J. Mat. Res. **3**, 563 (1988).

Beamline X7B

Kvick, A., "Applications of Synchrotron X-rays to Chemical Crystallography", Chemical Crystallography with Pulsed Neutrons and Synchrotron X-rays, NATO ASI Series C **221**, 187 (1988).

A. McLMathieson, "Small-Single-Crystal Diffractometry with Monochromated Synchrotron Radiation — The Wavelength-Dispersion Minimum Condition for Bragg Reflection Profile Measurement". Acta Cryst. **44**, 239 (1988).

Beamline X9

Change, B., Powers, L., Chance, M., Zhou, Y., Reddy, K.S., "Optical and X-ray Techniques in the Study of Rapid Ligand Binding: A Ligand 'docking' Site in the Reaction of Mb and CO at 40°", Adv. Biochemistry and Biophysics (A Symposium Honoring Tsoo E. King), C. Kim, et al., eds., Plenum, New York (1988).

Fischetti, R.F., Filipkowski, M., Garito, A.F., Blasie, J.K., "Profile Structures of Ultrathin Periodic and Nonperiodic Multilayer Films Containing a Disubstituted Diacetylene by High Resolution X-ray Diffraction", Phys. Rev. B **37**, 4714 (1988).

Fischetti, R.F., Skita, V., Garito, A.F., Blasie, J.K., "Asymmetry in the Interior Arachidic Acid Bilayers Within Ultrathin Multilayers Fabricated via the Langmuir Blodgett Technique", Phys. Rev. B. **37**, 4788 (1988).

Fontes, E., Heiney, P.A., Barois, P., Levelut, A.M., "Strong Incommensurate Fluctuations in a Smectic-A Phase", Phys. Rev. Lett. **60**, 1138 (1988).

McKeown, D.A., "Radiation Distribution Analysis of a Series of Silica Rich Sodium Aluminosilicate Glasses Using Energy Dispersive X-ray Diffraction", Physics & Chem. of Glasses **28**, 156 (1987).

Powers, L., Chance, B., Chance, M., Campbell, B., Friedman, J., Khalid, S., Kumar, C., Naqui, A., Reddy, K.S., and Zhou, Y., "Kinetic, Structural, and Spectroscopic Identification of Geminate States of Myoglobin: A Ligand Binding Site on the Reaction Pathway", Biochem. **26**, 4785 (1987).

Rosenbaum, G., Rock, L., Sullivan, M., "High-Flux, Elliptically-bent, UHV-Compatible Mirror with Simple External Bending Mechanism for Beam Line X9A at NSLS", Nucl. Instr. and Meth. **A266**, 399 (1988).

Rosenbaum, G., Sullivan, M., Rock, R., Khalid, S., "High-Flux, UHV-Compatible, Water-Cooled Double Crystal Monochromator for Beam Line X9 at NSLS", Nucl. Instr. and Meth. **A266**, 475 (1988).

Zhang, K., Bunker, G., Zhang, G., Zhao, Z.X., Chen, L.Q., Huang, Y.Z., "An EXAFS Experiment on the High T_c Superconductor $YBa_2Cu_3O_{7-\delta}$", Phys. Rev. B. **37**, 3375 (1988).

Beamline X10

Flannery, B.P, Deckman, H.W., Roberge, W.G., and D'Amico, K.L., "Three Dimensional X-ray Microtomography", Science **237**, 1389 (1987).

Liang, K.S., Sirota, E.B., D'Amico, K.L., Hughes, G.J., Sinha, S.K., and Unertl, W.N., "The Step Roughening of the Cu(113) Surface: A Grazing Incidence X-ray Scattering Study," *The Structure of Surfaces II*, Proceedings of the 2nd International Conference on the Structure of Surfaces (ICSOS II), Amsterdam, the Netherlands, 509 (1987).

Liang, K.S., Sirota, E.B., D'Amico, K.L., Hughes, G.J., and Sinha, S.K., "Roughening Transition of a Stepped Cu(113) Surface: A Synchrotron X-ray-Scattering Study", Phys. Rev. Lett. **59**, 2447 (1987).

Beamline X11

Barrera, E.V., Heald, S.M., and Marcus, H.L., "In situ Analysis of Monolayer Thick Metal-Metal Interfaces", Scripta Metallurgica **21**, 1633 (1987).

Bein, T., McLain, S.J., Corbin, D.R., Farlee, R.D., Moller, K., Stuckey, G.D., Woolery, G., and Sayers, D., "Intrazeolite Chemistry of Nickel (O) Complexes and Ni (0, 11) Clusters Studied by EXAFS, Solid-State NMR, and FT-IR Spectroscopy", J. Am. Chem. **110**, 1801 (1988).

Bianconi, A., Budnick,J., Flank, A.M., Fontaine, A., LaGarde, P., Marcelli, A., Tolentino, H., Chamberland, B., Michel, C., Raveau, B., and Demazeau, G., "Evidence of 4d9-Ligand Hole States in the Superconductor La(1.85)Sr(0.15)Cu(4) from L3 X-ray Absorption Spectroscopy", Phys. Lett. A **127**, 285 (1988).

Budnick, J.I., Sanchez, F.H., Zhang, Y.D., Choi, M., Hines, W.A., Zhang, Z.Y., Ge, S.H., and Hasegawa, R., "Study of the Local Structure of Metastable Crystalline Iron-Boron Alloys", IEEE Trans. on Magnetics **23**, 1938 (1987).

Bunker, B.A., "EXAFS Studies of Metastable Semiconductors", Mat. Res. Soc. **77**, 99 (1987).

Bunker, B.A., "EXAFS Studies of Semiconductor Structure", J. Vac. Sci. Tech. **A5**, 3003 (1987).

Bunker, B.A. and Sayers, D.E., "EXAFS Data Analysis", *Extended X-ray Asorption Fine Structure*, R. Prins and D. Koningsberger, eds. (1987).

Choi, M., Budnick, J.I., Hayes, G.H., Pease, D.M., Heald, S.M., Sayers, D.E., and Hasegawa, R., "Extended X-ray Absorption Fine-Structure of Amorphous $(Ni_xPt_{100-x})_{75}P_{25}$ Alloys", Phys. Rev. B **36**, 4613 (1987).

Heald, S.M., "Design of an EXAFS Experiment", *Extended X-ray Asorption Fine Structure*, R. Prins and D. Koningsberger, eds. (1987).

Islam, Q. and Bunker, B.A., "The Ferroelectric Transition in $Pb_{1-x}Ge_xTe$: Extended X-ray Absorption Fine-Structure Investigation of the Fe and Pb Sites", Phys. Rev. Lett. **59**, 2701 (1987).

Kelly, M.J., Fund, A.S., McDevitt, M.R., Tooley, P.A., and Gates, B.C., "Structure of Supported Metal Catalysts Derived from Molecular Bimetallic Clusters", Mat. Res. Symp. **111**, 23 (1988).

McBreen, J., O'Grady, W.E., and Pandya, K.I., "EXAFS: A New Tool for the Study of Battery and Fuel Cell Materials", J. of Power Sources **22**, 323 (1988).

Paesler, M.A., and Sayers, D.E., "X-ray Absorption Studies of Amorphous Semiconductors", *Disordered Semiconductors*, M. Kastner, G.A. Thomas, and S.R. Ovshinsky, eds. (1987).

Sarikaya, M. and Stern, E.A., "Local Structural Variations in $YBa_2Cu_3O_{7-x}$", Phys. Rev. B **37**, 9373 (1988).

Tranquada, J.M., Heald, S.M., and Moodenbaugh, A.R., "X-ray Absorption Near-Edge Structure Study of $La_{2-x}(Ba,Sr)_xCuO_{4-y}$ Superconductors", Phys. Rev. B **36**, 5263 (1987).

Tranquada, J.M., Heald, S.M., Moodenbaugh, A.R., and Suenaga, M., "X-ray Absorption Studies of $La_{2-x}(Ba,Sr)_xCuO_{4-y}$ Superconductors", Proceedings, Int. Wksp. on Novel Mechanisms in Superconducting, S.A. Wolf and V.Z. Kresin, eds. (1987).

Yang, C.Y., Paesler, M.A., and Sayers, D.E., "Quantitative Measurement of Structural Changes Associated with Photo-darkening in a-As_2S_3 Films", J. Non-Cryst. Solids **97**, 1119 (1987).

Yang, C.Y., Paesler, M.A., and Sayers, D.E., "X-ray Absorption Studies of Glassy As_2S_3: The Role of Rapid Quenching", Phys. Rev. B **36**, 8122 (1987).

Yang, C.Y., Paesler, M.A., and Sayers, D.E., "Measurements of Local Structural Configurations Associated with Reversible Photostructural Changes in Arsenic Trisulfide Films", Phys. Rev. B **36**, 9160 (1987).

Yang, C.Y., Paesler, M.A., and Sayers, D.E., "A New Method of Measuring Optical Phonons in Amorphous Solids: Analysis of the Mean Square Relative Displacement of the EXAFS", J. Non-Cryst. Solids **97**, 1151 (1987).

Yang, C.Y., Yang, X.Q., Heald, S.M., Reilly, J.J., Skotheim, T., Moodenbaugh, A.R., and Suenaga, M., "Superconducting $H_xYBa_2Cu_3O_7$: The Role of H", Phys. Rev. B **36**, 8798 (1987).

Beamline X12C

Badger, J., et al, "Structural Analysis of a Series of Antiviral Agents Complexed with Human Rhinovirus 14", National Academy of Science, USA **85**, 3304 (1988).

Beamline X14

Bommannavar, A.S., Sparks, C.J., Habenschuss, A., Ice, G.E., Dhere, A., Morkoc, H., and Zabel, H., "X-Ray Diffraction Study of a Thin GaAs Film on Si(100)", Mat. Res. Soc. Symp. Proc. **102**, 223 (1988).

Budai, J.D., Tischler, J.Z., Habenschuss, A., Ice, G.E., and Elser, V., "X-ray Diffraction Study of Phason Strain Field in Oriented Icosahedral Al-Mn", Phys. Rev. Lett. **58**, 2304 (1987).

DeAngelis, R.J., Dhere, A.G., Maginnis, M.A., Reucraft, P.J., Ice, G.E., and Habenschuss, A., "Synchrotron X-Ray Scattering for the Structural Characterization of Catalysts", Advances in X-Ray Analysis **30**, C.S. Barrett, J. V. Gilfrich, R. Jenkins, D.E. Leyden, J.C. Ross, and P.K. Predecki, eds., Plenum, New York, 389 (1987).

Dhere, A.G., DeAngelis, R.J., Reucroft, P.J., Bentley, J., Ice, G.E., and Habenschuss, A., "Morphological Developments of Nickel Particles in Supported Metal Catalysts," Advances in X-Ray Analysis **30**, C.S. Barrett, J.V. Gilfrich, R. Jenkins, D.E. Leyden, J.C. Ross, and P.K. Predecki, eds., Plenum, New York, 379 (1987).

Habenschuss, A., Ice, G.E., Sparks, C.J., and Neiser, R.A., Jr., "The ORNL Beam Line at the National Synchrotron Light Source", Nucl. Instr. and Meth. **A266**, 215 (1988).

Hwang, B., Houska, C.R., Ice, G.E., and Habenschuss, A., "Residual Strain Gradients in a Fully Stabilized Zirconia Sample", J. Appl. Phys. **63**, 11 (1988).

Hwang, B., Houska, C.R., Ice, G.E., and Habenschuss, A., "X-ray Analysis of the Near Surface Phase Distribution Applied to Wear on a PSZ Disk", Advanced Ceramic Mat. **3**, 180 (1988).

Ice, G.E., "Microdiffraction with Synchrotron Radiation", Nucl. Instr. and Meth. **B24**, 397 (1987).

Ice, G.E. and Sparks, C.J., "A Simple Cantilevered Mirror for Focusing Synchrotron Radiation", Nucl. Instr. and Meth. **A266**, 394 (1988).

Larson, B.C., Iida, S., Tischler, J.Z., Lewis, J.D., Ice, G.E., and Habenschuss, A., "X-Ray Diffuse Scattering from Cobalt Precipitates in Copper", Mat. Res. Soc. Symp. Proc. **82**, 73 (1987).

Sparks, C.J., Hasaka, M., Easton, D.S., Baik, S., Habenschuss, A., and Ice, G.E., "Structural Studies of Nickel Films and Their Interface with Sapphire Substrates", Mat. Res. Soc. Symp. Proc. **77**, 495 (1987).

Tischler, J.Z., Budai, J.D., Ice, G.E., and Habenschuss, A., "Multiple Scattering and the (200) Reflection in Silicon and Germanium", Acta Cryst. **A44**, 22 (1988).

Beamline X16A

Robinson, I.K., Waskiewicz, W.K., Fuoss, P.H., and Norton, L.J., "Observation of Strain in the Si(111) 7X7 Surface", Phy. Rev. B **37**, 4325 (1988).

Robinson, I.K., "The Role of Strain in Si(111)7X7 and Related Reconstructed Surfaces", J. Vac. Sci. Tech. **A6**, 1966 (1988).

Beamline X16B

Gibbs, D., Harshman, D.R., Isaacs, E.D., McWhan, D.B., Mills, D., and Vettier, C., "Polarization and Resonance Properties of Magnetic X-ray Scattering in Holmium", Phys. Rev. Lett. **61**, 1241 (1988).

Beamline X16C

Bates, F.S., Keith, H.D., and McWhan, D.B., "Isotope Effect on the Melting Temperature of Nonpolar Polymers", Macromolecules **20**, 3065 (1987).

Beamline X17B1

Brauer, E. and Thomlinson, W., "Experimental Verification of Photon: A Program for Use in X-Ray Shilding Calculations", Nucl. Instr. and Meth. **A266**, 195 (1988).

Brauer, E. and Thomlinson, W., "Experimental Verification of Photon: A Program for Use in X-Ray Sheilding Calculations", BNL 39793 (1988).

Chapman, D., Gmur, N., Lazarz, N., and Thomlinson, W., "Photon: A Program for Synchrotron Radiation Dose Calculations", Nucl. Instr. and Meth. **A266**, 191 (1988).

Chapman, D., "Photon: A User's Manual", BNL 40822, (1988).

Thomlinson, W., Chapman, D., Gmur, N., and Lazarz, N., "The Superconducting Wiggler Beam Port at the National Synchrotron Light Source", Nucl. Instr. and Meth. **A266**, 226 (1988).

Thomlinson, W., Chapman, D., Gmur, N., and Lazarz, N., "The Superconducting Wiggler Beam Port at the National Synchrotron Light Source", BNL 41158 (1988).

Beamline X18A

Dennison, J.R., Taub, H., Hansen, F.Y., Shechter, H., and Brener, R., "Anomalous Layering of $Fe(CO)_5$ Adsorbed on Graphite", Phys. Rev. B **37**, 2266 (1988).

Koo, Y.M., Cohen, J.B., Shapiro, S.M., and Tanner, L.E., "As Quenched Cu-10.9 at % Be", Acta Metall., **36**, 591 (1988).

Ohshima, K., Harada, J., Morinagba, M., Georgopoulos, P., and Cohen, J.B., "Distortion-Induced Scattering Due to Vacancies in NbC_O72", Acta Cryst. **A44**, 167 (1988).

Shen, Q. and Colella, R., "Solution of Phase Problem for Crystallography at a Wavelength of 3.5 A", Nature **329**, 232 (1987).

Shen, Q. and Colella, R., "Phase Observation in an Organic Crystal (Benzil: $C_{14}H_{10}O_2$) Using Long-Wavelength X-rays", Acta Cryst. **A44**, 17 (1988).

Beamline X18B

Alp, E., Goodman, G.L., Hinks, D.G., Veal, B.W., and Montano, P.A., "X-Ray Absorption Studies of $La_{2-x}Sr_yCuO_y$ and $Y_{1-x}Or_xBa_2Cu_3O_{7-}$", Mat. Res. Soc. Symp. Proc. **99**, 177 (1988).

Alp, E.E., Soderholm, L., Shenoy, G.K., Hinks, D.G., Veal, B.W., and Montano, P.A., "Valence Determination in High T_c Oxide Superconductors by XANES and Mossbauer Spectroscopy", Physica B **150**, 74 (1988).

Ramanathan, M., Engbretson, M., and Montano, P.A., "A Closed Loop Feedback System for Synchrotron Radiation Double Crystal Monochromators", Nucl. Instr. and Meth. **A266**, 471 (1988).

Robota, H.J., Cohn, M.J., Ringwelski, A.Z., and Eades, R.A., "Structural Transformation in PT Supported on α-alumina Studied by X-ray Absorbtion Spectroscopy", *Microstructure and Properties of Catalysts*, Mat. Res. Soc. Symp. Proc. **111**, 201 (1988).

Beamline X19C

Benci, J.E., Pope, D.P., and George, E.P., "Creep Damage Nucleation Sites in Ferrous Alloys", Mat. Sci. Eng. **A103**, 97 (1988).

Benci, J.E. and Pope, D.P., Met. Trans. **19A**, 837 (1988).

Chang, Y.S., Hsieh, I.J., and Chen, H., "Phase Transformation and Identification of an Epitaxial Fe-Ni Alloy Silicide", J. Appl. Phys. (1988).

Chen, H., "Studies of Diffusion by Diffraction/Scattering Techniques", in *Diffusion Analysis and Applications*, R.W. Heckel, A.D. Romi, and M.A. Dayananda, eds., Proc. of TMS-AIME Symp., Chicago, IL (1988).

Dudley, M., "Application of Synchrotron Radiation Topography to Dynamic Processes in Single Crystal Materials", Nucl. Instr. and Meth. **B24/25**, 1068 (1987).

Little, T.W. and Chen, H., "In-Situ X-ray Diffraction Measurement of Pd_2Si Transformation Kinetics Using a Linear Position-Sensitivity Detector", J. Appl. Phys. (1988).

Stock, S.R., Chen, H., and Birnbaum, H.K., "Growth of Thin Niobium Crystals by the Strain-Anneal Method", J. Cryst. Growth **84**, 419 (1987).

Beamline X20

Brock, J.D., "X-ray Scattering Study of Bond Orientational Order in Liquid Crystal Films", Ph.D. Dissertation, MIT (1987).

Chung, J.W., Evans-Lutterodt, K., Specht, E.D., Birgeneau, R.J., Estrup, P.J., and Kortan, A.R., "Grazing-Incidence X-ray Study of the Structures and Phase Transitions of Hydrogen on Tungsten(100)", Phys. Rev. Lett. **59**, 2192 (1987).

Goldman, A.I., Mohanty, K., Shirane, G., Horn, P.M., Greene, R.L., Peters, J.C., Thurston, T.R., and Birgeneau, R.J., "Magnetic X-ray Scattering Measurements on MnF_2", Phys. Rev. B **36**, 5609 (1987).

Greiser, M., Held, G.A., Frahm, R., Greene, R.L., Horn, P.M., and Suter, R.M., "Melting of Monolayer Xenon on Silver: The Hexatic Phase in the Weak-Substrate Limit", Phys. Rev. Lett. **59**, 1706 (1987).

Heiney, P.A., Bancel, P.A., Horn, P.M., Jordan, J.L., LaPlaca, S., Angilello, J., and Gayle, F.W., "Disorder in Al-Li-CU and Al-Mn-Si Icosahedral Alloys", Science **238**, 660 (1987).

Heiney, P.A., Bancel, P.A., and Horn, P.M., "Comment on 'So-called' Icosahedral and Decagonal Quasicrystals are Twins of an 820-Atom Cubic Crystal", Phys. Rev. Lett. **59**, 2119 (1987).

Held, G.A., Jordan-Sweet, J.L., Horn, P.M., Mak, A., and Birgeneau, R.J., "X-ray Scattering Study of the Thermal Roughening of Ag(110)", Phys. Rev. Lett. **59**, 2075 (1987).

Hong, H., Peters, C.J., Mak, A., Birgeneau, R.J., Horn, P.M., and Suematsu, H., "Commensurate-Incommensurate and Rotational Transitions of Monolayer Xenon on Single-Crystal Graphite", Phys. Rev. B **36**, 7311 (1987).

Hong, H., "Structures and Phase Transitions of Xenon Monolayers and Multilayers on Graphite Surfaces", Ph.D. dissertation, MIT (1988).

Horn, P.M., Malzfeldt, W., DiVencenzo, D.P., Toner, J., and Gambino, R., "Systematics of Disorder in Quasiperiodic Material", Phys. Rev. Lett. **57**, 1444 (1986).

Malzfeldt, W., Horn, P.M., DiVencenzo, D.P., Stephenson, B., Gambino, R., and Herd, S., "Structure Studies of Aluminum Based Quasicrystals", J. de Phys. **47**, C3-379 (1986).

Spect, E.D., Mak, A., Peters, C., Sutton, M., Birgeneau, R.J., D'Amico, K.L., Moncton, D.E., Nagler, S.E., and Horn, P.M., "Phase Diagram and Phase Transitions of Krypton on Graphite in the extended Monolayer Regime", Z. Phys. B **69**, 347 (1987).

Stephenson, G.B., "Time-Resolved X-ray Scattering Using A High-Intensity Multilayer Monochromator", Nucl. Instr. and Meth. **A266**, 447 (1988).

Sutton, M., Yang, Y.S., Mainville, J., Strom-Olsen, J.O., Altounian, Z., Stephenson, G.B., and Ludwig, K.F., "Crystallization of Amorphous $NiZr_2$", Mat. Sci. Eng. **97**, 307 (1988).

Beamline X22B

Braslau, A., Pershan, P.S., Swislow, G., Ocko, B.M., Als-Nielsen, J., "Capillary Waves on the Surface of Simple Liquids Measured by X-ray Reflectivity", Phys. Rev. A **38**, 2457 (1988).

Cohn, J.L., Lin, J.J., Lamelas, F.J., He, H., Clarke, R., and Uher, C., "Upper Critical Fields of Periodic and Quasiperiodic Nb-Ta Superlattices", Phys. Rev. B **38**, 2326 (1988).

Gibbs, D., Mohanty, K.M., and Bohr, J., "High-Resolution X-ray Scattering Study of Charge-Density-Wave Modulation in Chromium", Phys. Rev. B **37**, 562 (1988).

Pershan, P.S., "Liquid and Liquid Crystal Surfaces", Pro. Nat. Acad. Sci., USA **84**, 4692 (1987).

Beamline X22C

Blume, M. and Gibbs, D., "Polarization Dependence of Magnetic X-ray Scattering", Phys. Rev. B **37**, 1779 (1988).

Gibbs, D., Harshman, D.R., Isaacs, E., McWhan, D., Mills, D., Vettier, C., Phys. Rev. Lett. **61**, 1246 (1988).

Gibbs, D., Ocko, B., Zehner, D.M., Mochrie, S.J.G., Phys. Rev. B **38**, 7303 (1988).

Hannon, J.P., Trammell, G.T., Blume, M., and Gibbs, D., Phys. Rev. Lett. **61**, 1245 (1988).

Beamline X23

Bouldin, C.E., Forman, R.A., and Bell, M.I., "Silicon Photodiode Detector for Fluorescence EXAFS", Rev. Sci. Instr. **58**, 1891 (1987).

Jack, T., Novotny, D., Carver, G., Geist, J., and Spal, R.D., "An X-ray Monochromator Crystal which Detects the Bragg Condition", Nucl. Instr. and Meth. **A263**, 522 (1988).

Kennedy, J.J., Amirtharaj, P.M., Boyd, P.R., Qadri, S.B., Dobbyn, R.C., and Long, G.G., "Growth and Characterization of $Cd_{1-c}Zn_xTe$ and $Hg_{1-y}Zn_yTe$", J. Cryst. Growth **86**, 93 (1988).

Kuriyama, M., Dobbyn, R.C., Takagi, S., and Chow, L.C., "Microradiography with an X-ray Image Magnifier: Application to Dental Hard Tissue", Med. Phys. **14**, 968 (1987).

Kuriyama, M., "Advanced Techniques for Microstructure Characterization", Trans. Tech. Publ.: Materials Science Forum, T.R. Anatharaman and R. Krishnan, eds. (1988).

Long, G.G. and Kuriyama, M., "Local Atomic Environments in the Manganese-Aluminum Icosahedral Phase", in Incommensurate Crystals, Liquid Crystals, and Quasi-Crystals, J.F. Scott and N.A. Clark, eds., Plenum, New York, 337 (1987).

Skeath, P., Elam, W.T., and Burns, W.K., "Concentration Dependence of the Octahedral Ti^{4+} Center in LiN_6O_3: Its Effect on Refractive Indices", Phys. Rev. Lett. **59**, 1950 (1987).

Spal, R., "A CAMAC Handler for RT-11", Nucl. Instr. and Meth. **A270**, 462 (1988).

Steiner, B., Laor, U., Kuriyama, M., Long, G.G., and Dobbyn, R.C., "Diffraction Imaging of High Quality Bismuth Silicon Oxide with Monochromator Synchrotron Radiation: Implications for Crystal Growth", J. Cryst. Growth **87**, 79 (1988).

Steiner, B., Laor, U., Kuriyama, M., Long, G.G., and Dobbyn, R.C., J. Cryst. Growth **87**, 731 (1988).

Beamline X23B

Elam, W.T., Kirkland, J.P., Neiser, R.A., and Wolf, P.D., "Depth Dependence for Extended X-ray Absorption Fine Structure Spectroscopy Detected via Electron Yield in He and in Vacuum", Phys. Rev. B **38**, 26 (1988).

Kirkland, J.P., Gilfrich, J.V., and Elam, W.T., "Appearance Potential X-ray Fluorescence Analysis", Adv. in X-ray Analysis **B1**, C.S. Barrell, et al; eds., Plenum, New York (1988).

Neiser, R.A., Kirkland, J.P., and Elam, W.T., "Optical Performance at the Naval Research Laboratory's Materials Analysis Beam Line at the NSLS", Nucl. Instr. and Meth. **A266**, 220 (1988).

Shih, A., Hor, C., Mueller, D., Marrian, C.R.K., Elam, W.T., Wolf, P., Kirkland, J.P., and Neiser, R.A., "Surface Extended X-ray Absorption Fine Structure Study of Surface BaO Layers on Tungsten Surfaces", J. Vac. Sci. Tech. **A6**, 1058 (1988).

Beamline X24A

Deslattes, R.D., "Fluorescent and Scattered Spectra: Near-Threshold Excitation of Atoms, Molecules, and Solids", J. de Phys. **48**, C9-579 (1987).

Lindle, D.W., Cowan, P.L., LaVilla, R.E., Jach, T., Deslattes, R.D., Karlin, B., Sheehy, J.A., Gil, T.J., and Langhoff, P.W., "Polarization of Molecular X-ray Fluorescence", Phys. Rev. Lett. **60**, 1010 (1988).

Lindle, D.W., Cowan, P.L., LaVilla, R.E., Jach, T., Deslattes, R.D., Perera, R.C.C., and Karlin, B., "Polarization Effects in Molecular Fluorescence", J. de Phys. **48**, C9-761 (1987).

Lindle, D.W., Cowan, P.L., LaVilla, R.E., Jach, T., Deslattes, R.D., Perera, R.C.C., and Karlin, B., "Near-Threshold X-Ray Fluorescence Spectroscopy of Molecules", SPIE **911**, 54 (1988).

Perera, R.C.C., Cowan, P.L., Lindle, D.W., and LaVilla, R.E., "Sub-Threshold Excited Cl Kβ (KV) X-ray Fluorescence from CF>Cl Molecule", J. de Phys. **48**, C9-753 (1987).

Beamline X24C

Long, J.P., Instrumentation for Combined Laser-Synchrotron Photoemission Experiments", Nucl. Instr. and Meth. **A266**, 673 (1988).

Sadeghi, H.R. and Henrich, V.E., "Electron Interations in the Rhodium/TiO_2 System", J. Catal. **1097**, 1 (1988).

Beamline X26

Hanson, A.L., "A Method for Selecting Detector Apertures for Use in SRIXE", Nucl. Instr. and Meth. **A260**, 264 (1987).

Hanson, A.L., "The Calculation of Coherent and Incoherent Scattering Cross Sections for Polarized X-rays into an Arbitrarily Placed Circular Aperture", Nucl. Instr. and Meth. **A264**, 471 (1988).

Hanson, A.L., "An Easy and Accurate Approximation to the Integrated Compton Cross Section for the Scattering of Polarized X-Rays into an Arbitrarily Placed Circular Aperture", Nucl. Instr. and Meth. **A264**, 484 (1988).

Hanson, A.L. and Meron, M., "Errors Associated with the Measurement of Scattered Polarized X-Rays", Nucl. Instr. and Meth. **A264**, 488 (1988).

Hanson, A.L., Kwiatek, W., and Jones, K.W., "The Use of a SiTek Position Sensitive Detector for Synchrotron Radiation Beam Monitoring and Alignment", Nucl. Instr. and Meth. **A260**, 529 (1987).

Jones, K.W., Gordon, B.M., Hanson, A.L., Kwiatek, W.M., and Pounds, J.G., "X-Ray Fluorescence with Synchrotron Radiation", Ultramicroscopy **24**, 313 (1988).

Jones, K.W., Takacs, P.Z., Hastings, J.B., Casstevens, J.M., and Pionke, C.D., "Fabrication of an 8:1 Ellipsoidal Mirror for a Synchrotron X-Ray Microprobe", Proc. SPIE, **749,** 37 (1987).

Sutton, S.R., Delaney, J., Smith, J.V., and Prinz, M., "Copper and Nickel Partitioning in Iron Meteorites", Geochem. Cosmochem. Acta **51**, 2653 (1987).

Beamline X26A & C

Bockman, R., Repo, M., Warrell, R., Pounds, J.G., Kwiatek, W.M., Long, G.J., Schidlovsky, G., and Jones, K.W., "X-ray Microscopy Studies on the Pharmaco-Dynamics of Therapeutic Gallium in Rat Bones", *X-Ray Microscopy II*, D. Sayre, M. Howells, J. Kirz, and H. Rarback, eds., Springer-Verlag, New York, 391 (1988).

Chen, J.R., Back, J.M., Chao, E.C.T., Minkin, J.A., Hanson, A.L., Jones, K.W., Rivers, M.L., and Sutton, S.R., "Location and Mapping of Gold Sites in Unoxidized Carlin-Type Ores", *X-Ray Microscopy II*, D. Sayre, M. Howells, J. Kirz, and H. Rarback, eds., Springer-Verlag, New York, 395 (1988).

Church, D.A., Kravis, S.D., Meron, M., Johnson, B.M., Jones, K.W., Sellin, I.A., O, C.S., Levin, J.C., and Short, R.T., "Research with Stored Ions Produced Using Synchrotron Radiation", Nucl. Instr. and Meth. **B31**, 262 (1988).

Giauque, R.D., Thompson, A.C., Underwood, J.H., Wu, Y., Jones, K.W., and Rivers, M.L., "Measurement of Femtogram Quantities of Trace Elements Using an X-ray Microprobe", Anal. Chem. **60**, 855 (1988).

Gordon, B.M., Hanson, A.L., Jones, KJ.W., Kwiatek, W.M., Long, G.J., Pounds, J.G., Schidlovsky, G., Spanne, P., Rivers, M.L., and Sutton, S.R., "An X-ray Microprobe Beam Line for Trace Element Analysis", *X-Ray Microscopy II*, D. Sayre, M. Howells, J. Kirz, and H. Rarback, eds., Springer-Verlag, New York, 276 (1988).

Hanson, A.L., Gigante, G.E., and Meron, M., "Contours of Constant Scattering Angle", Phys. Rev. Lett. **61**, 135 (1988).

Jones, K.W., Kwiatek, W.M., Gordon, B.M., Hanson, A.L., Pounds, J.G., Rivers, M.L., Sutton, S.R., Thompson, A.C., Underwood, J.H., Giauque, R.D., and Wu, Y. "X-ray Microscopy using Collimated and Focussed Synchrotron Radiation", *Advances in X-Ray Analysis* **31**, C.S. Barrett, J.V. Gilfrich, R. Jenkins, J.C. Russ, J.W. Richardson, Jr., and P.K. Predecki, eds., Plenum, New York, 59 (1988).

Meron, M., Johnson, B.M., Jones, K.W., and Church, D.A., "Charge State Evolution in an Ion Trap Irradiated by VUV Synchrotron Radiation", Nucl. Instr. and Meth. **B31**, 256 (1988).

Pounds, J.G., Long, G.J., Kwiatek, W.M., Jones, K.W., Gordon, B.M., and Hanson, A.L., "The Role of High-Energy Synchrotron Radiation in Biomedical Trace Element Research", *X-Ray Microscopy II*, D. Sayre, M. Howells, J. Kirz, and H. Rarback, eds., Springer-Verlag, New York, 425 (1988).

Rivers, M.L., "X-Ray Fluorescence Imaging with Synchrotron Radiation", *X-Ray Microscopy II*, D. Sayre, M. Howells, J. Kirz, and H. Rarback, eds., Springer-Verlag, New York, 233 (1988).

Sutton, S.R. and Flynn, G.J., "Stratospheric Particles: Synchrotron X-Ray Fluorescence Determination of Trace Element Contents", *Proc. 18th Lunar and Planetary Science Conference*, Graham Ryder, ed., Cambridge University Press, 607 (1988).

Sutton, S.R., Rivers, M.L., Smith, J.V., and Jones, K.W., "Advances in Geochemistry and Cosmochemistry: Trace Element Microdistributions with the Synchrotron X-Ray Fluorescence Miroprobe", *X-Ray Microscopy II*, D. Sayre, M. Howells, J. Kirz, and H. Rarback, eds., Springer-Verlag, New York, 438 (1988).

Publications of the NSLS Staff During Fiscal Year 1988

Batchelor, K., Kirk, H., Sheehan, J., Woodle, M. and McDonald, K. Development of a High Brightness Electron Gun for the Accelerator Test Facility at Brookhaven National Laboratory. BNL 41767, August 1988.

Batchelor, K., Kirk, H., McDonald, K., Sheehan, J. and Woodle, M. Design and Modeling of a 5 MeV Radio Frequency Electron Gun. Informal Report BNL 41766, August 1988.

Batchelor, K., Pellegrini C. et al. The Brookhaven Accelerator Test Facility. *Proc. of the 1988 Linac Conference.* BNL 42020, September 1988.

Bozoki, E. Algorithms and Procedures in the Model Based Control of Accelerators. Informal Report BNL 40462, October 1987.

Bozoki, E. A Tool for Symmetry Studies in Circular Machines. Informal Report BNL 41444, October 1987.

Chapman, D. Photon: A User's Manual. Informal Report BNL 40822, January 1988.

Chou, T.S., Foerster, C., Halama, H. and Lanni, C. Measurements of a Prototype Synchrotron Radiation Pumped Absorber for Future Light Sources. *AIP Conference Proceedings No. 171, AVS Series 5, 334 (1988).* BNL 41566, August 1988.

Chou, T.S., Foerster, C., Halama, H. and Lanni, C. Proceedings of the Conf. on Vacuum Design of Advanced and Compact Light Sources, Upton, NY. *AIP Conference Proceedings No. 171, AVS Series 5 (1988).*

Cline, D. and Pellegrini, C. A High Luminosity B-B Factory. *Proc. of the Snowmass Workshop on High Energy Physics, Snowmass, Colorado, 1988.* BNL 42031, September 1988.

Cornacchia, M., Campagna, M., Fonda, L., Margaritondo, G., Pellegrini C., Rosei, R. and Rubbia, C. The Trieste Synchrotron Radiation Project. Nucl. Instr. and Meth. *A266,* 74 (1988).

Dutt, S.K., Friedman, A., Gover, A. and Pellegrini, C. Three Dimensional Simulation of High Harmonic Transverse Optical Klystron. Nucl. Instr. and Meth. *A272,* 564 (1988). BNL 42061, September 1988.

Faigel, G., Siddons, D.P., Hastings, J.B., Haustein, P.E, Grover, J.R., and Berman, L.E. Observation of the Full Time Evolution of the Nuclear Collective Decay Mode in Crystalline $^{57}Fe_2O_3$ Excited by Synchrotron Radiation. Physical Review Letters *61,* 2794 (1988). BNL 41715, August 1988.

Gallardo, J., Dattoli, G., Renieri, A., Hermsen, T. Integral Equation for the Laser Field Description of a Free-Electron Laser Oscillator. BNL 40844, January 1988.

Gallardo, J., Dattoli, G., Renieri, A., Torre, A., Hermsen, T. Lethargy. Super Modes in Free Electron Lasers: An Analytical Treatment (Part 1). Phys. Rev. A, Vol *37,* 4326 (1988). BNL 41104, February 1988.

Gallardo, J., Fernow, R., Palmer, R., Pellegrini, C. Theory of a Free-Electron Laser with a Gaussian Optical Undulator. IEEE J. Quantum Electronics *24,* 1557 (1988). BNL 41105, March 1988.

Gmur, N.F., Heese, R.N. and Knotek, M.L. Brookhaven: Superconducting X-ray Lithography Source. CERN Courier, Vol. *28,* (9), 24 (1988). BNL 41798, September 1988.

Halama, H. and Hsieh, H.C. Gauging Requirements and Practices for Storage Rings and Accelerators. Journal of Vacuum Science and Technology A5 (5) (1987). BNL 40597, February 1988.

Halama, H. Lifetime and Performance of NSLS Storage Rings. *AIP Conference Proceedings No. 171, AVS Series 5, 227 (1988).* BNL 41554, July 1988.

Halama, H., Johnson, B.M., Jones, K.W., Meron, M. and Schuchman, J. Vacuum Considerations for a Heavy-Ion Storage Ring with Synchrotron Light Source Attachment. *AIP Conference Proceedings No. 171, AVS Series 5, 275 (1988).*

Halama, H.J., Schuchman, J.C., Stefan, P.M. Editors, Vacuum Design of Advanced and Compact Synchrotron Light Sources. *AIP Conference Proceedings No. 171, AVS Series 5 (1988).*

Hohlwein, D., Siddons, D.P. and Hastings, J.B. A Graphite Double Crystal Monochromator for X-Ray Synchrotron Radiation. J. Appl. Cryst. *21*, 911-915 (1988) BNL 40855, March 1988.

Hulbert, S., Rotela, E. and Shleifer, M. A Manually-Operated Ultra-High Vacuum Water-Cooled Slit Mechanism for the U13U Wiggler/Undulator Spectroscopy Branch Line at the National Synchrotron Light Source. Informal Report BNL 41171, April 1988.

Johnson, E.D. and Chou, T.S. *In-Situ* Reactive Glow Discharge Cleaning of NSLS Distributed Ion Pumps. *AIP Conference Proceedings No. 171, AVS Series 5, 175 (1988).* BNL 41639, August 1988.

Johnson, E.D. Closing Remarks: A Perspective from the Advanced Synchrotron Light Source Conference on the Vacuum Design of Advanced and Compact Synchrotron Light Sources. *AIP Conference Proceedings No. 171, AVS Series 5, 376 (1988).* BNL 41640, August 1988.

Knotek, M. Synchrotron Radiation. Invited talk presented at the Third Symposium on Pan American Collaboration in Experimental Physics — Rio de Janiero, Brazil, October 19-23, 1987. BNL 41810, September 1988.

Krinsky, S. Experience with Synchrotron Radiation Sources. International Symposium on X-Ray Microscopy, Brookhaven National Laboratory, Aug. 31-Sept. 4, 1987. BNL 40632, December 1987.

Murphy, J.B. and Pellegrini, C. Introduction to the Physics of the Free Electron Laser, in Frontiers of Particle Beams, Lecture Notes in Physics, Vol. 296, p. 163, M. Month and S. Turner, Editors, Springer Verlag, Berlin, 1988.

Pan, X., Johnson, P.D., Weinert, M., Watson, R.E., Davenport, J.W., Fernando, G.W., and S.L. Hulbert. Localized states at metal-metal interfaces: An inverse photoemission study of Pd/Nb(110). Phys. Rev. B *38*, 7850 (1988).

Pellegrini, C. Progress Towards a Soft X-ray FEL. Nucl. Instr. and Meth. *A272*, 564 (1988). BNL 40985, March 1988.

Rarback, H., Jacobsen, C., Kirz, J. and McNulty, I. The Performance of the NSLS Mini-Undulator. Nucl. Instr. and Meth. *A266* 96-105 (1988).

Sagurton, M., Xu, P., Garrett, R.F. and Williams, G.P. Determination of the Energy of the Sigma Level for CO Adsorbed on Ni(001) Using Both Auger & Direct Photoemission. Surface Science *199*, 413 (1988). BNL 41312, April 1988.

Schuchman, J. and Sharma, S. Design of Vacuum Chambers Downstream of NSLS X-ray Ring Insertion Devices. *AIP Conference Proceedings No. 171, AVS Series 5, 311.* BNL 41555, July 1988.

Suortti, P., Thomlinson, W. A Bent Laue Crystal Monochromator for Angiography at the NSLS. Nuclear Instr. and Meth. *A269*, 639 (1988). BNL 41292, May 1988.

Takacs, P.Z., Feng, S.K., Church, E.L., Qian, S. and Liu, W. Long Trace Profile Measurements on Cylindrical Aspheres. Presented at SPIE 32nd Annual Int. Technical Symposium on Optical & Optoelectronic Applied Science & Engineering, San Diego, CA, August 14-19, 1988. BNL 40955, March 1988.

Thomlinson, W., D. Chapman, N. Gmur and N. Lazarz. The Superconducting Wiggler Beamport at the National Synchrotron Light Source. Nucl. Instr. and Meth. in Physics Res. *A266*, 226-233 (1988). BNL 41158, April 1988.

Tourillon, G., Mahatsekek, C., Andrieu, C., Williams, G.P., Garrett, R.F., and Braun, W. Electronic Structure and Orientation Studies of Undoped Poly3alkyethiophenes Electrochemically Deposited on Pt as Studied by NEXAFS. Surface Science *201*, 171 (1988). BNL 41290, November 1987.

Wachtel, J.M. On Bunch Lengthening Using the Fourth Harmonic Cavity in the NSLS VUV Ring. Informal Report BNL 40929, February 1988.

Weilandics, C., Rohrig, N. and Gmur, N. Ozone Production Due to Synchrotron Radiation. Nucl. Instr. and Meth. *A266*, 691. BNL 41385, July 1988.

White-DePace, S., Gmur, N. and Thomlinson, W. National Synchrotron Light Source Annual Report 1987. BNL 52131, October 1987.

Yu, L.H. and Krinsky, S. Gain Reduction Due to Betatron Oscillations in a Free Electron Laser. Physics Letters A Vol. *129*, 464 (1988). BNL 41107, March 1988.

Yu, L.H., Krinsky, S. Betatron Oscillation in a Free Electron Laser. Nucl. Instr. Meth. *A272*, 436 (1988). BNL 40507, November 1988.

☆ U.S. GOVERNMENT PRINTING OFFICE: 1989—614-571